Gerard van Koten
Robert A. Gossage *Editors*

The Privileged Pincer-Metal Platform: Coordination Chemistry & Applications

54
Topics in Organometallic Chemistry

Aims and Scope

The series *Topics in Organometallic Chemistry* presents critical overviews of research results in organometallic chemistry. As our understanding of organometallic structure, properties and mechanisms increases, new ways are opened for the design of organometallic compounds and reactions tailored to the needs of such diverse areas as organic synthesis, medical research, biology and materials science. Thus the scope of coverage includes a broad range of topics of pure and applied organometallic chemistry, where new breakthroughs are being achieved that are of significance to a larger scientific audience.

The individual volumes of *Topics in Organometallic Chemistry* are thematic. Review articles are generally invited by the volume editors. All chapters from Topics in Organometallic Chemistry are published OnlineFirst with an individual DOI. In references, Topics in Organometallic Chemistry is abbreviated as Top Organomet Chem and cited as a journal.

More information about this series at http://www.springer.com/series/3418

Gerard van Koten • Robert A. Gossage
Editors

The Privileged Pincer-Metal Platform: Coordination Chemistry & Applications

With contributions by

M. Albrecht · D.V. Aleksanyan · M. Asay · P.A. Chase ·
H.P. Dijkstra · K. Farrell · M. Font · L.H. Gade ·
A.S. Goldman · R.A. Gossage · M.M. Hänninen ·
P.G. Hayes · V.A. Kozlov · A. Kumar · A.R. McDonald ·
R.L. Melen · D. Morales-Morales · X. Ribas · G. van Koten ·
M.T. Zamora

Editors

Gerard van Koten
Organic Chemistry and Catalysis
Debye Institute for Nanomaterials
    Science
Utrecht University
Utrecht
The Netherlands

Robert A. Gossage
Department of Chemistry & Biology
Ryerson University
Toronto
Canada

Printed on acid-free paper

Preface

Pincer ligands are extensively used in many diverse areas of chemistry primarily as a means to direct and modulate the properties of a metal center to which it is bonded. The title framework emerged in the late 1970s during the pioneering organometallic chemical studies by Shaw and coworkers. In the present day, the pincer platform, with its tridentate arrangement of donor sites, is used with great success in both ligand-metal mediated catalysis, (bio)inorganic chemistry, and materials science. The first series of review papers on Pincer chemistry, published in *Topics in Organometallic Chemistry* (2013: Vol. 40), discussed primarily those aspects of the chemistry and applications of the prototypical monoanionic pincer-metal compounds. In this formulation, the metal center is covalently bonded via a central (sp^2 or sp^3 hybridized) C-metal bond in addition to two complementary interactions with neutral heteroatom donors.

An important characteristic of the pincer platform is the fact that its three ligating sites are well organized by the backbone of the ligand and hence this allows for the possible formation of five- or six-membered chelate rings which have the central metal-heteroatom bond in common. Recent developments have made use of this modular nature of the pincer platform. Up to now, a multifaceted combination of donor sets has been explored and includes combinations of, e.g., neutral, anionic, Lewis basic and acidic, arene, heteroaromatic, and carbene donor sites. Moreover, in some cases, the pincer platform itself acts as a non-innocent ligand (NIL) or provides, with its pincer-metal manifold, a system that is suitable for executing metal-ligand cooperative (MLC) behavior in, e.g., catalytic processes. At present, the number of possibilities seems to have no limit; most excitingly many of these novel pincer-ligand metal combinations lead to the discovery of new catalysts for, e.g., C–X bond forming processes in organic synthesis, new polymerization technologies, the chemical conversion of CO_2, and the activation of bonds that so far were considered as primarily unreactive. The present volume comprises a series of ten chapters, some of which touch on a variety of these issues.

First of all, it is a great pleasure to start with an introductory chapter that is dedicated to the celebration of the 85th birthday of Prof. Bernard L. Shaw. Prof. Shaw was the first, together with Dr. C.J. Moulton, to report examples of 2,6-bis [(diphenylphosphine)methyl]phenyl metal-d^8 halide compounds. We now recognize these materials as the benchmark pincer complexes.

The volume then continues with a chapter "Pincer Complexes of Lithium, Sodium, Magnesium and Copper: a Discussion of Solution and Solid-state Aggregated Structure and Reactivity" discussing the synthesis and structural features of pincer-metal (Li, Na, Mg, and Cu) compounds that, in some cases, are indispensable as transmetallation reagents for the clean preparation of the corresponding pincer-transition metal derivatives. Incorporation of N-heterocyclic carbenes in the donor set of the pincer platform gives rise to the pincer chemistry presented in chapter "Late Transition Metal Complexes with Pincer Ligands that Comprise N-Heterocyclic Carbene Donor Sites" and entails attractive benefits for the development of novel, robust catalysts and for uses in materials science and the medicinal chemistry areas.

A vast number of complexes based on combinations of novel pincer ligands and rare earth metals have been described in chapter "Rare Earth Pincer Complexes: Synthesis, Reaction Chemistry and Catalysis" with a special focus on the properties of these complexes as polymerization catalysts. Chapter "New Chemistry with Anionic NNN-Pincer Ligands" provides an overview of the synthesis of anionic pincer-metal catalysts based on a combination of three N-donor sites and includes their reactivity in organic synthesis.

The synthesis of pincer-metal complexes using a pincer platform that contains thione sulfur groupings as neutral donor sites is presented in chapter "Pincer Complexes with Thione Sulfur Donors." The high-yield syntheses of POCOP pincer nickel complexes and their application as catalysts in, e.g., selective organic synthesis are described in chapter "Recent Advances on the Chemistry of POCOP Nickel Pincer Compounds." It was at an early stage of pincer-metal chemistry that a unique property of some pincer platforms was recognized. The ability to stabilize uncommon (high or low) formal oxidation states of the bound metal center was observed and later exploited in catalysis. In chapter "Pincer-Like Cyclic Systems for Unraveling Fundamental Coinage Metal Redox Processes," the synthesis of rare arylcopper(II) and copper(III) species, in which the aryl anion is part of a cyclic pincer platform, is discussed. With these arylcopper species, the intimate steps of catalytic processes involving C–X bond formation are demonstrated.

In the final two chapters, the use of pincer-metal complexes in alkane dehydrogenation (chapter "Recent Advances in Alkane Dehydrogenation Catalyzed by Pincer Complexes") and the synthesis and properties of soluble nanomaterials with multiple, immobilized pincer metal units as homogenous catalysts (chapter "Tethered Pincer Complexes as Recyclable Homogeneous Catalysts") are discussed. It is obvious that the chemistry presented in the greater part of these chapters has only been possible due to the fascinating and unique high kinetic and thermal stability of the pincer-metal manifold.

It is with great pleasure that we present these chapters that have been submitted by many important players in the field. We hope that their results and discussions will be an inspiration to our many colleagues active in organometallic chemistry, organic synthesis, nanotechnology, and materials science.

Utrecht, The Netherlands   Gerard van Koten
Toronto, ON, Canada   Robert A. Gossage

Contents

Modern Organometallic Multidentate Ligand Design Strategies: The Birth of the Privileged "Pincer" Ligand Platform

Preston A. Chase, Robert A. Gossage, and Gerard van Koten

Abstract The seemingly simple tridentate ligand design, one that is now known as the "pincer," has gained increasing importance in metal–ligand chemistry and in other applications as diverse as organic synthesis, catalysis, and materials science. This chapter describes the historical context in which the pincer ligand platform developed and sketches how Shaw's research played a crucial early role. The original chemistry, emerging in the late 1970s and early 1980s, is presented which details the synthesis and properties of the first examples of pincer-based organometallic complexes along with a selection of related species. Finally, a connection is made from this early start to the excellent and striving studies that currently are ongoing in pincer chemistry and its applications thereof.

Contents

P.A. Chase and G. van Koten (✉)
Organic Chemistry and Catalysis, Debye Institute for Materials Science, Utrecht University, Universiteitsweg 99, 3584 CG Utrecht, The Netherlands
e-mail: g.vankoten@uu.nl

R.A. Gossage (✉)
Department of Chemistry and Biology, Ryerson University, 350 Victoria Street, Toronto, ON M5B 2K3, Canada
e-mail: gossage@ryerson.ca

1   Introduction

Figure 1 depicts the basic structure of the title ligand: hereafter referred to as the "pincer." As a preliminary descriptor, there are essentially two fundamental design elements for prototypical pincer ligands that will be discussed in this historical treatise: (1) an aryl ring which is σ-bonded to a given metal or metalloid (M) and (2) chains or rings incorporating donor atoms flanking the C–M bond. Most commonly, particularly in early pincer designs (from the late 1970s to the beginning of the 1980s), these donors are at *benzylic* positions with respect to the aryl ring, providing for the possibility for two coupled five-membered metallocycles. These rings further serve to stabilize and protect the M–C bond. The ability to easily vary the type of donor atoms, the appended groups at either the donor atom or within the ligated metallocycles, and to incorporate substituents remote to the metal center allows for a high level of control of the environment around M. While direct variation of the steric and electronic effects via the coordinating atoms of the pincers "arms" is obvious, significant remote modulation of the electron density at the metal is also simply accomplished by the groups in a *para* (i.e., for early pincers) position of the aryl ring. This position can also be utilized to link or anchor the ligand to surfaces, polymers, dendrimers, probe fragments, etc.

The term "pincer" was first coined by van Koten in 1989 [1]. This English word is itself derived from the Dutch word *tang*, which in that language refers to the common hardware tool known as a wretch or spanner. This phrase thus emphasizes the manner in which the ligand tightly grasps a metal center.

So why would one investigate ligands containing these specific properties? From the start, it was recognized that the potentially terdentate coordination mode could be employed to alter and control the properties of metal complexes in a superior fashion when compared to those with similar bidentate ligands. Also, enhanced complex stability was a key early observation and hence became a driving force for
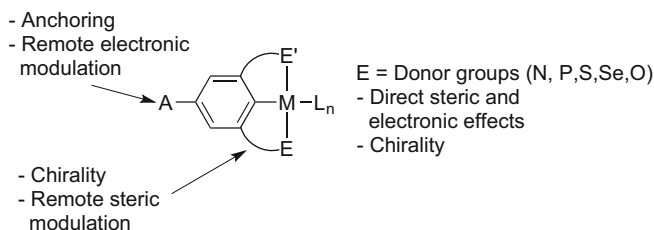
Fig. 1 Schematic structure of a prototypical ECE aryl pincer

exploring these systems. The simple synthesis of the parent ligands, often in only one or two steps from common commercial reagents, and the possibility for multiple routes to metal introduction were also a further selling point.

2 The Original Aryl Pincer Metal Complexes

2.1 Phosphine Containing "PCP" Aryl Pincers

Metal complexes of what we now refer to as the pincer ligands were first investigated in the mid-1970s in the groups of Bernard Shaw, Bill Kaska, and Gerard van Koten. In mid-1976, the seminal paper in the field was published by Shaw in *The Journal of the Chemical Society, Dalton Transactions* [2]. In an extension of his earlier studies on C–H activation and *ortho*-metalation of bulky, mixed aryl/alkyl phosphines [3–5], Shaw reasoned that 1,3-substitution of two bulky tBu_2PCH_2 groups on a benzene ring would result in preferential C–H activation in the mutually *ortho–ortho* position between the phosphine groups. Reaction of metal halide salts of Ni, Pd, Pt, Rh, or Ir in alcoholic solvents or mixtures of water and various alcohols resulted in the predicted C–H activation and formation of the resulting bis-cyclometalated metal complexes. For the platinum group metals, the simple PCP-M halide complexes were formed. With both Rh and Ir, PCP-MCl(H) hydride species were generated, as shown in Fig. 2. Even at this, the earliest stage of the investigation on aryl pincer metal complexes, the stability of these organometallic complexes was noteworthy. For instance, PCP-NiCl (**1**) was so thermally stable that it could be sublimed at 240°C and at atmospheric pressure *in air* without any visible decomposition. Similar thermal and air stability was noted for the other metalated PCP complexes **2–5** (Fig. 2).

Fig. 2 Synthesis of Shaw's original metallo-PCP aryl pincers [3–5]

1; M = Ni, L = H$_2$O, x = 6
2; M = Pd, L = PhCN, x = 2
3; M = Pt, L = PhCN, x = 2

4; M = Rh
5; M = Ir
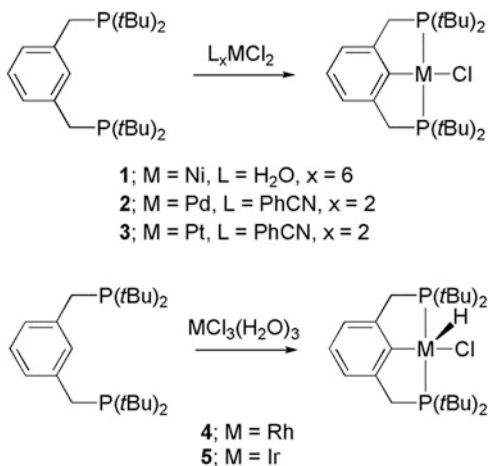
In addition, a fair degree of *chemical* stability for the Ni, Pd, and Pt PCP metallopincer complexes was also noted. Reaction of the PCP-MCl complex with $NaBH_4$ gave the corresponding PCP-MH hydrides in essentially quantitative yields. For the Pt species **3**, treatment of the hydride with ethanolic HCl regenerates the original chloro complex along with H_2 evolution without the rupturing of the aryl–Pt bond being observed. In addition, the halido ligands in complexes **1–3** could be replaced by either cyano or acetylenic groups via salt metathesis with NaCN or $LiC \equiv C-Ph$, respectively. Similarly, for PCP-NiCl **1**, salt metathesis with $NaBPh_4$ under an atmosphere of CO gives the ion-separated species [(PCP)Ni-CO][BPh_4] (**6**); see Fig. 3.

The coordinatively unsaturated Rh and Ir complexes **4** and **5**, respectively, also exhibit reactivity with CO (Fig. 4). Species **4** simply coordinates one molecule of CO, which by NMR and IR spectroscopy is positioned *trans* to the hydride ligand.
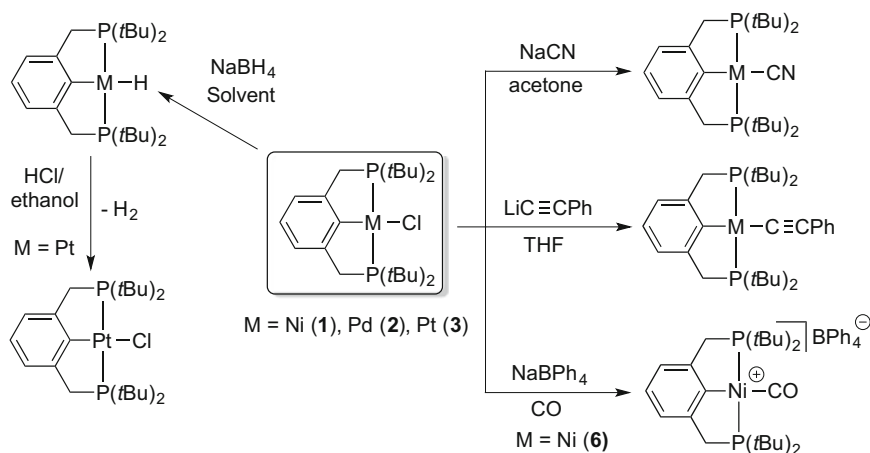
Fig. 3 Reactivity of original Ni, Pd, and Pt PCP aryl pincers
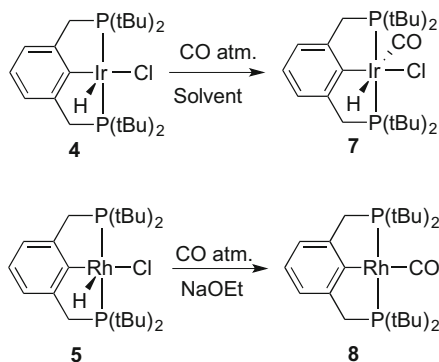
Fig. 4 Reactivity of original Ir (**4**) and Rh (**5**) PCP aryl pincers

Conversely, **5** exhibits decomposition to a Rh[I] dehydrochlorinated product PCP-Rh-CO (**8**) and a number of other, inseparable species. Pure **8** could be obtained by treatment of **5** with NaOEt in EtOH under an atmosphere of CO (*g*).

Reported in late 1978, the early study by Kaska also concerned PCP-type pincer complexes but in this case incorporating sterically moderate Me_2PCH_2 groups which flank the metal-aryl organometallic bond [6]. Clearly, the steric bulk needed for *ortho*-metalation of monomeric phosphines appeared to be unnecessary for facile C–H activation in these pincer systems. In analogous reactions to those of Shaw, Ni and Pd complexes were obtained in moderate yields (60 and 49%, respectively). In addition, a rather unusual (especially for the time) Fe hydride complex **9** was also synthesized. Treatment of $FeCl_2$ with the PMe_2-PCP ligand gave an insoluble solid, likely a coordination polymer of empirical formula $[PCP-FeCl_2]_x$. In the presence of additional coordinating ligands such as PMe_3 or 1,2-bis(dimethylphosphino)ethane (dmpe), the insoluble $[PCP-FeCl_2]_x$ complex reacts with Na/Hg amalgam to give the Fe–H species **9** (Fig. 5). It was proposed that a reduced, tetracoordinate Fe^0 species oxidatively adds across the C–H bond of the coordinated PCP ligand to generate the product. However, no yield or elemental analysis data was given at the time, presumably due to the high air and moisture sensitivity of the product. Hence, material **9** was only identified by NMR and IR spectroscopy.

2.2 Amine Containing Aryl Pincers of the "NCN" Type

Van Koten and Noltes reported the first metalloid complexes containing a prototypical NCN-type pincer in 1978. Published concurrently, a main group metal complex incorporating Sn [7] and a transition metal containing species with Pt [8] were revealed. The synthesis of both compounds employed a lithiated NCN pincer (**10**) as the key synthon. This material also serves as one of the early Group 1 pincer compounds to be structurally characterized [9]. The impetus for the Sn chemistry was based on previous studies exploring the mechanism and dynamics of stereoisomerism in chiral triorganotin halides [10]. These latter complexes
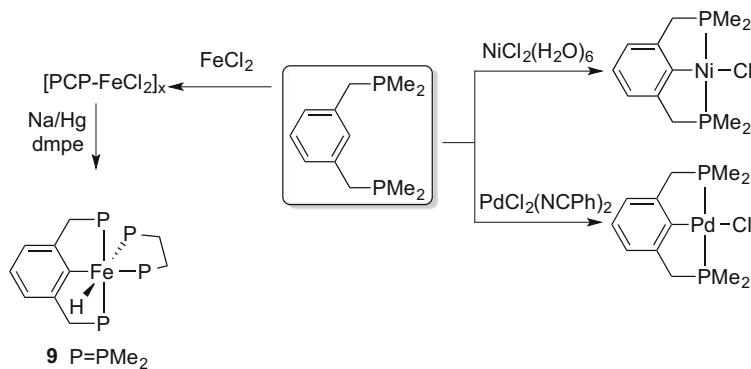
Fig. 5 Kaska's initial exploration of the Fe, Ni, and Pd PCP aryl pincer chemistry [6]

contained a cyclometalated, monoanionic 2-[(dimethylamino)methyl]-phenyl ligand, such as in compound **12** shown in Fig. 6. The [NCN-SnR₂]Br species **11** was one of the first examples of a stable pentacoordinate organotin cation, especially noteworthy since a relatively strongly potential coordinating anion, bromide, was ejected from the Sn center [7]. This was facilitated by the intramolecular coordination of the two appended amino groups. Most studies centering on Sn cations employ quite weakly coordinating anions, such as $[B(C_6F_5)_4]^-$. [NCN-SnRR′]Br complexes **11**, where R=R'=Me (Fig. 6), exhibit significant conductivity ($C = 84.8\,\Omega^{-1}cm^{-2}mol^{-1}$) in water, which was expected to improve their efficacy as a biocidal agent. This is in contrast to the generally low solubility of most other triorganotin halides in water. NMR experiments confirmed that the anion is indeed a Br⁻ and not a complex anion, such as, e.g., $[(NCN)SnR_2Br]^-$.

Recognizing the impact of the pincer ligand on the organometallic chemistry of Sn(IV), van Koten also investigated the transition metal chemistry of this NCN ligand with the Group 10 metals [8]. This work resulted in a synthesis and reactivity study of both NCN-PdBr and NCN-PtBr (Fig. 7). The synthesis of both complexes was achieved by a transmetalation reaction of an appropriate metal halide salt with the [NCN-Li]₂ dimer **10**. In accordance with the related PCP-PtCl complex described by Shaw, these materials were found to be quite thermally robust and indifferent toward both water and atmospheric oxygen.

The chemical reactivity of these early complexes would pave the way for a long series of parallel studies of these and other organometallic pincer complexes. This
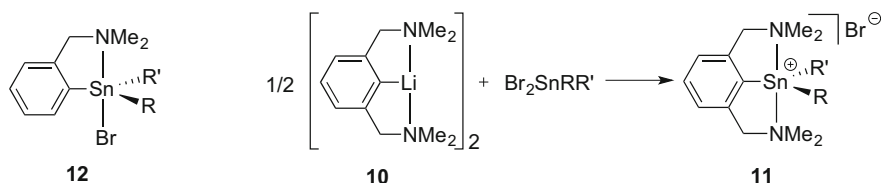
Fig. 6 Van Koten's cyclometalated Sn "pincer forbear" (**12**) [10] and the synthesis of the original NCN Sn(IV) aryl pincers (**11**) [7]
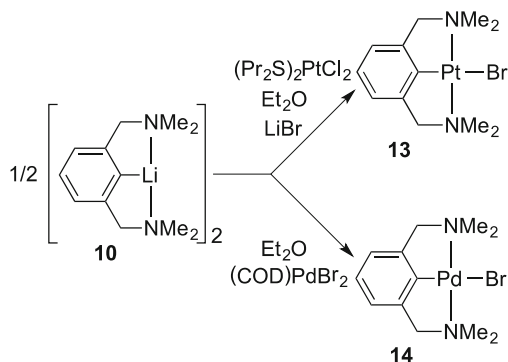
Fig. 7 Synthesis of original NCN-Pt and Pd aryl pincers [8]

was due to the observation of some very unusual reactivity and product profiles that were noted with these materials almost from the get-go. For example, the addition of two equiv. of PPh$_3$ or 1 equiv. of the bidentate phosphine (-)-Diop to NCN-PtBr (**13**) resulted in release of the chelating amino groups to give the corresponding phosphine adducts (**15** and **16,** respectively), but without concomitant rupture of the C–Pt bond, thus leaving the pincer ligand κ^1-*C*-bonded (Fig. 8). However, the NCN-PdBr did not form stable phosphine adducts under identical conditions. Both the NCN-Pd and -Pt species reacted smoothly with 1 equiv. of AgBF$_4$ to abstract the halido ligands and generate the resulting cationic metal complexes (**17**). The correct formulation of these materials as aqua adducts was only published after the initial early report [11]. The weakly bound water ligand is rapidly and quantitatively replaced by PPh$_3$ and, in the case of NCN-Pt, also by CO (Fig. 9, **18** and **19**, respectively) and even ethylene (not shown).

Surprising and unexpected results were noted in the attempted oxidative addition of MeI with the cationic NCN-Pt adduct. Instead of the expected pentacoordinate Pt^{IV} complex [NCN-PtI(Me)][BF$_4$], a unique arenium-like product was isolated quantitatively where, formally, the MeI molecule has added across the aryl–Pt bond (Fig. 9, **20**) [8]. In this case, the methyl unit has added to the aryl carbon atom and the iodide is coordinated to the Pt center as an iodido ligand (Fig. 9, **20**).
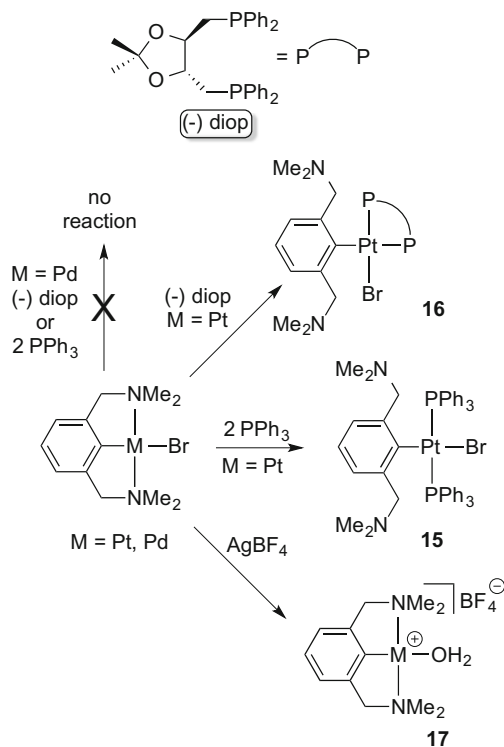
Fig. 8 The reactivity of [Pd(NCN)] and [Pt(NCN)] metallopincers [8]
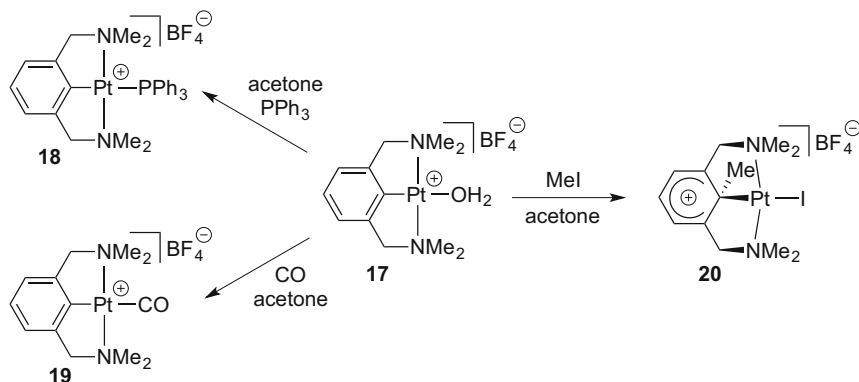
Fig. 9 The reactivity of cationic [Pt(NCN)(OH$_2$)][BF$_4$] species
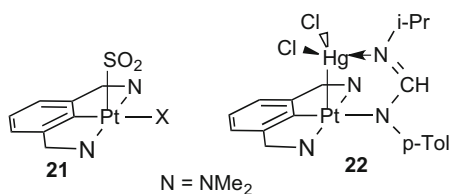
Fig. 10 NCN-Pt-X as a donor in donor–acceptor complexes with SO$_2$ (**21**) and mercury dichloride (**22**)

This highly unusual structure was confirmed by X-ray crystallography, still a relatively time-intensive technique at that time. As noted above for most of the pincer complexes known up to that time, this complex is also quite air stable and exhibits a ^{1}H NMR spectrum fully in line with the solid state structure, notably a disruption in the aromaticity of the aryl protons ($\delta_H = 8.47$ and 7.30 ppm) and a new signal for the methyl group at $\delta_H = 3.10$ ppm. The symmetry of the complex is also reduced from the starting material as the methyl substituents of the NMe$_2$ groups, and the protons of the benzylic CH$_2$ groups, were found to be magnetically inequivalent. Further work showed this to be an organometallic "Wheland intermediate" containing an arenium cation (Fig. 9) [12]. It was also shown that the formation of this arenium ion involves the initial formation of a Me-Pt(IV) cation that undergoes a subsequent 1,2-methyl shift which forms compound **20** [12]. Later studies revealed that the resulting C–C bond forming process is reversible. Moreover, reaction of the arenium ion with nucleophile afforded the corresponding, stable 2, 5- and 3, 5-hexadiene ("alkyl") pincer products depending on the size of the nucleophile [13].

Other surprises that so far seemed specific for the NCN pincer metal complexes includes the 1982 discovery that the NCN-PtX manifold could be used as a Lewis base via its filled d$_{z2}$ orbital; hence, this unit binds metals and small molecules (e.g., SO$_2$ and I$_2$) as demonstrated by the two complexes NCN-PtX with SO$_2$ (**21**, X = Cl) [14] and AgBr or HgCl$_2$ (see **22**, the κ^2-N, N′ monoanionic ligand bridging the Pt and Hg centers) [15]; see Fig. 10.
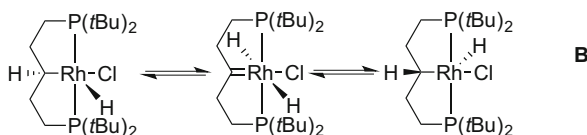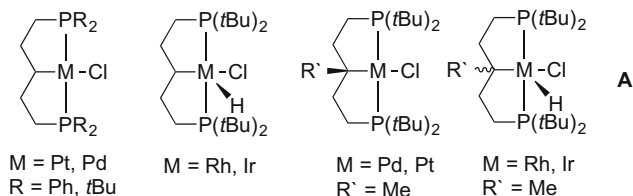
Fig. 11 Structures of σ-alkyl bound PCP metal complexes (**a**) and an example of a C–H activation process (**b**)

3 Early Metallo-Alkyl Pincer Complexes

Perhaps the most closely related ligand type is one where the aryl anion (sp^2 C–M) has been replaced by an alkyl (sp^3 C–M) bond (Fig. 11). In fact, these complexes were also initially investigated in the seminal work by Shaw [16–24], and they were reported almost concurrently with the aryl-based pincer ligands. However, these materials are generally much less stable due to additional kinetically facile C–H activation processes (Fig. 11). Hence, due in part to this characteristic, they did not initially receive the widespread attention of the aryl cousins. In recent years however, there have been many exciting developments that have clearly shown that the realm of alkyl pincer chemistry can yield compounds with surprisingly stable C(sp^3)-metal bonds [24].

4 How the Prototypical Aryl Pincer Platform Developed into a "Privileged" Ligand

During the years following this pioneering period, various closely related ligand motifs, with similar metal-binding pockets, began to be extensively explored. These showed that the typical κ^3-terdentate coordination mode and unique reactivity profiles exhibited by the prototypical PCP and NCN aryl and alkyl type metal complexes are not restricted to either phosphine or amino donor ligand arms nor to the more covalent central bond between the pincer manifold and the metal site. Some examples representing these developments, and some of the pioneers of these directions, will be briefly discussed.

4.1 Thioether Containing "SCS" Aryl Pincers

Subsequent to Shaw's seminal reports on PCP pincer complexes, the studies by Kaska, and those of the van Koten group on NCN pincer complexes, Shaw also described the first SCS aryl pincer complexes. These incorporate thioether-type (S-alkyl or S-aryl) coordinating heteroatom donor sites and were reported in 1980 [25]. This work was subsequently followed by the studies of Pfeffer and coworkers [26]. In accordance with Shaw's PCP systems, cyclopalladation proceeded exclusively between the pincer "arms" to give a predictable SCS-PdCl complex (Fig. 12). The X-ray crystal structure of one such material (**23**, Fig. 10) showed that the tBu group of the individual thioethers are oriented to opposite sides of the square planar metal core, giving a molecule with approximate C_2 point group symmetry. In addition, preliminary reactivity studies suggested that displacement of the intramolecular Pd-S coordination with PPh$_3$ only takes place in very concentrated solutions or in the solid state, cf. **24**; Pd-PPh$_3$ bonding interactions are virtually nonexistent in solution at NMR concentrations.

Other homoleptic aryl pincer ligands also exist, including those of the OCO and SeCSe formulation; however, these, at least up to the early 1990s, had not been utilized. In fact, it was only recently that the organometallic chemistry of the OCO-type pincer system has been investigated, owing in part to the weaker coordination ability of ethereal oxygen atoms vs. the other more popular pincer donor groups. Whereas the OCO pincer ligand has been known for some time (benzylic ethers are functionally masked benzylic bromides that are a cornerstone synthon in pincer chemistry), no transition metal complexes of the simple ligand have been reported to date. Complexes derived from Group 14 metals incorporating these ligands have been reported; see the work of Jambor and coworkers [27]. The SeCSe pincer was first disclosed by Yao in 2004 [28], and its late arrival is also somewhat surprising given the fact that organoselenium chemistry is well developed and that Se is known to be quite a strong electron donor. Interestingly, the palladation was achieved by reaction of a dimeric N,C-palladocycle with the bare SeCSe ligand, as shown in Fig. 13.

In addition to these homoleptic systems, at an early stage, a limited number of "mixed" pincers have also been reported, allowing for the probing of the effect of axial differentiating the ligand donor properties. Milstein and coworkers (Fig. 14) have synthesized a substituted PCN ligand **26** containing both a P(tBu)$_2$ unit and a
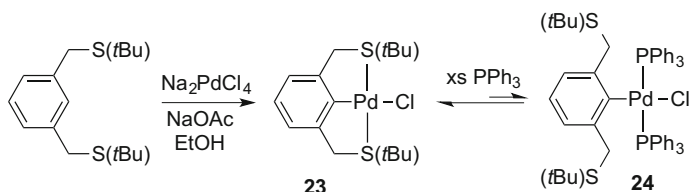
Fig. 12 Synthesis and reactivity of Shaw's original SCS Pd aryl pincer [26]
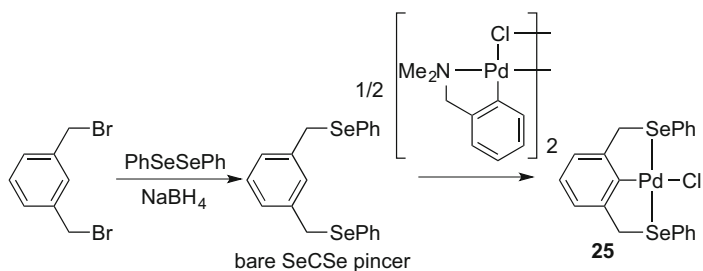
Fig. 13 Synthesis of original SeCSe Pd aryl pincer **25**
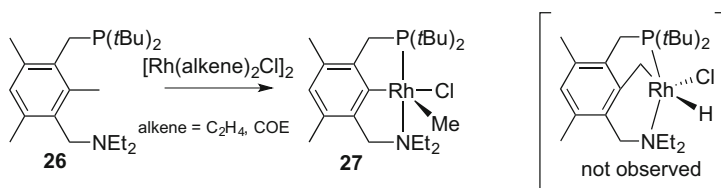
Fig. 14 Synthesis of Milstein's PCN aryl Rh pincer **27** involving C–C bond activation and cleavage [29]

NEt$_2$ group [29]. Studies on the comparative reactivity of this mixed system with related PCP pincers showed some subtle differences. For example, with [Rh (COE)$_2$Cl]$_2$ [COE = cyclooctene] or [Rh(C$_2$H$_4$)$_2$Cl]$_2$, products resulting from exclusive C–C activation are observed for the PCN ligand system, while reaction with PCP derivatives gives a mixture of both C–C and C–H inserted products. Both the altered steric and electronic properties of the coordinated heteroatoms would presumably have an influence on the relative barriers to selective C–C vs. C–H activation. Another potential explanation is that, due to the hemilabile nature of the PCN ligand, dissociation of the N donor from a C–H activated product helps promote a kinetically more rapid C–H reductive elimination.

Conversely, reaction with Pt(COD)Cl$_2$ [COD = cyclo-1,5-octadiene] results in distinctly divergent reactivity (Fig. 15). With the PCN ligand, the initial C–H oxidative addition product of Pt(IV) is trapped as the pendant amine acts as an internal base. This then abstracts a proton from the Pt–H unit, thus preventing HCl elimination and leading to the isolation of the C–H activation product (Fig. 15). Significantly, the methyl group situated between the donor groups is the exclusive site of reactivity, and hence the remaining methyl groups are presumably unaffected. This points to an important function of the amine in directing the regiochemistry of the activation. The latter two examples further emphasize the crucial role of the metal–ligand interactions that, in the case of Rh bis-cyclometalation, results in the formation of the κ^3-*PCN*-terdentate aryl pincer complex. In contrast, the reaction stops at the stage of the κ^2-*PC*-bidentate mono-cyclometalated alkyl Pt compound with a protonated trialkyl amino grouping in the reaction with PtCl(COD).

Fig. 15 Reactivity profile
of a PCN-pincer
incorporating Pt
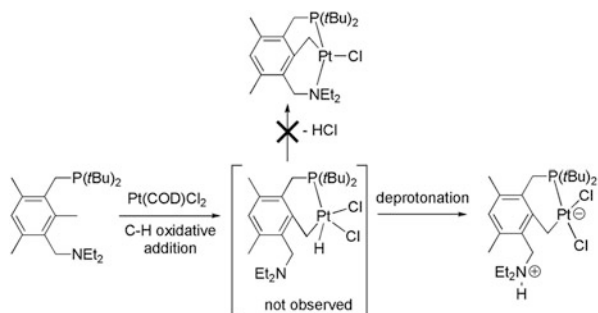
4.2 Other Similar Ligand Classes

At an early historical stage, Fryzuk and others began to extensively study ligand sets based on heteroatom complexation by a series of highly successful ligands derived from compounds of general formula $(R_2E-CH_2-SiMe_2)_2NH$ (E = P or N). These PNP/NNN systems offer a versatile scaffold as the charge, position of donor atoms and steric environment can all be systematically and simply varied. This allows for specific reactivities to be expressed, most impressive being the activation of dinitrogen in a variety of reactions such as hydrogenation, hydroboration, or hydrosilylation. Historical details on this chemistry can be found in reference [30–33].

Right from the beginning, the unique combination of metal complex stability and well-defined coordination environment has placed the pincer ligand platform in a leading role in the development of new and exciting areas of chemistry. This stability is coupled with the ability of organometallic pincer metal complexes to participate in numerous different types of reactions.

Examples of closely related ligand sets are those compounds shown in Fig. 16 including ligands such as the bis(imino)-phenyl/-pyridine; the bis(oxazolyl)-phenyl (phebox)/-pyridine (pybox), studied in detail by Nishiyama; as well as bis-pyridinephenyl/terpyridine (terpy) metal complexes. These latter materials differ only by replacement of the covalent M–C bond with a dative pyridine N-M linkage. This obviously gives a formally neutral ligand fragment as opposed to the monoanionic systems. Examples of applications of these novel complexes include their use in olefin polymerization (e.g., bis(imino)pyridine Fe and Co catalysts) [34], while the pybox systems are excellent chiral auxiliaries [35–39]. Both the terpy- and the bis-pyridinephenyl Ru complexes are also very widespread and studied [1, 40–42] and are noteworthy for their potent photochemical and physical properties [43]. Further to this, obvious ligand variations include the changing of the position of the monoanionic site to one of the other donor sites, the use of two or even three anionic ligand sites, etc. This leads to a much wider field than perhaps envisioned in the early days of the aryl and alkyl pincer metal complexes.

As perhaps a testament to the appeal of the concept of the pincer ligands, a recent search of academic publications utilizing the phrase "pincer" as keyword reveals
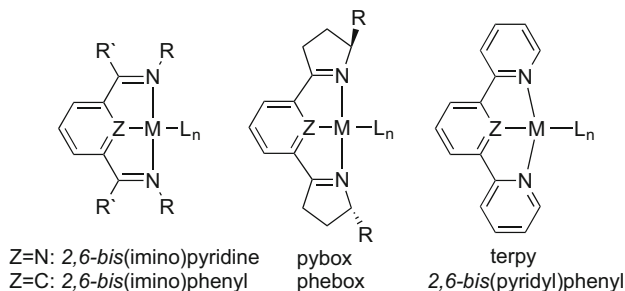
Fig. 16 Structures of some NNN-type coordination complexes

that, since Bernard Shaw's original publication in 1976, well over 1,900 scientific papers have appeared between 1996 (a mere 10 papers/year) and 2014 (250 papers/year, 6,000 citations).

In conclusion, this brief review has been presented in the hope that it provides a useful history of the multifaceted chemistry that is hinged on the use of metallopincer complexes. In addition, it is somewhat humbling to see the vast development in the last almost 40 years of an area of organometallic chemistry that began with just a few simple examples. Indeed, this class of organometallics is now reaching far beyond coordination chemistry and catalysis and into such realms as bio-inorganic chemistry, molecular labeling, and property-directed materials science. The authors of this historical perspective further hope that this discussion has served as a useful introduction to the other manuscripts in this volume, all presented by the new leaders in the field of pincer chemistry. References [44–56] provide some relevant reviews that give excellent and detailed overviews of previous and current developments in the field of pincer chemistry and its applications.

References

1. van Koten G (1989) Pure Appl Chem 61:1681
2. Moulton CJ, Shaw BL (1976) J Chem Soc Dalton Trans 1020
3. Jones CE, Shaw BL, Turtle BL (1974) J Chem Soc Dalton Trans 992
4. Mason R, Thomas KM, Empsall HD, Fletcher SR, Heys PN, Hyde EM, Jones CE, Shaw BL (1974) J Chem Soc Chem Commun 612
5. Miller EM, Shaw BL (1974) J Chem Soc Dalton Trans 480
6. Creaser CS, Kaska WC (1978) Inorg Chim Acta 30:L325
7. van Koten G, Jastrzebski JTBH, Noltes JG, Spek AL, Schoone JC (1978) J Organomet Chem 148:233
8. van Koten G, Timmer K, Noltes JG, Spek AL (1978) J Chem Soc Chem Commun 250
9. Jastrzebski JTBH, van Koten G, Konijn M, Stam CH (1982) J Am Chem Soc 104:5490
10. van Koten G, Noltes JG (1976) J Am Chem Soc 98:5393

11. Grove DM, van Koten G, Louwen JN, Noltes JG, Spek AL, Ubbels HJC (1982) J Am Chem Soc 104:6609
12. Terheijden J, van Koten G, Vinke IC, Spek AL (1985) J Am Chem Soc 107:2891
13. Grove DM, van Koten G, Ubbels HJC (1982) Organometallics 1:1366
14. Terheijden J, van Koten G, Mul WP, Stufkens DJ, Muller F, Stam CH (1986) Organometallics 5:519
15. van der Ploeg AFMJ, van Koten G, Vrieze K, Spek AL, Duidenberg AJM (1982) Organometallics 1:1066
16. Empsall HD, Hyde EM, Markham R, McDonald WS, Norton MC, Shaw BL, Weeks B (1977) J Chem Soc Chem Commun 589
17. Crocker C, Errington RJ, McDonald WS, Odell KJ, Shaw BL, Goodfellow RJ (1979) J Chem Soc Chem Commun 498
18. Crocker C, Errington RJ, Markham R, Moulton CJ, Odell KJ, Shaw BL (1980) J Am Chem Soc 102:4373
19. Al-Salem NA, McDonald WS, Markham R, Norton MC, Shaw BL (1980) J Chem Soc Dalton Trans 59
20. Errington RJ, McDonald WS, Shaw BL (1982) J Chem Soc Dalton Trans 1829
21. Briggs JR, Constable AG, McDonald WS, Shaw BL (1982) J Chem Soc Dalton Trans 1225
22. Crocker C, Empsall HD, Errington RJ, Hyde EM, McDonald WS, Markham R, Norton MC, Shaw BL, Weeks B (1982) J Chem Soc Dalton Trans 1217
23. Crocker C, Errington RJ, Markham R, Moulton CJ, Shaw BL (1982) J Chem Soc Dalton Trans 387
24. Gelman D, Romm R (2013) Top Organomet Chem 40:289
25. Errington J, McDonald WS, Shaw BL (1980) J Chem Soc Dalton Trans 2312
26. Dupont J, Beydoun N, Pfeffer M (1989) J Chem Soc Dalton Trans 1715
27. Jambor R, Dostal L, Cisarova I, Brus J, Holcapek M, Holecek J (2002) Organometallics 21:3996
28. Yao Q, Kinney EP, Zheng C (2004) Org Lett 6:2997
29. Gandelman M, Vigalok A, Shimon LJW, Milstein D (1997) Organometallics 16:3981
30. Fryzuk MD (1992) Can J Chem 70:2839
31. Fryzuk MD, Giesbrecht GR, Johnson SA, Kickham JE, Love JB (1998) Polyhedron 17:947
32. Fryzuk MD (2003) Chem Rec 3:2
33. Fryzuk MD (2009) Acc Chem Res 42:127
34. Gibson VC, Redshaw C, Solan GA (2007) Chem Rev 107:1745
35. Nishiyama H, Ito J (2010) Chem Commun 46:203
36. Nishiyama H, Ito J, Shiomi T, Hashimoto T, Miyakawa T, Kitase M (2008) Pure Appl Chem 80:743
37. Nishiyama H, Ito J (2007) Chem Rec 7:159
38. Gossage RA (2011) Dalton Trans 40:8755
39. Zhong LQ, Tang RR, Yang Q (2007) Prog Chem 19:902
40. Yuan SC, Chen HB, Wang HC (2009) Prog Chem 21:2132
41. Andres PR, Schubert US (2004) Adv Mater 16:1043
42. Constable EC (1986) Adv Inorg Chem Radiochem 30:69
43. Bomben PG, Robson KCD, Koivisto BD, Berlinguette CP (2012) Coord Chem Rev 256:1438
44. Rietveld MHP, Grove DM, van Koten G (1997) New J Chem 21:751
45. Rybtchinski B, Milstein D (1999) Angew Chem Int Ed 38:870
46. Albrecht M, van Koten G (2001) Angew Chem Int Ed 40:3750
47. van der Boom ME, Milstein D (2003) Chem Rev 103:1759
48. Singleton JT (2003) Tetrahedron 59:1837
49. Morales-Morales D, Jensen CM (2007) The chemistry of pincer compounds. Elsevier, Amsterdam
50. Selander N, Szabó KJ (2011) Chem Rev 111:2048
51. Choi J, MacArthur AHR, Brookhart M, Goldman AS (2011) Chem Rev 111:1761

52. van Koten G, Milstein D (2013) Topics in organometallic chemistry, vol 40. Springer, Heidelberg
53. Gunanathan C, Milstein D (2014) Chem Rev 114:12024
54. Szabo KJ, Wendt OF (2014) Pincer and pincer-type complexes: applications in organic synthesis and catalysis. Wiley-VCH, Weinheim
55. O'Reilly ME, Veige AS (2014) Chem Soc Rev 43:6325
56. Younus HA, Su W, Ahmad N, Chen S, Verpoort F (2015) Adv Synth Catal 357:283

Pincer Complexes of Lithium, Sodium, Magnesium and Related Metals: A Discussion of Solution and Solid-State Aggregated Structure and Reactivity

Robert A. Gossage

Abstract   An overview of the Li, Na, Mg and Cu complexes of the pincer ligands is presented. This discussion will include common techniques and advances in the synthesis of the title materials, their properties (notably in the solid state) and trends in their reactivity. In addition, a brief description of the known "mixed" or hetero-aggregated pincer complexes will also be given.

Keywords   Aggregates • Chelating ligands • Organocopper • Organolithium • Organomagnesium • Organosodium • Organozinc • Pincer • Structure • Tridentate ligands

Contents

R.A. Gossage (✉)

Department of Chemistry and Biology, Ryerson University, 350 Victoria Street, Toronto, ON, Canada, M5B 2K3

e-mail: gossage@ryerson.ca

1   Introduction

The Group 1 metals lithium (Li) and sodium (Na), the Group 2 element magnesium (Mg) and the later transition metals copper (Cu) and zinc (Zn) play unique roles in chemical synthesis [1, 2]. The discovery (Victor Grignard [3–6]) of the utility [3–11] of organomagnesium compounds, and the subsequent syntheses and applications of organolithium reagents by Schlenk, Ziegler, Wittig, Gilman and others [9–14] can now be seen as a pivotal turning point in modern synthetic chemistry [12–21]. In this regard, several excellent reviews by Seyferth on the early chemistry of organoalkali and organozinc chemistries has appeared [18–20]. Indeed, few total syntheses carried out today do not employ these classic reagents. In recent years, the milder (and often more selective) organocopper [21–28] and organozinc reagents [29–35] have become of widespread synthetic utility and accessibility. Given the rich history of the title elements in organic synthesis and organometallic chemistry in general, it is of little surprise that these elements have been investigated and utilised in the chemistry of the "pincer" ligands (Fig. 1).

   The pincer ligands are a class of binding agents in which the central (metal, transition metal or main group) atom is contained within an organic framework which typically consists of one or more formal anions (e.g. a formal C^- or O^- donor atom) linked to two or more (typically) heteroatom containing donor groups (i.e. –NR_2, –SR, –PR_2, –OR, etc.). A thorough introduction to this whole class of ligands can be found in the earlier reports and hence will not be repeated here; cf. [36–42]. This chapter will deal specifically with pincer ligands of the Group 1 elements (Li, Na) with some relationships drawn to the complexes of Mg, Cu and Zn where appropriate [43]. This monograph is not intended as a complete review of all compounds of the title elements that could be labelled as containing a pincer ligand. Instead, a general overview of the structural motifs and their relationship to the solid state and solution properties of these complexes will be given. It should be noted that a primary utility of pincer complexes with these elements are their
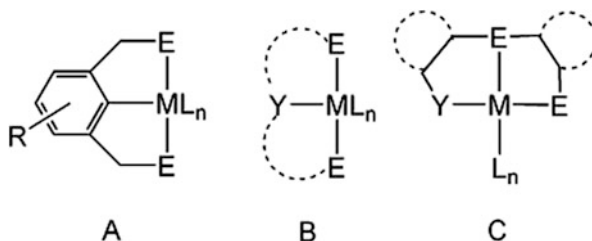
Fig. 1 A schematic illustration of "pincer" ligand scaffolds. Skeletal structure (**A**) represents the general formula of the "classical" aryl pincer ligand bound to (metallic) element "*M*" with appended functionality "*R*" on the aromatic ring and *n* number of accompanying ligands *L*. Structure (**B**) represents the more general pincer framework in which formally anionic central donor atom "*Y*" can be a carbon or other atom linked to two flanking "*E*" donor atoms. Structure "**C**" is the atypical pincer form in which the formal anion takes on the flanking or non-central donor atom position. Note that "*E*" can also be formally anionic

applications in the synthesis of other metal and non-metal pincer derivatives. Hence, metal metathesis reactions are their main use; this aspect has been discussed previously [38, 43].

2 Homo-Organo Pincers of Lithium

2.1 Introduction: Early Studies on Lithium Metal Reagents

Compounds that contain Li as the metal atom are by far the most common alkali metal complexes of the pincers. In addition, extensive studies have been carried out on the alkali metal chemistry of the pincer relative dimethylbenzylamine (DMBA: Fig. 2).

This molecule can be envisioned, in layman's terms, as a "one donor arm missing" pincer and is the obvious predecessor to the classic "NCN" pincer ligand 1,3-bis[(dimethylamino)methyl]benzene (Fig. 2). This latter molecule and a number of its derivatives have been investigated in detail by van Koten and others and will be described at length below. DMBA represents a very good model to put the later Li pincer chemistry into perspective. It was one of the early examples of a molecule that readily undergoes what is now termed "Directed *ortho*-Metalation" (DoM) [44–53]. This class of reactions was first described by Gilman in the late 1930s in his seminal investigations into the lithiation of anisole and other aromatic ethers ([54], also see (Li–Br exchange): [55]). Hauser and co-workers presented their study on the DoM of DMBA some 20 years later. It was shown that high yields of *ortho*-lithiated DMBA (DMBA-Li: Fig. 2: **1-A**) could be obtained upon reaction of the amine with *n*-BuLi in Et$_2$O solution [56, 57] or via Li–Br exchange from (*o*-bromobenzyl)dimethylamine [58]. Both of these methods yield synthetically useful quantities of DMBA-Li, but what is the actual solution and solid-state nature of this material?

To answer this question, it is probably first prudent to give a more detailed but general overview of the exact (solution and solid state) structural nature of organolithiums. This discussion will have a direct bearing on our later structural

Fig. 2 Schematic "representation" of DMBAs and the "NCN" pincer

DMBA: M = R = H;
DMBA-Li: **1-A**: M = Li; R = H;
1-B: M = Li; R = Me

"NCN" Pincer
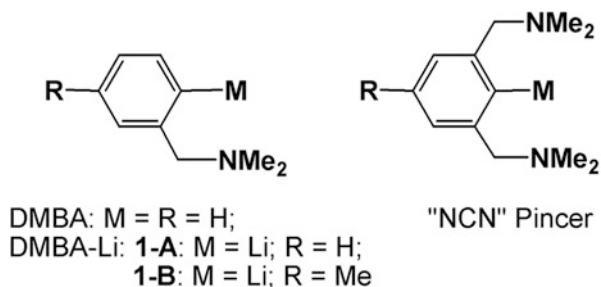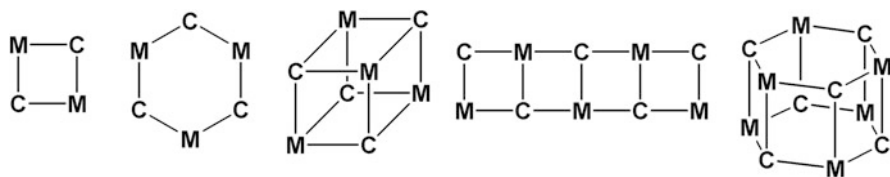
Fig. 3 Common (schematic) structural motifs of organolithium derivatives (from left to right): dimer (ring), trimer (ring), cubane, ladder and hexamer (prism). "M" represents the metal (Li) and "C" the organic fragment(s)

descriptions of alkali metal pincer chemistry. The schematic picture of DMBA-Li shown in Fig. 2 typifies the common "textbook" representation of an organolithium species. Indeed, most of us display these reagents in chemical equations simply as "RLi". For example, *n*-butyllithium is typically shown as "*n*-BuLi". This is certainly appropriate in terms of a functional description of the molecular content and nucleophilic properties of the formal butyl anion. However, as a structural description of the reagent itself, such designations are far from accurate. In truth, *n*-BuLi exists in a number of solid-state and solution forms, *none* of which are mononuclear nor do any contain the truly separated ions Li^+ and Bu^-. Organolithium chemistry is, of course, dominated by the phenomenon of *aggregation* [59–61]. These observations can be easily explained by the energetic desire of the Li atom(s) to complete an octet of electrons in their second quantum level. Due to the electron deficient nature of the Li atom ($1s^2 2s^1$), the multiple centred bonding motif (e.g. the three centred–two electron [3c–2e] bond) is commonplace in organolithium chemistry. Solid-state and solution structural forms vary widely with the dimer-, trimer (ring)-, cubane-, ladder- and hexamer (prism)-based forms being observed (Fig. 3) [18–20].

This aspect helps to explain the often pronounced solvent (cf. hexane vs. ether) or additive (e.g. TMEDA) effects that are observed in organolithium reactivity. This is due to the fact that the oligomeric nature of RLi complexes are perturbed by polar solvents since these can act as electron donors (i.e. ligands) to the Li nucleus. DMBA is in fact a very good example of this behaviour (Eq. 1). Van Koten's early structural study demonstrated the aggregated *tetrameric* (i.e. [DMBA-Li]₄: **1-A**) solid-state structure (Fig. 4). Thus, DMBA-Li was shown to possess a cubane-type arrangement (Fig. 3) of the Li and formal anionic carbon atoms with stabilisation provided via coordination of the –NMe₂ groups to lithium [62, 63].

This structural motif is retained (NMR) in *non*polar solvents like toluene (complex **1-B**: Fig. 2).[1] Very detailed studies (¹H, ¹³C, ⁶,⁷Li NMR, isotopic labelling, etc.) by Reich and co-workers have demonstrated how the addition of solvent

---

[1] Complex **1-A** lacks the solubility necessary for NMR characterisation.

Fig. 4 A schematic diagram (*left*) and a molecule (X-ray) of [DMBA-Li]₄, the methyl groups attached to the nitrogen atoms have been removed for clarity

Fig. 5 The identified low temperature solvated forms of [DMBA-Li]

(ligands) to *polar* solutions of **1-A** results in the establishment of a complex series of chemical equilibrium involving a number of DMBA-Li species (Eq. 1) [64, 65].

In pure THF solution at low temperature, *dimeric* [DMBA-Li]₂ predominates in no less than *three* structural forms (Fig. 5; **2-A**, **2-B** and **2-C**). Upon addition of TMEDA (Eq. 2), the complex [(DMBA-Li)₂(TMEDA)] (**3**: Fig. 6) can be isolated and has been structurally characterised [66]. Note that in this latter case only one of the Li atoms is bound in an intramolecular fashion to the dimethylamino groups.

Such observations can become important if one considers that reagent solutions of such RLi compounds can be mixtures of many isomers. Obviously, these mixtures can become different complexes if good donor ligands/solvents are present (cf. the use of (−)-sparteine [lupinidine] in enantioselective reactions involving RLi) [67–69]. One presumes that the isomeric forms must have very similar or identical reactivity patterns; otherwise, complex product mixtures would predominate the use of such reagents. A discussion below (Sect. 5) will describe

Complex 3

Fig. 6 Schematic diagram of the solid-state structure of [(DMBA-Li)$_2$(TMEDA)] (**3**)

some less common examples where additives or reaction by-products *does* affect such reactions. Having thus far established the complex nature of organolithiums and that of the pincer "ancestor" DMBA-Li, let us now consider the nature of Li pincers themselves.

2.2   Lithium NCN Pincers

The first synthesis and detailed characterisation of a Li(NCN) pincer was described by van Koten and co-workers during their investigations of the metalation of the aforementioned DMBA [62, 63]. The initial synthetic pathway used 2-bromo-1,3-bis[(dimethylamino)methyl]benzene (**4-Br**) and treated it with two equivalents of Li metal in Et$_2$O solution. Cryoscopy and NMR spectroscopic measurements suggested a dimeric formulation of the material (i.e. [Li$_2$(NCN)$_2$]: **5**) with a symmetrical C_2 point group structure. This unsubstituted NCN–Li complex (see Fig. 1, complex **A**; R = H) resisted characterisation by single crystal X-ray diffraction until 2008 [70], although several other examples of substituted analogues had been characterised by this technique over time. The solid-state structure (Fig. 7) of **5** parallels that observed in solution with each formal Li cation fulfilling its octet of electrons via bonding to both formal aryl anions (3c–2e bond) and one amino group from each of the two NCN fragments.

As stated previously, the original synthesis of **5** required a minimum of two equivalents of lithium metal. This is obviously not ideal for technical and atom economy reasons nor is it in fact necessity to use the 2-bromo NCN precursor (**4-Br**). It goes without saying that the best synthetic strategy for the formation of any Li pincer is via direct Li–H exchange of the desired aryl (or alkyl) position, in this case position-2 of 1,3-bis-[(dimethylamino)methyl]benzene (**4**). Reagents such as RLi are obviously more desirable than the application of excess neat Li metal. However, this process has some synthetic drawbacks (vide infra) that are not encountered in the related chemistry of DMBA. It took sometime before the use of a single equivalent of *n*-BuLi and **4** (direct Li–H exchange) to facilitate conversion to **5** was optimised. The key is that only *apolar* solvents can be used for the reaction. The use of ethers as solution media results in non-selective lithiation, likely due to the formation of different solution aggregates (vide supra) via either
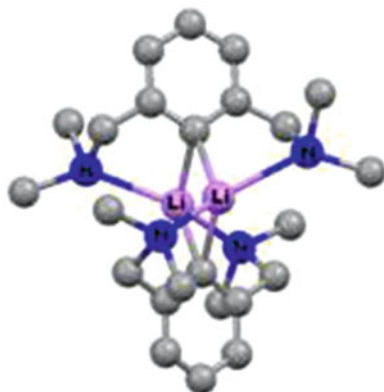
Fig. 7 Molecular diagram of the solid-state structure of a [Li$_2$(NCN)$_2$] (**5**) molecule [70]
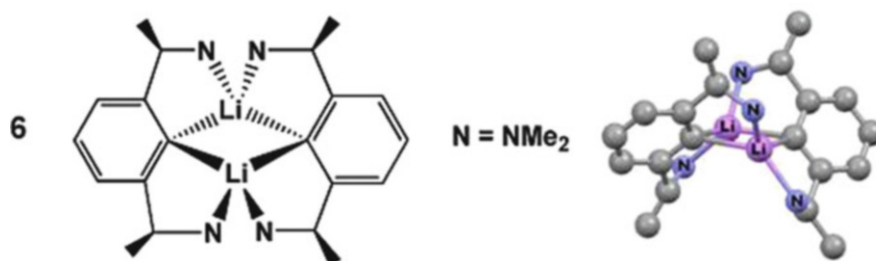
Fig. 8 The dimeric structure of a molecule of complex **6** (X-ray structure on the *right*): methyl groups attached to the nitrogen atoms have been removed for clarity

isomerisation or non-preferential kinetic selectivity [41, 71, 72]. Isolated complex **5** retains its dimeric structural integrity in polar solvents (THF) and in the presence of additives (TMEDA, NEt$_3$), the latter observation is in obvious contrast to that of DMBA-Li. Structurally characterised derivatives of **5** include the chiral dimeric complex derived from (*R, R*)-1,3-bis-[1-(dimethylamino)ethyl]benzene (**6**: Fig. 8), [Li$_2$(2,6-Me$_2$NCH$_2$)$_2$-4-Ph-C$_6$H$_2$)$_2$] (**7**: Fig. 9) [71, 73], [Li$_2${μ-κ^2-N^2,N^6-2,3,5,6-(Me$_2$NCH$_2$)$_4$C$_6$H}$_2$] [74–77] and the diethylamino and di-isopropylamino analogues of **5** [Li$_2${(2,6-R$_2$NCH$_2$)$_2$C$_6$H$_3$}$_2$] (**8a**: R = Et; **8b**: R = ^{i}Pr) [70, 78, 79]. NMR data suggests that **6**, **7** and **8** retain their dimeric structure in solution. A further discussion of the chemistry of **6** and **8a** will be detailed below in Sect. 5.

It is necessary to use excess (3 equiv.) *i*-Pr$_2$NLi (LDA) in the presence of TMEDA to convert bis-oxazoline **9** [80, 81] to lithium pincer derivative **10** [80]. A Li–Br exchange reaction (using *n*-BuLi) can also be used starting from the 2-bromo derivative of **9** (Fig. 10) [82]. Complex **10** cannot be obtained via a direct Li–H exchange reaction using alkyl or aryl lithium reagents [80]. Upon

Fig. 9 The dimeric
structure of a molecule of
complex **7** (X-ray structure
on the *bottom*): methyl
groups attached to the
nitrogen atoms have been
removed for clarity
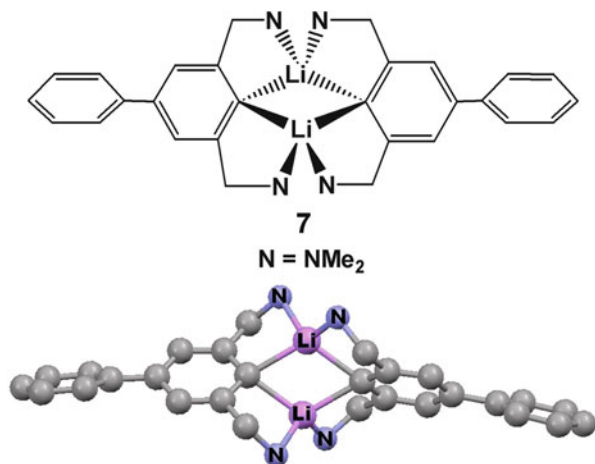
Fig. 10 The reaction
conditions used in the
formation of oxazoline **10**
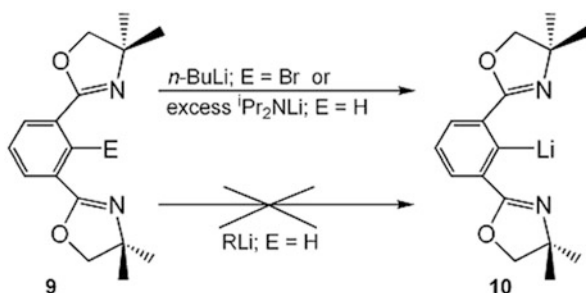
treatment of **9** with RLi (R = *n*-Bu, *sec*-Bu or Ph; benzene solution), products are
obtained which result from the attack of nucleophile R onto the aromatic ring [80].

Compound **10** has also been characterised by X-ray diffraction and the dimeric
nature of the species confirmed (Fig. 11) [82]. In a similar manner to **5**, complex **10**
is unaffected in solution (^{7}Li NMR) by the presence of added THF or NEt$_3$.

In contrast to the above examples, the first *trimeric* lithium compound was
isolated for the complex [2,6-bis(dimethylamino)phenyl] lithium (**11**: Fig. 12).
The absence of a methylene "linker" between the aryl group and the *N*-donor
atoms is thought to be the reason for this structural motif (i.e. increased steric
congestion). This material is formed via a Li–H exchange reaction upon treatment
of 1,3-(dimethylamino)benzene with *n*-BuLi [83]. The trimeric structure is retained
in benzene (cryoscopy) and implied in toluene-d_8 (NMR) solution at low temper-
ature. Experiments with **11** dissolved in THF suggest a partial breakdown of the
trimer with coordination of probably two THF molecules per lithium. The exact
aggregation state of this solvated form has not been unequivocally determined.

The syntheses and structural characterisation of the unusual lithium pincer
cluster [Li$_2$C(PPh$_2$NSiMe$_3$)$_2$]$_2$ (**12**: Fig. 13) were reported independently by both
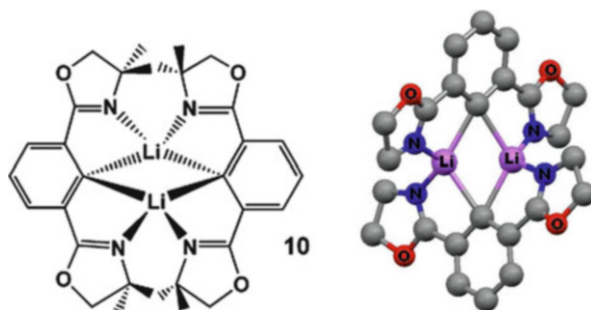
Fig. 11 The solid-state structure of a molecule of **10** (X-ray structure on the *right*; the methyl groups attached to the oxazoline rings have been removed for clarity)
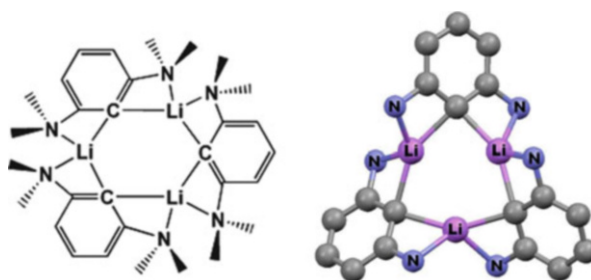
Fig. 12 Schematic diagram of the trimeric structure of [Li$_3$(C$_6$H$_3$\{NMe$_2$\}$_2$)$_3$] (**11**: *left*) and its structure in the solid state; Me groups attached to the N atoms have been removed for clarity
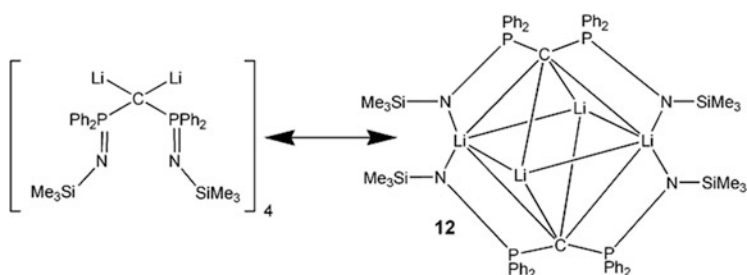
Fig. 13 Schematic diagram of the cluster [Li$_2$C(PPh$_2$NSiMe$_3$)$_2$]$_2$ (**12**)

Stephan [84] and Cavell [85–87]. This material retains its structure in solution and is a useful precursor for other organometallic derivatives [85–87].

The results documented in this section have shown some definitive trends in the chemistry of the general class of Li(NCN) pincers. All of the structurally characterised examples are dimeric (with the exception of **11** and **12**), and all feature intramolecular bonding of the nitrogen containing groups to the lithium centres. The materials are generally resistant to reaction (in solution) with additives

such as ethers and tertiary amines (TMEDA, NEt_3: cf. DMBA-Li: Sect. 2.1). Direct lithiation can be achieved regioselectively via Li–Br exchange (**5**, **8**, **9**) or in some cases by direct Li–H exchange (**5**–**7**, **11**, **12**). The latter process appears to be solvent dependent, and optimisation experiments are often required to find the specific conditions for selective product yields.

2.3 Lithium CNN Pincers

The class of bis-amino pincers in which the "central" binding atom is not the formal carbanion have received somewhat less attention in the literature. These materials can be viewed as a "tethered" version of Ph–Li linked to a TMEDA unit (Fig. 14).

Studies have centred on the lithiation of molecules of general formula o-BrC_6H_4-CH(R)-N(R')-$CH_2CH_2NR''_2$ (R $=$ H or Me, R' R'' $=$ Me or Et) utilising Li–Br exchange chemistry. Initial studies on the case of R $=$ H; R' $=$ R'' $=$ Me (**13**) revealed some interesting chemistry. The reaction of **13** with n-BuLi does indeed result in the expected Li–Br exchange reaction, and a dimeric (Sect. 2.2) species is obtained (**14**: cryoscopy). An interesting facet of this work is that the combination of two Li(CNN) moieties to produce dimeric [$Li_2(CNN)_2$] can produce *chiral* products. This is due to the fact that upon dimerisation, the fluxional nature of the benzylic N-atom substituents is arrested via strong coordination to a Li atom; hence, a rigid tetra-substituted nitrogen centre is created. This, by definition, is of course chiral. In addition, the Li centre can also become a chiral centre if the second bound (CNN) moiety has identical chirality at N than the first (Fig. 15). Thus, three possible products of this dimerisation can occur: an enantiomeric pair (R_{Li}, R_{Li}) and
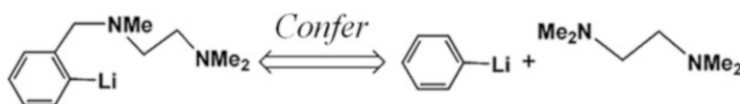
Fig. 14 A schematic representation of compound **14** (*left*) and its comparison to a PhLi/tmeda combination
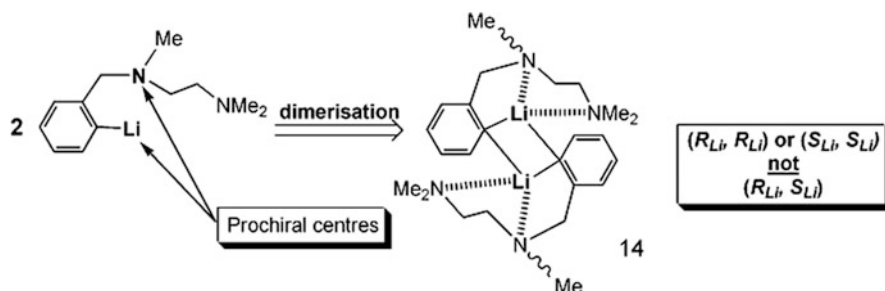
Fig. 15 Induced chirality upon dimerisation to form (R, R) or (S, S)-**14**

(S_{Li}, S_{Li}) or the *meso* (R_{Li}, S_{Li}) form of **14**. NMR and crystallographic measurements show that this latter species does not exist as the meso form and hence the enantiomeric pair results. This is an example of chiral "self-assembly" by aggregate formation in the absence of a secondary chiral centre (Fig. 15) [88]. This concept was later demonstrated in the chemistry of **6** (Sect. 5), in which again the meso form of the dimer is not a thermodynamic aggregate (Figs. 8 and 15) [73].

Expanding the possibility of further selectivity in aggregate formation involves an investigation of other external influences on the chiral self-assembly of such dimers. This is tested by (1) increasing the steric bulk of the molecule versus that of **14** and (2) adding the presence of a secondary fixed chiral centre (i.e. a chiral auxiliary group).

Steric effects are profiled by the replacement of all secondary Me groups on the N atoms of **12** by Et groups (i.e. using BrC_6H_4-$CH_2N(Et)CH_2CH_2NEt_2$: **15**). This action does little to the basicity of the *N*-donors but has a profound effect on the chiral aggregation properties. In this case, lithiation of **15** is followed by self-assembly (dimerisation), gives *only* the *meso* product (R, S)-**16** (i.e. (R_{Li}, S_{Li})-$[LiC_6H_4$-$CH_2N(Et)CH_2CH_2NEt_2]_2$), chirality in this case again being defined only at lithium [89]. Thus, steric effects can induce and control these self-assembled (chiral) organolithium pincer dimers.

The effect of the presence of a secondary fixed chiral centre can be determined by employing chiral precursors (R)-BrC_6H_4-$C^*H(Me)$-$CH_2N(Me)$-$CH_2CH_2NMe_2$ (i.e. (R)-**17**: the chiral carbon is marked with an asterisk for clarity) or its racemic (R/S) counterpart *rac*-**17** (chirality here being defined at the benzylic *C*-position). Upon lithiation of the enantiopure aryl-bromide (R)-**17**, the dimer which is formed is again exclusively *meso* at Li (like **16**), and hence this secondary chiral centre has no effect on the induced chirality at the Li centres [89]. *Rac*-**17** gives, upon lithiation, a different kind of self-assembly in which only Li centres of opposing chirality (at *C*) self-assemble to form the dimer. Further discussions of this unusual aggregation behaviour have been disclosed [89, 90].

2.4 Lithium PNP and PCP Pincers[2]

In the early 1980s, Fryzuk and co-workers introduced the first pincer amido ligand based on the de-protonation of the $HN(SiMe_2CH_2PR_2)_2$ skeleton (Fig. 16) [92]. The resulting formally anionic amidos have revealed a rich and diverse coordination chemistry with early, middle and late transition metal centres in addition to complexation with a vast array of lanthanide and main group elements [93]. Although the lithium materials have been used for some time, the attempted characterisation of these species in the solid state has been thwarted by the lack of

---

[2] The formally anionic, lithium bound $[HC\{PPh_2N(mesityl)\}_2]^-$ does not bind to the metal centre in a tridentate "pincer" fashion and hence is not discussed here (Hill et al. [91]).
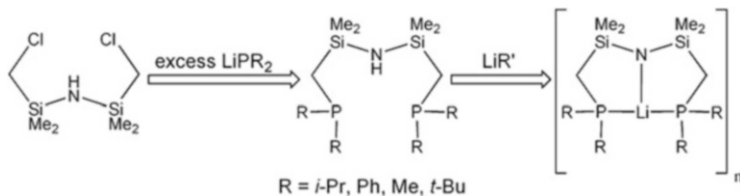
Fig. 16 The synthetic scheme to produce Fryzuk's Li amido pincers
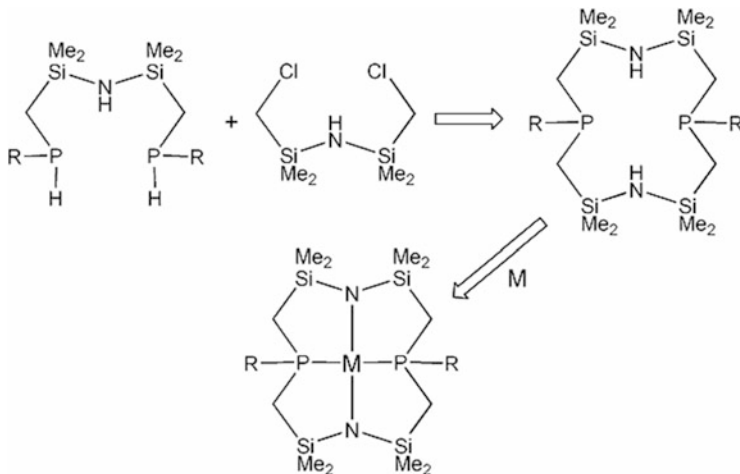
Fig. 17 General synthesis of "macrocyclic" bis-amido pincers

material suitable for X-ray analysis [93–95]. The materials do form crystalline adducts with other Li species however (this is detailed in Sect. 4).

Related "macrocyclic-" type amidos have also been reported by the Fryzuk group (Fig. 17) [96, 97].

The treatment of the macrocycle (Fig. 17: top right) with alkyllithium derivatives (Fig. 17; e.g. reagent M = n-BuLi) in THF solution gives rise to lithium species of intriguing structure. In the case of R = Ph, complexes can be isolated as one of two structurally unique THF adducts. The dimeric lithium amidos **18** and **19** are thus produced and can be isolated and separated (Fig. 18) [96–99].

The ratio of the production of these two materials is temperature dependent with the *anti* form being favoured at low temperature. Only the *syn* form **18** (isolated as a 1,4-dioxane adduct after work-up) is isolated if the solvent for the reaction is changed to Et_2O. This material can then be converted to solely **18** upon addition of THF [96, 97]. Other related examples of PNP complexes of Li have been disclosed [98, 99].

Although there is extensive transition metal chemistry of the PCP class of pincers [40, 100], there has been only two reports of lithium PCP complexes.
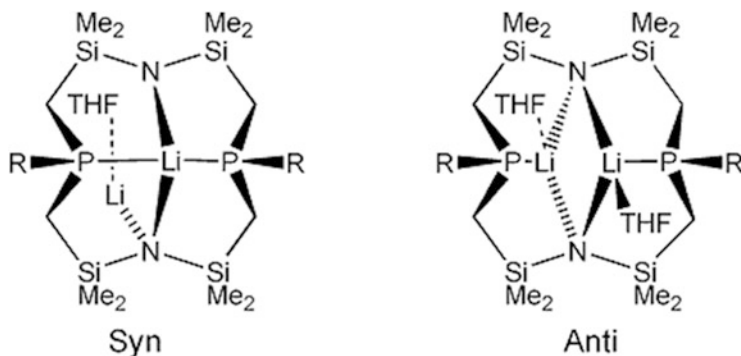
Fig. 18 Schematic diagram of *syn*-Li amido (**18**) and the *anti* derivative (**19**)

This is likely due to the propensity of this class of pincers to readily undergo DoM directly with *transition metal* precursors, hence negating the necessity to produce [Li(PCP)]$_n$ complexes for later metathesis.[3]A Li–Br exchange reaction was employed to produce [Li$_2$\{2,6-Me$_2$PCH$_2$)$_2$C$_6$H$_3$\}$_2$] (**20**) [104]. In the solid state, complex **20** strongly resembles the structure of the *N*-analogue **5** (Fig. 7). NMR spectroscopy has confirmed that **20** retains its dimeric structure (in toluene) up to room temperature, above which the dimer becomes fluxional on the NMR time-scale. This complex has been used to produce a magnesium derivative of PCP (Sect. 3).

The "caged" lithium complex [LiC(SiMe$_2$CH$_2$PPh$_2$)$_3$] (**21**) is produced via a selective de-protonation reaction of HC(SiMe$_2$CH$_2$PPh$_2$)$_3$ using MeLi. This species also retains its structural integrity in polar solvents such as THF [105].

2.5 Lithium OCO Pincers

There are a few examples of lithium pincer complexes containing ether-type functionalities that aid in bonding and stabilisation of the metal. The complex (2,6-dimethoxyphenyl)lithium (**22**) exists as a tetramer of cubic (Fig. 3) structure [106, 107]. The integrity of this motif is retained in apolar solvents (toluene), but in THF solution, this tetramer breaks down to a solvated monomer (cryoscopy, NMR). The more sterically bulky organic fragment 2,6-di-*tert*-butoxyphenyl results in the formation of a trimeric Li complex (**23**) of similar structure to that of **11**. The 3c–2e bonding motif is again seen. Theoretical calculations have suggested that the Li–O interaction is characterised by significant ionic character. No experiments were

---

[3] See, for example, Moulton and Shaw [101] and Rimml and Venanzi [102]. Regioselective ortholithiation of PCP pincers via Li–H exchange chemistry can be hampered by the acidity of the benzylic protons in, for example, 1,3-(R$_2$PCH$_2$)$_2$C$_6$H$_4$ derivatives; see, e.g. Gorla et al. [103] and Albrecht and van Koten [41].
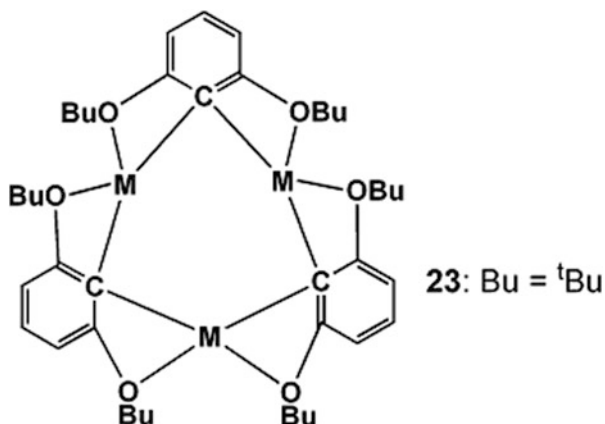
Fig. 19 Schematic diagram of complex **23** (M = Li)

carried out to test the stability of the complex to donor ligands, although it was noted that this material is highly soluble in both ether and hydrocarbon media (Fig. 19) [108].

A structural investigation of [2,6-(*tert*-butoxymethyl)$_2$C$_6$H$_3$Li] (**24**) has revealed that the material is dimeric in the solid state and is a close structural relative of **5**. This material appears to be dominated by an unusual monomeric form in dilute *apolar* (toluene) solutions (NMR, cryoscopy), but the dimer is present in more concentrated solutions [109]. This aspect is a rare observation within this class of materials.

Overall, it can be noted that the aggregation phenomena of the [OCO]Li class of pincers is greatly influenced by steric effects, solvation and ligand framework structure ([109, 110] and references therein).

2.6 Lithium Pincers with Hybrid Ligand Donor Sets

There are a few examples of Li pincers containing "hybrid" ligand donor atoms such as the "NCO" and "CPN" atom donor sets [111–113]. As part of their structural investigations of the OCO and NCN–Li materials, Harder and co-workers investigated the Li hybrid pincer complex [2-(dimethylamino)-6-(*tert*-butoxy)phenyl]lithium (**25**). This can be compared to **11** and **22**. Complex **25** is a trimer in the solid state, and this motif is retained in apolar solvents (NMR, cryoscopy). The trimer is dynamic, however, with ligand exchange processes between the Li centres being observed on the NMR timescale [111, 112].

The unusual complex **26** (Fig. 20), containing formally a "CPN" pincer donor atom set, is formed upon regioselective Li–H exchange (*t*-BuLi) from MeP
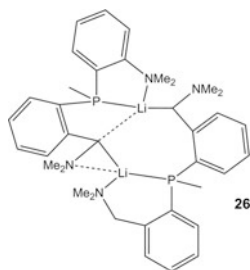
Fig. 20 Schematic diagram of complex **26**

({*o*-[dimethylamino]methyl}phenyl)$_2$. This dimeric structure is retained in apolar solvents (NMR) [114].

2.7 Lithium and Barium NON, SNS, SPS, OPO and NNN Pincers

The "NON" pincer skeleton can obviously be viewed as a chelate-stabilised (tridentate) phenolate. There are two structural examples of an Li(NON) pincer complex in addition to a rare case incorporating Ba.[4] The classic pincer design of 2,6-bis[(dimethylamino)methyl]-4-methylphenol (HOAr: Fig. 21: left-hand structure) forms quantitatively the slightly moisture-sensitive trimeric cluster [Li(OAr)]$_3$ upon treatment with *n*-BuLi [116, 117]. An earlier example of this structural formulation can be found in the related species derived from 2,6-bis(*N*-isopropyl-formimidoyl)-4-methylphenol. This trimeric species is formed from the free phenol upon reaction with LiOH (Fig. 21: right-hand structure) and is quite stable to hydrolysis [118, 119].

A Li complex of the formally monoanionic SNS ligand derived from the treatment of [(S=PPr^{i}CH$_2$)$_2$C$_5$H$_3$N-2,6] and *n*-BuLi has also been reported. The resulting monometallic complex has been structurally characterised and contains a sequestered solvent molecule (Et$_2$O). This material is formed via H$^+$ loss from one of the benzylic carbon atoms resulting in the formation of [Li{(S=PPr^{i}CH)(S=PPr^{i}CH$_2$)C$_5$H$_3$N-2,6-κ^3*S*,*N*,*S*′}(Et$_2$O-κ^1-*O*)] [118].

The unusual Li complex of an SPS pincer anion has been described by Mézailles and co-workers. Alkyllithium reagents form the solvent complex [Li(THF)$_2$] [SPS$^{(Me)}$-κ^3*S*,*P*,*S*′] (where SPS$^{(Me)}$ = a *P*-methyl derivative of 2,6-bis{diphenylphosphine sulphide}-3,5-diphenyl-phoshinine). This complex has been shown to be formed preferentially by slow cooling, a non-pincer κ^2*S*,*N*-bidentate isomer being obtained by solvent diffusion initiated crystallisation [119].

---

[4] A pincer-type "scorpionate" of Li has been reported; see Mutseneck et al. [115].
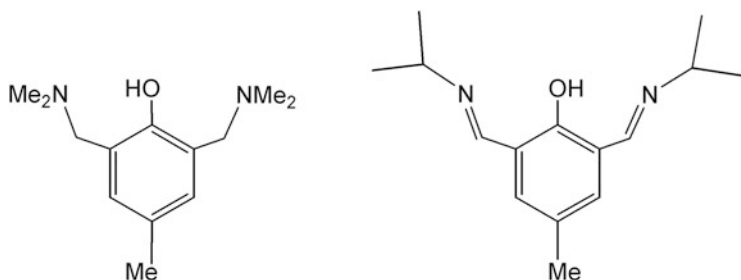
Fig. 21 Phenols (HOAr) used in the synthesis of trimeric [Li(OAr)]$_3$ clusters
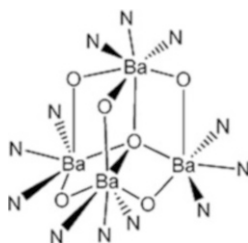
Fig. 22 Schematic diagram of the core structure of the cluster [Ba$_4$(μ_4-O)(μ_2-OC$_6$H$_2$\{CH$_2$NMe$_2$\}$_3$-2,4,6)$_6$]; aromatic rings have been removed for clarity; N represents the dimethylamino groups

An unusual Ba cluster, [Ba$_4$(μ_4-O)(μ_2-OC$_6$H$_2$\{CH$_2$NMe$_2$\}$_3$-2,4,6)$_6$], can be obtained from the treatment of K[OC$_6$H$_2$\{CH$_2$NMe$_2$\}$_3$-2,4,6] with BaI$_2$ in THF solution [120]. This material possesses a nearly perfect tetrahedral Ba$_4$ core (Fig. 22) with the oxo ligand being encapsulated within this tetrahedron. The arylphenolate ligands symmetrically bridge the edges of the Ba$_4$ tetrahedral unit with the two 2,6-positioned dimethylamino groups also coordinating to different Ba atoms; the third –NMe$_2$ functionality on aromatic position-4 is not metal bound.

Fryzuk has produced an NNN amido pincer which is a structural analogue of the PNP pincer amidos described earlier [121]. Thus, the treatment of HN(SiMe$_2$CH$_2$NMe$_2$)$_2$ with *n*-BuLi gives the dimeric lithium complex [Li$_2$\{N(SiMe$_2$CH$_2$NMe$_2$)$_2$\}$_2$] (**27**). The dimeric nature is reminiscent of **5** with the organic framework bridging the two metal atoms with a 3c–2e bond of the formal amido anion and concomitant coordination of the two dimethylamino groups of each NNN fragment to opposite metal centres. The structure appears to be retained in solution (toluene) despite the fluxional nature of the material. Compound **27** is a useful precursor to other metal NNN amido complexes [121].

The chemistry of the dianions with donor sets [OO′O]$^{2-}$ and [OPO]$^{2-}$ (i.e. Fig. 1: **B** with a neutral central donor atom and two phenolate anion donors "E") has appeared in the literature in recent years [122–125]. Lin and co-workers

have described [122] a number of structural motifs (dimeric, tetrameric and solvated adducts) for sterically bulky tridentate bis(phenolates) of Li and Na. These materials can also be employed in the ring-opening polymerisation of L-lactide. Fryzuk's [OPO]$^{2-}$ phosphine systems, also employing bulky phenolates, result in the formation of lithium oxide tetragons in either a face sharing half-cubane or stepform arrangements depending on the reaction conditions [123, 124].

A disclosure by Jenter and Roesky has revealed a dimeric Li species (i.e. [(DIP$_2$-pyr)Li$_2$]) resulting from the de-protonation (via n-BuLi) of 2,5-bis{N-(2,6-diisopropylphenyl)iminomethyl}pyrrole (DIP$_2$-pyrH) [126]. Analogous reactions of this precursor with NaH yield the Na dimer [(DIP$_2$-pyr)Na$_2$]) which possesses a related but not isostructural motif to that of the Li complex [126].

3 Sodium, Potassium and Magnesium Pincers

There are relatively few Na, K or Mg pincer compounds that have been isolated and studied [122, 124–131]. The complex 2,6-bis[(dimethylamino)methyl] phenylsodium] (**28**) is formed via Li–Na exchange from complex **5** (Sect. 2.1). However, it is structurally different from that of the Li congener. This complex adopts the less common (cf. **11**) trimeric structure (Fig. 3) [127]. Complex **28** itself is highly air, water and thermally sensitive with NMR characterisation having to be performed below −30°C to prevent decomposition.

Rabe et al. have described two [OCO]$^-$ pincer systems of Mg employing the carbanion derived from 1,3-bis(o-anisyl)benzene (DanipH) [128]. The isolation and structural characterisation of a monomeric complex Mg(Danip)$_2$ (cf. **29** below) and a THF-solvated dimer containing bridging phenolate groups (i.e. [DanipOMg(THF)$_2$]; DanipO = 2-{o-2-methoxynaphthyl}-6-{o-2-naphthoxide}phenyl) have been revealed.

There is a sole example of a phosphine pincer Mg complex. The reaction of **20** with anhydrous MgCl$_2$ results in the near quantitative formation of [bis{2,6-bis [(dimethylphosphino)methyl]phenyl}] magnesium ([Mg(PCP)$_2$]: **29**) [43, 100, 104]. Overall distorted octahedral coordination of the two pincer fragments to Mg is observed (Fig. 23). This material has high thermal stability. This latter observation is somewhat unusual considering the relative weakness of Mg–P dative bonds. Likely the formal anionic nature of the PCP fragment is partially responsible for these strong interactions. The structure is apparently preserved in solution (NMR, toluene).

Bickelhaupt's group has studied the magnesium coordination chemistry of a formally bis-anionic [COC]$^{2-}$ pincer and the classic [NCN]$^-$ pincer in terms of their Schlenk equilibria (i.e. 2 [XMgR] ↔ [MgR$_2$] + [MgX$_2$]) behaviour in THF solution. The preference for the [MgR$_2$] complex and [MgX$_2$] is pronounced. A crystal structure determination of mononuclear Mg(κ^3-C,O,C-[O{CH$_2$CH$_2$C$_6$H$_4$}$_2$])(κ^1-O-THF)$_2$ reveals an unusual five-coordinate ligand environment around the Mg atom [129].

Two equivalents of the formally anionic ligand 2,6-(MeOCH$_2$)$_2$phenyl (OCO) bind magnesium in an octahedral fashion (i.e. Mg(OCO)$_2$) which is a close structural relative to that of Mg(PCP)$_2$ [129].
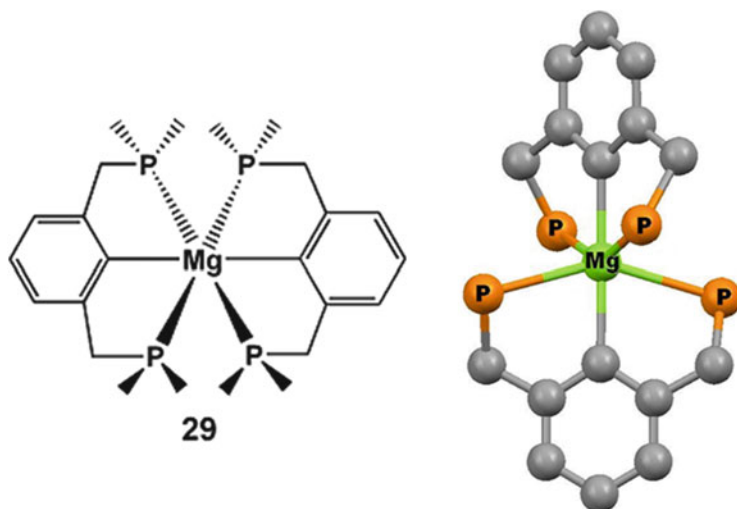
Fig. 23 The structure of [Mg(PCP)$_2$] (29); Me groups have been removed for clarity on the X-ray data (*right*)

The pincer 2,6-bis[(dimethylamino)methyl]-4-methylphenol (Fig. 21) gives a tetrameric sodium complex with a Na$_4$O$_4$ core unit upon reaction with NaOH (cf. [LiOAr]$_3$: Sect. 2.6) [116, 117, 130]. This material becomes dimeric in solution (cryoscopy) [130].

Finally, the κ^3-CON sodium complex of [C$_6$H$_4$OCH$_2$CH$_2$NMe$_2$]$^-$ is obtained by reaction of the tetrameric Li analogue with sodium-*tert*-amylate. This material is the first hexameric sodium complex to be isolated and features 4c–2e bonds from the organic fragments. This type of bonding is also found in the hexameric form of *n*-BuLi (i.e. [*n*-BuLi]$_6$) [131].

4 Zinc and Copper Pincers

Despite the large number of transition metal pincer complexes, relatively few studies until recently have focussed on the chemistry of copper or zinc. There appears to be no PCP compounds yet reported for either metal. Indeed, the NCN chemistry [25, 75] is somewhat limited and only includes one Zn and a few Cu compounds.[5] Gao and co-workers have reported on the NCN Zn complexes derived

---

[5] The compound H$_2$C(PPh$_2$NSiMe$_3$)$_2$ can be de-protonated by ZnMe$_2$ with loss of methane. The resulting zinc complex contains the formal anionic (NCN) ligand, but the binding mode of this fragment is revealed to be bidentate κ^2-*N,N'* not a κ^3-*N,C,N'* pincer motif, and hence [{κ^2-*N,N'*-HC (PPh$_2$NSiMe$_3$)$_2$}ZnMe] is formed: Kasani et al. [132]. In a similar way, the potentially tridentate NON pincers described by Wheaton and Hayes act as bidentate (κ^2-*N,N'*) ligands to Zn; see [133].

from the treatment of ZnEtCl with $[2,6\text{-}(ArN=CH)_2C_6H_3Li]_n$ derivatives (Ar = Ph, 2,6-$R_2C_6H_3$ {R = Me, Et or iPr}). The isopropyl pincer yields the predictable Zn(NCN)Et complex, while the other Li precursors yield Zn complexes with bidentate κ^2-NC formal NCN anions (cf. Footnote 5) in the solid state but with NMR evidence for κ^3-NCN coordination in solution [134].

The reactions of CuBr with **5** does not yield the expected Cu(NCN) material but instead $Cu_4Br_2(NCN)_2$ [135]. As in the lithium cases discussed above, 3c–2e bonding of the NCN fragment is common for the chemistry of Cu(I), but one also observes 4c–2e bonding of the bromide ions [25]. Thus, we have an unusual and highly distorted Br-bridged species of Cu(I) (**30**: Fig. 24).

The macrocyclic pincer **31** (Fig. 25) likewise forms an unusual cluster species with CuBr (**32**) ([136]; for other examples, NCN Pincer: [137], ONN Pincer: [138]).

Such structural motifs are not common in Li$^+$ chemistry [12–14]. However, the structure of **32** is reminiscent of *hetero-aggregated* lithium clusters containing organolithiums (cf. organocopper) and inorganic halides such as Li–Br (vide infra) [139]. Further examples of the "sequestering" of CuBr by organocopper pincers occur in the Cu clusters $[Cu_3Br\{C_6H_4(N(Me)CH_2CH_2NMe_2)\text{-}2\}_2]$ (**33**), $[Cu_4Br_2\{1\text{-}C_{10}H_6(N(Me)CH_2CH_2NMe_2)\text{-}2\}_2]$ (**34**) [140], $[Cu_8\{SC_6H_3(CH_2NMe_2)_2\text{-}2,6\}_3Br_5]$ (**35**) [141] and $[Cu_3\{C_6H_4(CH_2N(Me)CH_2CH_2Me_2)\text{-}2\}_3Br]$ (**36**) [142].

Recently the NNN pincer chemistry of Zn has begun to be explored in more detail [143–146]. Gladfelter has reported that the amido complex $Zn\{N(CH_2CH_2NMe_2)_2\}Cl$ likely exists as a μ,κ^3-$NN'N''$ bridged dimer [143], but this precursor yields a number of intriguing structurally characterised alkoxide bridging species upon treatment with alcohols or stoichiometric water [144]. In a similar fashion, a combination of dipicolylamine and PhC$\equiv$CH yields dimeric $[PhC\equiv CZn\{N(CH_2py)_2\}]_2$ upon treatment with ZnEt$_2$ and $[\{(Me_3Si)_2CHZn\}$
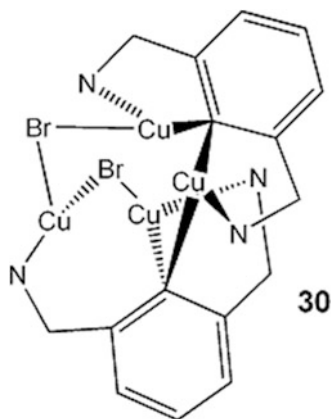
Fig. 24 The distorted nature of complex **30**: $[Cu_4Br_2(NCN)_2]$ (N = NMe$_2$)
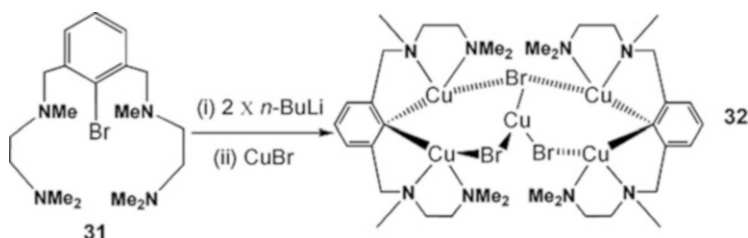
Fig. 25 The synthetic scheme to copper cluster **32**
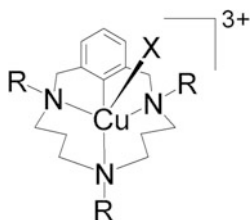
Fig. 26 Generic representation of the Cu-aryl macrocyclic pincers

($C \equiv CPh$) {$HN(CH_2py)_2$}] when reacted with $Zn(CH\{SiMe_3\}_2)$ [145]. The chemistry of both of these μ,κ^3-NN′N-complexes and related analogues has also been described [145]. In contrast, chiral bis-oxazoline (cf. **10**, isoindoline-based pincers) yield enantiopure monomeric $Zn(NN'N)_2$ derivatives [146].

In relation to complexes such as copper material **32**, structurally related organocopper macrocyclic pincers have recently been the subject of intense scrutiny (Fig. 26) and are described in some detail in the chapter by Font and Ribas found in this volume; cf. [147–154]. Hence, only a brief overview will be detailed here. Much of this work has centred around the observation and stabilisation of very unusual Cu^{3+} species that are derived from aryl C–H bond activation chemistry [147, 154]. Subsequent disproportion reactions of the initially formed Cu^{2+} species to give rise to diamagnetic Cu^+ and Cu^{3+} materials [147, 148]. The latter compounds have demonstrated a range of activities including aryl group transfer to form N–C bonds [149] and oxidative coupling to give N–C or O–C bonds [150, 151]. This work has led to the assignment of an unprecedented mechanism for C–H bond activation that includes a key rate-limiting proton-coupled electron transfer step [150, 154, 155]. It is of little doubt that some very interesting and novel chemistry has yet to be revealed by such pincer systems [154].

5 Hetero-Aggregated Li Pincers and Chiral Aggregate Formation

The concept of hetero-aggregation in organolithium chemistry occurs when two or more structurally distinct lithium species combine or "self-assemble" to form a new structural form containing all of the distinct Li containing units [139]. The new hetero-aggregate (e.g. $[RLi]_x[R'Li]_y[LiX]_z$) may have very different reactivity than either of the parent organolithiums. Although rarely recognised, this phenomenon has in fact been known for some time [155]. The familiar "LiCl effect" in organic synthesis is one typical example of this behaviour. This involves a kinetic or thermodynamic influence of the added salt to the reactivity involving an RLi or some other unit. In reality, the added salt is forming a hetero-aggregate with the source of nucleophile R, and this aggregate reacts along a different pathway (hopefully more selectively or at a modified rate) than RLi alone. Seebach has provided an excellent review and seminal work in this area [156, 157] in relation to lithium enolate chemistry, and the importance of such observations continues to surface routinely ([156–159] and references therein). Due to the oligomeric propensity of organolithiums, hetero-aggregated pincer materials are known. This has been the subject of an extensive review [90] and hence will only be briefly alluded to here.

Fryzuk has provided a number of interesting examples of hetero-aggregation using his amido-based pincer materials derived from $[LiN(SiMe_2CH_2PR_2)_2]_n$ (Fig. 16). Under the correct conditions, the *formation* of $[LiN(SiMe_2CH_2P^iPr_2)_2]$ can lead to a hetero-aggregate. Thus, the reaction of $HN(SiMe_2CH_2Cl)_2$ with LiP^iPr_2 in THF can lead to the isolation of $[LiN(SiMe_2CH_2P^iPr_2)_2]_2LiCl$ (**37**) [95]. This is not simply a molecule of LiCl "salt" trapped within the solid of the lithium amido but rather a trinuclear network material (Fig. 27).

The aggregated structure of **37** is retained in solution (NMR: C_6D_6), although site exchange between Li atoms was noted. "Salt" free $[LiN(SiMe_2CH_2P^iPr_2)_2]$

Fig. 27 Schematic diagram of the aggregated lithium amido complex [LiN(SiMe₂CH₂PⁱPr₂)₂]₂LiCl (**37**)

37: P = PⁱPr₂
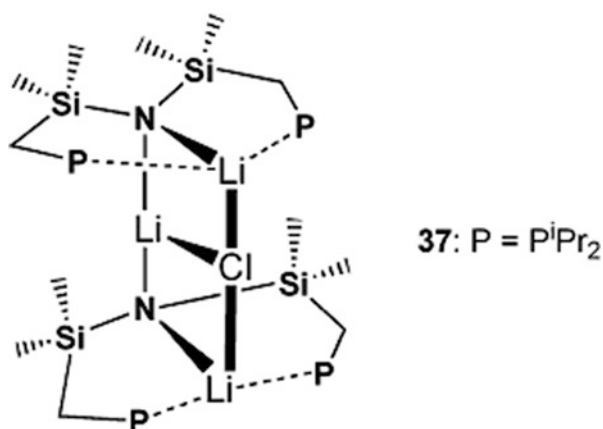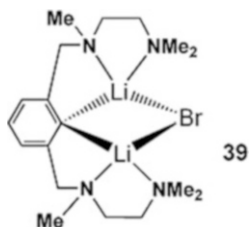
Fig. 28 The Li–Br adduct **39**

(**38**) will react cleanly with added LiCl in THF or toluene solution to regenerate **37**. Such an observation suggests that **37** is the thermodynamically stable hetero-aggregate complex and not simply a result of the "trapping" of a LiCl molecule during the formation of the two amido moieties. In a similar way, **38** forms complexes with LiAlEt$_4$, LiBEt$_4$, LiAlMe$_4$ and NaBEt$_4$. These latter two adducts have been characterised by X-ray diffraction. The LiAlMe$_4$ adduct is a 2:2 complex of **38** while the NaBEt$_4$ material is polymeric in nature with one equiv. of LiN (SiMe$_2$CH$_2$P^{i}Pr$_2$)$_2$ per unit of NaBEt$_4$. The structure of this adduct does not appear to be retained in solution [95]. The synthesis and stability of such adducts demonstrates that caution should be exercised when using RLi materials in the presence of other additives, especially if these additives can be quite reactive in themselves (e.g. "trapped" LiAlMe$_4$) or can be *formed* (e.g. LiX) during the course of a reaction. Such new hetero-aggregated materials could indeed alter the course of a desired synthesis [90, 139, 160].

Several pincer NCN and CNN complexes provide further examples of this behaviour. The reaction of **31** (Fig. 25) with 2 equiv. of *n*-BuLi does not give rise to the expected Li(CNNNN) complex, but instead one equiv. of the resulting *o*-LiC$_6$H$_3${CH$_2$CH$_2$N(Me)CH$_2$CH$_2$NMe$_2$}$_2$-2,6 material "sequesters" a molecule of the resulting by-product LiBr to form the mixed species **39** (Fig. 28) [160]. The structure of this material certainly reminds one of the copper halide complex **32**.

The first structurally elucidated "mixed" pure organolithium aggregate, [(*n*-BuLi)$_2$(2,4,6-*tert*-Bu$_3$C$_6$H$_2$Li)$_2$], was reported by Power's group in 1993 [161], although it was already well-established that such materials existed in solution [162, 163] and were also surmised to be involved in the chemistry of DMBA derivatives [164, 165]. The metalation of the carbon atom of the methyl group on position-2 of 2,4,6-trimethyl-1,3-[(dimethylamino)methyl]benzene (**40**) and the analogous methylene carbon at aromatic position-1 of 1-(2-trimethyl-silylethyl)-3,5-dimethyl-2,6-[(dimethylamino)methyl]benzene (**41**) by a variety of RLi reagents (R = *n*-Bu, Ph, *p*-tolyl, *tert*-Bu) all lead to the formation of 2:2 mixed aggregates [90, 166, 167].

Interestingly, complex **6** (Fig. 8) is a dimeric *homo-aggregate* of the two enantiopure moieties of (*R*)-1,3-bis-[1-(dimethylamino)ethyl] phenyllithium. However, the combination of an (*R*) and (*S*) fragment to make dimeric (*R*, *S*)-**16**

Fig. 29 The equilibria involving *n*-BuLi and Li(NCN). This figure is reproduced from [70] with permission of the Royal Society of Chemistry

(i.e. (R_{Li}, S_{Li})-[LiC$_6$H$_4$-CH$_2$N(Et)CH$_2$CH$_2$NEt$_2$]$_2$) is a *hetero-aggregate* by definition [89, 90].

A further example is demonstrated by the reaction of dimeric **8a** (i.e. [Li$_2$\{2,6-(Et$_2$NCH$_2$)$_2$C$_6$H$_3$\}$_2$] [70]) or **5** with *n*-BuLi in apolar solvents. This leads to *multiple* mixed aryl-alkyl aggregates [78]. These materials include the 2:2 aggregates \{[**8a**]$_2$[*n*-BuLi]$_2$\} (**42**) and \{[**8**]$_2$[*n*-BuLi]$_2$\} (**43**). Complex **42** and **43** have both been structurally characterised (NMR, X-ray, etc.). Of further interest is that solution studies suggest that 1:3 adducts are also present in solution, i.e. \{[**11**][*n*-BuLi]$_3$\} (**44**) and \{[**8**][*n*-BuLi]$_3$\} (**45**). Detailed NMR characterisation of solutions of either **5** or **8a** with varying amounts of *n*-BuLi reveals that a complex equilibrium exists (Fig. 29) between **42**, **44** and "free" [*n*-BuLi]$_6$ (for **8**) and the complexes derived from **5**: **43**, **45** and [*n*-BuLi]$_6$.

One can now imagine the potential difficulties faced by the synthetic chemist if such aggregates were to be employed in later metathesis reactions and the investigators were ignorant of the presence of "sequestered" *n*-BuLi. Such a situation may be commonplace when excess RLi reagents are employed in an attempt to force DoM to completion [90, 164, 166, 167].

6 Conclusions and Outlook

The chemistry of the pincer ligands is obviously diverse and structurally intriguing. The case of the metals Li, Na, Mg and others (notably Zn and Cu) represent the "classic" organometallic metals for use in synthesis. These materials are in themselves highly complex, and attention should be paid to these structures when unusual reactivity, such as noted in Sect. 5, or strange additive effects (e.g. LiBr) are noted. Certainly an area of little exploration thus far is the pincer chemistry of zinc. Given the historical and reactivity relationships between RLi, R$_2$Mg, RMgX, NaR and CuR materials, it is of little doubt that the chemistry of the pincer ligands with zinc [143–146] and other main group elements (a study detailing some intriguing pincer-Al chemistry has appeared: [168]) will be just as interesting and diverse.

References

1. Omae I (1998) Applications of organometallic compounds. Wiley, Toronto
2. de Meijere A, Diederich F (eds) (2004) Metal-catalyzed cross-coupling reactions, 2nd edn. Wiley-VCH, Weinheim
3. Grignard V (1900) Compt Rend 130:1322
4. Grignard V (1901) Ann Chim 24:433
5. Grignard V (1912) Nobel lecture, Stockholm. http://www.nobelprize.org/nobel_prizes/chemistry/laureates/1912/grignard-lecture.html
6. Seyferth D (2009) Organometallics 28:1598
7. Newbold B (2001) Can Chem News 25
8. Knochel P, Calaza MI, Hupe E (2004) Carbon-carbon bond forming reactions mediated by organozinc reagents. In: de Meijere A, Diederich F (eds) Metal-catalyzed cross-coupling reactions, 2nd edn. Wiley-VCH, Weinheim
9. Coates GE, Wade K (1967) The main group elements. In: Coates GE, Green MLH, Wade K (eds) Organometallic compounds, vol 1, 3rd edn. Methuen, London
10. Brown JM, Armstrong SK (1995) Magnesium. In: Abel EW, Stone FGA, Wilkinson G (eds) Comprehensive organometallic chemistry II. Elsevier, Amsterdam
11. Lindsell WE (1995) Magnesium, calcium, strontium and barium. In: Abel EW, Stone FGA, Wilkinson G (eds) Comprehensive organometallic chemistry II. Elsevier, Amsterdam
12. Wright DS, Beswick MA (1995) Alkali metals. In: Abel EW, Stone FGA, Wilkinson G (eds) Comprehensive organometallic chemistry II, vol 1. Elsevier, Amsterdam
13. Leroux F, Schlosser M, Zohar E, Marek I (2004) The preparation of organolithium reagents and intermediates. In: Rappoport Z, Marek I (eds) The chemistry of organolithium compounds. Wiley, Etobicoke
14. Langer AW (ed) (1974) Polyamine-chelated alkali metal compounds, Adv Chem Series 130. American Chemical Society, Washington
15. Snieckus V, Gray M, Tinki M (1995) Lithium. In: Abel EW, Stone FGA, Wilkinson G (eds) Comprehensive organometallic chemistry II. Elsevier, Amsterdam
16. Mordini A (1995) Sodium and potassium. In: Abel EW, Stone FGA, Wilkinson G (eds) Comprehensive organometallic chemistry II. Elsevier, Amsterdam
17. Wardell JL (1982) Alkali metals. In: Wilkinson G, Stone FGA, Abel EW (eds) Comprehensive organometallic chemistry. Elsevier, Amsterdam
18. Seyferth D (2009) Organometallics 28:2
19. Seyferth D (2006) Organometallics 25:2
20. Seyferth D (2001) Organometallics 20:2940
21. Wu G, Huang H (2006) Chem Rev 106:2596
22. Alexakis A (2002) Pure Appl Chem 74:37

23. Yang X, Knochel P (2006) Chem Commun 2486
24. Negishi E, Zeng X, Tan Z, Qian M, Hu Q, Huang Z (2004) Palladium- or nickel-catalyzed cross-coupling with organometals containing zinc, aluminum, and zirconium: the Negishi coupling. In: de Meijere A, Diederich F (eds) Metal-catalyzed cross-coupling reactions, 2nd edn. Wiley-VCH, Weinheim
25. van Koten G (1990) J Organomet Chem 400:283
26. van Koten G, James SL, Jastrzebski JTBH (1995) Copper and silver. In: Abel EW, Stone FGA, Wilkinson G (eds) Comprehensive organometallic chemistry II, vol 3. Elsevier, Amsterdam
27. Carruthers W (1982) Compounds of zinc, cadmium and mercury, and of copper, silver and gold in organic synthesis. In: Wilkinson G, Stone FGA, Abel EW (eds) Comprehensive organometallic chemistry. Elsevier, Amsterdam
28. Noltes JG, van Koten G (1982) Copper and silver. In: Wilkinson G, Stone FGA, Abel EW (eds) Comprehensive organometallic chemistry. Elsevier, Amsterdam
29. Knochel P, Sapounntzis I, Gommermann N (2004) Carbon-carbon bond forming reactions mediated by organomagnesium reagents. In: de Meijere A, Diederich F (eds) Metal-catalyzed cross-coupling reactions, 2nd edn. Wiley-VCH, Weinheim
30. Knochel P, Hupe E, Houte H (2004) L'actualité chimique 12
31. Knochel P, Hupe E, Dohle W, Lindsay DM, Bonnet V, Quéguiner G, Boudier A, Kopp F, Demay S, Seidel N, Calaza MI, Vu VA, Sapountzis I, Bunlaksananusorn T (2002) Pure Appl Chem 74:11
32. Knochel P, Singer RD (1993) Chem Rev 93:2117
33. Knochel P (1995) Cadmium and zinc. In: Abel EW, Stone FGA, Wilkinson G (eds) Comprehensive organometallic chemistry II, vol 11. Elsevier, Amsterdam
34. O'Brien P (1995) Cadmium and zinc. In: Abel EW, Stone FGA, Wilkinson G (eds) Comprehensive organometallic chemistry II, vol 3. Elsevier, Amsterdam
35. Boersma J (1982) Zinc and cadmium. In: Wilkinson G, Stone FGA, Abel EW (eds) Comprehensive organometallic chemistry. Elsevier, Amsterdam
36. van Koten G (1990) Pure Appl Chem 61:1681
37. van Koten G (2013) Top Organomet Chem 40:1
38. O'Reilly ME, Veige AS (2014) Chem Soc Rev 43:6325
39. Rietveld MHP, Grove DM, van Koten G (1997) New J Chem 21:751
40. van der Boom ME, Milstein D (2003) Chem Rev 103:1759
41. Albrecht M, van Koten G (2001) Angew Chem Int Ed 40:3750
42. Szabó K (2006) Synlett 811
43. Gruter G-JM, van Klink GPM, Akkerman OS, Bickelhaupt F (1995) Chem Rev 95:2405
44. Snieckus V (1990) Pure Appl Chem 62:671
45. Snieckus V (1990) Chem Rev 90:879
46. Snieckus V (1988) Bull Soc Chim Fr 67
47. Green L, Chauder B, Snieckus V (1999) J Heterocycl Chem 36:1453
48. Anctil EJ-G, Snieckus V (2002) J Organomet Chem 653:150
49. Omae I (1979) Chem Rev 79:287
50. Gschwend HW, Roderiquez HR (1979) Org React 26:1
51. Clayden J (2004) Directed metalation of aromatic compounds. In: Rappoport Z, Marek I (eds) The chemistry of organolithium compounds. Wiley, Etobicoke
52. Sotomayor N, Lete E (2003) Curr Org Chem 7:275
53. Anctil EJ-G, Snieckus V (2004) The directed ortho-metallation (DoM) cross-coupling nexus. Synthetic methodology for the formation of aryl-aryl and aryl-heteroatom-aryl bonds. In: de Meijere A, Diederich F (eds) Metal-catalyzed cross-coupling reactions, 2nd edn. Wiley-VCH, Weinheim
54. Gilman H, Bebb RL (1939) J Am Chem Soc 61:109
55. Ziegler K, Colonius H (1930) Justus Liebigs Ann Chem 479:135
56. Jones FN, Zinn MF, Hauser CR (1963) J Org Chem 28:663

57. Jones FN, Vaulx RL, Hauser CR (1963) J Org Chem 28:3461
58. Jones FN, Hauser CR (1962) J Org Chem 27:4389
59. Weiss E (1993) Angew Chem Int Ed Engl 32:1501
60. Bickelhaupt FM, van Eikema Hommes NJR, Guerra CF, Baerends EJ (1996) Organometallics 15:2923
61. Matito E, Poater J, Bickelhaupt FM, Solà M (2006) J Phys Chem B 110:7189
62. Jastrzebski JTBH, van Koten G, Konijn M, Stam CH (1982) J Am Chem Soc 104:5490
63. Wehman E, Jastrzebski JTBH, Ernsting J-M, Grove DM, van Koten G (1988) J Organomet Chem 353:145
64. Reich HJ, Goldenberg WS, Gudmundsson BÖ, Sanders AW, Kulicke KJ, Simon K, Guzei IA (2001) J Am Chem Soc 123:8067
65. Kalbarczyk-Bidelska E, Pasynkiewicz S (1991) J Organomet Chem 407:143
66. Reich HJ, Gudmundsson BÖ (1996) J Am Chem Soc 118:6074
67. Hoppe D, Christoph G (2004) Asymmetric deprotonation with alkyllithium-(−)-sparteine. In: Rappoport Z, Marek I (eds) The chemistry of organolithium compounds. Wiley, Etobicoke
68. Nájera C, Yus M (2003) Curr Org Chem 7:867
69. Goldfuss B (2005) Synthesis 2271
70. Chase PA, Lutz M, Spek AL, Gossage RA, van Koten G (2008) Dalton Trans 5783
71. Steenwinkel P, James SL, Grove DM, Veldman N, Spek AL, van Koten G (1996) Chem Eur J 2:1440
72. Albrecht M, Kocks BM, Spek AL, van Koten G (2001) J Organomet Chem 624:271
73. Donkervoort HG, Vicario JL, Rijnberg E, Jastrzebski JTBH, Kooijman H, Spek AL, van Koten G (1998) J Organomet Chem 550:463
74. Smeets WJJ, Spek AL, van der Zeijden AAH, van Koten G (1987) Acta Cryst C43:1429
75. van Koten G (1989) Pure Appl Chem 61:1681
76. Moene W, Vos M, de Kanter FJJ, Klumpp GW, Spek AL (1989) J Am Chem Soc 111:3463
77. van der Zeijden AAH, van Koten G (1988) Recl Trav Chim Pays Bas 107:431
78. Schlengermann R, Sieler J, Jelonek S, Hey-Hawkins E (1997) Chem Commun 197
79. Saito M, Matsumoto K, Fujita M, Minoura M (2014) Heteroatom Chem 25:354
80. Harris TD, Neuschwander B, Boekelheide V (1978) J Org Chem 43:727
81. Button KM, Gossage RA, Phillips RKR (2002) Synth Commun 32:363
82. Stol M, Snelders DJM, de Pater JJM, van Klink GPM, Kooijman H, Spek AL, van Koten G (2005) Organometallics 24:743
83. Harder S, Boersma J, Brandsma L, Kanters JA, Bauer W, von Ragué Schleyer P (1989) Organometallics 8:1696
84. Ong CM, Stephan DW (1999) J Am Chem Soc 121:2939
85. Kasani A, Babu RPK, McDonald R, Cavell RG (1999) Angew Chem Int Ed 38:1483
86. Jones ND, Cavell RG (2005) J Organomet Chem 690:5485
87. Cavell RG (2000) Curr Sci 78:440
88. Rietveld MHP, Wehman-Ooyevaar ICM, Kapteijn GM, Grove DM, Smeets WJJ, Kooijman H, Spek AL, van Koten G (1994) Organometallics 13:3782
89. Arink AM, Kronenburg CMP, Jastrzebski JTBH, Lutz M, Spek AL, Gossage RA, van Koten G (2004) J Am Chem Soc 126:16249
90. Gossage RA, Jastrzebski JTBH, van Koten G (2005) Angew Chem Int Ed 44:1448
91. Hill MS, Hitchcock PB, Karagouni SMA (2004) J Organomet Chem 689:722
92. Fryzuk MD, MacNeil PA (1981) J Am Chem Soc 103:3592
93. Fryzuk MD (1992) Can J Chem 70:2839
94. Fryzuk MD, Carter A, Westerhaus A (1985) Inorg Chem 24:642
95. Fryzuk MD, Giesbrecht GR, Rettig SJ (1997) Organometallics 16:725
96. Fryzuk MD, Love JB, Rettig SJ (1996) Chem Commun 2783
97. Fryzuk MD, Giesbrecht GR, Johnson SA, Kickham JE, Love JB (1998) Polyhedron 17:947
98. Liang L-C, Chien P-S, Lin J-M, Huang M-H, Huang Y-L, Liao J-H (2007) Organometallics 25:1399

99. Yurkerwich K, Parkin G (2010) Inorg Chim Acta 364:157
100. Izod K (2000) Adv Inorg Chem 50:33
101. Moulton CJ, Shaw BL (1976) J Chem Soc Dalton Trans 1020
102. Rimml H, Venanzi LM (1983) J Organomet Chem 259:C6
103. Gorla F, Venanzi LM, Albinati A (1994) Organometallics 13:43
104. Pape A, Lutz M, Müller G (1994) Angew Chem Int Ed Engl 33:2281
105. Avent AG, Bonafoux D, Eaborn C, Hill MS, Hitchcock PB, Smith JD (2000) J Chem Soc Dalton Trans 2183
106. Dietrich H, Mahdi W, Storck W (1988) J Organomet Chem 349:1
107. Harder S, Boersma J, Brandsma L, van Heteren A, Kanters JA, Bauer W, von Ragué Schleyer P (1988) J Am Chem Soc 110:7802
108. Harder S, Boersma J, Brandsma L, Kanters JA, Duisenberg AJM, van Lenthe JH (1991) Organometallics 10:1623
109. Jambor R, Dostál L, Císařová I, Růžička A, Holeček J (2005) Inorg Chim Acta 358:2422
110. Nakatsuji J-Y, Moriyama Y, Matsukawa S, Yamamoto Y, Akiba K-Y (2006) Main Group Chem 5:277
111. Harder S, Ekhart PF, Brandsma L, Kanters JA, Duisenberg AJM, von Ragué Schleyer P (1992) Organometallics 11:2623
112. den Besten R, Lakin MT, Veldman N, Spek AL, Brandsma L (1996) J Organomet Chem 514:191
113. Vrána J, Jambor R, Růžička A, Holeček J, Dostál L (2010) Collect Czech Chem Commun 75:1041
114. Clegg W, Izod K, McFarlane W, O'Shaughnessy P (1999) Organometallics 18:3950
115. Mutseneck EV, Bieller S, Bolte M, Lerner H-W, Wagner M (2010) Inorg Chem 49:3540
116. van der Schaaf PA, Hogerheide MP, Grove DM, Spek AL, van Koten G (1992) J Chem Soc Chem Commun 1703
117. Korobov MS, Minkin VI, Nivorozhkin LE, Kompan OE, Struchkov YuT (1987) Zh Obshchei Khim 59:429 (Russ J Inorg Chem 59:379)
118. Leung W-P, Kan K-W, Mak TCW (2010) Organometallics 29:1890
119. Doux M, Thuéry P, Blug M, Ricard L, Le Floch P, Arliguie T, Mézaiiles N (2007) Organometallics 26:5643
120. Tish KF, Hanusa TP (1991) J Chem Soc Chem Commun 879 (Corrigendum: J Chem Soc Chem Commun 1580)
121. Fryzuk MD, Hoffman V, Kickham JE, Rettig SJ, Gambarotta S (1997) Inorg Chem 36:3480
122. Huang Y, Tsai Y-H, Hung W-C, Lin C-S, Wang W, Huang J-H, Dutta S, Lin C-C (2010) Inorg Chem 49:9416
123. Carmichael CD, Fryzuk MD (2008) Dalton Trans 800
124. Chang Y-N, Liang L-C (2007) Inorg Chim Acta 360:136
125. Carmichael CD, Fryzuk MD (2010) Can J Chem 88:667
126. Jenter J, Roesky PW (2010) New J Chem 34:1541
127. den Besten R, Brandsma L, Spek AL, Kanters JA, Veldman N (1995) J Organomet Chem 498:C6
128. Rabe GW, Zheng-Preße M, Riederer FA, Rheingold AL (2010) Inorg Chim Acta 363:2341
129. Markies PR, Altink RM, Villena A, Akkerman OS, Bickelhaupt F, Smeets WJJ, Spek AL (1991) J Organomet Chem 402:289
130. van der Schaaf PA, Jastrzebski JTBH, Hogerheide MP, Smeets WJJ, Spek AL, Boersma J, van Koten G (1993) Inorg Chem 32:4111
131. Rappoport Z, Marek I (eds) (2004) The chemistry of organolithium compounds. Wiley, Etobicoke
132. Kasani A, McDonald R, Cavell RG (1999) Organometallics 18:3775
133. Wheaton CA, Hayes PG (2010) Dalton Trans 39:3861
134. Liu Z, Gao W, Zhang J, Cui D, Wu Q, Mu Y (2010) Organometallics 29:5783

135. Wehman E, van Koten G, Erkamp CJM, Knotter DM, Jastrzebski JTBH, Stam CH (1989) Organometallics 8:94
136. Kapteijn GM, Wehman-Ooyevaar ICM, Grove DM, Smeets WJJ, Spek AL, van Koten G (1993) Angew Chem Int Ed Engl 32:72
137. Wehman E, van Koten G, Knotter DM, Erkamp CJM, Mali ANS, Stam CH (1987) Recl Trav Chim Pays Bas 106:370
138. Rajendran U, Viswanathan R, Palaniandavar M, Lakshminarayanan M (1992) J Chem Soc Dalton Trans 3563
139. Pratt LM (2004) Mini Rev Org Chem 1:209
140. Janssen MD, Corsten MA, Spek AL, Grove DM, van Koten G (1996) Organometallics 15:2810
141. Janssen MD, Spek AL, Grove DM, van Koten G (1996) Inorg Chem 35:4078
142. Gerold A, Jastrzebski JTBH, Kronenberg CMP, Krause N, van Koten G (1997) Angew Chem Int Ed Engl 36:755
143. Luo B, Kucera BE, Gladfelter WL (2006) Polyhedron 25:279
144. Luo B, Kucera BE, Gladfelter WL (2010) Polyhedron 29:2795
145. Kahnes M, Görls H, Westerhausen M (2010) Organometallics 29:3490
146. Cryder JL, Killgore AJ, Moore C, Golen JA, Rheingold AL, Daley CJA (2010) Dalton Trans 39:10671
147. Ribas X, Jackson DA, Donnadieu B, Mahía J, Parella T, Xifra R, Hedman B, Hodgson KO, Llobet A, Stack TDP (2002) Angew Chem Int Ed 41:2991
148. Xifra R, Ribas X, Llobet A, Poater A, Duran M, Solà M, Stack TDP, Benet-Buchholz J, Donnadieu B, Mahía J, Parella T (2005) Chem Eur J 11:5146
149. Huffman LM, Stahl SS (2008) J Am Chem Soc 130:9196
150. Ribas X, Calle C, Poater A, Casitas A, Gómez L, Xifra R, Parella T, Benet-Buchholz J, Schweiger A, Mitrikas G, Solà M, Llobet A, Stack TDP (2010) J Am Chem Soc 132:12299
151. Casitas A, King AE, Parella T, Costas M, Stahl SS, Ribas X (2010) Chem Sci 1:326
152. Casitas A, Poater A, Solà M, Stahl SS, Costas M, Ribas X (2010) Dalton Trans 39:10458
153. King AE, Huffman LM, Casitas A, Costas M, Ribas X, Stahl SS (2010) J Am Chem Soc 132:12068
154. Casitas A, Ribas X (2013) Chem Sci 4:2301
155. Peascoe W, Applequist DE (1973) J Org Chem 38:1510
156. Seebach D (1988) Angew Chem Int Ed Engl 27:1624
157. Seebach D, Amstutz R, Dunitz JD (1981) Helv Chim Acta 64:2622
158. Briggs TF, Winemiller MD, Collum DB, Parsons RL, Davulcu AH, Harris GD, Fortunak JM, Confalone PN (1993) J Am Chem Soc 115:11353
159. Fraenkel G, Gallucci J, Liu H (2006) J Am Chem Soc 128:8211
160. Wehman-Ooyevaar ICM, Kapteijn GM, Grove DM, Spek AL, van Koten G (1993) J Organomet Chem 452:C1
161. Ruhlandt-Senge K, Ellison JJ, Wehmschulte RJ, Pauer F, Power PP (1993) J Am Chem Soc 115:11353
162. Curtin DY, Flynn EW (1959) J Am Chem Soc 81:4714
163. Glaze W, West R (1960) J Am Chem Soc 82:4437
164. van Koten G, Jastrzebski JTBH (1989) Tetrahedron 45:569
165. Kronenberg CMP, Rijnberg E, Jastrzebski JTBH, Kooijman H, Lutz M, Spek AL, Gossage RA, van Koten G (2005) Chem Eur J 11:253
166. Wijkens P, van Koten EM, Janssen MD, Jastrzebski JTBH, Spek AL, van Koten G (1995) Angew Chem Int Ed Engl 34:219
167. Wijkens P, Jastrzebski JTBH, Veldman N, Spek AL, van Koten G (1997) Chem Commun 2143
168. Koller J, Bergman RG (2010) Organometallics 29:3350

Late Transition Metal Complexes with Pincer Ligands that Comprise *N*-Heterocyclic Carbene Donor Sites

Kevin Farrell and Martin Albrecht

Abstract The incorporation of *N*-heterocyclic carbenes into the well-established pincer ligand platform entails a number of attractive benefits. For example, NHCs are strong donors, and the metal–carbene bond is often remarkably robust towards oxidative and hydrolytic conditions and thus sustains in air, moisture, and even highly acidic environments. Moreover, NHCs can be readily functionalized and modulated and thus provide excellent opportunities for fine-tuning the properties of a coordinated metal center. As a consequence, the combination of the concepts of pincer ligands and of NHCs has much appeal and continues to attract considerable interest. This chapter summarizes accomplishments over the last 5 years in the domain of pincer carbene complexes containing Group 8–10 metals, including synthetic aspects as well as application of these complexes, which has included in particular catalysis and to a lesser extent materials science and medicinal areas.

Keywords Catalysis · Late transition metals · *N*-heterocyclic carbenes · Photophysical applications · Pincer ligand · Platinum group metals · Synthesis

Contents

K. Farrell and M. Albrecht (✉)
School of Chemistry and Chemical Biology, University College Dublin, Belfield, Dublin 4, Ireland
e-mail: martin.albrecht@ucd.ie

1 Introduction

Pincer-type ligands have become a popular and most useful tool of modern organo-metallic chemistry [1–3], and pincer metal complexes have been very successfully employed for a wide variety of applications including supramolecular chemistry, as sensors, and of course for catalysis [4–10]. A great advantage of pincer ligands is their tridentate bonding mode, which enhances the integrity of the metal center and which allows specific ligand sites to be modified without altering the metal coordination environment significantly. This concept provides a methodology for rationally tailoring and tuning the properties and activity of the metal center by steric and electronic ligand modifications [11]. This approach has led to some of the most active systems known thus far, e.g., for catalytic alkane dehydrogenation [12] and oxidative alcohol/amine coupling [13]. At the other extreme, key intermediates have been stabilized to better understand fundamental processes such as oxidative addition [14], C–C bond formation [15, 16], and transmetalation [17].

Modification of the classic *E,C,E*-tridentate coordinating (ECE) pincer ligand (**A**, Fig. 1) includes, in particular, variation of the donor sites E as well as modification of the central carbanionic site. With the development of *N*-heterocyclic carbenes (NHCs) [18] as a versatile class of donor ligands to transition metals [19–23], and with their great impact on catalysis in their own rights [24–29], pincer ligands have received a new dimension. Specifically, since *N*-heterocyclic carbenes have significant mesoionic character [30], such carbenes can either be considered as neutral donors and hence as variables for the donor sites E, or as mesoionic systems that may substitute the central carbanionic site, thus leading to the generic carbene
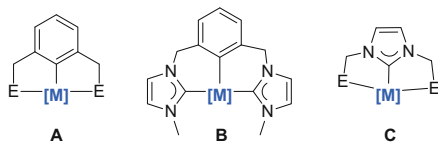
pincer scaffolds **B** and **C**, respectively (Fig. 1). Both modifications have been extensively investigated over the last 15 years [31–33]. As generic implication, the substitution of classic donor sites E such as phosphines, amines, imines, or sulfides in ECE pincer ligands by NHCs greatly enhances the electron density of the metal center, since NHCs are by far the strongest donors in this series. However, the strong *trans* effect attributed to NHC ligands is obviously attenuated in a ligand design such as in **B**. In contrast, replacing the central carbanion with a NHC donor site enables the full exploitation of the *trans* labelizing properties of these ligands, e.g., for accelerated product release in a potential catalytic cycle. In this ligand setup **C**, the type of NHC plays a significant role for the stabilization of specific coordination geometries. Thus, when using a five-membered NHC as core, the E–M–E angle becomes more acute and may disfavor a meridional coordination mode of the ECE pincer ligand and instead induce facial bonding.

The incorporation of NHCs into pincer ligand scaffolds entails a number of attractive benefits. For example, NHCs are remarkably strong donors [34–37] and generally highly robust to oxidation and hydrolysis and thus tolerate air, moisture, and often even strongly acidic conditions [38, 39]. Moreover, NHCs can be readily functionalized and modulated and thus provide an excellent platform for fine-tuning metal properties [19–23]. Moreover, the rather covalent bonding of carbenes to metal centers increases the stability of the metal–ligand bond and renders ligand dissociation less likely. Considering the attractiveness of pincer ligands and of NHCs, it is not surprising that the combination of these concepts has attracted much interest and continues to do so. Early activities in pincer carbene chemistry have been compiled in a number of reviews [40–47]. Here, we overview accomplishments over the last 5 years and concentrate specifically on complexes of Group 8–10 metals. The chemistry of pincer carbene complexes with early transition metals is much less developed [48], though recent reports demonstrate the great potential of this area [49–53].

2 Iron, Cobalt, and Nickel Complexes with Pincer Carbene Ligands

2.1 General Considerations

The synthesis of pincer carbene complexes with Fe, Co, and Ni has been strongly influenced by the success of bis(imino)pyridine complexes in polymerization

Fig. 2 Most abundant
generic pincer carbene
ligands used for Fe, Co, and
Ni complexation
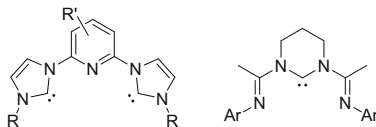
catalysis [54–56]. Accordingly variations include either the replacement of the imine arms with NHC donors thus providing CNC pincer complexes or the substitution of the central pyridine donor, thus leading to NCN pincer complexes (Fig. 2). The latter version requires the introduction of a six-membered NHC ligand in order to induce tridentate chelation [50, 56]. The majority of carbene pincer complexes contain however a CNC ligand motif. While Fe and Co pincer carbene complexes are relatively sparse, the chemistry of nickel pincer carbene complexes has developed considerably and a vast array of ligand designs has been reported, including chiral versions consisting of bicyclic imidazolylidenes [57, 58].

2.2   Pincer Carbene Iron Complexes

The primary strategy for complexation of the azolium salts with iron involves a basic metal precursor, such as $Fe[N(SiMe_3)_2]_2$, which engages in a simultaneous azolium deprotonation and $Fe–C_{carbene}$ bond formation process. Sometimes, a stepwise protocol has been applied, which includes initial deprotonation with a strong base such as KO*t*Bu and subsequently addition of the metal precursor salt. Accordingly, the iron(II) complexes **2a,b** have been synthesized from the pyridine-bridged bisimidazolium salt and $Fe[N(SiMe_3)_2]_2$ (Scheme 1) [59]. Reduction with amalgam gives quantitatively the corresponding iron(0) dinitrogen complexes **3a,b**. The carbene–carbon of complex **3b** appears at δ_C 204.6 ppm and the $\nu_{N\equiv N}$ absorption bands at 2,107 and 2,026 cm^{-1}. These stretch vibrations are 17–27 cm^{-1} lower in energy than in the corresponding NNN diimine analogue and indicate a more electron-rich iron center and more pronounced backbonding into the antibonding N_2 π^* orbital when the iron center is bound to NHC as opposed to an imine, consistent with the donor ability of these ligands. Rather unexpectedly analogous CO complexes, obtained after bubbling CO through a solution of **3a,b**, have revealed CO stretch vibrations up to 86 cm^{-1} higher in energy than those for an analogous PNP complex, indicating that the iron(0) center bound to a PNP pincer ligand (PNP = 2,6-bis(di-isopropyl-phosphinomethyl)-pyridine) is a stronger π base than iron(0) in a CNC pincer environment [60, 61]. DFT studies suggest a strong interaction between the $Fe–N_{pyr}$ bond and the antibonding orbitals of both Fe–CO bonds for the CNC complexes, but not for the PNP system. This orbital interaction results in delocalization of electron density to the pyridine and causes a reduction of the metal π-basicity to CO.

Under photolytic conditions, complex **3a** is a precursor for cyclometalation of benzylidene imines and induces selective $C(sp^2)$–H bond activation to yield
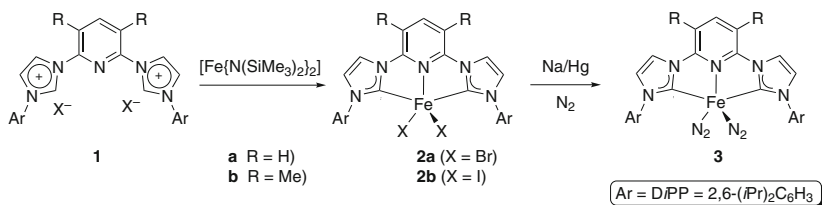
Scheme 1 Synthesis of iron(II) and iron(0) CNC pincer complexes
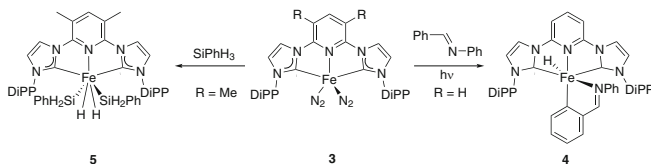
Scheme 2 Reactivity of CNC Fe(0) complexes with silanes and imines
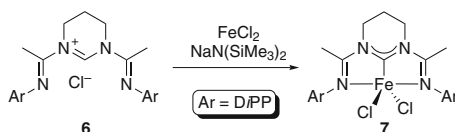
Scheme 3 Synthesis of the NCN pincer carbene complex **7**

complex **4** (Scheme 2). In the product, the hydride is in *cis* position to the activated phenyl group which is characteristic of oxidative C–H addition. Similar oxidative addition of silanes has been accomplished, affording the first example of an iron NHC complex with the iron in formal + IV oxidation state [62]. Notably, when Ph_2SiH_2 is used instead of $PhSiH_3$, the corresponding Fe(II) dihydrogen complex is formed rather than the dihydride Fe(IV) species.

Efforts towards replacing the central pyridine unit in bis(imino)pyridines with a five-membered NHC such as 2-imidazolylidene or 2-benzimidazolylidene have only resulted in complexes with a *C,N*-bidentate coordinating ligand [50, 56, 63, 64]. In contrast, metalation of ligand precursor **6** comprised of a six-membered NHC core affords the pincer complex **7** (Scheme 3) [56]. The complex is pentacoordinate and the Fe–C_{NHC} bond length is one of the shortest known thus far (1.812 Å). Electrochemical studies of the complex reveal four reversible redox events which are cathode-shifted in comparison to the bis(imino) pyridine analogue.

Based on the CNC coordination motif, Wärnmark and coworkers have developed homoleptic bis(tridentate) iron(II) complexes **9** for photophysical studies (Scheme 4) [65]. The NHC ligands efficiently prolong the ^{3}MLCT lifetime of iron(II) complexes to 9 ps which is almost twice as long as observed for [Fe (terpy)$_2$]$^{2+}$ (terpy = 2:2′,6′:2″-terpyridine). Complex **9b** with the *t*Bu wingtip

Scheme 4 Synthesis of homoleptic bis(tridentate) CNC pincer Fe complexes **9**
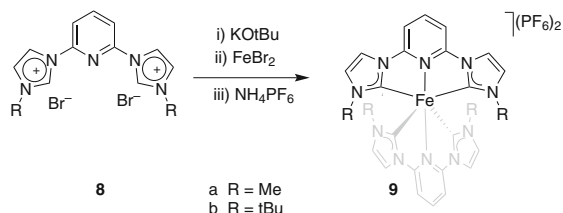
groups causes isotropic expansion of the coordination sphere relative to **9a**. Cyclic voltammetry indicates that the π* orbitals are much higher in energy in the NHC complex than in the terpy analogue.

The CNC pincer carbene complexes **3a** and analogues containing mesityl or xylyl substituents at the NHC (cf. Scheme 1, Ar = Mes, 2,6-Me$_2$C$_6$H$_3$) have been tested as catalysts for direct hydrogenation of a series of hindered tri- and tetra-substituted alkenes [54]. Remarkable activity has been noted towards a range of substrates at 5 mol% catalyst loading under 4 bar H$_2$. With *trans*-methylstilbene and 2-methyl-2-butene, the CNC pincer complexes show high activity and give >95% conversion within 1 h, while the analogous bis(imino)pyridine complexes are only poorly active. With larger substrates, the steric influence of the *N*-substituent becomes important. Complex **3a** with bulky D*i*PP substituents gives only low conversions, while smaller xylyl substituents induce full conversion of methyl cyclohexene after 1 h. With ethyl 3,3-dimethylacrylate as substrate, however, D*i*PP substituents provide better activity than xylyl or mesityl groups in complex **3**, most likely because the D*i*PP wingtip group shields the metal center and prevents oxygen coordination, hence revealing a subtle balance between metal shielding and poisoning substrate functionalities (such as carboxylate groups), yet providing sufficient space for bulky substrates to coordinate. Despite its similarity to the Gibson–Brookhart system, catalytic studies of the NCN pincer complex **7** have not been reported yet.

2.3 Pincer Carbene Cobalt Complexes

Only few examples of cobalt pincer carbene complexes have been reported thus far. The cobalt(I) CNC complex **10** has been synthesized from the corresponding CNC cobalt(II) dibromide complex and MeLi (Scheme 5) [66]. This complex eliminates methane under an atmosphere of H$_2$ (1 bar) and yields the corresponding hydride cobalt pincer complex **11** [55]. Deuterium studies suggest rapid deuteration at cobalt with the liberation of an 87:13 ratio of CH$_3$D and CH$_4$. Deuterium incorporation has also been observed, albeit less rapid, at the imidazolylidene carbon adjacent to the pyridine, at one of the isopropyl methyl groups, and, most notably, at the 4-position of pyridine, indicative of either fast hydride migration or intra- and intermolecular bond activation processes. When performing the reaction under N$_2$,

Scheme 5 Reactivity of pincer carbene cobalt complexes
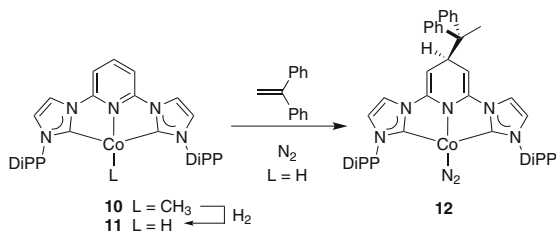
an IR absorption band at 2,048 cm^{-1} suggests N_2 coordination while two triplet signals at 3.57 and 4.31 ppm in the ^{1}H NMR spectrum point to the presence of allylic and vinylic protons due to hydride migration and dearomatization of the pyridine ring. When the hydride complex **11** is exposed to alkenes such as 1-butene, isobutene, or 1,1-diphenylethylene, formation of alkyl complexes has been detected by ^{1}H and ^{13}C NMR spectroscopy, although the low stability of such alkyl cobalt complexes precluded structural characterization of the products from 1-butene and isobutene. However, reaction of **11** with 1,1-diphenylethylene produces the stable complex **12** with a modified and dearomatized 1,4-dihydropyridine. The cooperativity of the metal and ligand in this formal insertion process may facilitate a radical process. Computation work further predicts that the bis(carbene)pyridine ligand is redox active and undergoes a formal one-electron reduction.

The methyl complex **10** is a highly active precatalyst for the hydrogenation of hindered tri- and tetra-substituted alkenes, such as *trans*-methylstilbene and 2,3-dimethyl-2-butene [55]. Activities are comparable to those of **3a** with less reaction time required to reach the same or higher conversion, and conditions are comparably mild (4 bar H_2, 22°C).

2.4 Synthesis of Pincer Carbene Nickel Complexes

In contrast to iron and cobalt, nickel pincer carbene work has developed at a far more rapid pace. Since the first pincer nickel(II) complex was reported by Inamoto and coworkers [67], a variety of coordination motifs have been investigated including CEC, ECE, and CEE ligand systems (E = C-, N-, O-, or P-donor). A recent review has covered some of the work on ECE Ni pincer complexes [68].

Metal–carbene bond formation has been achieved by a number of methods, providing a large synthetic flexibility. The most frequently applied procedures include transmetalation from a silver carbene intermediate and deprotonation with a base followed by addition of the metal precursor. Two representative examples are shown in Scheme 6. In addition, C–H bond activation with Ni (OAc)$_2$ [69] and, owing to the availability of a stable low-valent precursor, oxidative addition with [Ni(cod)$_2$] have also been employed [70]. Another interesting method is comprised of direct metalation of pincer carbene precursors with Raney nickel which affords the chelate complexes in excellent yields [71]. For example,
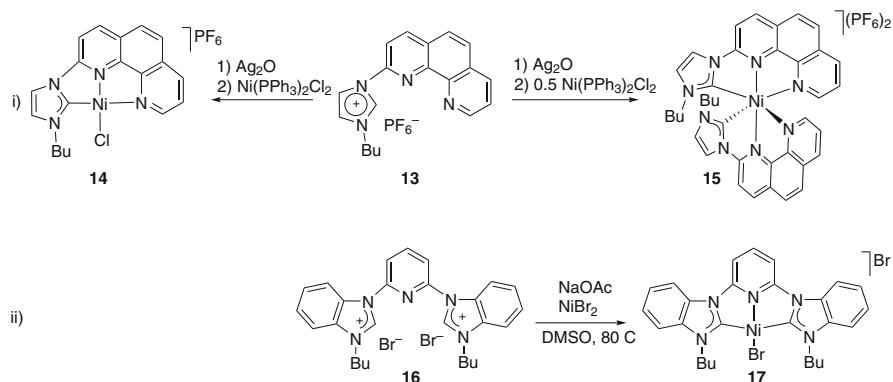
Scheme 6 Representative preparation of pincer carbene nickel complexes
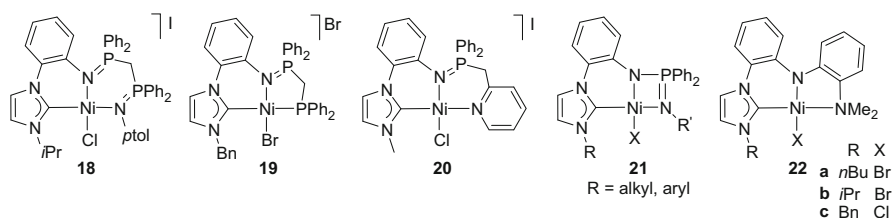
Fig. 3 CEE pincer carbene nickel complexes

Chen and coworkers synthesized the phenanthroline-functionalized 2-imidazolylidene nickel complexes **14** and **15** via a transmetalation procedure in 37% and 60% yield, respectively (Scheme 6) [72]. When utilizing Raney nickel, the yield of complex **15** raised to 93% [71]. Moreover, the latter method is highly tolerant to many functional groups.

2.4.1 CEE Pincer Complexes

A series of CEE pincer carbene nickel complexes **18–22** with a wide variety of donor ligands have been prepared by sequential deprotonation of the imidazolium salt with nBuLi and subsequent addition of the nickel precursor salt [NiCl$_2$(dme)] or [NiBr$_2$(dme)] (dme = dimethoxyethane, Fig. 3) [73–75]. An unusual protocol towards a CEE pincer carbene complex comprising a carbene, an aryl anion, and a phosphine donor setting has been reported by Zargarian and Chauvin. Starting from complex **23** comprising a NHC-stabilized phosphenium donor, extrusion of the Ph$_2$P$^+$ moiety has been achieved with Et$_4$NCl to yield the NHC pincer system **24** (Scheme 7) [76].

Scheme 7 Extrusion of Ph_2P^+ to give NHC complex **24**
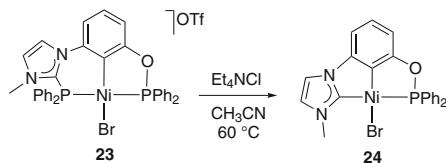
Scheme 8 Ethylene insertion into PCP nickel complex
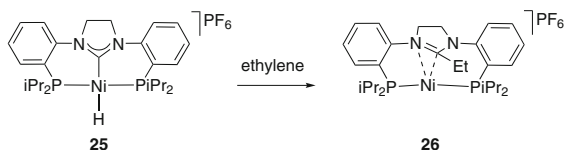
2.4.2 ECE Pincer Complexes

The PCP pincer carbene nickel complex **25**, formed by oxidative addition of the ligand precursor to $[Ni(cod)_2]$, reveals a unique reactivity pattern [70, 77]. Under an ethylene atmosphere, the yellow hydride is converted to the orange ethylimidazolinium species **26** arising from reductive C_{Et}–C_{NHC} and C_{Et}–H bond formation (Scheme 8). Mechanistic investigations using deuterium labeling experiments have unveiled H/D isotope scrambling due to repetitive β-H elimination, alkene rotation, and reinsertion steps. DFT calculations suggest that ethylene insertion into the Ni–H bond is significantly more favored than insertion into the C_{NHC}–Ni bond. The subsequent C–C bond forming reaction would be unfavored from the *trans* configuration, and rearrangement to an apical agostic ethyl complex has been calculated as a favorable pathway, which positions the ethyl group *cis* to the NHC ligand and which is induced by the steric congestion imparted by the phosphorus-bound iPr groups.

Arduengo and Runyon have developed an OCO pincer carbene ligand through alkylation of various N-heterocycles including imidazole, benzimidazole, and 1,2,3- and 1,2,4-triazole by ring opening of hexafluoroepoxide [78]. Deprotonation with KOtBu and subsequent metalation with $[NiCl_2(PPh_3)_2]$ yield a mixture of monocarbene complex **27a** and a bis-carbene species **27b** with one carbene featuring alcohol rather than alkoxide wingtip groups and hence a monodentate bonding mode (Fig. 4). Cavell has prepared a related NCN pincer carbene nickel complex **28** by oxidative addition to a chiral bicyclic trihydro-pyrimidine precursor, thus affording a 6-membered N-heterocyclic carbene [57].

2.4.3 CEC Pincer Complexes

Nickel complexes featuring a C_2-symmetric CNC pincer ligand with carbene arms are generally prepared by transmetalation from a silver carbene intermediate or by acetate-assisted C–Ni bond formation using $Ni(OAc)_2$ or a nickel(II) precursor in the presence of NaOAc (Fig. 5) [69]. Kemp and coworkers have observed an

27a L = PPh$_3$
b L = NHC

28
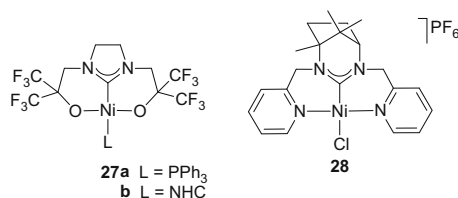
Fig. 4 OCO and NCN pincer carbene nickel complexes

X = anion
R = alkyl/aryl
n = 0 or 1

	NHC	n	R	X/X'
29a	imid	0	Mes	Cl/BF$_4$
29b	imid	0	DiPP	Cl/BF$_4$
29c	imid	0	Me	Br/Br
30a	imid	1	Mes	Cl/BF$_4$
30b	imid	1	DiPP	Cl/BF$_4$
31a	benzimid	0	Bu	Br/PF$_6$
31b	benzimid	0	Bu	Cl/PF$_6$

32

33
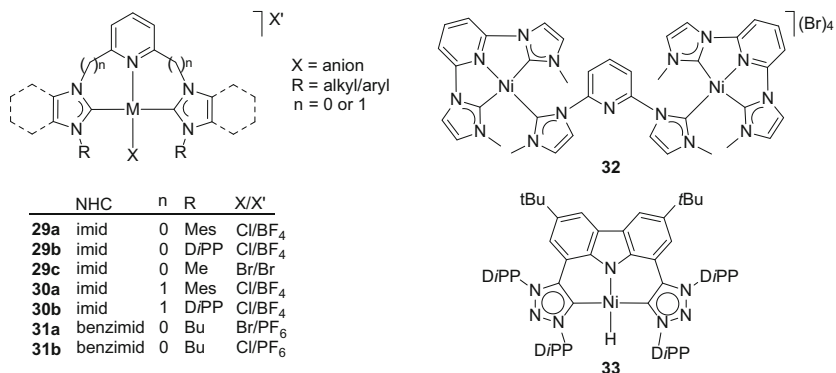
Fig. 5 CNC pincer carbene nickel complexes

unusual "reverse" Ni-to-Ag transmetalation when attempting to abstract the halides of complex **29c** with AgNO$_3$, indicating that the metal–carbene bond can be labile [79]. Reaction conditions in the nickelation step are delicate as illustrated by the isolation of a bimetallic system **32** comprised of two nickel CNC moieties that are bridged by a third CNC ligand when the nickelation is performed with Ni(OAc)$_2$ in the presence of Bu$_4$NBr (Fig. 5) [80]. Bertrand and coworkers have reported CNC pincer carbene nickel complex **33** based on 1,2,3-triazolylidenes, providing a first example of mesoionic carbene pincer system coordinating to nickel [81]. Despite the strong donor properties of the mesoionic carbenes and the anionic N-donor, the nickel hydride species has been successfully stabilized.

While pincer ligands with directly linked heterocycles produce coplanar metallacycles (cf. **29**), the CH$_2$-bridged heterocycles in **30** induce puckering and a twist of the central pyridine up to 47° out of the nickel square plane [82]. Space-filling models indicate that the nickel center is considerably more shielded when bound to the puckered CNC pincer ligand than in the planar system. When benzimidazolium-derived CNC ligand precursors are reacted with Ni(OAc)$_2$, pentacoordinate bis(halide) complexes are initially formed [83, 84]. One of the halides is readily exchanged with PF$_6^-$ to give the cationic square-planar complexes **31b** and **31c**.

A unique type of CCC pincer carbene nickel complex **35** has been synthesized from the alkyne-bridged bisimidazolium salt **34** via chloronickelation (Scheme 9) [85]. Presumably, the reaction sequence involves first the formation of one of the

Scheme 9
Chloronickelation of **34** to
give CCC pincer nickel
complex **35**

$$34 \qquad \begin{array}{l} \text{a } \text{Ar} = \text{Ph} \\ \text{b } \text{Ar} = \text{Mes} \end{array} \qquad 35$$
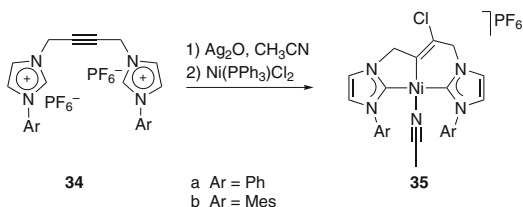
Ni–C$_{\text{NHC}}$ bonds by transmetalation from silver followed by coordination of the alkyne to nickel. Chloride nucleophilic addition on the activated alkyne may then take place to induce the second NHC transmetalation and tridentate chelation of the ligand.

2.5 Application of Pincer Carbene Nickel Complexes in Synthesis and Catalysis

Chen and coworkers have observed that the Ni–C bonds in complex **15** are labile despite the tridentate coordination mode of the ligand. By exploiting this reactivity, these complexes have been successfully used as carbene transfer agents to other metals including Pd, Pt, Ru, Co, and even different nickel centers [71]. This transmetalation procedure provides an alternative to the well-developed transmetalation of silver carbene systems and has demonstrated its efficacy for a vast array of mono- and polydentate ligand structures.

Catalysis is the most predominant application of pincer carbene nickel complexes, in particular C–C bond forming reactions involving the arylation of aryl halides with Grignard reagents (Kumada–Corriu-type), with aryl zinc species (Negishi-type), and with boronic acids and derivatives (Suzuki–Miyaura-type cross coupling) in an attempt to replace more precious palladium catalysts.

2.5.1 Kumada–Corriu Cross Coupling

The CNC pincer complexes **14** and **15** (cf. Scheme 6) efficiently catalyze the coupling of tolyl Grignards with various functionalized aryl chlorides [72]. The activity of the two complexes at 2 mol% loading is very similar, suggesting they lead to the same active species due presumably to dissociation of at least one of the pincer ligands in **15**. This reactivity pattern is surprising when considering the generally robust bonding mode of pincer ligands, yet it is in agreement with the ligand transfer activity developed for this type of complexes in transmetalation reactions (see above). Poor activities are observed however with deactivated substrates such as *p*-chloroanisole, giving less than 20% product within 24 h. Complexes **35a/b** featuring a CCC pincer ligand are more efficient and can be used at 0.5 mol% catalyst loading [85]. For example, the coupling of *p*-chloroanisole with

(*p*-tolyl)MgBr for 12 h affords up to 59% isolated yield of the diaryl product. This complex also catalyzes the coupling of bulky and heteroaryl chlorides in good to excellent isolated yields.

Likewise the CNN nickel complexes **22a–c** show high catalytic activity at 2 mol % catalyst loading (cf. Fig. 3) [73]. The carbene substituent has a distinct impact on the catalytic activity, and an *i*Pr group as in **22b** induces higher activity than *n*Bu or Bn substituents. This complex has been successfully used to prepare bi- and tri-aryl products. The CNN bonding mode has been suggested to be better for such cross-coupling catalysis than the CNP motif, since complex **19** affords only 51% yield upon arylation of *p*-tolyl chloride. The CNN pincer nickel complexes **18** and **20** give 70–80% conversion under similar conditions, albeit with different carbene substituents [75]. Along similar lines, the CNN pincer nickel complex **21** (R = Bn, R′ = *p*-tolyl, X = Br) efficiently catalyzes the arylation of activated and unactivated aryl chlorides and fluorides with aryl Grignard reagents with typical catalyst loading of 1 mol% [74]. The pentacoordinate dichloride precursor of complex **21** and its dibromide analogue are less active and produce only moderate yields of the cross-coupled products, and instead significant homocoupling has been noted [83, 84].

2.5.2 Negishi Cross Coupling

Complexes **18–20** also catalyze the Negishi coupling of aryl zinc reagents with aryl chlorides [75]. While the reaction proceeds sluggishly at room temperature, good conversions are achieved at 70°C with catalyst loadings as low as 0.05 mol%. When using the coupling of *p*-chloroanisole with (*p*-tolyl)ZnCl as a benchmark reaction, again the CNN pincer complexes are more efficient than the CNP analogue **19**, and complex **18** outperforms **20**.

2.5.3 Suzuki–Miyaura Cross Coupling

CNC pincer nickel complexes such as complexes **29** and **30** have been studied extensively in Suzuki–Miyaura cross coupling of phenylboronic acid with various aryl chlorides and bromides [82]. At 1 mol% of catalyst loading and elevated temperatures, complexes **29** comprised of 5-membered metalacycles and a planar ligand geometry are more efficient in the arylation of ArCl and ArBr substrates, while complexes **30** with 6-membered metalacycles and a puckered pincer ligand conformation are active for aryl tosylates and mesylates, suggesting a different rate-determining step in the catalytic cycles [86]. However, electron-rich or sterically hindered substrates give only poor yields of coupled products for both tosylates and mesylates. Notably, the catalytic procedure does not require any additive to accomplish good yields of coupled products.

The benzimidazolylidene complex **17** leads to similarly high catalytic activity and promotes the arylation of various functionalized (hetero)aryl bromides,

chlorides, tosylates, and mesylates at 2 mol% catalyst loading [69]. Addition of PPh$_3$ (10–20 mol%) is advantageous and efficiently suppresses homocoupling reactions that have been observed in the absence of phosphine. While yields for the coupled products are generally high (>90%), steric shielding of the Ar–X bond by *ortho* substituents leads to much lower yields. Moreover, complex **17** has been applied to catalyze the coupling of anthracen-9-yl esters and (hetero)arylboronic acids for the synthesis of fluorescent materials [87]. With only 0.5 mol% catalyst loading and 2 mol% PCy$_3$ as an additive, up to 96% product has been obtained via C–COOR bond activation. The related complex **29c** with imidazolylidene rather than benzimidazolylidene donors is slightly less active (83% yield). Interestingly, commercial [NiCl$_2$(PCy$_3$)$_2$] also catalyzes the reaction under the same conditions and with similarly high 93% yields [88]. Aliphatic esters give slightly inferior yields (71–86%), and sterically hindered substrates are converted poorly, e.g., mesitylcarboxylates give less than 35% product. This limitation can be overcome by increasing the catalyst loading to 5 mol% and that of PCy$_3$ to 20 mol%. Various (hetero)-arylboronic acids are converted well, except for those with strongly coordinating sites such as pyridylboronic acid.

3 Ruthenium and Osmium Complexes with Pincer Carbene Ligands

3.1 General Considerations

As with Fe, Co, and Ni, the dominant pincer carbene ligand system for Ru and Os is based on 2,6-bis(NHC)pyridine. While pincer carbene osmium complexes have not been investigated widely, the ruthenium analogues have been much more advanced and an array of different NHC systems have been incorporated including 2-(benz) imidazolylidenes and 1,2,4- and 1,2,3-triazolylidenes. A second predominant ligand system is based on appending NHC donors to privileged bidentate ligands such as bipyridine and phenanthroline. The N-donors incorporated into pincer carbene ruthenium complexes are almost exclusively sp^2-hybridized and aromatic.

   Metalation has been achieved predominantly via reductive C–H bond activation of the azolium salt with a metal halide salt such as RuCl$_3$ or [OsCl$_4$(bpy)] at high temperatures (140–190°C), sometimes with NaOAc as additive. Metal hydride precursors have also been used for Os and Ru complexation, while transmetalation from a silver carbene intermediate and base-assisted deprotonation have been applied for ruthenation only (see Scheme 10 for representative examples) [89].
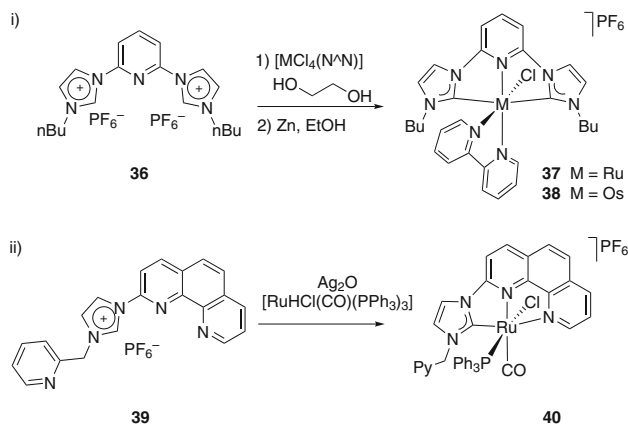
Scheme 10 Representative synthesis of CNC pincer Ru(II) and Os(II) complexes

3.2 CEC Pincer Ruthenium Complexes

The CNC motif is by far the most popular pincer ligand system with carbene ruthenium complexes. Modification of this general ligand includes the introduction of a methylene bridge between the NHC arms and the central pyridine unit and the introduction of functional groups in *para* position of the pyridine site, e.g., in pyrazines or by a carboxylate as pH-responsive group.

While the direct linkage of the NHC and the pyridine ligand as in **37** induce significant distortion of octahedral coordination geometries, addition of a methylene bridge accommodates octahedral ruthenium centers almost ideally (C–Ru–C bond angle ca. 173°) [90]. When compared to terpy as tridentate ligand, CNC pincer systems enhance the electron density at the ruthenium as demonstrated by the cathodic shift of the Ru^{II}/Ru^{III} oxidation potential. Despite their nearly ideal octahedral geometry and the anticipated increase of the ligand field splitting, homoleptic ruthenium complexes containing two methylene-bridged CNC pincer ligands are nonluminescent at room temperature [90, 91], presumably because the non-emissive and strongly antibonding ^{3}MC state is populated upon excitation. The stronger ligand field associated with less distortion from octahedral geometry is thus counterbalanced by the four carbene donors, which increase the ^{3}MLCT level. At 77 K, emission is observed with a lifetime of just 4 ns. Analogous heteroleptic [Ru(CNC)(terpy)]$^{2+}$ complexes are luminescent at room temperature [90], since the CNC ligand increases the energy of the ^{3}MC state while the terpy provides low-lying π* orbitals.

Another methylene-bridged CNC bis-imidazolylidene complex with larger alkyl N-wingtip substituents on the NHC nitrogen induces a facial coordination mode in ruthenium complexes **41a–c** (Fig. 6) [92]. Deprotonation of a benzylic proton with KO*t*Bu leads to pyridine dearomatization (see below).
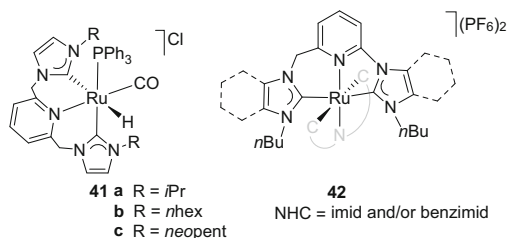
Fig. 6 Facial rather than meridional coordination of CNC pincer ligands in complex **41** and nonsymmetric CNC pincer ligands in complex **42**
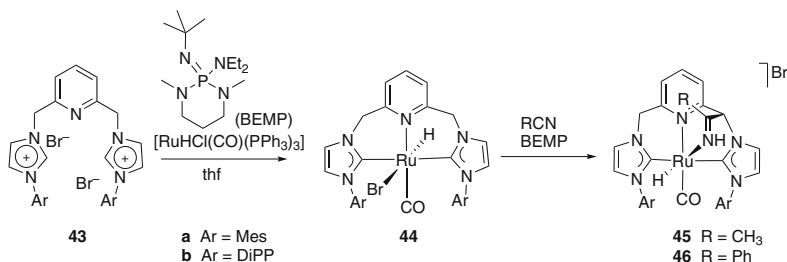
Scheme 11 Nitrile activation at a Ru(CNC) pincer carbene complex

Nonsymmetric CNC′ ligands containing a methylene linker only towards one of the NHC donors (2-imidazolylidene or 2-benzimidazolylidene) give rise to an acute bite angle (ca. 78°) and a second bite angle that is close to ideal for octahedral/square-planar geometries (ca. 90°) [93]. Such homoleptic [Ru(CNC′)$_2$]$^{2+}$ complexes **42** are luminescent at room temperature with a greater red shift of the ^{3}MLCT emission band if the methylene-bridged NHC is a 2-imidazolylidene rather than a benzimidazolylidene donor, irrespective of the nature of the directly linked NHC. DFT calculations confirm a larger ^{3}MLCT energy gap for the latter ligand configuration. All complexes have bi-exponential solid-state lifetimes in the microsecond range.

Similar methylene-bridged CNC pincer ligands have been coordinated to a neutral ruthenium(II) core by metalation of **43** with [RuHCl(CO)(PPh$_3$)$_3$] (Scheme 11) [94]. The bulky base BEMP together with LiBr is essential for successful metalation and formation of complexes **44**, while a C4-bound imidazolylidene complex is obtained in the absence of LiBr. Performing the metalation in MeCN affords complex **45**, presumably via base-assisted pyridine dearomatization and nucleophilic addition of the benzylic position to the nitrile group. Similarly, addition of PhCN to **44** in the presence of BEMP yields the corresponding adduct **46**. Notably, the nitrile is released again upon reaction of complex **45** with KO*t*Bu, which generates a dearomatized complex with an exocyclic double bond.

A variety of CNC pincer carbene ligands has been investigated with NHC donors directly linked to the pyridine center. Spectroscopic and time-dependent DFT studies on the CNC pincer carbene ruthenium complex **37** reveal a HOMO–
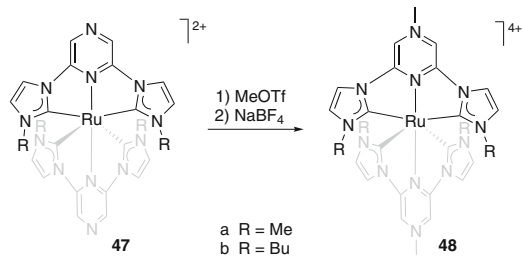
Scheme 12 Pyrazine-centered complexes **47** and **48**
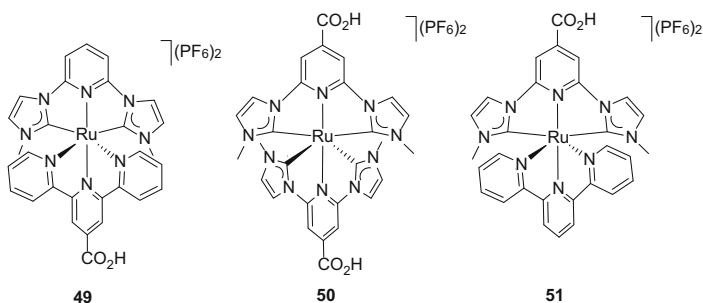
Fig. 7 Carboxylate-functionalized pincer carbene ruthenium complexes

LUMO gap that is constituted by a $d_\pi(Ru^{II}) \rightarrow \pi^*(bpy)$ MLCT [95]. In contrast, the lowest energy transition of the analogue containing a terpy instead of the CNC pincer ligand is a charge transfer to the terpy π^* molecular orbital.

The homoleptic bis(CNC) pincer ruthenium complexes **47** containing a central pyrazine unit (Scheme 12) [96] reveal red-shifted ^{1}MLCT bands in the absorption spectra when compared to analogues with a central pyridine ring [97]. Similarly, the enhanced electron-withdrawing character of pyrazine moves the $Ru^{II/III}$ oxidation by 140 mV to higher potential, consistent with a better π-acceptor character. Complexes **47** are emissive (^{3}MLCT-based luminescence) at room temperature. Reversible protonation of the pyrazine with $HClO_4$ leads to a further bathochromic shift of the absorption bands due likely to a lowering of the π^* LUMO energy upon protonation and hence a decreased HOMO–LUMO gap. Similar effects are observed when the pyrazine is methylated rather than protonated, as in complexes **48**. Proton abstraction with NEt_3 restores the absorption properties of complex **47**. Related proton-sensitive homo- and heteroleptic complexes with pH-dependent absorption and luminescence properties have been prepared by incorporating a pendant pyridine on the CNC or terpy ligand backbone [98].

The homo- and heteroleptic dicarbene ruthenium complexes **49–51** contain a pH-sensitive and electron-withdrawing carboxylic acid group (Fig. 7), which lowers the LUMO energy, while the strong σ-electron-donating NHC ligands increases the HOMO of the metal center when compared to bis(terpy) analogues

Fig. 8 Heteroleptic [Ru(CNC)(terpy)]$^{2+}$ complexes containing triazolylidene-based carbene pincer ligands

	R	R'
a	CH$_3$	H
b	CH$_3$	CO$_2$Me
c	CH$_3$	2-furyl
d	Br	2-furyl
e	PO(OH)$_2$	COOH
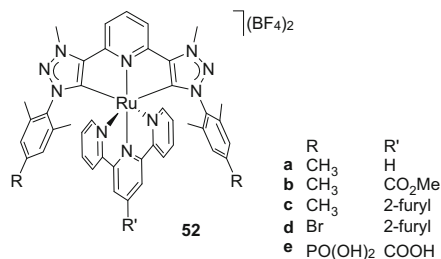
[99]. The net decrease of the HOMO–LUMO gap imparts a red shift of the absorption band, which is larger when two acid functionalities are present (**50**) rather than just one (**49**, **51**).

Complex **52a** has been prepared by a transmetalation involving a silver carbene intermediate and is a variation that features 1,2,3-triazolylidenes [27, 100] rather than imidazolylidenes as NHC ligands (Fig. 8) [101]. The strongly σ-donating and moderately π-accepting properties of triazolylidenes destabilize the ^{3}MC states and thus disfavor radiationless decays which compromise the excited-state lifetimes. The absorption spectrum shows only a minor blue shift in comparison to [Ru(terpy)$_2$](PF$_6$)$_2$, while the emission spectrum reveals an intense and unstructured red emission with quantum yields of 4.4% in deaerated MeCN. The excited-state lifetime is 633 ns and thus 2,500 times longer than that of [Ru(terpy)$_2$](PF$_6$)$_2$ and comparative with [(Ru(bpy)$_3$](PF$_6$)$_2$ (860 ns). As a bis(tridentate), heteroleptic system, this complex is rigid and isomer-free, an advantage over [Ru(bpy)$_3$]-derived systems. Fine-tuning of the ^{3}MLCT–^{3}MC separation and the HOMO–LUMO gap has been achieved by introducing electron-donating and withdrawing groups on the ligand scaffold [102]. According to electrochemical and computational studies, the incorporation of an electron-donating 2-furyl group in **52c** increases the π* orbital of the terpy ligand so much that the LUMO is shifted onto the CNC carbene ligand. Similarly, incorporation of an electron-withdrawing bromide on the carbene ligand (**52d**) lowers the HOMO, resulting in the longest excited-state lifetime (7.9 μs) observed thus far for mononuclear ruthenium complexes. Functionalization of the terpy backbone and the CNC pincer ligand at the wingtip groups with carboxylate and phosphonate anchoring groups, respectively, as in **52e** prompts the anchoring of the photosensitizer complex onto TiO$_2$ [103]. The tripodal anchoring is highly robust in aqueous media, maintains the beneficial photochemical properties, and allows efficient charge injection to the semiconductor. Power conversion efficiencies (PCE) have been measured, though they are rather low (<1%).

Phenyl-bridged bis-imidazolylidene complexes **54** featuring a CCC-tridentate pincer ligand motif have been synthesized from [Ru(cod)Cl$_2$]$_n$ at high temperatures in ethylene glycol (Scheme 13) [104]. The CO ligands originate from alcohol oxidation and decarbonylation during the reaction. The ancillary ligands have been substituted with bidentate N-donors such as bpy and 2-aminopyridine to give cationic complexes [Ru(CCC)(N^N)CO]$^+$ [104] or with derivatives of terpy to yield [Ru(CCC)(terpy)]$^+$ complexes [105]. While the absorption spectra show

Scheme 13 Synthesis of CCC pincer carbene ruthenium complexes

Fig. 9 Ruthenium CNN pincer complexes with benzylic and NH groups for deprotonation

MLCT transitions in the visible region, these complexes are poorly or non-emissive in solution at room temperature.

3.3 CEE and ECE Pincer Ruthenium Complexes

3.3.1 CEE Pincer Complexes

A series of CEE Ru complexes have been synthesized with various aromatic and aliphatic nitrogen donors (Fig. 9). The formation of complex **55** from the imidazole ligand and $RuCl_2(PPh_3)_2$ involves a chelate-assisted formal tautomerization [106] as the C2-bound proton migrates to N_{imi} [107]. An equimolar amount of base leads to reversible deprotonation of the pyrazole and forms a neutral pyrazolato complex. However, with 2 equiv. of base, a Ru–H species is formed in the presence of H_2 or 2-propanol. Presumably abstraction of the imidazolylidene N-*H* affords a reactive intermediate comprised of a Lewis acidic metal center and a basic imidazolyl group, which cooperatively facilitate the heterolytic cleavage of H_2 and the dehydrogenation of 2-propanol. Complex **56**, synthesized by reductive metalation, eliminates HI in the presence of K_2CO_3 and is thus transformed into the corresponding pyrazolato

complex [108]. This base-sensitive ligand platform is therefore predisposed for base-assisted catalytic procedures and may entail metal–ligand cooperation.

Milstein has developed the carbene-containing CNN pincer ruthenium complex **57** [109], which is an analogue of the catalytically highly active PNN system [110]. The complex is formed by sequential deprotonation of the azolium salt with a strong base and addition of RuH(Cl)CO(PPh$_3$)$_3$. The NHC ring in **57** is tilted out of the bpy plane as a consequence of the flexibility imparted by the methylene linker. The low CO stretch vibration ($\nu_{CO} = 1,932$ cm^{-1}) indicates considerable metal-to-ligand backbonding. Similar to the PNN system, deprotonation of the methylene linker with KHMDS yields a dearomatized complex with an exocyclic double bond [13]. This complex displays exceptional catalytic activity in the hydrogenation of esters to alcohols under mild conditions. A variation with larger steric flexibility includes complexes **58** [111], which undergo similar KHMDS-mediated dearomatization. Notably, deprotonation occurs exclusively at the NHC side of the pincer ligand, in agreement with the electron-withdrawing nature of the NHC. Complex **58b** requires the presence of PPh$_3$ to cleanly eliminate HBr, possibly to prevent aggregation. Similarly to Milstein's PNN system complex, the dearomatized versions of complexes **57** and **58** react with H$_2$ to yield a dihydride complex from hydrogen addition at the benzylic site and the metal center, thus re-aromatizing the pyridine ring. The dihydride complex is not stable and slowly loses H$_2$ and reverts to the dearomatized complex. Deuterium studies indicate isotope exchange at both benzylic positions of complex **58a**, suggesting that both pincer arms participate in reversible bond activation. A similar complex with a modified amine donor, viz., complex **59**, has been heterogenized on MCM-41, a mesoporous silica support [112, 113].

Complexes **60** and **61** contain a related CNN pincer ligand with a mesoionic 1,2,3-triazolylidene donor and have been synthesized from the corresponding triazolide complexes by *N*-alkylation after metalation (Fig. 10) [114]. Saponification of the ester groups on the terpy backbone affords **61b** with carboxylic acid functionalities for anchoring onto TiO$_2$. The incorporation of ester groups stabilizes the terpy-based π* orbitals and hence induces a shift of the MLCT bands to longer wavelengths. These complexes are emissive with excited-state lifetimes of 45, 133, and 117 ns, respectively, which are two orders of magnitude longer than the lifetime of the parent complex [Ru(terpy)$_2$](PF$_6$)$_2$. The significant influence of the carbene on the HOMO is obvious. The effect of the electron-withdrawing groups on the terpy backbone has been attributed to an increased ^{3}MLCT–^{3}MC gap entailed by the stabilization of the ^{3}MLCT state. The triazolide precursor has a 50% shorter excited-state lifetime, though protonation and formation of a protic triazolylidene impart characteristics similar to the alkylated triazolylidene complexes.

In contrast to CEE pincer complexes, only very few examples of ruthenium pincer complexes are known that contain a carbene donor in the center. Complex **62** features a NCN pincer carbene ligand [115], while complex **63** contains a NCO donor set (Fig. 11) [116]. Tridentate coordination of the latter has been concluded from the decreased CO vibration ($\nu_{CO} = 1,621$ vs. 1,693 cm^{-1} in the ligand precursor) and from X-ray diffraction. Notably the NCO ligand adopts a facial

Fig. 10 Ruthenium (II) complexes with a planar triazolylidene-derived CNN pincer ligand
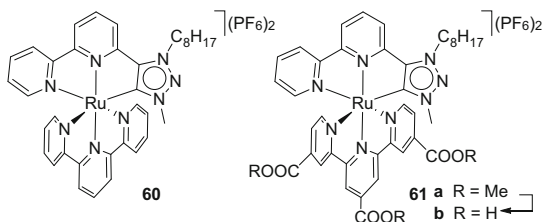
Fig. 11 Ruthenium complexes with an ECE pincer motif
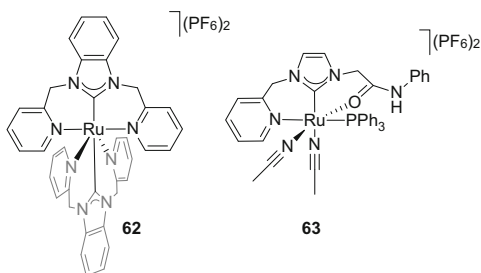
Fig. 12 Osmium complexes containing CNC and CCC pincer carbene ligands
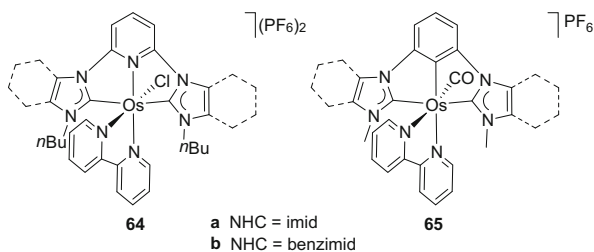
coordination mode, presumably due to unfavorable steric interactions between the *N*-bound phenyl group and the PPh₃ ligand. Ligand analogues with a secondary rather than a primary amide functionality only coordinate in a *C,N*-bidentate mode.

3.4　Pincer Carbene Osmium Complexes

Osmium has received considerably less attention than ruthenium in pincer carbene chemistry. (Benz)imidazolium-derived carbene complexes **64** have been synthesized from the corresponding azolium salts via C–H bond activation with [OsCl₄(bpy)] in ethylene glycol followed by reduction with Na₂S₂O₄ (Fig. 12) [117]. Spectroscopic and computational data indicate a low-energy absorption with predominant $d_\pi(Os^{II}) \rightarrow \pi^*$(diimine) MLCT character. In contrast to their ruthenium counterparts [95], these osmium complexes are non-emissive.
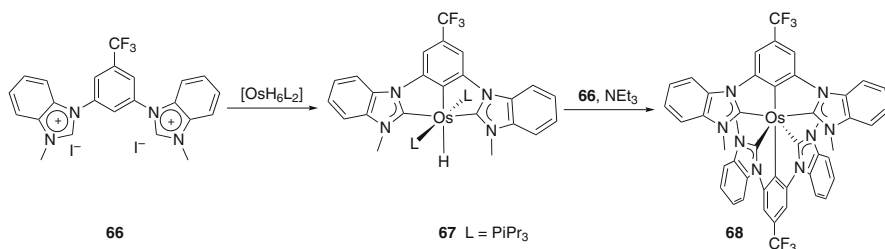
Scheme 14 Synthesis of mono- and bis(CCC) pincer osmium complexes via CH activation

Photoactivity is imparted however upon replacing the central pyridine with a phenyl group. For example, complexes **65**, obtained by a similar procedure as **64**, are red emitters [118]. The CO ligand originates from ethylene glycol oxidation and provides a sensitive probe that indicates stronger donation of the imidazolylidenes than of benzimidazolylidenes, $\nu_{CO} = 1{,}908(\pm 2)$ cm^{-1} vs. $1{,}926(\pm 2)$ cm^{-1}. Notably, little effects have been noted from changing the diimine ligand. Long excited-state lifetimes up to 6.1 μs have been measured for a pincer osmium complex with benzimidazolylidene donors and a phenanthroline spectator ligand.

Esteruelas and coworkers have developed an alternative method towards CCC-tridentate pincer osmium(II) complexes consisting of C–H bond activation of the azolium ligand precursor **66** with the polyhydride precursor [OsH$_6$(PiPr$_3$)$_2$] (Scheme 14) [119]. The intermediate osmium(IV) dihydride is reduced with KO*t*Bu to give the corresponding osmium(II) monohydride complex, e.g., **67**. Interestingly, only azolium iodides induce pincer-type ligand coordination, while analogous BF$_4$ salts result in bidentate coordination only due to C$_{phenyl}$–H bond activation in the *ortho,para* position, a reaction trajectory that is well established for pincer ligands [120]. Complex **67** reacts with another equivalent of ligand precursor to afford the homoleptic bis(pincer) complex **68**. The stepwise synthesis also enables the assembly of two different pincer ligands at one osmium center. Both the homo- and heteroleptic complexes are turquois emitters in the solid state. Excited-state lifetimes are in the range of 10–29 μs while quantum yields reach up to 62%. These complexes have been used for device fabrication, affording record-high electroluminescence efficiency for blue emissive osmium complexes, competitive to state-of-the-art iridium-based devices [121–123].

3.5 Application in (De)Hydrogenation Catalysis

3.5.1 Transfer Hydrogenation

Many ruthenium complexes such as complex **56** are active precursors for the catalytic hydrogen transfer from *i*PrOH to aliphatic and aromatic ketones and aldehydes in the presence of a base such as KOH or KO*t*Bu [104, 108, 124]. At
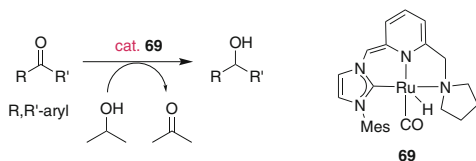
0.01 mol% catalyst loading, TOFs reach up to 3,300 h^{-1} and yields exceed 90% [104]. Post-catalytic analysis of complex **56** suggests that the CCC pincer ligand and the two CO ligands remain intact. In agreement with a robust catalyst, the same batch of complex **56** (1 mol%) has yielded >97% conversion over seven repetitive runs. While these CCC pincer carbene ruthenium complexes compare well with the most active NHC-based complexes in transfer hydrogenation, they do not reach the activity of ruthenium complexes with amine or phosphine donors [125]. The CNN pincer complex **69** with an exocyclic alkene in the pincer ligand displays interesting selectivity as aliphatic aldehydes and ketones are converted well, but not aromatic carbonyl groups (Scheme 15) [113].

3.5.2 Direct Hydrogenation

The CNN pincer ruthenium complexes **57–59**, which undergo reversible dearomatization, catalyze the hydrogenation of typically difficult substrates such as esters and amides [94, 109, 111–113, 126]. Complex **57** hydrogenates nonactivated esters to the corresponding alcohols under relatively mild conditions (5.2 bar H$_2$, 135°C) [109]. Almost quantitative yields are obtained after 2 h with 1 mol% catalyst loading. Decreasing the catalyst loading to 0.025 mol% and increasing the H$_2$ pressure to 50 bar produces almost 3,000 tons. This complex is also suitable for the hydrogenation of biomass-derived glycolide to ethylene glycol, though activity is lower than with an analogous PNN pincer ruthenium complex [126]. Complex **58** hydrogenates aromatic and aliphatic esters including bulky substrates such as *t*BuOAc in better yields (93% after 2 h) than the PNN analogue (11% after 24 h) [127]. Complexes **44–46** are active at lower loadings (0.1–0.5 mol %) for the hydrogenation of a range of aromatic and aliphatic esters under more mild conditions (50 bar H$_2$, 70–100°C) in the presence of a catalytic amount of base [94]. Imines are also hydrogenated at 0.1 mol% catalyst loading using the facially coordinating CCC pincer ruthenium complex **41** [92]. Complex **59** catalyzes the hydrogenation of prochiral alkenes under mild conditions (4 bar H$_2$, 40°C) [112]. When heterogenized on MCM-41, the catalyst shows higher activity than the homogeneous counterpart (TOF up to 1,400 h^{-1}, ee up to 99% with benzylidene succinate). Exchange of the carbene *N*-substituent from Mes to D*i*PP causes a considerable drop of activity.

3.5.3 Alcohol Oxidation

The ECE complex **63** catalyzes the oxidation of primary and secondary alcohols to the corresponding aldehydes and ketones, respectively (5 mol% catalyst loading) [116]. While benzyl alcohol is effectively dehydrogenated within 30 min, electron-withdrawing groups on the aromatic ring require longer reaction times. Complex **69** with a dearomatized CNN pincer ligand has been utilized in the oxidation of alcohols to the corresponding esters [113]. For example, *n*-butanol is fully converted within 3 h. The corresponding aromatized system is also active, though base is needed to activate the catalyst, and yields are usually lower, presumably because the catalyst slowly degrades in the presence of base. Heterogenization of the catalyst on MCM-41 allows for easy separation of the catalyst from the product solution, and catalyst recycling has been demonstrated over three consecutive runs without loss of activity, yet prolonged reaction times are necessary. A drastic decrease of activity has been observed in the fourth run, indicating some optimization potential.

3.6 Biological Applications

A homoleptic $[Ru(CNC)_2]^{2+}$ complex based on a benzimidazolylidene analogue of ligand **43** (cf. Scheme 11) shows modest in vitro cytotoxic properties against a number of cancer cell lines such as MCF7 (breast cancer), HCT116 (colon cancer), and A549 (lung cancer) [91, 115]. The IC_{50} values are considerably lower (0.06–1.25 μM) than those of cisplatin and carboplatin and hold thus promise for further developments.

4 Rhodium and Iridium Complexes with Pincer Carbene Ligands

4.1 General Considerations

The synthesis and properties of pincer carbene rhodium complexes is well documented, while iridium analogues have received attention only recently [40]. Over the last years, the chemistry of pincer carbene rhodium complexes has been significantly expanded from 2-imidazolylidene and 2-pyrimidylidene systems as NHC donors to less conventional heterocyclic carbenes such as 4-imidazolylidenes, bicyclic NHCs, and carbodicarbenes [26]. Various donor functionalities including P-, S-, C-, and N-donors have been incorporated, while the chemistry of iridium pincer carbene complexes is largely dominated by CCC pincer ligands involving a central phenyl anion binding site.

Scheme 16 Thermally induced P–C bond cleavage in PCP pincer rhodium complexes

Rhodium insertion into the pincer framework has been successfully achieved by transmetalation from the silver carbene precursor, by C–H bond activation, and by sequential or concerted deprotonation and metal coordination. Together with transmetalation, this latter method is prevalent in iridation, using [IrCl(cod)]$_2$ or a related precursor in the presence of a weak base such as NEt$_3$ or Cs$_2$CO$_3$ as proton scavenger.

4.2 ECE Pincer Rhodium and Iridium Complexes

Fryzuk and coworkers have prepared the PCP rhodium complex **70** via deprotonation of the imidazolium salt with KN(SiMe$_3$)$_2$ and subsequent addition of [RhCl(cod)]$_2$ [128]. Presumably due to rigid chelation, the C$_{carb}$–Rh bond is shorter (1.929 Å) than in other rhodium(I) complexes. Similar to related Pd, Ni, and Pt complexes [77], the NHC ring is twisted out of the PCP-metal plane. The chloro ligand in complex **70** is readily substituted upon reaction with KBEt$_3$H and MeLi, which yields the hydride and methyl complex **71a** and **71b**, respectively (Scheme 16). These complexes are thermally unstable and transform to the CCP pincer complexes **72** upon heating to 60°C through a C–P bond-breaking and R–P bond-making process. In contrast, the chloro precursor complex **70** is thermally stable up to 110°C. A suggested mechanism for this rearrangement is comprised of an oxidative addition of one of the C$_{aryl}$–P bonds followed by reductive elimination of the phosphido group with preferential P–R bond formation due to the absence of chelating constraints. Such a mechanism is in agreement with the observed first-order reaction kinetics, and the lability of the C–P bond flags potential complex deactivation pathways when considering catalytic application of this type of complexes.

Several rhodium and iridium complexes have been prepared that contain a ring-expanded NHC as central donor site. The pentacoordinate complexes **73** have been synthesized from the ligand precursor and [M(OMe)(cod)]$_2$ as a mixture of two stereoisomers (Fig. 13) [129]. Both the pyridines and the cod ligand are bound to the metal, and an X-ray diffraction analysis indicates a distorted trigonal bipyramidal structure with the carbene and one of the olefinic sites of cod in the axial positions. As a consequence, the Rh–C$_{cod}$ distances *trans* to the carbene are nearly 0.2 Å longer than those in *cis* position.

Fig. 13 Pincer rhodium complexes with ring-expanded NHC donors

73 a M = Rh
   b M = Ir

74

a R = Ph   **75**
b R = *i*Pr

Scheme 17 Hydride abstraction of PCP pincer iridium complex **76**

76   **77**

The pyrimidine-derived NHC pincer complexes **74** have been synthesized by chelate-assisted double C–H activation from [RhCl(PPh$_3$)$_3$] at ambient temperature with concomitant evolution of dihydrogen [130]. Mechanistic insights have been obtained from analogous reactions with the corresponding iridium precursor [IrCl (CO)(PPh$_3$)$_2$], which proceeds considerably slower. In this case, complex **76** has been observed as an intermediate after the first C–H bond activation, containing the methine proton and the iridium-bound hydrogen in antiperiplanar arrangement and thus likely representing the kinetic product of this bond activation step (Scheme 17). Such an arrangement prevents dihydrogen evolution, if bonding of the ligands is rigid. Chloride or phosphine dissociation may cause a rotation in the rhodium complex in order to facilitate H–H bond formation, though this process is apparently hindered in complex **76**. Attempts to remove the chloro ligand with a silver salt such as AgSbF$_6$ induce hydride abstraction and afford complex **77** instead. Complexes somewhat related to **77** comprising an acyclic carbene as central donor have been investigated by Piers and coworkers [131, 132].

Even larger ring-size carbene pincer complexes are accessible with carbodicarbene (bent allene) units [133]. Complexes **75a,b** are obtained by reaction of the ligand precursor with [RhCl(cod)]$_2$ in a formal oxidative addition and subsequent treatment with NaOMe to induce reductive elimination to rhodium (I) again (cf. Fig. 13). The carbene–carbon in these complexes resonates at extraordinarily high field (δ_C 73 ppm). Introduction of an ancillary CO ligand has been achieved upon metalation with [RhCl(CO)$_2$]$_2$, providing ν_{CO} frequencies at 1,986 cm^{-1} (R = Ph) and 1,970 cm^{-1} (R = *i*Pr).

Sterically and coordinatively very flexible pincer carbene complexes have been prepared from inserting allyl wingtip groups as *N*-substituents on imidazolylidenes. When metalated with [IrCl(cod)]$_2$, a pentacoordinate iridium cod complex is obtained with an all-carbon ligand environment [134]. At the other extreme, a sterically very rigid pincer carbene complex has been developed by Yamamoto
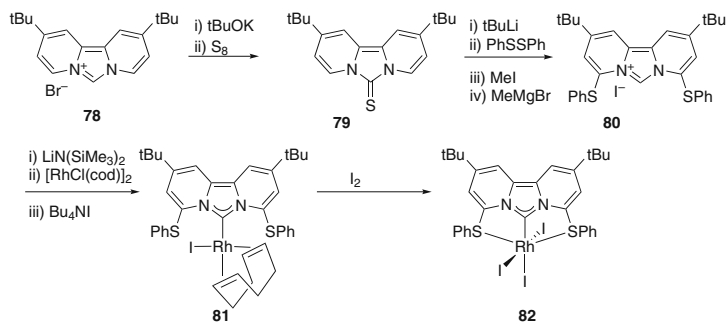
Scheme 18 Synthesis of the sterically rigid SCS pincer rhodium complex **82**
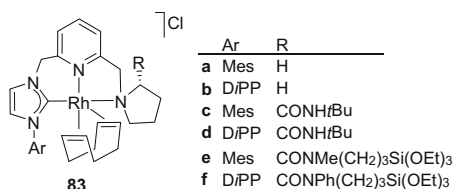
Fig. 14 Pincer carbene rhodium complexes **83** with remote functionality for immobilization

and coworkers based on *ortho*-substituted dipyrido-annulated NHCs [135]. Transient protection of the imidazolium C2 position of the azolium salt **78** and subsequent insertion of SPh substituents to the thiourea derivative **79** followed by deprotection of the pro-carbenic site affords the ligand precursor **80**. Deprotonation with LiN(SiMe₃)₂ and coordination to [RhCl(cod)]₂ yields a rhodium(I) complex **81** with a monodentate carbene ligand. Addition of iodine induces oxidation to rhodium(III) and SCS-tridentate coordination of the carbene ligand to give the pincer rhodium complex **82** (Scheme 18).

Monocarbene pincer complexes **83** with a CNN coordination pattern have been prepared via a transmetalation protocol (Fig. 14) [136, 137]. The flexibility of the ligand synthesis allows for a wide variation of substituents to be introduced at the pyrrolidine and carbene sites. In particular, the triethoxysilyl groups in complexes **83e** and **83f** have been used to graft the pincer rhodium complexes onto MCM-41.

4.3 CEC Pincer Rhodium and Iridium Complexes

The CNC pincer rhodium complex **84** based on a carbazole backbone has been prepared by deprotonation with LDA and subsequent addition of [Rh(CO)₂Cl]₂ [138]. The carbonyl stretch vibration is at remarkably low energy, $v_{CO} = 1,916$ cm^{-1}, indicating strong σ-donor and weak π-acceptor properties of the pyrrolyl binding site.

Scheme 19 Oxidative addition to the nucleophilic CNC pincer rhodium complex **84**
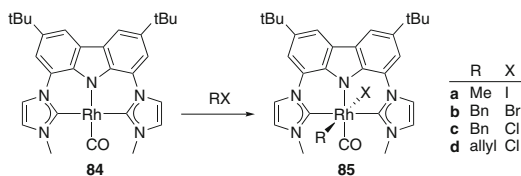
Crystallographic analyses, in particular the relatively small N_{pyr}–Rh–C_{CO} angle of 161.0°, suggest steric congestion caused by the NHC methyl substituents. The nucleophilic character of the metal center in **84** is also demonstrated by the facile oxidative addition of MeI, BnBr, and allyl chloride to give the corresponding rhodium(III) complexes **85** (Scheme 19). The reactivity sequence and the *trans* configuration in the product is in agreement with a S_N2'-type mechanism. While the shift of the v_{CO} to higher wave numbers (v_{CO} around 2,020 cm^{-1}) is expected due to the reduced backbonding of rhodium(III), it is worth noting that the allyl group is bound exclusively in an η^1-coordination mode [139]. While in complex **84** the carbazole backbone is only slightly bent, a related dicarbene complex with an aliphatic C-donor backbone is completely flexible and adopts a facial coordination mode when bound to a rhodium(III) center [140], indicating a broad range of steric patterns that are accessible with such CEC pincer carbene ligands.

CCC pincer complexes with a central phenyl donor and two carbene arms have been thoroughly investigated in iridium chemistry, stimulated in parts by the great success of related PCP iridium systems in alkane and amine borane dehydrogenation [12]. Early work has been compiled in 2009 [44, 141–143]. Sterically rigid complexes with the carbenes directly linked to the central aryl unit are accessible by multiple C–H activation using [IrCl(cod)]$_2$ and a base. They have also been synthesized via a stepwise procedure in which a monocarbene iridium(I) complex is first isolated as an intermediate, indicating a cascade of C–H bond activations [144]. The reaction outcome is delicately balanced by a number of factors including the solvent and in particular the substitution pattern on the ligand.

When using the pincer ligand precursor **86a** in the presence of [Ir(cod)Cl]$_2$, KI, and NEt$_3$, several products are obtained, with the diiodide complex **87b** as major species and minor quantities of the monohydride **87a** (Scheme 20) [145–147]. In addition, a bidentate complex originating from *ortho,para* rather than *ortho,ortho* C–H bond activation of the central phenyl ring is formed in considerable amounts [146]. Blocking these positions with methyl substituents effectively prevents the formation of the bidentate complex and instead promotes CCC tridentate pincer-type coordination of the ligand as in **87** along with formation of a monodentate iridium(I) NHC species and traces of a homoleptic bis(pincer) iridium complex. When using a large excess of base, the homoleptic bis(pincer) complex is formed selectively. Modification of the carbene wingtip group from butyl to adamantyl (Ad) promotes the formation of the 4-imidazolylidene complex **88** as the exclusive product, presumably due to steric congestion (Scheme 20) [144, 148]. This selectivity is independent of the presence or absence of *meta* methyl groups on the central aryl ring. Such a C4-bonding mode is obviously suppressed when
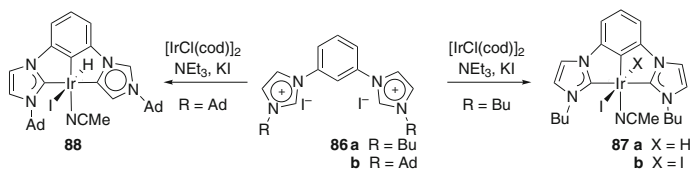
Scheme 20 Formation of CCC pincer iridium complexes
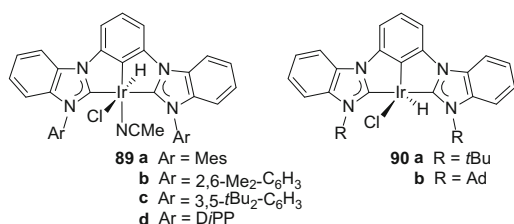
Fig. 15 Pincer iridium complexes with benzimidazolylidene donors
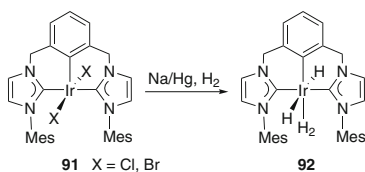
Scheme 21 Synthesis of pincer iridium polyhydride complex **92**

benzimidazolium rather than imidazolium groups are introduced as carbene precursors. The corresponding CCC iridium complexes **89** and **90** have been isolated as monohydrides akin to **87a** (Fig. 15) [149, 150]. In this ligand setting, bulky carbene substituents such as *t*Bu or Ad afford the pentacoordinate species **90**, while aryl substituents accommodate MeCN in the iridium coordination sphere. Obviously the solvent plays a critical role in the synthesis of these complexes. When nitriles different from MeCN such as isobutyronitrile, 2-chloroacetonitrile, or benzonitrile are used, the reaction does not proceed, whereas in toluene hydrolytic NHC ring opening has been observed [144].

Attempts to form di- and polyhydride complexes from these CCC pincer carbene iridium species have met only limited success. Reaction of complex **88** with NaO*t*Bu under a H_2 atmosphere suggests the generation of a dihydride species ($\delta_H - 34.9$ ppm compared to -23.4 ppm in the precursor) though isolation of this complex has failed thus far [148]. Similarly, reaction of complexes **89a** or **90b** with LiBEt$_3$H yields a spectroscopically observable polyhydride complex which could not yet be isolated [151]. Complex **89a** reacts with allylbenzene in the presence of NaOMe to give an η^3-allyl iridium hydride complex resulting from C$_{benzyl}$–H bond activation [152].

Well-defined hydride species are accessible upon changing the rigid pincer ligand to a more flexible platform by linking the carbenes and the central phenyl ring with methylene groups rather than a direct bond. Heinekey and coworkers have synthesized the pincer carbene iridium complex **91** by transmetalation from the silver intermediate (Scheme 21) [153]. The iridium precursor is critical, and while [IrCl(cod)]$_2$ and [IrCl(coe)$_2$]$_2$ fail, the simple olefin precursor [IrCl(C$_2$H$_4$)$_4$] yields complex **91**. Spectroscopic studies suggest a dynamic puckering that is relatively slow on the NMR time scale. Exchange of the ancillary halide ligands under a H$_2$ atmosphere and with amalgam readily affords the hydride complex **92**. This reaction is reversible in the presence of CCl$_4$. DFT and NMR data indicate a short H–H bond distance and a dihydride/dihydrogen complex, i.e., a smaller fraction of iridium(V) compared to the phosphine analogue [Ir(PCP) H$_4$]. Complex **92** undergoes H/D exchange in deuterated aromatic solvents such as benzene and toluene, but not in alkane solutions, indicating that only selected C–H bonds are activated. In the presence of a donor ligand such as PMe$_3$ or pyridine, the H$_2$ ligand is readily displaced.

4.4   Catalytic Application of Pincer Carbene Rhodium and Iridium Complexes

Much catalytic evaluation of rhodium and iridium complexes containing pincer carbene ligands has concentrated thus far on (transfer) hydrogenation and alkane dehydrogenation, which is undoubtedly inspired by the activity observed for classical PCP and related pincer complexes [12].

4.4.1   Direct and Transfer Hydrogenation

Complexes **83** are active catalyst precursors for the hydrogenation of *gem*-disubstituted olefins under mild conditions (40°C, 4 bar H$_2$), with turnover frequencies close to 5,000 h^{-1} at 0.1 mol% catalyst loading [136, 137]. With itaconate esters as substrates, enantioselectivity is poor (ee <20%), but with trisubstituted olefins such as 2-benzylidene succinate, the ee improves to 99% albeit at the cost of activity (TOF = 500 h^{-1}). Catalytic activity is substantially increased when complex **83e** or **83f** is supported on MCM-41, which induces up to 10 times higher turnover frequencies (TOF = 40,000 h^{-1}) [137]. Similar to the homogeneous catalysts, itaconate is hydrogenated with very low enantioselectivity, while hydrogenation of benzylidene succinate reaches >98% ee. Intriguingly, a change of the carbenic *N*-substituent from Mes to D*i*PP inverts the enantioselectivity of the homogeneous catalyst (from *S*- to *R*-selective), whereas the *S*-isomer is formed with the MCM-41-grafted system regardless of the carbene substituent.
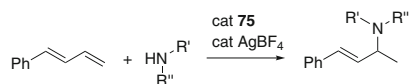
Scheme 22 Site-selective intermolecular hydroamination catalyzed by complex **75**

The ring-expanded carbene pincer complexes **73** display hydrogenation activity towards itaconate and acrylate esters under similar conditions (80°C, 5 bar H_2, 0.1 mol% complex). While conversions are complete, no enantioselectivity has been observed presumably because the chiral information is remote and poorly transferred to the catalytic center. The iridium complex **73b** also catalyzes ketone reduction by hydrogen transfer from *i*PrOH with good conversion of acetophenone but only moderate activity towards substituted aryl ketones.

4.4.2 Hydroamination

Upon activation with a halide scavenger such as $AgBF_4$, complexes **75** catalyze site-selective intermolecular hydroamination of dienes with aryl and alkyl amines to produce allylic amines (Scheme 22) [133]. Generally, Markovnikov selectivity is high (>98%), and alkyl amines require higher temperature than aryl amines. The catalytic process tolerates a large range of functional groups including alkenes, alcohols, esters, and tosyl amines, though sterically unbiased dienes tend to produce mixtures from α and γ addition.

4.4.3 Alkane Dehydrogenation and C–H Bond Activation

Stimulated by the unique activity of PCP iridium complexes in catalyzing the activation of alkane C–H bonds, the CCC pincer carbene complexes **87–90** have been evaluated in this reaction. In the absence of a hydrogen acceptor and after activation with NaO*t*Bu to promote reductive HCl elimination, complex **89a** accomplishes up to 100 turnovers in cyclooctane dehydrogenation [151], about an order of magnitude less than the corresponding PCP systems [12]. Introduction of a CF_3 substituent on the *para* position of the central phenyl ring of **89a** has no beneficial impact on the catalytic performance. The activity is fast initially though rapidly ceases due to catalyst decomposition. With alkyl or D*i*PP substituents on the carbene, the complexes are catalytically inactive.

In the presence of a hydrogen acceptor such as *t*Bu-CH=CH$_2$ or norbornene, complexes **89** and **87** fail to dehydrogenate cyclooctane, even when activated with a base [146, 150, 151]. In contrast, complex **88** containing a 4-imidazolylidene donor displays modest activity at 200°C with TOF = 0.36 h^{-1} [148]. Possibly, the stronger donor properties of 4-imidazolylidene in **88** vs. 2-(benz)imidazolylidenes in **87** or **89** promote the oxidative C–H bond activation to the transiently formed iridium (I) intermediate and may thus enable catalytic turnovers, albeit at very slow rate.

Scheme 23 Synthesis of hybrid CCP pincer complexes **94**

a R = Me
b R = *n*Bu
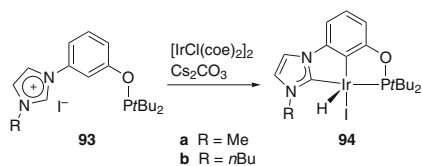
Fig. 16 Homoleptic bis CCC Ir^{III} complexes **95**

95 a X = I
b X = PF$_6$
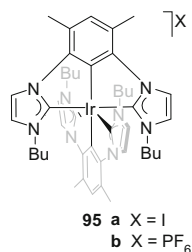
The low activity may also stem from the poor solubility of the complexes in apolar solvents. Complex **88** has a very narrow activity window, and catalytic performance drops sharply when the reaction temperature is either lowered or raised by 50°C [148].

When using 1-hexene as hydrogen acceptor, rapid alkene isomerization rather than alkane dehydrogenation is induced with complexes **89** and **90** [150, 152]. The process is fast even at lower temperature (100°C) and yields a mixture of isomers. Isomerization involves a π-allyl species, and H/D crossover experiments indicate that 1,3-hydrogen migration is exclusively intramolecular [152]. While C–H reductive elimination from the π-allyl intermediate is rapid, such an intermediate has been trapped and crystallized when using allylbenzene as ligand.

In general, NHC analogues of PCP-type pincer iridium complexes are considerably less competent alkane dehydrogenation catalysts than the phosphine and phosphinite originals [12]. Various arguments may account for this fact, including the lower solubility, the too strong donor properties of NHCs (thus inhibiting reductive elimination processes), and the intrinsic instability of the M–C$_{NHC}$ bond under reductive conditions, which often leads to imidazolium salt elimination. The advantageous properties of phosphorus donors are also underlined with the activity of the hybrid carbene/phosphinite complexes **94a,b**, which are substantially more active (TOF = 1.46 h^{-1}) than the dicarbene analogues but significantly less than PCP systems (Scheme 23) [154]. These complexes have been obtained by a base-assisted cyclometalation using **93** and [IrCl(coe)$_2$]$_2$, while transmetalation has failed thus far. When replacing the phosphinite donor in **93** with a phosphine, no C$_{aryl}$–H bond activation occurs and only bimetallic complexes are formed with the carbene and the phosphine coordinating to different iridium centers.

Complexes **89** together with 2 mol equiv. NaO*t*Bu activate C–H bonds in *meta*-xylene for borylation with B$_2$pin$_2$ (pin = pinacolate) [149]. Electron-rich aryl systems such as 1,3-(MeO)$_2$-C$_6$H$_4$ are converted only partially, while electron-deficient substrates such as 1,3-(CF$_3$)$_2$-C$_6$H$_4$ are borylated almost quantitatively even in the absence of NaO*t*Bu.

4.5 Photophysical Application of Pincer Carbene Iridium Complexes

The photophysical properties of homoleptic bis(pincer) complexes **95** have been investigated by De Cola and coworkers (Fig. 16) [155]. They have an intense emission in the near-UV region with quantum yields around 40%. The photophysical properties of these complexes have been exploited to build a near-UV electroluminescent device based on charged iridium complexes. Electroluminescence is observed with maxima at 386 and 406 nm with a turn-on voltage of ~8 V, and although the initial efficiency is rather low (<1%), this work constitutes a valuable proof of concept.

5 Palladium and Platinum Complexes with Pincer Carbene Ligands

5.1 Ligand Considerations

Since the last comprehensive reviews [40, 41, 44], a plethora of articles have been published relating to palladium and platinum pincer NHC complexes. Most of the synthetic procedures are well covered, and this section will thus focus more on applications. Expanding on earlier work, novel ligands have been designed incorporating a wide array of neutral and anionic S-, P-, O-, N-, and C-donor functionalities. The flexibility in donor atom and charge leads to variable (hemi-)lability which is relevant for tailoring catalytic activity, specifically the stabilization of active species.

Much work has centered on CEC-type pincer ligands comprised of pyridine- or phenyl-bridged dicarbene complexes (E = N, C$^-$), as well as ECE and CEE pincer systems. The position of the carbene in the pincer ligand is important due to its strong *trans* effect and the ensuing consequences for complex reactivity. A variety of carbenes have been implemented, including imidazolylidenes, benzimidazolylidenes, imidazolinylidenes, and 1,2,3- and 1,2,4-triazolylidenes. In elegant work, Lassaletta and coworkers have developed also chiral versions of SCS pincer ligands for palladium complexation [156].

5.2 Complexation

5.2.1 Synthetic Methodologies

In addition to C–H bond activation (see below), a very common route to pincer carbene palladium and platinum complexes is transmetalation from Ag, Ni, or Zr

Scheme 24 Representative examples for the different methodologies for introducing palladium and platinum into pincer carbene scaffolds
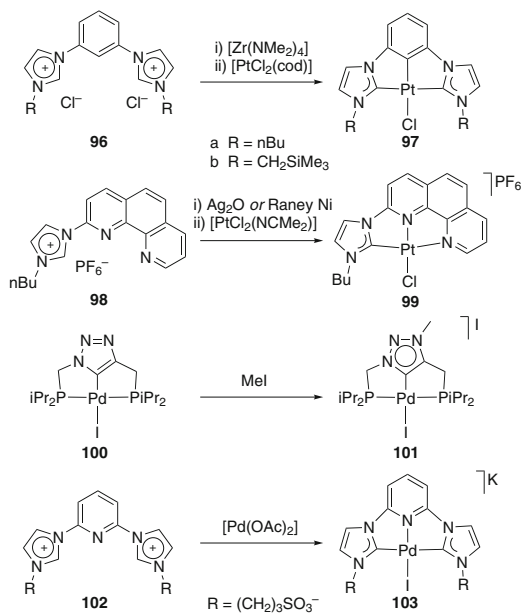
carbene precursors. Silver and nickel intermediates have been successfully used for generating both Pd and Pt complexes, while the procedure involving deprotonation with [Zr(NMe$_2$)$_4$] has thus far been reported exclusively for platination of CCC pincer precursors to give complexes **97** as well as benzimidazolylidene analogues (Scheme 24a) [157]. While transmetalation from silver carbenes is very well established, methods involving Raney nickel have emerged only recently. For example, complex **99** has been synthesized from the phenanthroline precursor **98** by both methods, though yields are higher when transmetalating from the nickel complex (96% vs. 85% from Ag; Scheme 24b) [71, 72]. Furthermore, obvious benefits arise from using considerably more abundant and cheaper metals. Similar to the silver route, carbene transfer from Ni and Zr can also be carried out in situ.

Other methods such as deprotonation of the azolium salt by a base and subsequent addition of the metal precursor and postmodification of a metal–alkyl complex have been demonstrated but are significantly less frequently used. Thus, 1,2,3-triazolylidene palladium complex **101** and homologous platinum systems have been synthesized by alkylation of the central triazolyl group of the PCP pincer ligand after complexation (Scheme 24c) [158]. This methodology offers access to pincer complexes bearing abnormal carbenes, which are known to be more basic donors than their normal counterparts [159], and it also avoids selectivity issues in the alkylation step since the phosphines are rigidly coordinating to the metal center. In a rare case, carbene bonding and formation of a CCP pincer complex comprising a central anionic phenyl group and a carbene donor arm has been accomplished via C$_{NHC}$–PPh$_2$ bond cleavage similar to nickel carbene bond formation (cf. Scheme 7) [160].
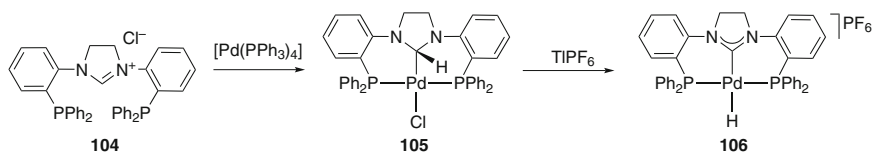
Scheme 25 Stepwise oxidative addition and carbene formation in the synthesis of complex **106**
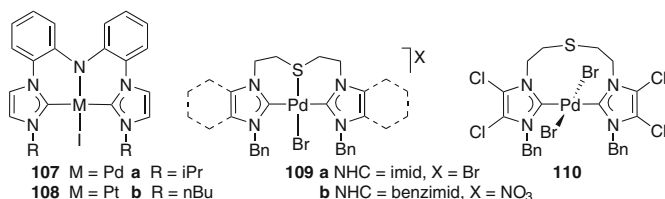
Scheme 26 Pincer ligation triggered by the carbene donor strength

By far the most widely used procedure for palladium complexation is C–H bond activation of the pincer ligand precursor with [Pd(OAc)$_2$] using microwave and/or thermal induction (Scheme 24d) [69, 161–167]. This method provides access to a diversity of pincer carbene complexes including triazolylidenes and (benz) imidazolylidenes, as well as methylene-bridged systems. It tolerates a variety of functionalities and enables, for example, the synthesis of water-soluble pincer complexes with carboxylate, sulfonate, and carbohydrate groups for aqueous cross-coupling reactions [161, 165, 167–169].

Mechanistically, the metalation with [Pd(OAc)$_2$] is generally assumed to follow classical cyclometalation principles [170]. When starting from [Pd(PPh$_3$)$_4$], however, Thomas and coworkers have spectroscopically and structurally identified initial formation of the metal adduct **105**, which formally implies a two-electron oxidation of the metal center and which is reminiscent to a Meisenheimer salt (Scheme 25) [171]. Subsequent C–H bond activation and halide dissociation gives the carbene complex **106** containing a metal-bound hydride. This reaction trajectory, which has also been observed for platinum complexation, diverges from the widely accepted mechanism for C–H bond activation involving an initial agostic C–H...M interaction and subsequent oxidative C–H bond cleavage. This result highlights the intriguing reactivity patterns induced by a rigidly chelating pincer ligand platform.

5.2.2 Ligand Reactivity

A range of pincer palladium complexes featuring an aliphatic sp^3-hybridized central donor site have been investigated in depth, including complexes **107** and **109** containing a central amine [172, 173] or a thioether [162–164]. The ligand
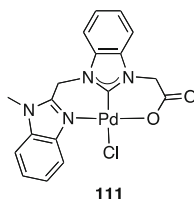
Fig. 17 NCO pincer palladium complex **111** with a hemilabile O-donor site
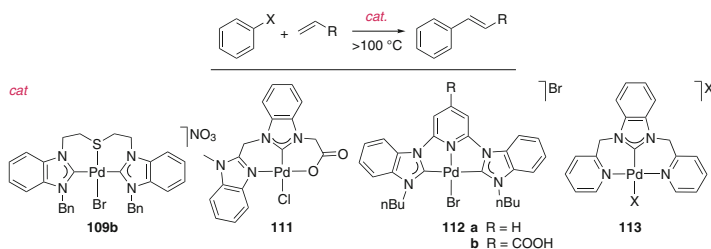
Scheme 27 Pincer carbene palladium complexes for catalytic Mizoroki–Heck arylation of olefins

bonding mode in the latter complexes is strongly dependent on the electronic nature of the carbene ligand. While the unsubstituted (benz)imidazolylidene-based ligand forms the expected tridentate chelate **109** upon palladium coordination (Scheme 26) [163, 164], electron-withdrawing chloro-substituents on the imidazolylidene induce only bidentate dicarbene coordination, yielding the neutral complex **110** with a pendant thioether [164]. This difference in coordination has been attributed to a better stabilization of the cationic palladium(II) center in complex **109** due to the stronger donation of the NHC ligands, while chloro-substituted carbenes increase the Pd–Br bond strength and hence prevent thioether coordination.

Our group has developed the NCO palladium complex **111** in which coordination of the carboxylate is reversible and dependent on the reaction conditions (Fig. 17) [174]. In acidic conditions, the protonation induces dissociation and affords a bidentate carbene complex while a basic environment leads to a tridentate pincer-type coordination mode. Ligand non-innocence has also been observed in a related indene-derived carbene ligand which may be useful for metal–ligand cooperativity [175].

5.3 Catalytic Application of Pincer Carbene Palladium and Platinum Complexes

Unsurprisingly, the vast majority of pincer carbene palladium complexes have been utilized as catalyst precursors in cross-coupling reactions. With a number of studies available, a general picture is emerging. In contrast, the catalytic application of pincer platinum complexes is much more limited and only three types of complexes have been reported to act as catalysts.

5.3.1 Mizoroki–Heck Coupling

Various complexes including **109b**, **111–113** have been successfully used as precursors for the arylation of olefins (Mizoroki–Heck coupling; Scheme 27) [161–167, 174, 176]. Generally, high temperatures are required ($>100°C$), and catalyst loadings can be very low (ppm levels), leading to turnover numbers in the 10^5–10^7 range. In several cases, addition of Bu$_4$NI or Bu$_4$NBr (Jeffery conditions [177]) has shown a positive effect.

The necessity of high temperatures for catalytic activity to ensue suggests either a difficult catalyst activation step or a (partial) heterogenization of the complex to form a colloidal phase as catalytically active species. In support of the latter notion, aryl chlorides are generally not converted and the substrate scope is limited to the more active aryl iodides and bromides. Moreover, pincer complex **109b** displays similar activity as related bidentate coordinated complexes [163], which may point to a similar active species due to complex decomposition. Mercury poisoning experiments with complexes **112** further indicate a heterogeneous phase to be relevant for catalytic turnover [165–167]. Thus, catalytic activity is effectively suppressed when mercury is added at the beginning (5% conversion after 5 h compared to 97% conversion in the absence of Hg). Likewise, addition of mercury during the reaction leads to a catalytic halt, indicating that ligand dissociation is possible, even when the carbene is bound to the metal in a tridentate pincer-type coordination mode.

The NCO complex **111** has been evaluated with deactivated aryl bromides at relatively low temperature (50°C) in an attempt to prevent the formation of colloidal particles [174]. The pincer coordination mode induces considerably higher activity than the bidentate ligand resulting from carboxylate protonation, suggesting some ability to tune the active site by the tridentate chelate. However, aryl chlorides are again not converted.

5.3.2 Sonogashira Coupling

Under copper-free conditions and with PPh$_3$ as an additive, complex **114** effectively couples a range of aryl bromides and iodides with terminal aryl acetylenes
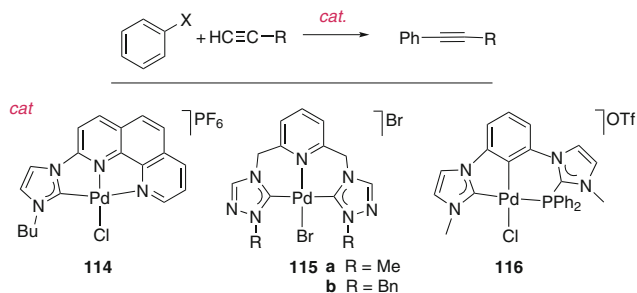
Scheme 28 Pincer carbene palladium complexes for catalytic Sonogashira coupling
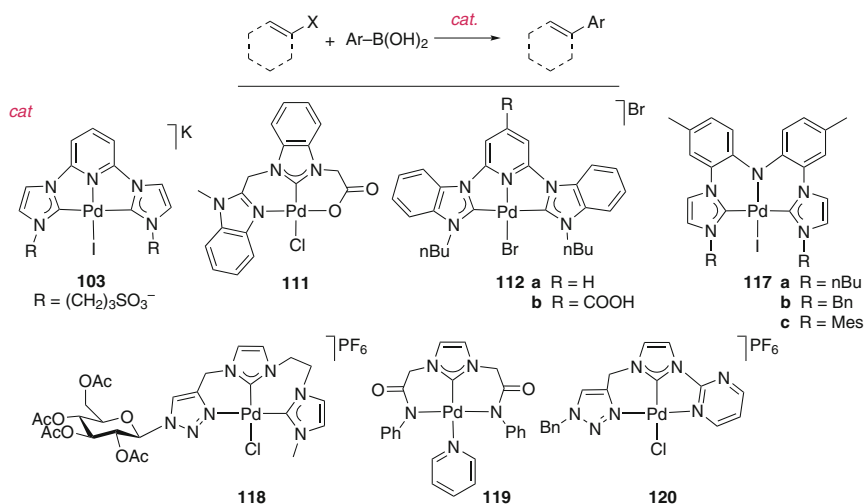
Scheme 29 Pincer carbene palladium complexes for catalytic Suzuki–Miyaura cross-coupling reactions

(Scheme 28) [72]. Aliphatic acetylenes only give moderate yields. Modification of the catalytic procedure allows the catalysis to be performed in neat water. Using the 1,2,4-triazolylidene palladium complexes **115** as catalyst, the coupling of 4-bromobenzaldehyde with phenylacetylene proceeds in the absence of phosphine and copper and with K_2CO_3 as base [162]. While the complex is stable under these conditions, NaOH as a base induces formation of palladium black, which is also catalytically active, albeit at a slower rate. The active species resulting from complex **115b** can be three times without a drop in activity and a further three times with slightly reduced performance to reach up to 75% conversion after the sixth run, affording a total TON of 56,000.

The carbene pincer complex **116** displays have been employed in the carbonylative Sonogashira reaction of phenyl iodide and phenylacetylene in an

Scheme 30 Pincer carbene palladium and platinum complexes for catalytic hydroamination of alkynes and alkenes
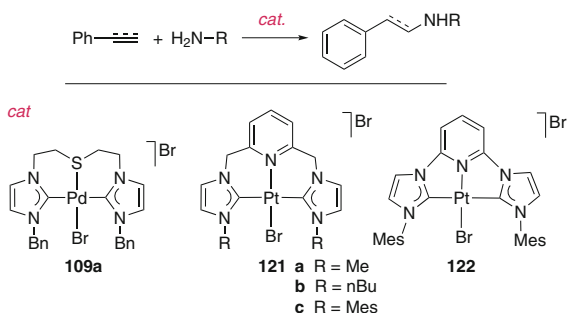
ionic liquid solvent [160]. The carbene complex displays only moderate activity when compared to mono- and bidentate phosphine palladium complexes.

5.3.3 Suzuki–Miyaura Coupling

A variety of complexes including **103**, **111**, **112**, and **117–120** have been used in Suzuki–Miyaura coupling reactions (Scheme 29) [161–169, 172–174, 178]. Extremely low catalyst loadings and very high TONs up to 2×10^8 have been accomplished with 1,1-dibromo-alkenes [169], and with aryl bromides and iodides [165, 166], though aryl chlorides require much higher catalyst loadings and give lower conversion. Ligand modifications influence the catalytic activity, as demonstrated by the different performance of the CNC pincer palladium complexes **117** [173].

Complexes **103**, **112**, and **118** are active in water, which enable the coupled biaryl products to be separated by simple filtration and to recycle the palladium-containing filtrate for further catalytic runs with no obvious loss in activity [165]. A mercury poisoning experiment with complex **112** does not stop the catalytic reaction but reduces the rate of product formation significantly, while the presence of polyvinyl pyridine as nanoparticle scavenger leads has a less inhibiting effect. The water-soluble complex **103** converts activated 4-chloro acetophenone in notable 52% yield when used at 0.1 mol% loading [161]. Interestingly, a related complex featuring two monodentate carbene ligands is more effective towards both aryl bromides and chlorides [161]. Similar conclusions have been drawn from comparing the pincer carbene palladium complex **119** with monodentate analogues [178]. Complex **111** with a hemilabile carboxylate donor is also less active than the bidentate analogue with a non-bound carboxylate group when using aryl bromides as substrates. However, the bi- and tridentate complexes display essentially the same activity when 4-chlorobenzaldehyde is used. This result may be rationalized by an acceleration of the oxidative addition step due to the presence of the anionic donor in the pincer complex, which is typically rate limiting with aryl chlorides but not with aryl bromides.

Scheme 31 Hydrovinylation of 2-methyl-2-butene
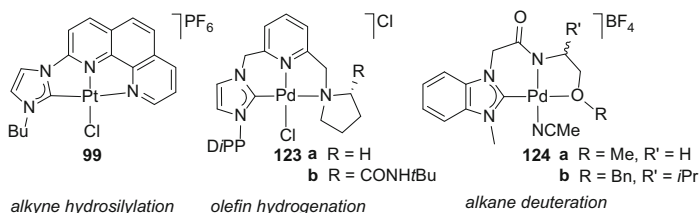
Fig. 18 Platinum and palladium pincer carbene complexes for various catalytic applications

5.3.4 Hydroamination

In the presence of triflic acid, complex **109a** catalyzes the hydroamination of phenyl acetylene with a range of anilines (Scheme 30) [164]. Conversions are moderate to good at 1 mol% complex loading, and 2,6-dimethylaniline gives the best yield. The bidentate complex **110** is less active than the tridentate pincer palladium complex **109** and does not achieve more than 60% conversion. Hydroamination has also been accomplished with pincer platinum complexes **121** and **122** [179]. The planar arrangement in **122** induces significantly higher catalytic activity than the puckered ligand in complexes **121**. In the presence of AgBF₄ as halide scavenger, this complex catalyzes the ethylene insertion into the N–H bond of primary amides, sulfonamides, and lactams. With morpholine, the reaction stops at an intermediate stage, which may provide some mechanistic hints. Higher alkenes such as propylene or styrene yield mixtures of branched and linear products.

An ethylene adduct of **122** has been successfully prepared, and while presumably highly relevant for hydroamination catalysis, this complex also catalyzes the hydrovinylation of olefins (Scheme 31) [180]. The reaction is slow (68% conversion after 8 days), but the selectivity is excellent.

5.3.5 Miscellaneous Catalytic Applications

Hydrosilylation catalysis has been reported with complex **99** (Fig. 18) [181]. The pincer complex is more active than other related bidentate and tetradentate analogues, allowing the catalyst loading to be reduced to 0.1 mol%. Under these conditions, high selectivity towards the *trans*-β-vinylsilane product is achieved.

The CNN pincer carbene complexes **123** induce the catalytic hydrogenation of geminally disubstituted and trisubstituted olefins, e.g., itaconate and benzylidene succinate esters (Fig 18) [136]. While they are less active than the Rh(I) analogues (see Sect. 4.4), up to 99% ee has been achieved with complex **123b** containing a

Scheme 32 Synthesis of the emissive complex **126** with vapochromic properties

125a R = Mes
b R = nBu

126
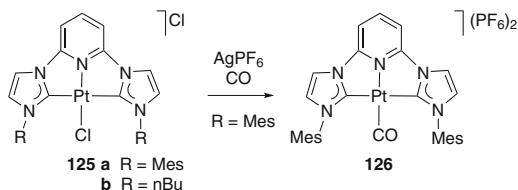
proline-derived N-donor arm. Interestingly a change of the carbene *N*-substituent from D*i*PP to Mes inverts the enantiopreference from *R* to *S* albeit at a lower 41% ee.

The water-soluble CNO benzimidazolylidene pincer palladium complexes **124** catalyze the H/D exchange of various hydrocarbons such as toluene and cyclohexane in water at 55°C (Fig. 18) [182, 183]. TONs up to 540% and 97% D-incorporation are accessible with cyclopentane, whereas only partial D-incorporation takes place with more difficult substrates such as THF and Et_2O. A related OCN rather than CNO pincer version gives much lower activity, possibly due to complex dimerization observed in solution.

5.4 Application of Pincer Carbene Palladium and Platinum Complexes in Materials

5.4.1 Photophysical Applications

Probably inspired by the photoemissive properties of a range of classical CNN pincer-type platinum complexes [184, 185], the photophysical properties of CCC and CNC pincer carbene platinum complexes have been investigated. In general, the formally neutral CNC pincer motif with a central pyridine moiety imparts longer excited-state lifetimes than the monoanionic CCC pincer ligand featuring a phenyl anion binding site.

The dicationic CNC pincer platinum complex **126** is emissive and has been obtained from **125a** by $AgPF_6$-mediated ligand exchange in the presence of CO (Scheme 32). This complex shows vapochromic behavior in the presence of small volatile molecules such as acetone and Et_2O, which changes the emission from blue to yellow [186]. Involvement of the Pt–CO unit in this sensing process has been confirmed in moist atmosphere by the formation of a Pt–COOH species. Small molecules with no donor atom as well as large molecules such as benzaldehyde have no effect on the emission properties. The photophysical properties of the related monocationic CNC pincer complex **125b** have unveiled that H_2O in the crystal lattice strongly affects the solid-state emission [187]. The hydrate complex shows an intense orange emission ($\lambda_{max} = 614$ nm) while the anhydrous complex is a green emitter ($\lambda_{max} = 550$ nm). The maximum emission wavelength is reversibly switched upon adding or removing water.

Fig. 19 Palladium pincer carbene complex **127** is a gelator, and the platinum CNC pincer carbene complex **128** is a moderate anticancer agent
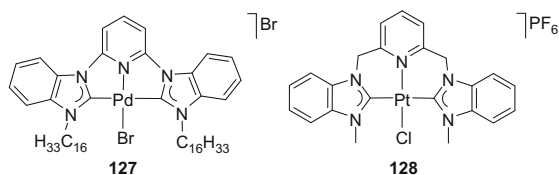
Exchange of the non-coordinating anion in complex **125b** from Cl^- to PF_6^- renders the complex non-emissive in degassed MeCN at room temperature, probably due to the presence of low-energy d–d ligand field states [188]. However, emission is switched on upon replacing the platinum-bound chloride with alkynyl ligands. These complexes are accessible upon reaction of complex **125** with various alkynes in the presence of NEt_3 and CuI. The emission energy can be readily tuned by varying the alkyne substituent; electron-donating MeO groups on the acetylide lower the emission energy compared to phenylacetylide (534 vs. 631 nm). Consistent with this shift, the emission bands have tentatively been assigned to ^{3}MLCT dπ (Pt) $\rightarrow \pi^*$(CNC) transitions with mixing of a ^{3}LLCT π(CCR) $\rightarrow \pi^*$(CNC) contribution. Accordingly, electron-donating alkynyl substituents raise the energy level of the dπ(Pt) and π(CCR) orbitals.

The CCC pincer platinum complexes **97a** (cf. Scheme 24) and its bromo analogue are blue light emitters in the solid state at room temperature [189]. Their emission is stable under continuous UV irradiation for 6 h (97% intensity retention), indicating a high resistance towards photobleaching in air. The benzimidazolylidene version of complex **97b** emits blue-green light in CH_2Cl_2 solution upon UV exposure. This complex displays a longer excited-state lifetime than the imidazolylidene analogue **97a**, perhaps due to the increased π-conjugation [157]. However, the emission intensity decreases by 14% over 6 h and thus indicates a lower photostability than complex **97a**.

Complex **97b** forms a Pt/Ag cluster when reacted with AgO_2CCF_3, which is emissive both in solution and in the solid state [190]. Highly concentrated solutions show emissions reminiscent of the solid-state features, while lower concentrations give significantly different emissions, perhaps due to dissociation of the cluster in solution.

5.4.2 Gelators

CNC palladium complexes such as **127** containing long alkyl substituents at the heterocyclic carbene serve as efficient low molecular mass organometallic gelators for a variety of protic and aprotic solvents (Fig. 19) [191, 192]. A combination of π-stacking of the heteroarenes, van der Waals forces between the alkyl chains, and metal–metal interactions may all play a role in imparting such gelation ability. Concentrations as low as 0.2 wt% are sufficient to induce gel formation. In the gel, the palladium centers remain active and have been demonstrated to catalyze Michael addition reactions.

5.5   Biological Application of Pincer Carbene Palladium and Platinum Complexes

Despite the established track record of platinum complexes in medicinal chemistry and in particular as antitumor agents, only little has been reported on pincer carbene complexes for biological applications. A single compound, CNC pincer platinum complex **128**, has been tested against several cancer cell lines, and its in vitro cytotoxicity is only modest [91]. Clearly, this field has large potential to further expand.

6   Conclusions

The merge of the concept of pincer ligands and *N*-heterocyclic carbenes as donors has led to exciting developments over the recent past. In particular, the role of *N*-heterocyclic carbenes as formally neutral ligands with very strong donor properties – a direct consequence of their mesoionic character – has prompted the development of variations of the archetypal ECE pincer ligand that contain the carbene ligand either as the core, i.e., a substitute of the central aryl unit, or as pincer arm ligand, i.e., as donor ligand E. In either setup, the carbene ligand fulfills a specific role that is unique to this type of donor systems. In pincer ligands with a central carbenic bonding site, the strong *trans* effect of the carbene is fully exploited, in particular when coordinated to square-planar metal centers. CEC pincer ligands with peripheral carbene bonding sites have distinct steric and electronic properties, imparted by the presence of two strongly donating carbene ligands, as well as the unique fanlike stereoelements entailed by *N*-heterocyclic carbenes. Subtle steric changes in the *N*-substituents of the carbene may induce significant changes, as demonstrated, for example, with complex **83**, where modification of the wingtip substituent from Mes to D*i*PP inverts the enantioselectivity of hydrogenation. Similarly, iron complexes show drastically different catalytic activity upon modification of these substituents.

The high stability of M–C$_{NHC}$ bonds entails further benefit of incorporating carbene ligands into pincer motifs. Especially when the ligand is non-innocent and reacts in concert with the metal in catalytic transformations, a robust bonding of the metal center is essential for achieving high turnover numbers and for preventing catalyst degradation. Along these lines, substantial progress has been made in incorporating pincer carbene complexes as active components into materials, e.g., as light emitters. While application in optical devices is still relatively scarce, this field will undoubtedly expand rapidly in the near future. The ability to tune the (photophysical) properties due to the various handles provided by *N*-heterocyclic carbenes and the pincer ligand platform provides excellent opportunities for further developments in catalysis, sensing, medicinal chemistry, and device fabrication.

References

1. Moulton CJ, Shaw BL (1976) J Chem Soc Dalton Trans 1020
2. van Koten G, Timmer K, Noltes JG, Spek AL (1978) J Chem Soc Chem Commun 250
3. Creaser CS, Kaska WC (1978) Inorg Chim Acta 30:L325
4. Albrecht M, van Koten G (2001) Angew Chem Int Ed 40:3750
5. Selander N, Szabó KJ (2011) Chem Rev 111:2048
6. van der Boom ME, Milstein D (2003) Chem Rev 103:1759
7. Albrecht M, Lindner MM (2011) Dalton Trans 40:8733
8. Rybtchinski B, Milstein D (1999) Angew Chem Int Ed 38:870
9. Morales-Morales D, Jensen CM (2007) The chemistry of pincer compounds. Elsevier, Amsterdam
10. van Koten G, Milstein D (2013) Organometallic pincer chemistry. Springer, Berlin
11. van Koten G (1989) Pure Appl Chem 61:1681
12. Choi J, MacArthur AHR, Brookhart M, Goldman AS (2011) Chem Rev 111:1761
13. Gunanathan C, Milstein D (2014) Chem Rev 114:12024
14. van Beek JAM, van Koten G, Smeets WJJ, Spek AL (1986) J Am Chem Soc 108:5010
15. Vigalok A, Uzan O, Shimon LJW, Ben-David Y, Martin JML, Milstein D (1998) J Am Chem Soc 120:12539
16. Albrecht M, Gossage RA, Spek AL, van Koten G (1999) J Am Chem Soc 121:11898
17. Abbenhuis HCL, Feiken N, Haarman HF, Grove DM, Horn E, Kooijman H, Spek AL, van Koten G (1991) Angew Chem Int Ed Engl 30:996
18. Arduengo AJ, Harlow RL, Kline M (1991) J Am Chem Soc 113:361
19. Bourissou D, Guerret O, Gabbaï FP, Bertrand G (2000) Chem Rev 100:39
20. Hahn FE, Jahnke MC (2008) Angew Chem Int Ed 47:3122
21. Nolan SP (2006) N-heterocyclic carbenes in synthesis. Wiley-VCH, Weinheim, p 297
22. Glorius F (2007) N-heterocyclic carbenes in transition metal catalysis. Springer, Berlin, p 1
23. Arduengo AJ, Bertrand G (2009) Chem Rev 109:3209
24. Díez-González S, Marion N, Nolan SP (2009) Chem Rev 109:3612
25. Herrmann WA (2002) Angew Chem Int Ed 41:1290
26. Schuster O, Yang L, Raubenheimer HG, Albrecht M (2009) Chem Rev 109:3445
27. Donnelly KF, Petronilho A, Albrecht M (2013) Chem Commun 49:1145
28. Kantchev EAB, O'Brien CJ, Organ MG (2007) Angew Chem Int Ed 46:2768
29. Vougioukalakis GC, Grubbs RH (2009) Chem Rev 110:1746
30. Albrecht M (2014) Adv Organomet Chem 62:111
31. Magill AM, McGuinness DS, Cavell KJ, Britovsek GJP, Gibson VC, White AJP, Williams DJ, White AH, Skelton BW (2001) J Organomet Chem 617–618:546
32. Gründemann S, Albrecht M, Loch JA, Faller JW, Crabtree RH (2001) Organometallics 20:5485
33. Peris E, Loch JA, Mata J, Crabtree RH (2001) Chem Commun 201
34. Perrin L, Clot E, Eisenstein O, Loch J, Crabtree RH (2001) Inorg Chem 40:5806
35. Chianese AR, Kovacevic A, Zeglis BM, Faller JW, Crabtree RH (2004) Organometallics 23:2461
36. Kelly RA III, Clavier H, Giudice S, Scott NM, Stevens ED, Bordner J, Samardjiev I, Hoff CD, Cavallo L, Nolan SP (2008) Organometallics 27:202

37. Gusev DG (2009) Organometallics 28:6458
38. Petronilho A, Woods JA, Mueller-Bunz H, Bernhard S, Albrecht M (2014) Chem Eur J 20:15775
39. Woods JA, Lalrempuia R, Petronilho A, McDaniel ND, Muller-Bunz H, Albrecht M, Bernhard S (2014) Energy Environ Sci 7:2316
40. Pugh D, Danopoulos AA (2007) Coord Chem Rev 251:610
41. Peris E, Crabtree RH (2004) Coord Chem Rev 248:2239
42. Mata JA, Poyatos M, Peris E (2007) Coord Chem Rev 251:841
43. Normand AT, Cavell KJ (2008) Eur J Inorg Chem 2781
44. Poyatos M, Mata JA, Peris E (2009) Chem Rev 109:3677
45. Edwards PG, Hahn FE (2011) Dalton Trans 40:10278
46. Budagumpi S, Haque RA, Salman AW (2012) Coord Chem Rev 256:1787
47. Bierenstiel M, Cross ED (2011) Coord Chem Rev 255:574
48. Bellemin-Laponnaz S, Dagorne S (2014) Chem Rev 114:8747
49. Helgert TR, Hollis TK, Oliver AG, Valle HU, Wu Y, Webster CE (2014) Organometallics 33:952
50. Thagfi JA, Lavoie GG (2012) Organometallics 31:7351
51. Romain C, Miqueu K, Sotiropoulos J-M, Bellemin-Laponnaz S, Dagorne S (2010) Angew Chem Int Ed 49:2198
52. Maron L, Bourissou D (2009) Organometallics 28:3686
53. Edworthy IS, Blake AJ, Wilson C, Arnold PL (2007) Organometallics 26:3684
54. Yu RP, Darmon JM, Hoyt JM, Margulieux GW, Turner ZR, Chirik PJ (2012) ACS Catal 2:1760
55. Yu RP, Darmon JM, Milsmann C, Margulieux GW, Stieber SCE, DeBeer S, Chirik PJ (2013) J Am Chem Soc 135:13168
56. Kaplan HZ, Li B, Byers JA (2012) Organometallics 31:7343
57. Newman PD, Cavell KJ, Kariuki BM (2010) Organometallics 29:2724
58. Yoshida K, Horiuchi S, Takeichi T, Shida H, Imamoto T, Yanagisawa A (2010) Org Lett 12:1764
59. Danopoulos AA, Pugh D, Smith H, Saßmannshausen J (2009) Chem Eur J 15:5491
60. Pelczar EM, Emge TJ, Krogh-Jespersen K, Goldman AS (2008) Organometallics 27:5759
61. Trovitch RJ, Lobkovsky E, Chirik PJ (2006) Inorg Chem 45:7252
62. Pugh D, Wells NJ, Evans DJ, Danopoulos AA (2009) Dalton Trans 7189
63. Al Thagfi J, Lavoie GG (2012) Organometallics 31:2463
64. Al Thagfi J, Dastgir S, Lough AJ, Lavoie GG (2010) Organometallics 29:3133
65. Liu Y, Harlang T, Canton SE, Chabera P, Suarez-Alcantara K, Fleckhaus A, Vithanage DA, Goransson E, Corani A, Lomoth R, Sundstrom V, Warnmark K (2013) Chem Commun 49:6412
66. Danopoulos AA, Wright JA, Motherwell WB, Ellwood S (2004) Organometallics 23:4807
67. Inamoto K, Kuroda J-I, Hiroya K, Noda Y, Watanabe M, Sakamoto T (2006) Organometallics 25:3095
68. Spasyuk DM, Castonguay A, Zargarian D (2013) Top Organomet Chem 40:131
69. Tu T, Mao H, Herbert C, Xu M, Dotz KH (2010) Chem Commun 46:7796
70. Steinke T, Shaw BK, Jong H, Patrick BO, Fryzuk MD, Green JC (2009) J Am Chem Soc 131:10461
71. Liu B, Liu X, Chen C, Chen C, Chen W (2012) Organometallics 31:282
72. Gu S, Chen W (2009) Organometallics 28:909
73. Sun Y, Li X, Sun H (2014) Dalton Trans 43:9410
74. Guo W-J, Wang Z-X (2013) J Org Chem 78:1054
75. Zhang C, Wang Z-X (2009) Organometallics 28:6507
76. Vabre B, Canac Y, Duhayon C, Chauvin R, Zargarian D (2012) Chem Commun 48:10446
77. Steinke T, Shaw BK, Jong H, Patrick BO, Fryzuk MD (2009) Organometallics 28:2830

78. Arduengo AJ 3rd, Dolphin JS, Gurau G, Marshall WJ, Nelson JC, Petrov VA, Runyon JW (2013) Angew Chem Int Ed Engl 52:5110
79. Mrutu A, Dickie DA, Goldberg KI, Kemp RA (2011) Inorg Chem 50:2729
80. Mrutu A, Goldberg KI, Kemp RA (2010) Inorg Chim Acta 364:115
81. Bezuidenhout DI, Kleinhans G, Guisado-Barrios G, Liles DC, Ung G, Bertrand G (2014) Chem Commun 50:2431
82. Inamoto K, Kuroda J-I, Kwon E, Hiroya K, Doi T (2009) J Organomet Chem 694:389
83. Brown DH, Skelton BW (2011) Dalton Trans 40:8849
84. MaGee KDM, Travers G, Skelton BW, Massi M, Payne AD, Brown DH (2012) Aust J Chem 65:823
85. Liu A, Zhang X, Chen W (2009) Organometallics 28:4868
86. Kuroda J-I, Inamoto K, Hiroya K, Doi T (2009) Eur J Org Chem 2251
87. Xu M, Li X, Sun Z, Tu T (2013) Chem Commun 49:11539
88. Quasdorf KW, Tian X, Garg NK (2008) J Am Chem Soc 130:14422
89. Gu S, Liu B, Chen J, Wu H, Chen W (2012) Dalton Trans 41:962
90. Dinda J, Liatard S, Chauvin J, Jouvenot D, Loiseau F (2011) Dalton Trans 40:3683
91. Dinda J, Adhikary SD, Roymahapatra G, Nakka KK, Santra MK (2014) Inorg Chim Acta 413:23
92. Hernandez-Juarez M, Vaquero M, Alvarez E, Salazar V, Suarez A (2013) Dalton Trans 42:351
93. Naziruddin AR, Kuo C-L, Lin W-J, Lo W-H, Lee C-S, Sun B-J, Chang AHH, Hwang W-S (2014) Organometallics 33:2575
94. Filonenko GA, Cosimi E, Lefort L, Conley MP, Copéret C, Lutz M, Hensen EJM, Pidko EA (2014) ACS Catal 4:2667
95. Chung L-H, Cho K-S, England J, Chan S-C, Wieghardt K, Wong C-Y (2013) Inorg Chem 52:9885
96. Lee C-S, Zhuang RR, Wang J-C, Hwang W-S, Lin IJB (2012) Organometallics 31:4980
97. Son SU, Park KH, Lee Y-S, Kim BY, Choi CH, Lah MS, Jang YH, Jang D-J, Chung YK (2004) Inorg Chem 43:6896
98. Park H-J, Chung YK (2012) Dalton Trans 41:5678
99. Park H-J, Kim KH, Choi SY, Kim H-M, Lee WI, Kang YK, Chung YK (2010) Inorg Chem 49:7340
100. Mathew P, Neels A, Albrecht M (2008) J Am Chem Soc 130:13534
101. Schulze B, Escudero D, Friebe C, Siebert R, Goerls H, Koehn U, Altuntas E, Baumgaertel A, Hager MD, Winter A, Dietzek B, Popp J, Gonzalez L, Schubert US (2011) Chem Eur J 17:5494
102. Brown DG, Sanguantrakun N, Schulze B, Schubert US, Berlinguette CP (2012) J Am Chem Soc 134:12354
103. Brown DG, Schauer PA, Borau-Garcia J, Fancy BR, Berlinguette CP (2013) J Am Chem Soc 135:1692
104. Naziruddin AR, Huang Z-J, Lai W-C, Lin W-J, Hwang W-S (2013) Dalton Trans 42:13161
105. Zhang Y-M, Shao J-Y, Yao C-J, Zhong Y-W (2012) Dalton Trans 41:9280
106. Hahn FE (2013) ChemCatChem 5:419
107. Toda T, Kuwata S, Ikariya T (2014) Chem Eur J 20:9539
108. Zeng F, Yu Z (2008) Organometallics 27:6025
109. Fogler E, Balaraman E, Ben-David Y, Leitus G, Shimon LJW, Milstein D (2011) Organometallics 30:3826
110. Balaraman E, Gnanaprakasam B, Shimon LJW, Milstein D (2010) J Am Chem Soc 132:16756
111. Sun Y, Koehler C, Tan R, Annibale VT, Song D (2011) Chem Commun 47:8349
112. del Pozo C, Corma A, Iglesias M, Sanchez F (2011) Green Chem 13:2471
113. del Pozo C, Iglesias M, Sanchez F (2011) Organometallics 30:2180

114. Sinn S, Schulze B, Friebe C, Brown DG, Jäger M, Altuntaş E, Kübel J, Guntner O, Berlinguette CP, Dietzek B, Schubert US (2014) Inorg Chem 53:2083
115. Das Adhikary S, Samanta T, Roymahapatra G, Loiseau F, Jouvenot D, Giri S, Chattaraj PK, Dinda J (2010) New J Chem 34:1974
116. Naziruddin AR, Zhuang C-S, Lin W-J, Hwang W-S (2014) Dalton Trans 43:5335
117. Wong C-Y, Lai L-M, Pat P-K, Chung L-H (2010) Organometallics 29:2533
118. Chung L-H, Chan S-C, Lee W-C, Wong C-Y (2012) Inorg Chem 51:8693
119. Alabau RG, Eguillor B, Esler J, Esteruelas MA, Oliván M, Oñate E, Tsai J-Y, Xia C (2014) Organometallics 33:5582
120. Trofimenko S (1971) J Am Chem Soc 93:1808
121. Adachi C, Kwong RC, Djorovich P, Adamovich V, Baldo MA, Thompson ME, Forrest SR (2001) Appl Phys Lett 79:2082
122. Holmes RJ, Forrest SR, Tung Y-J, Kwong RC, Brown JJ, Garon S, Thompson ME (2003) Appl Phys Lett 82:2422
123. Yook KS, Lee JY (2012) Adv Mater 24:3169
124. Li X-W, Chen F, Xu W-F, Li Y-Z, Chen X-T, Xue Z-L (2011) Inorg Chem Commun 14:1673
125. Baratta W, Chelucci G, Gladiali S, Siega K, Toniutti M, Zanette M, Zangrando E, Rigo P (2005) Angew Chem Int Ed 44:6214
126. Balaraman E, Fogler E, Milstein D (2012) Chem Commun 48:1111
127. Zhang J, Leitus G, Ben-David Y, Milstein D (2006) Angew Chem Int Ed 45:1113
128. Shaw BK, Patrick BO, Fryzuk MD (2012) Organometallics 31:783
129. Newman PD, Cavell KJ, Hallett AJ, Kariuki BM (2011) Dalton Trans 40:8807
130. Hill AF, McQueen CMA (2012) Organometallics 31:8051
131. Burford RJ, Piers WE, Parvez M (2012) Organometallics 31:2949
132. Burford RJ, Piers WE, Parvez M (2013) Eur J Inorg Chem 3826
133. Goldfogel MJ, Roberts CC, Meek SJ (2014) J Am Chem Soc 136:6227
134. Zanardi A, Peris E, Mata JA (2008) New J Chem 32:120
135. Fuku-en S-I, Yamamoto J, Minoura M, Kojima S, Yamamoto Y (2013) Inorg Chem 52:11700
136. Boronat M, Corma A, Gonzalez-Arellano C, Iglesias M, Sanchez F (2010) Organometallics 29:134
137. Del Pozo C, Corma A, Iglesias M, Sánchez FL (2010) Organometallics 29:4491
138. Moser M, Wucher B, Kunz D, Rominger F (2007) Organometallics 26:1024
139. Wucher B, Moser M, Schumacher SA, Rominger F, Kunz D (2009) Angew Chem Int Ed 48:4417
140. Kruger A, Haller LJL, Muller-Bunz H, Serada O, Neels A, Macgregor SA, Albrecht M (2011) Dalton Trans 40:9911
141. Danopoulos AA, Pugh D, Wright JA (2008) Angew Chem Int Ed 47:9765
142. Raynal M, Cazin CSJ, Vallee C, Olivier-Bourbigou H, Braunstein P (2008) Chem Commun 3983
143. Bauer EB, Andavan GTS, Hollis TK, Rubio RJ, Cho J, Kuchenbeiser GR, Helgert TR, Letko CS, Tham FS (2008) Org Lett 10:1175
144. Zuo W, Braunstein P (2012) Dalton Trans 41:636
145. Jagenbrein M, Danopoulos AA, Braunstein P (2015) J Organomet Chem 775:169
146. Raynal M, Pattacini R, Cazin CSJ, Vallee C, Olivier-Bourbigou H, Braunstein P (2009) Organometallics 28:4028
147. Zuo W, Braunstein P (2010) Organometallics 29:5535
148. Zuo W, Braunstein P (2012) Organometallics 31:2606
149. Chianese AR, Mo A, Lampland NL, Swartz RL, Bremer PT (2010) Organometallics 29:3019
150. Chianese AR, Shaner SE, Tendler JA, Pudalov DM, Shopov DY, Kim D, Rogers SL, Mo A (2012) Organometallics 31:7359
151. Chianese AR, Drance MJ, Jensen KH, McCollom SP, Yusufova N, Shaner SE, Shopov DY, Tendler JA (2014) Organometallics 33:457

152. Knapp SMM, Shaner SE, Kim D, Shopov DY, Tendler JA, Pudalov DM, Chianese AR (2014) Organometallics 33:473
153. Schultz KM, Goldberg KI, Gusev DG, Heinekey DM (2011) Organometallics 30:1429
154. Liu X, Braunstein P (2013) Inorg Chem 52:7367
155. Darmawan N, Yang C-H, Mauro M, Raynal M, Heun S, Pan J, Buchholz H, Braunstein P, De Cola L (2013) Inorg Chem 52:10756
156. Iglesias-Siguenza J, Ros A, Diez E, Magriz A, Vazquez A, Alvarez E, Fernandez R, Lassaletta JM (2009) Dalton Trans 8485
157. Huckaba AJ, Cao B, Hollis TK, Valle HU, Kelly JT, Hammer NI, Oliver AG, Webster CE (2013) Dalton Trans 42:8820
158. Schuster EM, Botoshansky M, Gandelman M (2011) Dalton Trans 40:8764
159. Yang L, Krüger A, Neels A, Albrecht M (2008) Organometallics 27:3161
160. Zhang J, Wang Y, Zhao X, Liu Y (2014) Eur J Inorg Chem 975
161. Godoy F, Segarra C, Poyatos M, Peris E (2011) Organometallics 30:684
162. Huynh HV, Lee C-S (2013) Dalton Trans 42:6803
163. Huynh HV, Yuan D, Han Y (2009) Dalton Trans 7262
164. Yuan D, Tang H, Xiao L, Huynh HV (2011) Dalton Trans 40:8788
165. Tu T, Feng X, Wang Z, Liu X (2010) Dalton Trans 39:10598
166. Tu T, Malineni J, Dötz KH (2008) Adv Synth Catal 350:1791
167. Wang Z, Feng X, Fang W, Tu T (2011) Synlett 951
168. Imanaka Y, Hashimoto H, Nishioka T (2014) Chem Lett 43:687
169. Gu S, Xu H, Zhang N, Chen W (2010) Chem Asian J 5:1677
170. Albrecht M (2009) Chem Rev 110:576
171. Pan B, Pierre S, Bezpalko MW, Napoline JW, Foxman BM, Thomas CM (2013) Organometallics 32:704
172. Cross WB, Daly CG, Ackerman RL, George IR, Singh K (2011) Dalton Trans 40:495
173. Wei W, Qin Y, Luo M, Xia P, Wong MS (2008) Organometallics 27:2268
174. Leigh V, Ghattas W, Mueller-Bunz H, Albrecht M (2014) J Organomet Chem 771:33
175. Oulié P, Nebra N, Ladeira S, Martin-Vaca B, Bourissou D (2011) Organometallics 30:6416
176. Jahnke MC, Pape T, Hahn FE (2009) Eur J Inorg Chem 1960
177. Jeffery T (1994) Tetrahedron Lett 35:3051
178. Liao C-Y, Chan K-T, Zeng J-Y, Hu C-H, Tu C-Y, Lee HM (2007) Organometallics 26:1692
179. Cao P, Cabrera J, Padilla R, Serra D, Rominger F, Limbach M (2012) Organometallics 31:921
180. Serra D, Cao P, Cabrera J, Padilla R, Rominger F, Limbach M (2011) Organometallics 30:1885
181. Lu C, Gu S, Chen W, Qiu H (2010) Dalton Trans 39:4198
182. Lee JH, Yoo KS, Park CP, Olsen JM, Sakaguchi S, Prakash GKS, Mathew T, Jung KW (2009) Adv Synth Catal 351:563
183. Sakaguchi S, Kawakami M, O'Neill J, Yoo KS, Jung KW (2010) J Organomet Chem 695:195
184. Chan C-W, Cheng L-K, Che C-M (1994) Coord Chem Rev 132:87
185. Lai S-W, Chan MC-W, Cheung K-K, Che C-M (1999) Organometallics 18:3327
186. Lee C-S, Zhuang RR, Sabiah S, Wang J-C, Hwang W-S, Lin IJB (2011) Organometallics 30:3897
187. Lee C-S, Sabiah S, Wang J-C, Hwang W-S, Lin IJB (2010) Organometallics 29:286
188. Leung SY-L, Lam ES-H, Lam WH, Wong KM-C, Wong W-T, Yam VW-W (2013) Chem Eur J 19:10360
189. Zhang X, Wright AM, DeYonker NJ, Hollis TK, Hammer NI, Webster CE, Valente EJ (2012) Organometallics 31:1664
190. Zhang X, Cao B, Valente EJ, Hollis TK (2013) Organometallics 32:752
191. Tu T, Assenmacher W, Peterlik H, Weisbarth R, Nieger M, Dötz KH (2007) Angew Chem Int Ed 46:6368
192. Tu T, Bao X, Assenmacher W, Peterlik H, Daniels J, Dötz KH (2009) Chem Eur J 15:1853

Rare Earth Pincer Complexes: Synthesis, Reaction Chemistry, and Catalysis

Mikko M. Hänninen, Matthew T. Zamora, and Paul G. Hayes

Abstract The research field surrounding rare earth pincer complexes has reached a stage where a comprehensive review about the reactivity and catalytic behavior of these species is justified. In this contribution, we begin with a brief introduction on common strategies for the preparation of rare earth pincer complexes, continuing with a section devoted to the versatile reactivity observed for this class of compound. Thereafter, several types of compounds are discussed, including extremely reactive hydrides, cationic species, and intriguing scandium imido complexes. Finally, the last portion of this chapter sums up the hitherto reported catalytic studies, including discussions on ring-opening polymerization of cyclic esters, polymerization of olefins and hydroamination reactions, as well as several examples of more infrequently encountered catalytic processes.

Keywords Catalysis · Lanthanides · Pincer ligands · Rare earth metals · Reactivity

Contents

M.M. Hänninen, M.T. Zamora, and P.G. Hayes (✉)
Department of Chemistry and Biochemistry, University of Lethbridge, 4401 University Dr W, Lethbridge, AB, Canada, T1K 3M4
e-mail: p.hayes@uleth.ca

1 Introduction

Although multifunctional pincer ligands have been widely exploited in organometallic transition metal chemistry for almost 40 years [1–7], rare earth pincer complexes have not received nearly as much attention. This paucity may be due to the general synthetic challenges associated with, and the high intrinsic reactivity of, the rare earth elements. However, the evolution of sophisticated experimental techniques and increasing availability of novel starting materials, particularly over the past decade, have paved the way for the preparation of numerous rare earth analogues of transition metal pincer counterparts.

The ubiquitous bis(cyclopentadienyl) moiety dominated early organometallic rare earth chemistry, as other types of ancillary ligands had difficulty protecting the voraciously reactive metals [8]. Given the extreme electropositive nature of the rare earth metals, the most sought-after ancillary properties typically include the ability to preclude Lewis base (e.g., THF) coordination and prevent dimerization/oligomerization, ligand redistribution, and "ate" complex formation. As such, the most prominent rare earth scaffolds generally feature electron-rich donors and substantial steric bulk. Furthermore, the charge of the ligand is of critical importance when considering intended applications as most rare earth metals exist almost exclusively in the +3 oxidation state. Given the electronic and steric variability of pincer ligands, it should be of little surprise that many such frameworks fulfill all of the preceding conditions and have thus become very popular.

The chemistry of pincer ligands with transition metals has been comprehensively surveyed in both the current and previous editions of this book; hence, readers interested in such work are directed to those sources. This contribution, which is the first to specifically address the synthesis, reactivity, and catalytic behavior of rare earth pincer complexes, has been prompted by the recent maturation of this field, such that a thorough review is now warranted. This chapter focuses primarily upon the reactivity and catalytic applications of well-defined and characterized rare earth complexes supported by pincer ancillaries. Hence, scientific contributions that merely describe the synthesis and/or solid-state structures of such species, while noteworthy and significant in their own right, are generally beyond the scope of this review. Furthermore, the extent of this chapter is limited to the definition that pincer ligands must be capable of binding to a metal center (usually in a meridional fashion) via exactly three main group donors. Finally, upon coordination to a metal, a five-membered or larger metallacycle must be formed
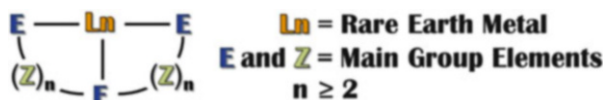
Fig. 1 General definition of a rare earth pincer complex

(Fig. 1). Though not bona fide organometallic, compounds without a metal–carbon bond have been included when they otherwise meet pincer complex criteria and are deemed to be sufficiently important.

2 Preparation of Rare Earth Complexes Supported by Pincer Ligands

Although the emphasis of this chapter is not on the preparation of rare earth metal complexes [2–5], it is worthwhile to briefly address typical metal attachment strategies. Hence, we begin by presenting, in chronological order, the most frequently encountered syntheses, procedures, and starting materials. The latter part of this section introduces the reader to various novel and often unexpected routes to pincer-supported rare earth metal complexes.

2.1 Common Synthetic Routes to Rare Earth Pincer Complexes

Synthetic methods for metal attachment are well known for rare earth and other metals with both pincer and non-pincer ligands. Such chemistry, corresponding reaction mechanisms, and various examples can be found in most inorganic and organometallic chemistry textbooks and, hence, will not be discussed at length. However, because of the overwhelming importance of such methodologies, the four most prevalent approaches for coordinating pincer ligands to rare earth metals are presented in Scheme 1. The advantages and disadvantages of each process are briefly addressed below.

2.1.1 Salt Metathesis

In 1988, Fryzuk synthesized one of the first rare earth pincer complexes by the straightforward salt metathesis reaction of anhydrous YCl_3 with 2 equiv. of $LiN(SiMe_2CH_2PMe_2)_2$ to generate the seven-coordinate monomeric complex $YCl[N(SiMe_2CH_2PMe_2)_2]_2$ [9]. This approach can also be employed with heavier halides, which are often desirable because of the lower reduction potential of the

Salt metathesis

$$LnX_3 + n\ M\mathbf{L} \xrightarrow[-n\ MX]{} \mathbf{L}_n LnX_{(3-n)}$$

Amine elimination

$$Ln(NR_2)_3 + n\ H\mathbf{L} \xrightarrow[-n\ HNR_2]{} \mathbf{L}_n Ln(NR_2)_{(3-n)}$$

Alcohol elimination

$$Ln(OAr)_3 + n\ H\mathbf{L} \xrightarrow[-n\ HOAr]{} \mathbf{L}_n Ln(OAr)_{(3-n)}$$

Alkane elimination

$$LnR_3(THF)_x + n\ H\mathbf{L} \xrightarrow[-n\ HR]{} \mathbf{L}_n LnR_{(3-n)}(THF)_y$$
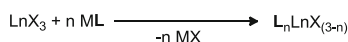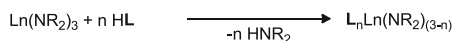
Ln = rare earth metal; M = alkali metal; X = halide
R = bulky alkyl group (e.g. CH$_2$SiMe$_3$)
Ar = bulky aromatic group (e.g. 3-^{t}Bu-5-MeC$_6$H$_2$)
L = monoanionic ancillary ligand; n ≤ 3; x = 2 or 3; y ≤ 3

Scheme 1 The four most commonly encountered rare earth metal (Ln) attachment strategies

corresponding metal complexes, as demonstrated by Evans et al. wherein SmI$_3$ was utilized to prepare chiral samarium complexes [10]. In addition, rare earth tris(borohydrides) Ln(BH$_4$)$_3$(THF)$_3$ can be utilized as a metal source in salt metathesis reactions because the BH$_4^-$ anion usually behaves as a pseudohalide with rare earth metals, although it occasionally takes part in redox reactions (vide infra) [11].

This synthetic methodology has proven exceedingly popular for metal complexes in general and is frequently used, though several other routes to rare earth pincer complexes are also typically employed. The most distinct advantage of this practice is the versatility of the resulting halide complexes. These species can be further reacted with virtually any amide, alkoxide, or alkyl salt to produce a wide range of novel compounds.

2.1.2 Amine Elimination

More than a decade after Fryzuk's first rare earth pincer complex was published, Mashima et al. prepared a series of yttrium pincer complexes, LY(N(SiMe$_3$)$_2$)$_2$ (L = 2,5-bis-[N-(2,6-Me$_2$C$_6$H$_3$)iminomethyl]pyrrolyl), by an amine elimination reaction between a bis(iminomethyl)pyrrolyl ligand and the homoleptic tris(amido) complex Y[N(SiMe$_3$)$_2$]$_3$ (Scheme 2) [12]. Conveniently, this procedure does not require initial conversion of the ligand into a metal salt. Furthermore, the extruded amine often exhibits high vapor pressure and is thus simple to remove from the reaction mixture. One potentially detractive aspect of this strategy, however, is the fact that the resultant product often bears one or more sterically demanding amido groups.
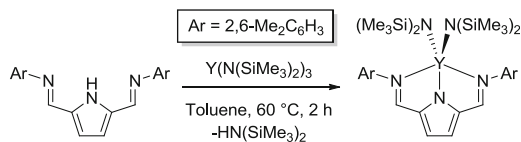
Scheme 2 Preparation of a bis(amido) yttrium complex by amine elimination

2.1.3 Alcohol Elimination

Another interesting, but not broadly utilized, synthetic pathway was introduced by Arnold and co-workers when they made mono- and dinuclear Sm(III) aryloxide complexes [LSm(OAr)(THF)] and [LSm(OAr)]$_2$ (L = 1,1'-S(2-O-3-^{t}Bu-5-MeC$_6$H$_2$)) bearing sulfur-bridged biphenolate ligands via an alcohol elimination protocol (Scheme 3) [13]. With proper aryl substituents, homoleptic rare earth tris(aryloxides) were produced as hydrocarbon-soluble crystalline solids. Such alkoxide ligands are desirable ancillaries in certain catalytic reactions, such as the ring-opening polymerization of cyclic ethers. However, alcohol elimination requires the use of ligands with a relatively acidic proton, and the by-product alcohol is fairly reactive and often difficult to remove (high boiling point and solubility).

2.1.4 Alkane Elimination

Highly reactive (LnR$_3$(THF)$_n$, R = CH$_2$Ph CH$_2$SiMe$_3$, CH(SiMe$_3$)$_2$, CH$_2$SiMe$_2$Ph, etc.) complexes of the rare earth metals, which feature sterically demanding alkyl groups, can be prepared from their trihalide precursors, and while these complexes have been known for many years, it was not until the beginning of the twenty-first century that alkane elimination became a common synthetic strategy for the preparation of organometallic pincer species. In 2003, Anwander et al. reacted Ln(CH$_2$SiMe$_3$)$_3$(THF)$_2$ (Ln = Sc, Y, Lu) trialkyl complexes with tridentate diamide ligands to produce the corresponding monoalkyl complexes LLn(CH$_2$SiMe$_3$)(THF)$_n$ (Ln = Sc, n = 1; Ln = Y, Lu, n = 2; L = 2,6-bis-[N-(2,6-^{i}Pr$_2$C$_6$H$_3$)aminomethyl]pyridine) (Scheme 4) [14].

Since Anwander's pioneering work, this technique has become increasingly popular, and many of the rare earth pincer complexes reported herein have been generated in this manner. Notably, the synthesis and isolation of the requisite trialkyl precursors is difficult, as most of these compounds are prone to decomposition at ambient temperature. Nonetheless, during the past decade, numerous new homoleptic compounds containing Ln–C σ-bonds that range in thermal stability have been reported; this area has recently been thoroughly reviewed [15]. In addition to the relative ease with which many alkane elimination reactions proceed, the released alkane is also inert and often sufficiently volatile to permit facile separation from the metal complex. However, the bulky alkyl group sometimes shuts down subsequent reaction chemistry, and it can be difficult to convert such moieties into other functionalities. A tactful balance is therefore required.
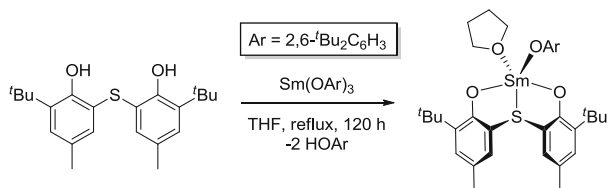
Scheme 3 An example of alcohol elimination for the synthesis of rare earth pincer complexes
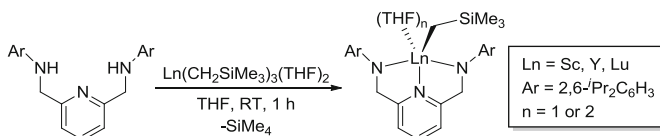
Scheme 4 Synthesis of monoalkyl rare earth pincer complexes by an alkane elimination protocol
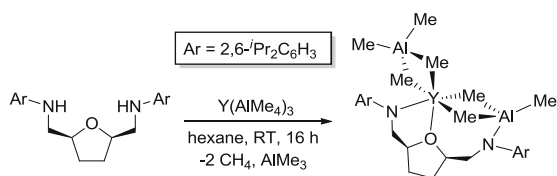
Scheme 5 An example of Ln(AlMe$_4$)$_3$ as a starting material for the synthesis of rare earth pincer complexes

In 2006, Anwander et al. described the use of Ln(AlMe$_4$)$_3$ in the preparation of postlanthanidocene complexes [16]. Similar to rare earth trialkyl compounds, homoleptic tetraalkylaluminate species can be used with proteo ligands in distinct metal attachment reactions to promote alkane elimination and complex formation. These reactions typically lead to heterodinuclear complexes, such as LY(AlMe$_4$)(AlMe$_3$) (L = *cis*-2,5-bis[*N,N*-((2,6-^{i}Pr$_2$C$_6$H$_3$)amino)methyl]tetrahydrofuran) (Scheme 5) with methane and trimethylaluminum eliminated as by-products.

2.2 Reactions of Metal Complexes That Produce Pincer Complexes

Although well-defined synthetic routes are normally utilized for generating metal complexes, occasionally unprecedented reactions can afford unique or unusual products that would be difficult or even impossible to prepare by conventional procedures. The following section is intended to showcase atypical reactions wherein transient rare earth complexes bearing non-pincer ligands can be transformed into species supported by a pincer ancillary.
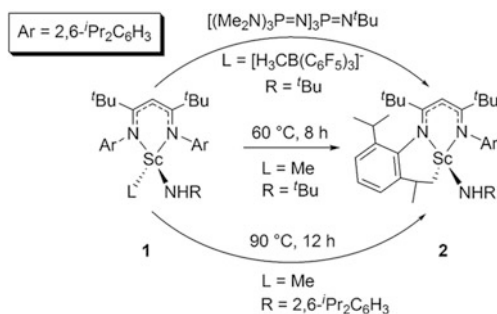
Scheme 6 Cyclometalation of β-diketiminato supported scandium complexes that leads to pincer-type complexes
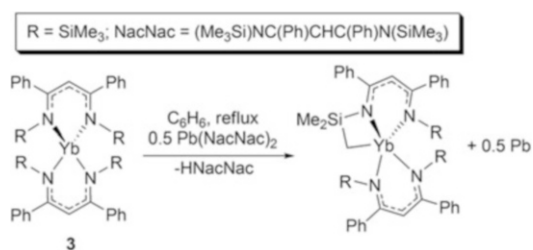
Scheme 7 Oxidative cyclometalation of a homoleptic Yb(II) complex

β-Diketiminate (NacNac) ligands are particularly popular auxiliaries that can form complexes with metals spanning the periodic table [17, 18]. Hence, numerous rare earth β-diketiminates have been prepared, some of which exhibit interesting reactivity patterns that produce pincer-type complexes relevant to this review. Most of these reactions begin with a C–H bond activation event, one of the most important and studied reactions in organometallic chemistry [19, 20].

Piers et al. were among the first to prepare rare earth metal complexes bearing β-diketiminato and related ligands, and it was quickly discovered that such species are prone to pincer-forming cyclometalation pathways [21]. In one particularly intriguing example, cyclometalated **2**, prepared by thermolysis of amido-methyl complex $LSc(CH_3)NHAr$ $(L = (Ar)NC(^tBu)CHC(^tBu)N(Ar)$, $Ar = 2,6\text{-}^iPr_2C_6H_3$; $R = {}^tBu$, or $2,6\text{-}^iPr_2C_6H_3)$, **1**, at temperatures between 60°C and 90°C (Scheme 6) [22, 23], was found to react with 4-N,N-dimethylaminopyridine (DMAP) to afford a remarkable imido complex $LSc=NAr \cdot DMAP$ [23]. Cyclometalated complex **2** is also formed upon reaction of complex **1** with a bulky phosphazene base $[(Me_2N)_3P=N]_3P=N^tBu$ [24]. Similar C–H bond activation occurs in the homoleptic Yb(II) NacNac complex $Yb(L)_2$ $(L = (Me_3Si)NC(Ph)CHC(Ph)N(SiMe_3))$, **3**, when it is heated, or if it is in the presence of either the analogous Pb(II)NacNac species PbL_2 or $Pb(N(SiMe_3)_2)_2$ (Scheme 7) [25].

Closely related phosphinimine-amido complexes studied by both Cui and co-workers [26] and Piers et al. [27] also revealed prevalent C–H bond activation
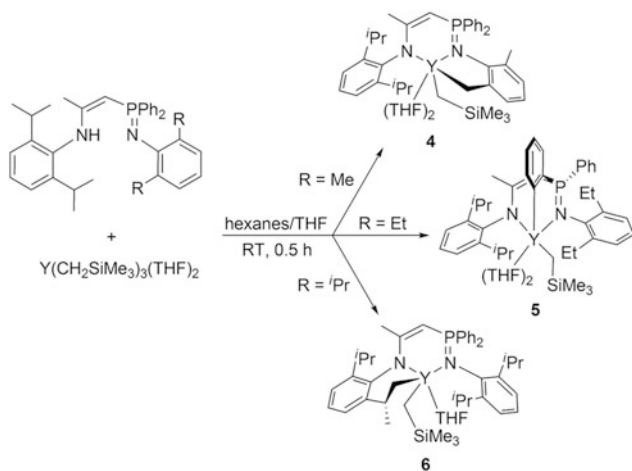
Scheme 8 Cyclometalation of phosphinimine-amido supported yttrium complexes
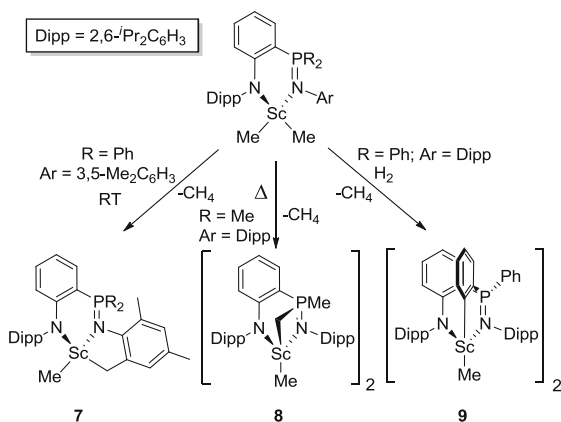
Scheme 9 Synthesis of scandium pincer complexes via ligand cyclometalation

chemistry. In both of these studies, cyclometalation occurred at multiple ligand sites, depending on the substituents and/or conditions of the specific reaction. In Cui's work, methyl, ethyl, and *iso*propyl substituents on the phenyl ring bound to the phosphinimine nitrogen triggered different cyclometalation behaviors upon complexation. Notably, when substituted with methyls, metalation of one of these groups occurred, affording the monoalkyl species **4**. However, the presence of ethyl or *iso*propyl substituents resulted in the activation of other moieties (i.e., *P*-phenyl, **5**, and *N*-2,6-^{i}Pr$_2$C$_6$H$_3$ (Dipp), **6**, groups, respectively) (Scheme 8).

Ligand substitution also played a key role in cyclometalation reported by Piers and co-workers (Scheme 9) [27]. For example, at ambient temperature, the activation of the *N*-mesityl group produced cyclometalated L^{1}ScMe (L^1 = 1-(NDipp)-2-
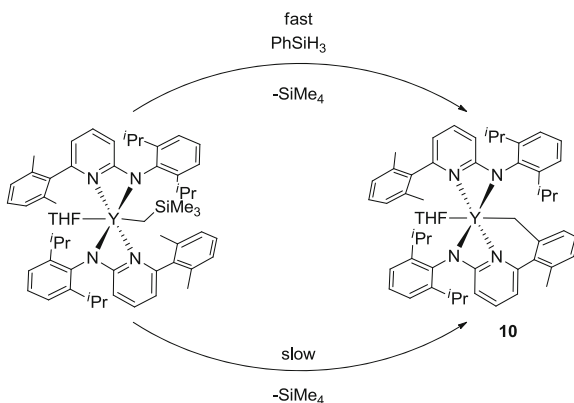
Scheme 10 Synthesis of complex **10**

(PR_2=NAr)C_6H_4; Dipp = 2,6-$^iPr_2C_6H_3$; R = Ph; Ar = 2,4-Me_2-6-$CH_2C_6H_2$), **7**. Conversely, complexes bearing the more sterically demanding 2,6-$^iPr_2C_6H_3$-substituted ligands required heating or the addition of dihydrogen before cyclometalation was observed. With these complexes, metalation occurred at the P–R (R = Me or Ph) group instead of the phosphinimine N-aryl moiety. Cyclometalation of PMe groups was rapid at 65°C to give L^2ScMe ($L^2 = 1$-(NDipp)-2-(PRR'=NDipp)C_6H_4; R = Me; R' = CH_2), **8**, whereas the analogous phenyl-substituted species, **9**, only cyclometalated when dihydrogen was added. The latter reaction presumably proceeds through a putative scandium hydride intermediate.

Substantial rates of C–H activation were also observed for the yttrium complex $L_2YCH_2SiMe_3$ (L = 2,6-($^iPr_2C_6H_3$)-[6-(2,6-dimethylphenyl)pyridin-2-yl]amine) which readily cyclometalated to give complex **10** (Scheme 10). Notably, the rate of cyclometalation was approximately 500 times greater upon the addition of 1 equiv. of $PhSiH_3$ [28]. Trifonov, Giambastiani, and co-workers observed similar pincer forming cyclometalation reactivity when related bidentate amidopyridinate ligands were reacted with trialkyl yttrium species. Interestingly, these complexes were active in ethylene polymerization; hence, a more detailed discussion is presented in Sect. 4 [29].

Cyclometalation reactions affording pincer complexes have also been reported for PN ligated lutetium and lanthanum complexes. Specifically, Cui et al. recently reported the metalated complex LLu(NCN)(THF) (L = 2-Me-6-CH_2-^iPrNC=N^iPr-C_6H_3-NCH(Ph)$CH_2P(Ph)_2$; NCN=$^iPrNC(CH_2SiMe_3)N^iPr$), **11**, which was postulated to have formed by an initial C–H activation of an NAr methyl, followed by the reaction with N,N'-diisopropylcarbodiimide (Scheme 11, top) [30]. Meanwhile, the bis(aminophosphide) lanthanum iodide complex [(CH(SiMe$_3$)$_2$)(C$_6$H$_4$-2-CH_2NMe_2)P]$_2$LnI was converted to the cyclometalated complex **12**, upon reaction with organopotassium salts (Scheme 11, bottom) [31]. Presumably, the expected
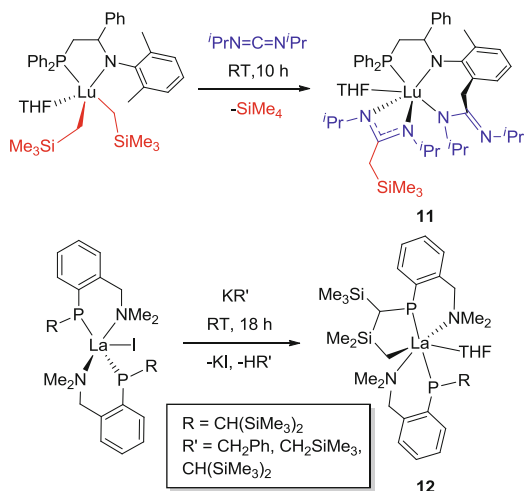
Scheme 11 Pincer complexes generated by C–H activation reactions in rare earth complexes supported by PN-donor ligands

organometallic intermediate formed but decomposed at a rate greater than its formation (i.e., $k_{decomposition} > k_{formation}$).

Cyclometalation of rare earth complexes is a prevalent decomposition pathway; hence, those species that bear bidentate scaffolds can give rise to unusual pincer-type complexes. These compounds tend to be particularly intriguing when they are formed in the presence of other reagents, such as carbodiimides, as they provide interesting options for creative ligand design. However, cyclometalation is customarily considered detrimental since it is typically undesirable and the resulting complexes are generally less reactive and/or less useful in targeted chemical transformations.

3 Reactivity and Chemical Transformations Induced by Rare Earth Pincer Complexes

The general reactivity of a metal complex is exceedingly important if one wishes to address the stability of the complex or survey potential applications. Since rare earth pincer chemistry is still quite new compared to the wealth of information on transition metal variants, the reaction chemistry of such complexes remains of special interest. In the following paragraphs, we review a wide variety of stoichiometric reactions reported to take place with rare earth pincer complexes. Judiciously selected examples were collected to compile this section, which is divided into three different subsections: stoichiometric bond activation reactions (**3.1**), alkane elimination and alkyl migration (**3.2**), and ligand metathesis reactions (**3.3**).
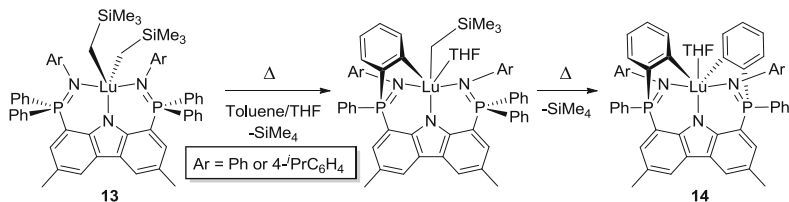
Scheme 12 Intramolecular decomposition of **13** to doubly cyclometalated complex **14**

3.1 Stoichiometric Bond Activation Reactions

3.1.1 C–H Bond Activation

The making and breaking of bonds are obviously central to synthetic chemistry; hence, the ability of a rare earth pincer complex to activate various types of bonds is of great importance and of vital significance for catalytic applications. The intrinsic reactivity of rare earth complexes can sometimes promote facile reaction at sp^2 and sp^3 C–H groups that are often considered to be quite inert. The intramolecular activation of C–H bonds generally leads to cyclometalated species that can be relevant to various catalytic transformations [32, 33]. These complexes also serve as excellent platforms from which unique bonding and reactivity patterns can be studied [20].

Ligand architecture has proven to be a determining factor as to where specific cyclometalated species reside on the reactivity spectrum, ranging from completely inert to transient intermediates that cannot be isolated. For example, when using a sterically demanding bis(phosphinimine) pincer ligand, Hayes et al. prepared lutetium dialkyl complexes $LLu(CH_2SiMe_3)_2$ (L = 1,8-$(Ph_2P=NAr)_2$-3,6-dimethylcarbazolide; Ar = Ph, 4-^{i}PrPh), **13**, which undergo a rapid two-stage metalation of the phosphine phenyl groups at temperatures above 0°C, to ultimately produce the doubly cyclometalated compound $LLu(THF)$ (L = 1,8-$(Ph(C_6H_4)P=NAr)_2$-3,6-dimethylcarbazolide), **14** (Scheme 12) [34].

Later on, the reactivity of complex **14** was probed, and it was found that methyl- or isopropyl-substituted anilines induce metallacycle ring opening of both metalated phenyl groups to generate the bis(anilide) products $LLu(NHAr)_2$ (Ar = 2,4,6-$Me_3C_6H_2$, 2,4,6-^{i}Pr$_3C_6H_2$). Notably, monoanilide products were not observed in these reactions, regardless of what experimental conditions and quantity of aniline were utilized. Conversely, when the more bulky 2,4,6-^{t}Bu$_3C_6H_2NH_2$ was employed, metallacycle ring opening was limited to only one of the *ortho*-metalated *P*-phenyl groups, leading to exclusive formation of the monoanilide complex $LLu(NHMes^*)$ (L = 1-$(Ph_2P=NAr)$-8-$(Ph(C_6H_4)P=NAr)$-3,6-dimethylcarbazolide; Ar = Ph, 4-^{i}PrPh; Mes* = 2,4,6-^{t}Bu$_3C_6H_2$), **15** (Scheme 13). Intriguingly, this species undergoes an unusual rearrangement to afford the *N*-aryl metalated isomer **15′**. Deuterium labeling and kinetic studies were conducted, establishing that this transformation does not involve an imido intermediate [35].
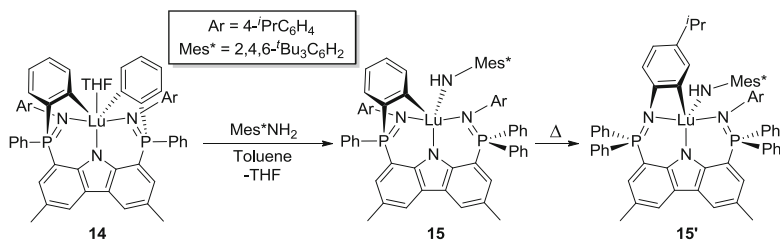
Scheme 13 Metallacycle ring-opening reaction of **14** with 1 equiv. of 2,4,6-^{t}Bu$_3$C$_6$H$_2$NH$_2$

As previously mentioned, cyclometalated rare earth complexes can be reactive species that are observed or postulated to be reaction intermediates. Hence, cyclometalated molecules can lead to unanticipated reactivity. Diaconescu and co-workers studied monoalkyl yttrium and lutetium complexes supported by a pyridine diamide scaffold 2,6-(CH$_2$N(2,6-^{i}Pr$_2$C$_6$H$_3$)$_2$)NC$_5$H$_3$ (L) [36]. Depending on the substrate, these complexes reacted with aromatic *N*-heterocycles via a diverse series of C–H activation, C–C coupling, or heterocycle dearomatization reactions. Mechanistic studies revealed that these reactions proceed through cyclometalated intermediates. Although both lutetium and yttrium complexes generally behaved in a similar fashion, considerable differences in reaction rates were observed. Interestingly, the reaction between LYCH$_2$Ar(THF) (Ar = Ph), **16**, and acridine afforded the alkyl migrated product LY(R)(THF) (R = 9-CH$_2$Ph-9-*H*-acridine), **18**, in which the benzyl group was transferred to the 9-position of acridine. However, the same reaction with lutetium complex **17** formed the stable cyclometalated compound **19** (Scheme 14).

As demonstrated by Shen et al., cyclometalation during metal attachment can also lead to new and unexpected ligand frameworks [37]. The amine elimination reaction between Ln(N(SiMe$_3$)$_2$)$_3$ (Ln = Y or Yb) and a salicylaldimine ligand (HL = 3,5-^{t}Bu$_2$-2-(OH)-C$_6$H$_2$CH=N-8-C$_9$H$_6$N) gave complex **20**, which was supported by a trianionic NOO-type ligand (Scheme 15). Complex **20** was hypothesized to have formed from the bis(ligand) species L$_2$LnN(SiMe$_3$)$_2$, **21**, which presumably undergoes cyclometalation of a ligand quinoline ring, **21′**, followed by subsequent nucleophilic attack by the metalated carbon on the imine group of the remaining monoanionic ligand. Complex **21** was independently prepared by slow addition of a toluene solution of HL onto Ln(N(SiMe$_3$)$_2$)$_3$ at −50°C. Heating **21** in THF at 40°C also produced complex **20**, thereby further substantiating the proposed mechanism.

Although C–H bond activation usually leads to well-defined cyclometalated products, in certain occasions, it can create a rigid framework that prevents intramolecular metallacycle formation. In a recent report, Chen et al. prepared scandium, yttrium, and lanthanum complexes of a β-diketiminate-derived pincer ligand that bears a pendant pyridyl donor (Scheme 16) [38]. When Sc(CH$_2$SiMe$_3$)$_3$(THF)$_2$ was allowed to react with the proteo ligand at ambient temperature, the expected dialkyl complex LSc(CH$_2$SiMe$_3$)$_2$ (L = CH$_3$C(NDippN)CHC(CH$_3$)-(NCH$_2$CNC$_5$H$_4$)), **22**, formed, but when the larger metal yttrium was utilized, an
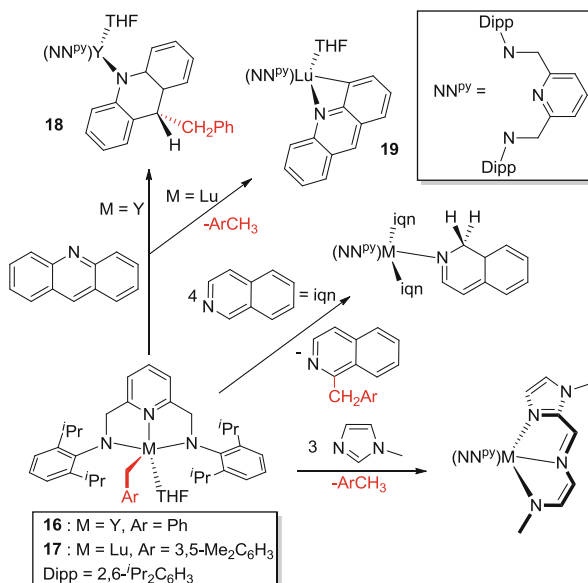
Scheme 14 Examples of C–H activation, C–C coupling, and heterocycle dearomatization
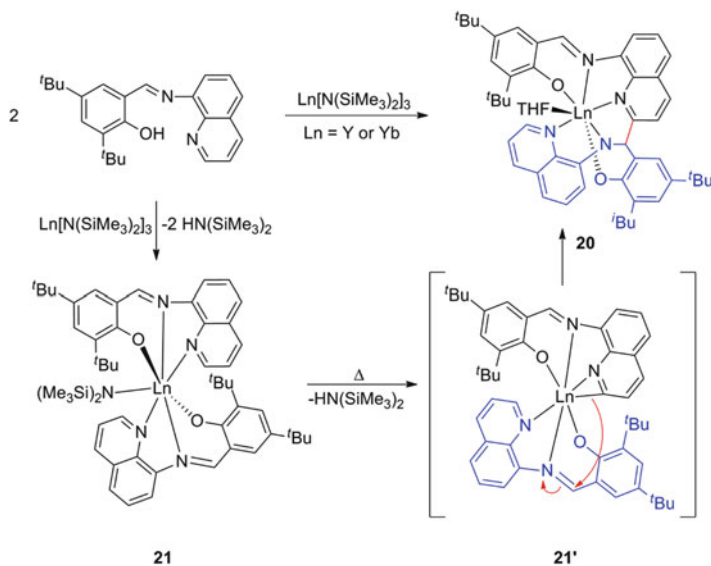
Scheme 15 Conversion of a monoanionic ligand into a macrocyclic trianionic framework via a putative cyclometalated intermediate
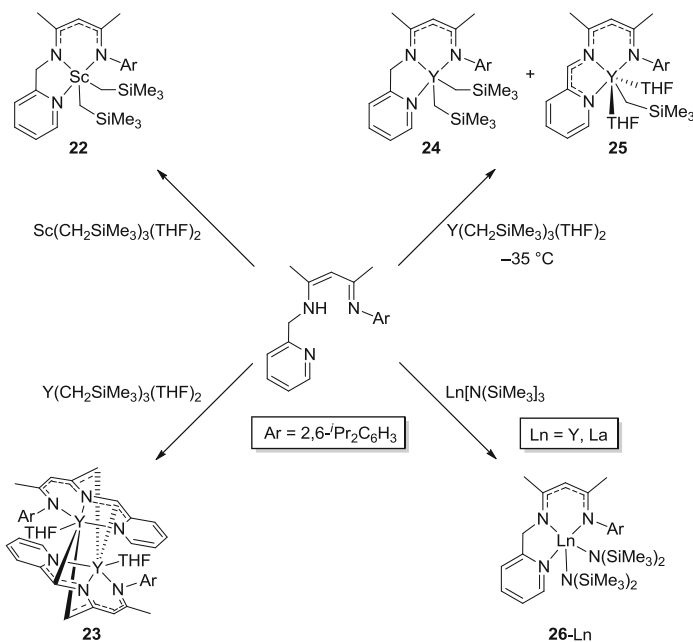
Scheme 16 Rare earth complexes supported by monoanionic, dianionic, and trianionic forms of a β-diketiminate-based pincer ligand

unusual dinuclear complex, **23**, which features two trianionic intermolecularly cyclometalated ligands, prevailed. When the temperature was lowered to −35°C, the reaction generated a mixture of yttrium complexes supported by either mono- or dianionic versions of the β-diketiminate ancillary, **24** and **25**, respectively. However, when $Ln[N(SiMe_3)_2]_3$ (Ln = Y, La) was used as the metal source, even the ambient temperature reaction gave the desired bis(amide) complexes $LLn(N(SiMe_3)_2)_2$, **26**-Ln.

3.1.2 Hydride Complexes: Formation and Reactivity

Metal hydrides are another type of influential complex prevalent in organometallic transition metal chemistry and homogenous catalysis [39, 40]. By comparison, non-Cp rare earth hydride complexes are relatively scarce [8, 41], and thus, the reports of molecules bearing pincer-type ligands are even less common. Nonetheless, in recent years, numerous novel polyhydride species have been reported [42], and perhaps unsurprisingly, many demonstrate unique reactivity and, hence, potential for catalysis [43, 44].

The activation of Si–H bonds by oxidative addition of silanes is a well-established synthetic strategy for preparing transition metal hydride species.
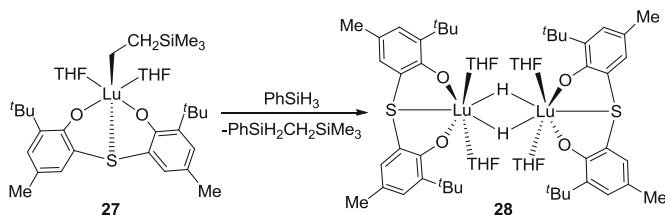
Scheme 17 Preparation of rare earth pincer supported hydride complexes **28**-Ln

However, since the majority of rare earth metals exist predominantly in the +3 oxidation state, they do not readily participate in redox reactions with silanes. Regardless, rare earth alkyl complexes typically react with silanes by σ-bond metathesis pathways to conveniently afford hydride species. In addition, hydrogenolysis reactions between rare earth alkyl complexes and H_2 also serve as a viable route to distinct polyhydride complexes [43].

Early examples of rare earth hydrides supported by pincer-type ligands were reported by Okuda and co-workers in 2007 [45]. The lutetium complex $LLu(CH_2SiMe_3)(THF)_2$ (L = 2,2′-thiobis(6-*tert*-butyl-4-methylphenolate)), **27**, reacted with $PhSiH_3$ to form dimeric hydride-bridged $[LLu(\mu\text{-}H)(THF)_2]_2$, **28** (Scheme 17). Bis(phenolate) ligated **28** readily reacted with phenyl acetylene (PhC≡CH) or benzophenone (Ph_2CO) at ambient temperature to form the corresponding insertion products. In addition, preliminary catalytic studies showed that in the presence of ^{i}PrOH complex, **27** exhibited modest activity as a catalyst for the ring-opening polymerization of L-lactide. Shortly thereafter, Sc, Y, and Ho derivatives of **27** were synthesized and their reactivity toward phenyl silane was studied. Unfortunately, the holmium complex **28**-Ho was the only isolable hydride species [46].

In late 2009, Giambastiani and Trifonov and Cui et al. reported similar cyclometalated rare earth complexes supported by amidopyridinate and anilido-phosphinimine ligands, respectively. They studied the utility of such compounds as precursors to rare earth hydrides [47, 48]. Although reactions with H_2 were not successful, the groups of Giambastiani and Trifonov isolated and characterized well-behaved dinuclear hydride-bridged yttrium complexes **29** and **30** via the reaction between the metalated monoalkyl complexes and phenylsilane (Scheme 18). Notably, the Y–C_{aryl} metallacycle appears inert, as it remained intact in all reported reactions. Unfortunately, preliminary investigations indicated these compounds were only modestly active catalysts for the polymerization of ethylene.

Cui and co-workers also attempted to prepare yttrium hydride species by the reaction of $LY(CH_2SiMe_3)(THF)$ (L = (2,6-^{i}Pr$_2$C$_6$H$_3$)NC$_6$H$_4$PPhC$_6$H$_4$N(2,4,6-C$_6$H$_2$Me$_3$), **31**, with phenyl silane [48]. In this case, the isolated methoxido-bridged dinuclear product, $[LY(\mu\text{-}OMe)]_2$, **32**, is the result of unpredicted C–O bond activation of dimethoxyethane (DME) (Scheme 19). It was proposed that the reaction mechanism proceeds via a transient terminal hydride intermediate, although the authors were unable to isolate such a species. However, in situ studies
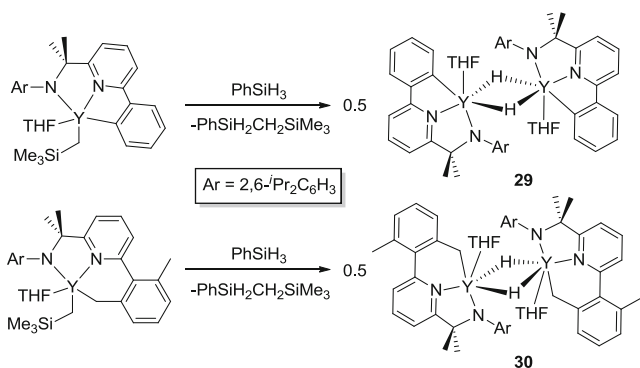
Scheme 18 Formation of yttrium dihydride complexes stabilized by a cyclometalated amidopyridinate ligand
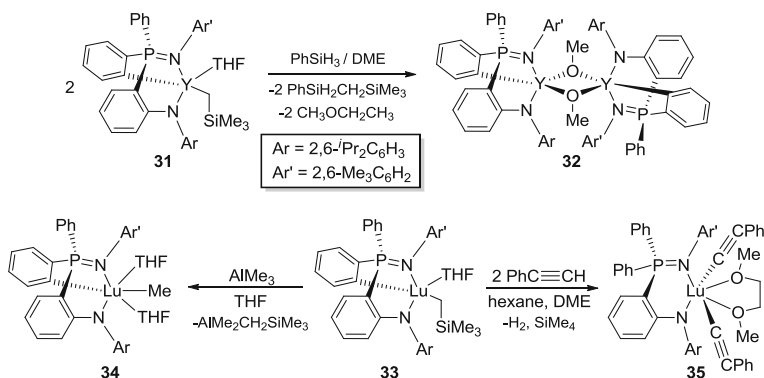
Scheme 19 Reaction of Y and Lu anilido-phosphinimine complexes with PhSiH₃, PhC≡CPh, and AlMe₃

with isoprene afforded a new compound identified as the η^3-pentenyl yttrium complex $LY(\eta^3$-$CH_2C(CH_3)CHCH_3)(THF)$. The solid-state structure of the pentenyl fragment suggested that an yttrium hydride species reacted with one molecule of isoprene via 1,4-addition. The lutetium analogue, **33**, of complex **31** reacted with $AlMe_3$ to produce the corresponding lutetium methyl complex **34**, again with the metalated Lu–C$_{aryl}$ linkage intact. Conversely, the addition of phenylacetylene cleaved the metallacycle bond and gave the bis(alkynyl) lutetium complex $LLu(C≡CPh)_2(DME)$, **35** (Scheme 19).

Shortly after the work of Gambastiani, Trifonov, and Cui, Chen et al. reported the synthesis and structure of dinuclear yttrium anilido hydride complexes **36** which exhibit a rich reaction chemistry with various unsaturated substrates (Scheme 20) [49]. Specifically, dinuclear species **36** reacts readily with a versatile selection of small molecules to give the expected Y–H addition products in good yields. Notably, no reaction was observed with the robust Y–N$_{anilido}$ bond.
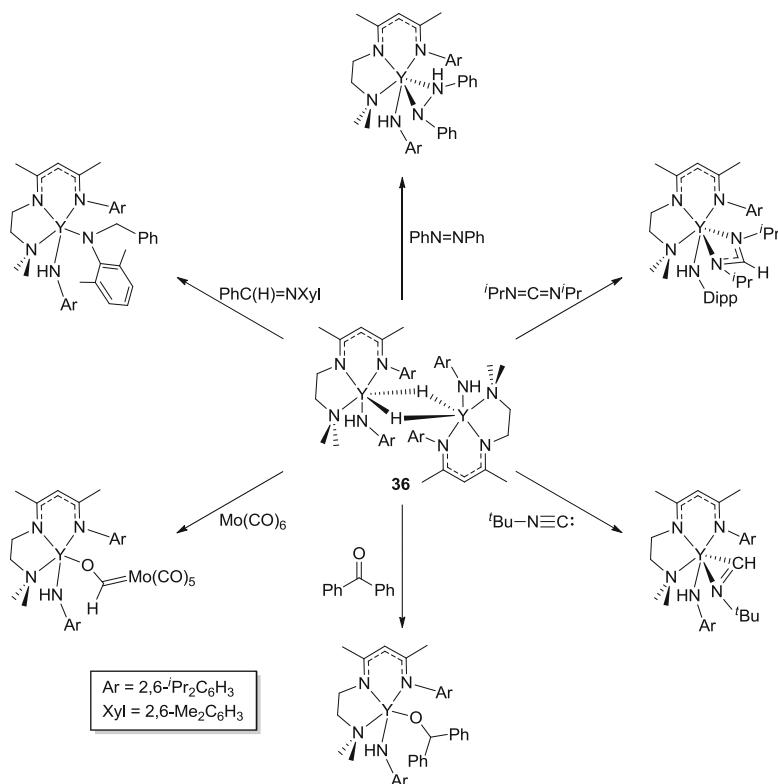
Scheme 20 Reactivity of hydride-bridged dinuclear yttrium anilido complexes **36** toward unsaturated substrates

More recently, Chen et al. extended the scope of dihydride **36** to reactions with phosphine oxides and sulfides [50]. Depending on the substrate, diverse reactivity patterns including C–P, C–H, or P–S bond cleavage was observed (Scheme 21). Furthermore, the reaction of **36** with $Ph_3P=O$ gave the first example of a rare earth diorganophosphinoyl complex via C–P bond cleavage.

Molecular rare earth polyhydride complexes having hydride-to-metal ratios larger than 1 have shown interesting and even unprecedented reactivity [43, 44]. Since the polyhydrides generally form as robust, polynuclear clusters, bulky ancillaries are often used to restrict the nuclearity and stabilize the resultant compounds.

Hou and co-workers demonstrated that hydrogenolysis of dialkyl yttrium and lutetium complexes **37**, which bear the rigid bis(phosphinophenyl)amido ligand, with H_2 produced structurally novel trinuclear hexahydrides **38** (Scheme 22). These complexes, upon the addition of $[NEt_3H][BPh_4]$ at ambient temperature, can be converted into the cationic pentahydrides **39** in high yields [51]. In addition, if the original hydrogenolysis reaction is conducted in the presence of 0.5 equiv. of $[NEt_3H][BPh_4]$, dinuclear trihydride complexes prevail.
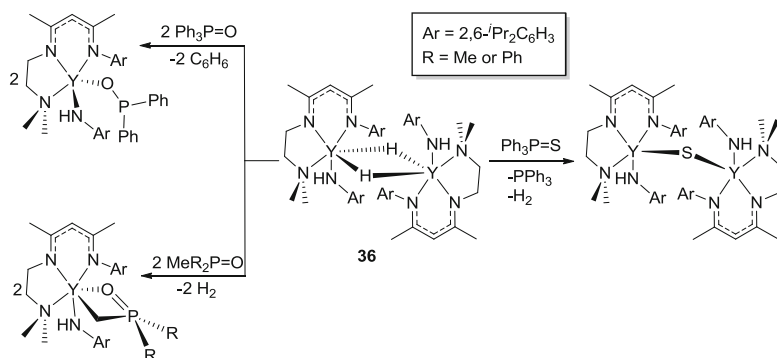
Scheme 21 Reaction of **36** with phosphine oxides and sulfides
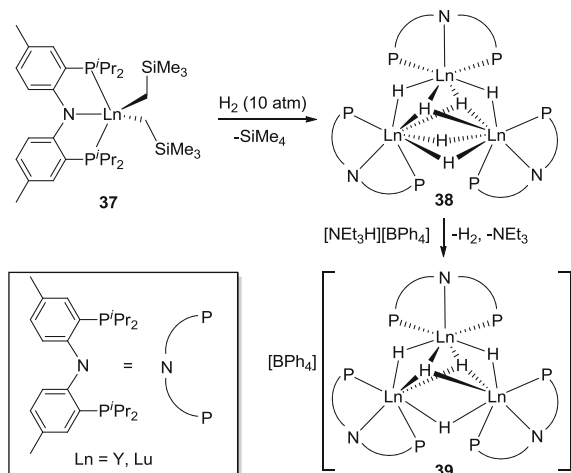
Scheme 22 Synthesis of hexahydride **38** and cationic **39**

A related neutral pentahydride species **40**, prepared by the hydrogenolysis of a bis(pyrazolyl)carbazole lutetium complex (Scheme 23), was recently reported by our group [52]. Unlike complex **38**, the putative hexahydride complex was transformed into the pentahydride variant upon C–H bond activation of one of the pyrazole donors.

3.1.3 Metal Complexes with Multiply Bonded Ligands

Despite the wide range of applications found for countless transition metal and actinide complexes that bear terminal multiply bonded ligands [53–55], rare earth counterparts of this type of complex are scarce. In fact, only three structurally characterized complexes containing terminal, *unsupported* (monodentate) multiply
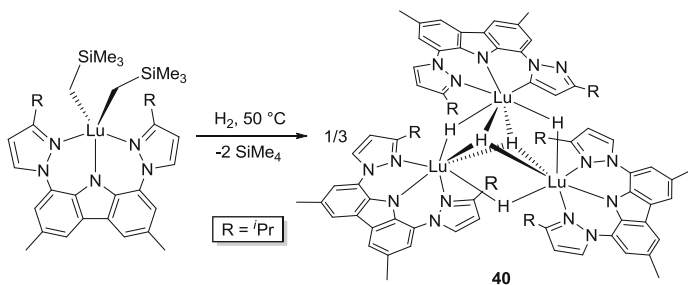
Scheme 23 Hydrogenolysis of a bis(pyrazolyl)carbazole lutetium dialkyl complex
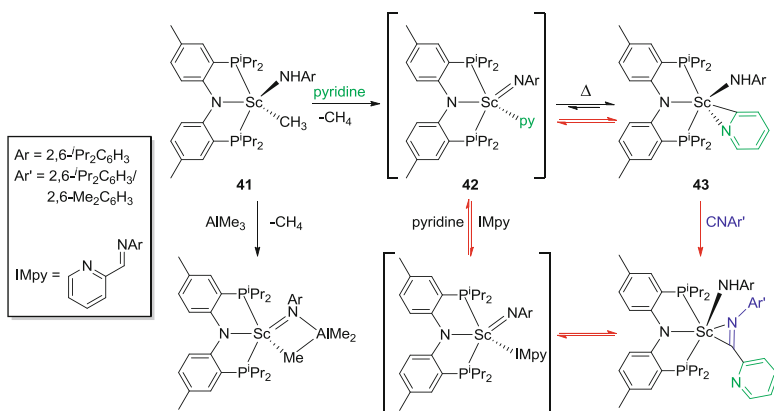
Scheme 24 Formation and reactivity of terminal scandium imido **41** and synthetic cycle for C–H activation and functionalization of pyridines (marked with *red arrows*)

bound main group element fragments have been reported to date [56, 57]. Notably, all of these examples are scandium(III) imido species supported by pincer-type or closely related ligands. In addition, Piers and colleagues isolated and spectroscopically characterized a scandium NacNac complex that exhibited reactivity which could be attributed to a terminal imido functionality [23]. Furthermore, elegant mechanistic studies have been reported that demonstrate the presence of Sc=NR-containing species in solution (vide infra).

Initial evidence for the formation of a terminal scandium imido group was delivered by Mindiola et al. in 2008. Alkane elimination from the alkyl amido complex LSc(Me)(NHAr) (L = N[2-P^{i}Pr$_2$-4-Me-C$_6$H$_3$]$_2$, Ar = 2,6,-^{i}Pr$_2$C$_6$H$_3$), **41**, purportedly afforded the transient imido intermediate LSc=NAr(py), **42**. The observation of intermolecular C–H activation of pyridine and benzene, as well as the isolation of an AlMe$_3$ trapped derivative, provided a strong argument for the presence of a Sc=NR species in the reaction mixture (Scheme 24) [58]. Later on, Mindiola reported that a scandium pyridyl-anilide compound LSc(NHAr)-(η^2-NC$_5$H$_4$), **43**, and an alleged pyridine adduct of an imido complex **42** were related

a)

Ar = 2,6-^{i}Pr$_2$C$_6$H$_3$
R = Me or CH$_2$SiMe$_3$
L = Lewis base, x = 1 or 2

b)

44   **45**   **46**
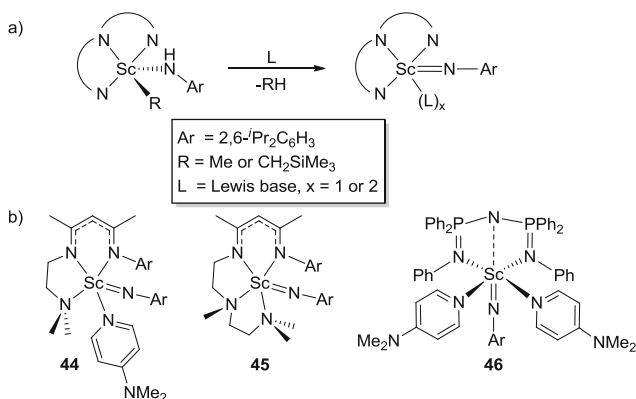
Scheme 25 (**a**) General route for the synthesis of LSc=NR complexes. (**b**) Schematic presentation of structurally characterized rare earth terminal imido complexes

by an interesting tautomeric equilibrium. As a result, his group capitalized on this process in order to facilitate the stoichiometric and catalytic functionalization of pyridines with isonitriles, establishing an atom economical route to mono- and bis(imino)-substituted pyridines (Scheme 24) [33].

In 2010, a seminal contribution by Chen et al. reported the first structurally characterized rare earth species bearing a terminal imido group LSc=NAr(DMAP) (L = MeC(NDippH)CHC(Me)(NCH$_2$CH$_2$NMe$_2$)); DMAP = 4-dimethylamino-pyridine; Dipp = 2,6-^{i}Pr$_2$C$_6$H$_3$), **44**. The scandium complex was prepared via methane elimination from the alkyl-amido precursor upon the introduction of the strongly coordinating base DMAP (Scheme 25) [59]. Shortly after, Chen and co-workers utilized a modified ligand framework with a pendant dimethylamino group that promoted alkane elimination in a similar fashion to DMAP, except it produced an imido complex (LSc=NDipp (L = MeC(DippNH)CHC(Me) (NCH$_2$CH$_2$N(Me)CH$_2$CH$_2$NMe$_2$)), **45**) devoid of coordinated external base [60]. The third example of a structurally characterized terminal rare earth imido complex was reported 3 years later, when Cui et al. synthesized the first hexacoordinate Sc=NR species, LSc=NDipp(DMAP)$_2$ (L = N(Ph$_2$P=NPh)$_2$), **46** [57].

Exploratory experiments of the scandium imido complex **44** with CuI and [M(COD)Cl]$_2$ (M = Rh, Ir) revealed intriguing chemistry at the imido group [61]. More specifically, the nucleophilic nitrogen coordinated to the Cu(I) cation of CuI to form the imido-bridged heterodinuclear complex LSc=NDipp(CuI)(DMAP) (L = MeC(NDipp)CHC(Me)(NCH$_2$CH$_2$NMe$_2$)), **47** (Scheme 26). Although reaction of **44** with [M(COD)Cl]$_2$ (M = Rh, Ir) released one molecule of DMAP which hampered the purification of the metal-containing products, the addition of **45** to [M(COD)Cl]$_2$ proceeded cleanly to one product after 1 h at ambient temperature. An X-ray diffraction study indicated that the electrophilic Sc center had abstracted a chloride anion from [M(COD)Cl]$_2$ and the resultant [M(COD)]$^+$ fragment coordinated to the aryl ring of the imido ligand, ultimately affording the unusual scandium–rhodium/iridium mixed metal species LSc=N(η^n-Dipp)M(COD) (M = Rh, n = 4; Ir,
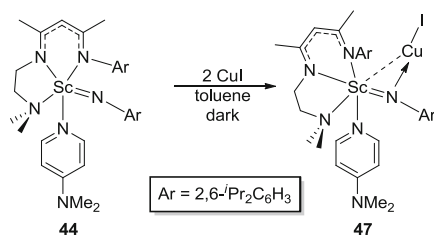
Scheme 26 Reactivity of complex **44** with CuI
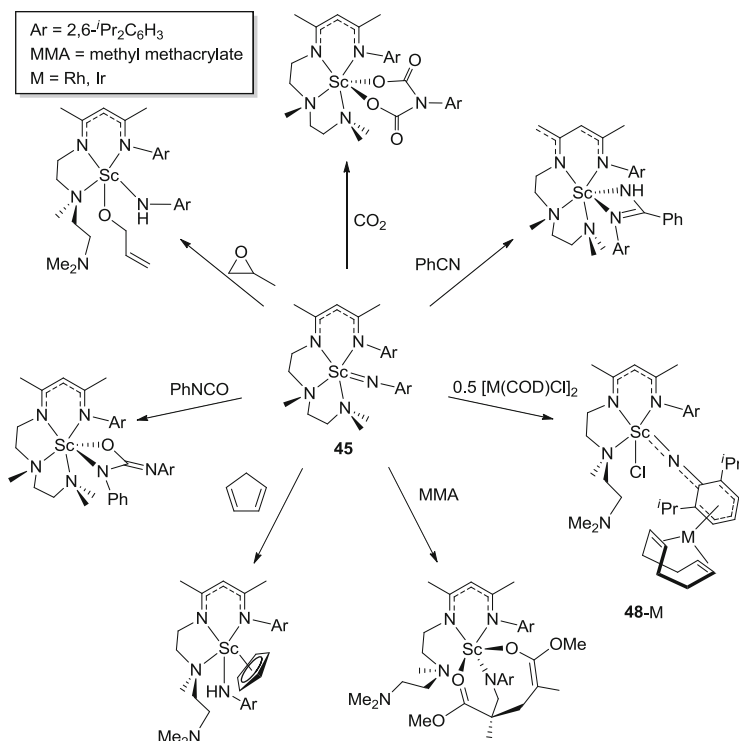
Scheme 27 Reactivity of imido **45** with various unsaturated substrates and transition metal complexes

$n = 3$–5; COD $= 1,5$-cyclooctadiene), **48**-M (Scheme 27). In addition to the remarkable structural features of the preceding complexes, **48**-Ir exhibited promising performance as an alkyne hydroboration catalyst.

After the first reports implicating the accessibility of rare earth imido species, the field flourished, confirming the expected versatility of this kind of complex. For example, Chen et al. demonstrated that elemental selenium reacted readily with Sc=NR fragments. Depending on the ancillary ligand, selenolation of one of the sp^2 aromatic or sp^3 NMe$_2$ carbons in DMAP was observed. Instead of the relatively

common activation of a coordinated DMAP C–H bond, the selenations were proposed to proceed through an unusual Sc–N–Se ring, formed upon [2 + 1] cyclo-addition of a Se atom to the Sc=N double bond [60]. In the follow-up paper, Chen et al. surveyed the cycloaddition chemistry of complex **45** with a wide selection of unsaturated substrates (Scheme 27) [62]. The imido functionality readily reacted with CO_2, benzonitrile (PhCN), methyl methacrylate (MMA), and phenyl isocya-nate (PhNCO) through [2 + 2] or [2 + 4] cycloadditions, highlighting the nucleophi-licity of the nitrogen atom but also the notable Lewis acidity of the Sc(III) center. The cycloadditions were often followed by subsequent reaction chemistry, such as Michael additions or isomerizations. Furthermore, imido complex **45** undergoes hydrogen transfer with cyclopentadiene and propylene oxide, again demonstrating the proton acceptor and ring-opening capability of the complex.

In addition to C–H bond activations, complex **45** also reversibly activated the Si–H bond of phenylsilane to give the corresponding scandium anilido hydride complex $LSc(H)[N(Dipp)(SiH_2Ph)]$ (L = MeC(NDipp)CHC(Me)-$(NCH_2CH_2NMe_2)$), **49**, which undergoes a rapid σ-bond metathesis process between the Sc–H and Si–H bonds of phenylsilane (demonstrated by deuterium-labeling experiments) [63]. The terminal hydrido complex **49** was not isolable per se, but upon trapping with diphenylcarbodiimide, a stable scandium anilido amidinate, $LSc[N(Dipp)(SiH_2Ph)](PhNCHNPh)$, was identified and structurally characterized. Furthermore, preliminary catalytic experiments showed that a 5 mol% loading of imido complex **45** selectively catalyzed the conversion of *N*-benzylidenepropan-1-amine to the corresponding monoaminosilane in 2 h at 50°C.

Recently, Chen and co-workers utilized **45** to prepare the first scandium nitrilimine derivative $LSc(NHDipp)(NNCSiMe_3)$ (L = MeC(NDipp)CHC(Me)-$(NCH_2CH_2NMe_2)$), **50** [64]. The thermal stability of this novel complex allowed for an in-depth analysis of its reactivity with a selection of unsaturated substrates, including aldehydes, ketones, nitriles, and allenes (Scheme 28). This work, which was complemented by sophisticated computational experiments, established the versatility of the nitrilimine species, as the reactivity of complex **50** is related to either diazoalkanes or organic nitrilimines, depending upon the given substrate.

To date, imido species are the only type of structurally characterized rare earth complex to feature terminal, multiply bonded, unsupported ligands. However, several other examples that have bridging and/or functionalities wherein the nature of the bonding is more ambiguous have also been reported [56]. For example, Mindiola et al. utilized Tebbe's strategy of trapping group 4 alkylidene species to prepare scandium complex $LSc(\mu_3\text{-}CH_2)(\mu_2\text{-}CH_3)_2[Al(CH_3)_2]_2$ (L = N[2-P^{i}Pr$_2$-4-Me-C$_6$H$_3$]$_2$), **51**, which contains a methylidene ligand supported by two coordinated $AlMe_3$ groups [65]. Notably, the methylidene ligand can be proton-ated with an excess of H_2NAr (Ar = 2,6-^{i}Pr$_2$C$_6$H$_3$) to form the alkyl complex $LSc(CH_3)(NHAr)$ or transferred to benzophenone to afford $H_2C=CPh_2$ and the scandium oxide complex $LSc(\mu_3\text{-}O)(\mu_2\text{-}CH_3)_2[Al(CH_3)_2]_2$, **52** (Scheme 29).

Thus far heavier rare earth analogues of scandium imido species remain unknown, likely because of the enhanced reactivity of larger metals. For example, Cui et al. were able to synthesize yttrium and lutetium analogues of the scandium
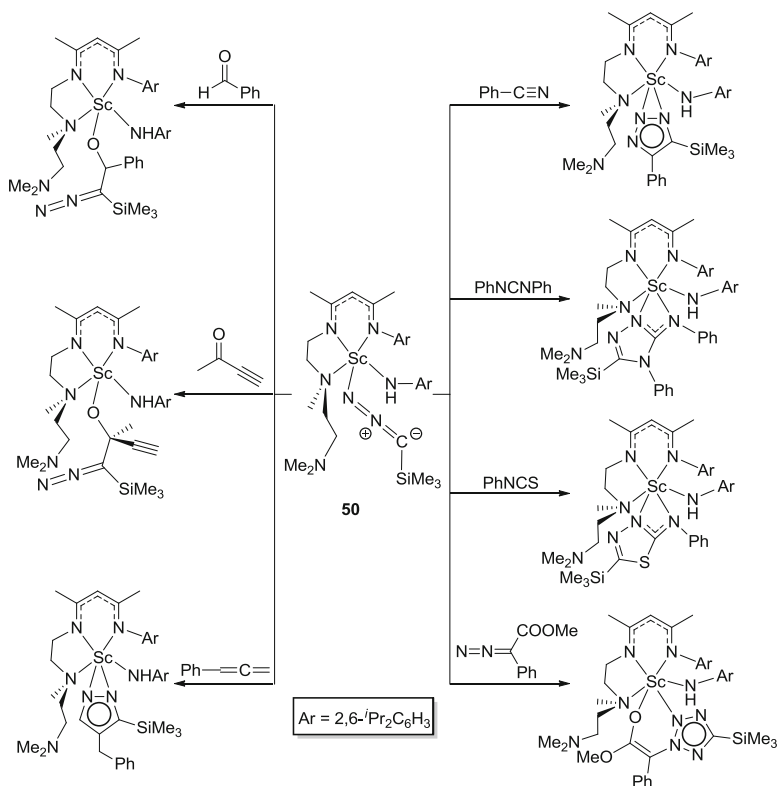
Scheme 28 Reactivity of **50** with unsaturated substrates
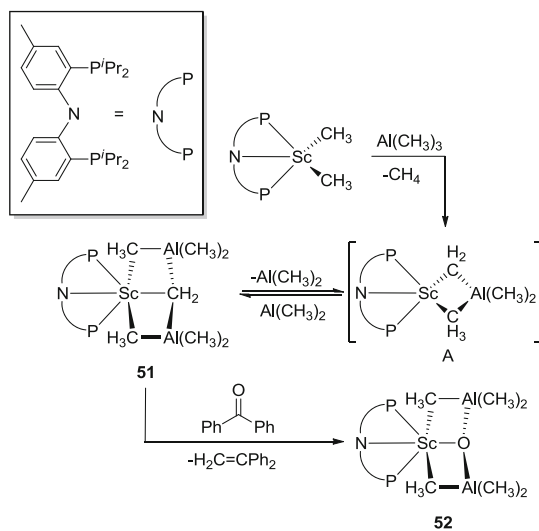
Scheme 29 Synthesis and reactivity of an AlMe$_3$ stabilized scandium methylidene complex

alkyl amido precursor to complex **46**; however, even in the presence of DMAP, only bis(anilido) and unidentified ligand redistribution products were generated [57]. Nonetheless, the rich reaction chemistry observed for scandium complexes bearing terminal imido moieties is sure to amplify future endeavors to prepare heavier rare earth congeners of these exceptional molecules.

3.2 Alkane Elimination and Alkyl Migration

Alkane elimination is a widely used method to coordinate pincer ligands to rare earth metals, and it is also frequently exploited when studying subsequent reactivity of such complexes. For example, imido and various amido functionalities are often prepared by alkane elimination (vide supra), as are cationic rare earth pincer compounds. Frequently, unanticipated alkyl migration reactions are observed and are responsible for the formation of many unusual complexes.

3.2.1 Cationic Rare Earth Complexes

Cationic rare earth complexes are commonly used in catalytic applications, such as olefin polymerization (see Sects. 4.2 and 4.3). These species tend to be extremely reactive and, thus, are often generated and used in situ. However, a handful of well-defined cationic rare earth pincer complexes have been reported, the details of which are summarized below.

In 2003, Gordon et al. isolated the first example of a cationic rare earth pincer complex, $[2\text{-}(2,6\text{-}^iPr_2C_6H_3N=CMe)\text{-}6\text{-}(2,6\text{-}^iPr_2C_6H_3NCMe_2)NC_5H_3Lu\text{-}(CH_2SiMe_2CH_2SiMe_3)(THF)][MeB(C_6F_5)_3]$, **54**. This anilido-pyridine-imine-supported species was prepared by the reaction of $B(C_6F_5)_3$ with $LLu(CH_2SiMe_3)_2$, **53**, wherein abstraction of a Si–Me group promoted migration of a CH_2SiMe_3 moiety to give rise to the $CH_2SiMe_2CH_2SiMe_3$ group in cationic complex **54** (Scheme 30) [66]. Presumably the steric bulk of this system prevented the Lewis acidic borane from abstracting the entire trimethylsilylmethyl group.
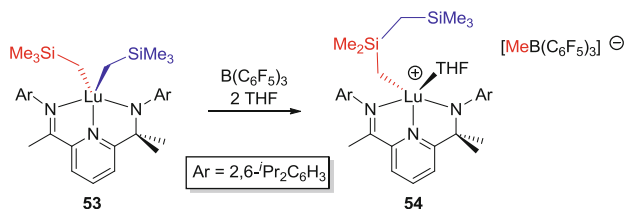
Scheme 30 Synthesis of cationic lutetium complex **54**

Cationic complexes with larger rare earth metals were reported by Berg et al. [67]. Dialkyl complexes $LLn(CH_2SiMe_3)_2$ (Ln = Y, Yb, Er; L = 1,8-bis(4′,4′-dimethyloxazolin-2′-yl)-3,6-di-*tert*butylcarbazole) were prepared either by straightforward alkane elimination or by the addition of the deprotonated ligand to $LnCl_3(THF)_n$ (n = 3 or 3.5), followed by reaction with 2 equiv. of $LiCH_2SiMe_3$. These dialkyl species were activated with $[Ph_3C][B(C_6F_5)_4]$ and tested for their ability to polymerize olefins. Aside from trace quantities of polymer produced solely by the trityl activator, no polymerization was observed. Nonetheless, multinuclear NMR spectroscopy confirmed that one of the alkyl groups of $LLn(CH_2SiMe_3)_2$ was indeed abstracted by $[Ph_3C]^+$ to generate the anticipated alkyl cation $[LLn(CH_2SiMe_3)_2][B(C_6F_5)_4]$. This compound is thermally stable in solution for more than a week, but all efforts to isolate it resulted in decomposition.

In 2009, Cui and co-workers examined the ability of the LiCl adduct of $[Ph_3C][B(C_6F_5)_4]$ to abstract an alkyl group from the lutetium analogue of anilido-phosphinimine complex **33** (see Sect. 3.1.2) [48]. The authors hypothesized that the putative complex $[LLu(DME)][B(C_6F_5)_4]$ (L = $(2,6-^iPr_2C_6H_3)NC_6H_4$-$PPhC_6H_4N(2,4,6-C_6H_2Me_3)$) formed upon alkyl abstraction by $[Ph_3C][B(C_6F_5)_4]$, and this ion pair was rapidly converted into the corresponding chloride complex LLuCl(DME) via metathesis with LiCl. This proposed mechanism was corroborated by the identification of $[Li(DME)_3][B(C_6F_5)_4]$ as a reaction by-product.

Although protonation is another well-known methodology utilized to create cationic metal species, this approach has rarely been reported for rare earth pincer complexes. Izod et al. protonated a cyclometalated lanthanum phosphide complex $[\{(Me_3Si)_2CH\}(C_6H_4\text{-}2\text{-}CH_2NMe_2)]PLa(THF)[P(C_6H_4\text{-}2\text{-}CH_2NMe_2)\{CH(SiMe_3)\text{-}(SiMe_2CH_2)\}]$ [31], **12** (see Sect. 2.2), with $[Et_3NH][BPh_4]$, generating the unusual alkyl cation $[(THF)_4LaP(C_6H_4\text{-}2\text{-}CH_2NMe_2)\{CH(SiMe_3)(SiMe_2CH_2)\}][BPh_4]$. Rather surprisingly, protonation occurred at the lanthanum–phosphorus bond, instead of the expected La–C bond. [68]. More recently, Hou and co-workers used $[NEt_3H][BPh_4]$ to prepare examples of cationic bi- and trinuclear polyhydrides (see Sect. 3.1.2) [51], while Hayes et al. treated dialkyl $LLu(CH_2SiMe_3)_2$ (L = 2,5-$((4\text{-}^iPrC_6H_4)N=PPh_2)_2NC_4H_2)$ with the oxonium acid ($[H(OEt_2)_2][B(C_6F_5)_4]$) to synthesize the cationic complex $[LLu(CH_2SiMe_3)(OEt_2)_2][B(C_6F_5)_4]$ [69].

3.2.2 Alkyl Migration

Reactive rare earth alkyl complexes can trigger diverse alkyl migration reactions which often result in functionalization of pincer ancillary ligands. For example, in 2006, Kiplinger et al. reported the 1,3-migration of a CH_2SiMe_3 group from lutetium to the *ortho* position of the central ring of a terpyridine ligand (Scheme 31) [70], resulting in loss of aromaticity and transformation of the neutral terpyridine pincer into an anionic ligand. A similar migration was also observed when the dialkyl lutetium complex $(Cp^*)Lu(CH_2SiMe_3)_2(THF)$ was used. The potential for this monoanionic tridentate NNN′ ligand system to support multiply bonded rare earth species was examined a few years later when the alkyl amido and bis(amido)
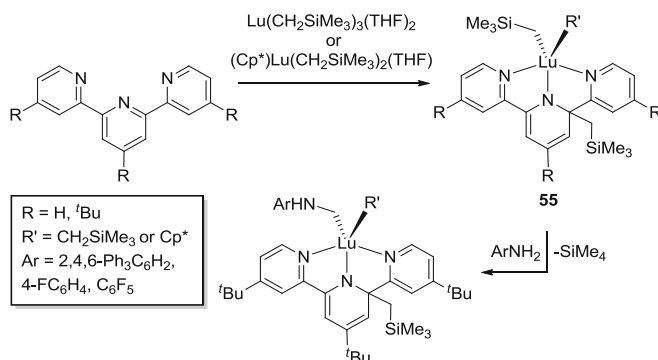
Scheme 31 Preparation of the alkyl migrated lutetium complex **55**
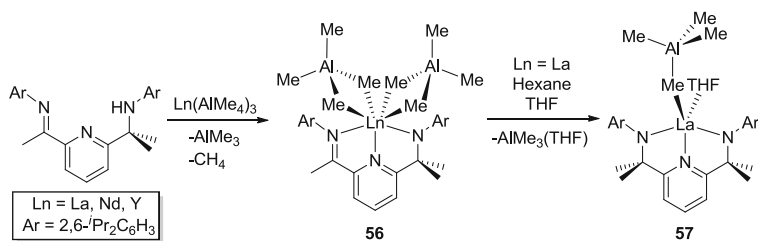
Scheme 32 Formation and reactivity of heterotrimetallic imino–amido complexes **56**

derivatives of complex **55** were prepared by alkane elimination reactions with different anilines. Unfortunately, thermolysis of the amido complexes did not result in the formation of the corresponding lutetium imido species, regardless of the nature of the anilide ligand [71].

Anwander and colleagues exploited $Ln(AlMe_4)_3$ as a novel metal precursor for the synthesis of heterotrimetallic imino–amido complexes $LLn(\eta^2-AlMe_4)_2$ (Ln = La, Nd, Y; L = 2-(2,6-^{i}Pr$_2$C$_6$H$_3$)NCMe$_2$-6-(2,6-^{i}Pr$_2$C$_6$H$_3$)N=C(Me)NC$_5$H$_3$), **56** (Scheme 32) [72]. Intriguingly, relatively modest yields prompted closer inspection of the reaction mixture, ultimately revealing the presence of two additional methyl aluminum complexes with alkylation of the remaining imino carbon atom transforming the original monoanionic ancillary into a dianionic bis(amido)pyridine ligand. Further experiments suggested that the alkylation occurred via an exceedingly reactive [Ln–Me] moiety, instead of AlMe$_3$ released during the reaction. Efforts to convert the heteroleptic complex into an organoaluminum-free methyl derivate only yielded the partially cleaved compound $LLa(\eta^1-AlMe_4)(THF)$ (L = 2,6-{(2,6-^{i}Pr$_2$C$_6$H$_3$)NCMe$_2$}$_2$NC$_5$H$_3$), **57** (Scheme 32). The formation of complex **57** is speculated to originate from a rapid process initiated by donor-induced loss of one tetramethylaluminate ligand to give a reactive [Ln–Me] species which then undergoes methyl migration from the metal center to the imino carbon of the supporting ligand.

Heterodinuclear Ln/Al complexes of dianionic NNN and NON donor ligands have typically been synthesized from $Ln(AlMe_4)_3$ metal sources [14, 72]. Rare
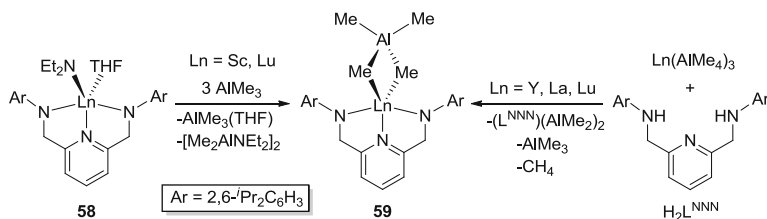
Scheme 33 Two different synthetic routes for the preparation of heterodinuclear **59**
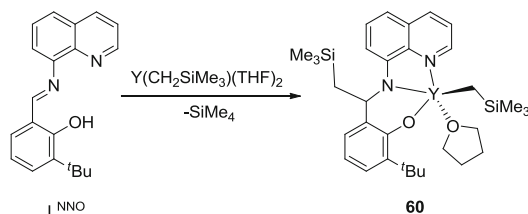
Scheme 34 Formation of yttrium complex **60**

earth metal tetramethylaluminate complexes bearing another [NNN]$^{2-}$-type bis(amido)pyridine pincer were obtained by trimethylaluminum promoted lanthanide-amide alkylation. Reaction of L^{NNN}Ln(NEt$_2$)(THF) (Ln = Sc, Lu; L^{NNN} = 2,6-{(2,6-^{i}Pr$_2$C$_6$H$_3$)NCH$_2$}$_2$NC$_5$H$_3$), **58**, with trimethylaluminum afforded complexes (L^{NNN}Ln(η^2-AlMe$_4$) (Ln = Sc, Lu), **59**) of scandium and lutetium. The corresponding yttrium and lanthanum analogues, **59**-Y and **59**-La, respectively, were prepared similarly to **56**-Ln via reaction of Ln(AlMe$_4$)$_3$ with the proteo ligand; however, these compounds were contaminated with (L^{NNN})(AlMe$_2$)$_2$ (Scheme 33) [73]. The solution state behavior of these complexes was studied by NMR spectroscopy which indicated dissociative (Sc) or associative (Lu) methyl group exchange of the AlMe$_4$ ligand depending on the size of the rare earth metal. Notably, in the presence of trimethylaluminum, the yttrium species **59**-Y underwent metalation of an isopropyl methyl group, whereas the isopropyl methine carbon was metalated when THF was added to **59**-Lu. Although these complexes exhibit complicated chemistry, they serve to shed insight into possible deactivation mechanisms for olefin polymerization catalysts that require an excess of organoaluminum co-catalyst.

Yttrium dihalide complexes of quinolone-imine-phenoxide NNO donor ligands L^{NNO} were prepared by the reaction of the deprotonated ligand with anhydrous YCl$_3$. However, attempts to prepare the corresponding dimethyl derivative L^{NNO}YMe$_2$ (L^{NNO} = 2-^{t}Bu-6-(quinolin-8-yliminomethyl)phenoxide) by the addition of the Grignard reagent MeMgBr gave the magnesium complex [Mg$_2$BrClL$^{NN(Me)O}$(THF)]$_2$ (L$^{NN(Me)O}$ = 2-^{t}Bu-6-[1-(quinolin-8-ylamido)ethyl]phenoxide as the only isolable product. Alternatively, reaction of HL^{NNO} with Y(CH$_2$SiMe$_3$)$_3$(THF)$_2$ afforded [Y(CH$_2$SiMe$_3$)L$^{NN(CH2SiMe3)O}$(THF)] (L$^{NN(CH2SiMe3)O}$ = 2-^{t}Bu-6-[1-(quinolin-8-
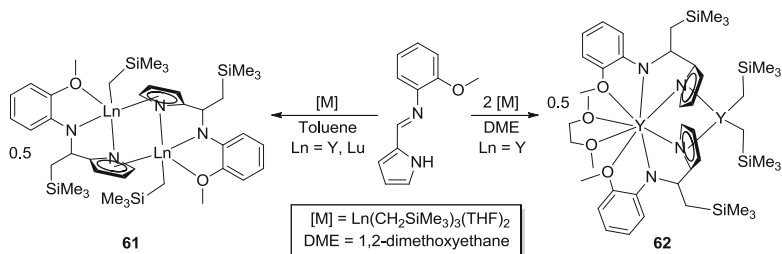
Scheme 35 Synthesis of alkyl migrated Y and Lu complexes **61** and **62**
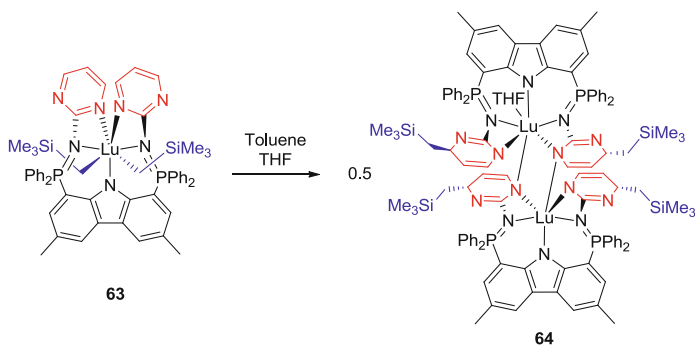
Scheme 36 Lutetium dialkyl **63** and its alkyl migration chemistry

ylamido)-2-trimethylsilanylethyl]phenoxide), **60**, the result of alkyl migration (Scheme 34) [74].

Similar alkyl shifts were reported in reactions involving the iminopyrrolyl ligand $(2\text{-}(2\text{-}CH_3OC_6H_3N=CH)C_4H_3NH)$ and $Ln(CH_2SiMe_3)_3(THF)_2$ (Ln = Y, Lu) (Scheme 35) [75]. Dinuclear monoalkyl, **61**, or dialkyl, **62**, species were formed depending upon which solvent (toluene or 1,2-dimethoxyethane) was used. Both complexes **61** and **62** feature amide donors formed upon nucleophilic attack by CH_2SiMe_3 groups on one or more imine carbons. Notably, benzophenone inserted into the Lu–CH_2SiMe_3 bond of **61**-Lu to afford the corresponding alkoxide species $[(2\text{-}(2\text{-}MeOC_6H_3NC(H)CH_2SiMe_3)C_4H_3N)LuOCPh_2CH_2SiMe_3]_2$.

Recently, Hayes et al. reported a pyrimidine-substituted bis(phosphinimine) carbazole ligand which reacted with $Lu(CH_2SiMe_3)_3(THF)_2$ to produce the thermally sensitive dialkyl lutetium complex $1,8\text{-}(N_2C_4H_3N=PPh_2)_2\text{-}3,6\text{-}dimethyl-$carbazole **63** (Scheme 36) [76]. Despite the fact that complex **63** was not prone to intramolecular C–H bond activation like Lu complexes supported by previous incarnations of the carbazole-based pincer [34], it undergoes double alkyl migration in which both of the alkyl groups bound to the lutetium center migrate to the ligand pyrimidine rings. The resultant product was an asymmetric dinuclear complex, **64**, wherein the now trianionic ligand was κ^5 coordinated to lutetium through five nitrogen atoms. The alkyl migration process was also studied with other rare
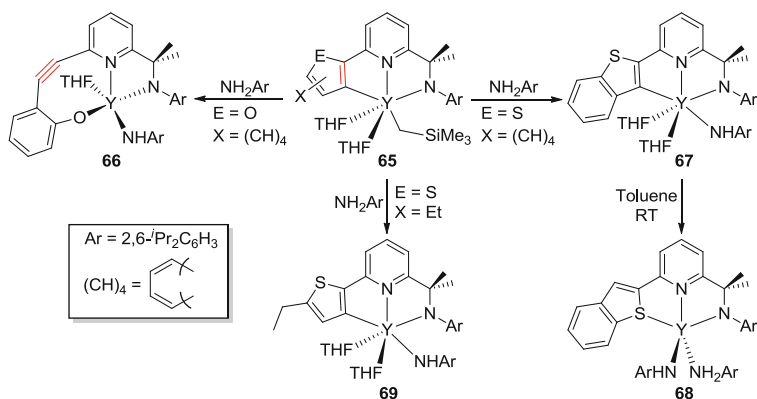
Scheme 37 Reaction of **65** with (2,6-^{i}Pr$_2$C$_6$H$_3$)NH$_2$

earth elements, but only intractable mixtures were obtained when scandium and yttrium derivatives of **63** decomposed.

Trifonov and Giambastiani et al. studied amine-triggered alkane elimination from LLn(CH$_2$SiMe$_3$)(THF)$_2$ (L = 2-(2,6-^{i}Pr$_2$C$_6$H$_3$)NCMe$_2$-6-R-NC$_5$H$_3$; R = benzofuran, benzothiophene, 2-ethylthiophene), **65** [29] in an effort to synthesize yttrium imido complexes [77]. Although reactions with equimolar quantities of 2,6-diisopropylaniline were proposed to proceed through a putative imido intermediate, only the resultant anilido or bis(anilido) products were observed (Scheme 37). The nature of the 6-R group bound to the pyridine donor greatly influenced the course of the reaction, as well as the stability of the resultant complex. In the case of the benzofuran derivative, the furan ring opened, leading to an unusual amido–yne–phenolate species, **66**. Meanwhile, no ring opening took place in the benzothiophene analogue, perhaps because of the difference between forming an Y–O vs. an Y–S bond. In toluene solution, Y–C bond protonolysis of LLn(NHAr)$_2$ (L = 2-(2,6-^{i}Pr$_2$C$_6$H$_3$)NCMe$_2$-6-C$_7$H$_4$S-NC$_5$H$_3$; Ar = 2,6-^{i}Pr$_2$C$_6$H$_3$), **67** gave bis (amido) **68**, which was supported by a monoanionic NNS pincer ligand. Conversely, anilido complex **69** proved to be relatively inert, with no evidence for ligand rearrangement at 100°C.

An example of the propensity for rare earth metals to form strong Ln–O bonds was recently demonstrated by the decomposition of an organolutetium complex bearing a bis(phosphinimine)carbazole ligand with flanking dioxaphospholane groups [78]. More specifically, dialkyl complex LLu(CH$_2$SiMe$_3$)$_2$ (L = 1,8-[4-^{i}PrC$_6$H$_4$N=P(O$_2$C$_2$H$_4$)$_2$]$_2$-3,6-dimethylcarbazole) **70** was found to undergo a cascading inter- and intramolecular ring-opening insertion reaction into Lu–C bonds, resulting in the formation of asymmetric bimetallic tetraalkoxide complex **71** (Scheme 38).

Mindiola et al. observed unique reactivity when 2,6-Me$_2$C$_6$H$_3$NC (XylNC) reacted with the coordinated pyridine/iminoacyl ligands in scandium complex **72** [58], resulting in the formation of novel indoline species (Scheme 39) [79]. Initially, complex **72** reacted with 1 equiv. of XylNC to afford an isolable iminoacyl complex
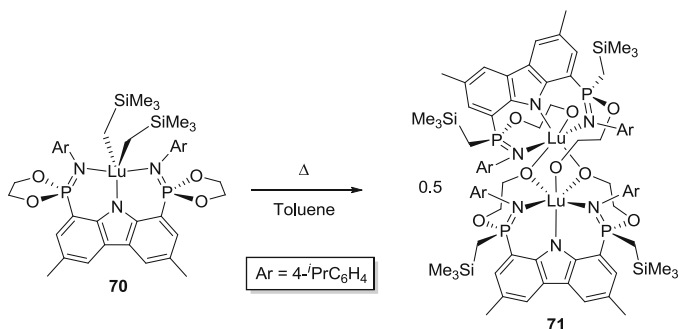
Scheme 38 Dioxaphospholane ring-opening reaction of **70**
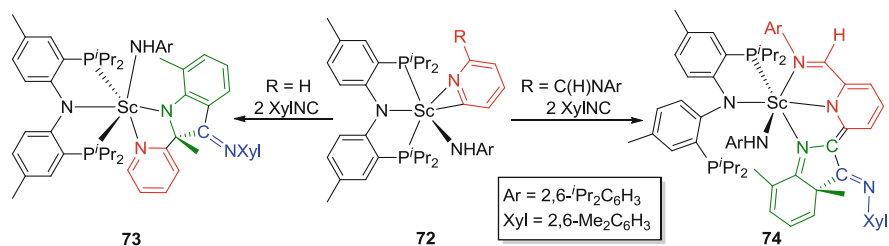
Scheme 39 Reaction of **72** with 2,6-Me$_2$C$_6$H$_3$NC. *Red* represents the initially coordinated pyridine, while *green* and *blue* denote the first and second inserted isocyanide molecules, respectively

which subsequently reacted with a second equivalent of XylNC to give either **73** or **74** depending on the substituents on the pyridine ligand. With the naked η^2-pyridine, a bidentate 2-indoline-pyridine ligand is formed by [3,5] migration of one of the methyl groups of a xylyl ring to the β-carbon of the former iminoacyl functionality, **73**. However, when the pyridine ligand is substituted with an imine group at the *ortho* position, an intermediate prior to methyl migration can be isolated. In this case, the imine nitrogen binds tightly to scandium, which interestingly prevents the relocation of the methyl group and leaves the tridentate 2-imino-6-indole-pyridine ligand intact, **74**.

The alkane elimination and alkyl migration reactions of rare earth pincer complexes presented above generally produce highly reactive complexes and/or low-coordinate intermediates that trigger further, and even more, peculiar reactivity. Although many such reactions are not targeted, they tend to produce unprecedented ligand transformations and exceptional compounds, which, in some

instances, reveal completely new types of reactivity not previously seen in those systems.

3.3 Ligand Metathesis Reactions

In coordination and organometallic chemistry, distinct ligand metathesis or exchange reactions commonly constitute the first attempts to scope chemical reactivity and potential catalytic properties of a metal complex. Thus, it is not surprising that these types of reactions are among the most studied in the field of rare earth pincer complexes. The pioneering work of Fryzuk et al. in this area on early rare earth pincer species has laid a solid foundation for many of the forthcoming studies in group 3 and lanthanide chemistry. The results from these initial reports are interwoven with more recent contributions from other authors and summarized below. This section then concludes with a discussion on related ligand exchange involving phosphorus-containing reagents.

3.3.1 Alkylation by Organoalkali Compounds

The salt metathesis chemistry of transition metal complexes is very well known and understood. In the late 1980s and early 1990s, Fryzuk et al. extended this reactivity to rare earth pincer species in a series of publications that reported numerous novel molecules prepared by alkylation with discrete organoalkali compounds. For example, the species $[N(SiMe_2CH_2PMe_2)]_2LnCl$ (Ln = Y, La, Ce, Lu), **75**, reacted readily with PhLi or $PhCH_2K$ to form the corresponding alkyl complexes **76**. While the Y and Lu analogues were isolated as stable compounds, cyclometalation of the ligand took place when Ln = La and Ce, producing 1 equiv. of hydrocarbon along with concomitant elimination of metalate **77** (Scheme 40) [9, 80, 81]. A series of comprehensive kinetic studies provided evidence for a four-centered σ-bond metathesis transition state, with prior η^2 to η^1-benzyl reorganization. In addition, the reaction rate increased proportionately with increasing ionic radius of the rare earth metal (i.e., from Lu, to Y, to La), thus suggesting that the proposed seven-
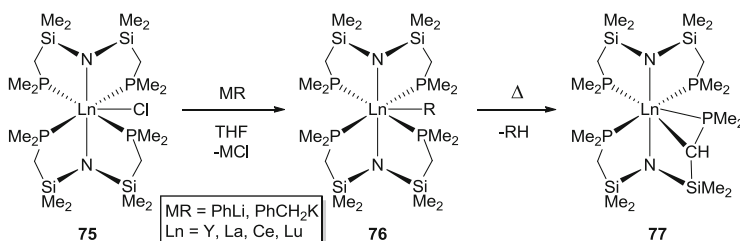
Scheme 40 Alkylation and subsequent cyclometalation of $LnCl[N(SiMe_2CH_2PMe_2)]_2$
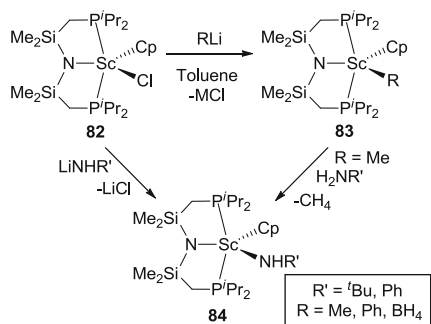
Scheme 41 Reactivity of scandium cyclopentadienyl halide complex **82**

coordinate transition state was more accessible for larger metal ions. Although most of the kinetic and reactivity studies have been performed on complexes supported by PNP ligands bearing methyl substituents at phosphorus, phenyl- and isopropyl-substituted species have also been prepared [82].

Fryzuk and co-workers also studied the salt metathesis chemistry of [N(SiMe$_2$CH$_2$PMe$_2$)]$_2$YCl with allyl Grignard reagents producing dimeric [[N(SiMe$_2$CH$_2$PMe$_2$)]$_2$Y(C$_3$H$_5$)(μ-Cl)]$_2$, **78**, and the corresponding bis(allyl) compound [N(SiMe$_2$CH$_2$PMe$_2$)$_2$]Y(C$_3$H$_5$)$_2$, **79**. Preliminary catalytic studies indicated that complex **79** was an active catalyst for the polymerization of ethylene, whereas neither **75**-Y nor **78** exhibited any catalytic activity [83].

Several years later, Fryzuk et al. extended the aforementioned salt metathesis chemistry to the smallest rare earth metal scandium [84]. Scandium readily formed the monomeric, dihalide complex [N(SiMe$_2$CH$_2$P^{i}Pr$_2$)$_2$]ScCl$_2$(THF), **80**, instead of the bis(ligand) derivatives observed for heavier congeners (vide supra). Reaction with a range of organolithium compounds invariably generated the expected dialkyl species [N(SiMe$_2$CH$_2$P^{i}Pr$_2$)$_2$]ScR$_2$(THF), **81** (R = Me, Et, CH$_2$SiMe$_3$), although some tendency for the incorporation of LiCl via the formation of "ate" complexes was observed. All reactions with small molecules (H$_2$, CH$_3$I, CO, CO$_2$, nitriles, isocyanides, silanes) caused decomposition. A computational study suggested that the frontier molecular orbitals of the scandium species are not well suited for strong σ donors, such as CO, hence hindering the reactivity of the complexes. The addition of an excess of ethylene gas to **81** produced polyethylene, but the catalytically active species could not be identified.

Reaction of the PNP scandium complex [N(SiMe$_2$CH$_2$P^{i}Pr$_2$)$_2$]ScCl$_2$(THF) with NaCp(DME) generated the robust alkylscandium species [N(SiMe$_2$CH$_2$P^{i}Pr$_2$)$_2$]-Sc(η^5-C$_5$H$_5$)Cl **82** [85]. The remaining chloride ligand in **82** could be readily exchanged for alkyl, aryl, borohydride, or amido groups by straightforward reaction with the requisite lithium reagents (Scheme 41). The addition of primary amines to [N(SiMe$_2$CH$_2$P^{i}Pr$_2$)$_2$]Sc(η^5-C$_5$H$_5$)Me, **83**-Me, yielded the same amido complexes, **84**, that were acquired by direct salt metathesis between complex **82** and LiNHR′ (R′ = ^{t}Bu, Ph). A ^{11}B NMR spectroscopic study of the borohydride derivate
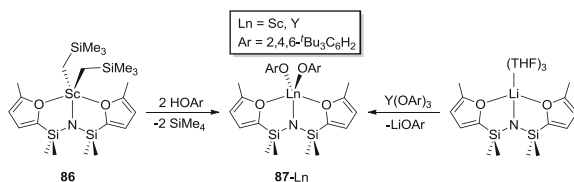
Scheme 42 Synthesis of bis(alkoxide) complexes **87**-Ln

$[N(SiMe_2CH_2P^iPr_2)_2]Sc(\eta^5\text{-}C_5H_5)BH_4$, **83**-$BH_4$, in the presence of excess PMe_3 indicated an equilibrium reaction between a putative hydride complex $[N(SiMe_2CH_2PiPr_2)_2]Sc(\eta^5\text{-}C_5H_5)(H)$, **85**, and the initial borohydride species. Further kinetic experiments suggested that it was unlikely that the scandium hydride species could be isolated since the equilibrium favored the borohydride complex even in the presence of a 100-fold excess of PMe_3 at $68°C$.

In 2010, Coles and Cloke reported a series of scandium and yttrium complexes supported by a furyl-substituted disilazide framework. Scandium dialkyl $LSc(CH_2\text{-}SiMe_3)_2$ (L = 1,3-bis(2-methylfuryl)-1,1′,3,3′-tetramethyldisilazide), **86**, was prepared by alkane elimination upon the reaction of HL and $Sc(CH_2SiMe)_3(THF)_2$ or by the combination of $LLi(THF)_3$ and $ScCl_3(THF)_2$, followed by the addition of 2 equiv. of $LiCH_2SiMe_3$ [86]. Subsequent reaction of complex **86** with 2 equiv. of $2,6\text{-}^tBu_2C_6H_2OH$ produced bis(alkoxide) **87**-Sc (Scheme 42). In contrast, reaction of $Y(CH_2SiMe)_3(THF)_2$ with the proteo ligand proceeded to an undesired yttrium species $((\eta^1\text{-}L)Y(CH_2SiMe_3)_2(THF)_2)$ wherein L was bound to the metal center by an η^1 bonding mode. Likewise, efforts to generate a κ^3-pincer-supported dialkyl complex by the reaction of a stoichiometric quantity of $LLi(THF)_3$ and $YCl_3(THF)_3$ were also fraught with failure. However, salt metathesis between $YCl_3(THF)_3$ and 2 equiv. of $LLi(THF)_3$ formed dimeric $[(\eta^2\text{-}L)_2Y(\mu\text{-}Cl)]_2$, from which the benzyl derivative $(\eta^2\text{-}L)(\eta^3\text{-}L)Y(CH_2Ph)$, **88**, was produced upon the addition of $PhCH_2K$. It was also discovered that the bis(alkoxide) complex $LY(OAr)_2$ (Ar = $2,6\text{-}^tBuC_6H_3$), **87**-Y, could be prepared by the reaction of $LLi(THF)_3$ and $Y(OAr)_3$, but this pathway necessitated harsh reaction conditions and extended reaction times to reach complete conversion.

The organometallic complexes **86** and **88** were briefly examined for their ability to catalyze ethylene polymerization and intramolecular hydroamination, respectively. Unfortunately, even upon in situ activation with Lewis or Brønsted acid co-catalysts, complex **86** proved to be a poor olefin polymerization catalyst. Although complex **88** did react with 2,2-dimethyl-1-aminopent-4-ene, it did not release the cyclized product [86].

Mononuclear complexes of the larger ionic radii, heavier rare earth metals that bear a single ancillary ligand are often challenging to prepare. However, Fryzuk and co-workers found success with their so-called NPN diamidophosphine pincer (Scheme 43) [87]. The dilithiated salt of this ligand reacts readily with the THF adducts of yttrium, samarium, holmium, ytterbium, and lutetium trichloride to give the desired halide complexes $LLn(Cl)(THF)$ (Ln = Y, Sm, Ho, Yb, Lu; L = PhP
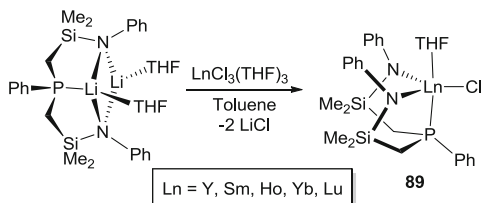
Scheme 43 Synthesis of mononuclear rare earth complexes **89**
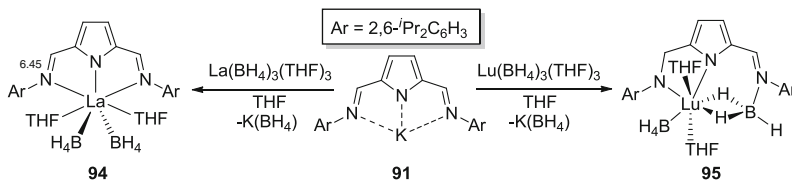
Scheme 44 Synthesis of complexes **94** and **95**

(CH$_2$SiMe$_2$NPh)$_2$) **89** in high yields. Unfortunately, most attempts to generate metal–carbon bonds resulted in mixtures of products, the only exception of which was a dinuclear, naphthalene bridging species, [(NPN)Lu]$_2$(μ-η^4:η^4-C$_{10}$H$_8$), that was formed under reducing conditions.

Mixed pincer–Cp complexes featuring an NNN-bis(iminomethyl)pyrrolyl ligand were reported by Roesky and colleagues [88]. Initial efforts to prepare well-behaved dihalide complexes of this ligand by the reaction of the lithium salt of the ligand with YCl$_3$ in THF proceeded to the "ate" complex LYCl$_2$(THF)-LiCl(THF)$_2$ (L = (2,5-(2,6-^{i}Pr$_2$C$_6$H$_3$)N=CH)$_2$NC$_4$H$_2$), **90**. Conversely, treatment of the potassium salt of the ligand, **91**, with anhydrous LnCl$_3$ (Ln = Y, Lu) in THF gave the anticipated dihalide complexes LLnCl$_2$(THF)$_2$, **92**. A subsequent reaction between NaC$_5$H$_5$ and yttrium derivatives **90** and **92** afforded the corresponding metallocene LLn(η^5-C$_5$H$_5$), **93**.

Later on, Scherer, Roesky, and co-workers synthesized lanthanide borohydride complexes using **91** and tris(borohydride) Ln(BH$_4$)$_3$(THF)$_3$ (Ln = La, Lu) as the starting materials (Scheme 44) [11]. Depending upon the size of the metal, the BH$_4^-$ group could be involved in redox chemistry. Generally, BH$_4^-$ behaves as a pseudohalide with rare earth metals, as was seen in the reaction of **91** with La(BH$_4$)$_3$(THF)$_3$, which afforded the anticipated bis(borohydride) complex LLa(BH$_4$)$_2$(THF)$_2$, **94**. However, when **91** reacted with Lu(BH$_4$)$_3$(THF)$_3$, one of the imine donors was reduced to an amide, leading to a product, **95**, that contained an N–BH$_3$ unit bound to lutetium in an unusual η^2-fashion. In later contributions, Roesky and colleagues have expanded such chemistry to divalent rare earth metals [89], as well as to mixed borohydride–chloride complexes [90].
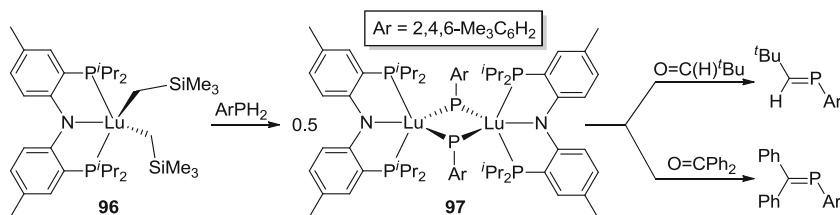
Scheme 45 Preparation and phospha-Wittig reactivity of complex **97**

3.3.2 Reactions with Phosphorus-Containing Molecules

Phosphines are one of the most well-known donors in coordination chemistry, and transition metal complexes with phosphorus-containing ligands are used as catalysts in a wide array of industrial processes [91]. Since rare earth elements can be considered as hard ions and phosphorus as soft, phosphorus-containing moieties are not generally considered to be good ligands for these metals. Regardless, rare earth complexes with phosphorus-based donor ligands have gained increasing attention over the past two decades [92, 93]. Although still scarce, a handful of studies on such compounds have been reported – the results from this work are presented below.

Similar to first row main group elements, attempts have been made to prepare rare earth species featuring terminal multiply bonded ligands of heavier p-block elements. The first rare earth phosphinidene was reported in 2008 by Kiplinger and co-workers. An alkane elimination between the primary phosphine $MesPH_2$ $(Mes = 2,4,6\text{-}Me_3C_6H_2)$ and $(PNP)Lu(CH_2SiMe_3)_2$ $(PNP = N(2\text{-}P^iPr_2\text{-}4\text{-}Me\text{-}C_6H_4)_2)$, **96**, produced dinuclear phosphinidene-bridged **97** (Scheme 45) [94]. Complex **97** readily reacts as a phospha-Wittig-type reagent with aldehydes and ketones to afford phosphaalkenes (Scheme 45). Unfortunately, all attempts to generate and stabilize a terminal phosphinidene complex via the introduction of different Lewis bases (e.g., PMe_3, tetramethylethylenediamine, DMAP, or bipyridines) resulted in decomposition. Nonetheless, it is important to note that kinetic stabilization using sterically demanding 2,4,6-tri-*tert*-butylphenylphosphine triggered the formation of phosphaindole, which has been interpreted as being indicative of the presence of transient phosphinidene species in certain transition metal systems.

In 2010, Mindiola and co-workers reported the synthesis of the related bridging phosphinidene scandium complex $[LSc(\mu\text{-}PAr)]_2$ $(L = N(2\text{-}P^iPr_2\text{-}4\text{-}MeC_6H_3)_2;$ $Ar = 2,4,6\text{-}{}^iPr_3C_6H_2)$, **98**. When more bulky phosphines were used, two remarkable mononuclear complexes, $LSc[\mu\text{-}P(DMP)](\mu\text{-}Br)Li$ $(DMP = 2,6\text{-}(2,4,6\text{-}Me_3C_6H_2)_2C_6H_3)$, **99**, and $LSc[\mu_2\text{-}P(DMP)](\mu\text{-}Br)Li(DME)$, **100**, that contained Lewis acid-supported phosphinidenes (Scheme 46) were prepared [95]. In a similar fashion to complex **97**, the mononuclear "ate" complex **100** exhibited well-behaved phospha-Wittig chemistry with ketones and dichlorophosphines. Intriguingly, complex **100** also seems to participate in a phosphinidene extrusion process that can be utilized to form the known phosphinidene complex $Cp_2Zr=P(DMP)PMe_3$.
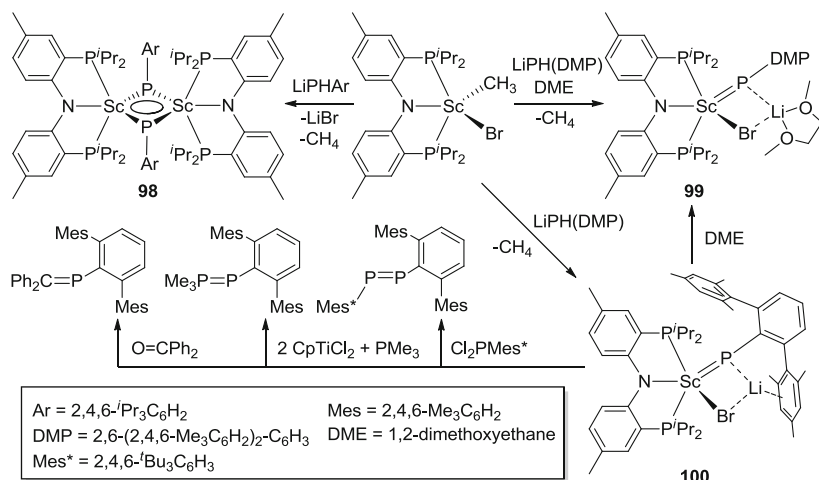
Scheme 46 Synthesis and reactivity of scandium phosphinidene complexes **98–100**
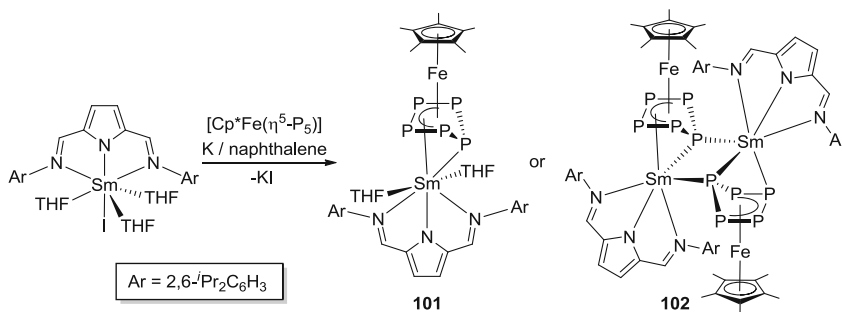
Scheme 47 Synthesis of polyphosphide complexes **101** and **102**

Unfortunately, decomposition products present in the reaction mixture prevented the separation of this species.

A particularly unusual example of rare earth phosphorus chemistry was recently reported by Roesky et al. wherein mixed metal polyphosphide complexes **101** and **102** were synthesized by the reduction of pentaphosphaferrocene [Cp*Fe(η^5-P$_5$)] in the presence of LSmI(THF)$_3$ (L = (2,5-(2,6-^{i}Pr$_2$C$_6$H$_3$)N=CH)$_2$NC$_4$H$_2$) (Scheme 47) [96]. Monomeric **101** was obtained by recrystallization from a THF/toluene mixture, whereas dimeric **102** was isolated by recrystallization from toluene/pentane. The reduction led to a [Cp*FeP$_5$]$^{2-}$ subunit, and the authors proposed that the phosphorous ligand could be considered a cyclo-P$_5$$^{3-}$ polyphosphide anion.

Berg et al. have also prepared divalent lanthanide complexes that contain phosphorus-based ligands [97]. Specifically, monohalide complexes LYbX(THF)$_2$ (L = 1,8-bis(4,4-dimethyloxazolin-2-yl)-3,6-di-*tert*-butylcarbazole; X = I, **103**-I, Cl, **103**-Cl) were prepared by the reaction of YbX$_2$ and NaL or by Na/Hg reduction
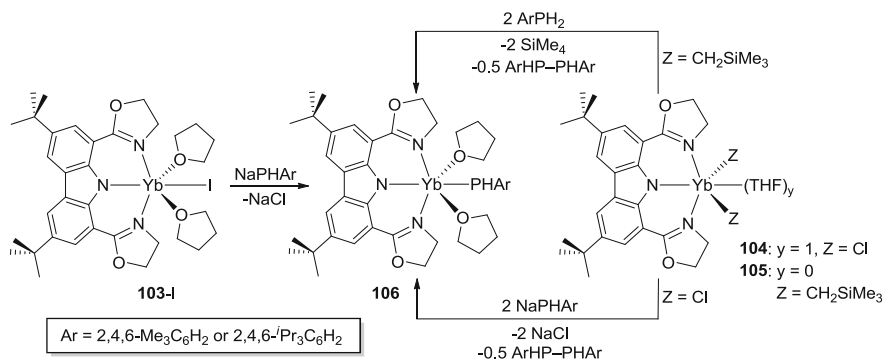
Scheme 48 Synthesis of phosphide complex **106** through salt metathesis or alkane elimination routes
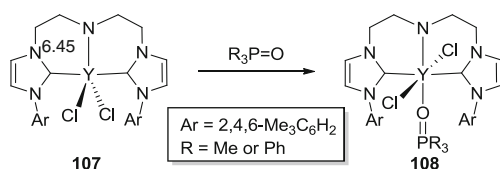
Scheme 49 Reactivity of dicarbene complex **107** with phosphine oxides

of the Yb(III) species LYbCl$_2$(THF), **104**. Notably, divalent silylamide, alkyl, and phosphide complexes could be prepared from complex **103**-I. Also noteworthy is the fact that the addition of LiCH$_2$SiMe$_3$ to LYbX(THF)$_2$ afforded the oxidized product LYb(CH$_2$SiMe$_3$)$_2$, **105**. Equally intriguing redox chemistry was observed upon the reaction of **104** and **105** with ArPH$_2$ and NaPHR, respectively (Scheme 48).

In addition to phosphine and phosphide reagents, phosphine oxides can also be used as suitable ligands for stabilizing rare earth pincer complexes. Arnold and colleagues employed the lithium chloride adduct of a tridentate amido-bridged di-*N*-heterocyclic carbene ligand, L (L = N{CH$_2$CH$_2$[1-C(NCHCHNAr)]}$_2$, Ar = 2,4,6-Me$_3$C$_6$H$_2$), in order to prepare the yttrium amidodicarbene pincer complex LYClN(SiMe$_3$)$_2$, by transamination. In addition, dihalide species LYCl$_2$, **107**, were prepared by salt metathesis between anhydrous YCl$_3$ and LLi. Although the addition of phosphine oxides to LYClN(SiMe$_3$)$_2$ resulted in decomposition, discrete, albeit somewhat thermally sensitive (when R = Ph), complexes LYCl$_2$(O=PR$_3$) (R = Me, Ph), **108**, were isolated when the same phosphine oxides were reacted with **107** (Scheme 49) [98].

4 Catalytic Properties of Rare Earth Pincer Complexes

As with other metals across the periodic table, the ultimate goal when preparing new rare earth pincer complexes is often the utilization of such species as catalysts in specific chemical transformations. Despite the fact that the number of reactions catalyzed by rare earth pincer complexes is somewhat limited when compared to transition metal analogues, rare earth pincer complexes have exhibited exceptional catalytic activity in polymerization reactions, especially in the ring-opening polymerization (ROP) of cyclic esters and the polymerization of dienes such as isoprene and butadiene. This section discusses these two research domains in separate segments and concludes with a review of reactions that are less prominent, but still noteworthy, in rare earth pincer complex catalysis (e.g., hydroamination).

4.1 Ring-Opening Polymerization of Cyclic Esters

The field of polymerization catalysis is a broad area with rich history [99]. At the turn of the twentieth century, chemists pioneered foundational work in this area, establishing the first synthetic-based polymers, such as Bakelite and rayon. The exhaustion of natural latex, wool, silk, and other resources during World War II sparked developments in alkene polymerization for the preparation of nylon, acrylic, neoprene, polyethylene, and other polymers. Subsequently, the development of high-polymer technology culminated with significant discoveries from Nobel laureates Karl Ziegler and Giulio Natta (1963) [100]. Meanwhile, the development of ring-opening processes of *cyclic* monomers garnered attention in the late 1970s and reached a climax with the popularity of ring-opening metathesis polymerization (ROMP), which ultimately led to Nobel Prizes for Richard Schrock, Robert Grubbs, and Yves Chauvin (2005) [101]. As a result of the modern renaissance in polymer technologies, contemporary studies have been initiated to develop single-site (homogeneous) catalysts for the polymerization of *hetero*cyclic monomers. Though many of these studies primarily involve transition metal catalysts, the polymerization of cyclic esters, especially lactide [102], a cyclic diester monomer, is frequently initiated by rare earth complexes [103, 104].

4.1.1 Polymerization of Lactide

Lactide (LA), which is a cyclic dimer of lactic acid, can be transformed into a biodegradable polymer, polylactide (PLA), via ring-opening polymerization. Lactide is one of, if not the most studied, monomers in the ROP of cyclic esters, and many rare earth metal complexes have been investigated for their ability to mediate this process [103].

High molecular weight PLA can be prepared via a coordination–insertion mechanism using metal catalysts that bear suitable initiating groups. Other mechanisms, such as cationic or anionic, are also viable, but these pathways often lead to low molecular weight polymers or problems in molecular weight distribution, respectively. The control of molecular weight distribution (polydispersity) is of special interest as it has major consequences on the physical properties of the resulting polymer. The measure of this property, known as the polydispersity index (PDI), is calculated by dividing the weight averaged molecular weight (M_w) by the number averaged quantity (M_n). Values close to unity represent polymer chains possessing uniform length, and higher values describe materials containing a wider range of molecular masses in the polymer.

Another important feature of the lactide precursor is the two stereogenic centers in the molecule's backbone. Hence, three different stereoisomers are possible: (S,S)-lactide (L-LA), (R,R)-lactide (D-LA), and (R,S)-lactide (*meso*-LA); a racemic mixture of the first two is known as *rac*-LA. The presence of chiral carbons in the monomer leads to the possibility of different tacticities of the resultant polymer. While many polymer microstructures are possible, isotactic (adjacent chiral centers possess the same configuration (R or S)), heterotactic (two adjacent stereogenic centers have the same configuration that are different from neighboring pairs (–RRSSRRSS–)), syndiotactic (alternating configurations (–RSRSRSRS–)), and atactic (no stereoregularity) are the most common.

In the transformation of lactide to PLA, the nature of the initiating group on the metal catalyst plays a key role in its activity, and alkoxides have generally proven to be the most effective. In addition to the role of the initiating group, steric factors of the ancillary ligands can have a major impact on the stereocontrol of the catalyst (via an enantiomorphic site-control mechanism). However, despite the prevalence of metal alkoxides as initiators in the ROP of lactide, the use of amides is more widespread in the area of rare earth pincer catalysis, and distinct alkyl complexes have also shown modest activity. Presumably, synthetic challenges and limited availability of the heteroleptic alkoxide species have limited their use. For example, these complexes can be prone to facile ligand redistribution, whereas a range of $Ln(NR_2)_3$ starting materials are well known. Furthermore, amine elimination strategies can be employed to easily attach a variety of ancillary ligands, whereas alcohol elimination routes from $Ln(OR)_3$ sources are infrequently encountered (see Sect. 2.1).

One of the first examples of rare earth pincer complexes initiating the ROP of LA was reported by Cui et al. when they prepared a dinuclear dialkyl yttrium complex $[L_2Y(THF)][Y(CH_2SiMe_3)]_2$ (L = 2-[(*N*-2-diphenylphosphinophenyl) iminomethyl]pyrrole), **109**, which was shown to be as efficient an initiator as previously reported (non-pincer) monoalkyl counterparts. The resultant PLA had lower molecular weights and broad molecular weight distributions since both alkyl groups supposedly participated in polymerization [105].

Cui and co-workers continued the exploration of yttrium pincer catalysts bearing modified β-diimines and anilido-imine ancillaries. In these studies, dialkyl $LY(CH_2SiMe_3)_2$, **110** and **111**, and diamido species $LY(NH-2,6-^iPr_2C_6H_3)_2$, **112**
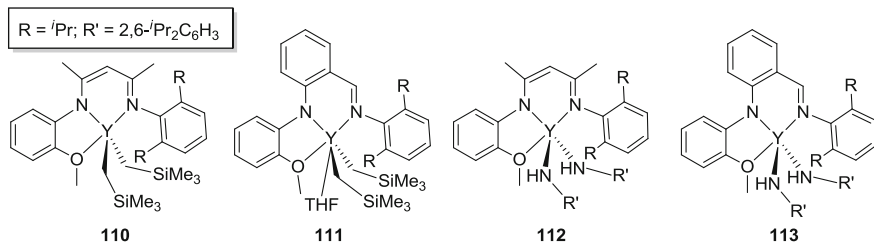
Chart 1 Dialkyl and diamido complexes **110–113** supported by NNO pincer ligands
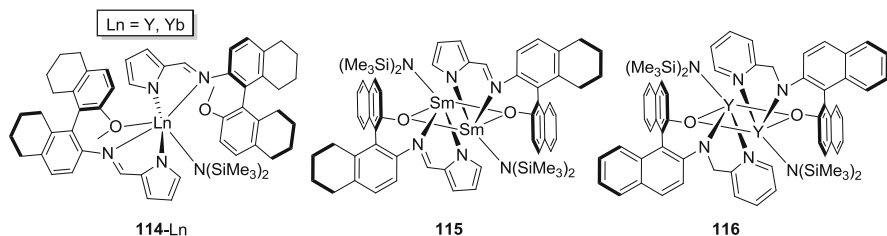
Chart 2 Rare earth amido **114**-Ln, **115**, and **116** complexes active in the ROP of LA

and **113** (**110** and **112**: L = 2-OMe-C$_6$H$_4$NCMeCHCMeNH-2,6-^{i}Pr$_2$C$_6$H$_4$; **111** and **113**: L = 2-OMeC$_6$H$_4$-NC$_6$H$_4$-CH=N-2,6-^{i}Pr$_2$C$_6$H$_3$) (Chart 1), were prepared and utilized in LA polymerization studies. All complexes exhibited high activity and gave high molecular weight PLA, although PDIs were somewhat broad in certain occasions (1.31–1.72). Despite the similarities in ligand framework, **110** and **112** behave as double-site catalysts, whereas **111** and **113** produced PLA with features that indicated the involvement of a single-site active species. For the dialkyl complexes **110** and **111**, this behavior was attributed to the unique arrangement of alkyl groups since the ancillary ligand adopted *mer*-coordination or *fac*-coordination, respectively. In the cases of **112** and **113**, the amido ligands were positioned similarly around the metal; hence, the difference in polymerization behavior was most likely electronic in origin. Moreover, the solvent used in these transformations had a notable effect on the molecular weight of the obtained polymer. In nonpolar solvents such as toluene or benzene, the polymerization was less controlled, producing higher than expected molecular weights and large PDIs. This behavior may be due to poor solubility of the monomer, which in turn might introduce heterogeneous features to the polymerization process [106, 107].

In 2008, Zi and colleagues used chiral ancillaries to prepare monoamido complexes L$_2$LnN(SiMe$_3$)$_2$ (Ln = Y or Yb; L = (*S*)-5,5′,6,6′,7,7′,8,8′-octahydro-2-(pyrrol-2-ylmethyleneamino)-2′-methoxy-1,1′-binaphthyl), **114**-Ln (Chart 2). Both species were active in the ROP of *rac*-LA under mild conditions. The yttrium complex **114**-Y produced isotactic-rich PLA with complete conversion of 500 equiv. of lactide to polymer in just over 1 h in THF solvent. By comparison, the ytterbium counterpart **114**-Yb reached 88% conversion under identical
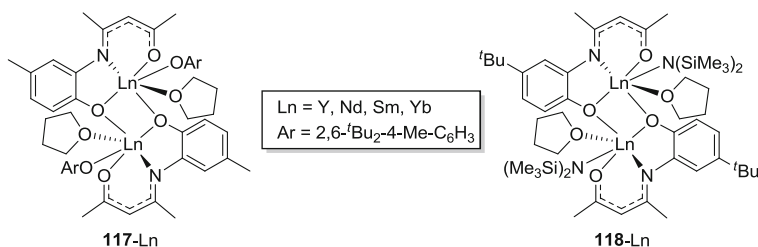
Chart 3 Dinuclear aryloxide **117**-Ln and amido **118**-Ln rare earth complexes

conditions. Interestingly, the relative activities were reversed when toluene was used as the solvent [108].

Shortly thereafter, Zi et al. synthesized the dinuclear samarium species, [LSmN-(SiMe$_3$)$_2$]$_2$ (L = (S)-5,5′,6,6′,7,7′,8,8′-octahydro-2-(pyrrol-2-ylmethyleneamino)-2′-hydroxy-1,1′-binaphthyl), **115**, and the closely related [LYN(SiMe$_3$)$_2$]$_2$ (L = (S)-2-(pyridin-2-ylmethylamino)-2′-hydroxy-1,1′-binaphthyl), **116** (Chart 2), and studied the performance of these complexes in the ROP of LA. The characteristics of the generated PLA were similar to polymers formed with **114**-Ln. The effect of ionic radius was again visible in reactions performed in toluene as the samarium species **115** was found to be more active. However, the difference in activities was minor when THF was used as a solvent, which is most likely because the effects of competitive coordination between the solvent and monomer (LA) are more pronounced with the smaller yttrium center [109].

Also in 2008, Yan, Cheng, and co-workers demonstrated that dinuclear aryloxide-bridged complexes [LLn(OAr)(THF)]$_2$ (Ln = Y, Nd, Sm, Yb; 4-(2-hydroxy-5-methylphenyl)imino-2-pentanone) **117**-Ln (Chart 3) were active in L-LA polymerization, although higher temperatures (70°C) and longer reaction times (4 h) were required to obtain close to complete conversion. The ionic radius of the metal was observed to have significant influence on the activity of the complexes, with **117**-Nd and **117**-Sm being the most active. All prepared PLA samples possessed high molecular weights, but the PDIs of the polymers were relatively large, suggesting that polymerization was not well controlled. These results indicate that initiation may be slow relative to propagation. This behavior seems consistent with **117**-Ln persisting as a dimer in solution, hindering monomer coordination [110].

Two years later, Yao and colleagues prepared monoamido analogues [LLnN-(SiMe$_3$)$_2$(THF)]$_2$ (Ln = Y, Nd, Sm, Yb; L = 4-(2-hydroxy-5-*tert*-butyl-phenyl)-imino-2-pentanone), **118**-Ln (Chart 3), which were capable of initiating the ROP of lactide, although with lower activities than the corresponding lanthanide aryloxide species **117**-Ln. The poor catalytic activity of **117**-Ln is most likely a consequence of the more electrophilic silylamide ligand, compared to the aryloxide in **118**-Ln, hampering nucleophilic attack at the carbonyl carbon of the coordinated lactide monomer [111].

Chart 4 Mono- and dinuclear rare earth complexes with chiral biaryl ligands

Chart 5 Mononuclear rare earth amido complexes supported by bis(naphtholate) ancillary ligands

Very recently, Zi et al. expanded their family of complexes bearing binaphthyl-derived ligands to include a series of monoamido species LYN(SiMe₃)₂(THF)₂, **119** (R = ^{t}Bu), LLnN(SiMe₃)₂(DME), **120**-Ln, [LLnN(SiMe₃)₂]₂, **121**-Ln, and **122**-Ln, (Ln = Y, Sm, Yb; L = (S)-2-amino-2′-hydroxy-6,6′-dimethyl-1,1′-biphenyl or differently substituted (S)-5,5′,6,6′,7,7′,8,8′-octahydro-2-amino-2′-hydroxy-1, 1′-binaphthyl) (Chart 4) [112]. All complexes promoted the ROP of *rac*-LA, but the mononuclear species were more active, converting 500 equiv. of lactide to PLA within 4 h at ambient temperature. In agreement with previous studies, metal cations with larger ionic radii were most active, and toluene was shown to be a better solvent than the more strongly coordinating THF (vide supra). The resulting PLA was isotactic rich with P_m values up to 0.74. In general, the activities of **119**–**122**-Ln were similar to that of complex **109**, and the polymer features were similar to the ones produced using catalysts **114**-Ln [105, 108].

Kirillov, Carpentier, and co-workers have prepared an impressive series of complexes of the form LLnN(SiHMe₂)₂(THF) (Ln = Sc, Y, La; L = silyl *ortho*-substituted 2,6-bis(naphtholate)pyridine or 2,5-bis(naphtholate)thiophene; see Chart 5), **123**–**125**-Ln, for the ROP of lactide, that feature N(SiHMe₂)₂ initiating groups. Compounds **123**–**125**-Ln were shown to be active initiators of *rac*-LA,

Chart 6 Dialkyl Sc and Y PNP complexes **126**-Ln

producing low PDI PLA with molecular weights similar to the predicted values. Conversion of 100–500 equiv. of *rac*-LA into PLA was achieved at ambient temperature in less than 12 h. Furthermore, immortal polymerization behavior was attained when isopropanol was added as a chain transfer agent. Interestingly, when reactions were performed in THF, ROP produced heterotactic-rich PLA with P_r values up to 0.93, whereas in toluene, all stereocontrol was lost with only atactic polymers formed. The ionic radius of the metal, as well as the identity of the donor atom in the ancillary backbone, appeared to affect the tacticity of the polymer, implying that the rigidity of the ancillary framework plays a role in stereocontrol. For example, with complexes **124**-Ln, the scandium derivative produced PLA with $P_r = 0.93$, whereas the use of the corresponding lanthanum compound resulted in atactic polymers. Notably, the trend was not uniform as it was inversed with complexes **123**-Ln, limiting definitive conclusions regarding the factors affecting stereochemistry. In addition to polymerization of LA, complexes **123**-Ln and **124**-Ln were also active in the ROP of *rac*-β-butyrolactone (BBL) (vide infra) [113].

Mononuclear PPP dialkyl complexes LLn(CH$_2$SiMe$_3$)$_2$(THF)$_n$ (Ln = Y, Sc; L = (4-methyl-6-PR$_2$-C$_6$H$_3$)$_2$P, R = Ph, ^{i}Pr) **126**-Ln-R were studied by Peters and Pellecchia for the ROP of L-LA (Chart 6) [114]. Yttrium derivatives were shown to be particularly active producing PLA almost quantitatively in 15 min at ambient temperature with a monomer to initiator ratio ([LA]$_0$/[I]$_0$) of 200. The phenyl-substituted **126**-Y-Ph was more active than **126**-^{i}Pr, perhaps because the weakly donating phenyl groups increased the metal's Lewis acidity. High molecular weight polymers were produced in 3 h at ambient temperature with 99% conversion when a [LA]$_0$/[I]$_0$ ratio of 1,000 was used. Unfortunately, the observed molecular weights were lower than theoretical values, accompanied by large PDIs. Mass spectrometric analysis of oligomers prepared with a [LA]$_0$/[I]$_0$ value of 20 revealed primarily linear oligomer formation, although cyclic species were also detected, confirming competitive transesterification during polymerization. More detailed kinetic analysis of the polymerization reactions indicated a single-site nature of the catalysts, which is consistent with "controlled-living" characteristics. A slight preference for heterotactic polymer formation (P_r values of 0.60–0.64) was observed when **126**-Ln-R was used to polymerize *rac*-LA. Analysis of solvent dependence determined that solvent effects were comparable with previous studies, i.e., higher catalytic activities were observed in toluene compared to THF. Solvent-free LA polymerization with **126**-Y-R as initiators reached satisfactory conversions in a controlled fashion. It is important to note, however, that measured molecular weights
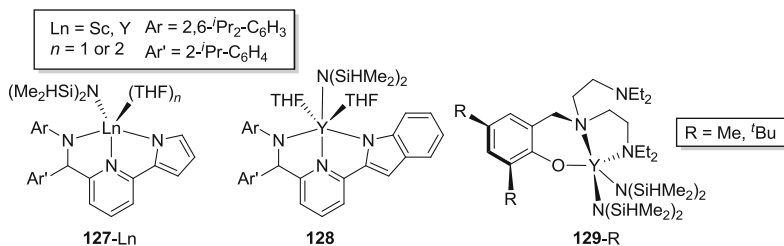
Chart 7 Monoamido, **127**-Ln and **128**, and diamido, **129**-R, rare earth complexes

suggested that both alkyl groups were active initiating groups in the absence of solvent.

Following these studies, the ROP of L-LA by **126**-Ln-R in the presence of isopropanol was investigated [115]. The addition of 2 equiv. of isopropanol to the reaction mixture of **126**-Ln-R and L-LA resulted in catalyst activity virtually identical to those conducted in the absence of alcohol, and the molecular weights of the formed PLA were in excellent agreement with theoretical values. An alcohol/initiator ratio of 5:1 resulted in reduced molecular weights and narrowed PDIs, confirming that excess isopropanol acts as an efficient chain-transfer agent. Furthermore, living polymerization was suggested owing to the rapid "growing chain to isopropanol" exchange.

Lamberti, Pellecchia, and co-workers investigated the scandium and yttrium complexes LLnN(SiHMe$_2$)$_2$(THF)$_n$ (Ln = Sc, Y; L = N-((6-(1H-pyrrol-2-yl)-pyridin-2-yl)(2-isopropylphenyl)methyl)-2,6-diisopropylaniline, **127**-Ln, and N-((6-(1H-indol-2-yl)pyridin-2-yl)(2-isopropylphenyl)methyl)-2,6-diisopropylaniline, **128**; n = 1 or 2) as initiators for the ROP of rac-LA (Chart 7) [116]. The yttrium species were again found to be highly active, converting 200 equiv. of monomer to PLA within minutes at ambient temperature. The polymerization rate also exhibited significant solvent dependence following the order CH$_2$Cl$_2$ > toluene > THF. Complex **127**-Y was found to be slightly more active than **128**, most likely originating from the steric protection and/or higher electron donating character offered by the indole group. Notably, **127**-Y was able to convert 1,050 equiv. of LA to PLA in 6 min at 20°C with a remarkable turnover frequency (TOF) of 1×10^4 mol$_{LA}$ mol$_Y^{-1}$ h^{-1}. The scandium derivative **127**-Sc displayed lower activity (vide infra), as observed in previous similar studies. The PDI values of the prepared PLA were relatively high, perhaps because of transesterification reactions.

In situ polymerization was studied at 130°C, with all complexes found to be active under these conditions, producing PLA with conversions up to 87% in 10 min. The molecular weights and PDIs were similar to those observed in solution state reactions, indicating well-controlled polymerization even in the absence of a solvent. All of the catalysts bestowed good to moderate heterotacticity on the polymer, with **127**-Y producing the best P_r values of up to 0.84 in THF. Polymerization experiments in the presence of isopropanol were also investigated in order to study the role of an alkoxide initiating group. In studies involving 1 equiv. of
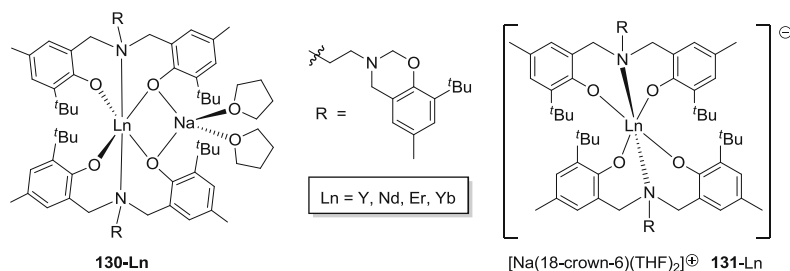
Chart 8 Heterodinuclear rare earth complexes **130**-Ln and **131**-Ln

isopropanol, complex **127**-Y polymerized 1,200 equiv. of LA in 2 min at 20°C with a remarkable TOF of 3.5×10^4 mol_{LA} $mol_Y^{-1} h^{-1}$. The addition of 5 equiv. of isopropanol resulted in immortal polymerization behavior, producing narrow PDI PLA with molecular weights proportional to the amount of added isopropanol. In addition, no silylamido end groups were observed, confirming that the isopropoxide ligand is the true initiating group.

Diamido yttrium complexes $LY(N(SiHMe_2)_2)_2$ (L = 2,4-dialkyl-6-bis-(2-(diethylamino)ethyl)aminomethlyphenol, R = Me, ^tBu) **129**-R (Chart 7) bearing unique pincer ligands were prepared by Arnold and co-workers [117]. Compounds **129**-Me and **129**-^tBu are active catalysts for the ROP of *rac*-LA, turning up to 1,000 equiv. of monomer into narrow PDI PLA within 30 min. Both complexes gave better conversion and more narrow PDI than $Y[N(SiMe_3)_2]_3$, demonstrating the influence imparted by the ancillary ligands. Notably, extended reaction times increased PDI values, suggesting competitive transesterification. No stereocontrol was observed during the polymerization of *rac*-LA, and the use of L-LA as the monomer resulted in atactic polymer growth, signifying epimerization processes during polymerization.

The heterodinuclear ate complexes $L_2LnNa(THF)_2$ (Ln = Y, Nd, Er, Yb; L = 6,6'-(2-(8-*tert*-butyl-6-methyl-2*H*-benzo[*e*][1,3]oxazin-3(4*H*)-yl)ethylazanediyl)-bis(methylene)bis(2-*tert*-butyl-4-methylphenolato)) **130**-Ln and their corresponding ion pairs $[L_2Ln][(18$-crown-6)Na(THF)_2]$ (Ln = Y, Yb) **131**-Ln (Chart 8) were prepared by Shen et al. [118]. The complexes were shown to be highly active in the polymerization of ε-CL (vide infra). In addition, the neodymium derivative **130**-Nd was shown to be a moderately active catalyst for the polymerization of L-LA at ambient temperature, resulting in virtually complete consumption of 100 equiv. of monomer in just over 6 h. Intriguingly, the corresponding yttrium complex **130**-Y did not exhibit any activity at 20°C, and only a mere 3% conversion was achieved after 24 h at 50°C.

Very recently, Ward and co-workers prepared an extensive series of dialkyl $LY(CH_2SiMe_2Ph)_2$, **132–134**, and diamido complexes $LLn(N(SiMe_3)_2)_2$, **135–137**-Ln (Ln = Y, La, Pr, Nd, Sm; L = bis(oxazolinylphenyl)amide) (Chart 9) [119]. Upon reaction with $[Ph_3C][B(C_6F_5)_4]$, the generated cationic yttrium, lanthanum, and samarium derivatives were utilized to polymerize *rac*-LA, while complexes of other metals were used as catalysts for hydroamination (vide infra).
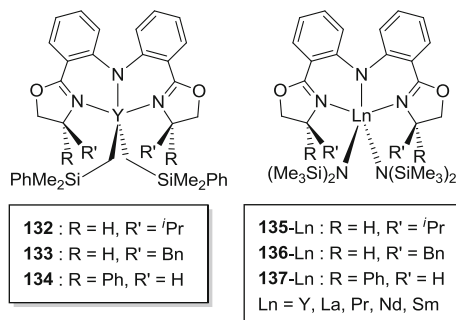
Chart 9 Ward's dialkyl and diamido complexes **132–134** and **135–137**-Ln

All compounds studied were found to be suitable initiators, with **132** being the most active, converting 100 equiv. of *rac*-LA into PLA in less than 2 min. Higher than predicted molecular weights and relatively broad molecular weight distributions indicated only moderate control, and notably, the alkyl species exhibited slightly higher activity than the corresponding amido complexes. The PLA obtained was shown to be heterotactic rich with P_r values of 0.66–0.81.

Despite the plethora of catalytic information provided above, comparing the performance of distinct rare earth metal complexes as initiators in the ROP of lactide is not straightforward. Polymerization experiments are often conducted under different conditions (temperature, reaction time, solvent, etc.) with variable monomer-to-initiator ratios. Nevertheless, a collection of data from representative runs has been tabulated in Table 1 (mononuclear initiators) and Table 2 (dinuclear initiators). For specific information regarding each distinct catalyst, the reader is directed to the corresponding reference. The disparate nature of experimental variables notwithstanding, certain conclusions can be drawn:

1. Pincer ligands can be used to effectively stabilize rare earth metal complexes to produce well-behaving, efficient initiators for the ROP of lactide.
2. Following the general trend inherent to rare earth complexes, larger ionic radii bring about more reactive species and thus more active ROP catalysts. On the other hand, there is often a trade-off between activity and control, wherein prior to optimization studies, the most active catalysts typically afford lower-quality polymers.
3. The solvent used in polymerization reactions has a major affect on the performance of the initiator. For example, coordinating solvents, such as THF, tend to hamper the activity of smaller metals, presumably by competitive coordination with the monomer. Conversely, poor solubility of lactide in noncoordinating solvents can decrease control over the polymerization, producing broader molecular weight distribution polymers (vide supra).

Table 1 Polymerization of *rac*-lactide or L-lactide by mononuclear rare earth pincer complexes

Entry	Complex	M	Solv.	T (°C)	Time (min)	[LA$_0$]/[I$_0$]	Conv. (%)	M_n^{calc} (×10^3)[a]	M_n^{obs} (×10^3)	M_w/M_n	P_r	References
1	**110**	Y	THF	20	2	300	100	21.6[b]	30.8	1.65	–	[106]
2	**110**	Y	THF	20	30	500	100	36.0[b]	45.7	1.72	0.69	[107]
3	**111**	Y	THF	20	60	300	100	43.2	46.4	1.46		[106]
4	**112**	Y	THF	20	2	300	100	21.6[b]	33.0	1.58		[106]
5	**113**	Y	THF	20	60	300	100	43.2	61.2	1.31		[106]
6	**114-Y**	Y	THF	20	60	500	100	72.1	76.4	1.29	0.62[c]	[108]
7	**114-Y**	Y	Tol	20	60	500	67	48.3	49.5	1.23	0.56[c]	[108]
8	**114-Yb**	Yb	THF	20	60	500	88	63.4	64.6	1.25	0.58[c]	[108]
9	**114-Yb**	Yb	Tol	20	60	500	76	54.8	56.3	1.27	0.54[c]	[108]
10	**119**	Y	Tol	20	240	500	100	72.1	72.3	1.23	0.70	[112]
11	**119**	Y	THF	20	240	500	65	46.8	46.2	1.28	0.71	[112]
12	**120-Y**	Y	Tol	20	240	500	100	72.1	72.3	1.21	0.74	[112]
13	**120-Y**	Y	THF	20	240	500	75	54.0	54.6	1.26	0.72	[112]
14	**120-Sm**	Sm	Tol	20	240	500	100	72.1	71.6	1.23	0.67	[112]
15	**120-Yb**	Yb	Tol	20	240	500	100	72.1	71.8	1.25	0.71	[112]
16	**123-Sc**	Sc	THF	20	700	100	100	14.4	16.2	1.55	0.65	[113]
17	**123-Y**	Y	THF	20	60	100	71	10.2	8.9	1.32	0.90	[113]
18	**123-Y**	Y	Tol	20	3	100	100	14.4	10.0	1.52	0.50	[113]
19	**123-La**	La	THF	20	40	100	87	12.5	12.7	1.43	–	[113]
20	**124-Sc**	Sc	THF	20	700	100	100	14.4	17.1	1.61	0.93	[113]
21	**124-Y**	Y	THF	20	700	100	100	14.4	17.3	1.52	0.84	[113]
22	**124-La**	La	THF	20	360	100	81	11.7	14.1	1.43	0.50	[113]
23	**125-Sc**	Sc	THF	20	700	100	100	14.4	13.1	1.42	0.66	[113]
24	**125-Y**	Y	THF	20	700	100	100	14.4	14.0	1.82	0.68	[113]
25	**125-La**	La	THF	20	700	100	100	14.4	11.6	1.51	0.75	[113]

(continued)

Table 1 (continued)

Entry	Complex	M	Solv.	T (°C)	Time (min)	[LA₀]/[I₀]	Conv. (%)	M_n^{calc} (×10³)[a]	M_n^{obs} (×10³)	M_w/M_n	P_r	References
26	**126-Sc-ⁱPr**	Sc	THF	RT	1,200	200	38	11.0	8.1	1.20	–	[114]
27	**126-Sc-ⁱPr**	Sc	Tol	RT	1,200	200	27	7.8	8.3	1.22	–	[114]
28	**126-Sc-Ph**	Sc	Tol	RT	1,200	200	23	6.6	6.4	1.50	–	[114]
29	**126-Sc-ⁱPr**	Sc	-	130	60	200	49	14.4	3.1	1.20	–	[114]
30	**126-Y-ⁱPr**	Y	THF	RT	15	200	65	18.7	15.9	1.25	–	[114]
31	**126-Y-ⁱPr**	Y	Tol	RT	15	200	82	23.6	20.4	1.47	–	[114]
32	**126-Y-Ph**	Y	THF	RT	15	200	79	22.8	21.5	1.25	–	[114]
33ᵈ	**126-Sc-Ph**	Sc	THF	RT	1,200	500	44	5.3ᵉ	4.0	1.06	–	[115]
34ᵈ	**126-Y-Ph**	Y	THF	RT	60	500	78	56.2ᵉ	47.0	1.26	–	[115]
35ᵈ	**126-Y-Ph**	Y	THF	RT	60	500	85	20.4ᵉ	23.7	1.13	–	[115]
36ᵈ	**126-Y-Ph**	Y	THF	RT	60	500	85	10.2ᵉ	10.0	1.07	–	[115]
37	**127-Sc**	Sc	THF	20	180	200	21	6.1	9.5	1.58	0.72	[116]
38	**127-Y**	Y	THF	20	5	200	89	25.7	25.4	2.23	0.77	[116]
39	**127-Y**	Y	Tol	20	5	200	88	25.4	14.9	2.23	0.57	[116]
40	**127-Y**	Y	DCM	20	2	200	100	28.8	25.2	1.54	0.64	[116]
41	**127Y**	Y	-	130	10	200	87	25.1	29.7	2.02	0.59	[116]
42	**128**	Y	THF	20	15	200	67	19.3	21.9	1.94	0.74	[116]
43	**129-Me**	Y	DCM	25	30	50	91	6.6	9.8	1.21	–	[117]
44	**129-ᵗBu**	Y	DCM	25	30	50	88	6.3	10.7	1.19	–	[117]
45	**129-ᵗBu**	Y	Tol	25	30	50	87	6.3	12.0	1.22	–	[117]
46	**129-ᵗBu**	Y	DCM	25	30	100	86	12.4	28.0	1.28	–	[117]
47	**130-Y**	Y	THF	20	1,440	100	0	–	–	–	–	[118]
48	**130-Nd**	Nd	THF	20	360	100	99	14.3	3.9	1.46	–	[118]
49	**132-Y**	Y	THF	25	0.5	100	95	13.8	32.0	1.18	0.72	[119]
50	**132-Y**	Y	THF	25	1.5	100	99	14.4	30.1	1.24	0.73	[119]
51	**133-Y**	Y	THF	25	1.5	100	95	13.9	35.5	1.38	0.76	[119]

52	134-Y	Y	THF	25	1.5	100	95	13.5	31.1	1.23	0.69	[119]
53	135-Y	Y	THF	25	300	100	88	12.8	17.9	1.55	0.70	[119]
54	135-Sm	Sm	THF	25	300	100	90	13.2	13.2	1.92	0.66	[119]
55	135-La	La	THF	25	10	100	88	12.8	22.8	2.15	0.68	[119]

[a] $M_n^{calc} = (144.13 \times [LA_0]/[I_0] \times \%conv.)$
[b] $M_n^{calc} = (144.13 \times [LA_0]/2[I_0] \times \%conv.)$
[c] P_m = probability of *meso* linkages between monomers
[d] Polymerization performed in the presence of ^{i}PrOH (5, 0, 2, and 5 equiv. compared to initiator for entries 33–36, respectively)
[e] $M_n^{calc} = (144.13 \times [LA_0]/[I_0 + ^iPrOH] \times \%conv.)$

Table 2 Polymerization of *rac*-lactide or L-lactide by dinuclear rare earth pincer complexes

Entry	Complex	M	Solv.	T (°C)	Time (min)	[LA$_0$]/[I$_0$]	Conv. (%)	M_n^{calc} (×10^3)^a	M_n^{obs} (×10^3)	M_w/M_n	P_r	References
1	**109**	Y	THF	20	60	300	93	40.2	24.4	1.49	–	[105]
2	**115**	Sm	THF	20	60	1,000	87	62.7	54.2	1.23	0.54	[109]
3	**115**	Sm	Tol	20	60	1,000	90	64.9	66.2	1.28	0.58	[109]
4	**116**	Y	THF	20	60	500	88	63.4	59.3	1.26	0.59	[109]
5	**116**	Y	Tol	20	60	500	100	72.1	72.9	1.21	0.68	[109]
6	**117**-Y	Y	Tol	70	240	400	35	20.2	70.8	1.35	–	[110]
7	**117**-Nd	Nd	Tol	70	240	400	96	55.3	84.7	1.73	–	[110]
8	**117**-Sm	Sm	Tol	70	240	400	97	55.9	13.1	1.61	–	[110]
9	**117**-Yb	Yb	Tol	70	240	100	40	5.8	19.7	2.37	–	[110]
10	**118**-Y	Y	Tol	70	240	100	52	7.5	12.6	2.03	–	[111]
11	**118**-Nd	Nd	Tol	70	240	200	95	27.4	80.8	2.02	–	[111]
12	**118**-Sm	Sm	Tol	70	240	200	64	18.4	32.2	1.68	–	[111]
13	**118**-Yb	Yb	Tol	70	240	100	20	2.9	7.5	2.44	–	[111]
14	**121**-Sm	Sm	Tol	20	240	500	93	67.0	66.5	1.24	0.68	[112]
15	**121**-Yb	Yb	Tol	20	240	500	90	64.9	64.4	1.22	0.66	[112]
16	**122**-Y	Y	Tol	20	240	500	78	56.2	56.8	1.21	0.69	[112]
17	**122**-Y	Y	THF	20	240	500	56	40.4	40.6	1.32	0.67	[112]
18	**122**-Yb-H	Yb	Tol	20	240	500	84	60.5	60.2	1.24	0.72	[112]
19	**122**-Yb-^{t}Bu	Yb	Tol	20	240	500	80	57.7	57.2	1.21	0.69	[112]

$^a M_n^{calc} = (144.13 \times [LA_0]/[I_0] \times \%conv.)$
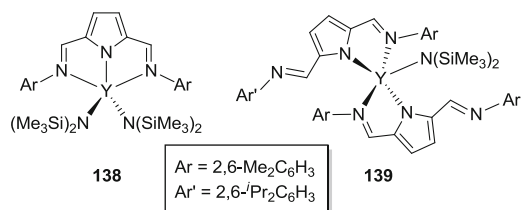
Chart 10 Mono- and bis(pyrrolyl) yttrium ε-caprolactone polymerization catalysts
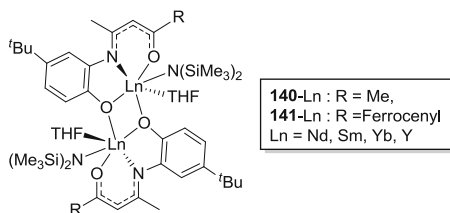
Chart 11 Dinuclear monoamido compounds **140**-Ln and **141**-Ln

4.1.2 Polymerization of ε-Caprolactone

Poly(ε-caprolactone) (PCL) is a highly attractive target for new plastics and commodity polymers owing to its properties as a biodegradable polymer. Supplementary to their popularity in the polymerization of PLA, rare earth metal complexes have garnered significant attention as catalysts for PCL production. As a result, many novel species which exhibit high or even exceptional catalytic activity have been reported [120]. The performance of pincer-supported rare earth complexes (with anionic initiating groups) as catalysts for the ROP of ε-caprolactone (ε-CL) is detailed below.

At the turn of the millennium, Mashima and co-workers prepared the heteroleptic diamido mono(pyrrolyl) complex $(Xyl_2\text{-pyr})Y(N(SiMe_3)_2)_2$, **138** $(Xyl_2\text{-pyr} = 2,5\text{-bis}[N\text{-}(2,6\text{-Me}_2C_6H_3)\text{iminomethyl}]\text{pyrrolyl})$. Although not a bona fide pincer complex, a bis(pyrrolyl) monoamido species $(Dipp_2\text{-pyr})_2YN(SiMe_3)_2$, **139**, $Dipp_2\text{-pyr} = 2,5\text{-bis}[N\text{-}(2,6\text{-}^iPr_2C_6H_3)\text{iminomethyl}]\text{pyrrolyl}$ was also obtained when $Dipp_2\text{-pyr}$ was used as the ancillary ligand (Chart 10). Catalytic studies indicated that complexes **138** and **139** initiated the ROP of ε-CL and also demonstrated that the monoamido complex **139** acted as a single-site initiator to give PCL with narrow molecular weight distribution (PDI = 1.2). It should also be noted that the homoleptic $Y(Xyl_2\text{-pyr})_3$ complex was shown to be virtually inactive [12].

In addition to their studies on the ROP of lactide (vide supra), Arnold et al. have also investigated mononuclear yttrium diamido complexes **129**-R in the ring-opening polymerization of ε-CL. Specifically, complex **129**-^{t}Bu produced PCL with low PDIs under mild experimental conditions. However, an undesirable
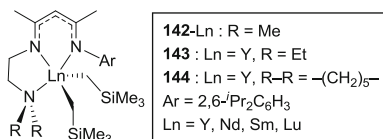
Chart 12 Mononuclear rare earth dialkyl complexes **142–144**
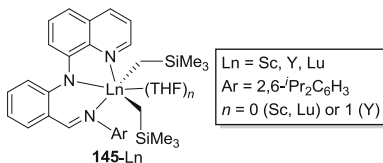
Chart 13 Sc, Y, and Lu dialkyl complexes **145**-Ln

range of chain lengths was observed when longer reaction times were employed, implying that **129**-R can also facilitate undesirable transesterifications [117].

Dinuclear monoamido complexes [LLnN(SiMe₃)₂(THF)]₂, **140**-Ln, (Ln = Nd, Sm, Yb, Y; L = MeCOCHC(Me)N(2-O-5-^{t}Bu-C₆H₃)) were prepared by Yao et al. (Chart 11) [121]. All **140**-Ln compounds initiated the ROP of ε-CL with modest activity, producing polymers with high molecular weight and relatively broad polydispersities. The size of the metal center clearly had an effect on polymerization as substantial loss in activity occurred with decreasing ionic radius. In an intriguing structural modification, the introduction of a ferrocenyl moiety into the ancillary ligand framework produced complexes **141**-Ln. Unfortunately, no increase in catalytic activity was observed, as **141**-Ln produced polycaprolactone in a similar fashion to its methyl-substituted brethren **140**-Ln [122].

In 2008, Chen and co-workers reported Y-, Lu-, Sm-, and Nd-dialkyl complexes that exhibit high ε-CL polymerization activities and relatively narrow PDIs, ranging from 1.34 to 1.39 (Chart 12) [123]. Interestingly, exchanging the metal in complexes **142**-Ln (Ln = Y, Lu, Sm, Nd) had little effect on catalytic activity, whereas modification of the ligand substituents had a pronounced impact. For example, replacement of the NMe₂ group in **142**-Ln for an NEt₂, **143**, or a piperidine moiety, **144**, resulted in improved catalytic activities and molecular weights without a noticeable increase in polydispersity.

Cui et al. reported the mononuclear dialkyl complexes LLn(CH₂SiMe₃)₂(THF)ₙ (Ln = Sc, Y, Lu, n = 0; Ln = Y, n = 0; L = N-(2-(((2,6-^{i}Pr₂C₆H₃)imino)methyl)-phenyl)quinolin-8-amine) **145**-Ln (Chart 13) [124]. Notably, the scandium and lutetium species **145**-Sc and **145**-Lu were THF-free with ancillaries arranged in a square-pyramidal geometry. Meanwhile, the geometry about the larger yttrium center in complex **145**-Y is best described as distorted octahedral with one coordinated THF molecule. All of the complexes were highly active living catalysts for the ROP of ε-caprolactone, but the Y and Lu species were the most active. The rigid and bulky nature of the ancillary ligand in **145**-Ln appears to suppress the
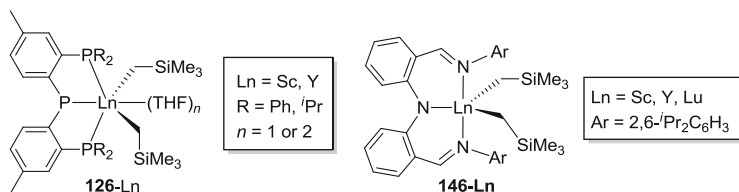
Chart 14 Rare earth dialkyl complexes bearing PPP, **126**-Ln, or NNN, **146**-Ln, pincer ligands
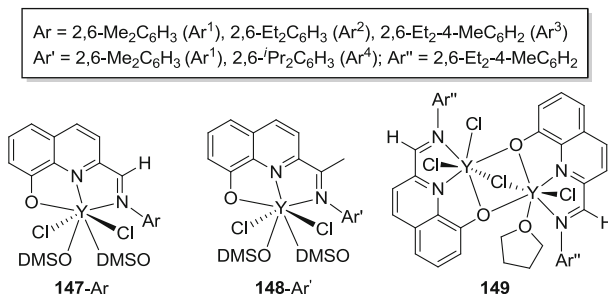
Chart 15 Mono- and dinuclear yttrium imino(methyl) quinolate complexes

backbiting and chain-transfer processes frequently observed in ε-CL polymerization catalyzed by dialkyl lanthanide complexes.

In addition to being active in lactide polymerization catalysis (vide supra), scandium and yttrium dialkyl complexes LLn(CH$_2$SiMe$_3$)$_2$(THF)$_n$ (Ln = Sc, Y; L = (4-methyl-6-PR$_2$-C$_6$H$_3$)$_2$P; R = ^{i}Pr, Ph, n = 1 or 2) **126**-Ln-R, which possess PPP donor ligands (Chart 14, left), catalyze ε-CL polymerization with very high TOFs [115]. The yttrium species **126**-Y-R were found to be more active than the scandium derivatives, which is not particularly surprising given the previous correlations noted between catalytic activity and ionic radius. Upon examining the substituents, the higher activity observed for **126**-Ln-Ph most likely originates from the weaker electron-donating ability of the phenyl groups attached to the phosphorus donors, thus increasing the Lewis acidity of the metal. Interestingly, living ROP of ε-CL was observed when complexes **126**-Ln-R were combined with 5 equiv. of isopropanol. Samples of PCL with close to predicted molecular weights and narrow PDIs were produced when appropriate ^{i}PrOH/initiator ratios were used.

Dialkyl complexes LLn(CH$_2$SiMe$_3$)$_2$ **146**-Ln (Ln = Sc, Lu, Y; L = (2,6-^{i}Pr$_2$C$_6$H$_3$–N=CH–C$_6$H$_4$)$_2$N) involving modified NNN ancillary frameworks (Chart 14, right), reported by Li et al., also proved to be highly active initiators for the polymerization of ε-CL polymerization [125]. Again, the yttrium derivative **146**-Y was the most active system, as it polymerized ε-CL in a rapid and living manner. In addition to the polymerization of ε-CL, **146**-Y was also active in the random copolymerization of ε-CL and γ-butyrolactone (γ-BL) (vide infra).

As a new contribution to the field, Sun, Glaser, and colleagues prepared a series of yttrium dihalide complexes of the form LYCl$_2$(DMSO)$_2$ (L = 2-((arylimino)

alkyl)quinolin-8-ol), **147**-Ar and **148**-Ar′ (Chart 15) [126]. Moreover, the stoichiometric reaction of potassium 2-((2,6-dimethylphenylimino)methyl)quinolin-8-olate with $YCl_3(THF)_3$ in the absence of DMSO resulted in the formation of dimeric yttrium species **149**. Subsequent in situ metathesis with $LiCH_2SiMe_3$ or $LiCH_2SiMe_3$ and benzyl alcohol (BzOH) produced catalytically active complexes that could facilitate polymerization of ε-CL with high efficiency. In the presence of BzOH, PCL possessing narrow molecular weight distribution was produced in a living manner. However, polymerization in the absence of alcohol resulted in higher than expected molecular weights, as well as broadened PDI values indicative of a more poorly controlled polymerization process. Differently substituted ancillaries (Ar = 2,6-$Me_2C_6H_3$ (Ar¹), 2,6-$Et_2C_6H_3$ (Ar²), 2,6-Et_2-4-MeC_6H_2 (Ar³); Ar′ = 2,6-$Me_2C_6H_3$ (Ar¹), 2,6-$^iPr_2C_6H_3$ (Ar⁴); Ar″ = 2,6-Et_2-4-MeC_6H_2) did not bring about major differences in catalytic behavior, and similar activities and polymer features were observed by both the aforementioned dinuclear species and their mononuclear analogues, thus suggesting that both precatalysts lead to the same catalytically active species.

In 2005, Huang et al. prepared the chloride-bridged dinuclear ate complex **150**, $LYCl_2(\mu-Cl_2)\cdot Li(OEt_2)_2$ (L = 2,5-$(CH_2NMe_2)_2C_4H_2N$). Unfortunately, this complex was not an active catalyst for the ROP of ε-caprolactone. Such inertness is not surprising, given the lack of precedent for chloride ligands to initiate ROP [127].

Although slow in the initiation of ROP of L-LA (vide supra) [118], complexes **130**-Ln were found to promote ROP of ε-CL under moderate experimental conditions (e.g., 90% conversion of 200 equiv. of monomer over 24 h at 70°C). Furthermore, the sodium cation in the ate complexes was shown to play a key role in the polymerization. As a result, studies on the effect of encapsulating the cation, to separate it from the lanthanide metal, were investigated by the addition of crown ether (18-crown-6) to a solution of **130**-Ln, generating new, discrete, ion pairs $[L_2Ln][(18$-crown-6)$Na(THF)_2]$ (Ln = Y, Yb) **131**-Ln. When compared to the aforementioned complexes, the catalytic activity of these "separated" ate complexes decreased considerably, indicating a bimetallic mechanism is most likely operative in polymerization mediated by these ate complexes.

Since most of the rare earth elements are relatively immune to reduction or oxidation, the +3 oxidation state dominates much of rare earth chemistry. However, divalent lanthanides, namely, samarium, europium, thulium, and ytterbium, are reasonably common. Accordingly, divalent Eu(II) and Yb(II) complexes were recently probed by Roesky and co-workers for their ability to polymerize ε-CL [128]. Heteroleptic complexes (Dipp₂-pyr)$Ln(BH_4)(THF)_3$ (Ln = Eu, Yb; Dipp₂-pyr = 2,5-bis[N-(2,6-$^iPr_2C_6H_3$)iminomethyl]pyrrolyl), **151**-Ln, were successfully prepared by a salt metathesis reaction between deprotonated ancillary Dipp₂-pyr and $[Ln(BH_4)_2(THF)_2]$. Out of the two complexes, **151**-Eu proved to be an active initiator, producing PCL with high molecular weight and good control over polymer features.

Similar to the ROP of lactide, polymerization of ε-caprolactone has been performed under various reaction conditions (temperatures, reaction times, etc.), using distinct monomer to initiator ratios. In general, the complexes noted above

Table 3 Polymerization of ε-caprolactone by mononuclear rare earth pincer complexes

Entry	Complex	M	Solv.	T (°C)	Time (min)	$[CL_0]/[I_0]$	Conv. (%)	M_n^{calc} ($\times 10^3$)[a]	M_n^{obs} ($\times 10^3$)	M_w/M_n	References
1	**129-*t*Bu**	Y	Tol	25	30	500	99	56.5	43.5	1.19	[117]
2	**129-*t*Bu**	Y	Tol	25	60	500	99	56.5	64.5	1.29	[117]
3	**129-*t*Bu**	Y	Tol	25	240	500	97	55.4	94.8	1.55	[117]
4	**130-Y**	Y	Tol	70	1,440	100	91	5.2	7.2	1.49	[118]
5	**130-Nd**	Nd	Tol	70	1,440	100	>99	5.6	8.9	1.39	[118]
6	**130-Er**	Er	Tol	70	1,440	100	66	3.8	3.9	1.44	[118]
7	**130-Yb**	Yb	Tol	70	1,440	100	95	5.4	6.2	1.56	[118]
8	**131-Y**	Y	Tol	70	1,440	100	40	2.3	2.7	1.17	[118]
9	**131-Yb**	Yb	Tol	70	1,440	100	39	2.2	2.4	1.13	[118]
10	**138**	Y	Tol	0	5	100	71	8.1	66.0	1.60	[12]
11	**139**	Y	Tol	0	5	100	99	11.3	61.3	1.20	[12]
12	**142-Y**	Y	Tol	26	20	2,000	89	203.2	23.7	1.37	[123]
13	**142-Nd**	Nd	Tol	26	20	2,000	89	203.2	29.4	1.35	[123]
14	**142-Sm**	Sm	Tol	26	20	2,000	85	194.0	28.7	1.35	[123]
15	**142-Lu**	Lu	Tol	26	20	2,000	95	216.9	46.9	1.35	[123]
16	**143**	Y	Tol	26	20	2,000	97	221.4	62.5	1.39	[123]
17	**144**	Y	Tol	26	20	2,000	98	223.7	67.8	1.34	[123]
18	**110**	Y	Tol	25	5	945	100	107.9	91.0	1.87	[124]
19	**145-Sc**	Sc	Tol	25	30	945	99	106.8	94.5	1.18	[124]
20	**145-Y**	Y	Tol	26	5	945	100	107.9	99.1	1.41	[124]
21	**145-Lu**	Lu	Tol	27	2	945	100	107.9	112.0	1.41	[124]
22	**126-Sc-Ph**	Sc	Tol	RT	5	1,000	80	91.3	69.5	1.34	[115]
23	**126-Sc-*i*Pr**	Sc	Tol	RT	5	1,000	67	76.5	63.7	1.45	[115]
24	**126-Y-Ph**	Y	Tol	RT	1	1,000	73	83.3	86.4	1.40	[115]
25	**126-Y-Ph**	Y	Tol	RT	30	1,000	100	114.1	132.8	1.71	[115]

(continued)

Table 3 (continued)

Entry	Complex	M	Solv.	T (°C)	Time (min)	$[CL_0]/[I_0]$	Conv. (%)	M_n^{calc} (×10³)[a]	M_n^{obs} (×10³)	M_w/M_n	References
26[b]	**126**-Y-Ph	Y	Tol	RT	30	1,000	100	38.0[c]	30.0	1.29	[115]
27[b]	**126**-Y-Ph	Y	Tol	RT	30	1,000	100	12.7[c]	13.7	1.16	[115]
28[b]	**126**-Y-Ph	Y	Tol	RT	30	1,000	85	2.4[c]	2.6	1.13	[115]
29	**126**-Y-^{i}Pr	Y	Tol	RT	5	1,000	91	103.9	61.4	1.46	[115]
30	**146**-Sc	Sc	Tol	25	120	2,000	100	228.3	170.0	1.26	[125]
31	**146**-Y	Y	Tol	25	5	2,000	100	228.3	240.0	1.25	[125]
32[d]	**146**-Y	Y	Tol	25	5	2,000	100	228.3	250.0	1.22	[125]
33	**146**-Lu	Lu	Tol	25	15	2,000	100	228.3	170.0	1.35	[125]
34[e]	**147**-Ar[1]	Y	Tol	20	30	500	89.7	51.2	65.7	1.68	[126]
35[e,f]	**147**-Ar[1]	Y	Tol	20	30	500	95.3	54.4	57.9	1.21	[126]
36[e,f]	**147**-Ar[2]	Y	Tol	20	30	500	98.4	56.2	58.4	1.14	[126]
37[e,f]	**147**-Ar[3]	Y	Tol	20	30	500	97.6	55.7	56.6	1.19	[126]
38[e,f]	**148**-Ar[1]	Y	Tol	20	30	500	94.4	53.9	52.0	1.09	[126]
39[e,f]	**148**-Ar[4]	Y	Tol	20	30	500	96.9	55.3	63.6	1.28	[126]
40	**151**-Eu	Eu	Tol	20	30	200	100	22.8	15.4	1.11	[128]

[a] $M_n^{calc} = (114.14 \times [CL_0]/[I_0] \times \%conv.)$
[b] Polymerization performed in the presence of ^{i}PrOH (2, 8, and 40 equiv. to initiator for entries 20–22, respectively)
[c] $M_n^{calc} = (144.13 \times [LA_0]/[I_0 + {}^i PrOH] \times \%conv.)$
[d] Polymerization of 1,000 equiv. of CL for 2 min followed by the addition of another 1,000 equiv. for 3 min
[e] Dihalides **147**–**148** were activated with 2 equiv. of LiCH$_2$SiMe$_3$
[f] Polymerization was performed in the presence of 1 equiv. of benzyl alcohol

Table 4 Polymerization of ε-caprolactone by dinuclear rare earth pincer complexes

Entry	Complex	M	Solv.	T (°C)	Time (min)	$[CL_0]/[I_0]$	Conv. (%)	M_n^{calc} ($\times 10^3$)[a]	M_n^{obs} ($\times 10^3$)	M_w/M_n	References
1	**140-Y**	Y	Tol	50	120	200	62	14.2	65.9	2.46	[121]
2	**140-Nd**	Nd	Tol	50	120	400	95	43.4	150.4	2.62	[121]
3	**140-Sm**	Sm	Tol	50	60	200	100	22.8	15.2	1.99	[121]
4	**140-Sm**	Sm	Tol	50	120	300	100	34.2	57.8	1.64	[121]
5	**140-Sm**	Sm	THF	50	120	300	52	17.8	67.1	1.56	[121]
6	**140-Yb**	Yb	Tol	50	120	200	17	3.9	10.9	1.66	[121]
7	**141-Y**	Y	Tol	50	120	300	70	24.0	82.3	1.85	[122]
8	**141-Nd**	Nd	Tol	50	120	200	98	22.4	78.5	1.73	[122]
9	**141-Nd**	Nd	Tol	50	120	400	90	41.1	167.7	1.69	[122]
10	**141-Nd**	Nd	THF	50	120	400	53	24.2	86.2	1.33	[122]
11	**141-Nd**	Nd	DCM	50	120	400	25	11.4	18.6	1.45	[122]
12	**141-Sm**	Sm	Tol	50	120	300	100	34.2	136.3	1.44	[122]
13	**141-Yb**	Yb	Tol	50	120	200	76	17.3	46.3	1.76	[122]
14[b,c]	**149**	Y	Tol	20	30	500	94.8	54.1	51.4	1.21	[126]
15	**150**	Y	Tol	RT	1,440	100	0	0.0	–	–	[127]

[a]$M_n^{calc} = (114.14 \times [CL_0]/[I_0] \times \%conv.)$

[b]Dihalide **132** was activated with 2 equiv. of $LiCH_2SiMe_3$

[c]Polymerization was performed in the presence of 1 equiv. of benzyl alcohol

are very active catalysts for the production of PCL in a relatively controlled manner with good, or occasionally even excellent, polymer properties. Alkyl variants appear to serve as better initiators compared to amido counterparts, whereas chloride species seem to be virtually inactive. Although examples of ε-CL polymerization in solvents other than toluene are few in number, the effect of solvent is similar to that observed in the ROP of lactide. Representative results from each reference are tabulated in Tables 3 and 4, which can be utilized to draw certain conclusions in regard to the performance of each individual rare earth pincer complex.

4.1.3 Polymerization of Other Cyclic Esters

Aside from recently popularized ROP of lactide and ε-caprolactone, only a few studies have been undertaken with other cyclic esters. The dialkyl complex **126**-Y (Chart 14) was shown to polymerize δ-valerolactone with comparable activity and a similar rate constant (pseudo first order) to that observed for the ROP of lactide. Consequently, it was surmised that the reactivity of cyclic esters toward ROP is dependent on the Lewis basicity of the carbonyl groups, which is inherently affected by the size of the ring [115]. Complexes **126**-Ln were also active in the ROP of *rac*-β-butyrolactone (BBL) at elevated temperatures, but the process was considerably slower when either ε-CL or LA was used as the monomer. The addition of isopropanol did not change the polymer features, whereas elongated reaction time and/or altering the quantity of monomer resulted in lower molecular weight polymers and broader molecular weight distributions [115].

Monoamido complexes **123**-Ln and **125**-Ln were also active in the ROP of BBL, whereas SiMe$_2$^{t}Bu-substituted **124**-Ln did not exhibit any polymerization activity (Chart 5). The lack of activity of this series is clearly related to the nature of the silyl substituents (SiMe$_2$^{t}Bu vs. SiPh$_3$), although the exact cause for inactivity remains unknown. However, **123**-Ln and **125**-Ln were able to facilitate polymerization of *rac*-BBL at ambient temperature. Also, the addition of isopropanol to presumably generate the Sc-isopropoxide species in situ led to faster rates of reaction, suggesting a slow initiation step when amido ligands are employed. Lanthanum complexes **123**-La and **125**-La demonstrated the highest polymerization activity, while the detrimental influence of THF solvent, compared to toluene, was identical
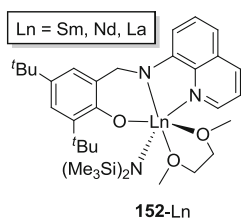
Chart 16 Monoamido lanthanide catalysts for the ROP of 1,4-dioxan-2-one

to that observed in LA catalysis. Relatively low PDI values indicated a good level of polymerization control. Finally, high stereoselectivities were observed in all cases, especially with **123**-Y and **123**-La [113].

Further contributions to the ROP of cyclic monomers were reported by Yao, Wang, and co-workers who investigated polymerization of 1,4-dioxan-2-one using monoamido complexes LLnN(SiMe$_3$)$_2$(DME) (Ln = Sm, Nd, La; L = (3,5-^{t}Bu$_2$-2-O-C$_6$H$_2$CH$_2$N-C$_9$H$_6$N)), **152**-Ln (Chart 16) [129]. All complexes produced high molecular weight polymers, but the neodymium species **152**-Nd was found to be the most active. Polymerization in the presence of a stoichiometric quantity of benzyl alcohol was also investigated, wherein higher activities than the corresponding amido complexes by themselves were observed, presumably because the initiating group had been converted to an alkoxide. Significantly, when reaction temperatures were higher than 60°C, lower conversion was observed and the isolated polymers had lower molecular weights.

4.1.4 Copolymerization Studies

Although more prevalent in the catalyses noted above, rare earth pincer complexes have also been tested as catalysts for the preparation of copolymers, exploiting ROP activity of two different cyclic esters. For example, complex **126**-Y, equipped with a phenyl substituted PPP donor ligand, produced PCL–PLA block copolymers via the addition of ε-CL followed by LA. Interestingly, when the order of monomer addition was reversed, no copolymer was observed whatsoever, and only the homopolymer PLA was formed. This seems somewhat contradictory since, as noted above, **126**-Y was more active for ε-CL homopolymerization than the ROP of lactide. Therefore, the reactivity order appears to be reversed for copolymerization of the two monomers. The origin of this reversal of monomer reactivity during copolymerization is not completely understood, but it may be rationalized by the combination of the stronger coordinative ability of lactide, combined with the electrophilic initiator **126**-Y [115].

Copolymerization experiments were also conducted with **146**-Y and **146**-Lu which bear NNN pincer ligands [125]. Although the lutetium derivative **146**-Lu exhibited higher activity than **146**-Y, both complexes initiated copolymerization of ε-CL and γ-BL, despite the fact that neither complex exhibited activity for the homopolymerization of γ-BL. The γ-BL content in poly(ε-CL-co-γ-BL) was determined to be less than 20 mol% even when a 1:3 ε-CL:γ-BL monomer ratio was used.

4.2 Polymerization of Dienes

Synthetic polymers play an extremely important role in our everyday life as they are used virtually everywhere, from food packaging to the automotive industry.
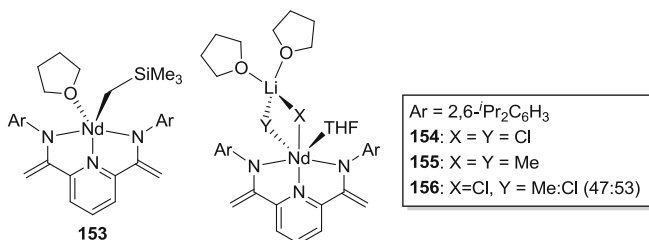
Chart 17 Yttrium pincer species **153–156** which are active catalysts for the polymerization of butadiene
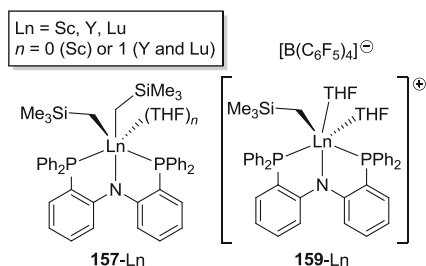
Chart 18 Neutral and cationic rare earth alkyl complexes **157**-Ln and **159**-Ln

Preparation of polymers with desired properties requires precise control over polymer microstructure. In the preparation of these desirable materials, the polymerization of 1,3-conjugated dienes serves as an excellent tool to convert simple monomers into materials with versatile properties. For example, *cis*-1,4-polybutadiene can be used as a component in the preparation of tires, and polyisoprene with high *cis*-1,4-regularity can be utilized as an alternative to natural rubber [130].

Wilson, Gambarotta, and colleagues were one of the first to study rare earth pincer complexes as diene polymerization catalysts [131]. Neodymium compounds LNd(CH$_2$SiMe$_3$)(THF), **153**, LNd(μ-X)$_2$[Li(THF)$_2$] X = Cl, **154**, and Me, **155**, Nd(μ-Cl)(μ-X)[Li(THF)$_2$](THF), X = Me:Cl in a 47:53 occupation ratio, **156**, (L = [2,6-(2,6-^{i}Pr$_2$C$_6$H$_3$)-N-C=(CH$_2$)]$_2$C$_5$H$_3$N) (Chart 17) were prepared, and their butadiene polymerization behavior was investigated. All ate complexes, **154–156**, were found to be highly active precatalysts for stereoselective *cis*-butadiene polymerization at 50°C, though they first needed to be activated with modified methylaluminoxane (MMAO). Meanwhile, the monoalkyl species **153** displayed negligible activity. Catalysts **154–156** were able to generate polybutadiene possessing a high *cis* content (95–97%), and polymer yields generally greater than 70%, except for the methyl-bridged complex **155**, which afforded a polymer yield less than 20%. The ancillary ligand was shown to be advantageous: complexes **154–156** were more active than NdCl$_3$(THF)$_2$. It should also be noted that complex **156** was found to be much more active in cyclohexane than in toluene.
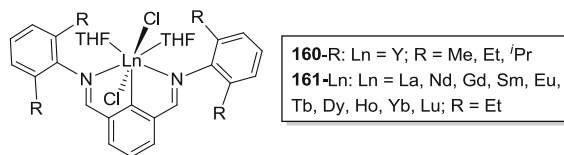
Chart 19 NCN-pincer-supported rare earth complexes **160**-R and **161**-Ln

The pincer-ligated Sc, Y, and Lu dialkyl complexes (PNP)Ln-$(CH_2SiMe_3)_2(THF)_n$ (Ln = Sc, Y, Lu; PNP = (2-Ph_2P-$C_6H_4)_2N$; Ln = Sc, $n = 0$; Ln = Y, Lu, $n = 1$), **157**-Ln (Chart 18), were prepared using straightforward alkane elimination protocols, while the subsequent cationic monoalkyl species **158**-Ln were generated from the neutral species by the addition of 1 equiv. of [$PhMe_2NH$]-[$B(C_6F_5)_4$]. Although these cationic complexes decompose rapidly in C_6D_5Cl solution, the corresponding bis(THF) adducts **159**-Ln [(PNP)Ln(CH_2SiMe_3)-$(THF)_2$][$B(C_6F_5)_4$] can be isolated when the reaction is carried out in THF solvent. All **158**-Ln compounds, generated in situ in C_6D_5Cl solution, showed excellent activity in the living polymerization of isoprene at ambient temperature. The polymer contained high *cis*-1,4 content (96.5–99.3%) with **158**-Y giving the most impressive values, coupled with narrow molecular weight distribution (PDIs < 1.11). These properties, selectivity and living character, can even be sustained at elevated temperatures (up to 80°C). In attempts to improve catalysis, Hou and co-workers discovered that the addition of [$PhMe_2NH$][$B(C_6F_5)_4$] to a solution of neutral **157**-Ln and isoprene improves catalyst activity by nearly twofold compared to polymerization results obtained from pregenerated **158**-Ln. Interestingly, the use of alternate activators (e.g., [Ph_3C][$B(C_6F_5)_4$] or $B(C_6F_5)_3$) resulted in substantially lower polymer yields and catalytically inactive complexes, respectively. Furthermore, the corresponding neutral **157**-Ln was not active under the same polymerization conditions. Finally, precatalysts **158**-Ln can also be utilized in the living *cis*-1,4 polymerization of butadiene and living *cis*-1,4-copolymerization of butadiene and isoprene to yield polymers with 99% *cis*-1,4 content and PDI values less than 1.13 [132].

Rare earth metal dichlorides possessing an aryldiimine NCN-pincer ligand $LLnCl_2(THF)_2$ (Ln = Y, **160**-R, La, Nd, Gd, Sm, Eu, Tb, Dy, Ho, Yb, Lu, **161**-Ln; L = 2,6-(2,6-$R_2C_6H_3N$=CH)$_2$-C_6H_3, R = Me, Et, ^iPr) (Chart 19) were synthesized via transmetalation between the lithiated ligand and [$LnCl_3(THF)_n$] [133]. Upon the addition of Al^{i}Bu$_3$ and [Ph_3C][$B(C_6F_5)_4$] activators, high activities and excellent *cis*-1,4 selectivities in the polymerization of butadiene and isoprene were observed. The yttrium species **160**-R were used to study the influence of the ligand *N*-aryl *ortho* substituent on catalytic activity. Significantly, **160**-Et was found to warrant the best activity, topping both methyl- and isopropyl-substituted compounds. Furthermore, the steric bulk of the alkylaluminum compounds was found to be critical to the catalytic behavior of the complexes. As seen in other studies, the high *cis*-1,4 selectivity endured at polymerization temperatures up to 80°C and did not vary with different lanthanide metals. In-depth mechanistic
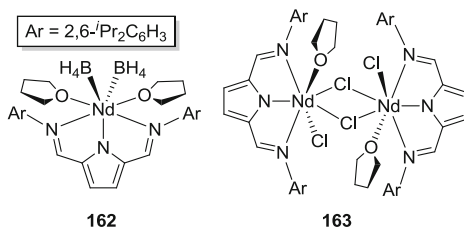
Chart 20 Mono- and dinuclear neodymium complexes **162** and **163**
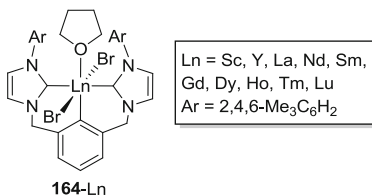
Chart 21 Xylenyl dicarbene rare earth metal dibromide complexes **164**-Ln

studies implied that alkyl-bridged Ln–Al bimetallic cations were the catalytically active species. It is important to note that **161**-Sm, **161**-Yb, and **161**-Eu did not initiate the polymerization reaction, likely because of the reducible nature of these elements.

Later on, Cui and colleagues studied the diene polymerization capabilities of **161**-Nd without the addition of [Ph₃C][B(C₆F₅)₄] activator [134]. Once again, this system exhibited high activity and high *cis*-1,4 selectivity for the polymerization of isoprene. Catalytic performance persisted over a wide range of temperatures, and monomer/catalyst ratios of 500 to 8,000 permitted the isolation of high molecular weight polymers with relatively narrow molecular weight distributions (PDI $\geq$ 1.68). Although the neodymium species appeared to be relatively robust, the catalytic activity does appear to be impacted by the steric bulk of the aluminum co-catalysts. Dynamic investigation of the reaction showed that the molecular weight of the resultant polymer had a near linear correlation with conversion.

Roesky, Eickerling, and co-workers prepared an intriguing neodymium bis(borohydride) LNd(BH₄)₂(THF)₂ complex, **162**, and its dinuclear chloride-bridged counterpart [LNdCl(μ-Cl)(THF)]₂ (L = 2,5-bis[*N*-(2,6-^{i}Pr₂C₆H₃)-iminomethyl]pyrrole), **163** (Chart 20), which they used as catalysts for the polymerization of 1,3-butadiene [135]. In the presence of various co-catalysts (MMAO, AlEt₃/B(C₆F₅)₃ or AlEt₃/[PhMe₂NH][B(C₆F₅)₄]), high activities and good *cis*-selectivities were observed, even when very low catalyst loadings were used (1:20,000–22,600).

In 2010, Cui et al. prepared a series of 2,6-xylenyl dicarbene-ligated rare earth metal dibromides LLnBr₂(THF) (Ln = Sc, Y, La, Nd, Sm, Gd, Dy, Ho, Tm, Lu; L = (2,6-(2,4,6-Me₃C₆H₂-NCHCHNCCH₂)₂-C₆H₃)), **164**-Ln (Chart 21). Using AlR₃ (R = Me, Et, ^{i}Bu) or [Ph₃C][B(C₆F₅)₄] as co-catalysts, a variety of complexes,
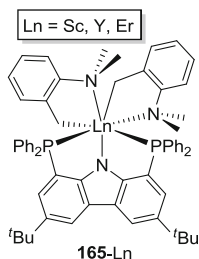
Chart 22 Rare earth bis(alkylamine) complexes **165**-Ln
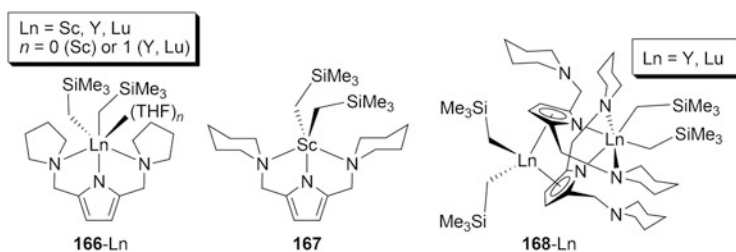
Chart 23 Dialkyl complexes **166**-Ln, **167**, and **168**-Ln

notably **164**-Y, **164**-Nd, and **164**-Dy, found success as catalysts for the polymerization of isoprene, wherein high activity and *cis*-1,4 selectivity (99.6%, 25°C) were noted. Selectivity remained unaffected by the identity of the metal itself and was only slightly influenced by the AlR$_3$, when temperatures were kept at 80°C (97.6%). In order to gain deeper mechanistic insight, a series of stoichiometric reactions were conducted which ultimately identified an yttrium hydrido aluminate cation [LY(μ-H)$_2$Al^{i}Bu$_2$]$^+$ as the catalytically active species [136].

The ligands in tris(aminobenzyl) rare earth complexes [Ln(CH$_2$C$_6$H$_4$-2-NMe$_2$)$_3$] can be replaced by diphosphinocarbazole ligands to afford the first bis(alkylamine) species LLn(CH$_2$C$_6$H$_4$-2-NMe$_2$)$_2$ (Ln = Sc, Y, Er; L = 3,6-^{t}Bu$_2$-1,8-(PPh$_2$)$_2$-carbazole), **165**-Ln (Chart 22). In the presence of [Ph$_3$C][B(C$_6$F$_5$)$_4$], **165**-Ln was transformed into a cationic variant that initiated the polymerization of isoprene and butadiene with high activities. In particular, the yttrium species **165**-Y displayed excellent *cis*-1,4-selectivity (>99%), as well as living polymerization character. This behavior was made evident by the linear relationship between polymer molecular weight and monomer/initiator ratio, which persisted over a wide range of temperatures (0–80°C). Notably, the active catalyst, presumably some form of yttrium diene complex, can further initiate the ROP of ε-caprolactone to selectively produce low PDI (1.15–1.47) poly(*cis*-1,4-diene)-*b*-polycaprolactone block copolymers with predetermined molecular weight ($M_n = 10$–70×10^4) [137].

Mononuclear dialkyl complexes L^{1}Ln(CH$_2$SiMe$_3$)$_2$(THF)$_n$ (Ln = Sc, $n = 0$; Ln = Y, Lu, $n = 1$; L^1 = 2,5-bis((pyrrolidin-1-yl)methylene)-1*H*-pyrrole), **166**-Ln,
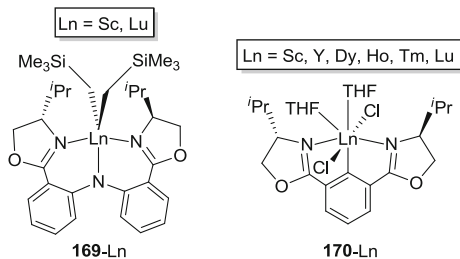
Chart 24 Chiral dialkyl **169**-Ln and dihalide **170**-Ln complexes

and $L^2Sc(CH_2SiMe_3)_2$ ($L^2 = 2,5$-bis((piperidino)methylene)-1H-pyrrole), **167**, or dinuclear tetra-alkyl $L_2^2Ln_2(CH_2SiMe_3)_4$, **168**-Ln (Chart 23), can be prepared in moderate to high yields by straightforward alkane elimination between the requisite proteo ligand and trialkyl rare earth complexes. Upon activation with the Lewis acid [Ph$_3$C][B(C$_6$F$_5$)$_4$], all complexes demonstrated controlled polymerization of isoprene, with complexes **167** and **168**-Ln exhibiting higher activity than **166**-Ln, in general. Complex **168**-Y (although not a bona fide pincer compound) gave high *cis*-1,4-selectivity (94.1%) and the highest activity for the polymerization of isoprene. Conversely, scandium species **166**-Sc and **167** gave high 3,4-selectivity (up to 87%) irrespective of the ancillary ligand, and **166**-Lu and **168**-Lu initiated atactic isoprene polymerization [138].

Zhang, Li, and colleagues utilized a chiral pincer ligand to generate the scandium and lutetium dialkyl complexes LLn(CH$_2$SiMe$_3$)$_2$ (Ln = Sc, Lu; L = (*S,S*)-bis(oxazolinylphenyl)amido), **169**-Ln (Chart 24). When combined with Lewis or Brønsted acid activators, complexes **169**-Ln afforded activities up to 6.8×10^5 g mol Ln^{-1} h^{-1} and atypical *trans*-1,4-selectivity (up to 100%) in the "quasi-living" polymerization of isoprene. The isolated polyisoprene had molecular weights of $M_n = 2$–10×10^4 g/mol and molecular weight distributions of $M_w/M_n = 1.02$–2.66 [139].

Finally, NCN-pincer-ligated rare earth dichlorides LLnCl$_2$(THF)$_2$ (Ln = Sc, Y, Dy, Ho, Tm, Lu; L = (*S,S*)-2,6-bis(4′-^{i}Pr-2′-oxazolinyl)phenyl), **170**-Ln, were generated by Xu, et al. via standard salt metathesis routes (Chart 24, right). Upon activation by [PhNHMe$_2$][B(C$_6$F$_5$)$_4$], together with Al^{i}Bu$_3$, Y, Dy, Ho, and Tm complexes exhibited impressive isoprene polymerization activity and noteworthy *cis*-1,4-selectivity (>98%). Interestingly, complexes involving Sc and Lu were virtually inactive in this process, while yttrium proved to be the most active. Polymers generated by this system were up to 99.5% *cis*-1,4, which seemed consistent regardless of reaction temperature (up to 80°C) [140].

Selected results from the aforementioned diene polymerization studies are gathered in Tables 5 and 6. In brief summary, neutral rare earth pincer species were not active for diene polymerization. Instead, complexes required activation by the addition of a Lewis or Brønsted acid. Once activated, rare earth pincer compounds showed excellent activities and high selectivities in the polymerization of both 1,3-butadiene and isoprene.

Table 5 Polymerization of 1,3-butadiene catalyzed by rare earth pincer complexes

Entry	Complex	Metal	T (°C)	Time (min)	Co-cat.	[BU]/[Al]/[X]/[Ln]	Conv. (%)	M_n ($\times 10^4$)	M_w/M_n	cis-1,4	trans-1,4	1,2	References
1	**153**	Nd	50	30	MMAO	998:303:0:1	75.0	4.40	2.18	61.8	36.4	1.8	[131]
2	**154**	Nd	50	10	MMAO	998:303:0:1	78.6	26.2	2.80	97.0	2.3	0.7	[131]
3	**155**	Nd	50	10	MMAO	998:303:0:1	17.2	15.5	4.90	95.9	3.3	0.8	[131]
4	**156**	Nd	50	15	MMAO	998:303:0:1	77.3	26.3	2.50	97.0	2.5	0.5	[131]
5	**156**	Nd	50	15	MMAO	998:303:0:1	67.5	16.4	2.31	95.0	4.5	0.5	[131]
6[a]	**156**	Nd	50	15	MMAO	998:303:0:1	84.8	16.4	2.34	96.1	4.5	3.4	[131]
7	**160**-Me	Y	25	60	Al^{i}Bu$_3$/ B	500:20:1:1	80.0	4.0	1.47	98.5	1.3	0.2	[133]
8	**160**-Et	Y	25	60	Al^{i}Bu$_3$/ B	500:20:1:1	100	8.6	2.23	99.7	0.3	0.0	[133]
9	**160**-^{i}Pr	Y	25	60	Al^{i}Bu$_3$/ B	500:20:1:1	68.0	2.6	1.31	95.3	4.2	0.5	[133]
10	**161**-La	La	25	60	Al^{i}Bu$_3$/ B	500:20:1:1	87.0	7.0	1.59	99.3	0.5	0.2	[133]
11	**161**-Nd	Nd	25	15	Al^{i}Bu$_3$/ B	500:20:1:1	100	18.0	2.08	99.5	0.4	0.1	[133]
12	**161**-Gd	Gd	25	10	Al^{i}Bu$_3$/ B	500:20:1:1	100	32.2	2.18	99.7	0.3	0.0	[133]
13	**161**-Sm	Sm	25	120	Al^{i}Bu$_3$/ B	500:20:1:1	0.0	–	–	–	–	–	[133]
14	**161**-Eu	Eu	25	120	Al^{i}Bu$_3$/ B	500:20:1:1	0.0	–	–	–	–	–	[133]
15	**161**-Tb	Tb	25	10	Al^{i}Bu$_3$/ B	500:20:1:1	100	21.0	2.43	99.7	0.3	0.0	[133]
16	**161**-Dy	Dy	25	10	Al^{i}Bu$_3$/ B	500:20:1:1	100	26.0	2.24	99.4	0.6	0.0	[133]

(continued)

Table 5 (continued)

Entry	Complex	Metal	T (°C)	Time (min)	Co-cat.	[BU]/[Al]/[X]/[Ln]	Conv. (%)	M_n ($\times 10^4$)	M_w/M_n	cis-1,4	trans-1,4	1,2	References
17	**161**-Ho	Ho	25	15	AlⁱBu₃/B	500:20:1:1	100	14.2	2.44	99.4	0.6	0.0	[133]
18	**161**-Yb	Yb	25	120	AlⁱBu₃/B	500:20:1:1	0.0	–	–	–	–	–	[133]
19	**161**-Lu	Lu	25	60	AlⁱBu₃/B	500:20:1:1	90.0	9.8	2.48	99.3	0.6	0.1	[133]
20[b]	**162**	Nd	65	60	MMAO	20,963:291:0:1	10.8	5.0	10.00	–	–	–	[135]
21[c]	**162**	Nd	65	60	AlEt₃	20,958:144:2:1	44.9	7.8	5.37	83.9	13.1	3.0	[135]
22[c]	**162**	Nd	65	60	AlEt₃	22,065:146:2:1	85.7	11.2	2.88	75.2	23.3	1.5	[135]
23[b]	**163**	Nd	65	60	MMAO	22,623:291:1	84.9	24.7	2.30	84.9	13.3	1.8	[135]
24[c]	**163**	Nd	65	60	AlEt₃	21,825:143:2:1	94.9	24.6	2.74	76.1	23.1	0.8	[135]
25[c]	**163**	Nd	65	60	AlEt₃	20,404:145:2:1	19.4	–	–	85.3	13.7	1.0	[135]
26	**165**-Y	Y	25	150	B	1,000:0:1:1	71.0	8.2	1.06	>99	–	–	[137]

A = [PhMe₂NH][B(C₆F₅)₄]; B = [Ph₃C][B(C₆F₅)₄]; C = B(C₆F₅)₃

[a] Order of the addition of MMAO and Nd was inverted

[b] Features based on polymer after 15 min reaction

[c] Features based on polymer after 10 min reaction

Table 6 Polymerization of isoprene catalyzed by rare earth pincer complexes

Entry	Complex	Metal	T (°C)	Time (min)	Co-cat.	[IP]/[Al]/[X]/[Ln]	Conv. (%)	M_n ($\times 10^4$)	M_w/M_n	cis-1,4	trans-1,4	1,2	References
1	**157**-Sc	Sc	RT	60	A	600:0:1:1	100	16.0	1.10	96.5	0.0	3.5	[132]
2	**157**-Y	Y	RT	60	A	600:0:1:1	100	23.0	1.10	99.3	0.0	0.7	[132]
3	**157**-Lu	Lu	RT	60	A	600:0:1:1	100	19.0	1.09	97.1	0.0	2.9	[132]
4	**157**-Y	Y	RT	60	B	600:0:1:1	79	32.0	1.11	99.3	0.0	0.7	[132]
5	**157**-Y	Y	RT	60	C	600:0:1:1	0	–	–	–	–	–	[132]
6[a]	**157**-Y	Y	RT	60	C	600:0:1:1	200	23.0	1.08	99.3	0.0	0.7	[132]
7	**160**-Me	Y	25	120	Al^{i}Bu$_3$/B	500:20:1:1	40	13.5	2.47	98.3	0.0	1.7	[133]
8	**160**-Et	Y	25	120	Al^{i}Bu$_3$/B	500:20:1:1	100	7.8	1.76	98.8	0.0	1.2	[133]
9	**160**-^{i}Pr	Y	25	120	Al^{i}Bu$_3$/B	500:20:1:1	28	14.3	3.63	91.0	0.0	9.0	[133]
10	**161**-La	La	25	120	Al^{i}Bu$_3$/B	500:20:1:1	54	7.0	2.06	98.6	0.0	1.4	[133]
11	**161**-Nd	Nd	25	15	Al^{i}Bu$_3$/B	500:20:1:1	100	4.3	1.70	97.6	0.0	2.4	[133]
12	**161**-Gd	Gd	25	10	Al^{i}Bu$_3$/B	500:20:1:1	100	5.7	2.49	98.3	0.0	1.7	[133]
13	**161**-Sm	Sm	25	120	Al^{i}Bu$_3$/B	500:20:1:1	0	–	–	–	–	–	[133]
14	**161**-Eu	Eu	25	120	Al^{i}Bu$_3$/B	500:20:1:1	0	–	–	–	–	–	[133]
15	**161**-Tb	Tb	25	60	Al^{i}Bu$_3$/B	500:20:1:1	100	8.9	2.44	92.9	0.0	7.1	[133]
16	**161**-Dy	Dy	25	15	Al^{i}Bu$_3$/B	500:20:1:1	100	5.3	2.64	98.4	0.0	1.6	[133]

(continued)

Table 6 (continued)

Entry	Complex	Metal	T (°C)	Time (min)	Co-cat.	[IP]/[Al]/[X]/[Ln]	Conv. (%)	M_n ($\times 10^4$)	M_w/M_n	cis-1,4	trans-1,4	1,2	References
17	**161**-Ho	Ho	25	15	Al^{i}Bu$_3$/B	500:20:1:1	90	5.1	2.59	98.5	0.0	1.5	[133]
18	**161**-Yb	Yb	25	15	Al^{i}Bu$_3$/B	500:20:1:1	0	–	–	–	–	–	[133]
19	**161**-Lu	Lu	25	60	Al^{i}Bu$_3$/B	500:20:1:1	80	6.2	2.43	98.6	0.0	1.4	[133]
20	**161**-Nd	Nd	20	240	Al^{i}Bu$_3$	1,000:2:0:1	0	–	–	–	–	–	[134]
21	**161**-Nd	Nd	20	240	Al^{i}Bu$_3$	1,000:3:0:1	35	71.7	2.09	97.6	0.0	2.4	[134]
22	**161**-Nd	Nd	20	240	Al^{i}Bu$_3$	1,000:4:0:1	93	75.6	2.00	97.8	0.0	2.2	[134]
23	**161**-Nd	Nd	20	240	Al^{i}Bu$_3$	1,000:10:0:1	100	28.8	2.41	98.1	0.0	1.8	[134]
24	**161**-Nd	Nd	20	240	AlEt$_3$	1,000:10:0:1	100	11.6	1.87	81.1	17.6	1.3	[134]
25	**161**-Nd	Nd	20	240	AlMe$_3$	1,000:10:0:1	94	36.7	4.67	97.2	1.0	1.8	[134]
26	**164**-Y	Y	25	300	Al^{i}Bu$_3$/B	500:20:1:1	50	14.4	3.81	99.6	0.0	0.4	[136]
27	**164**-Nd	Nd	25	90	Al^{i}Bu$_3$/B	500:20:1:1	100	28.0	3.09	97.3	0.0	2.7	[136]
28	**164**-Nd	Nd	25	15	AlEt$_3$/B	500:20:1:1	100	19.0	1.77	96.3	0.0	3.7	[136]
29	**164**-Nd	Nd	25	30	AlMe$_3$/B	500:20:1:1	100	62.2	1.70	96.7	0.0	3.3	[136]
30	**164**-Gd	Gd	25	180	Al^{i}Bu$_3$/B	500:20:1:1	100	23.7	3.87	98.6	0.0	1.4	[136]
31	**164**-Dy	Dy	25	200	Al^{i}Bu$_3$/B	500:20:1:1	100	15.1	2.61	99.3	0.0	0.7	[136]
32	**165**-Sc	Sc	25	5	B	1,000:0:1:1	100	11.6	1.49	98.3	–	–	[137]
33	**165**-Y	Y	25	10	B	1,000:0:1:1	100	11.7	1.07	>99	–	–	[137]
34	**165**-Y	Y	25	45	AlMe$_3$/B	1,000:10:1:1	100	7.6	1.11	98.8	–	–	[137]

35	**165-Y**	Y	25	45	AlEt$_3$/B	1,000:10:1:1	100	8.3	1.12	99.0	–	–	[137]
36	**165-Y**	Y	25	45	Al^{i}Bu$_3$/B	1,000:10:1:1	100	7.5	1.11	98.6	–	–	[137]
37	**165-Er**	Er	25	30	B	1,000:0:1:1	100	10.3	1.08	97.6	–	–	[137]
38	**166-Sc**	Sc	RT	360	B	1,000:0:1:1	100	17.4	1.14	–	–	85.5	[138]
39	**166-Y**	Y	RT	720	B	1,000:0:1:1	52	18.0	1.05	80.9	1.4	–	[138]
40	**166-Lu**	Lu	RT	360	B	1,000:0:1:1	100	47.0	1.31	–	–	42.2	[138]
41	**167**	Sc	RT	150	B	1,000:0:1:1	57	10.4	1.25	–	–	81.3	[138]
42	**168-Y**	Y	RT	150	B	1,000:0:1:1	100	10.3	1.22	94.1	0.9	–	[138]
43	**168-Lu**	Lu	RT	150	B	1,000:0:1:1	100	19.2	1.15	–	–	53.1	[138]
44	**169-Sc**	Sc	25	360	A	500:0:1:1	73	4.8	1.23	–	–	>99.5	[139]
45	**169-Sc**	Sc	25	360	B	500:0:1:1	80	3.3	1.25	–	–	>99.5	[139]
46	**169-Sc**	Sc	25	1,440	C	500:0:1:1	38	4.6	1.29	–	–	>99.5	[139]
47	**169-Sc**	Sc	25	360	Al^{i}Bu$_3$/B	1,000:2:1:1	100	3.1	1.47	–	–	99.0	[139]
48	**169-Sc**	Sc	25	360	Al^{i}Bu$_3$/A	1,200:2:1:1	50	2.5	1.59	–	–	99.0	[139]
49	**169-Sc**	Sc	25	360	Al^{i}Bu$_3$/B	1,200:2:1:1	77	3.0	1.70	–	–	99.0	[139]
50	**169-Sc**	Sc	25	360	Al^{i}Bu$_3$/C	1,200:2:1:1	21	2.0	1.31	–	–	99.0	[139]
51	**169-Lu**	Lu	25	180	Al^{i}Bu$_3$/B	500:0:1:1	100	6.4	1.38	–	–	99.5	[139]
52	**169-Lu**	Lu	25	360	Al^{i}Bu$_3$/B	1,000:2:1:1	100	3.7	1.45	–	–	99.0	[139]
53	**170-Sc**	Sc	30	60	Al^{i}Bu$_3$/A	500:10:1:1	0	–	–	–	–	–	[140]
54	**170-Y**	Y	30	30	Al^{i}Bu$_3$/A	500:10:1:1	100	11.6	2.12	98.6	0.8	0.6	[140]

(continued)

Table 6 (continued)

Entry	Complex	Metal	T (°C)	Time (min)	Co-cat.	[IP]/[Al]/[X]/[Ln]	Conv. (%)	M_n (×10^4)	M_w/M_n	cis-1,4	trans-1,4	1,2	References
55	**170**-Y	Y	30	30	AlMe$_3$/A	500:10:1:1	100	23.6	1.75	94.8	4.6	0.6	[140]
56	**170**-Y	Y	30	8	AlEt$_3$/A	500:10:1:1	100	12.9	1.74	90.7	8.4	0.9	[140]
57	**170**-Y	Y	30	30	Al^{i}Bu$_3$/B	500:10:1:1	100	7.4	4.13	97.1	1.6	1.3	[140]
58	**170**-Y	Y	30	90	Al^{i}Bu$_3$/C	500:10:1:1	91	8.2	3.14	98.9	0.3	0.8	[140]
59	**170**-Dy	Dy	30	15	Al^{i}Bu$_3$/A	500:10:1:1	100	11.0	2.34	98.9	0.6	0.5	[140]
60	**170**-Ho	Ho	30	30	Al^{i}Bu$_3$/A	500:10:1:1	100	13.9	3.21	99.2	0.4	0.4	[140]
61	**170**-Tm	Tb	30	60	Al^{i}Bu$_3$/A	500:10:1:1	78	12.0	3.69	98.3	0.9	0.8	[140]
62	**170**-Lu	Lu	30	60	Al^{i}Bu$_3$/A	500:10:1:1	7	–	–	–	–	–	[140]

A = [PhMe$_2$NH][B(C$_6$F$_5$)$_4$]; B = [Ph$_3$C][B(C$_6$F$_5$)$_4$]; C = B(C$_6$F$_5$)$_3$

[a]600 equiv. of isoprene was polymerized for 30 min after which another 600 equiv. was added. The activator was added to a solution of **157**-Y and isoprene

4.2.1 Rare Earth Metal Oxazoline Complexes in Asymmetric Catalysis

In addition to various polymerization reactions, rare earth complexes with various substituted 2,6-bis(oxazolinyl)-pyridine (pybox) and other oxazoline derived pincer-type ligands have been exploited for several other catalytic applications. For example, complexes with the general formula $Ln(pybox)(A)_3$ (A = monodentate anionic ligand) have been shown to catalyze a broad selection of reactions, such as enantioselective Diels–Alder [141] and nitrone cycloadditions [142], Friedel–Craft alkylations [143], asymmetric Mannich-type reactions [144], as well as a variety of ene-reactions [145]. It is important to note that most of these processes are catalyzed by in situ prepared complexes, rather than well-defined species, and thus remain out of the scope of this review. In addition, studies concerning rare earth metals with diverse oxazoline-based ligands have been recently and comprehensively reviewed. Thus, the interested reader is encouraged to procure further insight from that source [146].

4.3 Other Polymerization Reactions

Polyethylene (PE), the world's most common plastic, is generally produced by the polymerization of ethylene using well-established transition metal species, such as Ziegler–Natta or Phillips catalysts. However, in recent years, interest in rare earth pincer ethylene polymerization catalysts has increased. Selected results from these studies are gathered in Table 7 and briefly discussed in the paragraphs below.

In 2008, Waymouth, Anwander, and co-workers examined the use of the lanthanide dialkyl complexes $LLn(CH_2SiMe_3)_2$ (Ln = Sc, Lu; L = [2-{(2,6-^{i}Pr$_2$C$_6$H$_3$)-N=CMe}-6-{(2,6-^{i}Pr$_2$C$_6$H$_3$)NCMe$_2$}C$_5$H$_3$N]), **171**-Ln (Chart 25), in ethylene polymerization [147]. Although the neutral species **171**-Ln were inert toward ethylene, the cationic analogues, generated by reaction with $[PhMe_2NH][B(C_6F_5)_4]$ or $[Ph_3C][B(C_6F_5)_4]$, produced polyethylene in moderate yields. Meanwhile, the addition of the activator N-[tris(pentafluorophenyl)borane]-3H-indole to **171**-Ln led to species that were catalytically inactive. These binary catalytic systems were also tested in the polymerization of styrene and the copolymerization of styrene and ethylene, but no polymeric material was obtained.

Evans, Reid, and Tromp used a neutral SNS pincer ligand to create the scandium complex $LScCl_3$ (L = $HN(CH_2CH_2SC_{10}H_{21})_2$), **172** (Chart 25). The ability of this complex to catalyze ethylene polymerization was studied using two different modified methylaluminoxanes as co-catalysts [148].

In 2010 Trifonov, Giambastiani, and co-workers reported the ability of mononuclear cyclometalated yttrium amidopyridinate complexes $LY(CH_2SiMe_3)(THF)_2$ (L = [2-(C$_6$H$_4$)-6-{(2,6-^{i}Pr$_2$C$_6$H$_3$)NCMe$_2$}C$_5$H$_3$N]), **173**, [2-(2-Me-6-CH$_2$-C$_6$H$_3$)-6-{(2,6-^{i}Pr$_2$C$_6$H$_3$)NCMe$_2$}C$_5$H$_3$N], **174**, or [2-(C$_4$HR′S)-6-{(2,6-^{i}Pr$_2$C$_6$H$_3$)-NCMe$_2$}C$_5$H$_3$N], **175**-R′ (Chart 25), as well as dinuclear hydride-bridged species

Table 7 Selected results from ethylene polymerization experiments

Entry	Complex	Metal	T (°C)	Time (min)	Co-catalyst	[Al]/[X]/[Ln]	Pressure (bar)	Solvent	Activity[a]	References
1	**171-Sc**	Sc	25	60	A	0:1:1	10	Tol	33.0	[147]
2	**171-Sc**	Sc	25	60	B	0:1:1	10	Tol	25.0	[147]
3	**171-Sc**	Sc	25	60	D	0:1:1	10	Tol	–	[147]
4	**171-Lu**	Lu	25	60	A	0:1:1	10	Tol	13.0	[147]
5	**171-Lu**	Lu	25	60	B	0:1:1	10	Tol	15.0	[147]
6	**171-Lu**	Lu	25	60	D	0:1:1	10	Tol	–	[147]
7	**172**	Sc	60	17	MMAO-3A	500:0:1	40	C_6H_5Cl	18.1	[148]
8	**172**	Sc	60	10	PMAO-IP	500:0:1	40	C_6H_5Cl	0.6	[148]
9	**173**	Y	22	30	MAO	300:0:1	10	Tol	2.4	[29]
10	**173**	Y	50	30	MAO	300:0:1	10	Tol	1.6	[29]
11	**173**	Y	65	30	Al^iBu_3/A	200:1.2:1	10	Tol	0.8	[29]
12	**173**	Y	22	30	MAO	300:0:1	10	Tol	0.3	[29]
13	**175-H**	Y	22	30	MAO	300:0:1	10	Tol	2.2	[29]
14	**175-Et**	Y	22	30	MAO	300:0:1	10	Tol	3.1	[29]
15	**175-Et**	Y	50	30	MAO	300:0:1	10	Tol	2.7	[29]
16	**175-Et**	Y	65	30	Al^iBu_3/A	200:1.2:1	10	Tol	0.4	[29]
17	**30**	Y	22	30	MAO	300:0:1	10	Tol	traces	[29]
18	**30**	Y	65	30	Al^iBu_3/A	200:1.2:1	10	Tol	traces	[29]
19	**31**	Y	22	30	MAO	300:0:1	10	Tol	traces	[29]
20	**176**	Y	65	30	Al^iBu_3/A	200:1.2:1	10	Tol	traces	[29]

$A = [PhMe_2NH][B(C_6F_5)_4]$; $B = [Ph_3C][B(C_6F_5)_4]$; $D = N$-[tris(pentafluorophenyl)borane]-$3H$-indole
[a]Activity = [kg PE / (mol Ln bar h)$^{-1}$]
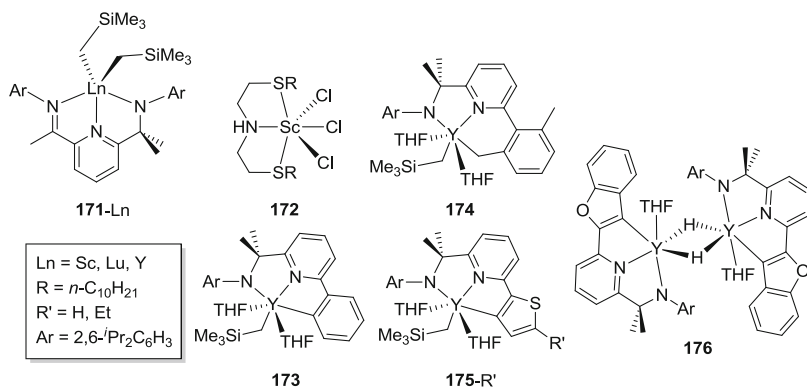
Chart 25 Chloride, alkyl, and hydride ethylene polymerization catalysts
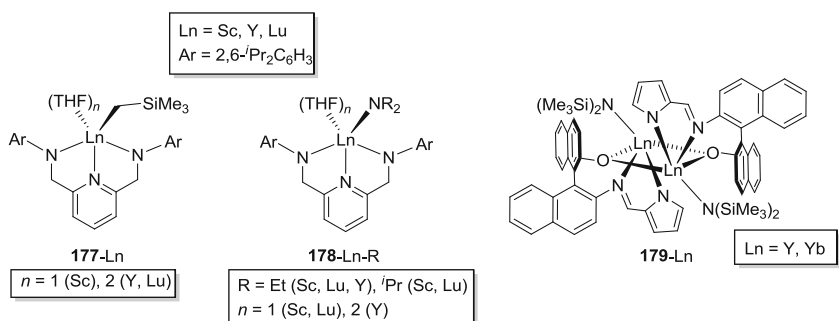
Chart 26 Alkyl and amido MMA polymerization catalysts

29 and **30** (see Sect. 3.1.2) and [LY(μ-H)(THF)]$_2$ (L = [2-C$_8$H$_4$O-6-{(2,6-^{i}Pr$_2$C$_6$H$_3$)-NCMe$_2$}C$_5$H$_3$N], **176**, to polymerize ethylene when activated with MAO or [PhMe$_2$NH][B(C$_6$F$_5$)$_4$]. More specifically, complexes **173** and **175**-Et were capable of producing up to 2.4 and 3.1 kg of PE [(mol of Y) bar h]$^{-1}$, respectively, at ambient temperature. A notable reduction in catalytic activity was observed when the metalated sp^2 carbon of the aryl substituent was replaced by an sp^3 hybridized carbon, **174**. Under all conditions tested, the dinuclear hydride complexes **29**, **30**, and **176** were completely inactive [29].

In addition to ethylene polymerization catalysis, rare earth pincer complexes have also been used to polymerize methyl methacrylate (MMA) to poly(methylmethacrylate) (PMMA), which is also known as acrylic glass. This exceedingly useful polymer is a transparent thermoplastic that is commonly used as an alternative for glass when more lightweight and durable material is required.

In 2003, Anwander published a series of alkyl complexes, LLn(CH$_2$SiMe$_3$)-(THF)$_n$ (Ln = Sc, n = 1; Y, Lu, n = 2; L = 2,6-bis(((2,6-^{i}Pr$_2$C$_6$H$_3$)amino)methyl)-pyridine), **177**-Ln, and amido LLn(NR$_2$)(THF)$_n$, **178**-Ln, that were used to polymerize MMA (Chart 26). The scandium complexes produced MMA that

featured narrow polydispersities ($M_w/M_n < 1.5$) and predominantly syndio- and heterotactic microstructures. Interestingly, the heavier yttrium and lutetium analogues gave only negligible conversions (Table 8) [14]. Likewise, even upon the addition of MAO, **171**-Ln gave only traces of PMMA, a fact which highlights the capacity of even seemingly subtle steric or electronic ligand modifications to dramatically impact catalyst performance [147].

A few years later, Zi et al. investigated dinuclear yttrium and ytterbium complexes of the formula [LLnN(SiMe$_3$)$_2$]$_2$ (Ln = Y, Yb; L = (*S*)-2-(pyrrol-2-ylmethyleneamino)-2′-hydroxy-1,1′-binaphthyl), **179**-Ln (Chart 26), as catalysts for the preparation of PMMA [149]. Both **179**-Y and **179**-Yb initiated MMA polymerization, affording syndiotactic-rich PMMA, although conversions were quite low (Table 8). As observed with heavier lanthanide metals, catalyst deactivation tends to kill MMA polymerization after several hours.

4.4   Hydroamination Reactions

Hydroamination, the formal addition of N–H across an unsaturated C–C fragment, offers an atom economical route to commercially important amines from relatively common alkenes or alkynes. Rare earth metals have consistently proven to be particularly useful in catalyzing this transformation [150]. A variety of examples of intramolecular hydroamination catalyzed by rare earth pincer complexes are presented both in the paragraphs below and in Table 9.

Hultzsch et al. [151, 156] reported the use of early rare earth pincer catalysts for hydroamination reactions in 2004. Yttrium complexes LYN(SiHMe$_2$)$_2$(THF) (L = (2,4,6-Me$_3$C$_6$H$_2$NCH$_2$CH$_2$)$_2$NMe), **180**, LYN(SiMe$_3$)$_2$, **181–183**, and LY-(2-NMe$_2$CH$_2$C$_6$H$_4$), **184–186**, (L = (ArNCH$_2$CH$_2$)$_2$NMe with Ar = 2,4,6-Me$_3$C$_6$H$_2$, **181**, **184**, 2,6-Et$_2$C$_6$H$_3$, **182**, **185**, or 2,6-Cl$_2$C$_6$H$_3$, **183**, **186**) (Chart 27) were shown to efficiently catalyze the intramolecular hydroamination of aminoalkenes and aminoalkynes. The nature of the leaving group was found to have a significant influence on the catalytic activity of the complexes. For example, systems possessing a bis(trimethylsilyl)amido or bidentate aryl amine functionality, **181–186**, displayed similar activities and TOFs, while catalysts equipped with a bis(dimethylsilyl)amido moiety, **180**, were much less active. Furthermore, the mesityl-substituted complex **184** quickly decomposed in solution ($t_{1/2} = 6$ h), whereas the corresponding 2,6-diethylphenyl and 2,6-dichlorophenyl-substituted species **185** and **186** were considerably more stable. The chloride substituents on the phenyl ring also appear to increase catalyst stability toward protonolysis, although the hydroamination activity of **183** and **186** suffered compared to their alkyl substituted counterparts (Table 9).

A few years later, Zi et al. [108, 109, 152] studied an extended series of rare earth complexes **114**-Ln (Ln = Y, Yb), **115–116**, **179**-Ln (Ln = Y, Yb), and L$_3$Ln ((Ln = Y, Yb; L = (*S*)-2-(pyrrol-2-ylmethyleneamino)-2′-hydroxy-1,1′-binaphthyl, **187**-Y and **187**-Yb, or Ln = Sm; L = (*S*)-5,5′,6,6′,7,7′,8,8′-octahydro-2-(pyrrol-2-

Table 8 Selected results from MMA polymerization studies

Entry	Complex	M	T (°C)	Time (h)	[MMA]/[Ln]	Conv. (%)	Mn (×10³)	Mw/Mn	Tacticity[a]			References
									mr	mm	rr	
1	**177**-Sc	Sc	40	48	500	95.0	81.0	1.60	44.0	6.5	49.5	[14]
2	**177**-Y	Y	40	48	500	12.0	58.0	29.90	25.0	37.0	38.0	[14]
3	**177**-Lu	Lu	40	48	500	11.0	60.0	86.50	27.0	20.0	53.0	[14]
4	**178**-Sc-Et	Sc	40	48	500	87.0	65.0	1.28	49.5	9.0	41.5	[14]
5	**178**-Sc-^{i}Pr	Sc	40	48	500	>99	67.0	1.56	47.5	8.0	44.5	[14]
6	**178**-Lu-^{i}Pr	Y	40	48	500	Trace	105.0	17.50	21.0	19.5	59.5	[14]
7	**179**-Y	Y	20	3	500	3.5	27.0	1.82	24.0	18.0^b	58.0	[149]
8	**179**-Y	Y	0	3	500	5.0	42.3	1.87	26.0	15.0^b	59.0	[149]
9	**179**-Y	Y	−20	3	500	7.0	47.8	1.99	25.0	21.0^b	54.0	[149]
10	**179**-Yb	Yb	20	3	500	3.2	32.6	2.28	28.0	27.0^b	45.0	[149]
11	**179**-Yb	Yb	0	3	500	3.7	34.8	2.32	25.0	18.0^b	57.0	[149]
12	**179**-Yb	Yb	−20	3	500	5.5	33.2	2.19	23.0	22.0^b	55.0	[149]

[a]mr, mm, and rr are hetero-, iso-, and syndiotactic triads, respectively
[b]Calculated as $mm = 100 - (mr + rr)$

Table 9 Selected results from the intramolecular hydroamination/cyclization of 2,2-dimethylpent-4-enylamine to 2,4,4,-trimethylpyrrolidine

Entry	Complex	Metal	T (°C)	Time (h)	[AA]/[Ln]	Conv. (%)	TOF[a]	ee	References
1	**180**	Y	40	13	25.0	41.0	0.8	–	[151]
2	**181**	Y	25	3.5	33.3	96.0	9.1	–	[151]
3	**182**	Y	25	4	33.3	98.0	8.2	–	[151]
4	**183**	Y	25	41	50.0	92.0	1.1	–	[151]
5	**184**	Y	25	3.65	95.0	95.0	24.7	–	[151]
6	**185**	Y	25	5	97.0	97.0	18.8	–	[151]
7	**186**	Y	25	25	96.0	96.0	3.7	–	[151]
8	**114**-Y	Y	20	48	20.0	93.0	0.4	39	[108]
9	**114**-Yb	Yb	60	48	20.0	65.0	0.3	44	[108]
10	**187**-Y	Y	120	160	20.0	–	–	–	[108]
11	**187**′	Sm	120	160	20.0	–	–	–	[108]
12	**187**-Yb	Yb	120	160	20.0	–	–	–	[108]
13	**115**	Sm	20	16	40.0	98.0	2.5	55	[109]
14	**116**	Y	20	16	40.0	95.0	2.4	54	[109]
15	**179**-Y	Y	23	48	20.0	81.0	0.3	5	[152]
16	**179**-Yb	Yb	120	160	20.0	–	–	–	[152]
17	**188**-Sm	Sm	23	48	20.0	100.0	0.4	37	[152]
18	**188**-Yb	Yb	23	48	20.0	55.0	0.2	43	[152]
19	**189**-Y	Y	60	48	20.0	46.0	0.2	11	[152]
20	**189**-Yb	Yb	120	60	20.0	31.0	0.1	61	[152]
21	**190**-Y	Y	40	4[b]	50.0	95.0	11.9	18	[153]
22	**190**-Lu	Lu	40	4[b]	50.0	95.0	11.9	52	[153]
23	**191**-Y	Y	40	5[b]	50.0	95.0	9.5	5	[153]
24	**192**-Sc	Sc	40	96[b]	25.0	95.0	0.2	18	[153]
25	**192**-Y	Y	40	3[b]	50.0	95.0	15.8	35	[153]
26	**192**-Lu	Lu	40	7[b]	71.4	95.0	9.7	62	[153]
27	**193**-Y	Y	40	12[b]	50.0	95.0	4.0	6	[153]
28	**193**-Lu	Lu	40	12[b]	50.0	95.0	4.0	10	[153]
29	**194**-Y	Y	40	7[b]	50.0	95.0	6.8	47	[153]
30	**194**-Lu	Lu	40	3[b]	50.0	95.0	15.8	63	[153]
31	**195**-Sc	Sc	60	24	100.0	<5	0.2	–	[154]
32	**195**-Y	Y	60	4	100.0	98.0	24.5	–	[154]
33	**195**-Lu	Lu	60	12	100.0	96.0	8.0	–	[154]
34	**196**-Y	Y	60	2	100.0	97.0	48.5	–	[154]
35	**196**-Nd	Nd	60	0.5	100.0	98.0	196.0	–	[154]
36	**196**-Nd	Nd	60	1	200.0	98.0	196.0	–	[154]
37	**196**-Gd	Gd	60	1	100.0	98.0	98.0	–	[154]
38	**196**-Dy	Dy	60	1	100.0	97.0	97.0	–	[154]
39	**197**	Y	60	1	40.0	96.0	38.4	–	[155]
40	**198**	Y	60	0.6	40.0	97.0	66.5	–	[155]
41	**199**	Y	60	2	40.0	97.0	19.4	–	[155]

(continued)

Table 9 (continued)

Entry	Complex	Metal	T (°C)	Time (h)	[AA]/[Ln]	Conv. (%)	TOF[a]	ee	References
42	**200**	Y	60	1.17	40.0	98.0	33.6	–	[155]
43	**132**	Y	50	168	10.0	0.0	0.0	–	[119]
44	**135**-La	La	30	72	10.0	99.0	0.6	7	[119]
45	**135**-Pr	Pr	22	12	10.0	99.0	0.8	14	[119]
46	**136**-Pr	Pr	22	12	10.0	99.0	0.8	16	[119]
47	**137**-Pr	Pr	22	12	10.0	99.0	0.8	10	[119]
48	**135**-Nd	Nd	22	168	10.0	0.0	0.0	–	[119]
49	**135**-Sm	Sm	22	12	10.0	99.0	0.8	14	[119]

[a]TOF = [%conv. × [AA]/[Ln] / time (in h)]
[b]Time to >95% conversion
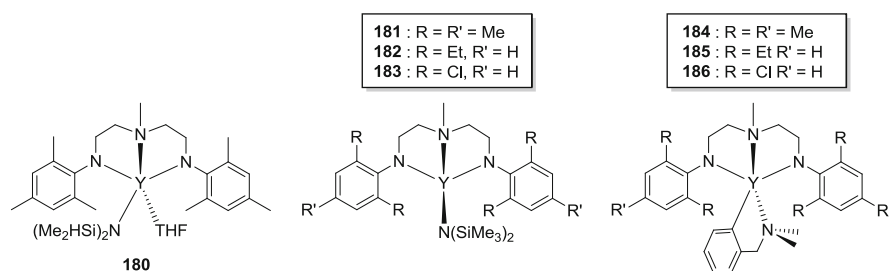
Chart 27 Amido and alkylamino hydroamination catalysts **180–186**

ylmethyleneamino)-2′-methoxy-1,1′-binaphthyl, **187′**, [LLnN(SiMe₃)₂]₂ (Ln = Sm, Yb; L = (S)-2-(pyrrol-2-ylmethyleneamino)-2′-hydroxy-6,6′-dimethyl-1,1′-biphe-nyl, **188**-Ln, and (L₂Ln)₂LnN(SiMe₃)₂ (Ln = Ym Yb; L = (S)-5,5′,6,6′,7, 7′,8,8′-octahydro-2-(pyrrol-2-ylmethyleneamino)-2′-methoxy-1,1′-binaphthyl, **189**-Ln (Chart 28), supported by 2-amino-2′-hydroxy-1,1′-binaphthyl)-based (NOBIN) ligands, as catalysts for the asymmetric hydroamination/cyclization of aminoalkenes. These complexes were capable of producing cyclic amines in good yield with moderate ee values. Notably, homoleptic complexes **187**-Ln and **187′** did not display any catalytic activity, even after heating at 120°C for 1 week.

More recently, Hultzsch and co-workers prepared a series of related rare earth complexes ligated by various substituted NOBIN-derived aminodiolates, LLn(NMe₂CH₂C₆H₄) (Ln = Sc, Y, Lu, L = 2-[(3,5-di-tert-butyl-2-hydroxybenzyl)-methylamino]-3-(triphenylsilyl)-1,1-binaphthalen-2-ol), **190–194**-Ln (Chart 29). These complexes achieved excellent catalytic activity in intramolecular hydroamination reactions and also boasted ee values up to 92%. However, when bound to scandium, the smallest rare earth metal, the steric bulk of these systems necessitated considerably longer reaction times to reach conversions comparable to that achieved by yttrium and lutetium derivatives. Significantly these complexes also catalyze asymmetric intermolecular hydroaminations with similarly impres-sive activities, although only moderate enantioselectivities were observed (up to
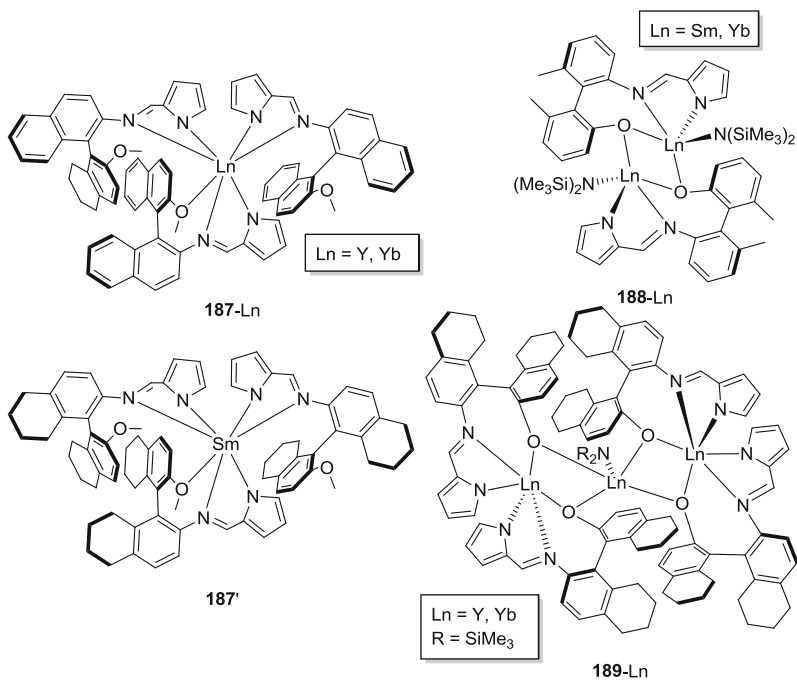
Chart 28 NOBIN supported rare earth complexes **187–189**-Ln
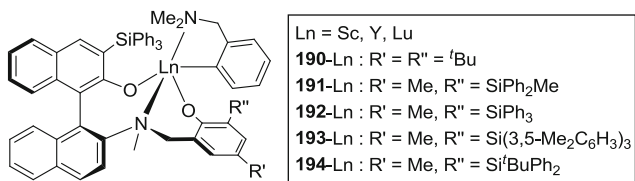
Chart 29 Selected examples of rare earth aminodiolate complexes

40% *ee*). As with the intramolecular catalysis, substituent effects played a major role. Specifically, the sterically demanding ligands that helped procure high enantioselectivities in intramolecular reactions completely shut down all activity in the intermolecular systems. Hence, less bulky ancillaries were required. Finally, it should be noted that these catalysts were less active than previously reported bidentate binaphtholate complexes [153].

Monoalkyl and monoamido rare earth complexes $LLn(CH_2SiMe_3)(THF)$ (Ln = Sc, Y, Lu; L = $MeC(2,6-{}^{i}Pr_2C_6H_3N)CHCMe(NCH_2CH_2NR)$, R = 2,6-$Me_2C_6H_3$, **195**-Ln, or 2,6-${}^{i}Pr_2C_6H_3$, **196**-Ln) and $LY(R)(THF)$ (L = 2-$SiMe_2CH_2$-6-CHC(Me)(2,6-${}^{i}Pr_2C_6H_3N)C_5H_3N$, R = CH_2SiMe_3, **197**, or R = NH-(2,6-${}^{i}Pr_2C_6H_3$), **198**, or L = 2-C_6H_4-6-CHC(Me)(2,6-${}^{i}Pr_2C_6H_3N)C_5H_3N$, R = CH_2SiMe_3, **199**, or R = NH(2,6-${}^{i}Pr_2C_6H_3$), **200**) (Chart 30) were also studied
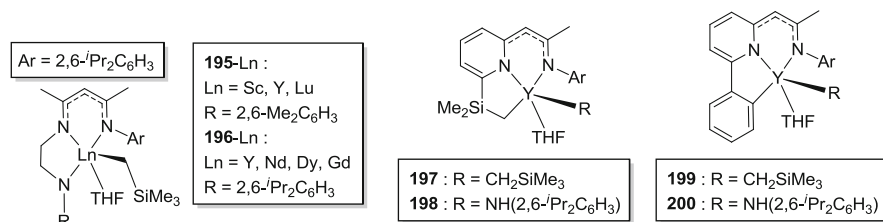
Chart 30 Monoalkyl complexes bearing β-diketiminato derived ancillary pincer ligands

by Chen and colleagues as catalysts for intramolecular hydroamination. All of the studied complexes were able to promote hydroamination catalysis with varying activity. In this work, the property with the most significant influence on catalytic behavior was the ionic radius of metal. For example, complex **196**-Nd, which contained the largest lanthanide examined, was found to convert 200 equiv. of 2,2-dimethylpent-4-enylamine into 2,4,4-trimethylpyrrolidine in 1 h at 60°C, while the yttrium analogue required twice as long for only 100 equiv. of starting material. Additionally, the yttrium alkyl species **197** and **199** were found to be slightly more active than their amido counterparts **198** and **200** [154, 155].

One of the most recent reports of rare earth hydroamination catalysis was that of Ward and Mountford in 2014, wherein metals bearing alkyl, **132–134**, and amido **135–137**-Ln, functionalities were found to catalyze both hydroamination and the ROP of LA [119]. The yttrium derivatives were inactive for the hydroamination of 2,2-dimethylpent-4-enylamine, even after being converted into the corresponding alkyl cations [LY(CH$_2$SiMe$_2$Ph)][B(C$_6$F$_5$)$_4$] (L = substituted bis(oxazolinylphenyl) amide). However, the yttrium species **132–134** were highly active when phenyl substituted 2,2-diphenylpent-4-enylamines were used as the hydroamination substrate. Complexes of larger metals (La, Pr, Nd, and Sm) catalyzed the hydroamination of 2,2-dimethylpent-4-enylamine more readily, although long reaction times (12 h or more) were still needed to reach complete conversion. Slightly better *ee* values were acquired when the phenyl-substituted **136**-Ln were used.

4.5 Other Catalytic Reactions

Rare earth pincer complexes have also proven useful in a number of other catalytic transformations. For example, Arnold reported dinuclear samarium species [LSmOAr]$_2$ (L = 1,1'-S(2-OC$_6$H$_2$-3-^{t}Bu-5-Me)$_2$, **201**, or 1,1'-S(2-OC$_{10}$H$_4$-3,6-^{t}Bu$_2$)$_2$, **202**), which were successfully proven to initiate the acylation of 1,2-diols, selectively converting 50% of substrate into the monoacyl product in 24 h at ambient temperature (Fig. 2) [13, 157].

Samarium has also been employed to catalyze other non-conventional chemical transformations, such as reports by Evans et al. in the early 1990s, wherein the

Monoacylation of *meso*-hydrobenzoin

Complex	Time (h)	Diol	Monoacyl	Diacyl
No cat.	24	84	14	0
201	24	50	50	0
201	48	34	66	0
202	24	50	50	0
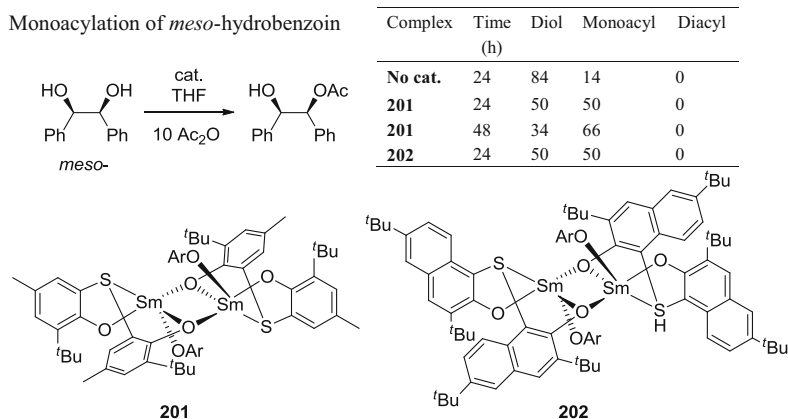
Fig. 2 Monoacylation of *meso*-hydrobenzoin catalyzed by dinuclear complexes **201** and **202**

Entry	Substrate		% ee (config)	Conv.(%)
1		X = Cl	97 (*R*)	100 (96)
2		X = H	96 (*R*)	83 (74)
3		X = OMe	96 (*R*)	100 (95)
4		X = Cl	94 (*R*)	91 (88)
5		X = OMe	92 (*R*)	43 (36)
6		X = NO$_2$	94 (*R*)	100 (77)
7		X = Cl	68 (*R*)	95 (78)
8		X = H	73 (*R*)	66 (63)
9			96 (*R*)	84 (82)
10			97 (*R*)	99 (95)
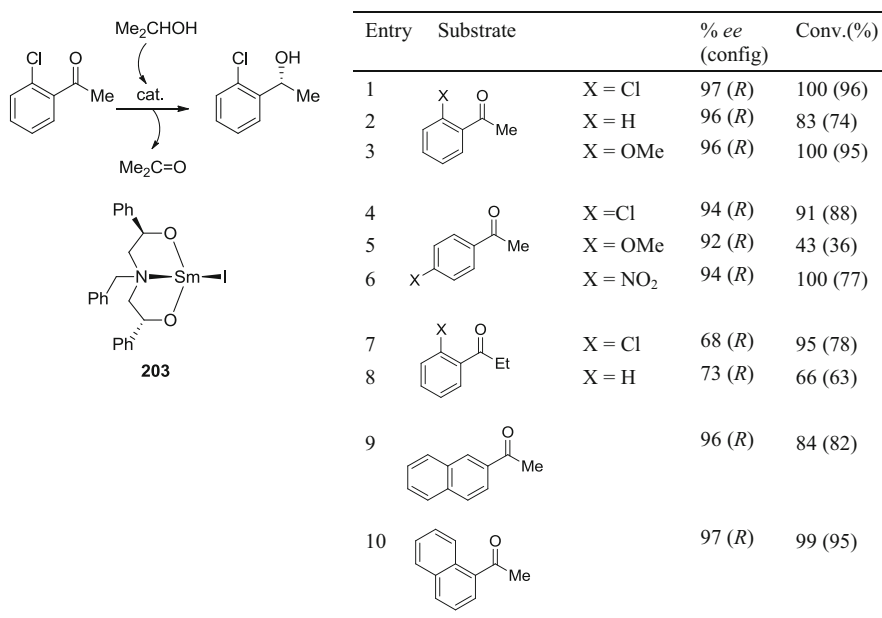
Fig. 3 Meerwein–Ponndorf–Verley reduction catalyzed by complex **203**

samarium iodo complex LSmI (L = PhCH(O)CH$_2$N(CH$_2$Ph)CH$_2$CH(O)Ph), **203**, catalyzed the Meerwein–Ponndorf–Verley reduction of various ketones (Fig. 3). Other lanthanide derivatives of **203** were also studied, with results suggesting that large metals (Y, Nd, Sm, Tb) were the most active, as well as the most enantioselective (*ee* >90%) [10].

Chart 31 Monoamido catalysts, **204**-Ln, for the addition of amines to carbodiimides

Finally, at a loading of 1%, monoamido rare earth complexes $L_2LnN(SiMe_3)_2$ (Ln = Y, La, Nd, Eu, Yb; L = 3,5-^{t}Bu$_2$-2-O-C$_6$H$_2$CH=N-8-C$_9$H$_6$N), **204**-Ln (Chart 31), efficiently catalyzed the transformation of amines into carbodiimides. The activity of **204**-Ln was dominated by the ionic radius of the metal. Detailed studies of different substrates demonstrated that the **204**-Nd complex was able to convert various substituted anilines into the corresponding guanidines in 1 h. Reaction times were not influenced by either electron-donating or electron-withdrawing substrates, although 2- and/or 6-substituted amine moieties required up to 24 h for complete conversion [158].

5 Conclusion

In this chapter, the chemistry of pincer-supported rare earth metal complexes has been thoroughly reviewed, with an emphasis upon small molecule reactivity and catalysis. Pincer complexes can be prepared by various well-known synthetic procedures including alkane, amine, or alcohol elimination, as well as by distinct salt metathesis (transmetalation) reactions. A wide array of pincer ligands has been reported, and many of these compounds can be easily fine-tuned, thus providing a broad spectrum of ligands that vary widely in their steric and electronic properties. As most of these ligands are either neutral or monoanionic, rare earth complexes bearing such scaffolds are typically equipped with one or more reactive groups that can be used for subsequent stoichiometric reactions or catalytic applications.

The reaction chemistry of these compounds is rich, originating from the intrinsic reactivity of lanthanide metals which can be effectively governed by sterically demanding pincer ligands that serve to generate well-behaved metal complexes. For example, a limited number of structurally characterized rare earth complexes that feature terminal multiply bonded ligands have all been supported by pincer, or closely related, ancillary ligands. Accordingly, pincer-ligated rare earth complexes have demonstrated application as catalysts in numerous industrially relevant

reactions, including the ring-opening polymerization of cyclic esters, the polymerization of dienes, and the hydroamination of alkenes and alkynes.

As novel pincer ligand designs continue to be applied to rare earth metals, we can realistically expect that unprecedented complexes with remarkable properties and reaction chemistry will be realized at an ever accelerating pace. As numerous examples of such complexes have demonstrated outstanding catalytic properties, such compounds are expected to play prominent roles in key areas of catalysis in the future.

References

1. Morales-Morales D, Jensen CM (2007) The chemistry of pincer compounds. Elsevier, Amsterdam
2. Albrecht M, van Koten G (2001) Angew Chem Int Ed 40:3750
3. Hogerheide MP, Grove DM, Boersma J, Jastrzebski JTBH, Kooijman H, Spek AL, van Koten G (1995) Chem Eur J 1:343
4. Hogerheide MP, Boersma J, Spek AL, van Koten G (1996) Organometallics 15:1505
5. Hogerheide MP, Boersma J, van Koten G (1996) Coord Chem Rev 155:87
6. Singleton JT (2003) Tetrahedron 59:1837
7. Boom ME, Milstein D (2003) Chem Rev 103:1759
8. Piers WE, Emslie DJH (2002) Coord Chem Rev 233:131
9. Fryzuk MD, Haddad TS (1988) J Am Chem Soc 110:8263
10. Evans DA, Nelson SG, Gagne MR, Muci AR (1993) J Am Chem Soc 115:9800
11. Meyer N, Jenter J, Roesky PW, Eickerling G, Scherer W (2009) Chem Commun 4693
12. Matsuo Y, Mashima K, Tani K (2001) Organometallics 20:3510
13. Arnold PL, Natrajan LS, Hall JJ, Bird SJ, Wilson C (2002) J Organomet Chem 647:205
14. Estler F, Eickerling G, Herdtweck E, Anwander R (2003) Organometallics 22:1212
15. Zimmermann M, Anwander R (2010) Chem Rev 110:6194
16. Zimmermann M, Tornroos KW, Anwander R (2006) Organometallics 25:3593
17. Bourget-Merle L, Lappert MF, Severn JR (2002) Chem Rev 102:3031
18. Tsai Y-C (2012) Coord Chem Rev 256:722
19. Crabtree RH (2005) The organometallic chemistry of the transition metals. Wiley, Hoboken
20. Johnson KRD, Hayes PG (2013) Chem Soc Rev 42:1947
21. Hayes PG, Piers WE, Lee LWM, Knight LK, Parvez M, Elsegood MRJ, Clegg W (2001) Organometallics 20:2533
22. Knight LK, Piers WE, Fleurat-Lessard P, Parvez M, McDonald R (2004) Organometallics 23:2087
23. Chu T, Piers WE, Dutton JL, Parvez M (2013) Organometallics 32:1159
24. Knight LK, Piers WE, McDonald R (2006) Organometallics 25:3289
25. Hitchcock PB, Lappert MF, Protchenko AV (2005) Chem Commun 951
26. Li D, Li S, Cui D, Zhang X (2010) J Organomet Chem 695:2781
27. Conroy KD, Piers WE, Parvez M (2008) J Organomet Chem 693:834
28. Skvortsov GG, Fukin GK, Trifonov AA, Noor A, Döring C, Kempe R (2007) Organometallics 26:5770

29. Luconi L, Lyubov DM, Bianchini C, Rossin A, Faggi C, Fukin GK, Cherkasov AV, Shavyrin AS, Trifonov AA, Giambastiani G (2010) Eur J Inorg Chem 2010:608
30. Liu B, Yang Y, Cui D, Tang T, Chen X, Jing X (2007) Dalton Trans 4252
31. Izod K, Liddle ST, McFarlane W, Clegg W (2004) Organometallics 23:2734
32. Roering AJ, Davidson JJ, MacMillan SN, Tanski JM, Waterman R (2008) Dalton Trans 4488
33. Wicker BF, Scott J, Fout AR, Pink M, Mindiola DJ (2011) Organometallics 30:2453
34. Johnson KRD, Hayes PG (2009) Organometallics 28:6352
35. Johnson KRD, Hayes PG (2011) Organometallics 30:58
36. Jie S, Diaconescu PL (2010) Organometallics 29:1222
37. Han F, Li B, Zhang Y, Wang Y, Shen Q (2010) Organometallics 29:3467
38. Xu X, Chen Y, Zou G, Sun J (2010) Dalton Trans 39:3952
39. Parshall GW, Ittel SD (1993) Homogeneous catalysis. Wiley, New York
40. van Leeuwen WNMP (2004) Homogeneous catalysis: understanding the art. Kluwer, Dordrecht
41. Konkol M, Okuda J (2008) Coord Chem Rev 252:1577
42. Fegler W, Venugopal A, Kramer M, Okuda J (2015) Angew Chem Int Ed 54:1724
43. Nishiura M, Hou Z (2010) Nat Chem 2:257
44. Cheng J, Saliu K, Ferguson MJ, McDonald R, Takats J (2010) J Organomet Chem 695:2696
45. Konkol M, Spaniol TP, Kondracka M, Okuda J (2007) Dalton Trans 4095
46. Konkol M, Kondracka M, Voth P, Spaniol TP, Okuda J (2008) Organometallics 27:3774
47. Lyubov DM, Fukin GK, Cherkasov AV, Shavyrin AS, Trifonov AA, Luconi L, Bianchini C, Meli A, Giambastiani G (2009) Organometallics 28:1227
48. Liu B, Liu X, Cui D, Liu L (2009) Organometallics 28:1453
49. Lu E, Chen Y, Leng X (2011) Organometallics 30:5433
50. Lu E, Chen Y, Zhou J, Leng X (2012) Organometallics 31:4574
51. Cheng J, Shima T, Hou Z (2011) Angew Chem Int Ed 50:1857
52. Johnson KRD, Kamenz BL, Hayes PG (2014) Organometallics 33:3005
53. Chauvin Y (2006) Angew Chem Int Ed 45:3740
54. Schrock RR (2006) Angew Chem Int Ed 45:3748
55. Grubbs RH (2006) Angew Chem Int Ed 45:3760
56. Summerscales OT, Gordon JC (2013) RSC Adv 3:6682
57. Rong W, Cheng J, Mou Z, Xie H, Cui D (2013) Organometallics 32:5523
58. Scott J, Basuli F, Fout AR, Huffman JC, Mindiola DJ (2008) Angew Chem Int Ed 47:8502
59. Lu E, Li Y, Chen Y (2010) Chem Commun 46:4469
60. Lu E, Chu J, Chen Y, Borzov MV, Li G (2011) Chem Commun 47:743
61. Lu E, Zhou Q, Li Y, Chu J, Chen Y, Leng X, Sun J (2012) Chem Commun 48:3403
62. Chu J, Lu E, Liu Z, Chen Y, Leng X, Song H (2011) Angew Chem Int Ed 50:7677
63. Chu J, Lu E, Chen Y, Leng X (2013) Organometallics 32:1137
64. Chu J, Kefalidis CE, Maron L, Leng X, Chen Y (2013) J Am Chem Soc 135:8165
65. Scott J, Fan H, Wicker BF, Fout AR, Baik MH, Mindiola DJ (2008) J Am Chem Soc 130:14438
66. Cameron TM, Gordon JC, Michalczyk R, Scott BL (2003) Chem Commun 2282
67. Zou J, Berg DJ, Stuart D, McDonald R, Twamley B (2011) Organometallics 30:4958
68. Izod K, Liddle ST, Clegg W (2004) Chem Commun 1748
69. Johnson KRD, Hannon MA, Ritch JS, Hayes PG (2012) Dalton Trans 41:7873
70. Jantunen KC, Scott BL, Hay PJ, Gordon JC, Kiplinger JL (2006) J Am Chem Soc 128:6322
71. Masuda JD, Jantunen KC, Scott BL, Kiplinger JL (2008) Organometallics 27:803
72. Zimmermann M, Tornroos KW, Anwander R (2007) Angew Chem Int Ed 46:3126
73. Zimmermann M, Estler F, Herdtweck E, Törnroos KW, Anwander R (2007) Organometallics 26:6029
74. Paolucci G, Bortoluzzi M, Bertolasi V (2008) Eur J Inorg Chem 2008:4126
75. Yang Y, Cui D, Chen X (2010) Dalton Trans 39:3959
76. Johnson KRD, Hayes PG (2013) Organometallics 32:4046

77. Karpov AA, Cherkasov AV, Fukin GK, Shavyrin AS, Luconi L, Giambastiani G, Trifonov AA (2013) Organometallics 32:2379
78. Johnson KRD, Hayes PG (2014) Dalton Trans 43:2448
79. Wicker BF, Pink M, Mindiola DJ (2011) Dalton Trans 40:9020
80. Fryzuk MD, Haddad TS (1990) J Chem Soc Chem Commun 1088
81. Fryzuk MD, Haddad TS, Berg DJ, Rettig SJ (1991) Pure Appl Chem 63:845
82. Fryzuk MD, Haddad TS, Rettig SJ (1991) Organometallics 10:2026
83. Fryzuk MD, Haddad TS, Rettig SJ (1992) Organometallics 11:2967
84. Fryzuk MD, Giesbrecht GR, Rettig SJ (1996) Organometallics 15:3329
85. Fryzuk MD, Giesbrecht GR, Rettig SJ (2000) Can J Chem 78:1003
86. Evans LTJ, Coles MP, Cloke FGN, Hitchcock PB (2010) Inorg Chim Acta 363:1114
87. Fryzuk MD, Yu P, Patrick BO (2001) Can J Chem 79:1194
88. Meyer N, Kuzdrowska M, Roesky PW (2008) Eur J Inorg Chem 2008:1475
89. Jenter J, Gamer MT, Roesky PW (2010) Organometallics 29:4410
90. Roesky PW, Jenter J, Koppe R (2010) C R Chim 13:603
91. Peruzzini M, Gonsalvi L (2011) Phosphorus compounds – advanced tools in catalysis and material sciences. Springer, Berlin
92. Nief F (1998) Coord Chem Rev 178–180, Part 1:13
93. Li T, Kaercher S, Roesky PW (2014) Chem Soc Rev 43:42
94. Masuda JD, Jantunen KC, Ozerov OV, Noonan KJ, Gates DP, Scott BL, Kiplinger JL (2008) J Am Chem Soc 130:2408
95. Wicker BF, Scott J, Andino JG, Gao X, Park H, Pink M, Mindiola DJ (2010) J Am Chem Soc 132:3691
96. Li T, Wiecko J, Pushkarevsky NA, Gamer MT, Köppe R, Konchenko SN, Scheer M, Roesky PW (2011) Angew Chem Int Ed 50:9491
97. Zou J, Berg DJ, Oliver A, Twamley B (2013) Organometallics 32:6532
98. Edworthy I, Blake A, Wilson C, Arnold P (2007) Organometallics 26:3684
99. Painter PC, Coleman MM (2009) Essentials of polymer science and engineering, 1st edn. DEStech Publications Inc., Lancaster, p 1
100. "The Nobel in Chemistry 1963" Nobelprize.org. Nobel Media AB 2014. http://www.nobelprize.org/nobel_prizes/chemistry/laureates/1963/. Accessed 29 Aug 2014
101. "The Nobel in Chemistry 2005" Nobelprize.org. Nobel Media AB 2014. http://www.nobelprize.org/nobel_prizes/chemistry/laureates/2005/. Accessed 29 Aug 2014
102. Dijkstra PJ, Du H, Feijen J (2011) Polym Chem 2:520
103. Amgoune A, Thomas CM, Carpentier JF (2007) Pure Appl Chem 79:2013
104. Dechy-Cabaret O, Martin-Vaca B, Bourissou D (2004) Chem Rev 104:6147
105. Yang Y, Li S, Cui D, Chen X, Jing X (2007) Organometallics 26:671
106. Shang X, Liu X, Cui D (2007) J Polym Sci A Polym Chem 45:5662
107. Liu X, Shang X, Tang T, Hu N, Pei F, Cui D, Chen X, Jing X (2007) Organometallics 26:2747
108. Zi G, Wang Q, Xiang L, Song H (2008) Dalton Trans 5930
109. Wang Q, Xiang L, Song H, Zi G (2009) J Organomet Chem 694:691
110. Peng H, Zhang Z, Qi R, Yao Y, Zhang Y, Shen Q, Cheng Y (2008) Inorg Chem 47:9828
111. Xu B, Han X, Yao Y, Zhang Y (2010) Chin J Chem 28:1013
112. Ren W, Chen L, Zhao N, Wang Q, Hou G, Zi G (2014) J Organomet Chem 758:65
113. Grunova E, Kirillov E, Roisnel T, Carpentier J (2010) Dalton Trans 39:6739
114. Mazzeo M, Lamberti M, D'Auria I, Milione S, Peters JC, Pellecchia C (2010) J Polym Sci A Polym Chem 48:1374
115. D'Auria I, Mazzeo M, Pappalardo D, Lamberti M, Pellecchia C (2011) J Polym Sci A Polym Chem 49:403
116. Li G, Lamberti M, Mazzeo M, Pappalardo D, Roviello G, Pellecchia C (2012) Organometallics 31:1180
117. Westmoreland I, Arnold J (2006) Dalton Trans 4155
118. Liang Z, Ni X, Li X, Shen Z (2012) Dalton Trans 41:2812

119. Bennett SD, Core BA, Blake MP, Pope SJA, Mountford P, Ward BD (2014) Dalton Trans 43:5871
120. Arbaoui A, Redshaw C (2010) Polym Chem 1:801
121. Han X, Wu L, Yao Y, Zhang Y, Shen Q (2009) Chin Sci Bull 54:3795
122. Huang L-L, Han X-Z, Yao Y-M, Zhang Y, Shen Q (2011) Appl Organomet Chem 25:464
123. Xu X, Xu X, Chen Y, Sun J (2008) Organometallics 27:758
124. Gao W, Cui D, Liu X, Zhang Y, Mu Y (2008) Organometallics 27:5889
125. Du G, Wei Y, Zhang W, Dong Y, Lin Z, He H, Zhang S, Li X (2013) Dalton Trans 42:1278
126. Zhang W, Liu S, Yang W, Hao X, Glaser R, Sun W-H (2012) Organometallics 31:8178
127. Kuo P, Chang J, Lee W, Lee HM, Huang J (2005) J Organomet Chem 690:4168
128. Schmid M, Guillaume SM, Roesky PW (2013) J Organomet Chem 744:68
129. Zhou H, Jiang Y, Chen M, Wang Y, Yao Y, Wu B, Cui D (2014) J Organomet Chem 763–764:52
130. Zhang Z, Cui D, Wang B, Liu B, Yang Y (2010) Men in blue. In: Roesky PW (ed) Molecular catalysis of rare-earth elements. Springer, Berlin, p 49
131. Sugiyama H, Gambarotta S, Yap GPA, Wilson DR, Thiele SKH (2004) Organometallics 23:5054
132. Zhang L, Suzuki T, Luo Y, Nishiura M, Hou Z (2007) Angew Chem Int Ed 46:1909
133. Gao W, Cui D (2008) J Am Chem Soc 130:4984
134. Liu D, Cui D, Gao W (2010) Sci Chin Chem 53:1641
135. Jenter J, Meyer N, Roesky PW, Thiele SK, Eickerling G, Scherer W (2010) Chem Eur J 16:5472
136. Lv K, Cui D (2010) Organometallics 29:2987
137. Wang L, Cui D, Hou Z, Li W, Li Y (2011) Organometallics 30:760
138. Wang L, Liu D, Cui D (2012) Organometallics 31:6014
139. Liu H, He J, Liu Z, Lin Z, Du G, Zhang S, Li X (2013) Macromolecules 46:3257
140. Pan Y, Xu T, Yang G-W, Jin K, Lu XB (2013) Inorg Chem 52:2802
141. Desimoni G, Faita G, Guala M, Pratelli C (2003) J Org Chem 68:7862
142. Evans DA, Song HJ, Fandrick KR (2006) Org Lett 8:3351
143. Evans DA, Fandrick KR, Song HJ (2005) J Am Chem Soc 127:8942
144. Morimoto H, Lu G, Aoyama N, Matsunaga S, Shibasaki M (2007) J Am Chem Soc 129:9588
145. Qian C, Wang L (2000) Tetrahedron Asymmetry 11:2347
146. Ward BD, Gade LH (2012) Chem Commun 48:10587
147. Zimmermann M, Törnroos KW, Waymouth RM, Anwander R (2008) Organometallics 27:4310
148. Bartlett SA, Cibin G, Dent AJ, Evans J, Hanton MJ, Reid G, Tooze RP, Tromp M (2013) Dalton Trans 42:2213
149. Wang Q, Xiang L, Zi G (2008) J Organomet Chem 693:68
150. Müller TE, Hultzsch KC, Yus M, Foubelo F, Tada M (2008) Chem Rev 108:3795
151. Hultzsch KC, Hampel F, Wagner T (2004) Organometallics 23:2601
152. Wang Q, Xiang L, Song H, Zi G (2008) Inorg Chem 47:4319
153. Reznichenko AL, Hultzsch KC (2013) Organometallics 32:1394
154. Lu E, Gan W, Chen Y (2009) Organometallics 28:2318
155. Lu E, Gan W, Chen Y (2011) Dalton Trans 40:2366
156. Hultzsch KC, Gribkov DV, Hampel F (2005) J Organomet Chem 690:4441
157. Natrajan LS, Hall JJ, Blake AJ, Wilson C, Arnold PL (2003) J Solid State Chem 171:90
158. Han F, Teng Q, Zhang Y, Wang Y, Shen Q (2011) Inorg Chem 50:2634

New Chemistry with Anionic NNN Pincer Ligands

Rebecca L. Melen and Lutz H. Gade

Abstract The use of tridentate anionic pincer ligands in organometallic chemistry has gained considerable importance, particularly in the field of homogenous catalysis. This chapter focuses on the recent developments of anionic tridentate NNN pincer ligands from their synthesis to coordination chemistry and their applications in forming stable transition metal complexes for applications in catalytic transformations.

Contents

R.L. Melen (✉) and L.H. Gade (✉)

Anorganisch-Chemisches-Institut, Universität Heidelberg, Im Neuenheimer Feld 270, 69120 Heidelberg, Germany
e-mail: MelenR@cardiff.ac.uk; lutz.gade@uni-heidelberg.de

Abbreviations

ATRP	Atom transfer radical polymerization
BOPA	Bis(oxazolinylphenyl)amine
BOX	Bis(oxazoline)
BOXMI	Bis(oxazolinylmethylidene)isoindoline
BPI	Bis(2-pyridylimino)isoindole
BQA	Bis(8-quinolinyl)amine
Cbzbox	Bis-oxazoline carbazole
DIPEA	Diisopropylethylamine
DMS	Dimethylsilane
iproxpH	Bis[2-(4,4-diisopropyl-4,5-dihydrooxazolyl)]pyrrole
NHK	Nozaki–Hiyama–Kishi
PDI	Polydispersity index
pyBOX	Pyridine bis(oxazoline)
PyrrMeBOX	2,5-Bis(2-oxazolinylmethyl)pyrrole
SIPr	1,3-Bis(2,6-di-i-propylphenyl)imidazolidin-2-ylidene
TBAF	Tetrabutylammonium fluoride
thq	Tetrahydroquinoline

1 Introduction

Mono-anionic, tridentate, meridionally coordinating ligands have been widely used in coordination chemistry to afford stable and robust complexes not only of transition metals but also lanthanides and main group elements [1–5]. The chelating nature of these polydentate ligands gives rise to kinetically and thermodynamically stable complexes which do not tend to undergo ligand displacement. This is important for the resulting coordination compounds that have applications in catalysis and materials chemistry. NNN pincer ligands have been used as ligands in organometallic chemistry and exhibit a range of applications in catalysis, including enantioselective catalysis, and in bond activation processes. Pincer ligands comprise a central formally anionic unit/moiety that donates two electrons from the donor atom (usually carbon or nitrogen) to the transition metal via a covalent bond and act as an "anchor." Located in either side of the central donor atom are two neutral pendant arms which donate a lone pair of electrons usually from heteroatoms such as oxygen, nitrogen, sulfur, or phosphorus. These aid in the stabilization of the metal center and play a role in defining the "active sector" in

the coordination sphere of the complex. In chiral complexes, the flanking donors in the "wingtip" positions are typically part of a heterocyclic unit and frequently possess the stereochemical information necessary for enantioselective catalysis. By changing the substituents on the chiral "wingtips," a large variety of optically pure ligands with a range of groups located close to the reactive metal center permit fine control of the steric effects close to the active site. Thus, large families of ligand variants have been designed which can allow for systematic investigations of the steric and electronic effects that control the selectivity and activity of catalytic systems. Often the groups on the periphery are identical resulting in ligands with twofold rotational symmetry.

chiral pincer ligand
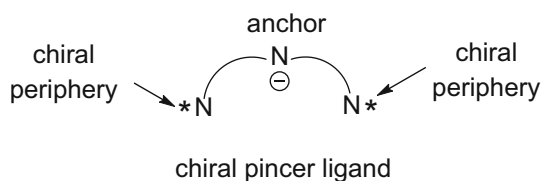
In this chapter, we review the recent developments in the synthesis, coordination chemistry, and applications of tridentate, anionic NNN pincer ligands. In the first section, we shall focus on the different classes of NNN pincers along with their design. This will then be followed by an introduction to the coordination modes of these ligands, and finally, the applications of NNN pincer complexes in catalysis (including enantioselective catalysis) will be reviewed.

2 Ligand Design

In this section, we focus on a selection of different types of tridentate anionic NNN pincer ligands which all contain a central anionic N-ligating unit with two pendant neutral N-donor arms connected to the central core via a 2- or 3-atom spacer unit (Fig. 1). While a great many chiral donor molecules are possible, only a few privileged ligands have been found to have broad application in catalysis. Among these, many chiral pincer ligands reported are of C_2-symmetry, although this has not precluded the use of other nonsymmetric chiral ligands that have also been reported and applied in coordination chemistry and catalysis. In fact, the presence of rotational symmetry can be considered desirable, and the benefits of C_2-symmetrical ligands based on bis(oxazoline)s have been reviewed in detail [6]. One series of NNN donor complexes is based upon the neutral BOX bis(oxazoline) bidentate framework in which the central CH_2 unit of BOX is replaced by pyridine (pyBOX) [7, 8]. In general, for BOX ligands and related systems, the substituent at the 4-position of the oxazoline ring blocks one enantiotopic face of the substrate, leading to chiral induction. Detailed studies of the stereochemical products of these reactions are consistent with a twisted square planar intermediate [9, 10].
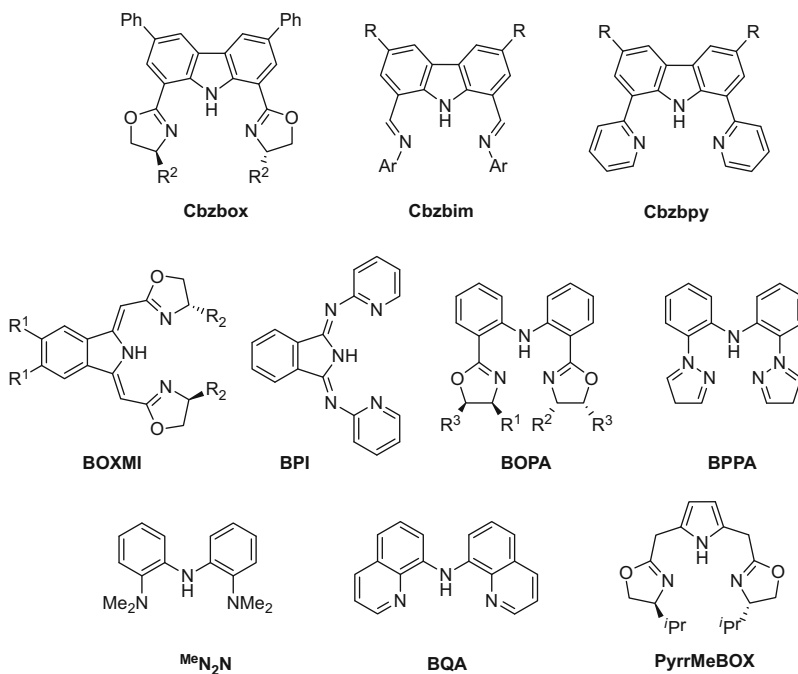
Fig. 1 Examples of tridentate NNN pincer ligands

Several different tridentate NNN pincer ligands contain the carbazole group as the anchor unit. The initial synthetic route to bis(oxazoline) carbazole (Cbzbox) ligands was reported in 2003 by Nakada from the reaction of dihalogenated diphenylcarbazoles with CuCN to form the dicyano diphenylcarbazoles which were reacted with amino alcohols and $ZnCl_2$ [11, 12]. Later, a new synthesis was developed in which the dihalogenated diphenylcarbazoles could be reacted with an amino alcohol and CO in the presence of Et_3N and catalytic $Pd(PPh_3)_4$ to yield the amide which could subsequently be cyclized using $BF_3 \cdot OEt_2$ or $MeSO_2Cl$ to give the ligand. Using these methods, several different derivatives could be obtained (Scheme 1) [13, 14]. The carbazolyl/bis(imino) ligands (Cbzbim) and carbazolyl/bis(pyridyl) (Cbzbpy) ligands were also synthesized from the dihalogenated carbazoles. In the former case, the 1,8-dibromocarbazole was converted into dialdehyde through lithiation and reaction with DMF. The 1,8-diformyl-3,6-dimethylcarbazoyl could then be converted to the corresponding imine by reaction with an amine [15–17]. Conversely, the 1,8-di(pyrid-2′-yl)carbazoles were synthesized through a Stille-type coupling reaction of the 1,8-dibromocarbazole with 2-(tri-*n*-butylstannyl)pyridine [18]. More recently, several other classes of tridentate anionic NNN pincers bearing the carbazolyl unit have been synthesized including carbazolyl/bis(phosphinimine) and carbazolyl/bis(pyrazolyl) ligands [19–21].
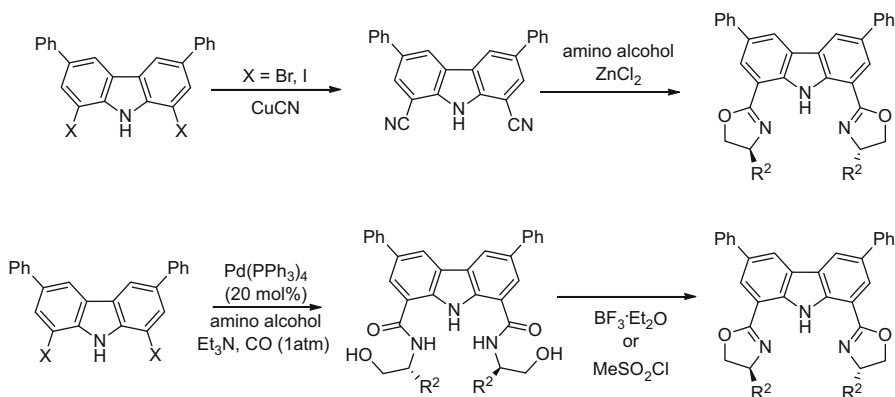
Scheme 1 Synthetic routes to Cbzbox ligands
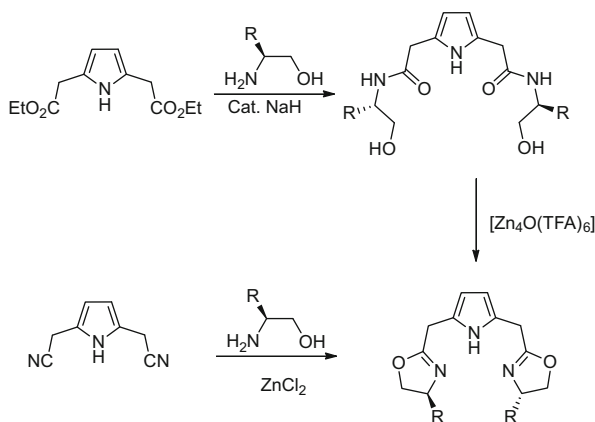
Scheme 2 Synthesis of bis(2-oxazolinylmethyl)pyrroles

In 2003, the tridentate ligand system 2,5-bis(2-oxazolinylmethyl)-pyrrole (PyrrMeBOX) was synthesized in which there is a 3-carbon linker between the nitrogen atoms [22]. This could be prepared starting from the 2,5-bis(cyanomethyl) pyrrole and reacting this with chiral alcohols in chlorobenzene under reflux with catalytic amounts of $ZnCl_2$, following the same synthetic methodology just described. However, for this reaction, the cyclization proved to be difficult, and in 2009, an alternative method was reported to synthesize this ligand [23]. The new method used diethyl pyrrole-2,5-diacetate which was condensed with an amino alcohol in the presence of catalytic NaH to yield the intermediate pyrrole-2,5-bis (acetamides) which could be cyclized in the presence of $Zn_4O(O_2CCF_3)_6$ (Scheme 2).

Another example of a pyrrole-based tridentate pincer ligand is 2,5-bis (3,5-dimethylpyrazolylmethyl)pyrrole (Scheme 3) synthesized from the pyrrole in a two-step reaction in moderate yields (56%). The pyrrole was initially reacted with
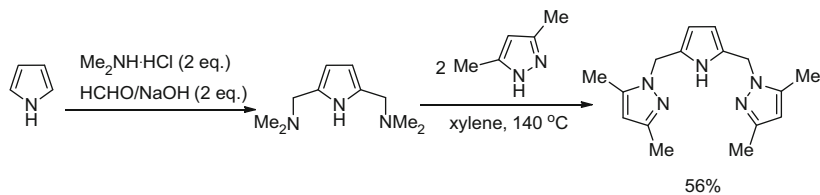
Scheme 3 Synthesis of the 2,5-bis(3,5-dimethylpyrazolylmethyl)pyrrole ligand
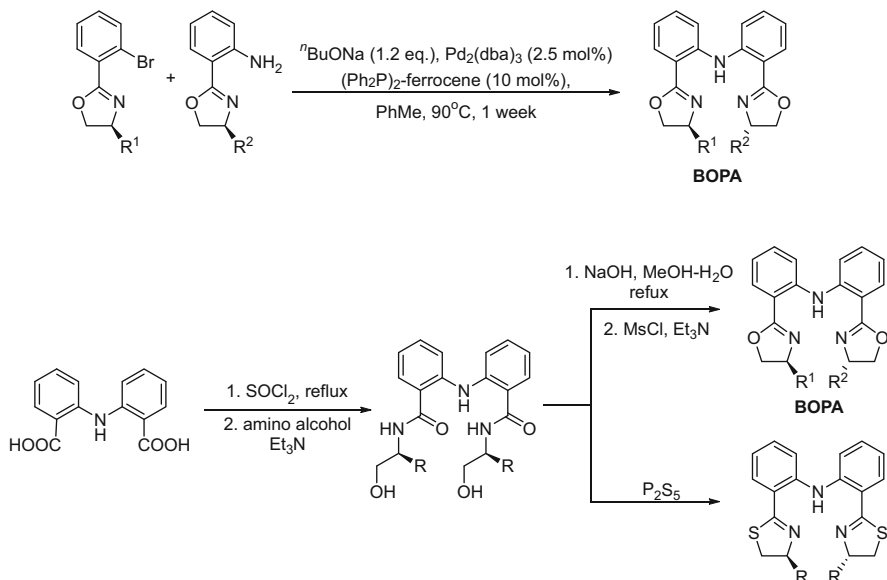
Scheme 4 Synthesis of BOPA ligands

formaldehyde and dimethylamine hydrochloride to give 2,5-bis(dimethylami-nomethyl)pyrrole via a Mannich reaction. Nucleophilic substitution using 3,5-dimethylpyrazole then afforded the 2,5-bis(3,5-dimethylpyrazolylmethyl)pyr-role ligand [24].

Several NNN ligands have been synthesized which have an *N*-diphenylaniline unit as a linker between two pendant N-containing groups (e.g., imines, oxazolines, pyrazoles, or amines). Tridentate bis(oxazoline) ligands (BOPA) [25,26] are impor-tant ligands to transition metals and have been used in a wide range of catalytic reactions. They were synthesized initially by Guiry in 2002 through a Pd-catalyzed Buchwald–Hartwig coupling between a 2-(2'-bromophenyl)oxazoline and a 2-(*o*-aminophenyl)oxazoline (Scheme 4, top). The bis(8-quinolinyl)amine (BQA) ligand [27] and amido bis(amine) ligand $^{Me}N_2N$ [28] were also synthesized by similar Pd-catalyzed C–N coupling reactions. Following the first synthesis of BOPA ligands, Du reported a different route to the ligands [26] that gave higher overall
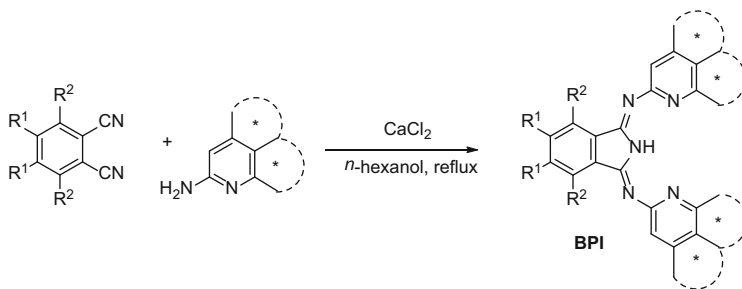
Scheme 5 Synthesis of BPI ligands

yields (41–83% cf. 40%) and did not require the use of palladium catalysts. In this synthesis, amino alcohols were reacted with dicarboxyl diphenylamine yielding β-hydroxyl amides which were then cyclized in the presence of base (Scheme 4, bottom). Conversely, if the β-hydroxyl amide was treated with P_2S_5, the corresponding bis-thiazoline ligands were formed in 41–61% yield (Scheme 4, bottom) [26]. The bis(2-pyrazolyl-*p*-tolyl)amine ligand (BPPA) was synthesized by a different route in two steps involving initial *ortho*-bromination of di(*p*-tolyl) amine using bromine to give the intermediate (2-Br-*p*-tolyl)$_2$NH. This is then converted into the anticipated product in 70% yield through a copper-catalyzed amination reaction with pyrazole [29].

Bis(2-pyridylimino)isoindole (BPI) ligands were first reported over 60 years ago [30–32] and are examples of tridentate pincer ligands which have found applications in catalysis and materials science [33]. The current preferred method of synthesis involves the reaction of commercially available phthalonitrile with 2-aminopyridines in a high boiling alcohol solvent in the presence of CaCl$_2$ (Scheme 5) [34–38].

Bis(oxazolinylmethylidene)isoindolines (BOXMI) have been recently reported and have already demonstrated their excellent potential as stereodirecting ligands. The three-step synthesis starts with the Wittig reaction of commercially available phthalimides with ethyl (triphenylphosphoranyliden)acetate [39]. The resulting intermediate could then be reacted with chiral amino alcohols and subsequently cyclized yielding the chiral C_2-symmetrical ligands (Scheme 6).

The significant advances in ligand synthesis described herein provide access to an extensive array of ancillary ligands in which the steric and electronic properties can be finely tuned to provide control of the Lewis acidity as well as regio- and stereoselectivity of transformations at the metal center. In the sections that follow, we focus in detail on the diversity of these ligands in their coordination chemistry and catalysis including enantioselective catalysis.
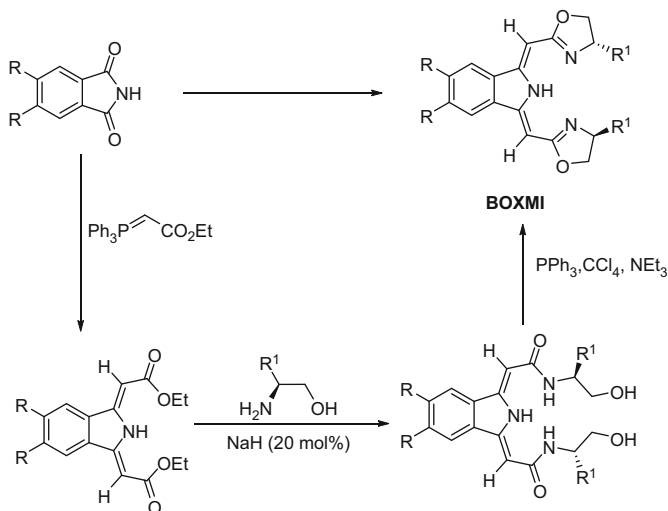
Scheme 6 Synthetic route to BOXMI ligands

3   Coordination Chemistry of NNN Pincer Ligands

The most common mode of coordination involves the three donor nitrogen atoms affording "homoleptic" (ML_2) or "heteroleptic" (LML'_n) complexes, although alternative coordination modes have also been observed. The synthesis of metal complexes is often achieved by one of two routes: either the ligand is initially deprotonated and reacted with MX_2 or the protio-ligand is directly reacted with the metal salt that usually contains weakly coordinating counter ions.

For applications in catalysis, heteroleptic complexes are often desired in which one meridionally coordinating, mono-anionic ligand coordinates to the metal center with the "reactive" coordination sites being occupied by other mono-dentate, often weakly coordinating ligands. The synthesis of heteroleptic [(NNN)M(X)n] complexes for four or five coordinate 4d or 3d metals is usually straightforward. Conversely, the synthesis of complexes where coordination numbers of six are favorable can sometimes be more challenging and may require bulky ligands and/or an excess of the metal salt to be used in order to avoid formation of the homoleptic complex of the tridentate donor, ML_2 [30, 34] (e.g., see [40–42]). This was observed, for example, in the synthesis of BPI complexes in which ligands are substituted adjacent to the pyridine nitrogen atom [43–45]. This results in steric shielding of the metal center in the complex, precluding the addition of a second ligand, and therefore, the heteroleptic complexes [(BPI)M(X)(S)$_n$)] could be obtained (Scheme 7) [43].

Heteroleptic complexes of BOXMI ligands with copper and nickel have been synthesized and structurally characterized, and both types of complexes adopt slightly distorted square planar coordination geometries (Fig. 2) [39, 46].
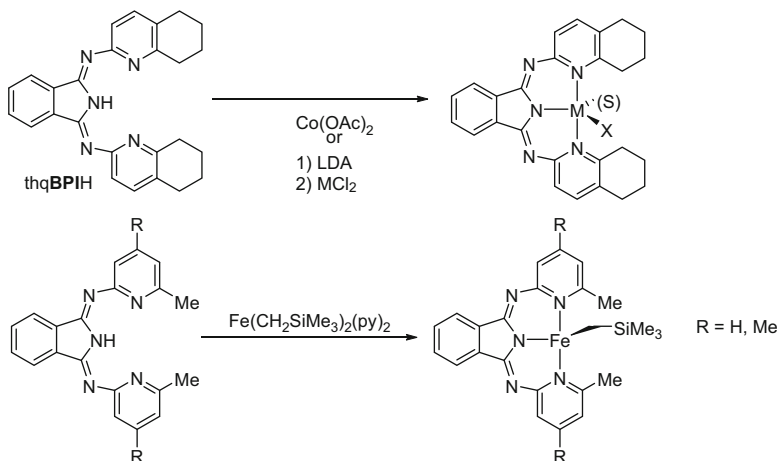
Scheme 7 Heteroleptic BPI complexes
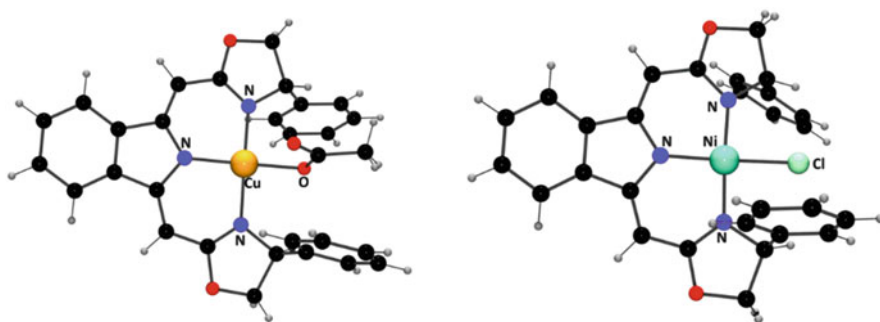
Fig. 2 BOXMI–copper and BOXMI–nickel complexes

The BQA ligand is also known to bind to metal centers in a planar manner yielding complexes which are stable even in the presence of water or acid [47–51]. For example, (BQA)NiCl was found to adopt a square planar structure with the BQA ligand coordinating in a κ^3-manner [27].

Complexes of the 4d and 5d metals are also known. For example, octahedral *trans*-(BQA)MX(PPh$_3$)$_2$ (M=Ru, Os; X=Cl, Br, N$_3$, OTf), *trans*-(BQA)RuH (PMe$_3$)$_2$, and *trans*-(BQA)RuMe(PMe$_3$)$_2$ as well as square planar (BQA)PtCl and (BQA)PdCl have been synthesized [27, 51]. Square planar platinum(II) complexes such as (BPI)Pt(L) using BPI and additional strong field ligands have also been prepared [52]. However, while BPI ligands typically act as chelating tridentate ligands, sometimes one of the pyridine rings may rotate out of the plane when other

bulky co-ligands are present [53]. This was observed in the isolation of [Ir(BPI)
(COD)] in which, as a result of the strong coordination of the cyclooctadiene (COD)
ligand, one of the pyridine rings does not coordinate to the metal center and is thus
twisted away [53]. On the other hand, if the smaller ethylene molecules are used
instead of COD, the BPI ligand coordinates in the usual manner (Fig. 3) [53]. Sim-
ilar results were observed with the asymmetrical pincer ligand o-(NMe$_2$)Ph-QAH
with (COD)PtCl$_2$. X-ray diffraction analysis of crystals formed during the reaction
showed that the ligand bound in a bidentate manner to give (o-(NMe$_2$)Ph-QA)Pt
(1,2-η^2-6-σ-cycloocta-1,4-dienyl) in which the NMe$_2$ group is not bound to the
metal center. In this reaction, the COD ligand has undergone C–H activation to give
an ionic ligand that occupies two coordination sites at the platinum center [27].
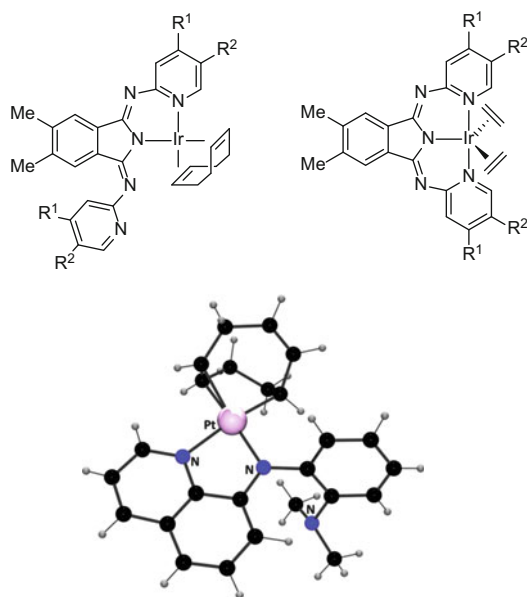
Fig. 3 Coordination of BPI ligands governed by the steric demand of the π-ligand (*top*) and the
crystal structure of (o-(NMe$_2$)Ph-QA)Pt(1,2-η^2-6-σ-cycloocta-1,4-dienyl) (*bottom*)

4 Applications in Catalysis

Many of the NNN pincer ligand types described above have been applied in catalytic reactions, including enantioselective catalysis. Control of the inherently chiral nature of the chemistry which underpins the biological processes necessary for life is central to the successful development of many pharmaceuticals. Recently, there has been much focus on chiral NNN pincer ligand complexes in asymmetric catalysis. In these complexes, a tridentate (anionic) N-donor ligand binds to the metal center with the ligand chirality promoting a preferred orientation of the substrate at the metal center, thereby inducing some degree of enantioselectivity in the reaction. Typically, the location of the chiral substituents in close proximity to the reactive center affords greater enantiomeric control in the product.

4.1 C–C Bond Formation

C–C bond formation plays a very important role in synthetic chemistry. The nickel amido bis(amine) ligand $^{Me}N_2N$ complex [$(^{Me}N_2N)$Ni-Cl] has been found to be an effective catalyst in C–H alkylation reactions and in the cross-coupling of unactivated alkyl halides with Grignard reagents (Scheme 8) [54–59]. The catalyst was found to be excellent at cleaving C–Cl bonds and in the subsequent C–C bond-forming reactions (Scheme 8). These reactions were found to go through [$(^{Me}N_2N)$Ni-R] intermediates [60]. For example, in sp^3–sp alkyl–alkynyl coupling, the alkynyl–nickel complex [$(^{Me}N_2N)$Ni-C≡CCH$_3$] has been structurally characterized, while in sp^3–sp^3 coupling, [$(^{Me}N_2N)$Ni-^{n}Pr] could be isolated (Fig. 4). Importantly, in alkyl–alkyl Kumada cross-coupling, it was found that β-H elimination was not favorable even at elevated temperature [61]. The alkyl–alkyl Kumada coupling reactions take place via a bimetallic radical mechanism involving two nickel centers in the oxidative addition of the alkyl halide [62]. More recently, the mechanism of alkyl–aryl coupling has been probed and shows a similar radical coupling mechanism to that in alkyl–alkyl coupling [63].
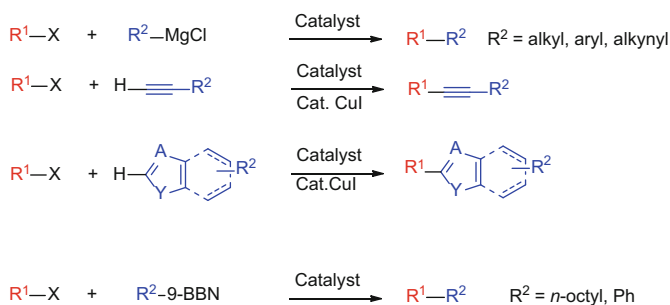
Scheme 8 Cross-coupling reactions and C–H alkylation reactions using the catalyst [$(^{Me}N_2N)$Ni-Cl]
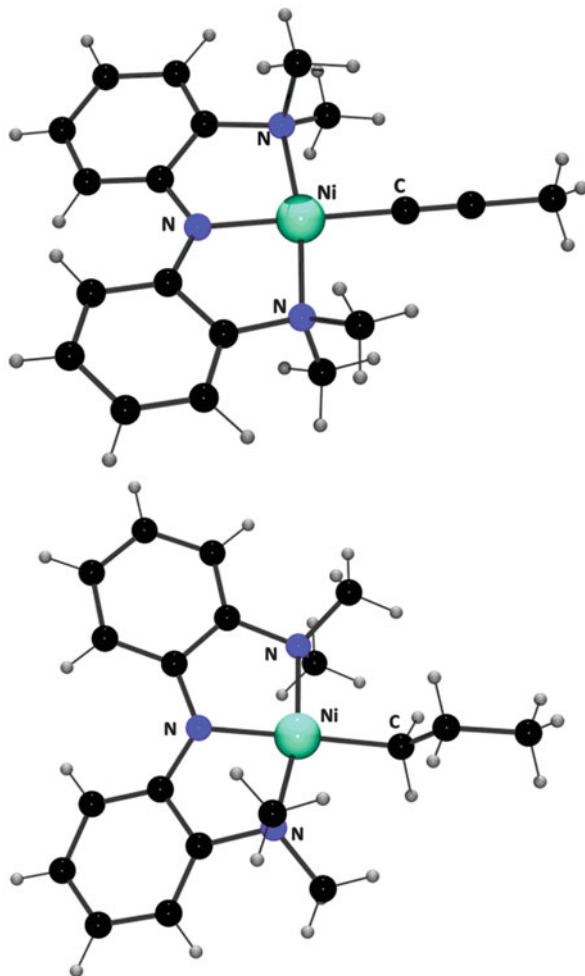
Fig. 4 Crystal structure of the nickel/alkynyl species [(^{Me}N$_2$N)Ni-C≡CCH$_3$] (*top*) and the nickel alkyl species [(^{Me}N$_2$N)Ni-^{n}Pr] (*bottom*)

In addition to alkyl–alkyl Kumada coupling, [(^{Me}N$_2$N)Ni-Cl] can also catalyze Suzuki–Miyaura cross-coupling reactions between a variety of alkyl bromides or iodides with *n*-octyl- or phenyl-(9-BBN) (Scheme 8) [64].
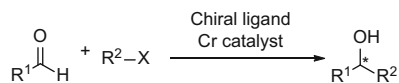
Scheme 9 NHK reactions using chiral chromium complexes

4.2 Nozaki–Hiyama–Kishi Reactions

Asymmetric C–C bond-forming reactions are very important for the construction of the backbone of many synthetic targets. One such method is the chromium-catalyzed Nozaki–Hiyama–Kishi (NHK) reaction (e.g., see [65–67]) which was first reported in the 1970s [68–70].

The incorporation of NNN pincer ligands has been found to be very effective in stabilizing the chromium catalyst while allowing for good control of the enantioselectivity in the addition of allyl, propargyl, and allenyl nucleophiles to aldehyde substrates (Scheme 9).

Among the possible NNN pincer ligands, Cbzbox, BOPA, and BOXMI ligands in combination with chromium chloride have all been employed in the asymmetric NHK reactions of allylic halides with aldehydes. These reactions included a wide substrate scope including a variety of allylation, methallylation, and crotylation reactions (Scheme 10). With Cbzbox, a variety of aldehydes were used in the addition reactions giving the products in good yields and enantioselectivities [11]. The allyl halide starting material used had an effect upon the yield and *ee* values of the reaction with the best results being observed with the chloride or bromide (up to 98% yield and 96% *ee*) with the iodide giving poorer yields and enantioselectivities (52% yield, 64% *ee*). Crotylation reactions of benzaldehyde with crotyl bromide resulted in poorer results with an *anti*/*syn* ratio of 2.7/1 with the reaction being *anti*-selective from the attack of the nucleophile onto the *Si*-face of the aldehyde [11]. BOPA ligands were subsequently employed in NHK reactions with varying results depending upon the ligand employed [71, 72]. The C_2-symmetric BOPA bearing ^{i}Pr groups on the oxazoline rings resulted in an enantiomeric excess of 69%, whereas the non-C_2-symmetrical ligand bearing two inequivalent oxazoline rings (one with a ^{t}Bu and one with a Bn substituent) gave an enantiomeric excess of 87% for the same reaction. In addition, the isomers formed in these reactions were also opposite: with *Si*-face attack occurring with the symmetrical ligand and *Re*-face attack occurring with the asymmetrical ligand. Notably, the effect of the halide was similar in both BOPA–Cr^{II}- and Cbzbox–Cr^{II}-catalyzed transformations, with the BOPA–Cr^{II}-catalyzed reactions of methallyl bromide affording higher yields (64% cf. 24%) albeit with lower enantioselectivities (95% cf. 99.5% *ee*) than the iodide. With BOPA ligands, rather than Cbzbox, higher *anti*/*syn* ratios (up to 4/1) and enantioselectivities (up to 92% *ee* for the major isomer) were observed in the crotylation reactions [71]. Finally, the BOXMI ligand family, in combination with CrCl$_2$, has also been exploited in the NHK reactions. These similarly afforded higher enantioselectivities when using allyl bromide [39]. Variations in both the bromide and aldehyde reagents were examined giving the
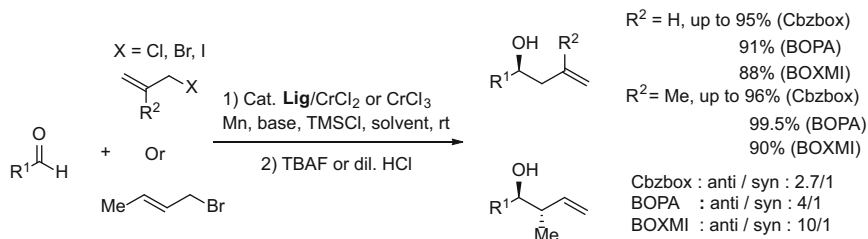
Scheme 10 Asymmetric NHK reactions catalyzed by Cr–tridentate pincer ligand complexes
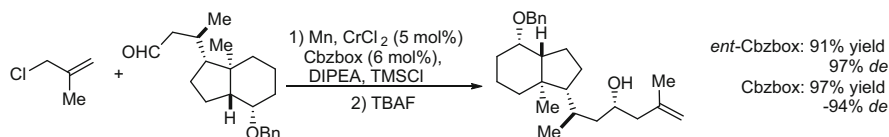
Scheme 11 An example of the use of chiral pincer ligands in natural product synthesis; formation of calcitriol lactone

products in good yields and high enantioselectivities (86–93 % *ee*) [39]. BOXMI–chromium complexes were also found to catalyze methallylation and crotylation reactions showing higher *anti/syn* ratios (10/1) relative to the Cbzbox and BOPA ligand/Cr^{II}-catalyzed transformations (Scheme 10) [39].

The NHK reaction using Cr–Cbzbox complexes was employed in the catalytic enantioselective methallylation of a key intermediate in the production of the vitamin D$_3$ metabolite calcitriol lactone (Scheme 11). The reaction was found to be highly selective giving a -94% *de* or a +97% *de* value depending upon which enantiomer of the ligand was used [11]. Additionally, the NHK reaction using Cbzbox/CrCl$_2$ has also been employed in two steps of the total synthesis of HMG-CoA reductase inhibitors FR901512 and FR901516 (Scheme 12) [73].

The asymmetric propargylation [74] and allenylation [75] reactions of aldehydes has also been achieved using Cbzbox ligands (Scheme 13). The ligand used in the former reaction was found to be influential in determining the stereochemistry of the product in these reactions similar to that described above for BOPA ligands in NHK reactions. Small substituents on the oxazoline rings (Me, ^{i}Pr) resulted in nucleophilic attack at the *Si*-face attack, while more bulky groups (^{t}Bu) favored the nucleophilic attack at the *Re*-face of the aldehyde [74]. Allenylation reactions of terminally silylated propargyl halides afforded 2-silylated allenic alcohols. In these reactions, smaller silyl groups on the propargyl halide performed better giving the *R*-alcohols in higher yields and *ee* values from attack at the *Si*-face of the aldehyde [75]. (4-Bromobut-2-ynyl)-trimethylsilane was also investigated as a substrate in the NHK allenylation of aldehydes affording [1-(silylmethyl)allenyl]methanols in yields up to 88% and enantioselectivities up to 78% *ee* using 5 mol% CrCl$_2$/Cbzbox ligand [76]. The silyl-containing products in the latter two reactions could be desilylated using tetrabutylammonium fluoride (TBAF) (or 2 M HCl) to give
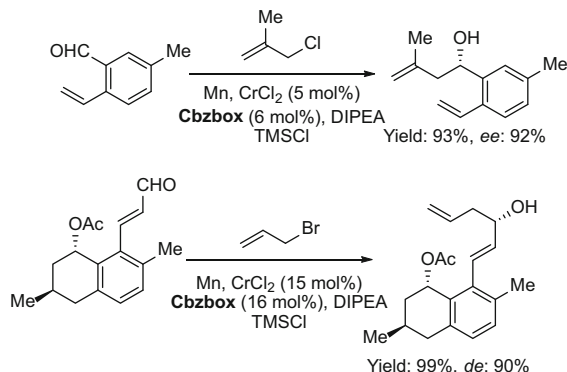
Scheme 12 Uses of Cbzbox ligands in the total synthesis of inhibitors HMG-CoA reductase
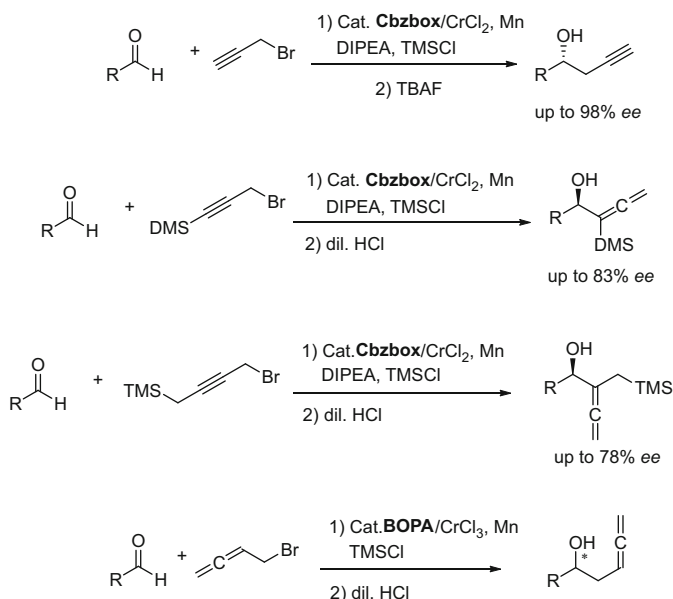
Scheme 13 Cbzbox ligands in the asymmetric propargylation, allenylation, and homoallenylation reactions of aldehydes

allenic alcohols and (butadienyl)methanols, respectively [75, 76]. Finally, the homoallenylation of aldehydes and ketones has been investigated employing chromium–BOPA complexes to prepare a range of (*R*)-β-allenols [77]. Interestingly, the preferred ligand for these reactions was found to be non-C_2-symmetric.
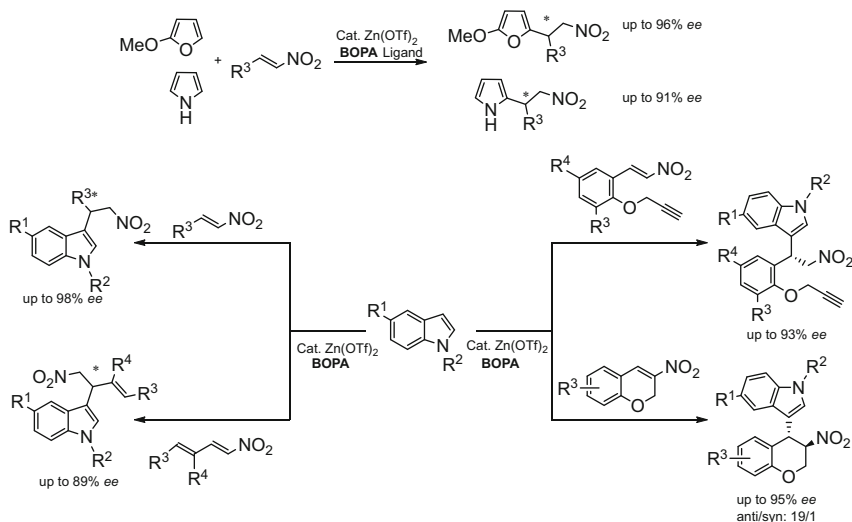
Scheme 14 BOPA–Zn(OTf)$_2$ complexes in asymmetric Friedel–Crafts alkylation of indoles, pyrroles, and 2-methoxyfurans

4.3 Friedel–Crafts Reactions

Friedel−Crafts reactions, first reported in the late nineteenth century, are not only important tools in C–C bond-forming reactions [78,79] but also classical textbook material for electrophilic substitution reactions of aromatics. The asymmetric Friedel−Crafts alkylations in which nitroalkenes are reacted with heterocyclic substrates such as indoles, pyrroles, and furans recently have received considerable attention [80–82], exemplified by the asymmetric Friedel–Crafts alkylation of nitroalkenes, nitrodienes, 2-propargyloxy-β-nitrostyrenes, and 3-nitro-2*H*-chromenes using chiral BOPA–Zn(OTf)$_2$ complexes (Scheme 14) [83–87]. In addition, highly derivatized chromenes have been generated via asymmetric tandem Friedel–Crafts alkylation/Michael addition reactions of nitro-olefin enolates to 1-methylindoles using a BOPA–Zn^{II} complex (Scheme 15) [88]. BOPA ligands immobilized on Fréchet-type dendrimers [89] have also been successfully implemented in Friedel–Crafts reactions, affording similar yields and enantioselectivities (93% *ee*) to the results to those observed without immobilization, and permitted recycling of the catalyst [90].

4.4 Addition of Fluorine-Containing Groups

The presence of fluorine in organic compounds (as R-F, R-CF$_3$, and R-SCF$_3$) often has a marked effect in the properties of the compounds [91]. This has resulted in the
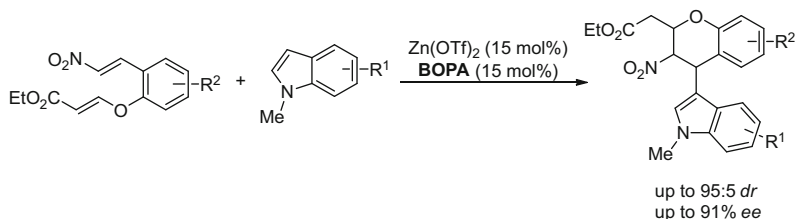
Scheme 15 Tandem reactions using Zn–BOPA complexes: Friedel–Crafts alkylation followed by Michael addition

use of fluorine-containing compounds in pharmaceuticals, polymers, and agro-chemicals [92–95]. Accordingly, many efforts have focused on the installation of F, CF_3, and SCF_3 groups into organic compounds. In this context, chiral BOXMI complexes have been employed in the catalytic electrophilic fluorination, trifluoromethylation, and trifluoromethylthiolation reactions in an enantioselective manner. Using nickel as the transition metal, the asymmetric fluorination of oxindoles and cyclic β-keto esters has been achieved with extremely high enantioselectivities (Scheme 16). This reaction has been applied in the synthesis of Maxipost™ (a pharmaceutical tested for the treatment of stroke) [96,97] to give selectively the N-Boc protected product as the *R*-enantiomer in 90% yield and in 99% *ee*. Using copper–BOXMI catalysts, electrophilic trifluoromethylations and trifluoromethylthiolations of cyclic β-keto esters using CF_3- or SCF_3-transfer reagents have also been performed [98, 99]. In both cases, the reaction yields were found to be high with extremely good enantioselectivities (up to 99% in both cases).

4.5 Enantioselective Azidations and Alkylations

Azidation and alkylation of β-keto esters and oxindoles were achieved in a similar manner to that described above this time using iron(II)–BOXMI or copper(II)–BOXMI complexes, respectively [46, 100]. In the azidation case, azido-iodinane was employed as a N_3-transfer agent to afford the 3-azido-oxindoles in up to 93% *ee* (Scheme 17). The azide-containing products could be transformed in subsequent reactions, for example, in the 1,3-dipolar copper-catalyzed azide-alkyne cycloaddition, to yield triazoles or in the palladium-catalyzed hydrogenolysis to give α-amino esters [100].

Likewise, the BOXMI–Cu(II)-catalyzed alkylation of β-keto esters with in situ-generated alkyl iodides yielded quaternary carbon-containing products stereoselectively (Scheme 18) [46]. The mechanism for this reaction proceeds through initial coordination of the β-keto ester to the (BOXMI)Cu complex resulting in intermediate **I**, which activates the β-keto ester to deprotonation by ${}^i Pr_2 NEt$ yielding the (BOXMI)Cu–enolate–ester complex **II**. Reaction of the copper-bound
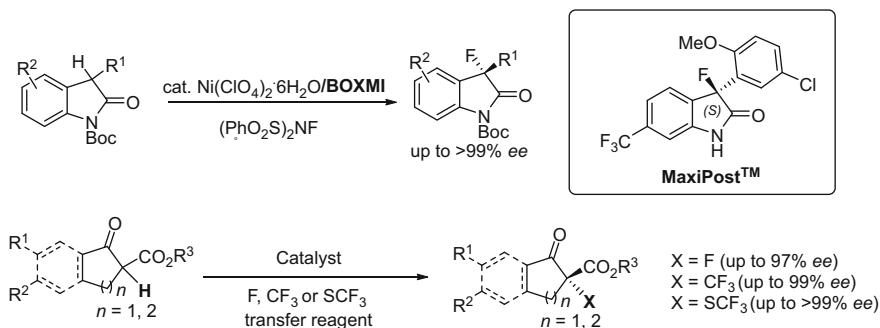
Scheme 16 Electrophilic fluorination, trifluoromethylation, and trifluoromethylthiolation reactions of β-keto esters and oxindoles
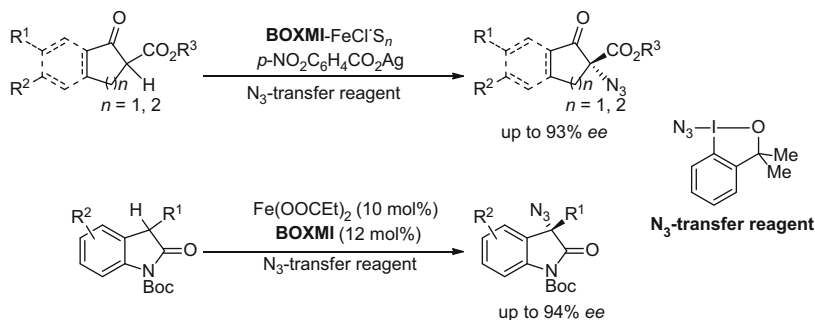
Scheme 17 Azidation of cyclic β-keto esters and 3-aryl oxindoles using a BOXMI–Fe catalyst
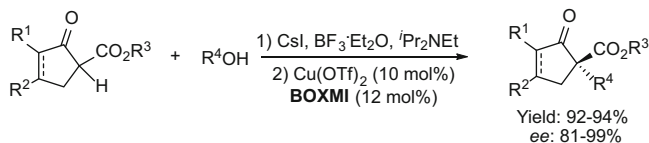
Scheme 18 Alkylation of cyclic β-keto esters using copper–BOXMI catalysts

enolate–ester **II** with the benzyl (or allyl) iodide generated in situ leads to the enantioselective formation of the alkylated copper-bound product **III**. Since the phenyl group in the oxazolinyl unit of the BOXMI ligand blocks the *Si*-face of the enolate–ester, the halide substrate approaches from the *Re*-face (Scheme 19, bottom) [46].
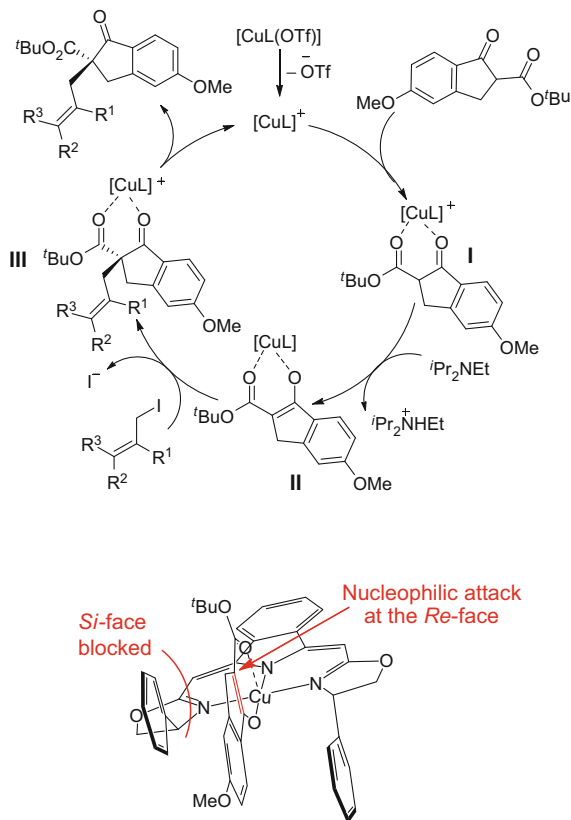
Scheme 19 Catalytic cycle for the alkylation of cyclic β-keto esters using (BOXMI)Cu complexes (*top*) and an explanation of the stereoselectivity (*bottom*)

4.6 [4+2] Cycloaddition Reactions

The Diels–Alder reaction and other [4+2] cycloadditions can be found in organic textbook undergraduate material and are classic ring-forming reactions which can be applied to both C-based and heterocyclic ring formation. They permit the construction of multiple chiral centers while retaining a high degree of control over chirality at each center. Recently, the [4+2] cycloadditions of 3-nitro-2*H*-chromenes with 1-benzyl-2-vinyl-1*H*-indoles have been achieved enantioselectively using catalytic Zn(OTf)$_2$/chiral BOPA ligand mixtures to generate fused tetra- and penta-cyclic structures (Scheme 20) [101]. The biologically relevant fused heterocyclic products were formed in up to 94% yield and in up to 95:5 *dr* and 96% *ee*.
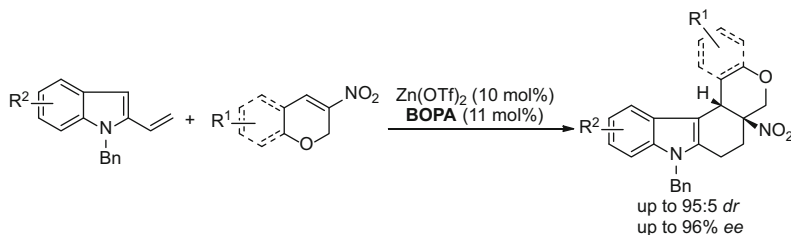
Scheme 20 [4+2] Cycloadditions using chiral $Zn(OTf)_2$/BOPA
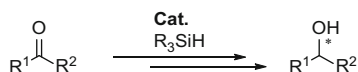
Scheme 21 Catalytic asymmetric hydrosilylation of ketones

4.7 Hydrosilylations of Ketones and Cyclopropanations of Alkenes

The asymmetric hydrosilylation of ketones using metal–BPI (M=Fe, Co) and Fe $(OAc)_2$/BOPA catalytic systems is an effective method for the synthesis of chiral alcohols following hydrolysis (Scheme 21) [37, 38, 102–104]. While the use of BPI–Co and BPI–Fe complexes resulted in hydride transfer to the *Si*-face to give the *R*-alcohol, the stereochemistry of the product with BOPA ligands was dependent upon the presence (or absence) of zinc powder. Thus, the combination of BOPA ligands with $Fe(OAc)_2$ gave the *R*-alcohol from *Si*-face attack, while the combination of BOPA ligands with $FeCl_2$/Zn resulted in *Re*-face attack to give the corresponding *S*-alcohol [102]. However, in both reactions, the enantioselectivities were high, giving the products in up to 93% *ee* (BPI) and 95% *ee* (BOPA), respectively.

The chiral BPI complex [Co(tetraphenyl-carBPI)(OAc)] was found to be an efficient catalyst for the asymmetric cyclopropanation of aryl- and alkyl-alkenes using ethyl diazo-acetate in which two chiral centers are generated at the alkene substrate carbon atoms [37]. These cyclopropanation reactions could also be undertaken in an intramolecular fashion, generating bicyclic rings (Scheme 22).

4.8 Conjugate Addition Reactions

The addition of a nucleophile to an α,β-unsaturated carbonyl is another common C–C bond-forming reaction and can generate new chiral centers in asymmetric additions. With respect to studies on NNN pincer ligands, palladium complexes of PyrrMeBOX ligands have been tested as Lewis acid catalysts in the asymmetric Michael addition reactions of ethyl-2-cyanopropionate to methyl vinyl ketone
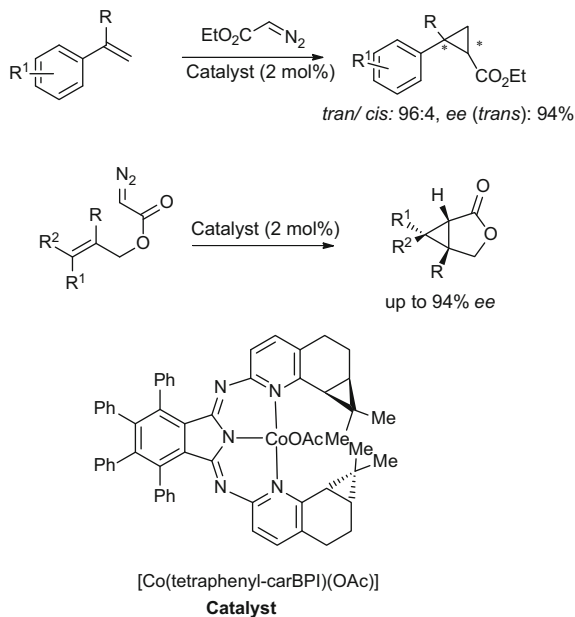
Scheme 22 [Co(tetraphenyl-carBPI)(OAc)]-catalyzed intermolecular (*top*) and intramolecular (*bottom*) cyclopropanation reactions
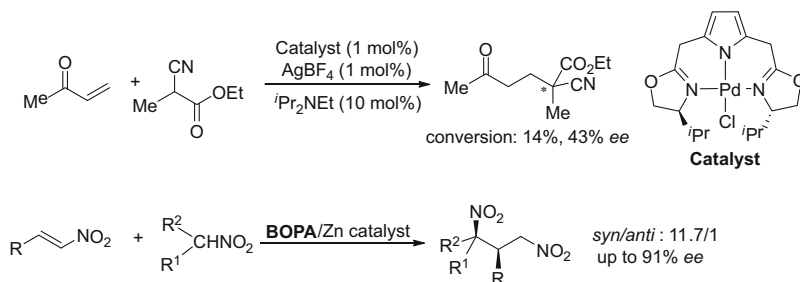
Scheme 23 2,5-Bis(2-oxazolinylmethyl)pyrroles and BOPA ligands in Michael addition reactions

albeit with only moderate *ee* values of 43% (Scheme 23) [22]. Zn-catalyzed Michael additions have also been reported using BOPA ligands which show much higher enantioselectivities (up to 95%) for the addition of nitroalkanes to a range of nitroalkenes (in which the alkene is conjugated to the nitro group in an analogous fashion to the conjugation of an alkene to a ketone) to give 1,3-dinitroalkanes (Scheme 23). These reactions were also found to be highly diastereoselective [105].
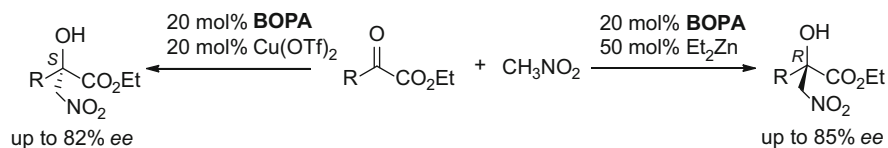
Scheme 24   Copper and zinc BOPA complexes in asymmetric Henry reactions

4.9   Henry Reactions

The nitro-aldol or Henry reaction between a nitroalkane and a carbonyl compound is an efficient route to synthetically useful β-nitro alcohols (e.g., see [106–111]). The BOPA and isoelectronic bis(thiazoline) ligands were used in Henry reactions with the Lewis acidic metals zinc(II) and copper(II) (Scheme 24). Both ligand and metal combinations resulted in the enantioselective formation of β-nitro alcohols (in up to 85% *ee*); however, the absolute configuration of the product formed was dependent upon the metal used. Thus, the copper system resulted in the *S*-enantiomer, whereas Zn afforded the *R*-enantiomer [112].

4.10   Hydrodehalogenation Reactions

The amido bis(amine) ligand $^{Me}N_2N$ complexes of nickel have been employed in the catalytic hydrodehalogenation of alkyl halides using catalytic amounts of $[(^{Me}N_2N)Ni-Cl]$ and either Ph_2SiH_2 or $Me(EtO)_2SiH$ as a silane source in the presence of a base [113]. The yields of the reactions were dependent upon the halides used and correlated with the C–X bond strength. Thus, reactions with alkyl chlorides gave the highest yields, while alkyl iodides gave the lowest yields. In the mechanism, the Ni–Cl complex is converted into the corresponding Ni–OR complex by reaction with the base RONa. This can then react with silane to form the Ni–H complex that catalyzes the hydrodehalogenation of alkyl halides (Scheme 25).

The mechanism of hydrodehalogenation is thought to take place by a radical process which is supported by the enantioselective PyrrMeBOX–Ni(II) hydride hydrodehalogenation. PyrrMeBOX ligand systems are known to undergo an isomerization rearrangement to afford stable planar $10\pi e$-conjugated systems. This isomer of PyrrMeBOX has been observed in PyrrMeBOX–Ni(II) hydride complexes which has been observed to reversibly eliminate H_2 to give PyrrMeBOX–Ni (I) species (Fig. 5) [114].

The Ni(II) complexes were found to be active in the hydrodehalogenations of geminal dihalogenides in an enantioselective fashion giving the product in up to 84% yield and 74% *ee* [114]. The mechanism for the reaction is shown in Scheme 26 and progresses through halogen abstraction from the substrate by the Ni^I complex to generate radical **I** and the Ni^{II} complex LigNiX (**II**). Reduction of **II** affords LigNiH (**III**) which then undergoes H abstraction by the reactive radical **I** to regenerate the active Ni^I complex [114].
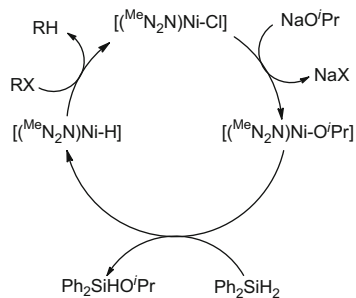
Scheme 25 Hydrodehalogenation of alkyl halides using [($^{Me}N_2N$)Ni-Cl]
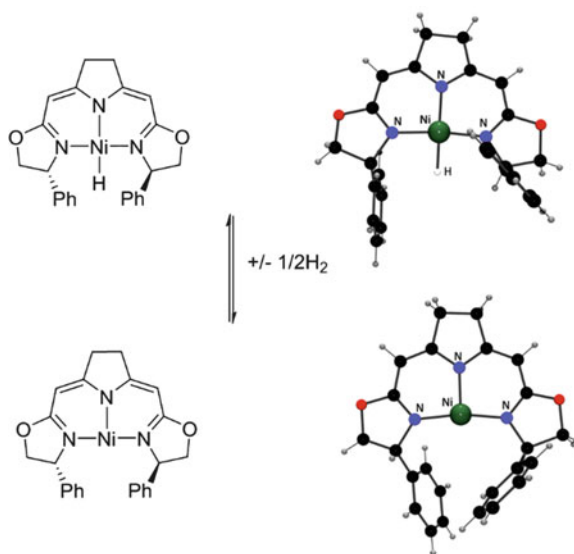
Fig. 5 Reversible addition/removal of H_2 between PyrrMeBOX-Ni(II)-H and PyrrMeBOX-Ni(I)
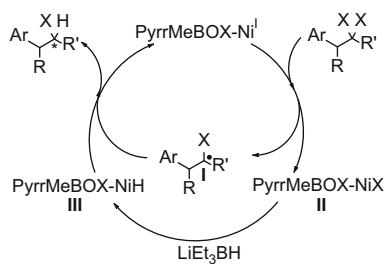
Scheme 26 Hydrodehalogenation reactions using Ni(I)
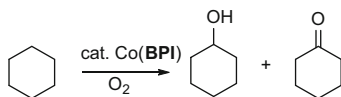
Scheme 27 Oxidation of cyclohexane using Co(BPI) complexes
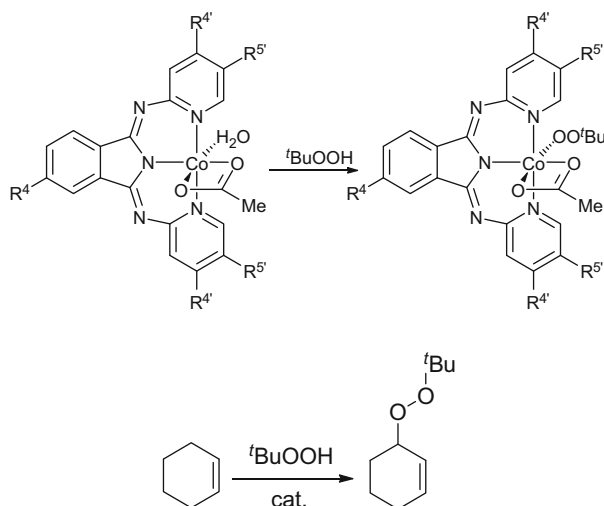
Scheme 28 [Co^{II}(BPI)(OAc)(H$_2$O)] and [Co^{III}(BPI)(OAc)(OO^{t}Bu)] complexes (*top*) tested in the allylic peroxylation of cyclohexene (*bottom*)

4.11 Oxidation Reactions

The industrial-scale catalytic oxidation of cyclohexane to cyclohexanol and cyclo-hexanone using cobalt(II)–BPI complexes (Scheme 27) was reported over 30 years ago [115]. Subsequent studies found the best catalyst with the highest activity and lifetime to be [Co(BPI)(OAc)] [116]. This catalyst was also found to be active in the hydroxylation of alkanes and alkenes [117].

The allylic peroxylation of olefins with *tert*-butyl hydroperoxide has been tested with several [Co^{II}(BPI)(OAc)] and Co^{III} *tert*-butylperoxy complexes (Scheme 28). The reactions were found to give a mixture of oxidized products: cyclohex-2-ene-1-*tert*-butylperoxide, cyclohex-2-en-1-one, cyclohex-2-en-1-ol, and epoxycyclohexane [118]. Improved selectivity was observed; however, if the temperature of the reaction was controlled and a 70% aqueous solution of ^{t}BuOOH was used, cyclohex-2-ene-1-*tert*-butylperoxide was formed selectively (Scheme 28). Copper–BPI complexes were also employed in this reaction although they were found to be less selective and active.

Copper catecholato and carboxylato complexes of the BPI ligands have been studied as mimics for enzyme active sites [119–121]. Catalytic reaction of copper–BPI complex [122] (Fig. 6) [Cu^{II}(BPI)(fla)] (flaH=flavonol) with oxygen afforded
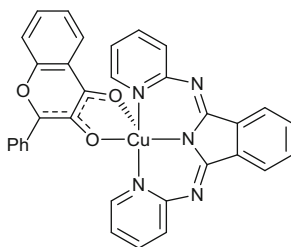
Fig. 6 [Cu^{II}(BPI)(fla)] complex as a model system for enzymes in flavonoid oxidation
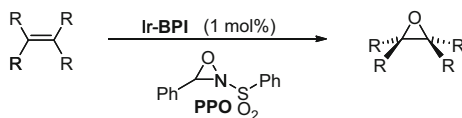
Scheme 29 Epoxidation of olefins using Ir–BPI catalysts
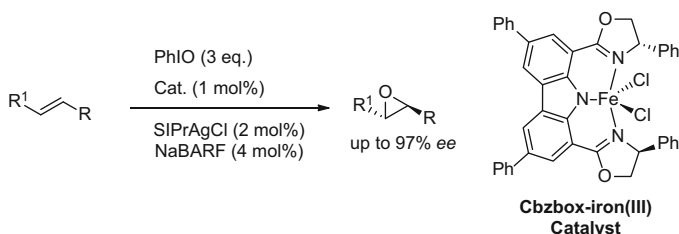
Scheme 30 Nonheme iron-catalyzed epoxidation reactions

benzoylsalicylic acid and its hydrolysate [121]. Dioxygenase models based upon Fe (BPI) have also been explored [123].

While iridium complexes are less well known in oxidation catalysis, iridium–BPI complexes were employed in the epoxidation of olefins using various oxidizing agents, the best being PPO (PPO=3-phenyl-2-(phenylsulfonyl)-1,2-oxaziridine) (Scheme 29) [53].

Asymmetric oxidation reactions have also been reported with other pincer ligands. Cbzbox–iron(III) complexes were found to have porphyrin-like properties in the asymmetric epoxidation of (*E*)-alkenes affording the epoxides catalytically in high enantioselectivities up to 97% *ee* (Scheme 30) [124]. The reaction occurs through a $2e^-$ oxidation process with the ligand undergoing a $1e^-$ oxidation and the cationic iron(III) complex undergoing a $1e^-$ oxidation to give an iron(IV) cation radical [124].

4.12 Reduction Chemistry

In addition to catalytic oxidations, reduction of alkenes is also possible using NNN pincer complexes. For example, (BPI)Pd^{II}–Cl complexes fixed to carbosilane or
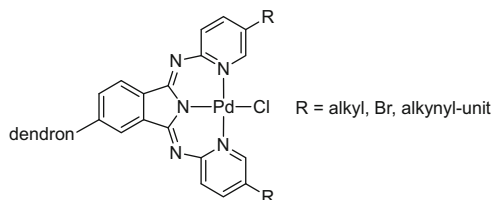
Fig. 7 Dendrimer-linked (BPI)Pd^{II}–Cl complexes

polyether dendrimers were highly active in the hydrogenation of alkenes such as styrene and had the advantage of being recycled without reduction in the catalytic activity (Fig. 7) [125–127].

4.13 Hydroamination Reactions

Emerging applications of tridentate NNN pincer ligands in catalysis are in the field of non-transition metal complexes for applications in enantioselective catalysis. For example, Ward prepared calcium [128] and lanthanide complexes [129, 130] of BOPA ligands. The presence of the extra N-donor between the oxazoline groups appears to favor the formation of selective and active catalysts [131]. Structure determination of [Ln(BOPA){N(SiMe$_3$)$_2$}$_2$] (Ln=Nd, Sm) by X-ray diffraction revealed that the two complexes were isomorphous, both being 5-coordinate with distorted trigonal bipyramidal geometries (Fig. 8). The silylamide ligands and the central nitrogen atom of the ligand adopt the equatorial positions in the coordination sphere, while the oxazoline nitrogen atoms lie in the axial positions. The BOPA ligand, however, deviates from planarity with the phenyl groups within the ligand framework being twisted relative to one another. This has given rise to two different diastereoisomers by virtue of the helical chirality (from the twisting of the diphenylamido backbone of the ligand) and the chirality on the oxazoline rings.

The Ca^{2+} complexes of BOPA have been employed in the catalytic intramolecular hydroamination of aminoalkenes containing geminal phenyl groups to generate the corresponding product with up to 50% *ee*, respectively (Scheme 31). Although the enantioselectivities are lower than those reported for typical transition metal catalysts, this is a significant advancement in enantioselective calcium catalysis that usually results in poor enantioselectivities due to redistributions of ligands. Lanthanide BOPA complexes (Ln=Y, La, Pr, Nd, Sm) were also employed in the intramolecular hydroamination of aminoalkenes containing geminal phenyl or methyl groups [129, 130].
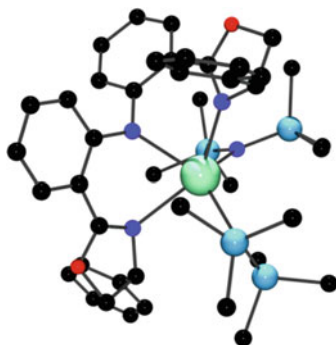
Fig. 8 Crystal structure of Sm(BOPA){N(SiMe$_3$)$_2$}$_2$
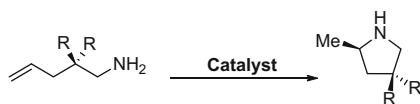
Scheme 31 Catalytic intramolecular hydroamination of aminoalkenes using calcium and lanthanide BOPA complexes

5 Conclusions

Various classes of NNN pincer ligands have been developed and have been used as tridentate ligands for a range of transition metals, group 2 metals, and lanthanides. Many of these complexes have been isolated and structurally characterized. In the case when these ligands contain two chiral wingtips (e.g., oxazoline or modified pyridine rings), chiral (usually C_2-symmetric) environments at the metal center result. Such chiral pincer complexes have been successfully employed in a variety of (stereo)selective organic transformations.

References

1. van Koten G (1989) Pure Appl Chem 61:1681
2. Peris E, Crabtree RH (2004) Coord Chem Rev 248:2239
3. Morales-Morales D, Jensen CGM (2007) The chemistry of pincer compounds. Elsevier, Amsterdam
4. Chase PA, van Koten G (2010) The pincer ligand: its chemistry and applications (Catalytic Science), 1st edn. Imperial College Press, London
5. van Koten G, Milstein D (eds.) (2013) Top Organomet Chem 40
6. Rasappan R, Laventine D, Reiser O (2008) Coord Chem Rev 252:702

7. Desimoni G, Faita G, Quadrelli P (2003) Chem Rev 103:3119
8. Desimoni G, Faita G, Jørgensen KA (2006) Chem Rev 106:3561
9. Evans DA, Miller SJ, Lectka T, von Matt P (1999) J Am Chem Soc 121:7559
10. Thorhauge J, Roberson M, Hazell RG, Jørgensen KA (2002) Chem Eur J 8:1888
11. Inoue M, Suzuki T, Nakada M (2003) J Am Chem Soc 125:1140
12. Suzuki T, Kinoshita A, Kawada H, Nakada M (2003) Synlett 2003:570
13. Inoue M, Nakada M (2007) Heterocycles 72:133
14. Durán-Galván M, Worlikar SA, Connell BT (2010) Tetrahedron 66:7707
15. Britovsek GJP, Gibson VC, Hoarau OD, Spitzmesser SK, White AJP, Williams DJ (2003) Inorg Chem 42:3454
16. Gibson VC, Spitzmesser SK, White AJP, Williams DJ (2003) Dalton Trans 2003:2718
17. Barbe J-M, Habermeyer B, Khoury T, Gros CP, Richard P, Chen P, Kadish KM (2010) Three-metal coordination by novel bisporphyrin architectures. Inorg Chem 49:8929–8940
18. Mudadu MS, Singh AN, Thummel RP (2008) J Org Chem 73:6513
19. Johnson KRD, Hayes PG (2009) Organometallics 28:6352
20. Wang L, Cui D, Hou Z, Li W, Li Y (2011) Organometallics 30:760
21. Johnson KRD, Kamenz BL, Hayes PG (2014) Organometallics 33:3005
22. Mazet C, Gade LH (2003) Chem Eur J 9:1759
23. Konrad F, Lloret Fillol J, Wadepohl H, Gade LH (2009) Inorg Chem 48:8523
24. Ghorai D, Kumar S, Mani G (2012) Dalton Trans 41:9503
25. McManus HA, Guiry PJ (2002) J Org Chem 67:8566
26. Lu S-F, Du D-M, Zhang S-W, Xu J (2004) Tetrahedron Asymmetry 15:3433
27. Peters JC, Harkins SB, Brown SD, Day MW (2001) Inorg Chem 40:5083
28. Csok Z, Vechorkin O, Harkins SB, Scopelliti R, Hu X (2008) J Am Chem Soc 130:8156
29. Wanniarachchi S, Liddle BJ, Toussainta J, Lindeman SV, Bennett B, Gardinier JR (2010) Dalton Trans 39:3167
30. Elvidge JA, Linstead RP (1952) J Chem Soc 5000
31. Elvidge JA, Linstead RP (1952) J Chem Soc 1952:5008
32. Clark PF, Elvidge JA, Linstead PR (1953) J Chem Soc 1953:3593
33. Sauer DC, Melen RL, Kruck M, Gade LH (2014) Eur J Inorg Chem 2014:4715
34. Siegl WO (1974) Inorg Nucl Chem Lett 10:825
35. Siegl WO (1977) J Org Chem 42:1872
36. Meder MB, Gade LH (2004) Eur J Inorg Chem 2004:2716
37. Langlotz BK, Wadepohl H, Gade LH (2008) Angew Chem Int Ed 47:4670
38. Sauer DC, Wadepohl H, Gade LH (2012) Inorg Chem 51:12948
39. Deng Q-H, Wadepohl H, Gade LH (2001) Chem Eur J 17:14922
40. Robinson MA, Trotz SI, Hurley TJ (1967) Inorg Chem 6:392
41. Beattie JK (1988) Adv Inorg Chem 132:1
42. Letcher RJ, Zhang W, Bensimon C, Crutchley RJ (1993) Inorg Chim Acta 210:183
43. Kruck M, Sauer DC, Enders M, Wadepohl H, Gade LH (2011) Dalton Trans 40:10406
44. Kruck M, Wadepohl H, Enders M, Gade LH (2013) Chem Eur J 19:1599
45. Sauer DC, Kruck M, Wadepohl H, Enders M, Gade LH (2013) Organometallics 32:885
46. Deng Q-H, Wadepohl H, Gade LH (2012) J Am Chem Soc 134:2946
47. Puzas JP, Nakon R, Pertersen JL (1986) Inorg Chem 25:3837
48. Maiti D, Paul H, Chanda N, Chakraborty S, Mondal B, Puranik VG, Lahiri GK (2004) Polyhedron 23:831
49. Fout AR, Basuli F, Fan H, Tomaszewski J, Huffman JC, Baik M-H, Mindiola DJ (2005) Angew Chem Int Ed 45:3291
50. Harkins SB, Peters JC (2006) Inorg Chem 45:4316
51. Betley TA, Qian BA, Peters JC (2008) Inorg Chem 47:11570
52. Wen H-M, Wang J-Y, Li B, Zhang L-Y, Chen C-N, Chen Z-N (2013) Eur J Inorg Chem 2013:4789
53. Camerano JA, Sämann C, Wadepohl H, Gade LH (2011) Organometallics 30:379

54. Vechorkin O, Hu X (2009) Angew Chem Int Ed 48:2937
55. Vechorkin O, Proust V, Hu X (2009) J Am Chem Soc 131:9756
56. Vechorkin O, Barmaz D, Proust V, Hu X (2009) J Am Chem Soc 131:12078
57. Vechorkin O, Proust V, Hu X (2010) Angew Chem Int Ed 49:3061
58. Hu X (2011) Chem Sci 2:1867
59. Vechorkin O, Godinat A, Scopelliti R, Hu X (2011) Angew Chem Int Ed 50:11777
60. Vechorkin O, Csok Z, Scopelliti R, Hu XL (2009) Chem Eur J 15:3889
61. Breitenfeld J, Vechorkin O, Corminboeuf C, Scopelliti R, Hu XL (2010) Organometallics 29:3686
62. Breitenfeld J, Ruiz J, Wodrich MD, Hu X (2013) J Am Chem Soc 135:12004
63. Breitenfeld J, Wodrich MD, Hu X (2014) Organometallics 33:5708
64. Di Franco T, Boutin N, Hu X (2013) Synthesis 45:2949
65. Fürstner A (1999) Chem Rev 99:991
66. Wessjohann LA, Scheid G (1999) Synthesis 1999:1
67. Avalos M, Babiano R, Cintas P, Jiménez JL, Palacios JC (1999) Chem Soc Rev 28:169
68. Okude Y, Hirano S, Hiyama T, Nozaki H (1977) J Am Chem Soc 99:3179
69. Okude Y, Hiyama T, Nozaki H (1977) Tetrahedron Lett 18:3829
70. Fürstner A, Shi N (1996) J Am Chem Soc 118:12349
71. McManus HA, Cozzi PG, Guiry PJ (2006) Adv Synth Catal 348:551
72. Hargaden GC, McManus HA, Giorgio Cozzi P, Guiry PJ (2007) Org Biomol Chem 5:763
73. Inoue M, Nakada M (2007) J Am Chem Soc 129:4164
74. Inoue M, Nakada M (2004) Org Lett 6:2977
75. Inoue M, Nakada M (2006) Angew Chem Int Ed 45:252
76. Durán-Galván M, Connell BT (2010) Eur J Org Chem 2010:2445
77. Coeffard V, Aylward M, Guiry PJ (2009) Angew Chem Int Ed 48:9152
78. Olah GA, Khrisnamurti R, Prakash GKS (1991) In: Trost BM, Fleming I (eds) Comprehensive organic synthesis, vol 3. 1st edn. Pergamon, Oxford, p 293
79. Roberts RM, Khalaf AA (1984) Friedel–Crafts alkylation chemistry. A century of discovery. Marcel Dekker, New York
80. Herrera RP, Sgarzani V, Bernardi L, Ricci A (2005) Angew Chem Int Ed 44:6576
81. Zhuang W, Hazell RG, Jørgensen KA (2005) Org Biomol Chem 3:2566
82. Jia Y-X, Zhu S-F, Yang Y, Zhou Q-L (2006) J Org Chem 71:75
83. Lu S-F, Du D-M, Xu, J (2006) Org Lett 8:2115
84. Liu H, Xu J, Du D-M (2007) Org Lett 9:4725
85. Liu H, Lu S-F, Xu J, Du D-M (2008) Chem Asian J 3:1111
86. Peng J, Du D-M (2012) Eur J Org Chem 2012:4042
87. Jia Y, Yang W, Du D-M (2012) Org Biomol Chem 10:4739
88. Li C, Liu F-L, Zou Y-Q Lu L-Q, Chen J-R, Xiao W-J (2013) Synthesis 45:601
89. Kassube JK, Gade LH (2006) Top Organomet Chem 20:61
90. Liu H, Du D-M (2010) Eur J Org Chem 2010:2121
91. Purser S, Moore PR, Swallow S, Gouverneur V (2008) Chem Soc Rev 37:320
92. Tressaud A (ed) (2006) Fluorine and the environment – agrochemicals, archaeology, green chemistry & water. Adv Fluorine Sci 2
93. Leo A, Hansch C, Elkins D (1971) Chem Rev 71:525
94. Yagupolskii LM, Ilchenko AY, Kondratenko NV (1974) Russ Chem Rev 43:32
95. Filler R, Kobayashi Y (1982) Biomedical aspects of fluorine chemistry. Elsevier, Amsterdam
96. Gribkoff VK, Starrett JE, Dworetzky SI, Hewawasam P, Boissard CG, Cook DA, Frantz SW, Heman K, Hibbard JR, Huston K, Johnson G, Krishnan BS, Kinney GG, Lombardo LA, Meanwell NA, Molinoff PB, Myers RA, Moon SL, Ortiz A, Pajor L, Pieschl RL, Post-Munson DJ, Signor LJ, Srinivas N, Taber MT, Thalody G, Trojnacki JT, Wiener H, Yeleswaram K, Yeola SW (2001) Nature Med 7:471
97. Hewawasam P, Gribkoff VK, Pendri Y, Dworetzky SI, Meanwell NA, Martinez E, Boissard CG, Post-Munson DJ, Trojnacki JT, Yeleswaram K, Pajor LM, Knipe J, Gao Q, Perrone R, Starrett JE (2002) Bioorg Med Chem Lett 12:1023
98. Deng Q-H, Wadepohl H, Gade LH (2012) J Am Chem Soc 134:10769

99. Deng Q-H, Rettenmeier C, Wadepohl H, Gade LH (2014) Chem Eur J 20:93
100. Deng Q-H, Bleith T, Wadepohl H, Gade LH (2013) J Am Chem Soc 135:5356
101. Tan F, Xiao C, Cheng H-G, Wu W, Ding K-R, Xiao W-J (2012) Chem Asian J 7:493
102. Inagaki T, Ito A, Ito J-I, Nishiyama H (2010) Angew Chem Int Ed 49:9384
103. Nishiyama H, Furuta A (2007) Chem Commun 2007:760
104. Inagaki T, Phong LT, Furuta A, Ito J-i, Nishiyama H (2010) Chem Eur J 16:3090
105. Lu S-F, Du D-M, Xu J, Zhang S-W (2006) J Am Chem Soc 128:7418
106. Rosini G (1991) In: Trost BM, Heathcock CH (eds) Comprehensive organic synthesis, vol. 2. Pergamon, Oxford, pp 321–340
107. Ono N (2001) The nitro group in organic synthesis. Wiley-VCH, New York, Chap 3, pp 30–69
108. Shibasaki M, Gröger H (1999) In: Jacobsen EN, Pfaltz A, Yamamoto H (eds) Comprehensive asymmetric catalysis. Springer-Verlag, Berlin, Heidelberg, Ch. 29.3
109. Shibasaki M, Sasai H, Arai T (1997) Angew Chem Int Ed 36:1236
110. Luzzio FA (2001) Tetrahedron 57:915
111. Westermann B (2003) Angew Chem Int Ed 42:151
112. Du D-M, Lu S-F, Fang T, Xu J (2005) J Org Chem 70:3712
113. Breitenfeld J, Scopelliti R, Hu X (2012) Organometallics 31:2128
114. Rettenmeier C, Wadepohl H, Gade LH (2014) Chem Eur J 20:9657
115. Druliner JD, Ittel SD, Krusic PJ, Tolman CA (1982) Process for producing a mixture containing cyclohexanol and cyclohexanone from cyclohexane. US Patent 4 326 084
116. Tolman CA, Druliner JD, Krusic PJ, Nappa MJ, Seidel WC, Williams ID, Ittel SD (1988) J Mol Catal 48:129
117. Saussine L, Brazi E, Robine A, Mimoun H, Fischer J, Weiss R (1985) J Am Chem Soc 107:3534
118. Meder MB, Siggelkow BA, Gade LH (2004) Z Anorg Allg Chem 630:1962
119. Kaizer J, Pap J, Speier G, Párkányi L (2004) Z Kristallogr NCS 219:141
120. Csay T, Kripli B, Giorgi M, Kaizer J, Speier G (2010) Inorg Chem Commun 254:781
121. Kaizer J, Pap J, Speier G, Réglier M, Giorgi M (2004) Trans Met Chem 29:630
122. Balogh-Hergovich É, Kaizer J, Speier G, Huttner G, Jacobi A (2000) Inorg Chem 39:4224
123. Váradi T, Pap JS, Giorgi M, Párkányi L, Csay T, Speier G, Kaizer J (2013) Inorg Chem 52:1559
124. Niwa T, Nakada M (2012) J Am Chem Soc 134:13538
125. Siggelkow B, Meder MB, Galka CH, Gade LH (2004) Eur J Inorg Chem 2004:3424
126. Meder MB, Haller I, Gade LH (2005) Dalton Trans 2005:1403
127. Siggelkow BA, Gade LH (2005) Z Anorg Allg Chem 631:2575
128. Nixon TD, Ward BD (2012) Chem Commun 48:11790
129. Bennett SD, Pope SJA, Ward BD (2013) Chem Commun 49:6072
130. Bennett SD, Core BA, Blake MP, Pope SJA, Mountford P, Ward BD (2014) Dalton Trans 43:5871
131. Sanchez-Blanco AI, Gothelf KV, Jørgensen KA (1997) Tetrahedron Lett 38:7923

Pincer Complexes with Thione Sulfur Donors

Diana V. Aleksanyan and Vladimir A. Kozlov

Abstract Rapid development of pincer chemistry over the last several decades made a substantial contribution in extension of theoretical and practical organometallic chemistry as well as organic synthesis, catalysis, and materials science. This review is devoted to relatively new types of nonclassical pincer compounds bearing thione sulfur donors incorporated into thiophosphoryl and/or thioamide groups. The discussion is focused on synthetic aspects and structural features of symmetrical and hybrid *S,C,S*-pincer ligands and complexes with particular attention to the practically valuable properties.

Keywords Catalysis · Cyclometallation · Luminescence · Organothiophosphorus compounds · Pincer complexes · Sulfur donors · Thioamides

Contents

D.V. Aleksanyan (✉) and V.A. Kozlov
A. N. Nesmeyanov Institute of Organoelement Compounds, Russian Academy of Sciences, ul. Vavilova 28, Moscow 119991, Russia
e-mail: aleksanyan.diana@ineos.ac.ru

1 Introduction

Progress in coordination and organometallic chemistry is often connected with the creation of tailor-made ligands allowing for fine-tuning of electronic and steric properties of a whole system. In this respect, of particular interest are the so-called pincer complexes having a specific tridentate framework that offers multiple options for directed structural modifications and rigid control of the properties of a metal center. Since the pioneering work of B. Shaw in 1976 [1], pincer complexes have emerged as a privileged class of organometallic compounds, finding extensive use in organic synthesis, catalysis, materials science, and so on. A series of excellent reviews [2–12] and two recently published special treatises [13, 14] cover synthetic aspects, structural features, as well as different applications of pincer complexes, showing rapid development of this area of organometallic chemistry.

   For a long period of time, the most popular types of pincer ligands were bis(phosphine), bis(thioether), and bis(amine) derivatives with the benzene core and methylene units connecting donor groups with the central aromatic ring. However, over the years, a classical structure of a pincer ligand has been significantly modified, and different groups, including phosphinite, imine, thioamide, etc., as well as heterocyclic fragments, were successfully introduced as coordinating arms into a pincer framework, extending the boundaries of pincer chemistry. While phosphorus- and nitrogen-donor systems have been extensively reviewed [4, 15–28], their sulfur-containing analogs of S,E,S-types (E=C, N, P) received markedly less attention. However, the main achievements in the field of thioether-based sulfur-donor systems have been summarized by P. Le Floch and N. Mézailles [29]. Taking this into account, the present chapter will focus on the chemistry of nonclassical pincer complexes with thione sulfur donors based on bis(thioamides), bis(phosphinosulfides), and related organothiophosphorus compounds[1] as well as hybrid derivatives having at least one thione sulfur-donor group, where the central unit is a metallated or nonmetallated (hetero)aromatic ring. Representing relatively new types of pincer compounds, these soft-donor derivatives often feature air- and moisture-resistance, which essentially simplifies their production, isolation, and handling in contrast to widely recognized P,C,P-counterparts. Furthermore, S,E,S-pincer complexes with thione sulfur donors, as will be shown below, exhibit interesting chemical and physical properties which make them attractive research objects.

---

[1] Due to peculiar structure and coordination chemistry, bis(diphenylphosphinosulfide)methane derivatives seem to represent a subject for separate discussion and are beyond the scope of the current review.

2 Bis(thioamide) Pincer Compounds

One of the main classes of pincer compounds with thione sulfur donors is the bis(thioamide) derivatives. Introduction of readily tunable and strongly coordinating thioamide groups into a pincer framework opened the way to several series of neutral, mono-, and dianionic ligands which complexes display prominent photo- and electroluminescence properties as well as unique reactivity and high catalytic activity in cross-coupling reactions.

In 1995, M. Nonoyama et al. reported the first example of bis(thioamide) pincer ligand, namely, $N,N,N'N'$-tetramethyl thioamide of isophthalic acid **1** and its S,C,S-palladium(II) complex **2** (Scheme 1) [30]. At that time, the fundamental aspects of direct cyclometallation of sulfur-donor ligands were poorly explored compared to their nitrogen- and phosphorus-containing analogs. Investigating the factors directing the site of cyclopalladation in (hetero)aromatic carbothioamides, the authors showed that the presence of two C=S donor groups in 1,3-positions of the benzene ring facilitates the metallation at the C2-carbon atom owing to the formation of two stable fused five-membered metallacycles. Therewith, direct cyclopalladation of **1** can be readily performed either under action of in situ generated Li_2PdCl_4 in a CH_2Cl_2/MeOH mixture or $PdCl_2$ in hot DMSO. In turn, ligand **1** was obtained in comparable yields both by thionation of a bis(amide) predecessor with the Lawesson reagent [31] and by the modified Willgerodt–Kindler reaction of isophthalaldehyde and dimethylamine hydrochloride in the presence of elemental sulfur and NaOAc [32] (Scheme 1). Subsequently, the mentioned synthetic routes became two general approaches to bis(thioamide) pincer ligands.

The chloride ion in complex **2** can be readily substituted for iodide, isothiocyanate, and N,N-diethyldithiocarbamate ion (complexes **3–5**) as well as for tri-n-butylphosphine and 4-$tert$-butylpyridine (cationic derivatives **6** and **7**), in all cases leaving S,C,S-tridentate monoanionic coordination mode of the ligand intact (Scheme 2) [30].

Direct cyclopalladation of thioamide-based pincer ligands proceeded smoothly also in the case of ligands **8a–c** bearing sterically hindered pyrrolidine, piperidine, and morpholine units, leading to complexes **9a–c** in high yields (Scheme 3) [33, 34].
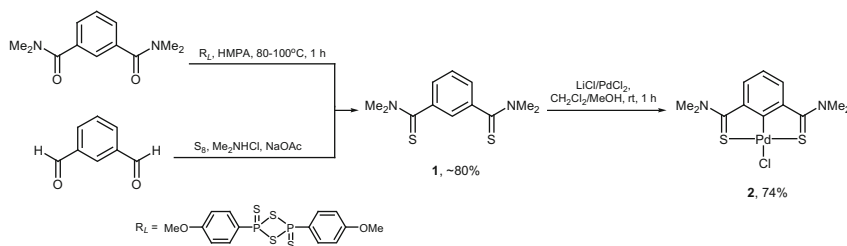
Scheme 1 Synthesis of $N,N,N'N'$-tetramethylisophthalthioamide and its pincer Pd(II) complex
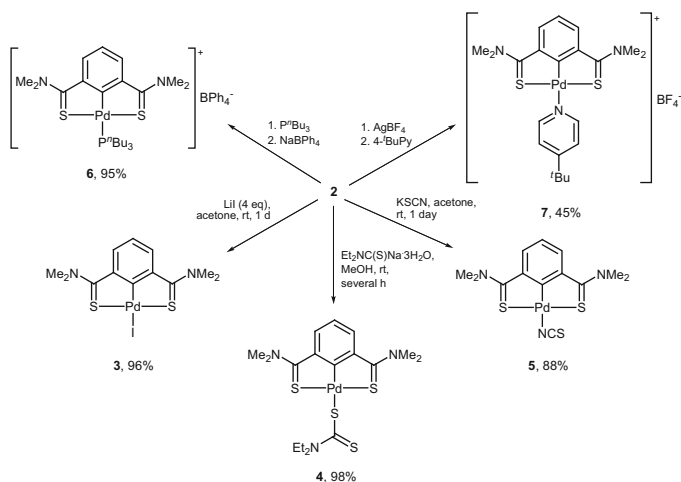
Scheme 2 Neutral and cationic pincer complexes obtained by substitution of the chloro ligand of palladacycle **2**
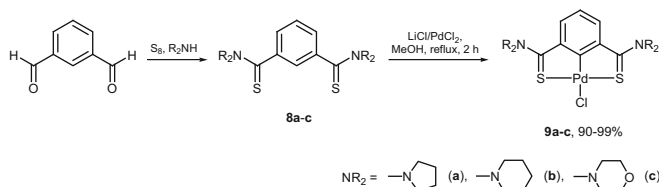
Scheme 3 *S,C,S*-pincer compounds with sterically hindered substituents at the thioamide coordinating arms

Besides the fundamental aspects of formation, *S,C,S*-pincer complexes based on bis(thioamide) derivatives provoked considerable interest owing to their remarkable photophysical properties [35, 36]. Thus, palladium(II) complexes **2** and **9b,c** with tertiary thioamide donor groups were shown to exhibit strong photoluminescence in the glassy frozen state with relatively long lifetimes indicative of phosphorescence (80–90 μs), which was assigned to emission from the ^{3}MLCT excited state [34]. More importantly, they were also light-emissive in the solid state at room temperature. At the same time, complex **10** bearing secondary thioamide units demonstrated only weak photoluminescence in the solid state ($\Phi_{em} < 0.001$) presumably having excimeric nature [37]. However, incorporation of **10** into hybrid films with poly(vinylpyrrolidone) matrix markedly enhanced its emission owing to hydrogen bonding interactions elucidated from the IR spectral and X-ray crystallographic data [37]. Furthermore, in order to evaluate the effect of molecular arrangement in crystals on the intensity of emission, several kinds of crystals of complex **10** were obtained from different solvents [38]. Taking into account the presence of secondary thioamide group that can be used as a hydrogen-bond donor, the solvents were chosen to be capable of serving as hydrogen-bond acceptors

(DMF, NMP, DMAc, and DMSO). Aggregation-induced emission (AIE) was detected only for densely packed crystals featuring hydrogen bonds between complex and solvent molecules [38].

10
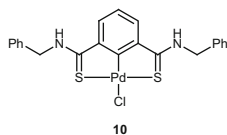
From the viewpoint of optical and electroluminescence applications, of special attention are various cyclometallated platinum derivatives [39]. A series of bis(thioamide) Pt(II) pincer complexes possessing valuable luminescence properties were reported by T. Kanbara et al. [40–43]. A platinum(II) counterpart of complex **9a** readily obtained by direct cyclometallation of **8a** with PtCl$_2$(PhCN)$_2$ (Scheme 4) exhibited strong photoluminescence in the glassy frozen state as well as in the solid state at room temperature [40]. Modification of **11** via replacement of the chloride ligand can either improve or impair luminescence properties of thioamide-based *S,C,S*-pincer complexes. For example, alkynyl derivative **12** along with platinacycle **11** was successfully used in fabrication of light-emitting diodes (LEDs), providing red (**12**) or reddish orange (**11**) electroluminescence, while their iodide analog **13** was not emissive at all.

Platinum(II) pincer complex **15** with secondary thioamide groups obtained by direct cyclometallation of ligand **14** under action of K$_2$PtCl$_4$ (Scheme 5) also exhibited intensive photoluminescence in the frozen matrix and in the solid state at room temperature [41]. Bis(thioamide) pincer ligand **14** can be obtained by treatment of the Grignard reagent of *m*-dibromotoluene with phenylisothiocyanate (Scheme 5). Furthermore, it can be readily converted into bis(benzothiazole) derivative **16** which affords light-emissive *N,C,N*-pincer complex **17** [41].

Unlike palladium complex **10**, related platinacycle **18** bearing benzyl-substituted secondary thioamide group was shown to be light-emissive also in solution at room temperature [42]. Generally, secondary thioamides can exist as amino-thione and
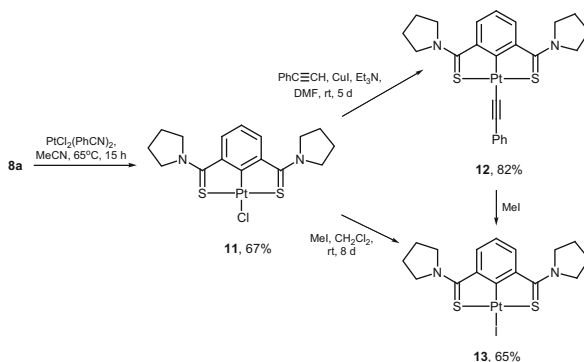
Scheme 4 Pincer platinum(II) complexes with tertiary thioamide units
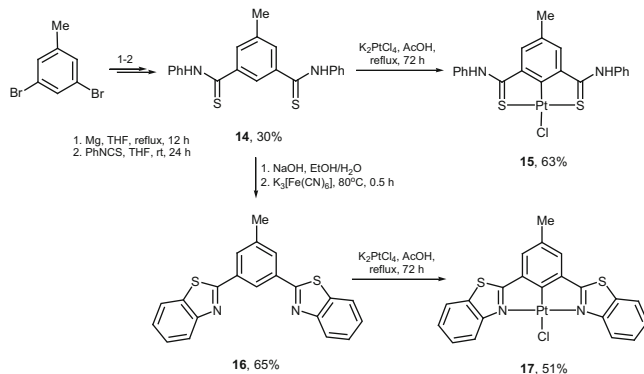
Scheme 5 *S,C,S*- and *N,C,N*-pincer Pt(II) complexes derived from ligand **14** with secondary thioamide donor groups
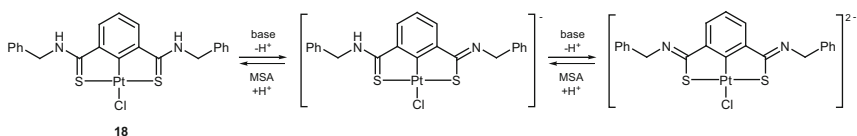
Scheme 6 Reversible deprotonation/protonation of Pt(II) pincer complex **18** with secondary thioamide units under action of chemical reagents
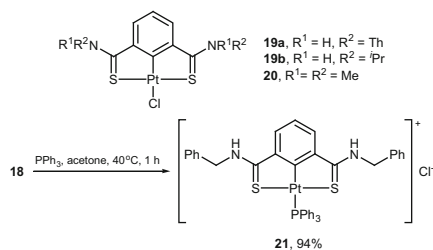
Scheme 7 Synthesis of cationic secondary thioamide-based pincer platinum(II) complex

imino-thiol tautomers. This important feature found reflection in the chemistry of *S,C,S*-thioamide-based pincer systems. Thus, NHC(S) fragments of **18** were used as reactive sites for modulation of the complex absorption and emission properties upon exposure to chemical stimuli [42]. Treatment of **18** with different bases (DBU, DBN, etc.) resulted in stepwise deprotonation of the coordinated pincer ligand, accompanied by quenching of luminescence, while addition of methanesulfonic acid (MSA) led to the recovery of the initial light-emissive complex (Scheme 6). Furthermore, owing to hydrogen bonding interactions, addition of different anions (as tetra-*n*-butylammonium or tetraphenylphosphonium salts) induced an enhancement in the emission intensity of **18** and related complexes **19a,b** with NHC(S) moiety, while no effect was observed for their tertiary thioamide counterpart **20**. For cationic platinum(II) complex **21** (Scheme 7), the AIE-activity was
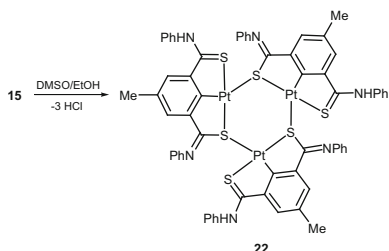
Scheme 8 Formation of a cluster from bis(thioamide) pincer Pt(II) complex **15**
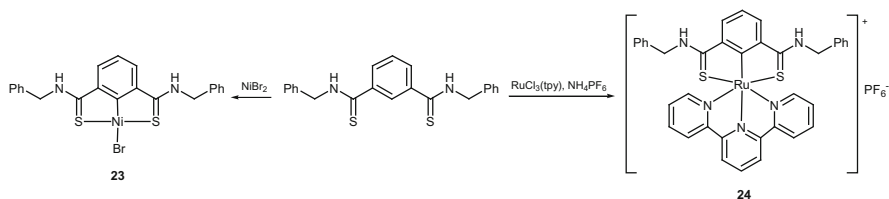
Scheme 9 Synthesis of Ni(II) and Ru(II) *S,C,S*-bis(thioamide) pincer complexes

observed upon addition of hexane into chloroform solution or water into methanol solution of the platinacycle, resulting in formation of nanosized aggregates [43]. The detected improvement of luminescence properties was again attributed to hydrogen bonding and interionic interactions characteristic for the system.

Thioamide coordinating arms of *S,C,S*-pincer Pt(II) complex in iminothiolate tautomeric form were also utilized as bridging ligands for the formation of trimetallic cluster **22** upon crystallization of complex **15** from a DMSO/EtOH mixture (Scheme 8) [44].

Investigation of electrochemical behavior of neutral nickel and cationic ruthenium pincer complexes **23** [45] and **24** [46] having secondary thioamide units (Scheme 9) revealed that their deprotonation with a base leads to reduction in the redox potentials compared to the initial complexes, which may be used in creation of novel catalytic systems. Introduction of different substituents at the peripheral phenyl and pyridine rings of ruthenium(II) complex **24** allowed for modulation of the second-order nonlinear optical properties of the resulting system [47]. Interestingly, Ni(II) [48] and Ru(II) [46] complexes with the pyrrole core (compounds **25a–c** and **26**, Scheme 10) featured lower electron donating ability of the monoanionic ligand than their benzene-centered counterparts **23** and **24**. Note that the first examples of *S,N,S*-pyrrole-based thioamide-containing pincer ligands and their transition metal complexes (M=Ni (**25a**), Pt (**27**), Pd (**28**)) were reported as early as 2006 [49]. Scheme 10 outlines general synthetic approaches to such derivatives.

An important field of application of bis(thioamide) pincer complexes appeared to be catalysis. Thus, palladium(II) complex **30** (Scheme 11) and its ditopic counterpart **32** (Scheme 12) readily available by cyclopalladation of the corresponding ligands with K_2PdCl_4 demonstrated high catalytic activity in the
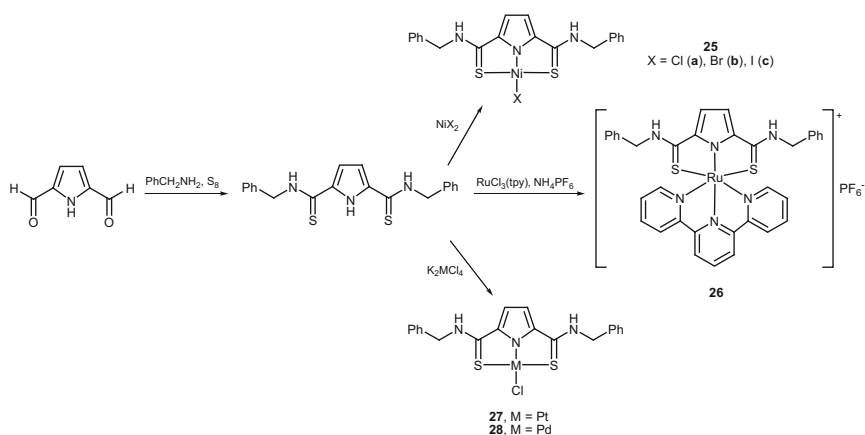
Scheme 10 Thioamide-based pincer compounds with the pyrrole central unit
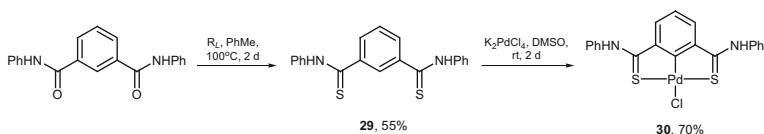
Scheme 11 Synthesis of S,C,S-bis(thioamide) palladacycle with phenyl substituents
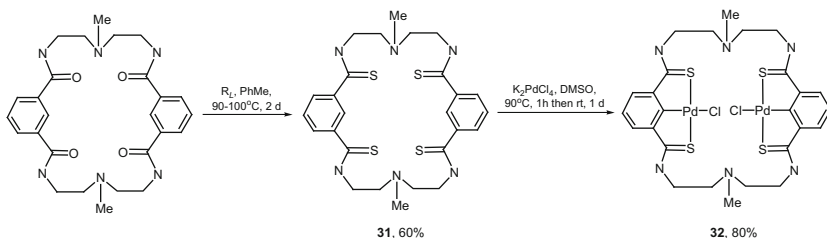
Scheme 12 Ditopic pincer compounds with thioamide donor groups

Heck reaction between iodotoluene and styrene at low catalyst loading, providing high turnover numbers in relatively short reaction times [50]. Ligands **29**, **31** were obtained by thionation of the corresponding amide precursors under action of the Lawesson reagent (Schemes 11 and 12). Note that complex **32** was the first example of transition metal complexes containing a thioamide-based macrocycle.

Substitution of the benzene core for pyridine ring afforded S,N,S-pincer ligands, lacking potential metallated CH-unit. However, the acidity of secondary thioamide groups leads to internal charge versatility of this system capable of loosing NH-protons in the absence of a base. Thus, treatment of thioamide-based ligand **33** with $ML_2(PhCN)_2$ led to unsymmetrical amino-thione/iminothiolate palladium(II)
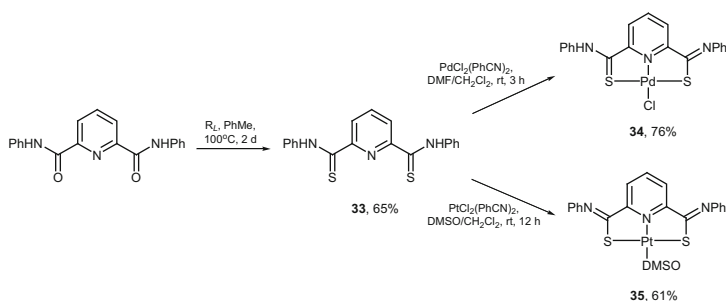
Scheme 13 Synthesis of *S,N,S*-pincer ligand with the pyridine core and its metal complexes
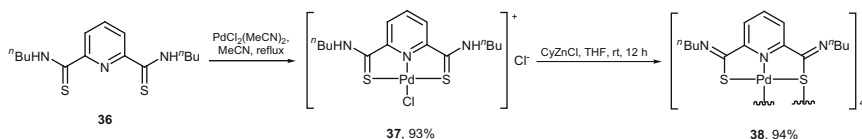
Scheme 14 Formation of polynuclear palladium(II) complex with the *S,N,S*-pincer scaffold

complex **34** and symmetrical bis(iminothiolate) platinum(II) counterpart **35**, resulting from spontaneous deprotonation of one and two NHC(S) moiety, respectively (Scheme 13) [51]. Complexes **34** and **35** were also tested as catalysts for the Heck reaction under conditions used for *S,C,S*-palladacycles **30**, **32** but provided low (**34**) or trace (**35**) amounts of the coupling product.

Interestingly, only slight changes in the nature of a ligand and metal precursor can affect the course of complexation. Thus, *n*-butyl-substituted analog of ligand **33** (compound **36**) afforded bis(thioamide) cationic complex **37** instead of a neutral mixed amino-thione/iminothiolate product [52]. Reaction of **37** with cyclohexylzinc chloride led to the formation of polynuclear bis(thioimide) species **38**. Both palladium complexes **37** and **38** demonstrated high catalytic activity in the Negishi cross-coupling of primary and secondary alkyl zinc reagents bearing the β-hydrogen atom. At the low catalyst loading (0.1–0.5 mol%), both catalysts promoted the reactions at room temperature or even at 0°C and provided high turnover numbers up to 6,100,000 [52]. Additional experiments showed that an active catalyst was an alkylated adduct generated from the catalyst precursor and basic metal reagents under reaction conditions (Scheme 14) [53].

Recently, thioimide pincer tetramer **38** was found to efficiently promote the cleavage of aryl-iodo bonds under mild conditions [54]. Stoichiometric reaction of **38** with thiourea **39** bearing ArI-fragment in THF solution at room temperature proceeded as dissociation of the initial cluster, resulting in complex **40** with *S*-coordinated thiourea and aryl-iodo moiety remaining intact. Subsequent heating of **40** in DME without any additive smoothly led to the formation of thiazole **41** and a precipitate which was proven to be iodo complex **42** (Scheme 15). This transformation was successfully accomplished in the catalytic version for a range of
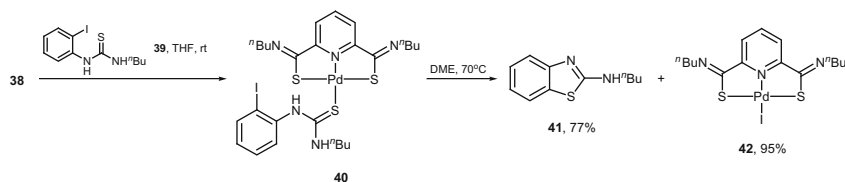
Scheme 15 Cleavage of the C(Ar)–I bond under action of thioimide pincer cluster **38**

$R^1 = H, R^2 = {}^nBu$ $R^1 = COOEt, R^2 = {}^nBu$
$R^1 = Me, R^2 = {}^nBu$ $R^1 = H, R^2 = Me$
$R^1 = Cl, R^2 = {}^nBu$ $R^1 = H, R^2 = CH_2CH=CH_2$
$R^1 = Br, R^2 = {}^nBu$
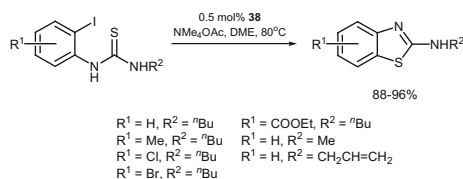
Scheme 16 Synthesis of benzothiazoles catalyzed by thioimide pincer cluster **38**
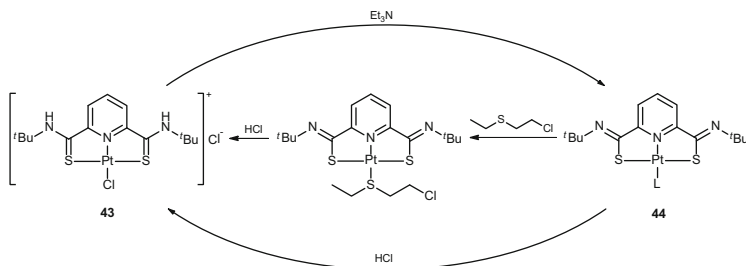
Scheme 17 Pincer-type platinacycle as a molecular switch for half sulfur mustard

thioureas bearing additional substituents in the aryl-iodo fragment using only 0.5 mol% of complex **38** (Scheme 16).

Utilizing a possibility of reversible transformation between bis(thioamide) and bis(iminothiolate) forms under slightly acidic and basic conditions, platinum(II) system with the secondary thioamide groups and pyridine central unit (compounds **43** and **44**, Scheme 17) was shown to reversibly bind and release the surrogate half sulfur mustard – 2-chloroethyl ethyl sulfide – serving as a molecular switch [55].

Dynamic behavior of *S,N,S*-pincer Ru(II) complex **45** upon successive deprotonation of the thioamide groups opened the way to novel mono- (**46**) and dinuclear (**47**) compounds (Scheme 18) [56]. The authors noticed that the change in coordination mode of the ligand from neutral to mono- and dianionic strongly affects the electron density at the metal center.

Recently, T. Kanbara et al. synthesized and characterized *S,C,S*-platinum(II) and palladium(II) bis(thioamide) pincer complexes with the azulene central unit, featuring interesting structural and optical properties (Scheme 19) [57]. The azulene core affects the electron density of the thioamide moiety in complexes **49**, **50** in such a way that the MLCT band in the UV/vis spectra appeared at the longer wavelengths compared to its counterparts with the benzene and pyrrole core.
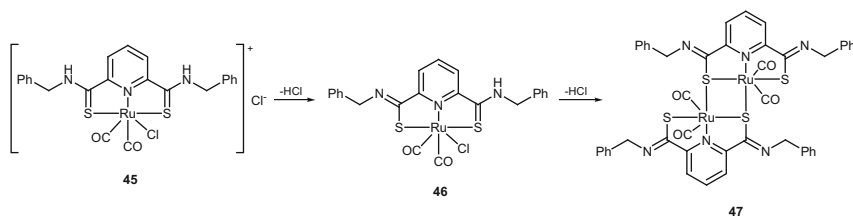
Scheme 18 Deprotonation-induced reactivity of *S,N,S*-pincer ruthenium complexes
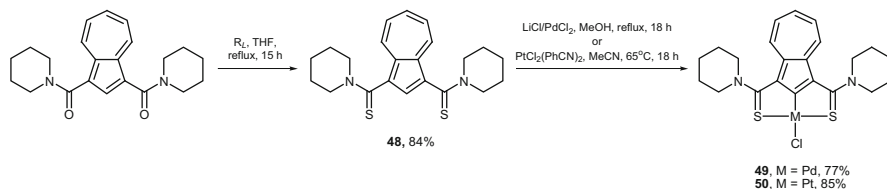
Scheme 19 Bis(thioamide) pincer compounds with the azulene central unit

Hence, thioamide ancillary groups in a pincer framework offer structural and charge versatility, resulting in a diversity of complexes with valuable chemical and physical properties.

3 Bis(thiophosphoryl) Pincer Compounds

Compounds containing thiophosphoryl groups ($R^1R^2P=S$, where R^1 and R^2 are alkyl, aryl, alkoxy, etc.) comprise another important class of pincer complexes with thione sulfur donors. A variety of methods for construction of the P–C bonds makes phosphorus-containing groups readily introduced coordinating arms. Generally, organophosphorus ligands are very popular in the creation of pincer complexes, but this concerns mainly various trivalent phosphorus derivatives [4, 15–26]. Nevertheless, recent studies on organothiophosphorus pincer systems have led to a considerable progress in this area, and a great diversity of bis(thiophosphoryl) pincer complexes with a benzene, toluene, pyridine, pyrrole, indene, and indole central core featuring promising luminescence properties, intriguing chemical behavior, as well as remarkable catalytic activity in different processes have been developed.

One of the first examples of pincer ligands bearing thiophosphoryl donor groups was symmetrical bis(diphenylphosphinosulfide)toluene **51** obtained by palladium-catalyzed phosphination of 3,5-dibromotoluene with Ph_2PH followed by addition of elemental sulfur (Scheme 20) [58]. The direct cyclometallation of **51** was shown to
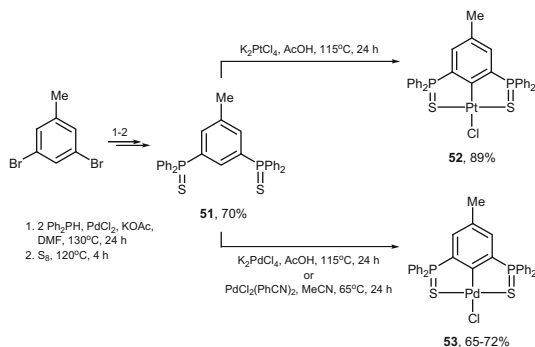
Scheme 20 Pincer complexes of 3,5-bis(thiophosphorylated) toluene
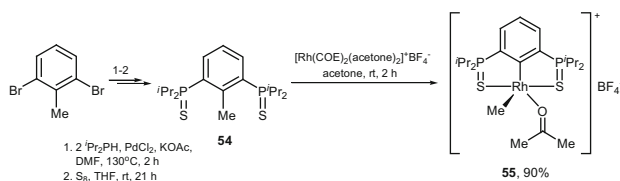
Scheme 21 Synthesis of rhodium pincer complex of 2,6-bis(thiophosphoryl)toluene via C–C bond activation

readily proceed under heating either with K_2MCl_4 (M=Pd, Pt) in acetic acid or with $PdCl_2(PhCN)_2$ in acetonitrile (Scheme 20). As their thioamide analogs, the resulting *S,C,S*-metallacycles **52** and **53** exhibited photoluminescence properties in the frozen state (77 K). Furthermore, Pt(II) complex **52** was also light-emissive in the solid state at room temperature. In all cases, the observed luminescence was attributed to emission from the ^{3}MLCT excited state, showing the potential of application of pincer complexes with organothiophosphorus ligands in luminescence devices.

Isomeric 2,6-bis(thiophosphorylated) toluene **54** prepared via the same synthetic protocol (Scheme 21) was used as a convenient model for investigation of C–C vs. C–H bond activation with cationic Rh(I) precursor, studied previously for other pincer systems [59]. It was found that the reaction of **54** with $[Rh(COE)_2(acetone)_2]^+BF_4^-$ under mild conditions exclusively results in the C–C bond oxidative addition (complex **55**, Scheme 21) instead of the cleavage of seemingly more accessible $C(sp^3)$–H bond [60]. According to the DFT calculations, a key feature of the *S,C,S*-bis(thiophosphoryl) system is the significant π-repulsion between the rhodium and sulfur atoms. The higher electronegativity of the methyl ligand compared to the hydride one allows for more effective release of the excessive π-electron density, leading to thermodynamic preference of the strong $C(sp^2)$–$C(sp^3)$ bond activation. Therewith, a novel η^3-C–C–H agostic intermediate was observed.

Further peculiarities of *S,C,S*-bis(thiophosphoryl) pincer system were revealed upon exploration of the reactivity of Rh(III) methyl complex **55** toward CO [61]. In
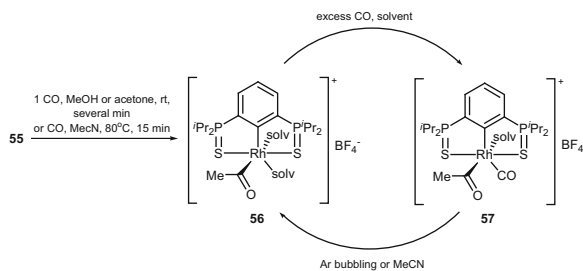
Scheme 22 Interaction of *S,C,S*-pincer rhodium complexes with CO
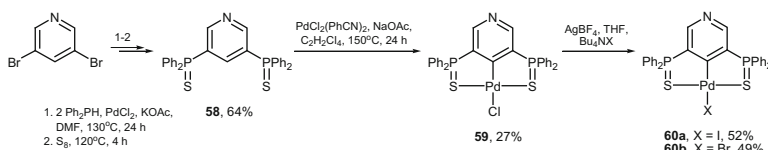
Scheme 23 *S,C,S*-pincer compounds with 3,5-substituted pyridine as the central unit

61a X = I, R = Me, 64%
61b X = Br, R = PhCH₂, 77%
61c X = Br, R = σ-All, 64%
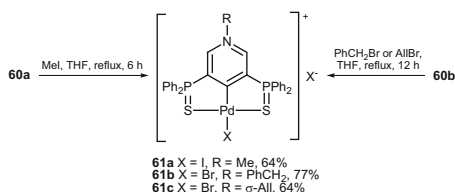
Scheme 24 Quaternization of 3,5-bis(thiophosphoryl)pyridine pincer complexes

reaction with an equivalent of CO, it undergoes migratory insertion giving acetyl derivative **56** (Scheme 22). Subsequent treatment of **56** with excess CO results in carbonyl complex **57** which can be recovered into **56** (Scheme 22). Note that *P,C,P*- and *P,C,N*-analogs of metallacycle **55** lead to Rh(I) agostic adducts due to the C–C reductive elimination [59]. A sharp distinction in the properties of these systems was attributed to the higher electrophilicity of the sulfur atoms compared to the phosphorus ones, which weakens π-back donation from the rhodium atom to the CO ligand, facilitating metal-to-CO direction of methyl migration. An important conclusion is that the bonding scheme in the *S,C,S*-pincer system is best described by single, polar covalent P–S bonds and formal Rh(V) oxidation state.

Substitution of the central toluene ring for the pyridine unit afforded a pincer-type ligand with additional coordination-active site (compound **58**, Scheme 23), opening the way to new pincer complexes [62]. Thus, palladacycles **59**, **60** obtained by direct cyclometallation of this ligand (Scheme 23) can be used to prepare *N*-quaternized pyridinium complexes **61** via treatment with alkyl or allyl halides (Scheme 24) and hetero-binuclear complexes **62**, **63** by reaction with the corresponding metal precursors (Scheme 25). Note that unlike palladacycle **53**,

Scheme 25 Synthesis of hetero-binuclear derivatives based on *S,C,S*-bis-(thiophosphoryl) pincer complexes
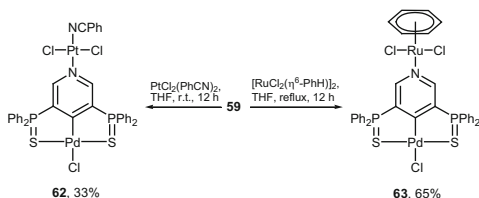
Scheme 26 Rhenium(I) *S,N,S*-pincer complexes based on (thio) phosphorylated pyridine
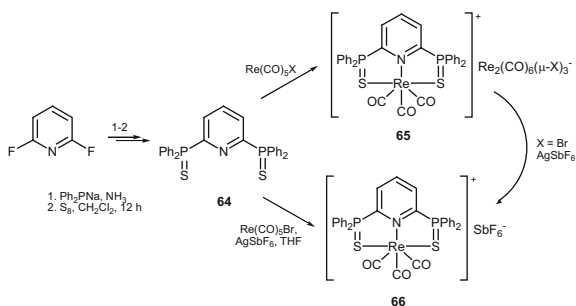
complex **59** exhibited only weak emission in the frozen state (77 K) and its functionalization did not improve photophysical properties.

Potentially tridentate ligand – 2,6-bis(diphenylphosphinosulfide)pyridine **64**, isomeric to the abovementioned *S,C,S*-ligand **58** – was synthesized by the reaction of 2,6-difluoropyridine with Ph$_2$PNa in liquid ammonia followed by sulfurization with S$_8$ (Scheme 26) [63]. It was assumed that, in contrast to the classical monoanionic pincer systems, this neutral ligand would show fluxional behavior upon complexation with transition metal ions due to less strong bonding. However, in reactions with rhenium(I) carbonyl halides, the title ligand afforded *S,N,S*-cationic pincer-type complexes **65** and **66** (Scheme 26) in all cases adopting stereochemically rigid tridentate coordination mode. This confirms the strong donating and directing ability of thiophosphoryl pendant arms in pincer systems.

A more flexible counterpart of ligand **64** bearing elongated thiophosphoryl coordinating arms, 2,6-bis(diphenylphosphinosulfide)lutidine **67**, was derived from the corresponding dibromide under action of ^{i}Pr$_2$PLi followed by treatment with elemental sulfur (Scheme 27) [64]. Interaction of **67** with ^{n}BuLi resulted in monolithium salt **68** featuring *S,N,S*-coordination mode. The latter was used as a ligand-transfer reagent in the synthesis of heavier group 14 metal complexes, in which, nevertheless, the pincer structure was not preserved (Scheme 27).

An elegant route to *S,N,S*-pincer ligand with the pyrrole central unit was devised using two sequential phospho-Fries rearrangements, consisting in based-induced conversion of *N*-thiophosphorylated pyrroles into 2- and 2,6-thiophosphoryl-substituted derivatives (Scheme 28) [65]. What is important is that this method avoids the intermediate formation of a P(III)-precursor and allows for the introduction of thiophosphoryl group with alkoxy substituents instead of popular aryl or alkyl groups (thiophosphonate coordinating arm). Direct cyclometallation of **69**
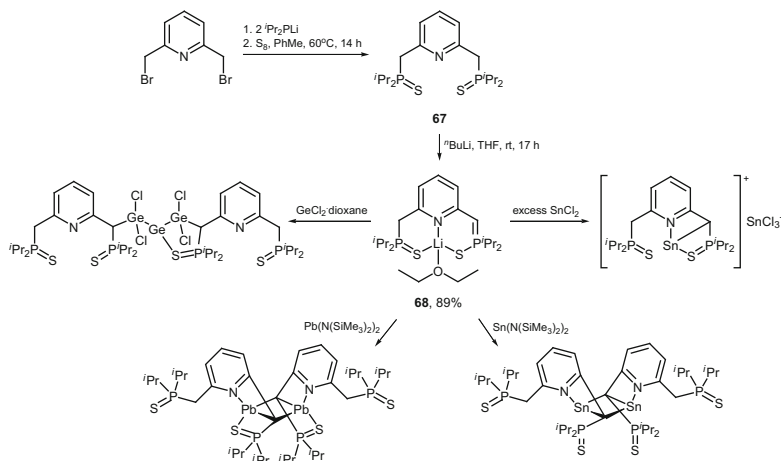
Scheme 27 Synthesis of bis(thiophosphorylated) lutidine and its metal complexes
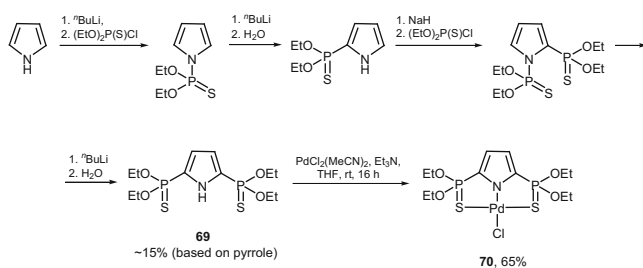
Scheme 28 *S,N,S*-bis(thiophosphoryl) pincer compounds with the pyrrole core

was readily accomplished under action of PdCl$_2$(MeCN)$_2$ in THF solution at room temperature, affording *S,N,S*-pincer palladium(II) complex **70** (Scheme 28). This example demonstrates the potential of organophosphorus chemistry methods in creation of new pincer systems, which, in our opinion, is still underappreciated.

(Bis)thiophosphorylated *S,P,S*-pincer ligands with the λ^4-phosphinine core were shown to serve as versatile ligands for a wide range of metals, including f-elements, affording complexes with interesting structural properties and reactivity (Fig. 1). Due to the unusual charge distribution and the presence of low-lying π^*-systems, these poor σ-donor/strong π-acceptor ligands are of special interest for stabilization of electron-excessive metal centers. The synthesis and electronic properties of the ligand and the main results of its coordination chemistry were reviewed in paper [29].

A particularly interesting pincer system appeared to be 1,3-bis(thiophosphorylated) indene. Compound **71** was prepared from indene via repeated treatment with an equivalent of ^{n}BuLi and quenching with Ph$_2$PCl followed by addition of elemental sulfur to the resulting bis(phosphine) derivative (Scheme 29) [66]. Of note is the high

R = Me, Bu, Cl, Br, OH, OMe

M = Li, K, Ni, Pd, Pt, Ir, Mo,
Rh, Mn, Re, Au, Ce, U
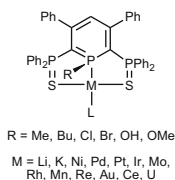
Fig. 1 *S,P,S*-Pincer complexes with the phosphinine core
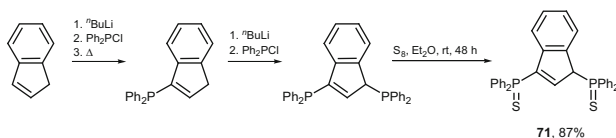
Scheme 29 Synthesis of 1,3-bis(phosphinosulfide)indene
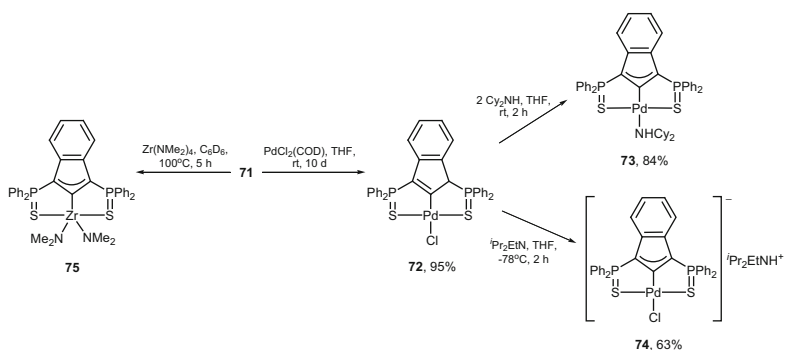
Scheme 30 Symmetrical and unsymmetrical pincer complexes of 1,3-bis(thiophosphorylated) indene

selectivity of formation of 1,3-disubstituted product, which was attributed to the steric bulkiness of the Ph_2P moiety and thermodynamic stability of 3-substituted phosphinoindenes. D. Bourissou et al. showed that the reaction of **71** with $PdCl_2(COD)$ or $PdCl_2(PhCN)_2$ under mild conditions affords unsymmetrical complex **72** featuring *S,C,S*-pincer-type coordination of 2-indenyl ligand (Scheme 30) [67]. Furthermore, dehydrochlorination of palladacycle **72** under action of Cy_2NH or its treatment with $^iPr_2EtN$ resulted in palladacycle **73** and its anionic counterpart **74**, respectively, in which an unusual 2-indenylidene pincer-type backbone was observed. 1,3-Bis (thiophosphoryl)-substituted indene **71** adopted the same dianionic tridentate coordination mode also in zirconium complex **75** (Scheme 30) [67]. According to the DFT calculations, the metal–carbon interaction in compounds **73–75** is best described as a single bond with essential σ-bonding and weak (if any) π-interaction.
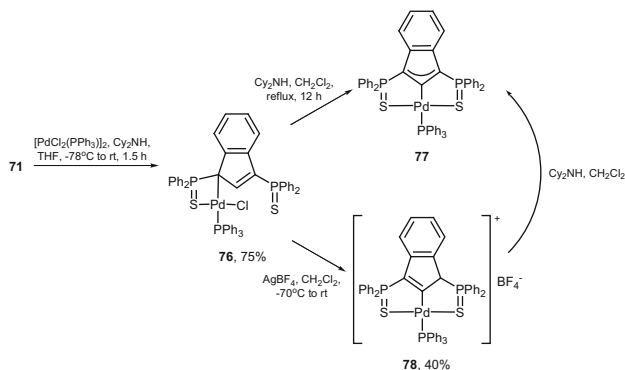
Scheme 31 Mechanism of formation of 2-indenylidene pincer complexes with thiophosphoryl pendant arms
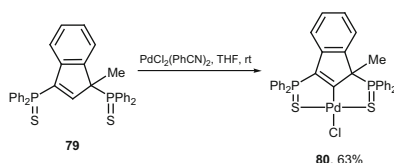
Scheme 32 Direct $C(sp^2)$–H bond activation in S,C,S'-pincer ligand with the indene central unit

Trying to elucidate the mechanism of formation 2-indenylidene complexes using additional experiments, it was shown that the $C(sp^2)$–H bond activation actually results from the preliminary activation of the $C(sp^3)$–H bond followed by the Pd/H exchange at the C1/C2 atoms [68]. Thus, interaction of 1,3-bis(phosphinosulfide)indene **71** with $[PdCl_2(PPh_3)]_2$ in the presence of an equivalent of Cy_2NH at room temperature afforded stable four-membered palladacycle **76**. The latter can be converted to pincer-type complex **77** with 2-indenylidene ligand either directly under action of Cy_2NH or through the intermediate formation of cationic derivative **78** with a monoanionic tridentately bound ligand via treatment with $AgBF_4$ (Scheme 31). Direct activation of the indene $C(sp^2)$–bond can be promoted by coordination of thiophosphoryl pendant arms only in the case of the absence of a possible competitive $C(sp^3)$–H bond activation route, as was the case with 1-methyl-substituted ligand **79** leading to unsymmetrical S,C,S'-pincer complex **80** immediately after mixing with the Pd(II) precursor (Scheme 32). The methyl-substituted analog was prepared using the synthetic route previously suggested for ligand **71**.

Owing to the presence of sulfur-donor atoms capable of acting as bridging ligands, anionic palladacycle **74** can be used as a precursor for homo- and heteropolymetallic complexes (Scheme 33) [69]. Note that compounds **81**–**83** feature $d^8 \ldots d^8$ interactions.

Furthermore, an analog of chloropalladate **74** with another countercation (compound **84**, Scheme 34), introduced to increase solubility and prevent undesirable side reactions, exhibited versatile reactivity toward nucleophilic and electrophilic
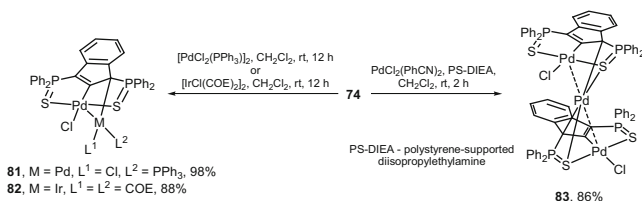
Scheme 33 Homo- and heteropolymetallic complexes based on bis(thiophosphorylated) indenylidene pincer complexes
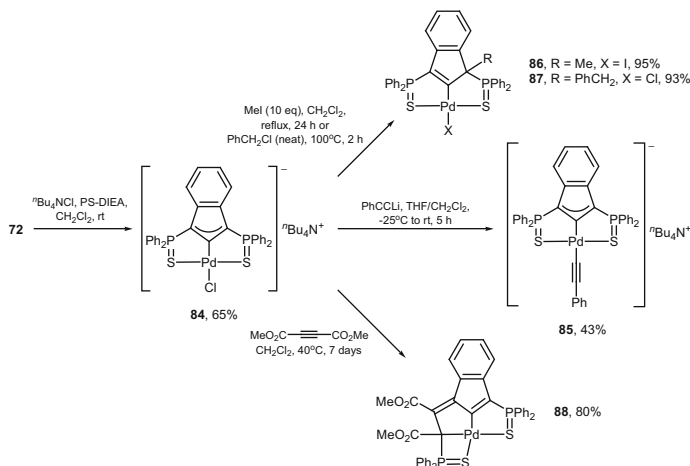
Scheme 34 Chemical reactivity of palladium(II) *S,C,S*-indenylidene pincer complex

organic reagents [70]. Thus, treatment of **84** with such nucleophiles as PPh$_3$ or Cy$_2$NH proceeded as the displacement of chloride ligand at the palladium ion, resulting in the previously reported complexes **77** and **73**, respectively. In addition, reaction of **84** with lithium phenylacetylide afforded complex **85** – the first example of isolated alkynylpalladate (Scheme 34). Electrophilic reagents, namely, alkyl halides, affected predominantly the ligand backbone, affording unsymmetrical 2-indenyl complexes **86**, **87** owing to the alkylation at the C3-carbon atom. Finally, dimethyl acetylenedicarboxylate inserted into the C–P bond of one of the pendant thiophosphoryl arms to give complex **88** featuring three fused metallacycles.

In continuation of the studies on bis(thiophosphorylated) indenyl and indenylidene complexes, D. Bourissou et al. recently reported the related ligand with the indole core [71]. The title compound **89** was prepared using a one-pot synthetic procedure including sequential phosphination at the C3 and N atoms followed by treatment with elemental sulfur (Scheme 35). Cyclopalladation of **89** was accomplished using in situ generated cationic palladium(II) precursor, leading to unsymmetrical *S,C,S'*-pincer complex **90** with monoanionic tridentate coordination mode of the indolyl ligand.

Scheme 35 Synthesis and
direct cyclopalladation
of unsymmetrical
bis(thiophosphoryl)indole
pincer ligand
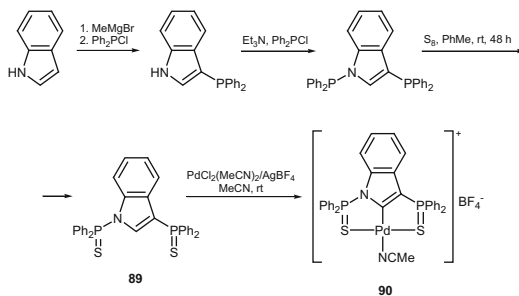
Scheme 36 Pincer
complexes of bis
(phosphinosulfide)indolyl
ligand
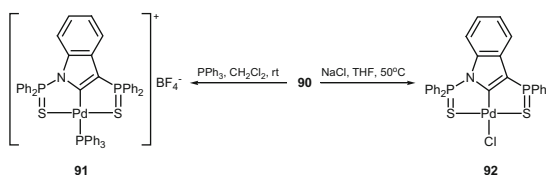
Fig. 2 *S,C,S*-Palladium
carbonyl pincer complexes
featuring indolyl, indenyl,
and indenylidene ligand
framework
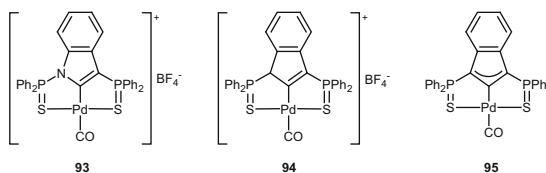
Treatment of **90** with triphenylphosphine and sodium chloride afforded palladacycles **91** and **92**, respectively, which cannot be obtained directly from the corresponding ligand (Scheme 36) [71].

To compare the electronic properties of indolyl, indenyl, and indenylidene pincer systems bearing phosphine sulfide donating groups, metallacycles **93–95** were synthesized that represent the rare example of palladium carbonyl pincer complexes (Fig. 2) [71]. The IR spectra of complexes **93**, **94**, and **95** recorded under CO atmosphere showed ν_{CO} bands at 2,151, 2,161, and 2,121 cm^{-1}, respectively. This corresponds to the following series of an increase in electron density at the palladium center: indenyl $\leq$ indolyl $<$ indenylidene.

The difference in electronic effect of the ligand backbone was also reflected in the catalytic performance of chloro complexes **80**, **84**, and **92** in reaction of phenyl tosylimine with Bu$_3$SnAll. Under optimized reaction conditions (Scheme 37), indenylidene derivative **84** substantially surpassed in the activity its counterparts **92** and **80**, providing allyl tosyl amine in 83%, 33%, and 51% yield, respectively [71]. The higher electron density at the palladium center induced by the indenylidene backbone is likely to result in the increased nucleophilicity of η^1-allyl intermediate which is supposed to serve as a key intermediate in allylation of imines catalyzed by pincer complexes. It is noteworthy that, despite the presence of

Scheme 37 Allylation of phenyl tosyl imine catalyzed by *S,C,S*-pincer Pd(II) complexes

Pd cat.	**84**	**92**	**80**
Yield of allyl tosyl amine	83%	33%	51%
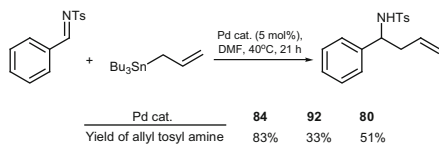
Scheme 38 1-Thiophosphoryloxy-3-thiophosphorylbenzene pincer compounds
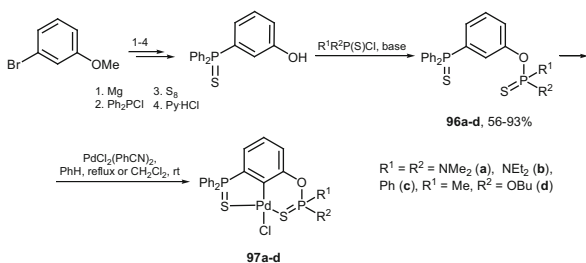
weaker donor groups, palladacycle **84** shows the same level of activity as the previously reported *P,C,P*-analogs.

Recent theoretical studies on activation of the X–H bonds (X=O, N, S, and P) with *S,C,S*-bis(thiophosphorylated) indenylidene pincer complexes showed their potential for application in other catalytic transformations, for example, hydrofunctionalization reactions [72].

A series of unsymmetrical thiophosphoryloxy-thiophosphoryl pincer ligands **96a–d** was prepared using *m*-thiophosphoryl-substituted phenol as a single key precursor (Scheme 38). Direct cyclopalladation of **96a–d** under action of PdCl$_2$(PhCN)$_2$ afforded rare examples of pincer complexes with five- and six-membered fused metallacycles (Scheme 38) [73]. Compounds **97a–d** demonstrated high catalytic activity in the Suzuki–Miyaura cross-coupling of aryl bromides with phenylboronic acid providing turnover numbers up to 38,000 [73].

4 Hybrid Pincer Compounds with Thione Sulfur Donors

Over the years, a classical structure of pincer compounds has been significantly modified. Nowadays, hybrid systems bearing donor groups of different nature are of particular interest since they offer additional possibilities for fine-tuning electronic and steric properties. Pincer metallacycles based on such unsymmetrical ligands were shown to combine characteristics of several symmetrical prototypes or manifest unique properties [8, 12, 74–77]. Despite an increasing number of publications devoted to the hybrid pincer complexes, only several examples containing thione sulfur donors have been described to date. Nevertheless, the available literature data on reactivity and catalytic activity of these systems allows considering further development of this area of pincer chemistry very promising.
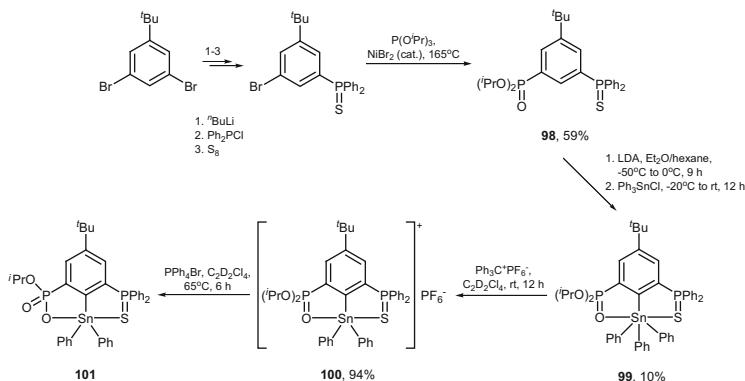
Scheme 39 Thiophosphoryl-phosphoryl hybrid pincer compounds

Exploring a possibility of application of pincer-type ligands in the chemistry of hypervalent main group elements (tin, silicon, etc.) [78], K. Jurkschat et al. reported the first example of a hybrid pincer ligand combining the soft thione sulfur atom of the thiophosphoryl group with the hard oxygen atom of the phosphoryl group as coordination sites [79]. A convenient synthetic route to the desired ligand consisted in the stepwise introduction of the P=S and P=O pendant arms via one-pot sequential treatment of 1,3-dibromo-5-*tert*-butylbenzene with ^{n}BuLi, chlorodiphenylphosphine, and elemental sulfur followed by reaction of the resulting monobromide with trialkylphosphite in the presence of catalytic amount of NiBr$_2$ (compound **98**, Scheme 39). Metallation of **98** with LDA followed by treatment with Ph$_3$SnCl afforded tetraorganotin(IV) complex **99** featuring tridentate monoanionic coordination mode of the ligand. The latter was preserved also in triorganotin cationic complex **100** readily derived from the interaction of **99** with Ph$_3$C$^+$PF$_6^-$. Reaction of **100** with tetraphenylphosphonium bromide resulted in benzoxaphosphastannole derivative **101** similar to the previously reported tin derivatives [80]. This investigation contributed to the general understanding of the structure and reactivity of hypercoordinated organotin compounds.

The first examples of pincer compounds bearing two thione sulfur donors of different nature were elaborated in our group in 2008 [81]. Hybrid ligands **102a**,**b** having thiophosphoryl and thioamide coordinating arms were synthesized from readily available 3-diphenylphosphorylbenzoic acid via aminolysis of the corresponding acid chloride followed by thionation with the Lawesson reagent (Scheme 40). Compounds **102a**,**b** readily underwent cyclopalladation in reaction with PdCl$_2$(PhCN)$_2$ in dichloromethane solution at room temperature, affording *S,C,S'*-pincer complexes **103a**,**b** in high yields (Scheme 40). As well as their symmetrical bis(thioamide) and bis(thiophosphoryl) prototypes, hybrid palladacycles **103a**,**b** are light-emissive in the frozen matrix and in the solid state at 77 K. Based on the literature and experimental data, the bands observed in the photoluminescence spectra were assigned to emission from the MLCT excited
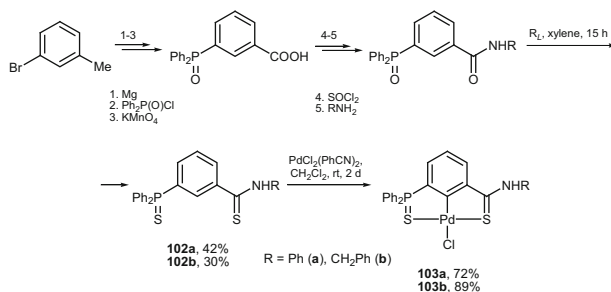
Scheme 40 Synthesis of thiophosphoryl-thioamide pincer ligands and their 5,5-membered palladacycles
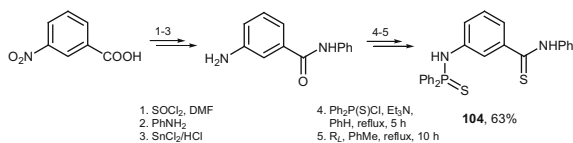
Scheme 41 Synthesis of thiophosphorylamino-thioamide pincer ligand
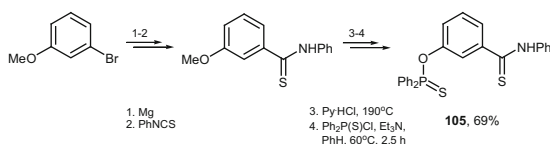
Scheme 42 Synthesis of thiophosphoryloxy-thioamide pincer ligand

state. Note that only weak luminescence was detected for one of crystallosolvates of complex **103a** in the solid state at room temperature. In addition, complexes **103a,b** were found to efficiently promote the Suzuki–Miyaura cross-coupling of aryl bromides with PhB(OH)$_2$.

To study the effect of structure modifications on the properties of hybrid thioamide-thiophosphoryl pincer system, it seemed interesting to develop the analogs of compounds **102a,b** bearing elongated thiophosphoryl pendant arms, which would afford upon cyclometallation fused metallacycles of different sizes. *S,C,S'*-Pincer ligand **104** with the NH bridge between the P=S group and central benzene ring was obtained by thiophosphorylation of 3-aminobenzoic acid anilide followed by thionation of the resulting *S,O*-derivative under action of the Lawesson reagent (Scheme 41) [82]. Its counterpart containing thiophosphoryloxy donating group (compound **105**) was derived from 3-hydroxybenzoic acid thioanilide (Scheme 42) [82]. Cyclopalladation of ligands **104** and **105** was smoothly accomplished under action of PdCl$_2$(PhCN)$_2$ in CH$_2$Cl$_2$ or MeCN at room temperature (Scheme 43). Therewith, the rate of cyclopalladation of hybrid thiophosphoryl-thioamide derivatives under optimized conditions reduced from 2 days for ligands

Scheme 43 Complexation of thiophosphoryl-thioamide pincer ligands having elongated thiophosphoryl arms with the Pd(II) and Pt(II) ions

104 or **105**

MCl₂(PhCN)₂

M = Pd: MeCN, rt, 5 min
M = Pt: MeCN, reflux, 4 h

M = Pd: CH₂Cl₂, rt, 1 d
M = Pt: PhCN, 120°C, 3 h

106a, 93%
106b, 74%

107a, 82%
107b, 67%

M = Pd (**a**), Pt (**b**)
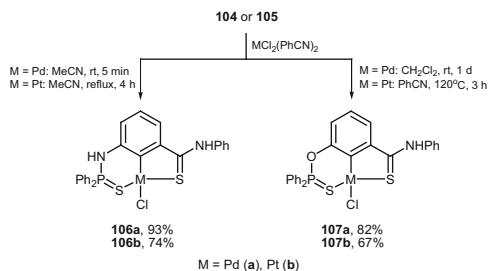
102 a,b to 5 min for their counterpart with the thiophosphorylamino group, suggesting stronger coordinating ability of the latter. Reaction of **104** with PdCl₂(PhCN)₂ in MeCN appeared to be one of the fastest examples of direct cyclopalladation in pincer systems reported to date. A difference in the reactivity of phosphine sulfide derivatives **102a,b** and its analogs with the elongated thiophosphoryl arms was further revealed in reactions with PtCl₂(PhCN)₂. Thus, interaction of ligands **104** and **105** with this platinum(II) precursor under heating in MeCN or PhCN led to cycloplatinated complexes **106b** and **107b** in moderate yields (Scheme 43). At the same time, 3-thiophosphorylbenzoic acid thioamides **102a,b** did not afford pincer products, giving only several nonmetallated complexes (³¹P monitoring).

Whereas ligands **102a**,b are not light-emissive at all, their counterparts **104** and **105** with the elongated thiophosphoryl arm exhibit fluorescent emission both at 77 or 300 K, which originates from the ligand-centered π–π* transition [82]. Unlike 5,5-membered complexes **103 a,b**, all their counterparts with the fused metallacycles of different sizes (compounds **106 a,b** and **107 a,b**) possess luminescence properties in the solid state at room temperature. The emission of platinum derivatives **106b**, **107b** is likely to occur from the MLCT excited states, while in the case of the palladium complexes, it involves ligand-centered levels. However, it is obvious that *desymmetrization* of a pincer ligand structure positively affects the luminescence properties of *S,C,S'*-pincer complexes and search for new effective luminophores among hybrid thiophosphoryl-thioamide derivatives seems to be promising. Furthermore, palladacycles **106a**, **107a** were also shown to catalyze the Suzuki–Miyaura cross-coupling of a range of electronically varied aryl bromides with PhB(OH)₂ [82]. Therewith, the high level of activity toward both activated and deactivated substrates was observed at significantly lower concentrations of the palladium(II) (pre)catalyst than in the case of 5,5-membered counterpart **103a** (e.g., 0.01 vs. 3 mol% for the coupling of 4-bromoacetophenone).

Since the hemilabile nature of ligands is often mentioned as a reason for better catalytic performance of palladium pincer complexes [83–86], we turned to ligand systems combining the soft thione sulfur atoms with the hard nitrogen-donor centers. *N,C,S*-Pincer ligands with acyclic and cyclic imine moiety and phosphinosulfide group (compounds **108a–e**) were prepared by the condensation of 3-thiophosphorylbenzaldehyde with primary amines or metallation of
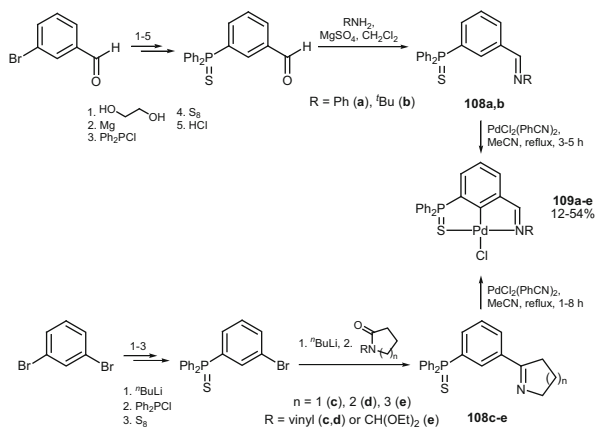
Scheme 44 *N,C,S*-Pincer compounds with the imine and thiophosphoryl pendant arms
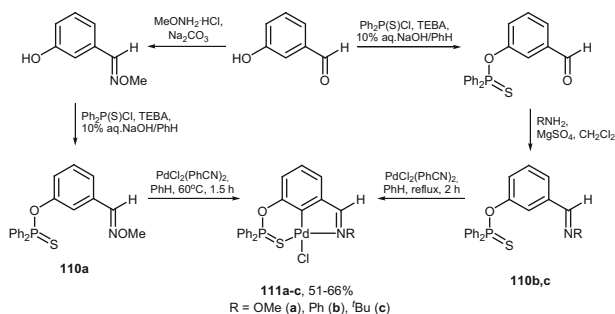
Scheme 45 3-(Thiophosphoryloxy)benzaldimine pincer compounds

m-thiophosphorylated bromobenzene with ^{n}BuLi followed by treatment with an equivalent of appropriate lactam (Scheme 44) [87]. The most favorable conditions for direct cyclopalladation of the resulting ligands appeared to be refluxing in MeCN for several hours (Scheme 44). However, even under these optimized conditions, the yields of 5,5-membered pincer complexes **109a–e** hardly exceeded 50%. These results are consistent with the literature data on low efficiency of direct cyclopalladation in symmetrical bis(imine) pincer systems, stemming from the kinetically preferred metallation at the other positions of the benzene core [88–90].

In order to estimate the effect of the length of pendant thiophosphoryl arm on direct cyclopalladation in *N,C,S*-pincer systems, the analogs of compounds **108a–e** bearing the oxygen bridge between the P=S group and the central benzene ring (compounds **110a–c**) were synthesized in two steps starting from commercially available 3-hydroxybenzaldehyde (Scheme 45) [91]. Therewith, the sequence of thiophosphorylation and Schiff-base condensation stages depended on the nature of the amine component. *N,C,S*-Pincer complexes with five- and six-membered fused palladacycles were derived from the reactions of **110a–c** with PdCl$_2$(PhCN)$_2$ in

benzene at elevated temperatures (Scheme 45). The yields of complexes **111a–c** were indeed higher than those achieved for 5,5-membered palladacycles **109a–e**. Interestingly, the reaction of **110a,b** with the same palladium precursor performed in CH$_2$Cl$_2$/MeOH at room temperature was accompanied by the formation of the *N,C,O*-complexes along with *N,C,S*-palladacycles **111a,b** due to the transformation of the thiophosphoryl group into the phosphoryl one. This oxygenation was suggested to proceed in the metal ion coordination sphere of the coordinated intermediate species; however, the detailed mechanism is still unclear. It should be mentioned that the *N,C,O*-complexes obtained represent the rare examples of noble metal pincer metallacycles with the coordinated phosphoryl group [92].

In general, 5,5- and 5,6-membered palladium(II) pincer complexes **109b–e** and **111a,c** displayed higher level of catalytic activity in the Suzuki–Miyaura cross-coupling of aryl bromides with PhB(OH)$_2$ compared to *S,C,S′*-thioamide-thiophosphoryl derivatives **106a**, **107a** (higher yields of biphenyl products at the same concentration of the Pd(II) (pre)catalysts). Encouraged by the results on catalytic activity of *N,C,S*-palladacycles with hybrid thiophosphoryl-imine ligands, we decided to incorporate the imine functionality into the bulky benzothiazole moiety. This heterocyclic system was chosen, in particular, owing to a possibility of transformation of secondary thioamide group into benzothiazole fragment previously performed for bis(thioamide) prototype **14** (see Sect. 2). Moreover, monocyclic benzothiazole-based palladium(II) complexes were shown to possess high catalytic activity in different reactions, including Heck vinylation of aryl iodides [93–96]. Therewith, adjusting the position of an additional linker between the donating groups and central benzene ring would give access to 5,6-membered complexes with either imine- or thiophosphoryl-containing six-membered metallacycles.

Ligand **112** with the thiophosphoryl and benzothiazole fragments directly attached to the central benzene ring was obtained by oxidative cyclization of secondary thioamide **102a** (Scheme 46) [97]. Convenient synthetic routes to its analogs **113** and **114** with the thiophosphoryl arms connected with the benzene core via NH- or O-bridge (compounds) were based on thiophosphorylation of *m*-benzothiazole-substituted phenol and aniline (Scheme 47) [97]. Finally, compound **115** having the oxygen linker between the benzothiazole moiety and benzene core was derived from the reaction of sodium salt of *m*-thiophosphorylated phenol with 2-chlorobenzothiazole (Scheme 48) [97]. Reactions of ligands **112–115** with PdCl$_2$(PhCN)$_2$ under heating in aceto- or benzonitrile for several hours afforded pincer complexes **116**, **117**, **118a**, **119** (Scheme 49). Cycloplatination was accomplished only in the case of the most active thiophosphorylamino derivative **114**.
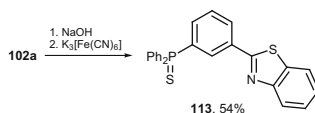
Scheme 46 Synthesis of thiophosphoryl-benzothiazole pincer ligand
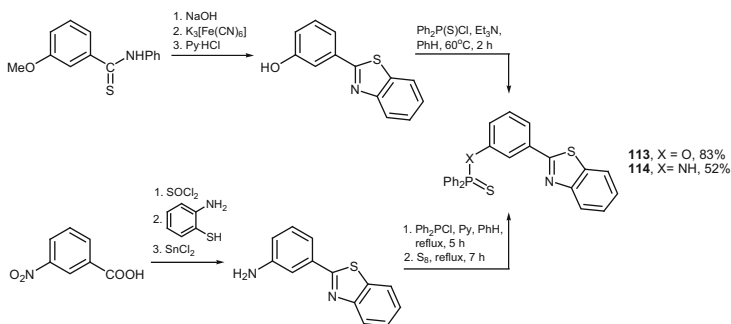
Scheme 47 Synthesis of *N,C,S*-pincer ligand with the elongated thiophosphoryl arms
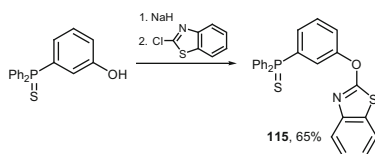
Scheme 48 Synthesis of *N,C,S*-pincer ligand with the elongated benzothiazole arm
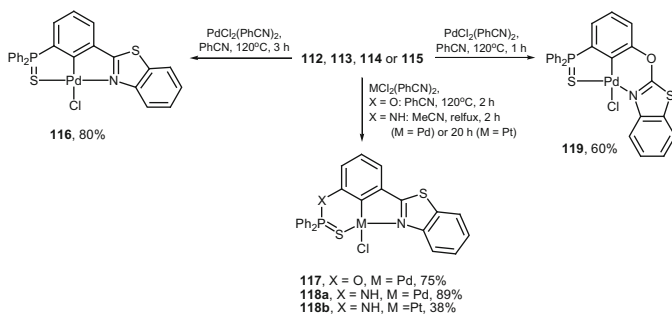
Scheme 49 Cyclometallation of thiophosphoryl-benzothiazole hybrid pincer ligands

Similar to the other palladacycles with the thiophosphoryl donating group, complexes **116**, **117**, **118a**, **119** were tested as (pre)catalysts for the Suzuki–Miyaura cross-coupling of aryl halides with $PhB(OH)_2$ under the same reaction conditions. Unlike the abovementioned *N,C,S*-complexes **109a–e** and **111a–c**, the benzothiazole-based palladacycles efficiently promoted the coupling of deactivated 4-bromoanisole at the concentration of Pd(II) (pre)catalyst as low as 0.01 mol%. Furthermore, complex **118a** showed remarkable activity also in the reaction with 4-chloroacetophenone, ranking among the best pincer (pre)catalysts reported to date.

Interestingly, palladium complexes **116–119** can be also prepared via thermally induced C–H bond activation in the nonmetallated precursors or homogeneous mixtures of the corresponding ligand and $PdCl_2(PhCN)_2$ obtained by grinding of

the reagents in a mortar [98]. These reactions appeared to be the first examples of *solid-phase synthesis* of pincer complexes. Recently, the *solid-phase strategy* has been successfully used for synthesis of S,C,S'-pincer systems with different thione sulfur donors [99].

5   Conclusions

In this review, we summarized recent advances in the chemistry of thiophosphoryl- and thioamide-containing derivatives as relatively new, nonclassical types of pincer ligands. The presented data on reactivity, catalytic activity, and physical properties of pincer complexes with thione sulfur donors show the potential of search for effective catalysts and functional materials, especially among metallacycles with new backbones and combinations of donating groups.

References

1. Shaw BL, Moulton CJ (1976) J Chem Soc Dalton Trans 1020
2. Albrecht M, van Koten G (2001) Angew Chem Int Ed 40:3750
3. Singleton JT (2003) Tetrahedron 59:1837
4. van der Boom ME, Milstein D (2003) Chem Rev 103:1759
5. Morales-Morales D (2004) Rev Soc Quím Méx 48:338
6. Beletskaya IP, Cheprakov AV (2004) J Organomet Chem 689:4055
7. Dupont J, Consorti CS, Spencer J (2005) Chem Rev 105:2527
8. Moreno I, SanMartin R, Inés B, Herrero MT, Domínguez E (2009) Curr Org Chem 13:878
9. Albrecht M (2010) Chem Rev 110:576
10. Odinets IL, Aleksanyan DV, Kozlov VA (2010) Lett Org Chem 7:583
11. Selander N, Szabó KJ (2011) Chem Rev 111:2048
12. Niu J-L, Hao X-Q, Gong J-F, Song M-P (2011) Dalton Trans 40:5135
13. Morales-Morales D, Jensen CM (eds) (2007) The chemistry of pincer compounds. Elsevier, Oxford
14. van Koten G, Milstein D (eds) (2013) Organometallic pincer chemistry. Topics in Organometallic Chemistry, vol 40. Springer, Heidelberg
15. Dunina VV, Gorunova ON (2004) Russ Chem Rev 73:309
16. Dunina VV, Gorunova ON (2005) Russ Chem Rev 74:871
17. Torres-Nieto J, Garcia JJ (2007) Desulfurization catalyzed by nickel PCP-pincer compounds 79. In: Morales-Morales D, Jensen CM (eds) The chemistry of pincer compounds. Elsevier, Oxford
18. Morales-Morales D (2007) The chemistry of PCP pincer phosphinite transition metal complexes 151. In: Morales-Morales D, Jensen CM (eds) The chemistry of pincer compounds. Elsevier, Oxford

19. Ozerov OV (2007) Rigid PNP pincer ligands and their transition metal complexes 287. In: Morales-Morales D, Jensen CM (eds) The chemistry of pincer compounds. Elsevier, Oxford
20. Morales-Morales D (2008) Mini Rev Org Chem 5:141
21. Leis W, Mayer HA, Kaska WC (2008) Coord Chem Rev 252:1787
22. Serrano-Becerra JM, Morales-Morales D (2009) Curr Org Synth 6:169
23. van der Vlugt JI, Reek JNH (2009) Angew Chem Int Ed 48:8832
24. Poverenov E, Milstein D (2013) Noninnocent behavior of PCP and PCN ligands of late metal complexes 21. In: van Koten G, Milstein D (eds) Organometallic pincer chemistry. Topics in Organometallic Chemistry, vol 40. Springer, Heidelberg
25. Roddick DM (2013) Tuning of PCP pincer ligand electronic and steric properties 49. In: van Koten G, Milstein D (eds) Organometallic pincer chemistry. Topics in organometallic chemistry, vol 40. Springer, Heidelberg
26. Gelman D, Romm R (2013) PC(sp^3)P transition metal pincer complexes: properties and catalytic applications 289. In: van Koten G, Milstein D (eds) Organometallic pincer chemistry. Topics in organometallic chemistry, vol 40. Springer, Heidelberg
27. Chase PA, van Koten G (2007) Nitrogen-based pincers: a versatile platform for organometallic chemistry 181. In: Morales-Morales D, Jensen CM (eds) The chemistry of pincer compounds. Elsevier, Oxford
28. Ito J-I, Nishiyama H (2013) Optically active bis(oxazolinyl)phenyl metal complexes as multiponent catalysts 243. In: van Koten G, Milstein D (eds) Organometallic pincer chemistry. Topics in organometallic chemistry, vol 40. Springer, Heidelberg
29. Mézailles N, Le Floch P (2007) S-P-S and S-C-S pincer ligands in coordination chemistry and catalysis 235. In: Morales-Morales D, Jensen CM (eds) The chemistry of pincer compounds. Elsevier, Oxford
30. Takahashi S, Nonoyama M, Kita M (1995) Trans Met Chem 20:528
31. Scheibye S, Pedersen BS, Lawesson S-O (1978) Bull Soc Chim Belg 87:229
32. Amupitan JO (1983) Synthesis 730
33. Nojima Y, Nonoyama M, Nakajima K (1996) Polyhedron 15:3795
34. Akaiwa M, Kanbara T, Fukumoto H, Yamamoto T (2005) J Organomet Chem 690:4192
35. Kuwabara J, Kanbara T (2008) J Photopolym Sci Technol 21:349
36. Freeman GR, Williams JAG (2013) Metal complexes of pincer ligands: excited states, photochemistry, and luminescence 89. In: van Koten G, Milstein D (eds) Organometallic pincer chemistry. Topics in Organometallic Chemistry, vol. 40. Springer, Heidelberg
37. Ogawa Y, Taketoshi A, Kuwabara J, Okamoto K, Fukuda T, Kanbara T (2010) Chem Lett 39:385
38. Kuwabara J, Ogawa Y, Taketoshi A, Kanbara T (2011) J Organomet Chem 696:1289
39. Williams JAG, Develay S, Rochester DL, Murphy L (2008) Coord Chem Rev 252:2596
40. Kanbara T, Okada K, Yamamoto T, Ogawa H, Inoue T (2004) J Organomet Chem 689:1860
41. Okamoto K, Kanbara T, Yamamoto T, Wada A (2006) Organometallics 25:4026
42. Okamoto K, Yamamoto T, Akita M, Wada A, Kanbara T (2009) Organometallics 28:3307
43. Honda H, Ogawa Y, Kuwabara J, Kanbara T (2014) Eur J Inorg Chem 1865
44. Okamoto K, Kuwabara J, Kanbara T (2011) J Organomet Chem 696:1305
45. Teratani T, Koizumi T-a, Yamamoto T, Kanbara T (2011) Inorg Chem Commun 14:836
46. Teratani T, Koizumi T, Yamamoto T, Tanaka K, Kanbara T (2011) Dalton Trans 40:8879
47. Wang C-H, Ma N-N, Sun X-X, Sun S-L, Qiu Y-Q, Liu P-J (2012) J Phys Chem A 116:10496
48. Koizumi T-a, Teratani T, Okamoto K, Yamamoto T, Shimoi Y, Kanbara T (2010) Inorg Chim Acta 363:2474
49. Okamoto K, Kanbara T, Yamamoto T (2006) Chem Lett 35:558
50. Hossain MdA, Lucarini S, Powell D, Bowman-James K (2004) Inorg Chem 43:7275
51. Begum RA, Powell D, Bowman-James K (2006) Inorg Chem 45:964
52. Wang H, Liu J, Deng Y, Min T, Yu G, Wu X, Yang Z, Lei A (2009) Chem Eur J 15:1499
53. Liu J, Wang H, Zhang H, Wu X, Zhang H, Deng Y, Yang Z, Lei A (2009) Chem Eur J 15:4437
54. Liu J, Deng Y, Lin C, Lei A (2012) Chem Sci 3:1211

55. Wang Q-Q, Begum RA, Day VW, Bowman-James K (2012) Inorg Chem 51:760
56. Komiyama Y, Kuwabara J, Kanbara T (2014) Organometallics 33:885
57. Kuwabara J, Munezawa G, Okamoto K, Kanbara T (2010) Dalton Trans 39:6255
58. Kanbara T, Yamamoto T (2003) J Organomet Chem 688:15
59. Rybtchinski B, Milstein D (2007) Pincer systems as models for the activation of strong bonds: scope and mechanism 87. In: Morales-Morales D, Jensen CM (eds) The chemistry of pincer compounds. Elsevier, Oxford
60. Montag M, Efremenko I, Diskin-Posner Y, Ben-David Y, Martin JML, Milstein D (2012) Organometallics 31:505
61. Montag M, Efremenko I, Leitus G, Ben-David Y, Martin JML, Milstein D (2013) Organometallics 32:7163
62. Meguro H, Koizumi T-A, Yamamoto T, Kanbara T (2008) J Organomet Chem 693:1109
63. Heard PJ, Aliev AE (1998) Polyhedron 17:3981
64. Leung W-P, Kan K-W, Mak TCW (2010) Organometallics 29:1890
65. Fraix A, Lutz M, Spek AL, Klein Gebbink RJM, van Koten G, Salaün J-Y, Jaffrès P-A (2010) Dalton Trans 39:2942
66. Stradiotto M, Kozak CM, McGlinchey MJ (1998) J Organomet Chem 564:101
67. Oulié P, Nebra N, Saffon N, Maron L, Martin-Vaca B, Bourissou D (2009) J Am Chem Soc 131:3493
68. Nebra N, Lisena J, Saffon N, Maron L, Martin-Vaca B, Bourissou D (2011) Dalton Trans 40:8912
69. Nebra N, Saffon N, Maron L, Martin-Vaca B, Bourissou D (2011) Inorg Chem 50:6378
70. Oulié P, Nebra N, Ladeira S, Martin-Vaca B, Bourissou D (2011) Organometallics 30:6416
71. Lisena J, Monot J, Mallet-Ladeira S, Martin-Vaca B, Bourissou D (2013) Organometallics 32:4301
72. Nicolas E, Martin-Vaca B, Mézailles N, Bourissou D, Maron L (2013) Eur J Inorg Chem 4068
73. Kozlov VA, Aleksanyan DV, Nelyubina YV, Lyssenko KA, Gutsul EI, Vasil'ev AA, Petrovskii PV, Odinets IL (2009) Dalton Trans 8657
74. Wang Z, Eberhard MR, Jensen CM, Matsukawa S, Yamamoto Y (2003) J Organomet Chem 681:189
75. Gagliardo M, Selander N, Mehendale NC, van Koten G, Klein Gebbink RJM, Szabó KJ (2008) Chem Eur J 14:4800
76. Zhang B-S, Wang C, Gong J-F, Song M-P (2009) J Organomet Chem 694:2555
77. Hao X-Q, Wang Y-N, Liu J-R, Wang K-L, Gong J-F, Song M-P (2010) J Organomet Chem 695:82
78. Jambor R, Dostál L (2007) Hypervalent organotin, aluminum, antimony and bismuth Y,C,Y-chelate complexes 357. In: Morales-Morales D, Jensen CM (eds) The chemistry of pincer compounds. Elsevier, Oxford
79. Fisher J, Schürman M, Mehring M, Zachwieja U, Jurkschat K (2006) Organometallics 25:2886
80. Peveling K, Henn M, Löw C, Mehring M, Schürmann M, Costisella B, Jurkschat K (2004) Organometallics 23:1501
81. Kozlov VA, Aleksanyan DV, Nelyubina YV, Lyssenko KA, Gutsul EI, Puntus LN, Vasil'ev AA, Petrovskii PV, Odinets IL (2008) Organometallics 27:4062
82. Aleksanyan DV, Kozlov VA, Nelyubina YV, Lyssenko KA, Puntus LN, Gutsul EI, Shepel NE, Vasil'ev AA, Petrovskii PV, Odinets IL (2011) Dalton Trans 40:1535
83. Zhang J, Leitus G, Ben-David Y, Milstein D (2006) Angew Chem Int Ed 45:1113
84. Inés B, Moreno I, SanMartin R, Domínguez E (2008) J Org Chem 73:8448
85. Yorke J, Sanford J, Decken A, Xia A (2010) Inorg Chim Acta 363:961
86. Lindner R, van den Bosch B, Lutz M, Reek JNH, van der Vlugt JI (2011) Organometallics 30:499
87. Aleksanyan DV, Kozlov VA, Shevchenko NE, Nenajdenko VG, Vasil'ev AA, Nelyubina YV, Ananyev IV, Petrovskii PV, Odinets IL (2012) J Organomet Chem 711:52
88. Chakladar S, Paul P, Venkatsubramanian K, Nag K (1991) J Chem Soc Dalton Trans 2669

89. Chakladar S, Paul P, Nag K (1991) Polyhedron 10:1513
90. Fernandez A, Pereira E, Fernandez JJ, Lopez-Torres M, Suarez A, Mosteiro R, Pereira MT, Vila JM (2002) New J Chem 26:895
91. Kozlov VA, Aleksanyan DV, Nelyubina YV, Lyssenko KA, Vasil'ev AA, Petrovskii PV, Odinets IL (2010) Organometallics 29:2054
92. Poverenov E, Efremenko I, Frenkel AI, Ben-David Y, Shimon LJW, Leitus G, Konstantinovski L, Martin JML, Milstein D (2008) Nature 455:1093
93. Gai X, Grigg R, Collard S, Muir JE (2000) Chem Commun 1765
94. Grigg R, Khamnaen T, Rajviroongit S, Sridharan V (2002) Tetrahedron Lett 43:2601
95. Gai X, Grigg R, Koppen I, Marchbank J, Sridharan V (2003) Tetrahedron Lett 44:7445
96. Gai X, Grigg R, Ramzan MI, Sridharan V, Collard S, Muir JE (2000) Chem Commun 2053
97. Kozlov VA, Aleksanyan DV, Nelyubina YV, Lyssenko KA, Petrovskii PV, Vasil'ev AA, Odinets IL (2011) Organometallics 30:2920
98. Kozlov VA, Aleksanyan DV, Korobov MV, Avramenko NV, Aysin RR, Maloshitskaya OA, Korlyukov AS, Odinets IL (2011) Dalton Trans 40:8768
99. Aleksanyan DV, Klemenkova ZS, Vasil'ev AA, Gorenberg AY, Nelyubina YV, Kozlov VA (2015) Dalton Trans 44:3216

Recent Advances on the Chemistry of POCOP–Nickel Pincer Compounds

Matthew Asay and David Morales-Morales

Abstract A description of the vertiginous development of the chemistry of POCOP–Ni complexes and their applications is described. Recent advances include the discovery and initially challenging synthesis of these species to the high-yield green procedures recently developed. The various applications of these compounds, particularly in catalysis, are discussed in detail.

Contents

M. Asay and D. Morales-Morales (✉)
Instituto de Química, Universidad Nacional Autónoma de México, Circuito Exterior s/n, Ciudad Universitaria 04510, Mexico
e-mail: damor@unam.mx

1 Introduction

Pincer compounds have seen a tremendous amount of development in the last two decades [1–3]. This has been promoted, in part, by the creation and discovery of novel procedures for the synthesis of both the ligands and the corresponding complexes. The richness of pincer chemistry initially with rhodium [4–6] and reaching its peak with their iridium derivatives for the catalytic aliphatic C–H bond activation processes [4–10] has evolved to many different catalytic transformations [11–17], which is an important ingredient in the generation of hydrogen technology and the study of alternative energy sources [18, 19] and many other potentially relevant industrial transformations (see, for instance, [20]).

The increasing interest for these complexes has led to the exploration of other transition metals (see, for instance, [21, 22]). Initially this was done under the vain excuse of lowering the price of the catalyst, but later it became clear that the potential of "cheaper" metals such as iron or nickel could be found in a variety of aspects including the advantageous redox properties and the ability of these metals to produce alternative reaction mechanisms, for instance, for well-known and ubiquitous cross-coupling reactions, which are widely used in organic synthesis (see, for instance, [23] and references therein).

Thus, as it has been with the iridium and palladium pincer derivatives, POCOP–Ni compounds came to accelerate the discovery and improvement of different catalytic applications of organometallic nickel compounds, due to the ease of their synthesis, the comparatively low price of the metal due to its intrinsic earth abundance and the remarkable chemical properties and thermal stability of the complexes.

Although there have been some excellent recent reviews dealing with pincer complexes of nickel in a general manner [24–26], the increasing interest and research development on POCOP–Ni compounds and the study of their chemistry and catalytic applications have accelerated in the last lustrum, which is due to an improved comprehension of these systems and the discovery of novel applications. These developments have, in a way, served as inspiration for the study of similar systems based on other metals such as iron and cobalt. Thus, this chapter will review the chemistry of POCOP–Ni complexes from the synthesis of the first compound in 2006 [27] to the present day along with the catalytic applications that these species have had in the "almost" last decade.

Fig. 1 Potential points of modifications and tuning of pincer compounds
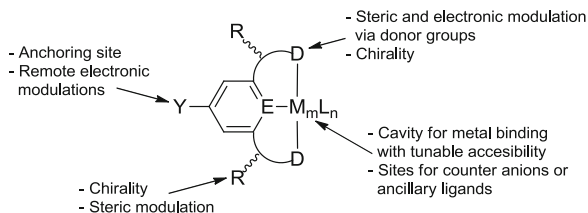
2 Synthesis

In 1976, Moulton and Shaw [28] reported the first examples of compounds that, due to the geometry that the ligands adopt around the metal centre, would be later labelled as "pincer complexes or pincer compounds" (Fig. 1). The thermal properties of these compounds (melting points above $200°C$) allowed these species to withstand continuous heating for prolonged periods without any apparent decomposition. The relevance of these properties and the versatility of this simple backbone were not exploited until recently. Nowadays, pincer compounds are a popular type of ligand widely employed in different areas of chemistry, from chemical sensors to extremely efficient catalysts for the activation of strong chemical bonds and for their use as synthons for the synthesis of dendrimers and nanomaterials to complexes with potential pharmaceutical applications (Fig. 1) [29].

Pincer structures have been modified to give a rich variety of chemical motifs that range from simple phosphines to N-heterocyclic carbenes (NHCs), thioethers, oxazolines and other more complex moieties. This structural diversity is only matched by the numerous applications that these complexes have found so far, particularly in the case of homogeneous catalysis [30–43].

Very often one of the caveats on the use of these complexes has been the sometimes difficult or tedious synthesis of the pincer ligands themselves and, in some cases, the inherent difficulty to C–H activate the ligand for the formation of their complexes, leading in many occasions to the synthesis of ligands including halogens or more acidic atom–H bonds to favour the oxidative addition process. This later concept has led to the discovery of a vast variety of different pincer ligands beyond the traditional aromatic PCP backbone. One large step forward was provided by Morales-Morales and Jensen and by Bedford [44, 45] in 2000 when they, independently, reported the synthesis of the first POCOP–phosphinite pincer systems (Fig. 2), thus providing a convenient answer to this synthetic problem.

Following these reports, the synthesis of the first POCOP–iridium species was done in 2004 [46, 47], and the rhodium [48], ruthenium [49, 50] and platinum [51] examples were subsequently reported in 2006. In the same year, Morales-Morales et al. reported for the first time the synthesis of a POCOP–nickel complex [NiCl$\{C_6H_3$-2,6-$(OPPh_2)_2\}$] [27]. This compound was obtained in a very facile manner from the reaction of the ligand [C_6H_4-1,3-$(OPPh_2)_2$] with $NiCl_2$ under reflux

Fig. 2 A schematic illustration of POCOP–Pd pincer compounds

Morales-Morales
&
Jensen

Bedford
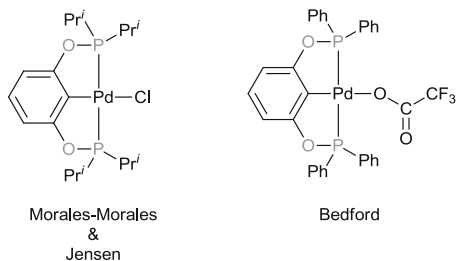
Fig. 3 Synthesis of the first $^{Ph}POCO^{Ph}P$–NiCl pincer compound
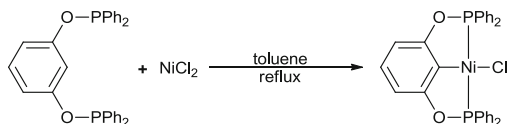
conditions in toluene in good yields (Fig. 3). The green compound $NiCl\{C_6H_3$-2,6-$(OPPh_2)_2\}$ is stable both to air and moisture.

The synthesis of the $[NiCl\{C_6H_3$-2,6-$(OPPh_2)_2\}]$ has been fundamental for the development of the chemistry of POCOP–Ni pincer compounds since it has served as the starting material of choice for most of the chemistry that has been developed to date. Thus, although there have been some modifications in order to generate this complex more rapidly, the ease of this initial procedure and the availability and low cost of the starting materials employed make it the preferred methodology. Most of the modifications to this protocol include the changing of the nickel source ($NiBr_2$, $[Ni(OAc)_2]$, $[Ni(NO_3)_2]$, etc.) or the use of more activated starting materials like $[NiBr_2L_n]$ (L=THF or MeCN; $n = 1.5$ or higher depending on the conditions of preparation) along with the use of bases [52]. However, no significant increase in yield has been reported.

It is worth mentioning that there are three other methods that have been reported recently. Although the approaches are very similar, these procedures may define the further progress of the POCOP–Ni pincer chemistry. The first one uses Ni(0) powder in a one-pot procedure [53]. The reasoning behind this method is very interesting; if the reaction to synthesize the ligand produces HCl, its reaction with the Ni (0) powder may actually generate $NiCl_2$ in situ which in turn reacts with the POCHOP ligand to generate the POCOP–NiCl complex plus hydrogen and more HCl (Fig. 4). However, this method suffers from some limitations, since it is not general for the synthesis of POCOP–Ni complexes and specifically it is unpractical for the synthesis of $^{Ph}POCO^{Ph}P$ derivatives (low yields) and only works in the case of nickel, this being attributed to the intrinsic redox properties of palladium, for instance (difficult to oxidize).

The second approach first reported for palladium and recently reported for nickel (2012) consists in another one-pot synthesis [54, 55]. This is more similar to the traditional procedure with subtle changes, such as the solvent and the bases employed, essentially furnishing the same yields. Interestingly, this procedure

Fig. 4 Synthesis of POCOP–NiCl complexes from Ni(0)

R= ^{i}Pr, R'= 4-H, 4-MeO, 4-COOMe, 3,5-^{t}Bu
R= Ph, R'= 4-H
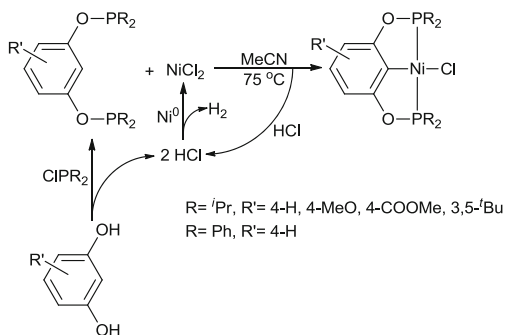
Fig. 5 One-pot synthesis of POCOP–NiCl compounds

R= cyPe, Me
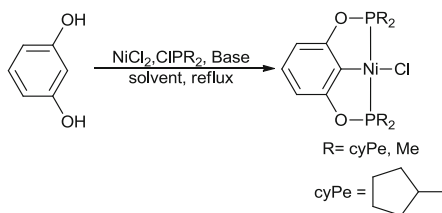
cyPe =

allowed the synthesis of the P-alkyl-substituted ^{cyPe}POCO^{cyPe}P–NiCl (DMAP, THF) and ^{Me}POCO^{Me}P–NiCl (NaH, toluene) derivatives (Fig. 5).

The third method, although not in a single pot, offers, for the first time, the possibility of further functionalization at the aromatic moiety of the complexes obtained by introducing a –OH functionality at the *para*-position of the pincer complex [56]. This hydroxyl group can subsequently be derivatized with any of a variety of functionalities including groups that allow the POCOP–Ni complexes available to be supported on common polymeric supports. The principle is simple; in a typical procedure, stoichiometric control of the chlorophosphine over phloroglucinol (2:1 ratio) furnishes cleanly the *p*-hydroxy PO^{3-OH}CHOP ligands, which upon further reaction with NiCl$_2$ afford the corresponding 4-hydroxy-substituted PO^{4-OH}COP–NiCl complexes in good yields. Although this framework was already known and employed successfully to support iridium derivatives over silica [10], the reported method was long and tedious and limited to iridium thus hampering the further progress of this chemistry. The present procedure allowed the facile synthesis of three ligands ^{R}PO^{4-OH}CHO^{R}P (R=Ph, ^{i}Pr, ^{t}Bu) and their corresponding nickel derivatives ^{R}PO^{4-OH}CO^{R}P–NiCl (R=Ph, ^{i}Pr, ^{t}Bu). As a proof of concept, the complex ^{tBu}PO^{4-OH}CO^{tBu}P–NiCl was easily functionalized with different acid chlorides to produce four different derivatives (Fig. 6).

In order to have a complete vision of the procedures used for the synthesis of POCOP–Ni complexes, two more examples are worth mentioning. The first one uses a method reported earlier by Uozumi [57] for palladium complexes, which involves the use of an iodoresorcinol derivative and low oxidation state metal complex to promote the oxidative addition. A variant of this method directly reacts iodoresorcinol with the metal complex, which upon oxidative addition produces an
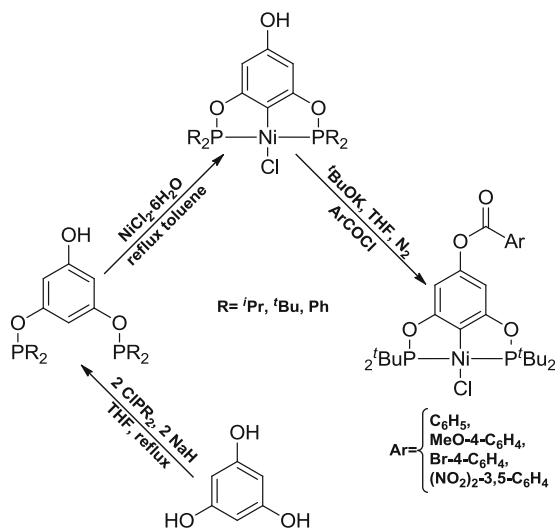
Fig. 6 Synthesis and functionalization of *para*-hydroxy-functionalized POCOP–NiCl
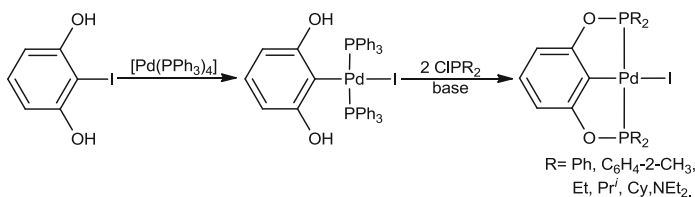
Fig. 7 Uozumi's procedure for the synthesis of POCOP–PdI complexes

aryl metal iodide intermediate that is further reacted with the corresponding chlorophosphine derivative in the presence of a base to afford the desired pincer complex (Fig. 7). This method becomes relevant when acid labile, thermally unstable or sterically bulky substituents are included on the pincer ligand, since direct cyclometallation by C–H activation often requires high temperatures and prolonged reaction times formally releasing acid. Using this procedure, Balakrishna [58] produced a series of cyclodiphosphazane-based pincer complexes of group 10 metals including the Ni(II) derivative (Fig. 8).

In contrast, the somewhat similar phosphoramidate species were cleanly obtained in high yield by Hartwig and Driess [59] by reacting the corresponding phosphoramidate pincer ligand with [NiBr$_2$(dme)] via C–H activation (Fig. 9).

Thus, it becomes clear that there is no general method to obtain POCOP–Ni complexes and that the structure of the backbone of the pincer, substituents at the phosphorus donors, the use or not of base, nickel starting material and the solvent used are determinants in the production of these most interesting species.
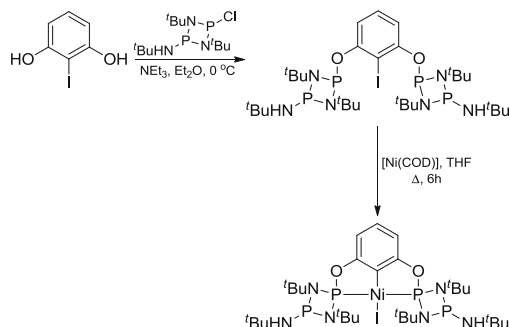
Fig. 8 Synthesis of cyclodiphosphazane POCOP–NiI complexes by Uozumi's method
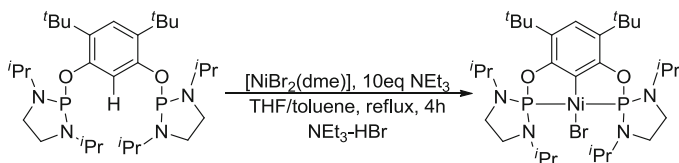
Fig. 9 Synthesis of a phosphoramidate POCOP–Ni compound

3 Reactivity

As with most of the known pincer compounds, POCOP–Ni pincer derivatives have been used as catalysts for different organic transformations. During this process, the understanding of how the substrates bind to the metal centre and the properties of the ligands that can affect these reactivities has been the motif of different studies. These studies have driven the rationalized synthesis of some of these complexes, while a better comprehension of the tuning of both steric and electronic effects has allowed their performance to be improved in some catalytic reactions. Thus, most of the reactivity studies have focus on the variation of R groups at the P donors, substitution reactions of the counter ion for other counter ions or labile substituents in order to promote substitution reactions or to promote the reactivity of these reactants and finally modifications to the backbone of the POCOP ligand. Although this later point has mostly been limited to the commercially available resorcinols, a few examples have involved the synthesis of other novel resorcinol structures. However, this has not hampered the synthesis of a myriad of POCOP–Ni pincer derivatives (Fig. 10).

Figure 10 illustrates the different possible combinations that have been achieved (it is important to mention that not all combinations have been possible, and for concrete combinations, one has to refer to the corresponding references), some of which have been fully characterized inclusive by single crystal X-ray diffraction analysis.
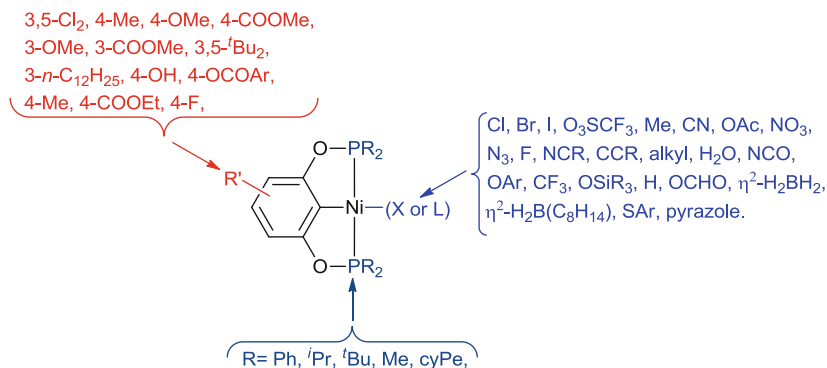
Fig. 10 A schematic illustration of substitution points and substituents known in POCOP–Ni pincer compounds
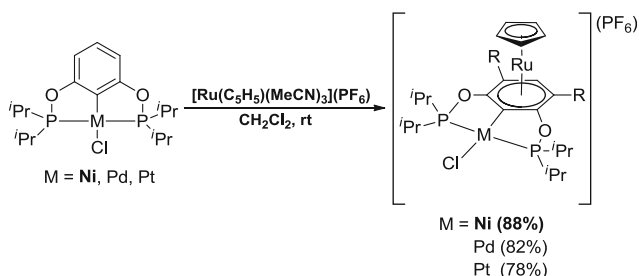
Fig. 11 Synthesis of bimetallic sandwich POCOP–Ni compounds

In general, variations of X or L have been achieved by the addition of silver salts AgX [e.g. Ag(SO$_3$CF$_3$)], which exchange the anionic ligand (generally a halogen) for a labile counter anion, which promotes the subsequent substitution by potentially coordinative solvents (e.g. MeCN, H$_2$O, etc.) or substrates (e.g. $^-$SAr, etc.). For the alkyl, $-$OSiR, $-$CF$_3$, $-$N$_3$ and hydride substituents, a more direct approach can be used by reacting Grignard reagents, Me$_3$SiL (L=$-$OK, $-$CF$_3$, $-$N$_3$) and LiAlH$_4$, respectively, directly with the nickel halide [60–68].

These compounds will become relevant in the next section for the catalytic applications of these compounds.

Thus far, the functionalization of POCOP–Ni pincer compounds has been carried out in a traditional manner. However, two examples worthy of highlighting include the use of the aromatic ring on the POCOP backbone as an arene functional group. Although this idea was first reported for the case of POCOP complexes, the concept is not new and has been exploited before for NCN, SNS and PCP [69–79] pincer compounds. Thus, taking advantage of the arenophilicity of the fragment [CpRu]$^+$, its reaction with ^{iPr}POCO^{iPr}P–NiCl produced in a simple manner η^6,η^1-bimetallic complexes in good yields [80] (Fig. 11). This coordination of the ruthenium moiety makes the two faces of the ^{iPr}POCO^{iPr}P–NiCl nonequivalent,
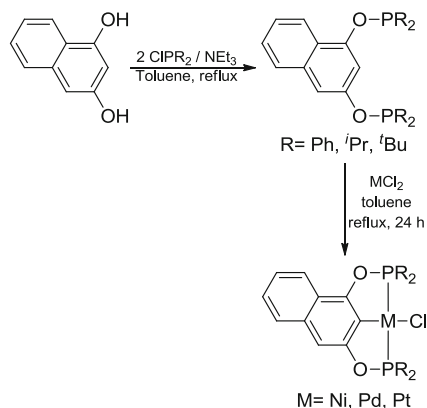
Fig. 12 Synthesis of POCOP compounds derived from naphthoresorcinol

[M] = [Cp*Ru(NCMe)$_3$]PF$_6$ (3) or [CpRu(NCMe)$_3$]PF$_6$ (4); CH$_2$Cl$_2$, R.T./24 hrs
[M] = [Cp$_2$Fe]; a) AlCl$_3$/ClCH$_2$CH$_2$Cl, Reflux/2hrs, b) NH$_4$PF$_6$/H$_2$O
[M] = [Cr(C$_{10}$H$_8$)(CO)$_3$]; THF, R.T./24 hrs
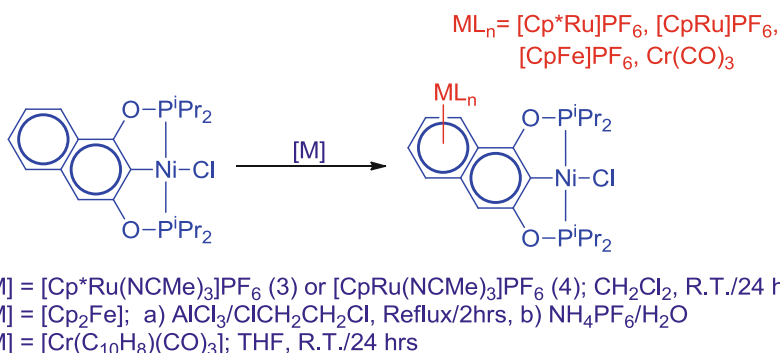
Fig. 13 Synthesis of bimetallic sandwich PO^{Naph}COP–Ni compounds

and thus the P-isopropyl groups become stereotopic. This reactivity could be very important in terms of catalysis since the introduction of another metal may produce cooperative effects, which in turn might be relevant in tandem catalytic processes.

This concept has been further exploited, and the same group has introduced a novel naphthalene backbone to the rich series of PO^{naph}COP–Ni compounds [81] (Fig. 12).

The structure of these ^{R}P^{naph}CO^{R}P–NiCl pincer compounds is very interesting since it renders the two phosphorus donor nuclei nonequivalent as determined by NMR experiments and confirmed by single crystal X-ray diffraction analyses. The nonsymmetry of these compounds brings consequences since the products of the reactions between the *iso*propyl derivatives ^{iPr}PO^{Naph}CO^{iPr}P–NiCl and [RuCp*], [RuCp]$^+$, [FeCp]$^+$ or [Cr(CO)$_3$] produced a series of chiral heterobimetallic complexes [82] (Fig. 13). Moreover, the reaction is regiospecific, and only coordination on the non-cyclometallated ring is observed. These bimetallic complexes have not yet been tested as catalysts.

An examination of the reactivity of POCOP–NiCl complexes clearly shows that modification of the ligand, neutral or anionic, bound to the Ni centre of different POCOP complexes is not only possible but easy and a rich variety of ligands can be used. Although some of these species were identified during the study of different POCOP–Ni-catalysed reactions, others were synthesized with the aim of further developing catalytic processes or promoting the activation of small molecules such as H_2 or CO_2, building the foundation to further develop interesting catalytic transformations. Some of which will be discussed in the following section.

4 Catalysis

Among the vast number of applications that pincer compounds have found in different areas of chemistry, their use as catalysts is perhaps one of the most popular due to their well-known physical properties and chemical reactivity, and POCOP–Ni complexes have not been an exception. These compounds have become more relevant in recent times due to the fact that, among precious metals, the use of nickel reduces costs, but more importantly nickel compounds can undergo facile oxidative addition and provide ready access to multiple oxidation states, facts that have allowed the development of a broad range of innovative reactions. These inherent properties of nickel in combination with the properties that the pincer framework confers to their derivatives have been increasingly understood in recent years and used to perform transformations long considered exceptionally challenging. Thus, in this section, we discuss some of the most recent and significant developments in homogeneous catalysis using POCOP–Ni compounds. The different catalytic applications are presented in chronological order more than classifying the reactions in groups, e.g. cross-coupling reactions.

4.1 Thiolation (C–S Cross-Coupling)

The synthesis of the first POCOP–Ni complex was accompanied by the first catalytic application of these complexes. Thus, the $^{Ph}POCO^{Ph}P$–NiCl compound was employed successfully as catalyst for the C–S cross-coupling of iodobenzene with a broad scope of disulphides [27]. This process required the presence of metallic zinc to afford nonsymmetric sulphides in good to excellent yields. The yields of the reactions were affected by the size of the substituents at the disulphide; thus, small substituents such as methyl afforded the higher yields (methyl phenyl sulphide), while *tert*-butyl disulphide only afforded 49% yield of the *tert*-butyl phenyl sulphide and a considerable percentage of biphenyl as the homocoupling by-product (Fig. 14).

A mechanism was proposed for this process (Fig. 15).
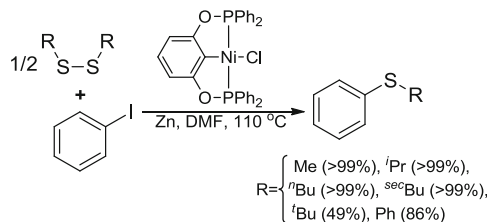
Fig. 14 Thiolation of iodobenzene with disulfides catalysed by POCOP–NiCl
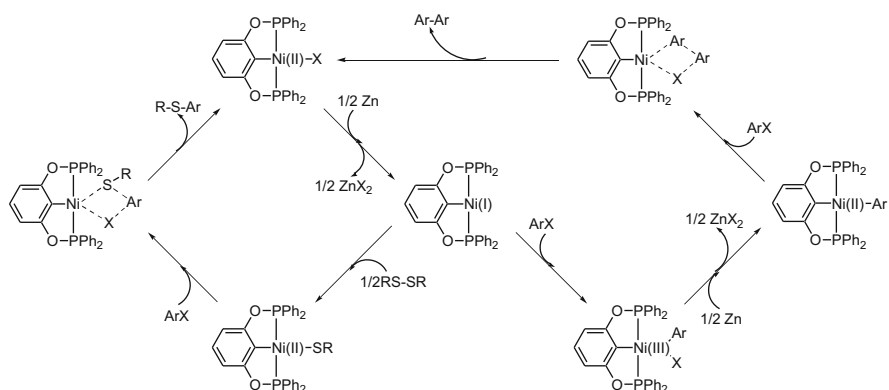
Fig. 15 Proposed mechanism for the thiolation of iodobenzene with disulphides catalysed by a POCOP–NiCl pincer compound

R_1= Me, OMe,CF$_3$, CN
R_2= 4-Me, 3-Me, 2-Me, 4-OMe
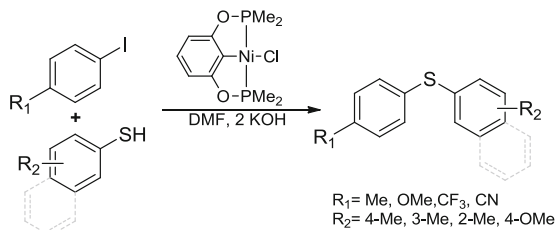
Fig. 16 Thiolation of iodobenzenes with thiophenols catalysed by POCOP–NiCl in the presence of NaOH

By changing the substituents at the P donors by an alkyl substituent, this process was later optimized (yields to the nonsymmetric disulphides >90% in all examples reported) for different iodobenzenes *albeit* using thiophenols instead of disulphides and KOH as base [54, 55] (Fig. 16). However, the change of the conditions also led to the degradation of the catalyst ^{Me}POCO^{Me}P–NiCl, reaching the conclusion that most likely these cross-couplings are catalysed by secondary phosphine oxide Ni (0) species rather than the pincer catalyst.

Fig. 17 Thiolate pincer
compound, synthesis and
reactivity
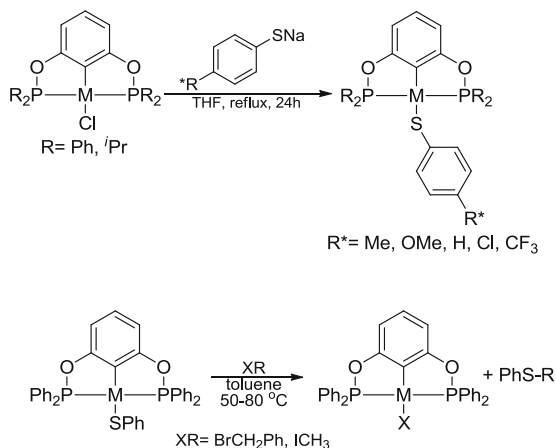
Related to these later results, several thiolate POCOP–NiSR complexes were synthesized (Fig. 16), where the substituents at the phosphorus donors and on the thiolates were varied and further alkylated under controlled conditions, for instance, with MeI [83] (Fig. 17).

These compounds were also crystallized, and the Ni–S distances compared systematically the finding that for most of the complexes obtained, the Ni–S distances are neither affected by the basicity of the thiolate nor by the pincer P-substituents, but certainly affected by the electronic effect of the *para*-substituent at the thiolate, leading to stronger Ni–S bonds when electron-withdrawing groups are present. Moreover, when the POCOP ligand is less electron donating, the Ni–S is more sensitive to changes in the thiolate substituent, which was attributed to the increased electrostatic contribution in bonding. These observations in combination with mechanistic studies lead to the conclusion that either an S_N2-type mechanism or a σ-bond-metathesis-like mechanism is taking place [83].

4.2 *Hydroamination and Alcoholysis of Unsaturated Nitriles (Michael Additions)*

Alkynes and alkenes are recognized as two of the most important building blocks for the synthesis of a wide variety of derivatives relevant in both industry and fine chemistry [84, 85]. The direct addition of amines to alkynes and alkenes (hydroamination) [86] represents a convenient, straightforward and high atom economy method for the synthesis of N-derivatives such as amines, imines and enamines in one step. In general, intramolecular hydroamination proceeds faster than intermolecular reactions both thermodynamically and kinetically. In order to promote the hydroamination of C–C unsaturations, a wide variety of catalysts have been developed [87, 88].
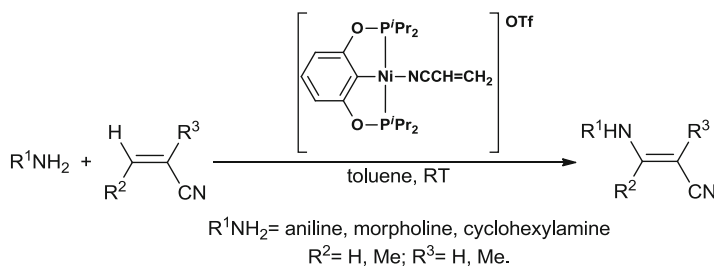
Fig. 18 Hydroamination of unsaturated nitriles catalysed by POCOP–Ni compounds

In the case of POCOP–Ni complexes, the first reports employing these compounds as catalysts for the hydroamination of unsaturated nitriles were reported in 2007 [89]. Although preliminary, the results showed that [^{iPr}POCO^{iPr}P-Ni-(acrylonitrile)]OTf efficiently catalysed the hydroamination (Michael addition) of morpholine, CyNH$_2$ and PhNH$_2$ to acrylonitrile, crotonitrile and methacrylonitrile, respectively (Fig. 18). The reaction of the more nucleophilic amine, morpholine, proceeds at room temperature with a high TON in the range of 10^3.

Further studies by the same group examined the potential effects of substituents on the aromatic backbone of the POCOP–Ni catalyst [90]. Thus, introduction of electron-withdrawing chloride substituents was installed to give ^{iPr}PO$^{3,5-}$^{Cl2}CO^{iPr}P–NiBr. Initial comparison of the parent compounds ^{iPr}POCO^{iPr}P–NiBr and ^{iPr}PO$^{3,5-Cl2}$CO^{iPr}P–NiBr by cyclic voltammetry and X-ray indicates that indeed the introduction of chlorides on the aromatic moiety reduces the Ni centre's electron richness. However, this effect is subtle, since, in the solid state, parameters such as Ni–C and Ni–P bond distances do not significantly vary as a consequence of this substitution. In fact, these catalysts are most sensitive to factors such as the choice of solvent and the amine–olefin ratio, rather than substituents on the backbone. Furthermore, reactivity studies have shown that these structural differences have little impact on the catalytic performance of the cationic complexes in the hydroamination of acrylonitrile with aniline (Fig. 19). The results obtained suggest that the cationic POCOP–Ni catalysts employed may follow a mechanism where the nickel centre is simply acting as a Lewis acid activating the olefin towards nucleophilic attack, thus efficiently promoting the hydroamination process, and base on the results obtained, a reaction mechanism was proposed (Fig. 20).

The above-mentioned results have served to set the grounds for further applications of these cationic catalysts in other similar transformations. In fact, given the close similarity of amines with alcohols and phenols, the addition of the latter was also envisioned with the use of the very same catalysts. This idea came out based on the above-mentioned mechanistic proposal (Fig. 20). Thus, the reasoning was that POCOP–Ni precatalysts based on a less nucleophilic POCOP ligand should generate more electrophilic cationic intermediates wherein the coordinated cyano-olefin should experience greater activation towards nucleophiles. Thus, the catalytic activity of the in situ-generated [(^{iPr}POCO^{iPr}P–Ni–NCR*)OTf] and [^{Ph}POCO^{Ph}P–Ni–NCR(OTf)] complexes was examined. The parent [^{iPr}POCO^{iPr}P–NiOTf] and
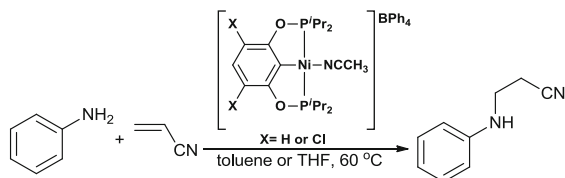
Fig. 19 Effect of substituents in the aromatic backbone over the hydroamination of unsaturated nitriles catalysed by POCOP–Ni compounds
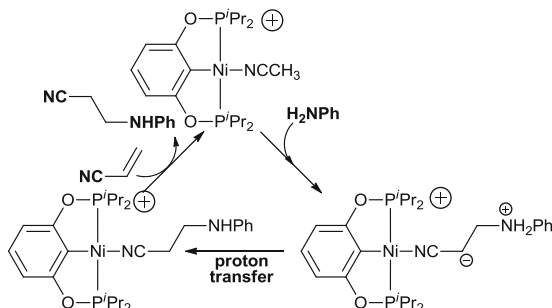
Fig. 20 A mechanism proposal for the hydroamination catalysed by POCOP–Ni compounds (Lewis acid approach)
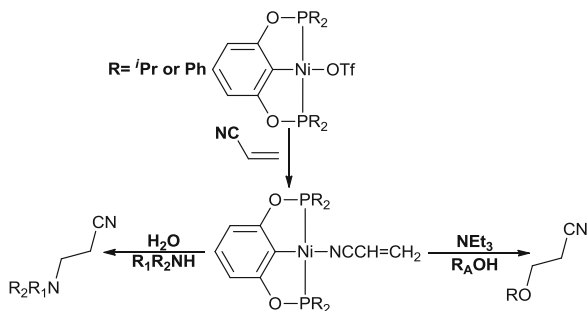
Fig. 21 Hydroamination and alcoholysis of unsaturated nitriles catalysed by POCOP–Ni complexes

[^{Ph}POCO^{Ph}P–NiOTf] complexes served as precatalysts for the regioselective, anti-Markovnikov addition of aliphatic and aromatic amines and alcohols to acrylonitrile, crotonitrile and methacrylonitrile [91, 92] (Fig. 21). Additionally, the influence of additives in the catalytic activities was also explored. Initially the first clues were provided by infrared spectroscopy, where a small but significant difference between the ν(CN) of [^{R}POCO^{R}P–Ni–NCR*)]$^{+}$ (R=Ph, 2,297 cm^{-1}, and ^{i}Pr, 2,292 cm^{-1}) indicates greater N → Ni σ-donation to the [^{Ph}POCO^{Ph}P–Ni–NCR*)]$^{+}$ fragment, which indicates these cationic adducts are more electrophilic.

Fig. 22 Effect of O_2/H_2O over the $^{Ph}POCO^{Ph}P$–NiOTf catalyst [92]

crystal structure
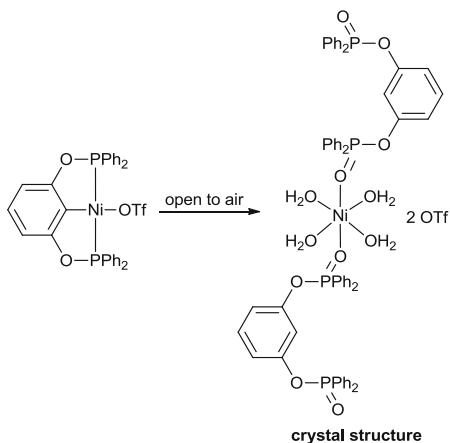
In spite of this, the complex [$^{iPr}POCO^{iPr}P$–NiOTf] is a better catalyst for the hydroamination of acrylonitrile. However, as predicted, the complex [$^{Ph}POCO^{Ph}P$–NiOTf] is a much more effective catalyst in the same process when water is used as a proton-transfer agent instead of NEt_3. In fact, [$^{Ph}POCO^{Ph}P$–NiOTf] also proved to be a better precatalyst for the alcoholysis of acrylonitrile. Another important difference is that hydroamination works better with more nucleophilic amines, while the alcoholysis process works better with ArOH, CF_3CH_2OH and $ArCH_2OH$ and does not proceed with more nucleophilic aliphatic alcohols such as MeOH, EtOH and $^{i}PrOH$. In terms of the nitriles, both hydroamination and alcoholysis work best with acrylonitrile (Fig. 21).

In addition, the reactivity of both catalysts [$^{R}POCO^{R}P$–Ni–NCR*)]$^+$ (R=Ph, ^{i}Pr) was strongly related to their reactivity with the additives NEt_3 and H_2O [92]. The competitive binding of NEt_3 to the nickel centre is more effective in [$^{Ph}POCO^{Ph}P$–Ni–NCR*)]$^+$ and therefore hampers the catalytic activity of this species. In contrast, the combination of this compound with water makes this system highly efficient in promoting hydroamination reactions despite the fact that this species is more prone to hydrolysis than the ^{i}Pr analogue [92] (Fig. 22).

It is noteworthy that the catalytic cycle for the alcoholysis reactions presumably does not proceed by the same Lewis acid mechanism proposed for the hydroaminations reactions (Fig. 23).

Fig. 23 Mechanistic proposal for the alcoholysis of unsaturated nitriles catalysed by POCOP–Ni complexes
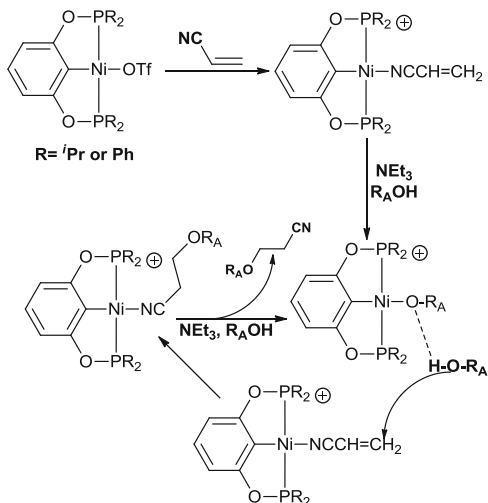
4.3 Hydrosilylation of Aldehydes and Ketones

The hydrosilylation reaction of aldehydes and ketones generates silyl ethers with Si–H bond addition to carbonyl compounds. The hydrolysis of the silyl ether gives rise to the corresponding alcohol. This process can be used as a convenient, mild alternative for the reduction of unsaturated compounds. The reduction of aldehydes and ketones is one of the most important transformations in organic synthesis and in the pharmaceutical industry. Thus, this reaction has not escaped the broad scope of applications of pincer compounds or of POCOP–Ni complexes.

In this sense, the application of POCOP–Ni complexes in this process was a consequence of another significant discovery, the synthesis and characterization of the first POCOP–NiH hydride complex [93]. As we will see later, this compound has opened a number of possibilities for further interesting applications; some of them derived from these first observations.

Thus in 2009, the reaction of ^{R}POCO^{R}P–NiCl (R=Ph, ^{i}Pr or ^{t}Bu) with LiAlH$_4$ cleanly gave the hydride species POCOP–NiH (Fig. 24), except in the case of ^{Ph}POCO^{Ph}P–NiCl, which when reduced with LiAlH$_4$, NaBH$_4$ or LiEt$_3$BH only gave intractable mixtures of products [93].

Initial reactivity studies of ^{R}POCO^{R}P–NiH (R=^{i}Pr, ^{t}Bu) with benzaldehyde were carried out observing a fast insertion of the C=O bond to produce the benzyloxide derivative [93]. As expected, ketones were less reactive than PhCHO. In order to complete the catalytic cycle, the complex ^{iPr}POCO^{iPr}P–Ni–OCH$_2$Ph was reacted with silanes, which reformed the parent compound ^{iPr}POCO^{iPr}P–Ni–H. Both PhSiH$_3$ and Ph$_2$SiH$_2$ worked perfectly for the complete regeneration of the hydride compound releasing the corresponding silyl ether. Under the established conditions, a series of hydrides were examined, and all gave good to excellent yields, and a catalytic cycle was subsequently proposed [93] (Fig. 25).

Fig. 24 Synthesis of hydride POCOP–NiH pincer compounds

R= ^{i}Pr, ^{t}Bu, Ph   R= ^{i}Pr, ^{t}Bu, Ph (*not isolated*)
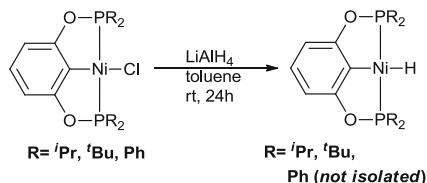
Fig. 25 Proposed catalytic cycle for the hydrosilylation of aldehydes catalysed by POCOP–NiH complexes
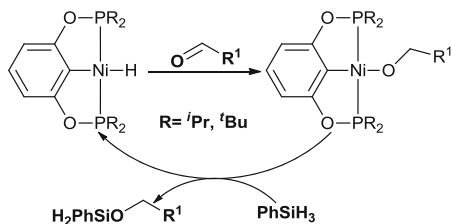
These results established the bases for the following process to be discussed where the greenhouse gas CO_2 is reduced.

4.4 Carbon Dioxide Reduction

Climate change influenced by human activities has led to a significant increase in greenhouse gas emissions, which has led to emphatic actions from decision-making bodies and policymakers. In order to avoid potential catastrophic consequences of global warming, a political consensus was established concerning the rise of temperatures limited to 2°C above pre-industrial levels as a global target. As an effect of the Kyoto Protocol, industrialized countries were committed to reducing greenhouse gas emissions to 8% below "base year" 1990 levels before 2012. Further decreases of emissions are planned by the year 2020.

The use of CO_2 in chemical processes cannot provide a global solution to the reduction of anthropogenic carbon dioxide emission. It is, however, an attractive option to decrease emissions. Thus, the recycling of carbon dioxide with the possibility to make valuable products seems an economic and environmentally friendly alternative. CO_2 can be a source of carbon for production of hydrocarbons, monomers for polymers (e.g. polycarbonates), synthetic fuels (alcohols, hydrocarbons), fertilizers and food. Several routes and technological schemes that involve CO_2 conversion into valuable, commercial products are taken into account. The existing conversion pathways include production of such chemicals as urea, methanol, cyclic carbonates and salicylic acid. The emerging strategies embrace CO_2-based polymers, dry reforming or hydrogenation to formic acid; and other conversion routes like production of isocyanates, organic carbonates, lactone and carboxylic acids and their synthesis are currently being explored. While catalysts for the synthesis of some of these compounds, like formic acid or methanol, already exist,
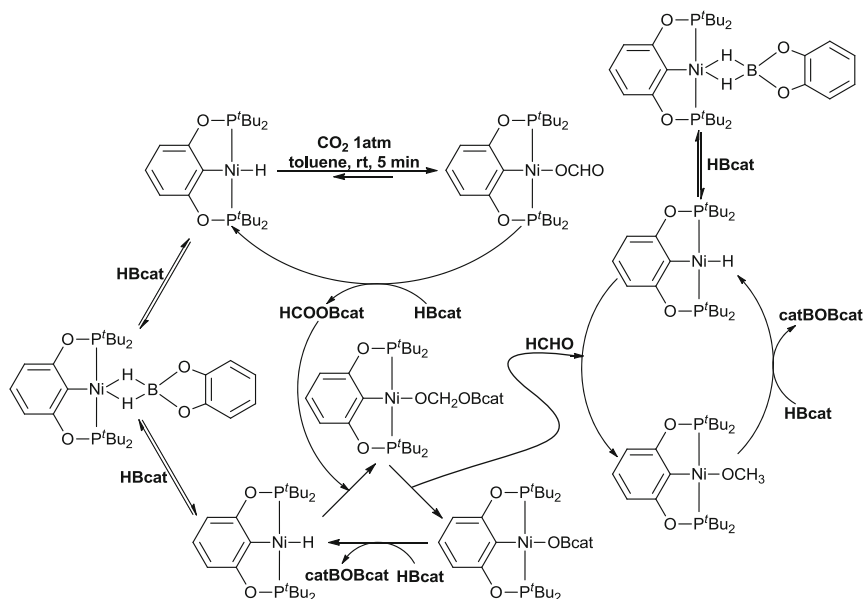
Fig. 26 A proposed mechanism for catalysed reduction of carbon dioxide by POCOP–NiH complexes

future research may focus on attaining synergistic catalysts based on combining more powerful catalysts with high catalytic activity.

In this sense, and based on the results presented in the previous section, the potential activation of CO_2 was conceived. Thus, despite the high thermodynamic stability of CO_2, the reaction of this compound with the pincer complex $^{tBu}POCO^{tBu}P$–Ni–H proceeds rapidly at room temperature to afford the nickel formate complex $^{tBu}POCO^{tBu}P$–Ni–OCHO (this process being reversible) [94]. Based on these results and as it was the case for the hydrosilylation of aldehydes (vide supra), regeneration of $^{tBu}POCO^{tBu}P$–Ni–H from $^{tBu}POCO^{tBu}P$–Ni–OCHO would complete the potential catalytic cycle for the reduction of CO_2. Indeed, reaction of $^{tBu}POCO^{tBu}P$–Ni–OCHO with 1 equiv. of catecholborane (HBcat) afforded $^{tBu}POCO^{tBu}P$–Ni–H with a new boron species identified as HCOOBcat. Interestingly, when HBcat was employed in a large excess, another species was formed and identified as a methanol derivative CH_3OBcat. CH_3OBcat proved to be hygroscopic absorbing moisture quickly from air to generate CH_3OH. It was also discovered that the reduction of CO_2 with HBcat was catalytic in nickel. Thus, a mixture of HBcat and $^{tBu}POCO^{tBu}P$–Ni–H in a 500:1 ratio under 1 atm of CO_2 generates CH_3OBcat (495 TON-based on B-H) in 1 h with a boron by-product (catBOBcat) that precipitates from the reaction media. The results allowed the proposal of a catalytic cycle (Fig. 26), where the catalytic reduction of CO_2 begins with a reversible insertion of CO_2 into the Ni–H bond of $^{tBu}POCO^{tBu}P$–Ni–H. Then, the cleavage of the Ni–O bond with HBcat regenerates $^{tBu}POCO^{tBu}P$–Ni–H and

releases HCOOBcat, which in turn is reduced by another HBcat (Fig. 26). A second cycle involves the hydroboration of the formaldehyde, analogously to the nickel-catalysed hydrosilylation of aldehydes presented above (vide supra). Thus, reduction of paraformaldehyde with HBcat in the presence of $^{t\text{Bu}}POCO^{t\text{Bu}}P$–Ni–H yields CH_3OBcat. A catalytic cycle for the whole process was also proposed (Fig. 26). This mechanism was also examined by the means of computational studies leading to the conclusion that the choice of hydrogen source for the reduction of CO_2 is strongly dependant on the catalyst employed [95, 96]. Further experimental mechanistic analysis of this process revealed that the substituents at the P donor atoms as well as of the type of borane employed strongly effect the process. Thus, the catalytic reactions are fast when the nickel catalyst contains bulky substituents on the phosphorus donor atoms. The primary benefit of bulky P-substituents is that they provide protection to the P–O bonds of the pincer ligand from the borane attack, which minimizes catalyst degradation [55, 97].

4.5 Cyanomethylation of Aldehydes

POCOP–Ni pincer compounds have also found application in a process that is interesting in its own right, cyanomethylation. This procedure provides easy access to a large variety of pharmaceutically important compounds through the resultant β-hydroxy nitriles [98–101]. Although some synthetic methods are available, issues such as the use of highly toxic cyanide salts (for the ring opening of epoxides), difficulty in using unactivated simple alkyl nitriles and incompatible reaction conditions with base-sensitive substrates often leading to the loss of the hydroxy group by dehydration have limited the development and wide application of this process and are still to be solved.

In order to produce better results, transition metal catalysts have been employed. The hypothesis behind this idea is that a Lewis acidic metal centre would substantially lower the pKa value of acetonitrile once it is coordinated to the metal. To this end, the compound $^{i\text{Pr}}POCO^{i\text{Pr}}P$–Ni–$CH_2CN$ was synthesized and used as a catalyst for the cyanomethylation of a variety of aldehydes in good to excellent yields at room temperature in the absence of base [102]. The catalyst was easily obtained from the reaction of $^{i\text{Pr}}POCO^{i\text{Pr}}P$–NiCl with $LiCH_2CN$; the compound is air and moisture stable both in the solid state and in solution [102] (Fig. 27). Mechanistic studies suggest a reversible insertion of the aldehydes into a C-bound cyanomethyl complex and subsequent activation of acetonitrile with the resulting nickel alkoxide intermediate. A catalytic cycle was proposed [102] (Fig. 28).

Fig. 27 Synthesis of the catalyst ^{iPr}POCO^{iPr}P–Ni–CH$_2$CN
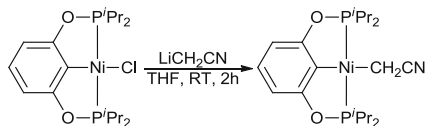
Fig. 28 Mechanistic proposal for the cyanomethylation of aldehydes catalysed by ^{iPr}POCO^{iPr}P–Ni–CH$_2$CN
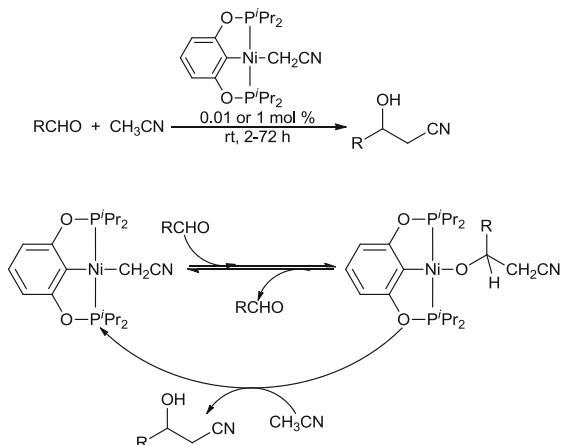
4.6 Alkyl–Alkynyl Cross-Coupling Reactions

Due to the relevance that palladium compounds have had in cross-coupling reactions, it should come as no surprise that researchers would explore the reactivity of analogous nickel derivatives for this kind of reaction. This area of chemistry has advanced significantly in recent years. However, as it was for palladium, optimization of the processes, softening the reaction conditions and reducing the catalyst loading, among other modifications, are still to be resolved. In this sense and due to the high degree of success that pincer compounds have had in cross-coupling processes, in recent years different research groups have turned their attention to the use of POCOP–Ni complexes as catalysts for these important transformations.

One example is the use of the compound ^{Ph}POCO^{Ph}P–NiCl as a highly efficient catalyst for the cross-coupling of alkyl and alkynyl groups. Over the past decades, the alkynylation of Csp^2 halides conducted either with alkynylmetal reagents or directly with terminal alkynes has emerged as an extremely powerful method for the synthesis of alkynes. Unfortunately, nonactivated alkyl halides have been a challenge since the oxidative addition process of these compounds is far more difficult and because alkyl metal intermediates may undergo side reactions like β-H elimination. Thus, to date most of the research efforts have focused on the use of alkyl and aryl metal nucleophiles, and only a few examples of coupling reactions with alkynyl nucleophiles have been reported.
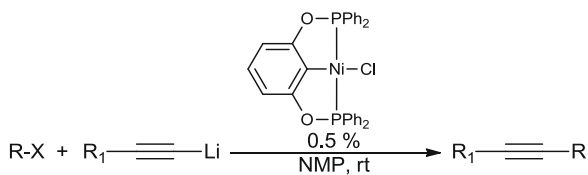
Fig. 29 Alkyl–alkynyl coupling reactions catalysed by $^{Ph}POCO^{Ph}P$–NiCl
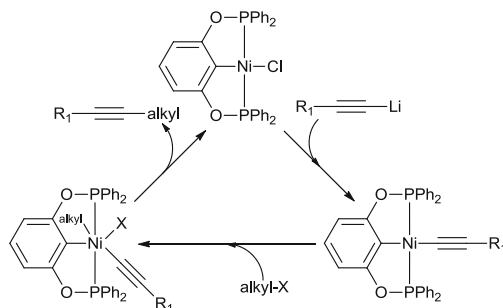
Fig. 30 Mechanistic proposal for the alkyl–alkynyl coupling reactions catalysed by $^{Ph}POCO^{Ph}P$–NiCl

Thus, the complex $^{Ph}POCO^{Ph}P$–NiCl was used as a catalyst for the cross-coupling of a series of unactivated alkyl halides with alkynyllithium reagents at room temperature, affording good to excellent yields in most of the cases explored, giving better results as compared to Sonogashira protocols, for instance [103] (Fig. 29). A catalytic cycle was proposed invoking a Ni(IV) active species, although no evidence was provided to support the generation of such a species (Fig. 30).

4.7 Homocoupling of Benzyl Halides

Organic molecules including dibenzyl motifs in their structure have been used as key intermediates for the synthesis of dyes, polymers, agrochemicals and pharmaceuticals. The synthesis of these compounds has been carried out usually employing low oxidation state transition metal catalysts; however, the use of well-defined complexes has been scarce. Thus, a series of POCOP–Ni–X complexes were used as catalysts in the presence of zinc powder for the homocoupling of a number of bromobenzyl derivatives in good to excellent yields [104] (Fig. 31). Variations on the structure of the benzene moiety of the pincer catalyst revealed that the substituents at the *para*-position have little effect on their catalytic activity. The same

Fig. 31 Homocoupling of benzyl halides catalysed by POCOP–NiCl pincer complexes
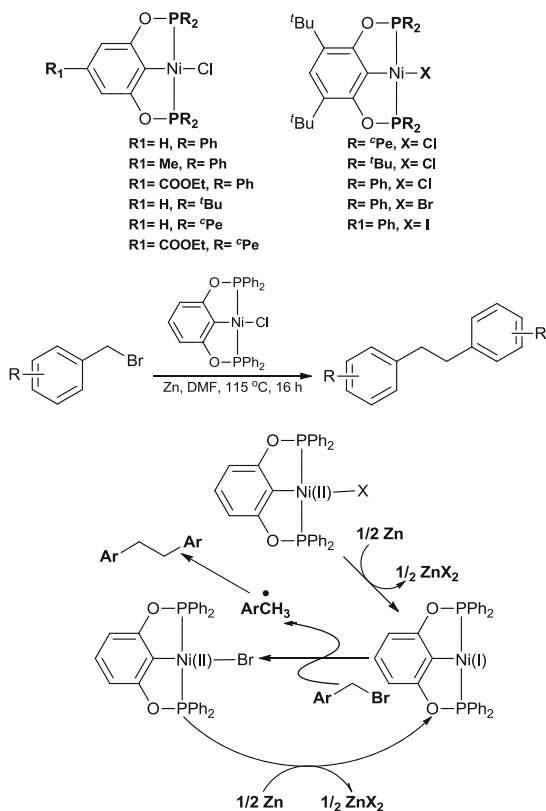
null effect was observed for the catalyst with sterically hindered substituents at the benzene moiety of the compounds. However, the activity of the catalyst was clearly influenced by the substituents at the phosphorus donors; thus, the complexes with the more electron-rich phosphine donors afforded lower yields of homocoupling products. Different halides bound to the nickel centre make no difference in the reactivity of the catalysts. Based on these observations, $^{Ph}POCO^{Ph}P$–NiCl was chosen as the preferred catalyst for this process, and a catalytic cycle was proposed (Fig. 31).

4.8 Suzuki–Miyaura Couplings

Among the cross-coupling reactions, the Suzuki–Miyaura protocol stands out as one of the most important transformations in organic chemistry and has been considered a cornerstone of modern organic synthesis [105]. The evolution of this
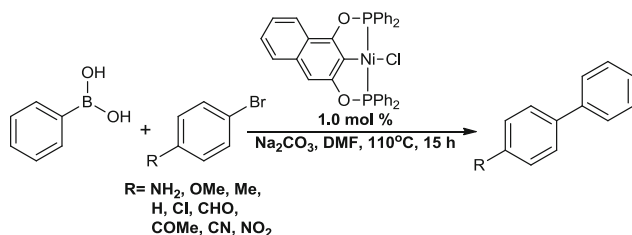
Fig. 32 Suzuki–Miyaura couplings catalysed by PO^{naph}COP–NiCl

reaction has led to the discovery of extremely active and compatible catalysts with a large variety of substrates; however, all of the most efficient examples require the use of expensive palladium catalysts. This has led to the development of cheaper nickel-based catalysts for this important catalytic reaction. Pincer complexes of palladium are among the best catalysts for Suzuki–Miyaura couplings [106] because of the physical and electronic properties that the pincer complexes have, and therefore, it is a natural extension to test their nickel counterparts. However, it is certainly curious that not many POCOP–Ni complexes have been tested in this reaction. In fact, the only report known on the use of POCOP–Ni complexes as catalyst in the Suzuki–Miyaura couplings is PO^{naph}COP–NiCl [81] (Fig. 32). These species efficiently catalyse the coupling of a series of activated and unactivated bromobenzenes with phenylboronic acid under relatively soft reaction conditions, attaining good to excellent yields. The yields being strongly dependant of the electronic effect of the *para*-substituent at the bromobenzene, with better yields obtained when electron-withdrawing substituents are present and relatively lower yields as their donor capabilities increase (related to the Hammett parameter). Experiments probed the process does indeed proceed in a homogenous manner.

4.9 Electrocatalytic Production of Hydrogen

Sustainable production of hydrogen is currently sought in the context of alternative energy strategies, and thus the design of low-cost proton reduction catalysts is of interest. In this context, ^{tBu}PC^{tBu}P–NiCl and ^{Ph}POCO^{Ph}P–NiCl were used as catalysts for the efficient electrocatalysis for proton reduction [19] (Fig. 33). For both compounds, the rates of H$_2$ production were measured, showing catalyst ^{tBu}PC^{tBu}P–NiCl to be faster in comparison with ^{Ph}POCO^{Ph}P–NiCl producing a TOF of 209 s^{-1} and 54.6 s^{-1}, respectively, although the Faradaic yield of H$_2$ production for both complexes is very similar, being close to 90% in both cases. Experiments performed with both catalytic systems found that in both cases the hydrogen

Fig. 33 ^{Ph}POCO^{Ph}P–NiCl catalyst employed for the electrocatalytic production of hydrogen
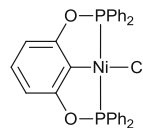
generation takes place in a homogenous environment. Due to the fact that the ^{t}BuPC^{t}BuP–NiCl catalyst was faster, all further studies focused on this species, including theoretical calculations that allowed the authors to make a mechanistic proposal; however, this will not be shown here because direct comparison may not be straightforward despite the similarity of both pincer frameworks. In this process the pincer compounds only serve as precatalysts, and the active species may be a solvent adduct of the type [^{Ph}POCO^{Ph}P–Ni(II)–NCMe]$^{+}$ that is reduced to the Ni (I) species [^{Ph}POCO^{Ph}P–Ni(I)–NCMe] which upon protonation affords the Ni(III) species [^{Ph}POCO^{Ph}P–Ni(III)–H]$^{+}$ further reduction to [^{Ph}POCO^{Ph}P–Ni(II)–H], and final protonations lead to the formation of the hydrogen complex [^{Ph}POCO^{Ph}P–Ni (II)–H$_2$] that upon release of the H$_2$ produces [^{Ph}POCO^{Ph}P–Ni(II)–NCMe]$^{+}$ to start the cycle again.

4.10 Sonogashira Cross-Coupling Reactions

The phosphoramidate species shown in Fig. 9 were synthesized and employed as catalysts in Sonogashira cross-couplings [59]. Despite the fact that the report was focused on the silicon and germanium derivatives, reactions with the phosphorus complex were also performed. These results clearly demonstrate that the operational mechanism is different for the phosphorus species when compared to that of the silicon and germanium analogues, although the yields are similar. It seems like the phosphorus compound follows the typical mechanism determined for the palladium-catalysed Sonogashira couplings, while the Ge and Si derivatives may actually follow a different mechanism or the reactive intermediates are substantially different or a combination of both as presently the case (Fig. 34).

In general, this difference in reactivity was explained by the higher electron density at the Ni centre in the silicon and germanium derivatives that enables a stronger π-back-bonding interaction with the C≡C bond, leading to a higher stability of the transmetallation product as revealed by the isolated intermediates shown in Fig. 35. This intermediate was not isolated nor observed for the case of the phosphorus analogue.
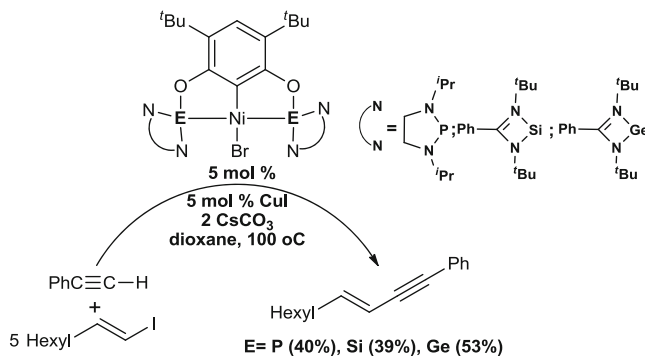
Fig. 34 Mechanistic proposal for Sonogashira cross-couplings catalysed by POCOP–Ni phosphoramidate pincer compounds
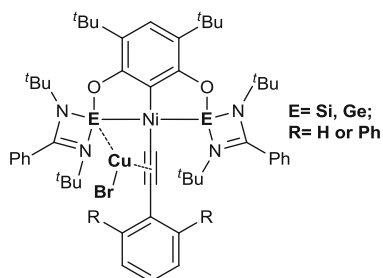
Fig. 35 Isolated intermediates in the Sonogashira couplings catalysed by Si and Ge analogues of POCOP–Ni phosphoramidate pincer compounds

4.11 Fluorination and Direct Benzylation of Unactivated Arenes

Organofluorine compounds play prominent roles in pharmaceuticals, medical imaging, material science, agrochemicals, and other disciplines. Nevertheless, the breadth and scope of methods available for preparing fluorinated molecules by means of direct C–F bond construction has lagged behind technologies for the molecular incorporation of other heteroatoms. In this sense, the field of transition metal-catalysed fluorination reactions has also experienced a rapid growth.

In the interest of this paper, the previously described $^{iPr}POCO^{iPr}P$–NiBr and $^{iPr}PO^{MeO}CO^{iPr}P$–NiBr (see Sect. 2) were used for catalytic fluorination of benzylbromides and chlorides [107]. The results obtained revealed that complex $^{iPr}PO^{MeO}CO^{iPr}P$–NiBr (the more electron-rich pincer backbone) produces the higher yields of fluorinated products. The reaction is affected, not only by the nature of the pincer catalyst. The process is completely inhibited by residual moisture and is sensitive to the nature of the *para*-substituents and leaving groups

Fig. 36 Catalytic cycle proposed for the fluorination of benzyl halides catalysed by $^{iPr}POCO^{iPr}P$–NiX and $^{iPr}PO^{MeO}CO^{iPr}P$–NiX
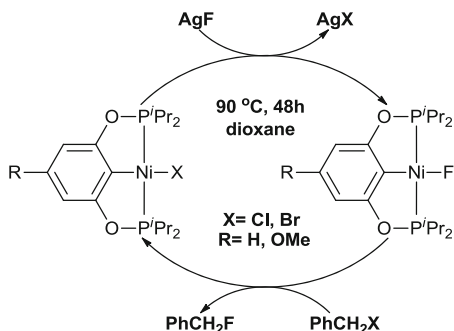
on the substrate. Even the rate of stirring plays a role *albeit* only slightly beneficial for the transformation. It should be noted that NMR experiments indicate the regeneration of the parent bromo- or chloro-derivatives, indicating that the POCOP framework is stable towards decomposition during the catalytic process. A mechanistic proposal was described (Fig. 36).

Motivated by these results and having the $^{iPr}POCO^{iPr}P$–Ni–CF_3 and $^{iPr}PO^{MeO}CO^{iPr}P$–Ni–CF_3 complexes on hand, authors envisioned the possibility of a similar trifluoromethylation process. Thus, under the same conditions as those used in the fluorination of benzylbromides and chlorides and CF_3SiMe_3 as the source of –CF_3, no trifluoromethylation products were obtained, changing the solvent for benzene did not afford trifluoromethylated products either, and instead an unexpected benzylation process occurred to afford $PhCH_2C_6H_5$. This reactivity is general and reproducible, and reactions of benzylbromide in toluene, *m*-xylene and bromobenzene afford the corresponding benzylation products $PhCH_2(tolyl)$, $PhCH_2(xylyl)$ and $PhCH_2C_6H_4Br$. This observed reactivity seemed to be limited to aromatic substrates and was sensitive to solvent, as reactions in hexane do not proceed.

5 Conclusions and Outlook

The chemistry of POCOP–Ni complexes has evolved rapidly in the last decade. The structural diversity and applications that these complexes have achieved in this short period of time is enormous. The reactivity of these species with fundamentally important substrates like CO_2 allows us to foresee future developments and creation of new catalytic processes employing POCOP–Ni catalysts. The possibility of easily synthesizing bimetallic species derived from POCOP–Ni complexes may allow the exploration of tandem catalytic processes; at the same time, this may also allow the synthesis of planar chiral POCOP–Ni motifs of potential relevance in asymmetric catalysis, while the facile generation of *para*-hydroxy $^{R}PO^{OH}CO^{R}P$–Ni may represent a key to unleashing the potential of these compounds by permitting the functionalization of the backbone with an endless number of substrates and

solid supports. Thus, the future development of the chemistry of POCOP–Ni compounds looks bright and promising with multiple applications yet to be discovered.

References

1. Morales-Morales D, Jensen CM (2007) The chemistry of pincer compounds. Elsevier, Amsterdam
2. van Koten G, Milstein D (eds) (2013) Organometallic pincer chemistry, vol 40, Topics in organometallic chemistry. Springer, Heidelberg
3. Chase PA, van Koten G (2010) The pincer ligand: its chemistry and applications (catalytic science), 1st edn. Imperial College, London
4. van der Boom ME, Milstein D (2003) Chem Rev 103:1759
5. Jensen CM (1999) Chem Commun 2443–2449
6. van Koten G (1989) Pure Appl Chem 61:1681
7. Goldberg KI, Goldman AS (eds) (2004) Activation and functionalization of C–H bonds, vol 885, ACS symposium series. American Chemical Society, Washington, DC
8. Morales-Morales D (2009) Iridium-mediated alkane dehydrogenation. In: Oro LA, Claver C (eds) Iridium complexes in organic synthesis, 1st edn. Wiley-VCH, Weinheim, ch 13
9. Choi J, MacArthur AHR, Brookhart M, Goldman AS (2011) Chem Rev 111:1761
10. Haibach MC, Kundu S, Brookhart M, Goldman AS (2012) Acc Chem Res 45:947
11. Szabo JK, Wendt OF (eds) (2014) Pincer and pincer-type complexes: applications in organic synthesis and catalysis, 1st edn. Wiley-VCH, Weinheim
12. Albrecht M, Morales-Morales D (2009) Pincer-type iridium complexes for organic transformations. In: Oro LA, Claver C (eds) Iridium complexes in organic synthesis, 1st edn. Wiley-VCH, Weinheim, Chap 12
13. Morales-Morales D (2004) Rev Soc Quim Mex 48:338
14. Serrano-Becerra JM, Morales-Morales D (2009) Curr Org Synth 6:169
15. Singleton JT (2003) Tetrahedron 59:1837
16. Selander N, Szabo KJ (2011) Chem Rev 111:2048
17. Dupont J, Consorti CS, Spencer J (2005) Chem Rev 105:2527
18. Jensen CM, Sun D, Lewandowski B, Kumashiro KK, Niemczura WP, Morales-Morales D, Wang Z (2001) In: Proceedings of the 2001 U.S. DOE hydrogen program review; National Renewable Energy Laboratory, Golden, CO, p 2500
19. Luca OR, Blakemore JD, Konezny SJ, Praetorius JM, Schmeier TJ, Hunsinger GB, Batista VS, Brudvig GW, Hazari N, Crabtree RH (2012) Inorg Chem 51:8704
20. Torres-Nieto J, Garcia JJ (2007) Desulfurization catalyzed by nickel PCP-pincer compounds. In: Morales-Morales D, Jensen CM (eds) The chemistry of pincer compounds. Elsevier, Oxford, Chap 4
21. Bauer G, Kirchner KA (2011) Angew Chem Int Ed 50:5798
22. Bhattacharya P, Guan H (2011) Comment Inorg Chem 32:88
23. Wang Z-X, Liu N (2012) Eur J Inorg Chem 901
24. Campora J, Melero C (2004) The role of redox processes in reactions catalyzed by nickel and palladium complexes with anionic pincer ligands. In: Szabo JK, Wendt OF (eds) Pincer and pincer-type complexes: applications in organic synthesis and catalysis, 1st edn. Wiley-VCH, Weinheim, Chap 2

25. Adhikary A, Guan H (2014) Nickel-catalysed cross-coupling reactions. In: Szabo JK, Wendt OF (eds) (2014) Pincer and pincer-type complexes: applications in organic synthesis and catalysis, 1st edn. Wiley-VCH, Weinheim, Chap 5
26. Zargarian D, Castonguay A, Spasyuk DM (2013) Top Organomet Chem 40:131
27. Gómez-Benítez V, Baldovino-Pantaleón O, Herrera-Álvarez C, Toscano RA, Morales-Morales D (2006) Tetrahedron Lett 47:5059
28. Shaw BL, Moulton CJ (1976) J Chem Soc Dalton Trans 1020
29. Albrecht M, van Koten G (2001) Angew Chem Int Ed 40:3750
30. Morales-Morales D, Redón R, Yung C, Jensen CM (2000) Chem Commun 1619
31. Morales-Morales D, Cramer RE, Jensen CM (2002) J Organomet Chem 654:44
32. Morales-Morales D (2008) Mini Rev Org Chem 5:141
33. Hahn FE, Jahnke MC, Gómez-Benítez V, Morales-Morales D, Pape T (2005) Organometallics 24:6458
34. Baldovino-Pantaleón O, Hernández-Ortega S, Morales-Morales D (2006) Adv Synth Catal 348:236
35. Basauri-Molina M, Hernández-Ortega S, Morales-Morales D (2014) Eur J Inorg Chem 4619
36. Gómez-Benítez V, Hernández-Ortega S, Toscano RA, Morales-Morales D (2007) Inorg Chim Acta 360:2128
37. Avila-Sorrosa A, Estudiante-Negrete F, Hernández-Ortega S, Toscano RA, Morales-Morales D (2010) Inorg Chim Acta 363:1262
38. Baldovino-Pantaleón O, Hernández-Ortega S, Morales-Morales D (2005) Inorg Chem Commun 8:955
39. Naghipour A, Sabounchei SJ, Morales-Morales D, Canseco-González D, Jensen CM (2007) Polyhedron 26:1445
40. Ramírez-Rave S, Estudiante-Negrete F, Toscano RA, Hernández-Ortega S, Morales-Morales D, Grévy J-M (2014) J Organomet Chem 749:287
41. Crisóstomo-Lucas C, Toscano RA, Morales-Morales D (2014) Tetrahedron Lett 55:5841
42. Serrano-Becerra JM, Hernández-Ortega S, Morales-Morales D (2010) Inorg Chim Acta 363:1306
43. Brayton DF, Beaumont PR, Fukushima EY, Sartain HT, Morales-Morales D, Jensen CM (2014) Organometallics 33:5198
44. Morales-Morales D, Grause C, Kasaoka K, Redón R, Cramer RE, Jensen CM (2000) Inorg Chim Acta 958:300–302
45. Bedford RB, Draper SM, Scully PN, Welch SL (2000) New J Chem 24:745
46. Morales-Morales D, Redon R, Yung C, Jensen CM (2004) Inorg Chim Acta 357:2953
47. Göttker-Schnetmann I, White P, Brookhart M (2004) J Am Chem Soc 126:1804
48. Salem H, Ben-David Y, Shimon LJW, Milstein D (2006) Organometallics 25:2292
49. Cerón-Camacho R, Gómez-Benítez V, Le Lagadec R, Morales-Morales D, Toscano RA (2006) J Mol Catal A 247:124
50. Bedford RB, Betham M, Blake ME, Coles SJ, Draper SM, Hursthouse MB, Scully PN (2006) Inorg Chim Acta 359:1870
51. Wang Z, Sugiarti S, Morales CM, Jensen CM, Morales-Morales D (2006) Inorg Chim Acta 359:1923
52. Pandarus V, Zargarian D (2007) Chem Commun 978
53. Vabre B, Lindeperg F, Zargarian D (2013) Green Chem 15:3188
54. Zhang J, Medley CHM, Krause JA, Guan H (2010) Organometallics 29:6393
55. Chakraborty S, Patel YJ, Krause JA, Guan H (2012) Polyhedron 32:30
56. García-Eleno MA, Padilla-Mata E, Estudiante-Negrete F, Pichal-Cerda F, Hernández-Ortega S, Toscano RA, Morales-Morales D (2015) New J Chem 39:3361
57. Kimura T, Uozumi Y (2006) Organometallics 25:4883
58. Ananthnag GS, Mague JT, Balakrishna MJ (2015) Dalton Trans 44:3785
59. Gallego D, Brück A, Irran E, Meier F, Kaupp M, Driess M, Hartwig JF (2013) J Am Chem Soc 135:15617

60. Salah AB, Zargarian D (2011) Dalton Trans 40:8977
61. Lefèvre X, Spasyuk DM, Zargarian D (2011) J Organomet Chem 696:864
62. Zargarian D, Salah AB (2011) Acta Crystallogr E67:m940
63. Salah AB, Zargarian D (2011) Acta Crystallogr E67:m437
64. Vabre B, Spasyuk DM, Zargarian D (2012) Organometallics 31:8561
65. Hao J, Vabre B, Zargarian D (2014) Organometallics 33:6568
66. Wilson GLO, Abraha M, Krause JA, Guan H (2015) Dalton Trans. doi:10.1039/c5dt00161g
67. Kwan M-L, Conry SJ, Carfagna CHS, Press LP, Ozerov OV, Hoffman NW, Sykora RE (2012) Acta Crystallogr E68:m1282
68. Salah A, Corpet M, Khan NU-H, Zargarian D, Spasyuk D (2015) New J Chem. doi:10.1039/C5NJ00807G
69. Farrington EJ, Martinez EV, Williams BS, van Koten G, Brown JM (2002) Chem Commun 308
70. Koridze AA, Kuklin SA, Sheloumov AM, Dolgushin FM, Lagunova VY, Petukhova II, Ezerniskaya MG, Peregudov AS, Petrovskii PV, Vorontsov EV, Baya M, Poli R (2004) Organometallics 23:4585
71. Kuklin SA, Sheloumov AM, Dolgushin FM, Ezerniskaya MG, Peregudov AS, Petrovskii PV, Koridze AA (2006) Organometallics 25:5466
72. Koridze AA, Sheloumov AM, Kuklin SA, Lagunova VY, Petukhova II, Dolgushin FM, Ezerniskaya MG, Peregudov AS, Petrovskii PV, Macharashvili AA, Chedia RV (2002) Russ Chem Bull Int Ed 51:1077
73. Koridze AA, Polezhaev AV, Safronov SV, Sheloumov AM, Dolgushin FM, Ezernitskaya MG, Lokshin BV, Petrovskii PV, Peregudov AS (2010) Organometallics 29:4360
74. Bonnet S, Lutz M, Spek AL, van Koten G, Gebbink RJM (2008) Organometallics 27:159
75. Bonnet S, Li J, Siegler MA, von Chrzanowski LS, van Koten G, Gebbink RJMK (2009) Chem Eur J 15:3340
76. Bonnet S, van Lenthe JH, Siegler MA, Spek AL, van Koten G, Gebbink RJMK (2009) Organometallics 28:2325
77. Bonnet S, Lutz M, Spek AL, van Koten G, Gebbink RJMK (2010) Organometallics 29:1157
78. Bonnet S, Siegler MA, van Lenthe JH, Lutz M, Spek AL, van Koten G, Gebbink RJMK (2010) Eur J Inorg Chem 4667
79. Walter MC, White PS (2011) New J Chem 35:1842
80. Espinosa-Jalapa NA, Hernández-Ortega S, Morales-Morales D, Le Lagadec R (2012) J Organomet Chem 716:103
81. Estudiante-Negrete F, Hernández-Ortega S, Morales-Morales D (2012) Inorg Chim Acta 387:58
82. Espinosa-Jalapa NA, Hernández-Ortega S, Le Goff X-F, Morales-Morales D, Djukic J-P, Le Lagadec R (2013) Organometallics 32:2661
83. Zhang J, Adhikary A, King KM, Krause JA, Guan H (2012) Dalton Trans 41:7959
84. Lindsley CW (2013) ACS Chem Neurosci 4:905
85. Lawrence SA (2004) Amines: synthesis properties and applications. Cambridge University, Cambridge
86. Yim JCH, Schafer LL (2014) Eur J Org Chem 6825
87. Huang L, Arndt M, Gooßen K, Heydt H, Gooßen LJ (2015) Chem Rev 115:2596
88. Bernoud E, Lepori C, Mellah M, Schulzab E, Hannedouche J (2015) Catal Sci Technol 5:2017
89. Pandarus V, Zargarian D (2007) Organometallics 26:4321
90. Castonguay A, Spasyuk DM, Madern N, Beauchamp AL, Zargarian D (2009) Organometallics 28:2134
91. Lefèvre X, Durieux G, Lesturgez S, Zargarian D (2011) J Mol Catal A Chem 335:1
92. Salah AB, Offenstein C, Zargarian D (2011) Organometallics 30:5352
93. Chakraborty S, Krause JA, Guan H (2009) Organometallics 28:582
94. Chakraborty S, Zhang J, Krause JA, Guan H (2010) J Am Chem Soc 132:8872

95. Huang F, Zhang CH, Jiang J, Wang Z-X, Guan H (2011) Inorg Chem 50:3816
96. Wang L, Guo J, Wen J, He H, Zhang J (2013) Eur Phys J D 67:241
97. Chakraborty S, Zhang J, Patel YJ, Krause JA, Guan H (2013) Inorg Chem 52:37
98. Corey EJ, Wu YJ (1993) J Am Chem Soc 115:8871
99. Fleming FF, Shook BC (2002) Tetrahedron 58:1
100. Fukuda Y, Okamoto Y (2002) Tetrahedron 58:2513
101. Fan Y-CH, Du GF, Sun W-F, Kang W, Kang W, He L (2012) Tetrahedron Lett 53:2231
102. Chakraborty S, Patel YJ, Krause JA, Guan H (2013) Angew Chem Int Ed 52:7523
103. Xu G, Li X, Sun H (2011) J Organomet Chem 696:3011
104. Chen T, Yang L, Li L, Huang K-W (2012) Tetrahedron 68:6152
105. Miyaura N, Suzuki A (1995) Chem Rev 95:2457
106. Solano-Prado MA, Estudiante-Negrete F, Morales-Morales D (2010) Polyhedron 29:592
107. Vabre B, Petiot P, Declercq R, Zargarian D (2014) Organometallics 33:5173

Pincerlike Cyclic Systems for Unraveling Fundamental Coinage Metal Redox Processes

Marc Font and Xavi Ribas

Abstract Pincerlike cyclic ligands have overcome the high instability of transition metals in their higher oxidation states and have permitted the isolation of such species and the exhaustive study of their properties and reactivity. The formation and isolation of organometallic Cu^{II} and M^{III} (M=Cu, Ag, Au) complexes stabilized by NCPs, carbaporphyrins, carbaporphyrinoids, heterocalixarenes, and triaza macrocyclic ligands will be discussed in this chapter. The study of these complexes have led to the discovery of unprecedented reactivity and proved the plausibility of often invoked pathways in copper-catalyzed cross-coupling reactions. Aryl-M^{III} (M=Cu, Ag) stable species have been implicated as the key intermediate species that operate in coupling catalysis through two-electron redox cycles involving oxidative addition and reductive elimination fundamental steps.

Keywords Copper, Cross-coupling catalysis, Gold, Group 11 metals, High oxidation states, Reaction mechanisms, Silver

Contents

M. Font and X. Ribas (✉)
QBIS-CAT Research Group, Institut de Química Computacional i Catàlisi (IQCC), Girona, 17071 Catalonia, Spain

Departament de Química, Universitat de Girona, Campus Montilivi, Girona, 17071 Catalonia, Spain
e-mail: xavi.ribas@udg.edu

Abbreviations

Ac	Acetyl
Ar	Aryl
AT	Atom transfer
cal	Calories
cat	Catalytic
Cp	Cyclopentadienyl
DDQ	2,3-Dichloro-5,6-dicyano-1,4-benzoquinone
DFT	Density functional theory
DMF	Dimethylformamide
DMSO	Dimethyl sulfoxide
equiv	Equivalent(s)
Et	Ethyl
h	Hour(s)
i-Bu	*Iso*butyl
L	Ligand
Me	Methyl
min	Minute(s)
mol	Mole(s)
N_2CP	Doubly N-confused porphyrin
Naph	Naphthalene
n-Bu	Butyl
NCP	N-confused porphyrin
NMR	Nuclear magnetic resonance
n-Pr	Propyl
Nuc	Nucleophile
[O]	Oxidant
Ph	Phenyl
phen	Phenanthroline
py	Pyridine
rt	Room temperature

s	Second(s)
SET	Single-electron transfer
t-Bu	*Tert*-butyl
TEMPO	(2,2,6,6-Tetramethylpiperidin-1-yl)oxyl
Tf	Trifluoromethanesulfonyl (triflyl)
TFA	Trifluoroacetic acid
THF	Tetrahydrofuran
Tol	4-Methylphenyl
UV–Vis	Ultraviolet–visible spectroscopy
V	Volt(s)
xyl	Xylyl

1   Introduction

Macrocyclic pincerlike ligands have proven to be privileged motifs for the stabilization of organometallic high-valent metal species [1–7]. Such ligands define a conformational and electronic environment suitable for accommodating high oxidation states of Group 11 transition metals, i.e., copper, silver, and gold, enabling the isolation and full characterization of these rare metal species. Among the privileged architectures capable of achieving this purpose, NCPs, carbaporphyrins, carbaporphyrinoids, porphyrin hybrid structures, arene triazamacrocyclic scaffolds and heterocalixarenes are highlighted. The high stability of these high-valent model systems has been exploited to understand the mechanism of certain reactions involving such species.

Stabilizing and studying metal high-valent species is of great importance not only because it allows the study of the uncommon electronic properties of these complexes around the metal center but also provides understanding about the features of the ligand that confer this stability. Given the fact that some reactions are known to proceed through these high-valent intermediate species, the understanding of the electronic and geometric environment of those species provides valuable insight for the rational design of ligands capable of favoring the formation of high-valent species and accelerating its reactivity.

In the same line, stable metal high-valent species enable the study of the formation and reactivity of these species. Unprecedented reactivity of the three coinage metals has been extracted from such systems but also metal high-valent species have served to corroborate long time invoked mechanistic hypothesis for known reactions. In this context, copper(III) complexes bearing pincerlike cyclic ligands have been exploited as models to elucidate the fundamental pathways of copper-catalyzed cross-coupling reactions [8–10].

Thus, this chapter gathers the recent progress in the application of pincer-related ligands in the fundamental understanding of the behavior of coinage metals in high oxidation states. The discussion will focus on their synthesis, characterization, and

reactivity centred on the understanding of Group 11-catalyzed cross-coupling reactions.

The discussion is organized into different sections: Sect. 2 covers the synthesis and characterization of the rare stable complexes of high oxidation state transition metals bearing pincerlike cyclized ligands. It is organized based on the family of ligands featured in the complexes. Section 3 describes the application of some of the copper complexes presented in the first section towards the fundamental understanding of copper-catalyzed cross-coupling reactions. The discussion is structured into subsections depending on the nature of the bond formed during the process. Section 4 is devoted to the unprecedented cross-coupling chemistry of aryl–Ag[III] model platforms operated through two-electron processes. Finally Sect. 5 summarizes the scope of the present chapter and discusses the most important challenges remaining in this field.

2 Stabilization and Reactivity of Organometallic High-Valent Group 11 Metal Species with Pincerlike Cyclic Ligands

2.1 N-Confused Porphyrins (NCPs)

While organocuprate species containing Cu[I]–C bonds have become a basic tool in organic transformations since its discovery in the beginning of the last century and Cu[III] organometallic complexes bearing perfluorinated alkyl moieties are known since the late 1980s [11], the first organometallic Cu[II] compound was not isolated until 2000, when Latos-Grażyński, Chmielewski, and coworkers reported Cu[II](NCP) stable complexes (**1a**-Cu[II] and **1b**-Cu[II]) [12]. NCPs, namely, porphyrin isomers wherein at least one of the four pyrrole rings is inverted, thus placing one or more carbon atoms into the inner cavity of the macrocycle, show an extraordinary ability to stabilize unusual organometallic Cu[II], Cu[III], Ag[III], and Au[III] complexes in a square-planar fashion. The Cu[II]–C example described by the Latos-Grażyński group was synthesized by simply reacting Cu[II](OAc)$_2$ and the porphyrin containing one inverted pyrrole (Scheme 1). Later, in 2005, Schweiger and coworkers studied in closer detail the electronic structure of the metal center and the nature of the Cu[II]–C bond, by studying the magnetic properties of the unpaired electrons surrounding the nitrogen nuclei. Based on continuous-wave (CW) EPR and pulse EPR experiments, they determined that Cu–C bond presents a very strong σ character and that the inversion of the pyrrole ring results on a strong asymmetric distribution of the electron spin densities on the three nitrogen atoms, thus breaking the D_4h symmetry of the original porphyrin molecule. This observation is of great relevance for the understanding of the reactivity of organometallic NCP complexes [13, 14]. Also, Furuta's group reported the synthesis, characterization, and X-ray

Scheme 1 Metalation reaction of $Cu^{II}(OAc)_2$ over NCP ligands

R^1 = H, R^2 = Ph; **1a**
R^1 = Me, R^2 = Ph; **1b**
R^1 = H, R^2 = C$_6$F$_5$; **1c**

1a-Cu^{II}; 70%
1b-Cu^{II}; 80%
1c-Cu^{II}; 78%
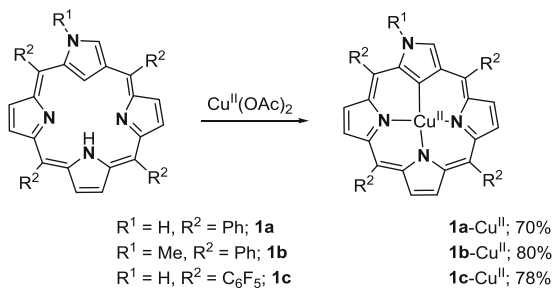
Fig. 1 Organometallic family of Cu^{II} complexes **1**-Cu^{II} and **2**-Cu^{II} bearing NCP ligands

R^1 = H, R^2 = Ph; **1a**-Cu^{II}
R^1 = Me, R^2 = Ph; **1b**-Cu^{II}
R^1 = H, R^2 = C$_6$F$_5$; **1c**-Cu^{II}

2-Cu^{II}

1c-Cu^{II}

− e$^-$, − H$^+$ (DDQ)
+ e$^-$, + H$^+$
(p-toluenesulfonylhydrazine)
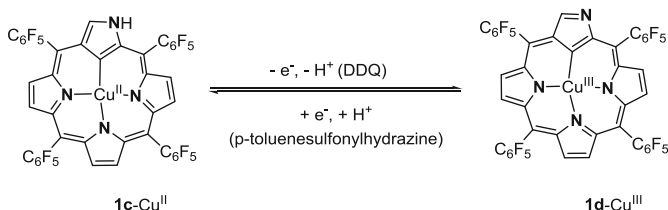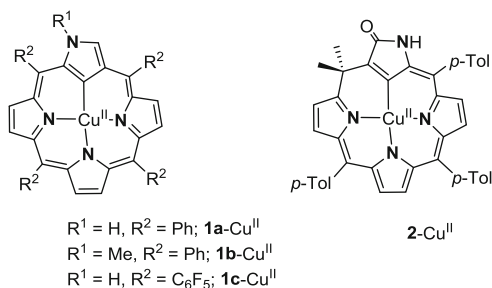
1d-Cu^{III}

Scheme 2 Interconversion between Cu^{II} (**1c**-Cu^{II}) and Cu^{III} (**1d**-Cu^{III}) species accompanied by the protonation and deprotonation of the peripheral nitrogen

diffraction of related Cu^{II}–NCP complexes **2**-Cu^{II} [15] and **1c**-Cu^{II}; see Scheme 1 and Fig. 1 [16].

The same research group published in 2003 the quantitative interconversion between Cu^{II} and Cu^{III} species in the frame of an NCP system. The authors described a one-electron oxidation of the Cu^{II} center associated to the deprotonation of the inverted pyrrole nitrogen of the NCP in the neutral **1c**-Cu^{II} complex triggered by the addition of DDQ to yield an again neutral Cu^{III}–NCP complex **1d**-Cu^{III} that could be fully characterized by means of NMR, UV–Vis, and X-ray diffraction spectroscopies. Upon addition of *p*-toluenesulfonylhydrazide, the Cu^{III} complex is capable of accepting one electron and protonating the outer N of the ligand to regenerate the Cu^{II}–NCP complex (Scheme 2).

Staying on Cu^{III} systems, the first reported example of a Cu^{III} organometallic complex that takes advantage of NCP frameworks, complex **3**-Cu^{III}, was based on the use of a doubly confused porphyrin ligand (N$_2$CP) analogous to the NCPs

employed for the formation of organometallic Cu^{II} complexes but bearing two proximal inverted pyrrole moieties (Fig. 2) [17]. The analogous *trans* complex **4**-Cu^{III} that bear two pyrroles at opposite sides of the porphyrin were also reported few years later [18]. Interestingly, this complex adopts a linear chain network in the solid state by intermolecular hydrogen bonding. In either case, when $Cu^{II}(OAc)_2$ was reacted with the ligand in the presence of a base, a neutral square-planar Cu^{II} complex was obtained quantitatively. Interestingly, ligands that contain three (*cis*-N_2CP) or four sites (*trans*-N_2CP) susceptible to deprotonation into the inner core give rise indistinctly to a trianionic ligand that stabilizes Cu^{III} cations resulting in a neutral complexes (Fig. 2). Although the mechanism of the oxidation of copper is not well understood, the second pyrrolic confusion site clearly assists in the stabilization of higher oxidation states of the coordinated metal affording complexes that present two Cu–C bonds. The spectroelectrochemical properties of the *cis*-N_2CP Cu^{III} complex **3**-Cu^{III} (Cu^{III}/Cu^{II} redox process and ligand oxidation) were studied in detail at different pH to discuss the protonation/deprotonation equilibria of the complex [19].

Regarding silver chemistry with NCP ligands, Ag behaves differently compared to Cu. While copper(II) and copper(III) species can be stabilized by NCP ligands, only silver(III) complexes bearing NCP ligands are known to date, despite silver (I) precursors are always employed as the metal source for the metalation reaction. The first example is complex **1e**-Ag^{III}, reported in 1999 by Furuta's group and that was synthesized by reacting $Ag^{I}(TFA)$ with the N-confused tetraphenylporphyrin ligand (Fig. 3) [20]. Later, its analogous complexes, **1d**-Ag^{III}, bearing perfluorinated arene moieties [16] and **1f**-Ag^{III} with *p*-toluene rings [21] were reported (Fig. 3). Also, the aforementioned doubly confused porphyrin system capable of

Fig. 2 Organometallic Cu^{III} complexes bearing N_2CP ligands

3-Cu^{III}

R = Me; **4a**-Cu^{III}
R = Et; **4b**-Cu^{III}
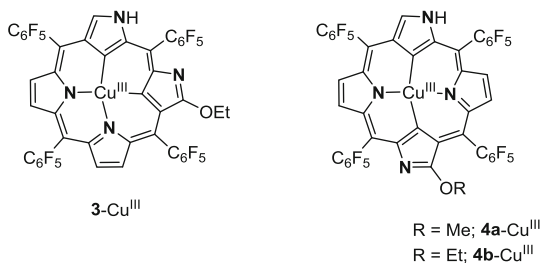
Fig. 3 Organometallic Ag^{III} complexes bearing NCP and N_2CP ligands

R = Ph; **1e**-Ag^{III}
R = C_6F_5; **1d**-Ag^{III}
R = *p*-Tol; **1f**-Ag^{III}
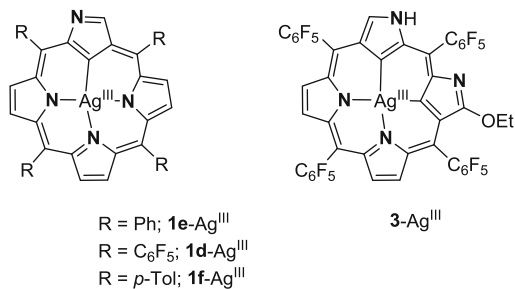
3-Ag^{III}

stabilizing Cu^{III} cations was proven to stabilize Ag^{III} neutral organometallic complex (3-Ag^{III}) by reaction of $Ag^{I}(OAc)$ with the ligand in the presence of a base (Fig. 3) [17]. The last example involving stabilization of silver(III) with NCPs was reported in 2008. In the study, it was described that unexpectedly, the inverted pyrrole moiety undergoes the nucleophilic attack of a molecule of water to form an alcohol that consecutively is oxidized by the excess of $Ag^{I}(OAc)$ to eventually form the corresponding Ag^{III}–NCP lactam products **5c**-Ag^{III} and **5d**-Ag^{III} (Scheme 3) [22]. Interestingly, the metalation reactions with Ni^{II} and Pd^{II} salts formed the square-planar organometallic compounds but did not form the lactam product.

Regarding the 3rd row transition metal of Group 11, +3 oxidation state is stable for gold, and a vast number of organometallic complexes of gold in that oxidation state have been reported to date. Therefore, one would expect that NCPs could be also suitable ligands for Au^{III} complexes. In fact, $Au^{III}(OAc)_3$ presents a reactivity analogous to that for $Ag^{I}(OAc)$ in front of the *meso*-unsubstituted NCP described above, but affords very poor yields of the analogous Au^{III}–NCP lactam product **5c**-Au^{III} (Scheme 4) [22]. Also in 2008, another example of Au^{III}–NCP was published by Furuta and coworkers. Nonetheless, in contrast to silver systems, reaction of Au^{I} salt and the NCP ligand gave rise to side reactions, and no product was observed. However, if the inverted pyrrole is modified and its inner carbon is brominated, when it is reacted with $Au^{I}Cl•SMe_2$, 37% yield of the organometallic **1e**-Au^{III} complex is formed, by what appears to be a formal oxidative addition of Au^{I} over a C–Br bond (Scheme 5), although no details are given in the manuscript and the
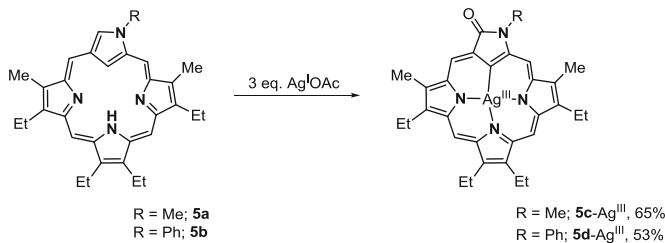
Scheme 3 Formation of the lactam–Ag^{III} complexes **5c**-Ag^{III} and **5d**-Ag^{III} by reaction of the NCP ligands **5a-b** and excess of $Ag^{I}OAc$
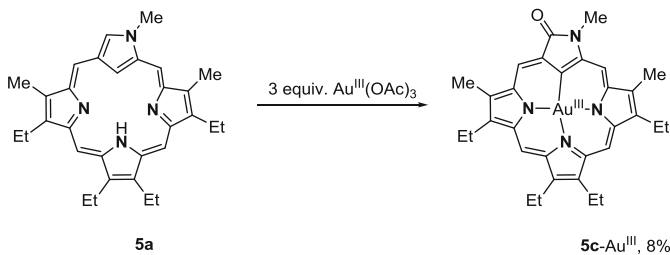
Scheme 4 Formation of the lactam–Au^{III} complex **5c**-Au^{III} by reaction of the NCP ligand **5a** and excess of $Au^{III}(OAc)_3$

Scheme 5 Synthesis of the NCP-Au^{III} complex **1e**-Au^{III} presumably via oxidative addition over brominated NCP ligand **1e**-Br

3.3 equiv. Au^{I}Cl·SMe$_3$

1e-Br   **1e**-Au^{III}, 37%
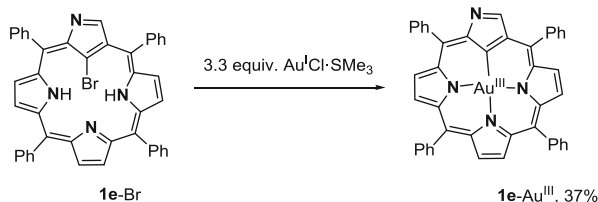
low yields found might argue in favor of another mechanism [23]. Besides its structural interest, this complex presents unique luminescence properties.

2.2 Carbaporphyrins and Carbaporphyrinoids

Carbaporphyrins and carbaporphyrinoids present very similar features compared to NCP ligands and have also shown to be suitable ligands for the stabilization of rare high oxidation states of transition metals. Carbaporphyrins are porphyrin-related compounds that arise from the substitution of one or more of the pyrrolic nitrogens by carbon atoms, whereas carbaporphyrinoids result from the replacement of one or more of the pyrrolic rings by other carbocyclic moieties. In both cases, like NCPs, carbaporphyrins and carbaporphyrinoids also place a carbon in the inner core of the porphyrin leading to attractive ligands to attempt the formation of organometallic complexes. To our knowledge there are no examples of copper carbaporphyrin complexes, whereas copper carbaporphyrinoid complexes are very rare, yet few examples have been reported. In 2007, Latos-Grażyński and coworkers reported the isolation of Cu^{II} and Cu^{III}–oxycarbaporphyrin complexes. Complex **6a**-Cu^{III} is obtained quantitatively by reaction of Cu^{II}(OAc)$_2$ with ligand **6a** in THF. However, it is extremely unstable in aerobic conditions, and its reaction with oxygen results in the formation of the paramagnetic complex **6b**-Cu^{II}. The latter can also be obtained by direct insertion of Cu^{II} in its corresponding ligand **6b**-Cu^{II} (Scheme 6) [24]. Latos-Grażyński communicated and subsequently expanded the synthesis and spectroscopic characterization of copper(II) complexes bearing 21-phosphoryl and 21-thiophosphoryl NCP hybrid ligands, namely, compounds **7**-Cu^{II}, **8a**-Cu^{II}, to **8d**-Cu^{II} (Fig. 4) [25, 26]. The spectroscopic data, in addition to DFT calculations, showed that copper(II) affords square-pyramidal complexes with 21-phosphoryl NHC ligands presenting apical coordination of the oxygen atom from the phosphonyl moiety, whereas the copper(II) center does not coordinate sulfur atoms with thiophosphoryl hybrids (**8c**-Cu^{II} and **8d**-Cu^{II}).

Concerning silver species in high oxidation states bearing carbaporphyrin ligands, in 2002, Lash and colleagues published the isolation of the family of complexes **9**-Ag^{III} upon reaction of Ag^I(OAc) with the corresponding benzocarbaporphyrin ligands in a mixture of MeOH:CH$_2$Cl$_2$ at room temperature (Fig. 5)[27–29]. Later, in 2004, Lash's research group reported the isolation of structural derivatives of the previously detailed benzocarbaporphyrin compounds with
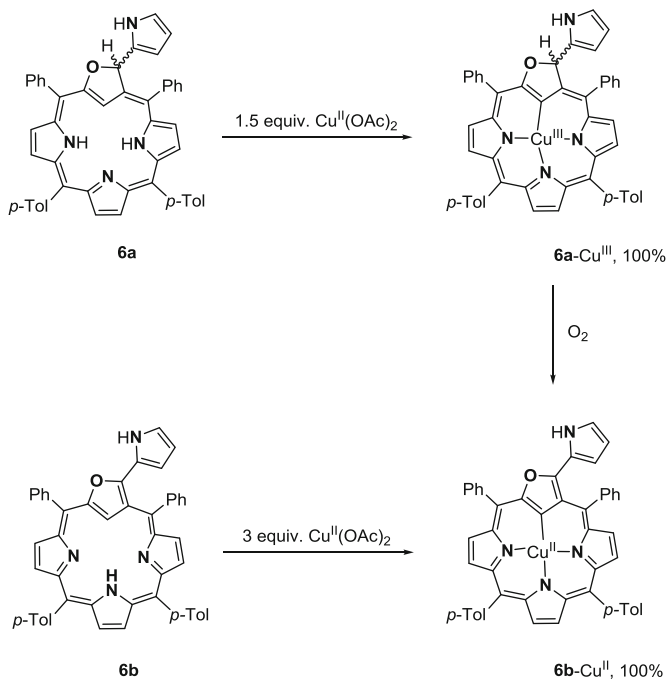
Scheme 6 Reactivity of Cu(II) over **6a** and **6b** and stability of **6b**-Cu^{II} under aerobic conditions
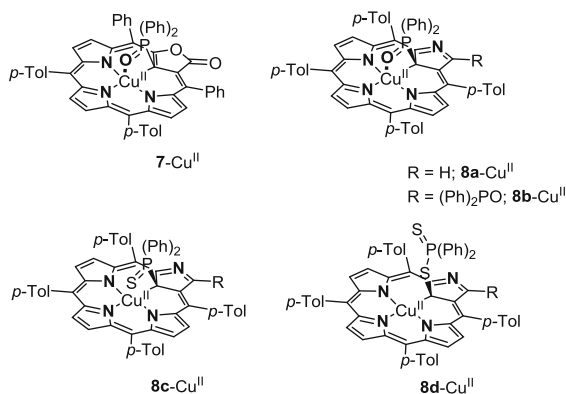
Fig. 4 Organometallic Cu^{II} complexes bearing **21**-P and **21**-S-substituted hybrid NCP ligands

modified R groups in one of the pyrrole rings to explore the effect of larger alkyl groups on the solubility of its organometallic complexes in organic solvents (Fig. 5) [28]. Also in 2004, the same research group described the isolation and full characterization of Ag^{III} complexes embedded in tropiporphyrin (**10**-Ag^{III}) [28, 30], oxybenziporphyrins (**11**-Ag^{III} and **12**-Ag^{III}) [31, 32], and oxynaphtiporphyrin ligands (**13**-Ag^{III}) [29] (Fig. 5).

R^1 = R^3 = Et, R^2 = H, R^4 = Me; **9a**-Ag^{III}
R^1 = Ph, R^2 = H, R^3 = Et, R^4 = Me; **9b**-Ag^{III}
R^1 = Et, R^2 = H, R^3 = t-Bu, R^4 = Me; **9c**-Ag^{III}
R^1 = Et, R^2 = H, R^3 = Me, R^4 = n-Pr; **9d**-Ag^{III}
R^1 = Et, R^2 = H, R^3 = Me, R^4 = i-Bu; **9e**-Ag^{III}
R^1 = R^3 = R^4 = H, R^2 = Ph; **9f**-Ag^{III}
R^1 = R^3 = R^4 = H, R^2 = p-ClC$_6$H$_4$; **9g**-Ag^{III}

R = Et; **10a**-Ag^{III}
R = Ph; **10b**-Ag^{III}

X = OH; **11a**-Ag^{III}
X = Br; **11b**-Ag^{III}

R^1 = Et, R^2 = H; **12a**-Ag^{III}
R^1 = Ph, R^2 = H; **12b**-Ag^{III}
R^1 = H, R^2 = Ph; **12c**-Ag^{III}

13a-Ag^{III}

13b-Ag^{III}
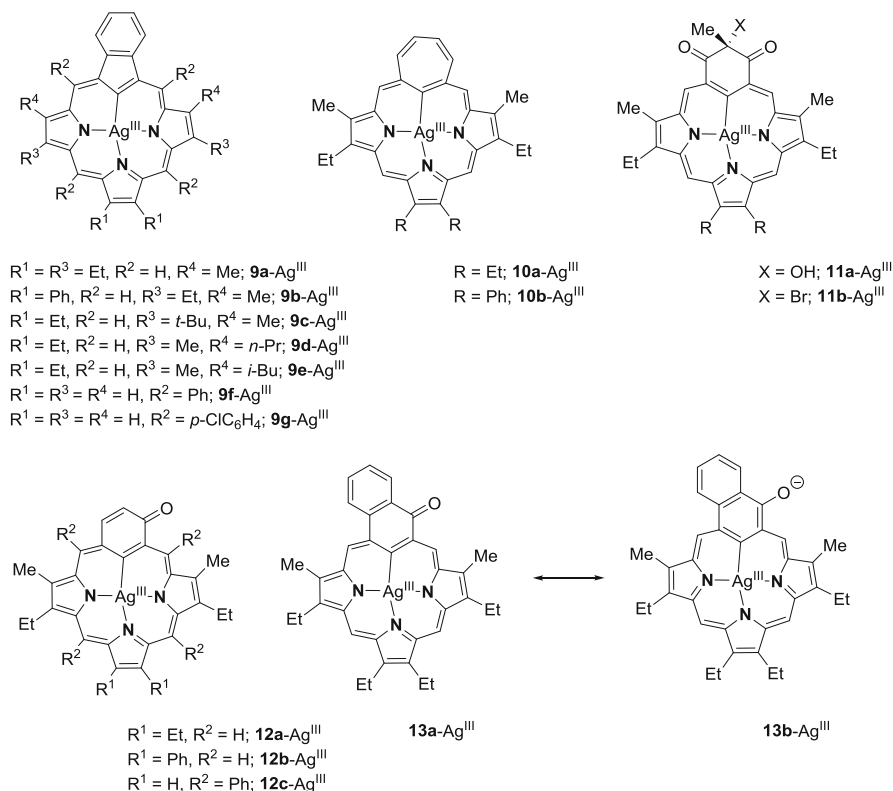
Fig. 5 Organometallic Ag^{III} complexes bearing benzocarbaporphyrin, tropiporphyrin, oxybenzi-porphyrin, and oxynaphtiporphyrin ligands

Latos-Grażyński and Chmielewski also covered the chemistry of silver complexes bearing carbaporphyrinoid ligands. First, Latos-Grażyński and coworkers reported the synthesis of complexes **6c**-Ag^{III} and **6d**-Ag^{III} in an O-confused oxaporphyrin ligand bearing a pyrrole at C(3) position (Scheme 7). Complex **6d**-Ag^{III} was found to undergo exocyclic C(3)-O cleavage and eliminate ethanol to result in **6e**-Ag^{III}, which was able to tautomerize to restore the aromaticity of the macrocycle (Scheme 7b). The addition of sodium ethoxide to the solution reverts the process recovering the starting material **6d**-Ag^{III} [33]. Two years later, the authors extended the study of Ag^{III}–oxyporphyrins by synthesizing by metalation of its original ligands, the related **6h**-Ag^{III} and **6i**-Ag^{III} complexes. Interestingly, these two complexes can interconvert controlling the pH conditions analogously as observed with complex **6d**-Ag^{III}. Further, and in a related manner as mentioned above in the reactions described by Lash's group to yield **5**-Ag^{III} complexes, ligands **6i** and **6j** were reacted with Ag^{I}OAc to yield the corresponding lactone–Ag^{III} complex **6k**-Ag^{III} regardless of the starting ligand (Scheme 8) [34].
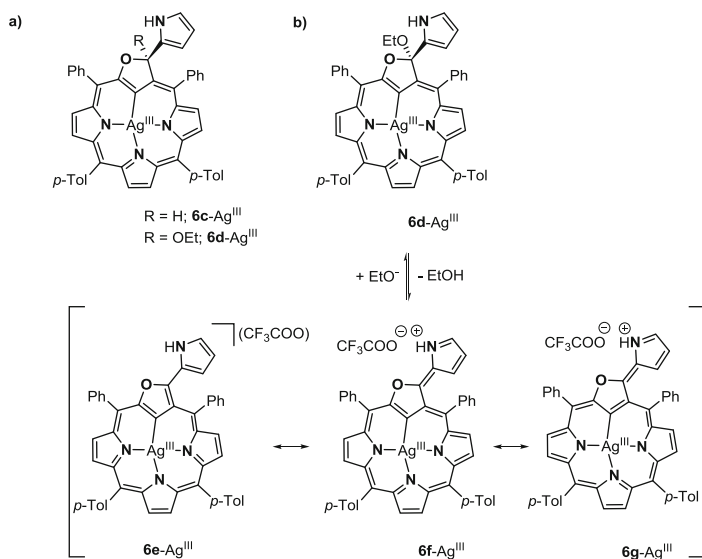
Scheme 7 (**a**) Organometallic Ag^III complexes bearing furan-substituted oxaporphyrin ligands. (**b**) Reversible pH-controlled elimination of ethanol in **6d**-Ag^III complex
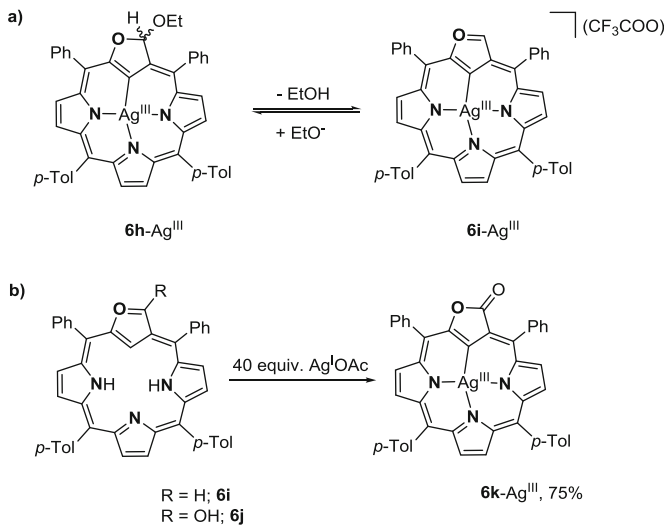
Scheme 8 (**a**) Reversible pH-controlled elimination of ethanol in **6h**-Ag^III complex. (**b**) Formation of the lactone–Ag^III complex **6k**-Ag^III by treating oxyporphyrin ligands **6i** and **6k** with excess of Ag^I OAc

Furthermore, Chmielewski also contributed to this field by appending *o*-xylyl moieties to classical NCP ligands. That led to two different ligands, **14** and **15**. The reaction of **14** with Ag^I BF$_4$ resulted in the formation of **14a**-Ag^III complex, in
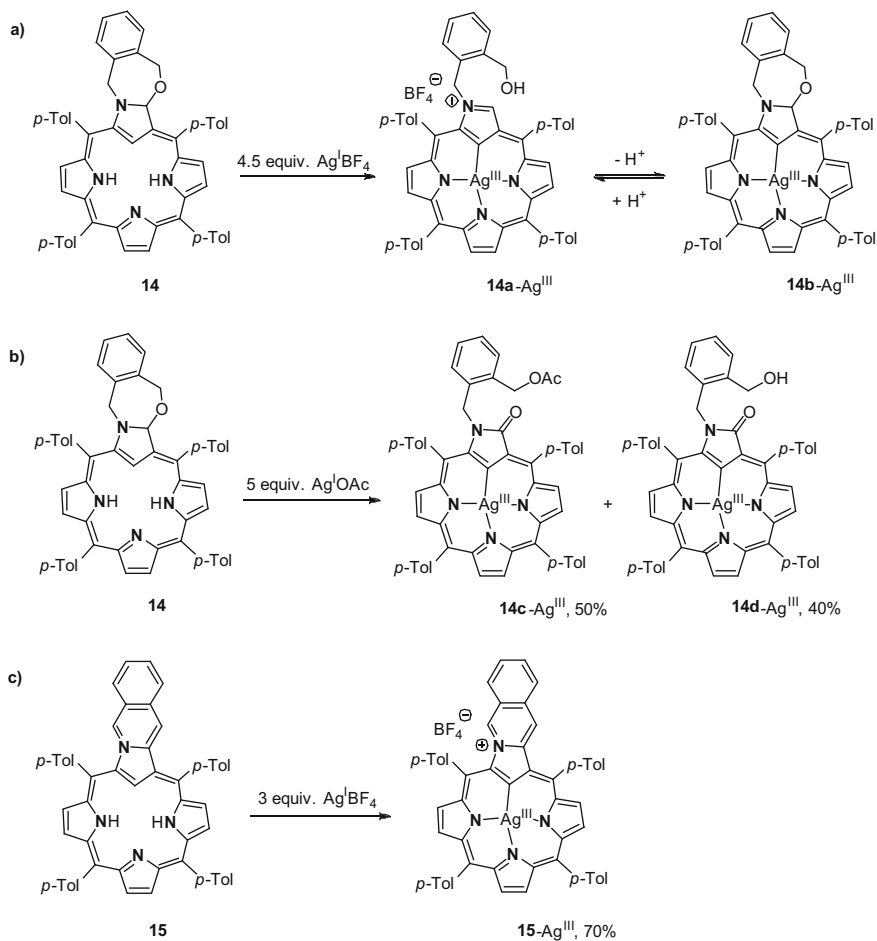
Scheme 9 (**a**) Metalation reaction of Ag^{I}BF$_4$ for the synthesis of **14a**-Ag^{III} that presents a pH-controlled equilibrium between the opening/closure of the 7-membered oxazole ring. (**b**) Formation of **14c**-Ag^{III} and **14d**-Ag^{III} upon complexation of Ag^{I}OAc over ligand **14** and subsequent oxidation. (**c**) Metalation reaction of Ag^{I}BF$_4$ over ligand **15** to yield complex **15**-Ag^{III}

which the oxazole cycle has been opened during the complexation. However, the addition of a base promotes the ring closure obtaining complex **14b**-Ag^{III} (Scheme 9a). When a less acidic silver(I) source such as Ag^I(OAc) is employed, the reaction leads to a mixture of complexes from which **14c**-Ag^{III} and **14d**-Ag^{III} could be separated (Scheme 9b). On the other hand, metalation of **15** with Ag^{I}BF$_4$ proceeds readily to produce the cationic complex **15**-Ag^{III} (Scheme 9c) [35].

Lash and coworkers also demonstrated that carbaporphyrins and carbaporphyrinoids are capable of stabilizing gold(III) complexes successfully. Most of the ligands that afforded silver(III) species proved good ligands for gold(III) species. Specifically, the reaction of Au^{III}(OAc)$_3$ with the previously described

carbaporphyrins afforded good yields of its resulting organometallic Au^{III} complexes **9b**-Au^{III}, **9f**-Au^{III}, and **9g**-Au^{III} (Fig. 6) [28]. It was demonstrated that the outcomes of the reactions using Au^{I} sources were significantly lower. Similarly, Au^{III}(OAc)$_3$ can undergo metalation into oxybenziporphyrins to provide the corresponding organometallic Au^{III} complex **12c**-Au^{III} (Fig. 6) [32].

Very recently, a ring contraction reaction mediated by Au^{III} has been observed in benziporphyrins and naphthiporphyrins. When Na[Au^{III}Cl$_4$]•2H$_2$O was reacted with ligands **16a-c**, complexes **17a**-Au^{III}, **17b**-Au^{III}, and **17c**-Au^{III} were isolated (Scheme 10) [36]. The reaction leads to the contraction of the benzene and naphthalene units into cyclopentadiene and benzocyclopentadiene, respectively, thus providing an alternative route toward the formation of the former ones out of the previously described [28]. Further, complexes **17a**-Au^{III} and **17b**-Au^{III} are susceptible to reversible protonation to interconvert between **17a**-Au^{III} and **17b**-Au^{III} to **18a**-Au^{III} and **18b**-Au^{III} (Scheme 10).

R = Ph, R^1 = Me, R^2 = Et, R^3 = H; **9b**-Au^{III}
R = R^1 = R^2 = H, R^3 = Ph; **9f**-Au^{III}
R = R^1 = R^2 = H, R^3 = p-ClC$_6$H$_4$; **9g**-Au^{III}
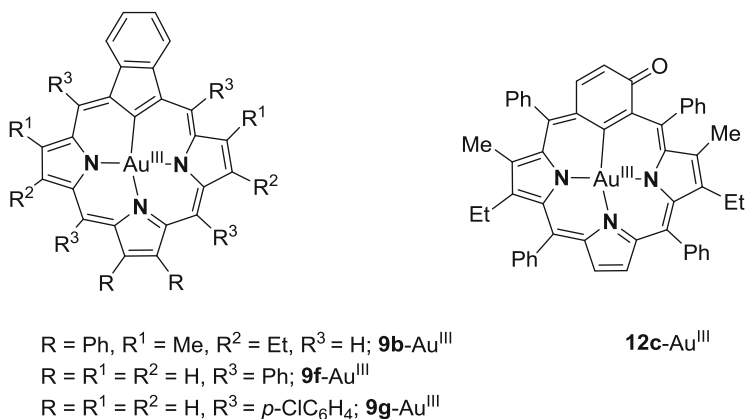
12c-Au^{III}

Fig. 6 Organometallic Au^{III} complexes bearing benzocarbaporphyrin and oxybenziporphyrin ligands

R = Ph, Ar = p-xyl; **16a**
R = p-NO$_2$Ph, Ar = p-xyl; **16b**
R = Ph, Ar = p-Naph; **16c**

R = Ph, Ar = m-Cp; **17a**-Au^{III}, 10%
R = p-NO$_2$Ph, Ar = m-Cp; **17b**-Au^{III}, 14%
R = Ph, Ar = m-PhCp; **17c**-Au^{III}, 32%

R = p-NO$_2$Ph; **18a**-Au^{III}
R = Ph; **18b**-Au^{III}
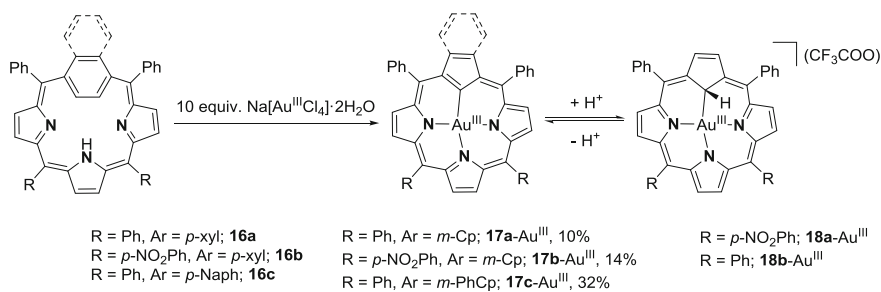
Scheme 10 Au^{III}-mediated ring contraction reactions of **16a–c** ligands. Complexes **17a**-Au^{III} and **17b**-Au^{III} are susceptible to reversible protonation

2.3   Triazamacrocyclic Aryl-X and Aryl-H Ligands

Triazamacrocyclic families of ligands containing an arene moiety have proven to be one of the few non-porphyrinic models that exhibit exceptional abilities to form organometallic square-planar Cu^{III} complexes (see complexes **19**-Cu^{III} and **19**-Cu^{III}–X in Fig. 7). Classically, these two families of complexes are synthesized by reacting the arene ligand with Cu^{II} salts under O_2 atmosphere [37–41]. Its three amine coordination sites within a macrocyclic environment direct the metal center toward the C–H bond facilitating its activation resulting in the organometallic Cu^{III} complex that contains a Cu^{III}–C bond [7, 42].

Nonetheless, **19**-Cu^{III}–X complexes, bearing a halide ligand in the apical position, could be obtained also by oxidative addition of copper(I) salts over the corresponding aryl halide macrocyclic ligand [43]. Further, Ribas and coworkers have recently demonstrated that the aryl–Ag^{III} **19e**-Ag^{III} organometallic complex, analogous to **19e**-Cu^{III}, can also be synthesized by oxidative addition over the aryl iodide and aryl bromide macrocyclic ligand (Scheme 11) [44].

The rich reactivity of these systems will be expanded in Sects. 3 and 4.

$^*X$ = OTf or ClO_4

R^1 = H, R^2 = H, n = 0; **19a**-Cu^{III}
R^1 = H, R^2 = H, n = 1; **19b**-Cu^{III}
R^1 = H, R^2 = Me, n = 1; **19c**-Cu^{III}
R^1 = H, R^2 = NO_2, n = 1; **19d**-Cu^{III}
R^1 = Me, R^2 = H, n = 1; **19e**-Cu^{III}
R^1 = Me, R^2 = Me, n = 1; **19f**-Cu^{III}
R^1 = Me, R^2 = NO_2, n = 1; **19g**-Cu^{III}

R^1 = H, Y = Cl; **19b**-Cu^{III}-Cl
R^1 = H, Y = Br; **19b**-Cu^{III}-Br
R^1 = H, Y = I; **19b**-Cu^{III}-I
R^1 = Me, Y = Cl; **19e**-Cu^{III}-Cl
R^1 = Me, Y = Br; **19e**-Cu^{III}-Br
R^1 = Me, Y = I; **19e**-Cu^{III}-I
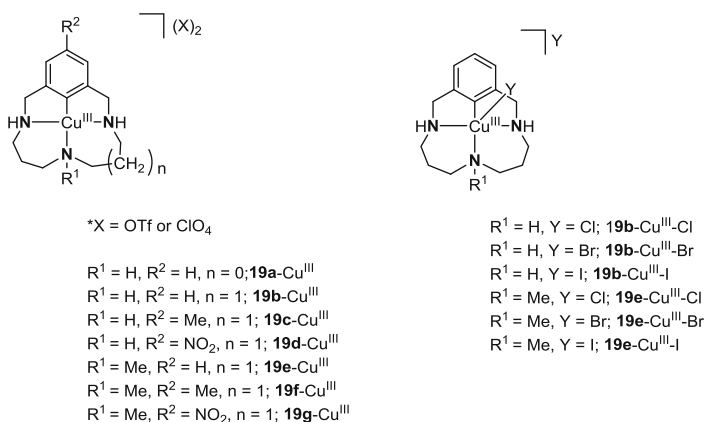
Fig. 7 Organometallic Cu^{III} complexes bearing triazamacrocyclic arene ligands
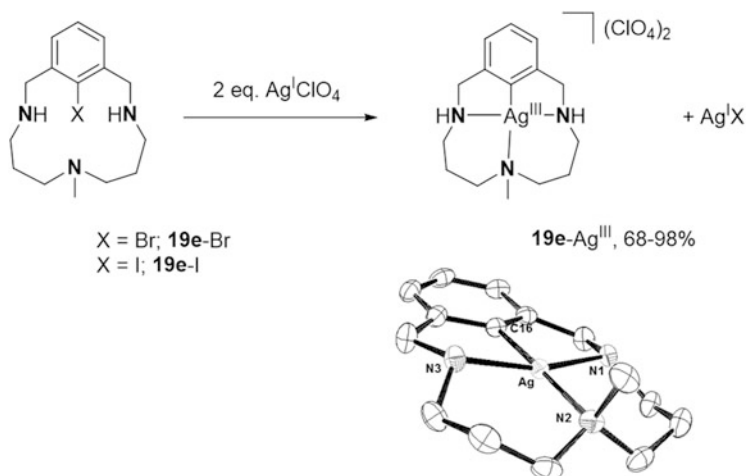
Scheme 11 Synthesis of **19e**-Ag^{III} complex (crystal structure ellipsoid diagram included, H atoms and counterions omitted for clarity) by oxidative addition of silver(I) perchlorate over macrocyclic aryl halide ligands **19e**-X (X=Br, I)

R = H; **20a**-Cu^{II}
R = OMe; **20b**-Cu^{II}
R = Me; **20c**-Cu^{II}
R = F; **20d**-Cu^{II}
R = Cl; **20e**-Cu^{II}
R = CO$_2$Me; **20f**-Cu^{II}
R = CN; **20g**-Cu^{II}
R = NO$_2$; **20h**-Cu^{II}

R = H; **20a**-Cu^{III}
R = OMe; **20b**-Cu^{III}
R = Me; **20c**-Cu^{III}
R = F; **20d**-Cu^{III}
R = Cl; **20e**-Cu^{III}
R = CO$_2$Me; **20f**-Cu^{III}
R = CN; **20g**-Cu^{III}
R = NO$_2$; **20h**-Cu^{III}
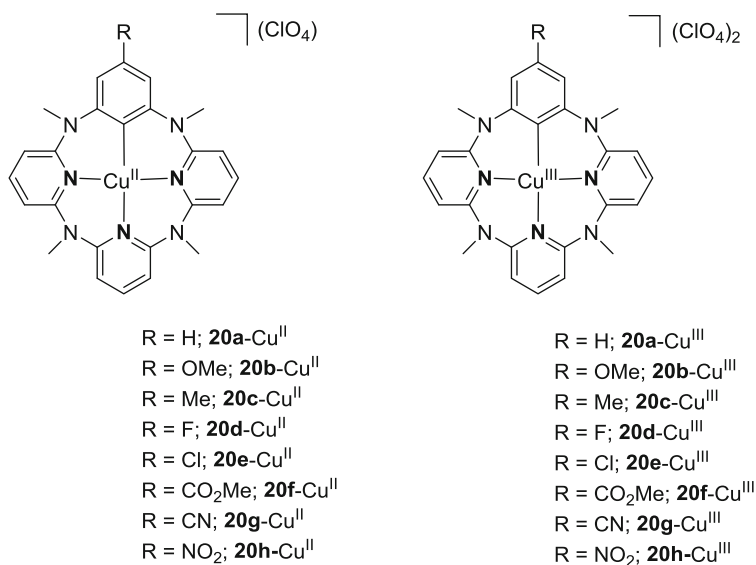
Fig. 8 Organometallic aryl–Cu^{II} and aryl–Cu^{III} family of complexes bearing substituted tetraazacalix[2]arene[3]pyridine ligands

2.4 Tetraazacalix[1]arene[3]pyridine Ligands

The last examples of pincerlike cyclic ligands capable of stabilizing Group 11 high-valent species are an heterocalixaromatic macrocycles, in particular, the family of

tetraazacalix[1]arene[3]pyridines (Fig. 8). Similarly to the aforementioned triazamacrocyclic ligands, Cu^{II} salts can activate the internal arene C–H bond in the substituted heterocalixarenes generating the unique family of aryl–Cu^{II} complexes **20**-Cu^{II} under anaerobic conditions, which could eventually furnish the corresponding family of aryl–Cu^{III} organometallic complexes **20**-Cu^{III} upon oxidation with Cu^{II} salts or Oxone® [45, 46].

3 Pincerlike Cyclized Mononuclear Aryl–Cu^{III} Model Platforms for the Understanding of Cross-Coupling Chemistry

Even though copper in its oxidation state +3 is postulated to have an active role in organic transformations such as nucleophilic organocuprate reactions for C–C bond formation, C-nucleophile cross-coupling reactions, and direct C–H bond functionalization processes, the instability of Cu^{III} species precluded its detection and identification as reaction intermediates until recently. The detection of the first copper(III) intermediate species operating in coupling chemistry was not realized until 2007 by Bertz, Ogle, and Murphy when rapid injection NMR techniques were applied to elucidate the mechanisms of these transformations [47]. Yet another strategy that flourished over the last lustrum to study cross-coupling reactions was the use of macrocyclic substrates containing an arene moiety and bearing chelating anchors to stabilize these elusive and often invoked aryl–Cu^{III} species (see Fig. 7). The study of the formation and reactivity of those model systems led to a deeper understanding of key mechanistic aspects of copper-catalyzed cross-coupling chemistry and proved the plausibility of Cu^{I}/Cu^{III} redox cycles operating on these processes in a wide range of coupling reactions.

3.1 Observation of Oxidative Addition and Reductive Elimination Fundamental Steps and Mechanistic Insights on the Catalytic Halide Exchange Reactivity

The family of aryl–Cu^{III}–X (X=Cl, Br, I) complexes **19**-Cu^{III}–X allowed to characterize for the first time a reductive elimination step from a Cu^{III} center resulting in the formation of a C_{aryl}–halide bond. Moreover, the reversibility of this process and the feasibility of the aryl halide oxidative addition to Cu^{I} resulting in the regeneration of the initial aryl–Cu^{III}–X complex were shown. By UV–Vis monitoring of the characteristic band at 420 nm corresponding to **19**-Cu^{III}–Br complex, it was demonstrated that the addition of triflic acid triggered the reductive elimination, effecting the bromination of the phenyl moiety and releasing the Cu^{I} from the macrocyclic pocket. The band at 420 nm was fully recovered by addition
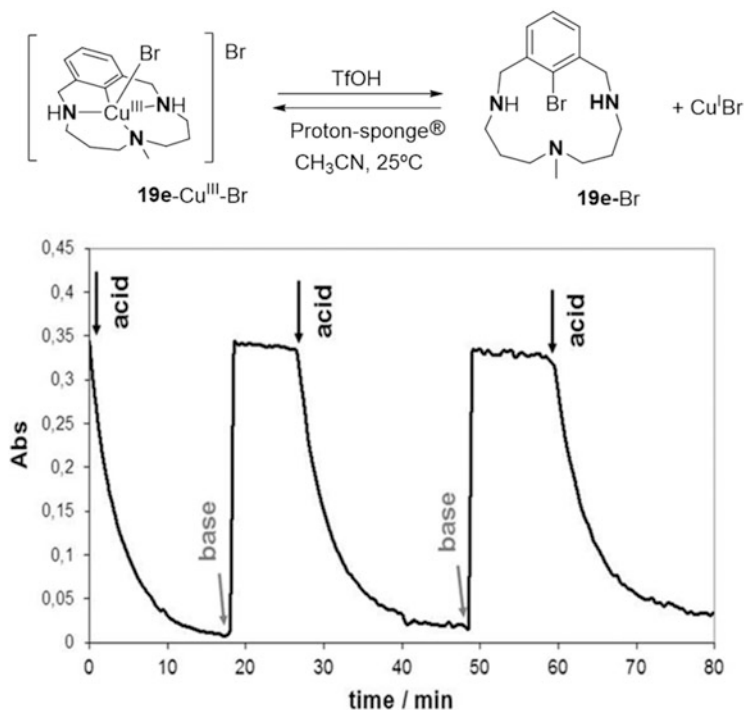
Fig. 9 UV–Vis monitoring of the sequential interconversion between Cu^{III}/Cu^I redox states by addition of acid or base

of Proton-sponge® (base) to the solution, being the first observation of aryl halide oxidative addition to Cu^I ever reported (Fig. 9). The interconversion between Cu^I and Cu^{III} redox states by sequential addition of acid and base was repeated several times without significant loss of the **19**-Cu^{III}–Br complex (Fig. 9) [39].

A detailed computational study served to reason that the protonation of one of the amines of the macrocyclic ligand causes its decoordination from the very electron-deficient Cu^{III} center, thus strongly destabilizing the complex and triggering the reductive elimination [48].

An equally effective strategy to trigger the reductive elimination and displace the equilibrium toward the halogenated ligand and Cu^I species is the use of 1,10-phenanthroline. The presence of excess of 1,10-phenanthroline that presents a large affinity for Cu^I ions drives the formation of **19e**-X (X=Cl, Br, I) coupling products and $[Cu^I(phen)]^+$ from the corresponding aryl–Cu^{III}–X species exhibiting faster rates for the stronger C–X bond formed[43].

Moreover, Wang and coworkers also described in 2009 the ability of aryl–Cu^{III} heterocalixaromatic **20a**-Cu^{III} complex to undergo halogenation reactions except fluorination upon reaction with equimolar amounts of the corresponding Et_4NX (X=Cl ,Br, I) in less than one min [45].
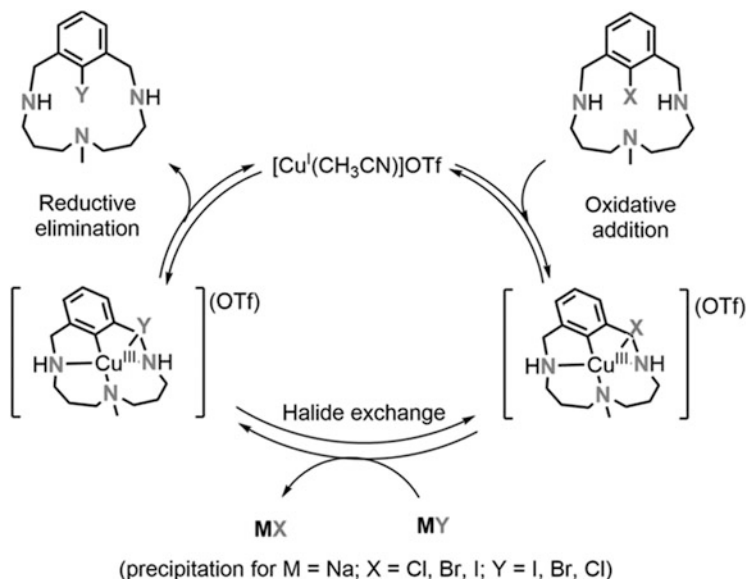
Scheme 12 General mechanistic scenario operating in Cu-catalyzed halide exchange reaction within model aryl halide model platform **19e**-X

Inspiration arose from the observation of the aforementioned acid-triggered halogenation coupling reactions of aryl–Cu^{III}–X complexes and prompted an study on the catalytic exchange of halides [43]. Aryl halide model substrates **19e**-X (X=Cl, Br, I) could be interconverted between them by employing catalytic amounts of [Cu^I(CH$_3$CN)$_4$]OTf and an excess of the desired halide MY salt (M=Na, n-Bu$_4$N; Y=Cl, Br, I). The conversion to aryl moieties bearing lighter halides from aryl moieties containing heavier ones is achieved in excellent to quantitative yields using acetonitrile as solvent and soluble n-Bu$_4$NX salts, as, for instance, in the transformation of **19e**-I to **19e**-Cl. These reactions are driven by the formation of stronger C–halide bonds. However, when the same types of reactions are run toward the opposite direction, i.e., formation of weaker C–halide bonds, the reactions resulted unsuccessful. In order to overcome this obstacle, the reaction needed a driving force other than the relative strength of the bond formed. The precipitation of the undesired halide as a sodium salt (instead of using tetra-butylammonium halide salts) turned out to be the solution to this limitation, affording exchanged products in good to excellent yields. Importantly, the resting state of this transformation was well characterized and found to be the product of oxidative addition plus halide exchange, strongly suggesting that reductive elimination is the rate-limiting step of the reactions (Scheme 12).

The size of the macrocyclic platform is a key factor for the stabilization of the copper center in +3 oxidation state, although the same reactivity pattern has been observed for smaller analogous systems. For instance, **19e**-Cu^{III} complex defines a 14-membered cavity suitable for accommodating copper(III) ions and observing
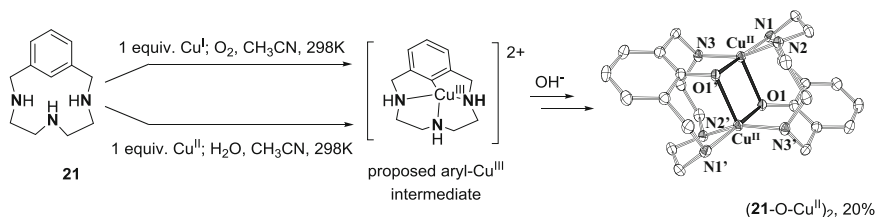
Scheme 13 Aromatic hydroxylation of **21** ligand via aryl–Cu^{III} species resulting in the final isolation of bis-phenoxo–Cu^{II} complex (crystal structure ellipsoid diagram included, H atoms omitted for clarity)

Scheme 14 Catalytic fluorination of N-permethylated aryl halide substrates **22**-X (X = Cl, Br)
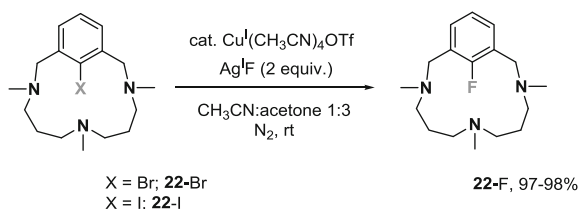
subsequent couplings on the ring upon addition of nucleophiles. In contrast, ligand **21**, analogous to **19e** but defining a 12-membered cavity, reacts either with Cu^{II} or Cu^{I} in the presence of molecular O$_2$ to generate elusive intermediate species that are able to perform the coupling of hydroxide anions affording eventually a dinuclear bis-phenoxo-Cu^{II} compound ((**21**-O-Cu^{II})$_2$) in moderate yields presumably after a reductive elimination from a putative aryl–Cu^{III}–OH species (Scheme 13) [5, 49]. In both cases, the coupling chemistry is related, but the size of the cavity defined by the ligand is crucial for the stabilization of the aryl–Cu^{III} key intermediate species. Our reasoning to explain the superior ability of macrocycle **19e** to stabilize Cu^{III} ions is that the copper center is coordinated with the 3 nitrogens of the macrocyclic system in the same plane and directs the metal center toward the phenyl moiety eventually effecting the C–H bond activation resulting in a square-planar complex, whereas ligand **21** provides a facial coordination in which copper lies farther from the carbon of the aryl and also disfavors the formation of square-planar complexes.

Fluorination reactions were more challenging and only tolerated silver fluoride and KF (although obtaining poorer yields) as the fluoride source. Slow addition of the fluorinating agent increased substantially the outcome of the reactions by reducing undesired deprotonation of the secondary amines of the aryl–Cu^{III}–X (X = Cl, Br) species by the basic fluoride anions. To further improve the yields of fluorinated arenes, structurally related N-permethylated macrocyclic **22**-Cl and **22**-Br substrates were prepared. After optimization, quantitative conversion of **22**-Cl and **22**-Br to **22**-F was accomplished in a 1:3 mixture of CH$_3$CN–acetone at room temperature using 2 equiv. of Ag^{I}F (Scheme 14).

The stoichiometric activation of C_{aryl}–F bonds, that is, the defluorination reaction, was also carried out successfully and by reacting equimolar amounts of **19e**-F and $[Cu^I(CH_3CN)_4]OTf$ in acetone in the presence of excess of *n*-Bu$_4$NCl furnished the aryl–Cu^{III}–Cl complex **19e**-Cu^{III}–Cl in 75% yield.

Wang and coworkers showed recently and for the first time that aryl pseudohalides such as aryl triflates embedded in heterocalixaromatics can undergo this same copper-catalyzed two-electron redox chemistry described for aryl halides in halogenation and acyloxilation reactions. In their study, the oxidative addition step of copper(I) over the C–O bond of the aryl triflate and the reductive elimination from this complex to furnish aryl halides and aryl acyloxilates have been proven individually [50].

The oxidative addition and reductive elimination redox steps have been fully characterized for the first time, allowing to further investigate their implication in catalytic processes (see Sect. 3.2).

3.2 Mechanistic Insights on Ullmann-Type Coupling Reactions

Copper-catalyzed C_{aryl}–nucleophile bond forming cross-coupling reactions, known as Ullmann-type chemistry, has emerged as a powerful tool to effect the arylation of amines, amides, alcohols, carboxylic acids, and thiophenols among the wide range of nucleophiles able to participate in these couplings. These reactions have been known for more than a century, although its practicality was very limited until the late 1990s, when the harsh conditions and stoichiometric amounts of metal required in the original reports were improved by the addition of auxiliary ligands [7, 51]. Despite the extensive development of Ullmann methodologies in the late 1990s, the fundamental steps governing the coupling reactions remained obscure. To put forward Ullmann-type chemistry and to base its development on rational grounds, there was a need for the understanding of its mechanistic pathways. In this sense, many proposals were drawn, including radical and non-radical processes (Scheme 15). The two radical pathways postulate the formation of aryl radicals that can recombine with Cu^{II}–nucleophile species to form the product of coupling and Cu^I. Among the non-radical processes, the most invoked mechanism is the one that proceeds through oxidative addition/reductive elimination processes, although σ-bond metathesis and S$_E$Ar processes driven by the π-complexation of Cu^I have also been proposed (Scheme 15).

Our research group and others have demonstrated the capability of aryl–Cu^{III} complexes to generate C_{aryl}–heteroatom bonds upon reaction with nitrogen-based nucleophiles [41] (lactams, imides, sulfonamides, oxazolidone, and benzamides), oxygen-based nucleophiles [45, 52–54] (carboxylic acids, alcohols), sulfur-based nucleophiles [45, 55] (thiols, thiocyanate), selenium-based nucleophiles [55] (benzeneselenol), and phosphorus-based nucleophiles [55] (H-phosphonate
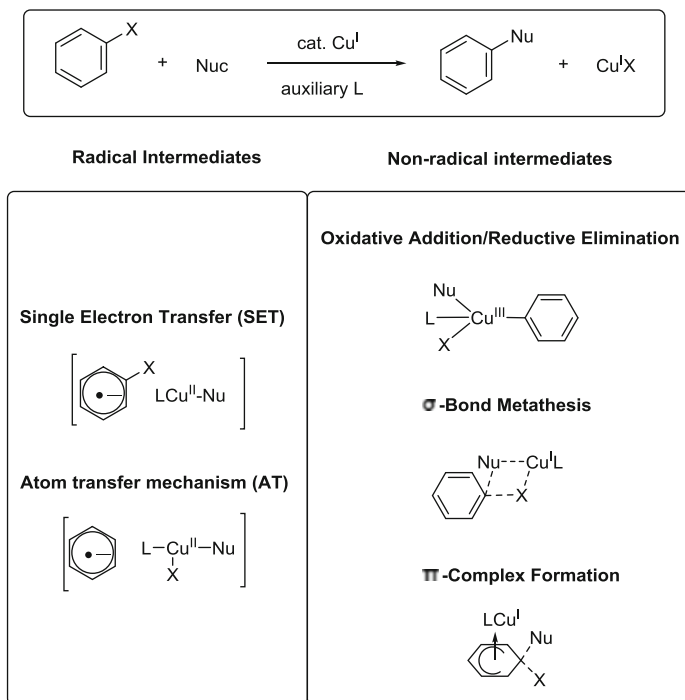
Scheme 15 Radical and non-radical reaction intermediates postulated to operate in Ullmann-type coupling reactions

diesters). This step can be envisioned to occur through two possible mechanisms: (1) a three-centered C-nucleophile reductive elimination from the non observed aryl–Cu^{III}–nucleophile intermediate or (2) a bimolecular nucleophilic attack of a deprotonated nucleophile on the ipso carbon of the aryl ligand. While for halogenation reactions it is clear that the first pathway is functional, being aryl–Cu^{III}–X complexes isolated and fully characterized, for C-nucleophile reactions, the authors have only been able to detect by low-temperature UV–Vis and NMR techniques aryl–Cu^{III}–nucleophile adducts prior to the nucleophile deprotonation step [52, 55]. Further, both oxidative addition and coupling steps could be merged to realize a catalytic process with the whole range of nucleophiles (Scheme 16). In all cases, the presence of aryl–Cu^{III}–halide species has been identified as the resting state of the catalysis and thus has been detected spectroscopically during the course of the reaction.

Stahl's group showed in 2008 that the aryl–Cu^{III} complexes **19e**-Cu^{III}, **19f**-Cu^{III}, and **19g**-Cu^{III} (Fig. 7) react readily with nitrogen-based nucleophiles resulting in the eventual C_{aryl}–N bond formation. Interestingly, the more electron-withdrawing is the substituent on the aryl moiety of the Cu^{III} complex, the fastest is the reaction, indicating that more electrophilic aryl–Cu^{III} reacts best with the nucleophile. Regarding the electronic effects on the nitrogen nucleophile, a Brønsted plot
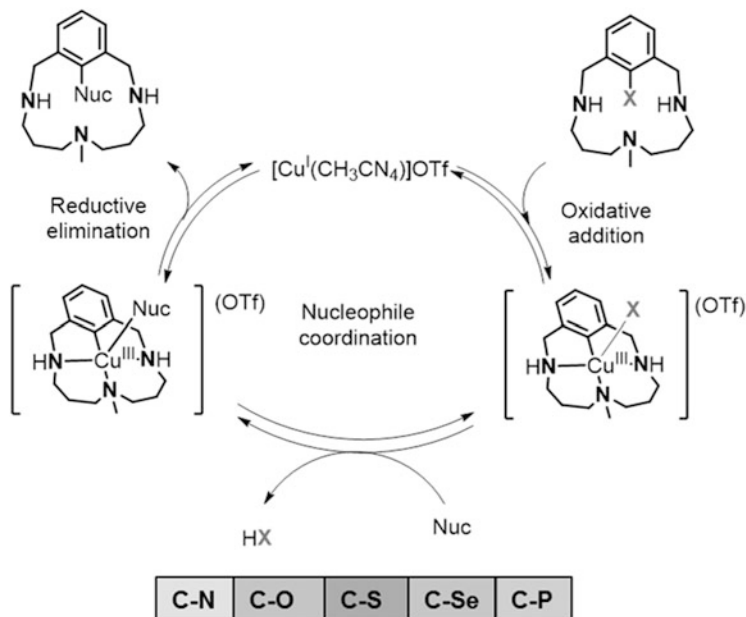
Scheme 16 General mechanistic scenario operating in Cu-catalyzed C–N, C–O, C–S, C–Se, and C–P cross-coupling reactions within model aryl halide model platform **19e**-X

reflected that the reaction was dependent on the pK_a of the nucleophile indicating that the deprotonation step occurs before or during the rate-limiting step [41]. Later in 2010, Ribas and Stahl's groups demonstrated that the final C–N coupling products could be achieved in a catalytic fashion by employing $[Cu^I(CH_3CN)_4]$ PF_6 as catalyst (<5 mol%) and the macrocyclic aryl bromide **19e**-Br as substrate via aryl–Cu^{III}–Br intermediates [39].

The same operative Cu^I/Cu^{III} catalytic cycle has been now validated for O-, S-, Se-, and P-nucleophiles (Scheme 16) [52, 55].

The propensity of **19e**-Cu^{III} complex to undergo facile reductive elimination was strengthened by the observation of a *trans* intramolecular C–N coupling when it was heated in acetonitrile in the absence of a nucleophile [56]. In this case, the high reactivity of the complex led to an unusual *trans* reductive elimination with the tertiary amine of the ligand, presumably after the coordination of one acetonitrile to facilitate the isomerization of the macrocyclic ligand into the *cis* aryl amine configuration required for reductive elimination to occur.

3.3   Mechanistic Insights on Hurtley Coupling Reactions

The coupling of aryl halides with active methylenes catalyzed by copper-bronze or copper(II) acetate was discovered by Hurtley in 1929 [57]. From the late 1990s, diverse research groups put their efforts on improving the reaction conditions and expanding the scope of Hurtley couplings and reached these objectives by employing bidentate ligands and Cu^I salts as catalysts [51]. Despite the advances on the development of methods for Hurtley couplings, the mechanistic details of these reactions have been rarely explored, and there was no consensus on its reaction pathways. In 2012, Hartwig and Huang shed light into the mechanism of Hurtley condensations by studying the behavior of isolated Cu^I–enolate complexes in the presence of aryl iodides [58]. This work described the facile α-arylation of the enolates upon addition of aryl iodides in DMSO under mild reaction conditions. *Ortho* and *para* competition reactions together with radical clock experiments ruled out the formation of radical intermediates during the reaction disfavoring a mechanism requiring an electron transfer step to effect the cleavage C–halide bond. In addition, the authors, supporting their arguments on DFT grounds, proposed a catalytic cycle involving an aryl halide oxidative addition step to a C-bound form of the Cu^I–enolate complex followed by a reductive elimination to release the coupling product. Yet the field raised another precedent that pointed in the direction of two-electron redox transformations to afford the coupling products. This was the work published by Wang and coworkers that same year, in which they reported the C_{sp2}–C_{sp3} bond condensation between aryl–Cu^{III} complex **20a**-Cu^{III} and ethyl cyanoacetate and diethyl malonate showing that the reductive elimination process can account for the formation of the products of condensation although in moderate yields [59]. However, it was not until 2013 that the first experimental evidence of a Hurtley condensation reaction that operates through a well-characterized Cu^I/Cu^{III} redox catalytic cycle was reported [60]. The macrocyclic platforms capable of stabilizing high oxidation states provided by **19** ligands were also exploited to gain mechanistic insight on copper-catalyzed C–C couplings. For instance, aryl–Cu^{III} complex **19e**-Cu^{III} proved the versatility of its reactivity upon reaction with substrates containing active methylenes such as malononitrile, dimethyl malonate, and acetylacetone. Ribas and coworkers observed the coupling of aryl–Cu^{III} complex **19e**-Cu^{III} and activated methylene containing substrates that in this case is accompanied by a subsequent intramolecular cyclization triggered by the nucleophilic attack of one of the secondary amines over one of the unsaturations of the coupled product. More importantly, the catalytic version of these reactions proved successful yielding the corresponding **P1**, **P2**, and **P3** heterocyclic products in moderate to excellent yields (Scheme 17). The UV–Vis monitoring of the cross-coupling reaction of **19e**-Br with malononitrile employing catalytic amounts of [Cu^I(CH_3CN)$_4$]OTf revealed the formation of the well-defined aryl–Cu^{III}–Br species as the resting state of the catalyst under the reaction conditions suggesting a rate-limiting replacement of the apical halide ligand by the nucleophile. A detailed mechanistic proposal for the formation of the final **P1** product bearing a 1,2-dihydroisoquinoline scaffold is shown in Scheme 18.
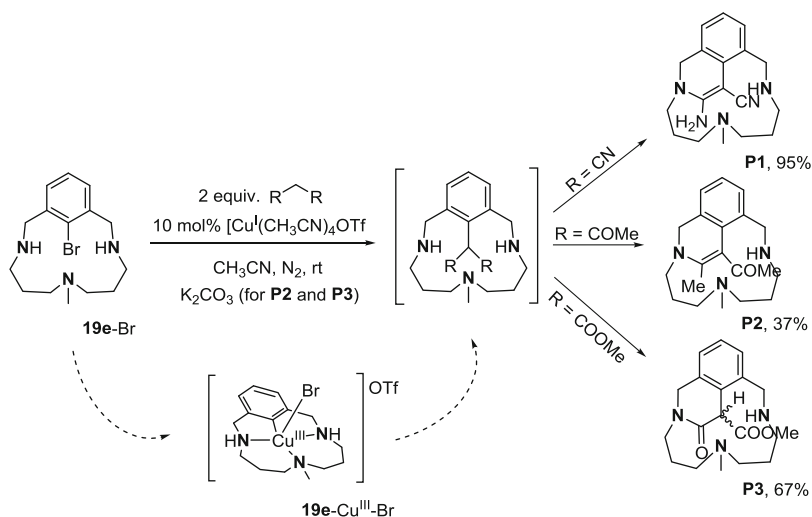
Scheme 17 Model catalytic Hurtley-type reactivity of Cu^I species within macrocyclic pincerlike ligand **19**-Br upon reaction with activated methylene substrates giving rise to the corresponding coupling plus intramolecular cyclization products **P1**-**P3** through well-defined **19e**-Cu^{III}–Br species
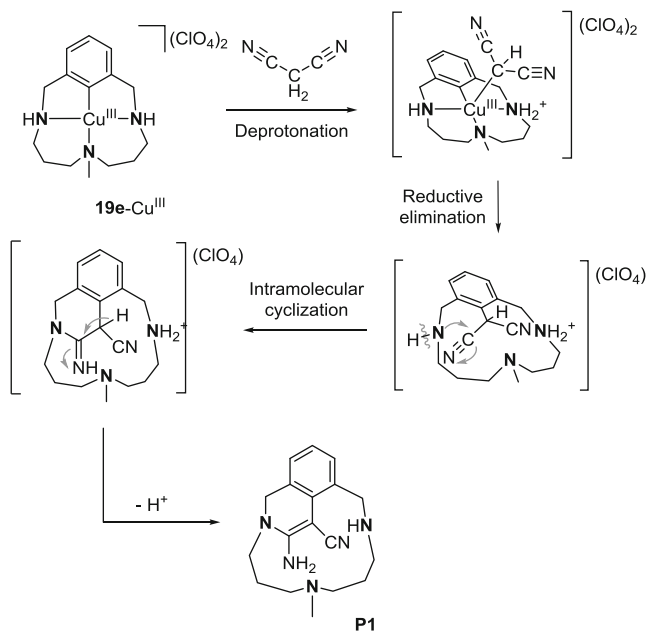
Scheme 18 Proposed mechanism for the coupling of aryl–Cu^{III} **19e**-Cu^{III} species with malononitrile followed by intramolecular reorganization to afford product **P1**

In summary, the studies presented in this section show that the two electron Cu^I/Cu^{III} redox cycles already established in some examples of Ullmann-type cross-coupling reactions are also extensive to reactions where C–C bonds are formed.

3.4 Mechanistic Insights on Stephens–Castro Coupling Reactions

Researchers, in their continued effort to replace palladium in cross-coupling methodologies by more abundant metals that present reduced toxicity, such as copper or iron, have developed some examples of palladium-free Sonogashira couplings. Stephens and Castro were the first to observe the coupling between aryl halides and copper(I) acetylides under N_2 atmosphere [61]. Moreover, when the aryl halide is *ortho*-substituted with a nucleophile, the heterocyclic product is produced, giving access to indoles, benzofurans, and isocoumarins. Miura's group discovered thirty years later that the process can be achieved catalytically by using copper iodide and triphenylphosphine (1:2 ratio) instead of stoichiometric amounts of copper(I) acetylide [62]. Both authors proposed a mechanism operating via σ-bond metathesis, although no experimental evidence was provided to support their claim.

Nevertheless, in 2012, Wang's group put their efforts in exploring the mechanism of Stephens–Castro reaction. First they tested the conditions for the Stephens–Castro catalysis in their pincerlike cyclized platform **20**. Thus, the corresponding aryl iodide substrate **20**-I was submitted to reaction with phenylacetylene in the presence of substoichiometric amounts [$Cu^I(CH_3CN)_4$]OTf, triphenylphosphine, as the auxiliary ligand and excess of a base in DMF to finally afford the coupling product **P4** in 76% yield after 12 h that is reminiscent of the coupling products to which Stephens–Castro reaction gives access (Scheme 19). Alternatively, the two steps of the catalysis, i.e., the activation of C–I bond of the aryl iodide and the acetylide couplings, were attempted independently. On one side, the authors were able to isolate the aryl–Cu^{III} species **20a**-Cu^{III} upon reaction of **20a**-I with 2 equiv. of [$Cu^I(CH_3CN)_4$]OTf. On the other hand, they showed that the isolable aryl–Cu^{III} complex **20a**-Cu^{III} complex reacts with phenyl acetylene to yield the C_{aryl}–$C_{alkynyl}$ coupling product (Scheme 19). All this data enabled the authors to postulate an alternative mechanism to the long established σ-bond metathesis scheme involving two-electron Cu^I/Cu^{III} redox cycles comprising oxidative addition and reductive elimination fundamental steps.

Very recently, Ribas's group showed parallel results to those reported by Wang with complex **19e**-Cu^{III}, which reacted in the same fashion observed for heterocalixarene aryl–-Cu^{III} complex **20a**-Cu^{III} in the presence of acetylenes at 0°C in CH_3CN. After 30 min. reacting with *p*-ethynyl-α,α,α-trifluorotoluene, full formation of the C_{aryl}–$C_{alkynyl}$ coupling product **I1** was attained and was fully characterized [63]. However, after 18 h at 0°C, this product completely reverted to the
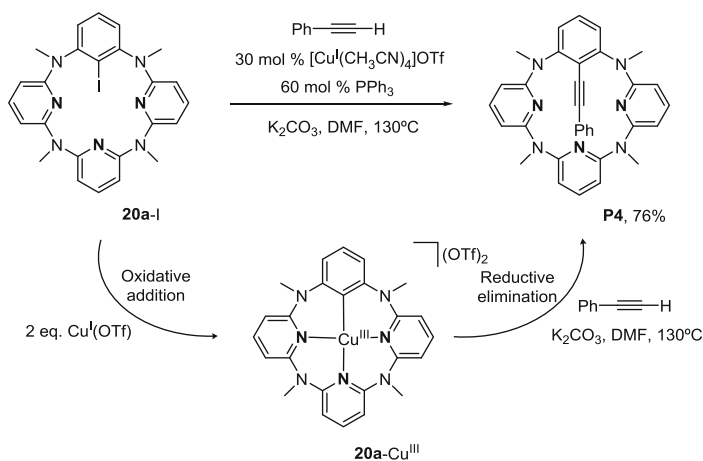
Scheme 19 Stephens–Castro chemistry operated by a Cu^I/Cu^{III} redox cycle within the pincerlike cyclized platform **20**

intramolecular reorganization product **P6**, reminiscent of the reactivity observed previously with active methylene substrates (Sect. 3.3) [60]. This is also in line with the cascade chemistry used by Stephens and Castro [61] and others [62, 64, 65] that takes advantage of the capacity of alkynes to act as electrophiles to prepare heterocyclic scaffolds. The authors proposed the nucleophilic attack of one of the secondary amines over the unsaturation of the inserted acetylide, which is activated by the liberated Cu^I into the solution, to eventually afford 5-membered ring 2*H*-isoindole products (Scheme 20). However, the nucleophilic attack could take place on both carbons of the triple bond. This is not observed for the two acetylenes bearing electron-withdrawing groups tested, i.e., *p*-ethynylnitrobenzene and *p*-ethynyl-α,α,-α-trifluorotoluene, but phenylacetylene shows a nearly 1:1 mixture of the 5- and 6-membered rings **P5a** and **P5b**. The computed representation of the frontier orbitals of the C–C coupling products **I1**, **I2**, and **I3** showed that only phenylacetylene presents a LUMO orbital that involves the contribution of the orbitals of both carbons of the alkyne and thus is the only residue among the alkynyl substrates that can undergo nucleophilic attack on both carbons of the triple bond.

Overall, these two examples of mechanistic studies that exploit the ability to stabilize aryl–Cu^{III} species open up alternative explanations to rationalize the pathways through which Stephens–Castro reactions proceed and confirm again the plausibility of Cu^I/Cu^{III} processes including oxidative addition and reductive elimination steps in palladium-free Sonogashira C–C bond-forming cross-couplings reactions catalyzed by copper.
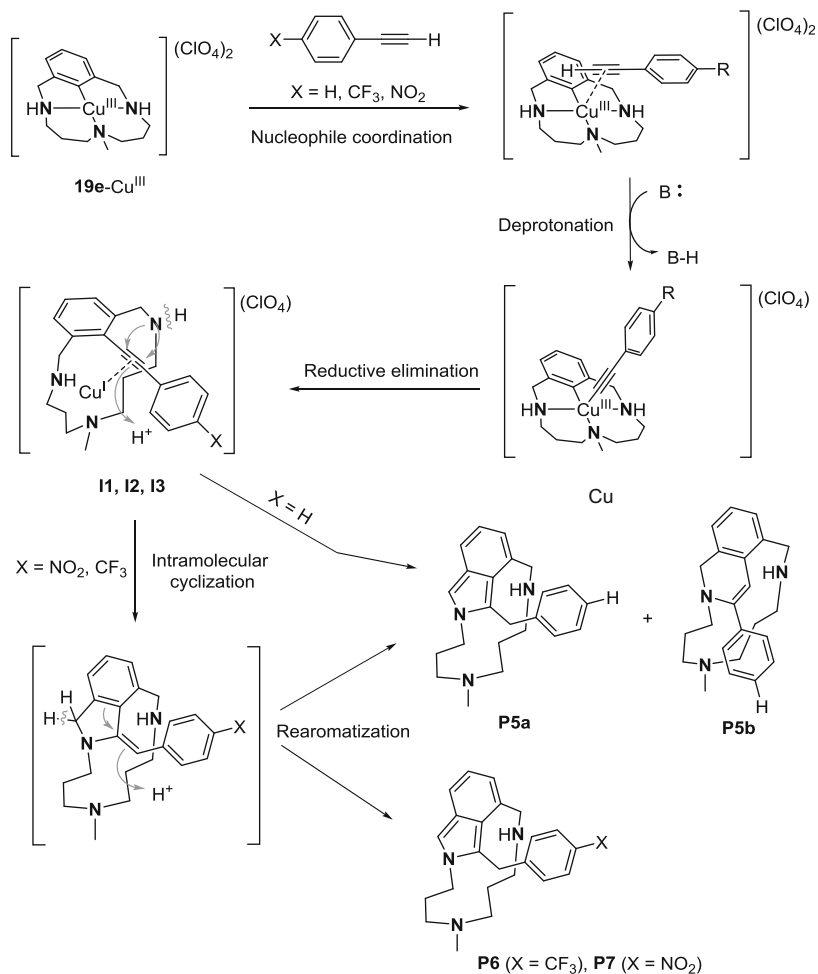
Scheme 20 Mechanistic proposal for the formation of coupling plus intramolecular reorganization products **P5**-**P7** via the aryl–Cu[III] species **19e**-Cu[III]

3.5 Mechanistic Insights on Copper-Promoted C–H Functionalizations

Selective activation of ubiquitous C–H bonds is becoming one of the major achievements of modern chemistry despite the fact that there are still grand challenges to overcome to reach this goal with all its plenitude. The direct access to molecules from common hydrocarbon feedstocks, namely, the functionalization of non-prefunctionalized raw materials, would have a tremendous relevance in terms of simpler, more effective, and less costly routes in organic synthesis as well as the reduction of waste generation. The vast majority of C–H
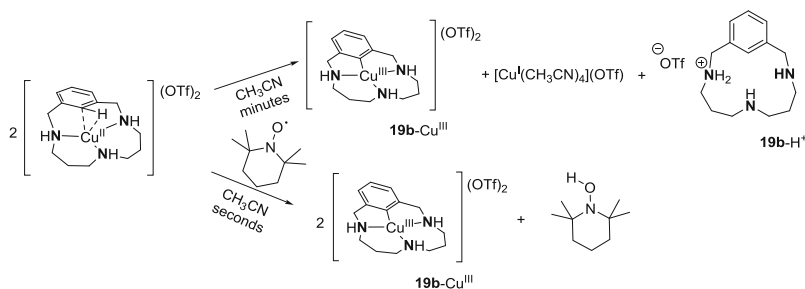
Scheme 21 Formation of **19b**-Cu^{III} complex after rate-limiting C–H cleavage by PCET favored by free Cu^{II} or TEMPO species

functionalizations require the use of metal catalysts to effect the transformation. Within the context of coinage metals, copper-catalyzed C–H functionalization has been widely explored since the seminal work from Yu's group, on the C–H functionalization of phenylpyridine type of substrates [66, 67]. Despite the large amount of resources spent on this purpose, the mechanisms that govern the C–H activation steps remain poorly understood. However, the reactions to generate aryl–Cu^{III} complexes within pincerlike cyclic systems through C–H bond cleavage have been deeply studied by their authors.

In this regard, Ribas et al. studied by means of pulse electron paramagnetic resonance (EPR) spectroscopy, DFT calculations, and kinetic studies the rate-limiting Cu^{II}-mediated C–H cleavage step in the formation of the aryl–Cu^{III} complex **19b**-Cu^{III} (Scheme 21) [42]. The reaction of Cu^{II}(OTf)$_2$ with ligand **19b** in acetonitrile under N$_2$ atmosphere yielded equimolar amounts of **19b**-Cu^{III} and [Cu^I(CH$_3$CN)$_4$]OTf by formal disproportionation reaction of Cu^{II}. A rate-limiting C–H bond cleavage step was confirmed by the measured kinetic isotope effect (KIE) k_H/k_D of 3.0 for the formation of **19b**-Cu^{III} with ligand **19b** and its deuterated analog **19b-D**. A three-center three-electron C–H···Cu^{II} interaction previous to the C–H bond cleavage was identified by low-temperature pulse EPR spectroscopy and found support on DFT calculations. Kinetic data pointed toward a rate-limiting proton-coupled electron transfer (PCET) that is coupled with the protonation of a molecule of free ligand and the oxidation of copper to aryl–Cu^{III} by another equivalent of Cu^{II}. The accelerated rates and quantitative formation of **19b**-Cu^{III} of the reaction when TEMPO, a good proton and electron acceptor, was employed bolster the proposal of a rate-limiting PCET pathway (Scheme 21).

Interestingly, Cu^{II}-catalyzed C–H functionalization of triazamacrocyclic arene ligands can be effected analogously to the Cu^I-catalyzed functionalization of C–halide bonds discussed in previous sections. In a copper(II)-catalyzed aerobic functionalization of an arene moiety, substrate **19e** and catalytic amounts of Cu^{II}(ClO$_4$)$_2$ or Cu^{II}Br$_2$ promoted the C–N bond forming coupling with pyridone and the methoxylation reactions in excellent yields; indeed, aryl–Cu^{III} species were
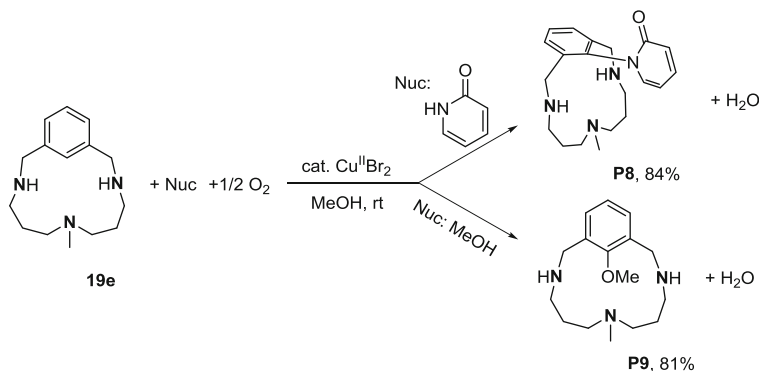
Scheme 22 Copper(II)-catalyzed C–H functionalization of **19e** ligand using pyridine and methanol as the coupling partners

detected during the course of the reaction by UV–Vis spectroscopy (Scheme 22) [40].

A strikingly different scenario was found by Wang and coworkers on the fundamental pathways that govern the C–H activation of tetraazacalix[1]arene[3] pyridines to afford aryl–Cu^{II} complexes and the corresponding aryl–Cu^{III} complexes after electron transfer. Under anaerobic conditions and the presence of excess of collidine as a base, the family of Cu^{II} complexes **20**-Cu^{II} was obtained in yields ranging from 74% to 88% after mixing equimolar amounts of Cu^{II}(ClO$_4$)$_2$•6H$_2$O and the family of tetraazacalix[1]arene[3]pyridine ligands **20**. These complexes appear stable under atmospheric conditions, exhibiting no self-disproportionation, but are rapidly oxidized to its corresponding aryl–Cu^{III} complexes **20**-Cu^{III} in the presence of 1 equiv. of Cu^{II}ClO$_4$•6H$_2$O, which was quantitatively reduced to Cu^{I}(CH$_3$CN)$_4$ClO$_4$ (Scheme 23). Oxone$^®$ was also used as oxidant with similar reaction outcomes.

To investigate how the C–H bond cleavage step takes place, experiments including reaction kinetics, Hammett plots, and KIE measurements were carried out. UV–Vis measurements of the reaction rates of the reactions of **20** heterocalixarene ligands and Cu^{II}(ClO$_4$)$_2$•6H$_2$O with excess of collidine using stopped-flow techniques afforded a Hammett plot showing excellent linearity and a slope of −1.56. The latter value strongly suggested the development of a positive charge during the rate-limiting step of the reaction. The KIE obtained by measuring the reaction rate of the macrocyclic platform in which the activated proton is replaced by deuterium is 1.13, indicating a low primary effect. These studies served as rational ground for the authors to draw a plausible mechanism to sustain the observed reactivity. The mechanistic proposal, which is supported on DFT calculations, is initiated by a rate-limiting nucleophilic attack of the arene moiety over the Cu^{II} already coordinated to the three pyridine residues of the ligand, giving rise to the Wheland intermediate **II**. The subsequent step is the deprotonative rearomatization of the arene effected by a base eventually affording **20**-Cu^{II} complexes. Further oxidation of the generated Cu^{II} species by free Cu^{II} or Oxone$^®$ finally furnishes **20**–Cu^{III} complexes (Scheme 24).
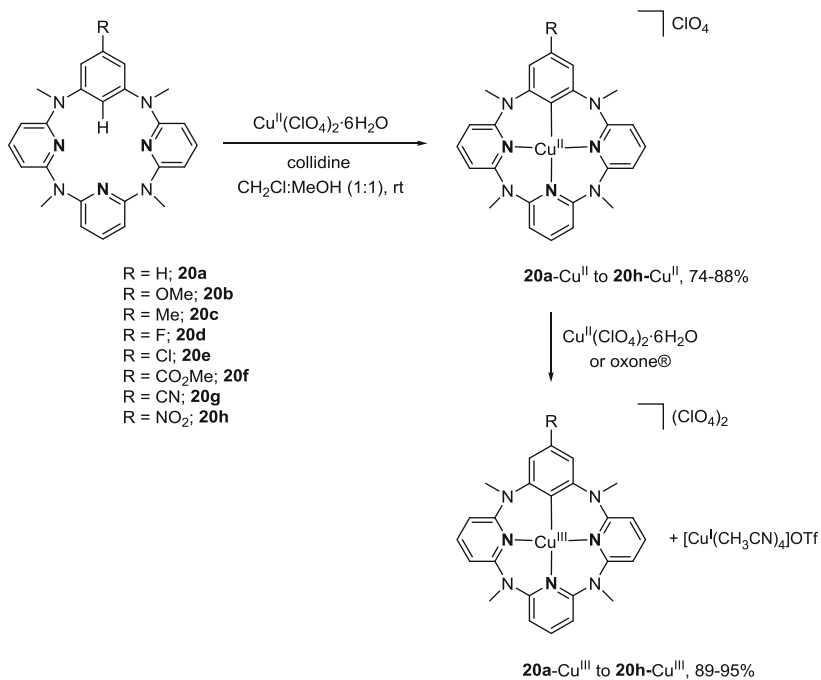
Scheme 23 Synthesis of the family of aryl–Cu^{II} complexes **20**-Cu^{II} and their conversion to aryl–Cu^{III} complexes **20**-Cu^{III}
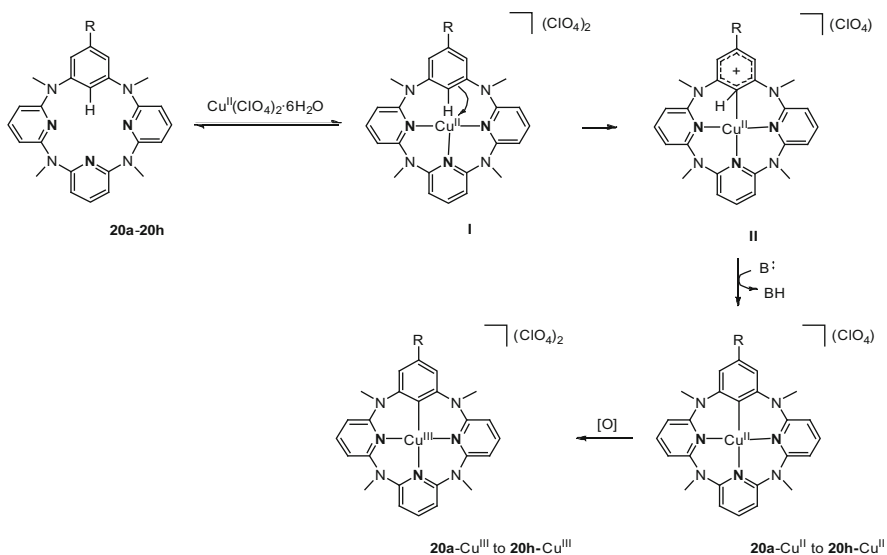
Scheme 24 Proposal of the C–H metalation mechanism of heterocalixarene **20a–20h** ligands to form complexes **20**-Cu^{II} and **20**-Cu^{III}

4 Pincerlike Cyclized Mononuclear Aryl–Ag^{III} Model Platforms for the Understanding of Cross-Coupling Chemistry

Pincerlike cyclic scaffolds have clearly shown to be privileged architectures for the study of the behavior and reactivity of copper. The potential of these structures to study the reaction pathways in copper-catalyzed cross-coupling processes has been largely exploited, and the knowledge gained has led to the development of new concepts on copper reactivity. However, the utility of pincerlike cyclic systems is not confined to copper chemistry, and recently studies with other group 11 metals as silver have emerged. In fact, silver holds the most unexplored chemistry among the coinage metals, and its redox chemistry is the least understood [68–72]. Silver redox chemistry is generally thought to stem exclusively from one-electron redox reactivity, in contrast to the two other coinage metals, copper and gold, which are known to undergo two-electron redox chemistry [73, 74]. Nevertheless, silver effectively catalyzes typically two-electron-operated cross-coupling reactions such as palladium-free Sonogashira-type couplings [75] and copper-free Ullmann-type C–heteroatom bond forming reactions [76]. However, no mechanistic ground has been reported on silver-catalyzed cross-coupling reactions, hampering the development and design of new synthetic methodologies based on silver. Very recently, pincerlike cyclic structures containing aryl halide moieties have also been utilized to gain insight on the reactivity of silver.

The first examples of such chemistry consisted in the regioselective acetoxylation and pyridination of a carbaporphyrinoid, specifically a benziporphyrin. Treatment of the benziporphyrin scaffold **23** with a large excess of Ag^{I}BF$_4$ in refluxing pyridine produced the product of pyridination of the inner C–H bond of the arene moiety to afford the aryl pyridinium **P10** product (Scheme 25) [77]. Similarly when the reaction is carried out with excess of Ag^{I}OAc, the analogous acetoxylation product was obtained [78].

Since the reaction occurred with complete regioselectivity on the inner carbon of the carbaporphyrin, a mechanism involving radical intermediates was ruled out. Hence, a mechanism operated through aryl–Ag^{III} intermediates was proposed, although no evidence was provided to support these pathways. Indeed, a first C–H activation of the inner C–H of the aryl is proposed to generate the aryl–Ag^{III}
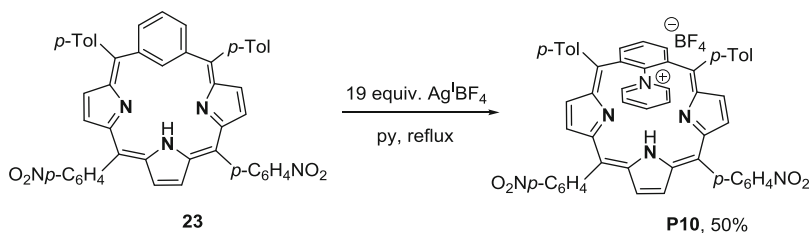
Scheme 25 Ag^I-mediated pyridination of benziporphyrin **23**
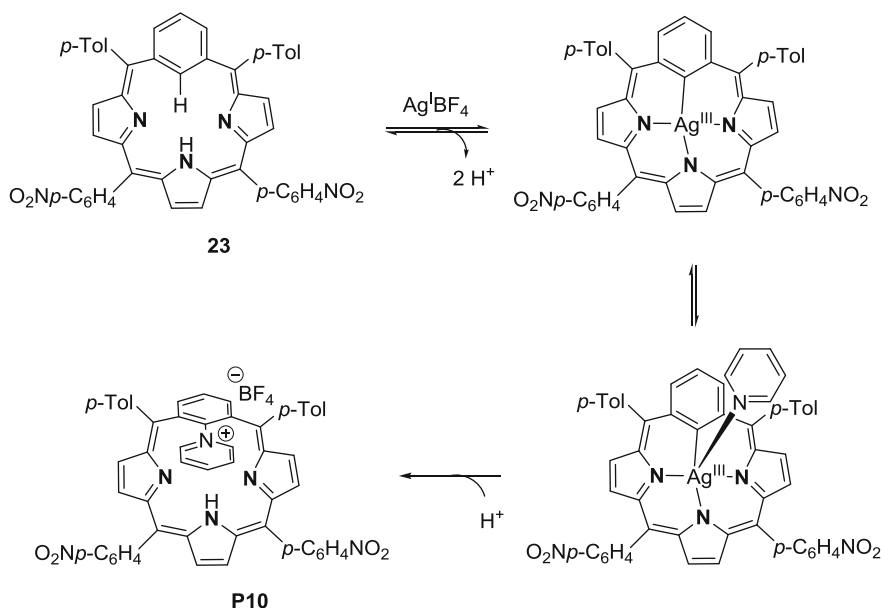
Scheme 26 Mechanistic proposal involving aryl–Ag^{III} to rationalize the regioselective pyridination of benziporphyrin **23**

species that after coordination of the pyridine and subsequent reductive elimination afforded product **P10** and Ag^I (Scheme 26). The Ag$^\circ$ formed during the reaction might suggest that the large excess of Ag^I is needed to reach Ag^{III} redox states by a disproportionation process.

Moreover, the example reported by the same group in 2009 consisting in reductive elimination from organometallic Ag^{III}–C$_{sp2}$ species resulting in the coupling of a nucleophile in the frame of the furanone–Ag^{III} complex **6k**-Ag^{III} bearing a pincerlike macrocyclic ligand demonstrates the plausibility of the proposal involving key aryl–Ag^{III} intermediate species in the C–H pyridination of **23**. This study describes the phosphonylation of complex **6k**-Ag^{III} upon treatment with potassium diphenylphosphide to furnish the desired formation of product **P11** and its corresponding diphenylphosphoryl analog (**P12**) generated by oxidation of **P11** (Scheme 27) [25]. Three years later, the same authors reported a study that showed that the phosphorylation reaction is effected in the same conditions for complex **1f**-Ag^{III} (Fig. 3) and also the products of thiophosphorylation of the complex are accessible by parallel routes affording a family of rare NCP hybrid ligands [21].

Recent studies by Ribas and coworkers corroborate that aryl–Ag^{III} species can perform couplings with a wide range of nucleophiles of a different nature through reductive elimination. Moreover, the same study proves that silver is not only capable of effecting C–H bonds but also can functionalize molecules through the
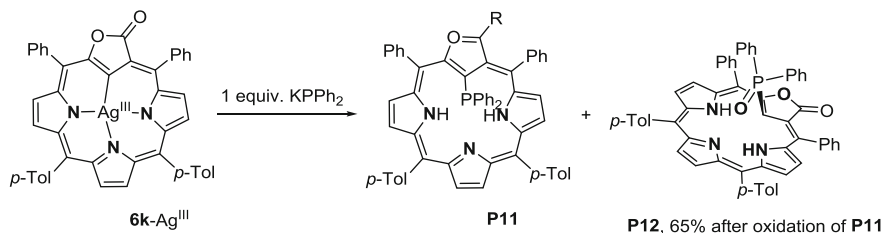
Scheme 27 Phosphonylation of the furanone–Ag^{III} complex **6k**-Ag^{III} through a reductive elimination pathway

activation of C–halide bonds [44]. As observed for copper(I), silver(I) salts can activate the aromatic C–X bonds (X=Br, I) of the **19e**-X family of ligands to furnish isolable and benchtop stable aryl–Ag^{III} complex **19e**-Ag^{III} (Scheme 11). This transformation can proceed up to excellent yields by using 2 equiv. of a Ag^I salt, suggesting the C–X cleavage by one of the equivalents of Ag^I plus the precipitation of the remaining equivalent with the halide released in the solution. The formation of the complex in excellent yields was also attained by using 1 equiv. of Ag^I salt in the presence of excess of Tl(OTf) as halide scavenger to compete with silver for the precipitation of the halides. This observation discredits bimetallic pathways for the C–halogen bond activation and supports the proposal of an oxidative addition process, which was also strengthened by the plausible energy barriers computed for the reaction profiles of the oxidative addition steps.

Complex **19e**-Ag^{III} exhibited parallel reactivity to its analogous copper complex (**19e**-Cu^{III}), i.e., undergoes coupling to functionalize its C$_{aryl}$–Ag^{III} bond in the presence of a wide range of nucleophiles of different nature. Reaction of **19e**-Ag^{III} with sulfonamides, carboxylic acids, phenols, thiophenols, cyanide, malononitrile, aryl boronic acids, and tetrabutylammonium chloride, bromide, and iodide proceeded smoothly to afford the coupling products in excellent to quantitative yields. Very importantly, the complex showed coupling with aryl boronic acids indicating that these substrates can effectively transmetalate over high oxidation states of silver before the coupling step. Also of interest is the fact that these reactions were proved to be unaffected by the addition of radical scavengers such as TEMPO, ruling out a mechanism involving free diffusing radicals. Despite the good results obtained for all the aforementioned substrates, tetrabutylammonium fluoride afforded the fluorination of the aryl only in low yields (<40%). In that case, deprotonation of one of the secondary amines of the ligand resulted detrimental for the reaction outcome. To overcome deprotonation pathways, the corresponding N-permethylated family of ligands **22**-X (Scheme 14) was employed in fluorination reactions. Reaction of **22**-Br with 2 equiv. of Ag^{I}F proceeded to quantitative conversion to **22**-F within 24 h.

Both individually understood steps were merged to realize a catalytic process. This goal, though, presented the challenge of overcoming the inherent proclivity of silver(I) species to precipitate as silver halides. However, the catalytic reactivity of 10 mol% of Ag^I(OTf) using catalytic amounts of triphenylphosphine as the

a) C-O and C-C bond-forming catalysis
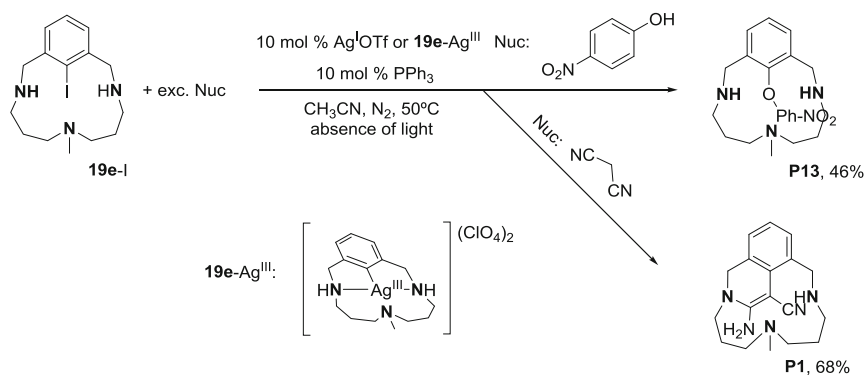
b) Halide exchange catalysis
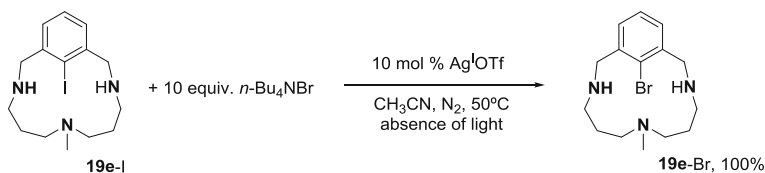
Scheme 28 (**a**) Silver-catalyzed C–O and C–C bond-forming cross-coupling reactions using model substrate **19e**-I. (**b**) Silver-catalyzed bromination of model aryl iodide substrate **19e**-I

auxiliary ligand and large excess of the nucleophile coupling partner resulted in the transformation of **19e**-I into either the C–O coupling product **P13** in 46% yield when *p*-nitrophenol was employed or the C–C coupling product **P1** in 68% yield when malononitrile was used. When 10 mol% of aryl–Ag^{III} complex **19e**-Ag^{III} was used as catalyst C–O coupling product **P13** was formed in the same yield as using Ag^{I}(OTf) under the same conditions of catalysis, indicating that aryl–Ag^{III} species is a competent intermediate in the catalytic cycle (Scheme 28a). However, the success of these catalytic transformations cannot be explained without referring to the ability of large excesses of phenols to delay the precipitation of silver(I) ions in the presence of halides in the solution as demonstrated by turbidity measurements. This phenomenon is due most likely to the formation of coordination complexes with phenol and phenolate species. Moreover, the excess of the halide led to the formation of monoanionic Ag^{I}X$_2^-$ species completely quenching the precipitation of the Ag^{I}X salts. In fact, monoanionic dihalide silver(I) species can participate in the cross-coupling reactions as demonstrated by the catalytic quantitative halide exchange reaction obtained using **19e**-I model substrate, 10 mol% Ag^{I}(OTf), and 10 equiv. of *n*-Bu$_4$NBr (Scheme 28b).

Further investigations were needed to substantiate the two-electron nature of the coupling step. Cyclic voltammetry measurements indicate that the Ag^{III}/Ag^{II} couple is electrochemically irreversible and presents a reduction potential of −0.6 V versus nonaqueous Ag/AgNO$_3$ reference electrode. This value is 1.9 V farther from
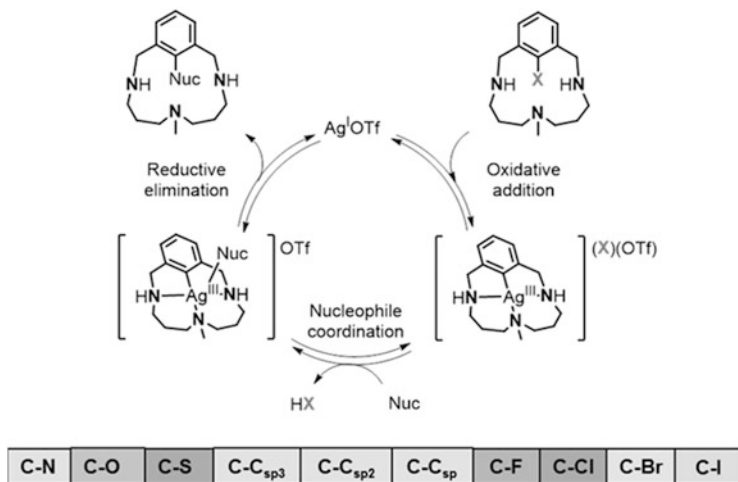
Scheme 29 General mechanistic scenario operating in Ag-catalyzed C–N, C–O, C–S, C–C, and C–halide cross-coupling reactions within model aryl halide model platform **19e**-X

the oxidation potential of *p*-nitrophenol which represents a $\Delta G° = 43.8$ kcal mol^{-1}. This high barrier argues against a SET from the *p*-nitrophenol to Ag^{III} to generate phenoxyl radical and an aryl–Ag^{II} species that would initiate a radical coupling pathway. In addition, DFT calculations are in close agreement with these results showing a barrier of 41.6 kcal mol^{-1} for the SET step. Conversely, the DFT-computed pathway for a reductive elimination of a putative aryl–Ag^{III}-(*p*-nitrophenol) intermediate to afford the final C–O coupling product and Ag^{I} provides a small energy barrier of 16.6 kcal mol^{-1}.

Overall, experimental and theoretical information obtained for this system showed that two-electron transitions are feasible both in the activation of the C–halogen bond and the coupling steps. Scheme 29 puts together all the mechanistic information gathered in this study in a catalytic cycle that rationalizes the nature of the transformations that have been studied.

All the information provided by this study demonstrates that the canonical one-electron redox chemistry generally accepted for silver can be surpassed. The oxidative addition and reductive elimination fundamental steps in Ag^{I}/Ag^{III} redox chemistry are demonstrated providing new mechanistic grounds for an unprecedented reactivity of silver. This brings new concepts in the fundamental understanding of silver's redox chemistry and opens new avenues for designing Ag-catalyzed tools in organic synthesis.

Very interestingly, silver and copper present some different features in the context of the described macrocyclic pincerlike platform. For instance, silver is only capable of furnishing complex **19e**-Ag^{III} upon reaction with macrocyclic aryl halide ligands containing weak C–Br and C–I, while copper can also activate the corresponding **19e**-Cl ligand to generate **19e**-Cu^{III} complex. Another fundamental divergence between the behavior of silver and copper originates in terms of

selectivity. Analogous complexes **19e**-Ag^{III} and **19e**-Cu^{III} react upon treatment of aryl boronic acid to form different coupling products. **19e**-Ag^{III} affords the corresponding C–C$_{sp2}$ coupling product arising from the transmetalation of the aryl boronic acid and subsequent reductive elimination to produce a biaryl scaffold, whereas **19e**-Cu^{III} forms the C–O coupling product coming from the coupling with methanol, the cosolvent employed in the reaction. This observation proves a complementary reactivity of silver with respect to copper that offers perspectives on using their orthogonality in organic synthesis.

5   Conclusions and Outlooks

In this chapter, we aimed at providing a general overview of the richness in terms of reactivity presented by high-valent organometallic species of coinage metals stabilized within pincerlike cyclic scaffolds. It has been discussed how researchers have made use of pincerlike cyclic structures that impart an ideal environment for the accommodation of these high-valent species, conferring enough stability to its complexes to reach the long sought goal that is studying its properties and reactivity. In the porphyrin derivative chemistry, the introduction of transition metals at the inner core that they define led to the development of functionalization methods to tune the porphyrin derivative motifs that are otherwise unattainable. Moreover, it has been demonstrated that the nature of the reactivity of the complex depends largely on the environment of the metal as well as on its intrinsic behavior. Thus, a myriad of different sorts of chemistry has been exhibited from such complexes such as reorganization of the conjugation of the porphyrin derivative ligand promoted by the metal, nucleophilic attack of water or hydroxide over the insaturations of the porphyrinoid, ring-opening reactions, elimination reactions to generate an insaturation upon release of a leaving group, ring contraction reactions, functionalization of C–H bonds mediated by the metal, and coupling reactions triggered by a reductive elimination undergone by the high-valent metal species. The predictability of this chemistry remains as one of the grand challenges to control the nature of the transformations effected.

Different kinds of ligands, triazamacrocyclic aryl ligands and heterocalix-aromatics, have also proven suitable for the stabilization of organometallic complexes of coinage metals in high oxidation states. The importance of these complexes is not only restricted to the opportunity that they offer for studying the fundamental properties of high-valent species but have been applied for mechanistic studies of C–H bond activation and functionalization and a wide variety of cross-coupling reactions. The resemblance of their aryl–M^{III} complexes (M=Cu, Ag) to the intermediate species proposed to effect this chemistry offered a unique platform to demonstrate that these transformations can plausibly proceed through aryl–M^{III} intermediates. Within the environment conferred by pincerlike cyclic ligands, copper(III) and silver(III) have been implicated in cross-coupling catalysis, but no aryl–Au^{III} species have been isolated so far. The flourishing of gold-catalyzed

coupling catalysis, especially in oxidative couplings and the gaps already to fill in the understanding of this chemistry make pincerlike cyclic systems very attractive options to overcome this limitations.

References

1. Harvey JD, Ziegler CJ (2003) Coord Chem Rev 247:1
2. Chmielewski PJ, Latos-Grażyński L (2005) Coord Chem Rev 249:2510
3. Stepień M, Latos- Grażyński L (2005) Acc Chem Res 38:88
4. Srinivasan A, Furuta H (2005) Acc Chem Res 38:10
5. Ribas X, Casitas A (2010) The bioinorganic and organometallic chemistry of copper(III). In: Pignataro B (ed) Ideas in chemistry and molecular science. Where chemistry meets life. Wiley-VCH, Weinheim
6. Wang M-X (2012) Acc Chem Res 45:182
7. Casitas A, Ribas X (2013) Chem Sci 4:2301
8. Casitas A (2013) Mechanistic understanding of copper-catalyzed aryl-heteroatom bond formation: dependence on ancillary ligands. In: Ribas X (ed) C-H C-X bond functionalization: transition metal mediation. Royal Society of Chemistry, Cambridge
9. Casitas A, Ribas X (2014) Aromatic/vinylic Finkelstein reaction. In: Evano G, Blanchard N (eds) Copper-mediated cross-coupling reactions. Wiley, Hoboken
10. Casitas A, Ribas X (2014) Insights into the mechanism of modern Ullmann-Goldberg coupling reactions. In: Evano G, Blanchard N (eds) Copper-mediated cross-coupling reactions. Wiley, Hoboken
11. Naumann D, Roy T, Tebbe K-F, Crump W (1993) Angew Chem Int Ed Engl 32:1482
12. Chmielewski PJ, Latos-Grazyński L, Schmidt I (2000) Inorg Chem 39:5475
13. Mitrikas G, Calle C, Schweiger A (2005) Angew Chem Int Ed Engl 44:3301
14. Calle C, Schweiger A, Mitrikas G (2007) Inorg Chem 46:1847
15. Furuta H, Ishizuka T, Osuka A, Uwatoko Y, Ishikawa Y (2001) Angew Chem Int Ed Engl 40:2323
16. Maeda H, Osuka A, Ishikawa Y, Aritome I, Hisaeda Y, Furuta H (2003) Org Lett 5:1293
17. Furuta H, Maeda H, Osuka A (2000) J Am Chem Soc 122:803
18. Maeda H, Osuka A, Furuta H (2003) J Am Chem Soc 125:15690
19. Araki K, Winnischofer H, Toma HE, Maeda H, Osuka A, Furuta H (2001) Inorg Chem 40:2020
20. Furuta H, Ogawa T, Uwatoko Y, Araki K (1999) Inorg Chem 38:2676
21. Grzegorzek N, Latos-Grażyński L, Szterenberg L (2012) Org Biomol Chem 10:8064
22. Lash TD, von Ruden AL (2008) J Org Chem 73:9417
23. Toganoh M, Niino T, Furuta H (2008) Chem Commun 4070
24. Pawlicki M, Kańska I, Latos-Grażyński L (2007) Inorg Chem 46:6575
25. Grzegorzek N, Pawlicki M, Szterenberg L, Latos-Grażyński L (2009) J Am Chem Soc 131:7224
26. Grzegorzek N, Nojman E, Szterenberg L, Latos-Grażyński L (2013) Inorg Chem 52:2599
27. Muckey MA, Szczepura LF, Ferrence GM, Lash TD (2002) Inorg Chem 41:4840–4842
28. Lash TD, Colby DA, Szczepura LF (2004) Inorg Chem 43:1246
29. Lash TD, Rasmussen JM, Bergman KM, Colby DA (2004) Org Lett 6:549
30. Bergman KM, Ferrence GM, Lash TD (2004) J Org Chem 69:7888
31. Miyake K, Lash TD (2004) Chem Commun 178
32. El-beck JA, Lash TD (2006) Org Lett 8:5263
33. Pawlicki M, Latos-Grażyński L (2003) Chem Eur J 9:4650
34. Pawlicki M, Latos-Grażyński L (2005) J Org Chem 70:9123

35. Chmielewski PJ (2005) Org Lett 7:1789
36. Szyszko B, Kupietz K, Szterenberg L, Latos-Grażyński L (2014) Chem Eur J 20:1376
37. Ribas X, Jackson DA, Donnadieu B, Mahía J, Parella T, Xifra R, Hedman B, Hodgson KO, Llobet A, Stack TDP (2002) Angew Chem Int Ed Engl 41:2991
38. Xifra R, Ribas X, Llobet A, Poater A, Duran M, Solà M, Stack TDP, Benet-Buchholz J, Donnadieu B, Mahía J, Parella T (2005) Chem Eur J 11:5146
39. Casitas A, King AE, Parella T, Costas M, Stahl SS, Ribas X (2010) Chem Sci 1:326
40. King AE, Huffman LM, Casitas A, Costas M, Ribas X, Stahl SS (2010) J Am Chem Soc 132:12068
41. Huffman LM, Stahl SS (2008) J Am Chem Soc 130:9196
42. Ribas X, Calle C, Poater A, Casitas A, Gómez L, Xifra R, Parella T, Benet-Buchholz J, Schweiger A, Mitrikas G, Solà M, Llobet A, Stack TDP (2010) J Am Chem Soc 132:12299
43. Casitas A, Canta M, Solà M, Costas M, Ribas X (2011) J Am Chem Soc 133:19386
44. Font M, Acuña-Parés F, Parella T, Serra J, Luis JM, Lloret-Fillol J, Costas M, Ribas X (2014) Nat Commun 5:4373. doi:10.1038/ncomms5373
45. Yao B, Wang D-X, Huang Z-T, Wang M-X (2009) Chem Commun 2899
46. Zhang H, Yao B, Zhao L, Wang D, Xu B, Wang M (2014) J Am Chem Soc 136:6326
47. Bertz SH, Cope S, Murphy M, Ogle CA, Taylor BJ (2007) J Am Chem Soc 129:7208
48. Casitas A, Poater A, Solà M, Stahl SS, Costas M, Ribas X (2010) Dalton Trans 39:10458
49. Fusi V, Llobet A, Mahía J, Micheloni M, Paoli P, Ribas X, Rossi P (2002) Eur J Inorg Chem 2002:987
50. Long C, Zhao L, You J, Wang M (2014) Organometallics 33:1061
51. Evano G, Blanchard N, Toumi M (2008) Chem Rev 108:3054
52. Huffman LM, Casitas A, Font M, Canta M, Costas M (2011) Chem Eur J 17:10643
53. Wang J, Sánchez-Roselló M, Aceña JL, Del Pozo C, Sorochinsky AE, Fustero S, Soloshonok VA, Liu H (2014) Chem Rev 114:2432
54. Wang Z-L, Zhao L, Wang M-X (2011) Org Lett 13:6560
55. Font M, Parella T, Costas M, Ribas X (2012) Organometallics 31:7976
56. Huffman LM, Stahl SS (2011) Dalton Trans 40:8959
57. Hurtley WRH (1929) J Chem Soc 1929:1870
58. Huang Z, Hartwig JF (2012) Angew Chem Int Ed Engl 51:1028
59. Wang Z-L, Zhao L, Wang M-X (2012) Chem Commun 48:9418
60. Rovira M, Font M, Ribas X (2013) Chem Cat Chem 5:687
61. Stephens RD, Castro CE (1963) J Org Chem 28:3133
62. Okuro K, Furuune M, Enna M, Miura M, Nomura M (1993) J Org Chem 58:4716
63. Rovira M, Font M, Acuña-Parés F, Parella T, Luis JM, Lloret-Fillol J, Ribas X (2014) Chem Eur J 20:10005
64. Saejueng P, Bates CG, Venkataraman D (2005) Synthesis 2005:1706
65. Yang Y, Ren H, Wang D, Shi F, Wu C (2013) RSC Adv 3:10434
66. Chen X, Hao X-S, Goodhue CE, Yu J-Q (2006) J Am Chem Soc 128:6790
67. Wendlandt AE, Suess AM, Stahl SS (2011) Angew Chem Int Ed Engl 50:11062
68. Lipshutz BH, Yamamoto Y (2008) Chem Rev 108:2793
69. Naodovic M, Yamamoto H (2008) Chem Rev 108:3132
70. Weibel J-M, Blanc A, Pale P (2008) Chem Rev 108:3149
71. Álvarez-Corral M, Muñoz-Dorado M, Rodríguez-García I (2008) Chem Rev 108:3174
72. Hashmi ASK (2010) A critical comparison: copper, silver and gold. In: Harmata M (ed) Silver in organic chemistry. Wiley, Hoboken
73. Tang P, Furuya T, Ritter T (2010) J Am Chem Soc 132:12150
74. Seo S, Taylor JB, Greaney MF (2013) Chem Commun 49:6385
75. Li P, Wang L (2006) Synlett 14:2261
76. Das R, Mandal M, Chakraborty D (2013) Asian J Org Chem 2:579
77. Stepień M, Latos-Grażyński L (2003) Org Lett 5:3379
78. Stepień M, Latos-Grażyński L (2001) Chem Eur J 7:5113

Recent Advances in Alkane Dehydrogenation Catalyzed by Pincer Complexes

Akshai Kumar and Alan S. Goldman

Abstract Olefins are ubiquitous intermediates in the production of fuels and commodity chemicals. Accordingly, the development of methods for the selective dehydrogenation of alkanes to give olefins is a goal with great potential value. Molecular (homogeneous) catalysts appear quite promising in this respect. Great advances have been seen with pincer-ligated catalysts since the mid-1990s, particularly (but not exclusively) with iridium complexes. In this chapter we give an overview of this productive area of research, with emphasis on recent progress.

Contents

A. Kumar (✉)
Department of Chemistry, Indian Institute of Technology Guwahati, Guwahati, 781039, Assam, India
e-mail: akshaikumara@gmail.com

A.S. Goldman (✉)
Department of Chemistry and Chemical Biology, Rutgers-The State University of New Jersey, 610 Taylor Road, Piscataway, NJ 08854-8087, USA
e-mail: alan.goldman@rutgers.edu

1   Introduction to Alkane Dehydrogenation

Alkanes are the major constituent of petroleum and natural gas liquids or conden-sates, as well as being the major product of Fischer–Tropsch conversion of gas, coal, or biomass to liquids. With regard to their use as a chemical feedstock, however, alkanes are notoriously resistant to selective chemical transformations. Olefins, by contrast, are perhaps the most chemically versatile class of organic molecules and are intermediates, isolated or otherwise, in perhaps the majority of fuel- and commodity-chemical syntheses. The conversion of alkanes to olefins is accordingly one of the most widely practiced reactions in the petrochemical industry. Conventional, heterogeneous, catalysts, however, for the most part lack the ability to effect such reactions with selectivity, especially selectivity for limited dehydrogenation, e.g., the conversion of higher alkanes to monoolefins. Further, the ability to control regioselectivity with the use of such catalysts, e.g., the conversion of higher alkanes to α-olefins, is essentially nonexistent. Homogeneous (molecular) catalysts are known for their high selectivity. Thus, the first reported examples of alkane dehydrogenation by well-defined soluble transition metal complexes were met with great interest [1–6]. Soon thereafter reports of remarkable selectivity in the stoichiometric oxidative addition of C–H bonds appeared, serving to highlight the potential offered by molecular dehydrogenation catalysts [7–15] (for some reviews of alkane C–H bond activation by organometallic complexes, see [16–21]).
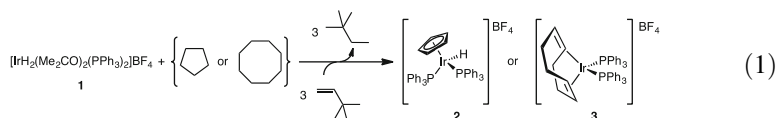
In 1979, Crabtree reported the first example of stoichiometric alkane dehydro-genation by a transition metal complex [1]. The cationic Ir(III) complex **1** reacted with either cyclopentane or cyclooctane (COA) in refluxing 1,2-dichloroethane containing 3,3-dimethyl-1-butene (TBE) resulting in the formation of the corresponding cyclopentadienyl and cyclooctadiene iridium complexes (**2 and 3,** respectively) (1) [1–3]. Baudry, Ephritikhine, and Felkin subsequently reported that L_2ReH_7 (L=PPh$_3$ and PEt$_2$Ph) dehydrogenates alkanes in the presence of TBE to give rhenium complexes of the corresponding unsaturated hydrocarbons [4–6]. Cycloalkanes were reported to be catalytically dehydrogenated by this group, although turnovers were low; COA gave the highest turnover number (9 TO after 10 min at 80°C) [22].

TBE acts as a sacrificial hydrogen acceptor in these reactions. It offers a high degree of steric bulk, mitigating inhibition due to olefin binding, as well as the inability to undergo double-bond isomerization; it has thus continued to be the most widely used species for this purpose in the 35 years since its introduction by Crabtree [1]. Likewise, cyclooctane, with an anomalously low enthalpy of dehy-drogenation as compared with linear alkanes or cyclohexane, is still the alkane most commonly used in research in this field. While this makes perfectly good sense for

exploratory studies, the use of the atypical alkane COA as a "model" alkane is perhaps now questionable since (as will be seen below) good catalysts routinely effect the dehydrogenation of linear alkanes in high yield and, moreover, COA is not in all cases more reactive than *n*-alkanes [23].

With the addition of base (1,8-bis(dimethylamino)naphthalene, Eq. 1.1) to $[IrH_2(Me_2CO)_2(PR_3)_2][SbF_6]$(**4**)(R=*p*-F$C_6H_4$, cyclohexyl), Crabtree achieved COA/TBE transfer dehydrogenation in a catalytic fashion [24]. Crabtree proposed that the role of base was to deprotonate the cationic species. If it is assumed that the acetone is labile, this would effectively give neutral $IrH(PR_3)_2$(R=*p*-F-C_6H_4, cyclohexyl), a species that is at least formally very closely related to pincer complexes of the type (PCP)Ir (vide infra). Independently, Felkin and coworkers reported several polyhydride systems based on iridium and ruthenium, which could also accomplish catalytic transfer dehydrogenation of COA with TBE [25, 26]. The most effective were $(PR_3)_2IrH_5$complexes (R=*p*-F-C_6H_4, ^iPr), proposed, in this case too, to give $IrH(PR_3)_2$ as the active species that actually adds the alkane C–H bond.

Alkane dehydrogenation is highly endothermic, e.g., ca. 23 kcal/mol for COA, ca. 28 kcal/mol for typical cycloalkanes and the internal position of *n*-alkanes, and ca. 30 kcal/mol for the terminal position of *n*-alkanes [27]. Thus it was quite noteworthy that Crabtree reported that $Ir(PR_3)_2(CF_3CO_2)$ (**5**)(R=p-F-C_6H_4, cyclohexyl) complexes catalyzed photochemical alkane dehydrogenation without the requirement of a sacrificial acceptor [28, 29]. Light was proposed to provide the necessary thermodynamic driving force by dissociating H_2 from $H_2Ir(PR_3)_2(\kappa^2$-$CF_3CO_2)$(**6**)(R=p-F-C_6H_4, cyclohexyl). The C–H bond-activating species was proposed to be $Ir(PR_3)_2(\kappa^1$-$CF_3CO_2)$(**5**)(R=p-F-C_6H_4, cyclohexyl), which constituted another example of a 3-coordinate bisphosphine Ir(I) species analogous to complexes of the type (PCP)Ir.

Inspired by Crabtree's photocatalytic systems and the development of alkane carbonylation catalysts reported by Eisenberg [30, 31], the groups of Tanaka [32–35], Saito [36–38], and Goldman [39–41] found that $Rh(PMe_3)_2Cl(CO)$(**7**) could effect photochemical dehydrogenation with unprecedentedly high turnover numbers. The Goldman group showed that this reaction proceeded via C–H addition to $Rh(PMe_3)_2Cl$ (**10**), another example of an active 3-coordinate d^8 bis-phosphine complex. The role of light was proposed to be dissociation of CO from Rh$(PMe_3)_2Cl(CO)$ (**7**); the resulting fragment then reacted with alkane to give alkene and $H_2Rh(PMe_3)_2Cl$ (**9**), which then reacted with the photo-liberated CO to give back $Rh(PMe_3)_2Cl(CO)$ (**7**) and free H_2. Very recently, the Beller group reported substantial further improvement in TONs obtained in the acceptorless photochemical dehydrogenation of *n*-octane catalyzed by $Rh(PMe_3)_2Cl(CO)$ (**7**) based largely on innovative reactor design [42].

$$R \diagdown\diagup R + R' \diagdown\diagup\diagup R' \xrightarrow[\Delta]{\mathbf{7}, H_2} R \diagdown\diagup\diagup R + R' \diagdown\diagup R'$$

$$H_2 + Rh(PMe_3)_2Cl(CO) \rightleftharpoons H_2Rh(PMe_3)_2Cl(CO) \rightleftharpoons CO + H_2Rh(PMe_3)_2Cl$$
$$\mathbf{7} \qquad\qquad\qquad \mathbf{8} \qquad\qquad\qquad\qquad \mathbf{9}$$

Acceptor   H₂•Acceptor

Rh(PMe₃)₂Cl
10

alkene   alkane

(2)
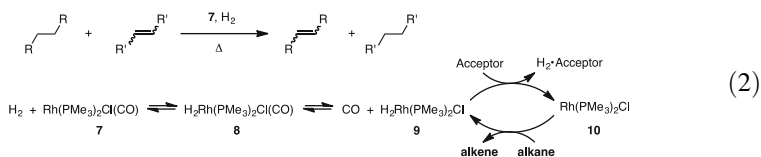
Remarkably $Rh(PMe_3)_2Cl(CO)(\mathbf{7})$ was found to be highly active for thermochemical alkane transfer dehydrogenation but only in the presence of H_2 atmosphere (2). Other $Rh(PMe_3)_2Cl(L)$ ($L=P^iPr_3, PCy_3$ and PMe_3) complexes, as well as $[Rh(PMe_3)_2Cl]_2$, were also found to be thermochemically active under H_2. The role of H_2 is believed to add to these precursors to give $H_2Rh(PMe_3)_2Cl$ (**9**), which is then dehydrogenated by sacrificial acceptor to give the active fragment $Rh(PMe_3)_2Cl$ (**10**) (2). Unfortunately, the presence of H_2 also results in simple hydrogenation of acceptor and the loss of several mol per mol dehydrogenated alkane, precluding practical applications of this system. Based on the high activity of the $Rh(PMe_3)_2Cl$ (**7**) fragment, the Goldman group synthesized and investigated precursors of the isoelectronic fragment (PCP)Rh [43]. Some transfer dehydrogenation was observed but turnover numbers were very low.

2 Dehydrogenation of Alkanes by Pincer-Iridium Complexes

In 1996, Kaska and Jensen reported (^{tBu4}PCP)IrH$_2$(**11-H$_2$**) to be a remarkably robust catalyst and stable at relatively high temperatures at which it afforded very high turnover rates and numbers for COA/TBE catalytic transfer dehydrogenation [44, 45]. Since those seminal reports, work in the area of organometallic-catalyzed alkane dehydrogenation has been dominated by pincer-ligated complexes [46–48].

Transfer dehydrogenation by **11-H$_2$** was found to be inhibited by excess TBE (>350 mM) but the complex exhibited excellent activity at temperatures as high as 200°C. For example, the dehydrogenation of cyclooctane with 0.36 M TBE catalyzed by **11-H$_2$** (1 mM) proceeded at a rate of 12 TO min^{-1} at 200°C [44]. Periodic additions of 0.36 M TBE resulted in high TON as the reaction continued to proceed at 12 TO min^{-1}. In this manner, a maximum of 1,000 TON is obtained after which the catalytic system is inhibited by TBE. The remarkable stability prompted Kaska, Jensen, and Goldman to investigate (^{tBu4}PCP)IrH$_2$(**11-H$_2$**) for acceptorless dehydrogenation. A refluxed (201°C) cyclodecane solution of 1.0 mM **11-H$_2$** afforded 360 turnovers after 24 h [49].
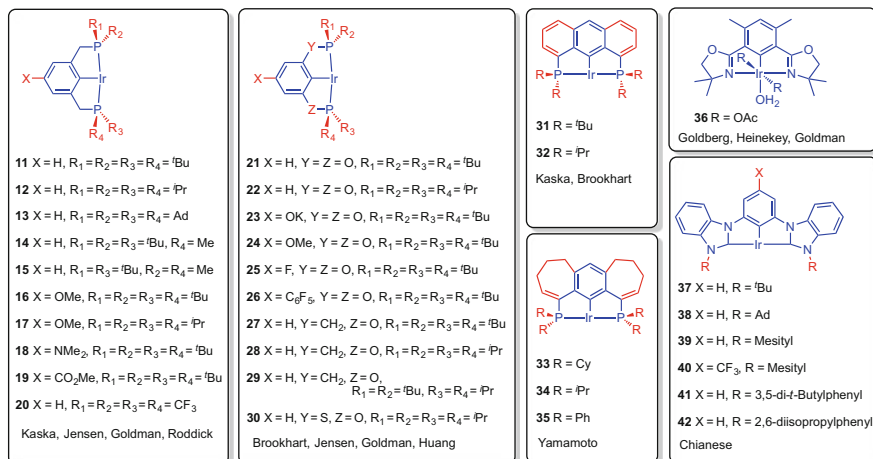
Fig. 1 Examples of pincer-iridium complexes that have been investigated for alkane dehydrogenation

(3)
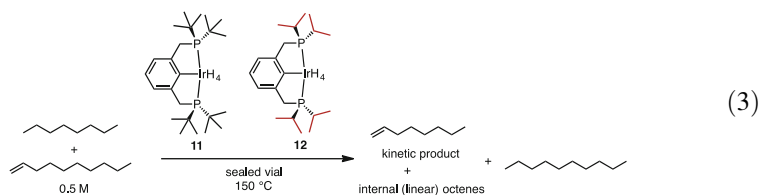
In 1999, Jensen and Goldman followed up these results with the important observation that both **11-H$_4$** and its isopropyl analogue (^{iPr4}PCP)IrH$_4$(**12-H$_4$**) gave high kinetic selectivity for the formation of α-olefin from the transfer dehydrogenation of *n*-alkane (3). (Note that dihydride and tetrahydride complexes are used interchangeably in the case of complex **11**; H$_2$ is very readily lost from the tetrahydride complex under dehydrogenation conditions.) Unfortunately, olefin isomerization occurred concomitantly, and as a result total yields of α-olefin greater than ca. 100 mM were never obtained [50].

Catalyst (^{iPr4}PCP)IrH$_4$(**12-H$_4$**) was found to be more effective than (^{tBu4}PCP) IrH$_2$(**11-H$_2$**) for the acceptorless dehydrogenation of both *n*-alkanes and cycloalkanes [49, 51]. These studies led to the design of numerous pincer-based catalytic systems for alkane dehydrogenation (Fig. 1). Hall, Kaska, and coworkers reported that the pincer-iridium complex (**31-H$_2$**, Fig. 1) based on the rigid anthraphos ligand was found to be thermally more stable than **11-H$_2$**, tolerating temperatures up to 250°C [52]. Goldman and coworkers observed that the use of adamantyl groups on P (Fig. 1) also enhanced thermal stability, making complex **13** a particularly effective catalyst for acceptorless dehydrogenation (which generally requires higher temperatures than transfer dehydrogenation) [53].

Over the years many research groups have reported variants of **11** where either the aryl backbone has been altered [54–57] or the CH$_2$ linkers and the ligating

groups have been modified (Fig. 1) [58–70]. The Brookhart and Jensen groups reported a new class of catalysts wherein the benzylic CH_2 linkers of the PCP backbone were replaced by O linkers to obtain the (^{R}POCOP)Ir (**21**, R=*t*-Bu;**22**, R=*i*-Pr) systems [58–60, 66]. Notably, (^{tBu4}POCOP)IrH$_2$(**21-H$_2$**) showed greater activity than (^{tBu4}PCP)IrH$_2$(**11-H$_2$**) for COA/TBE transfer dehydrogenation, although the latter was found to be significantly more active for the transfer dehydrogenation of linear alkanes [46–48, 71]. As will be discussed later in this chapter, these phosphine, phosphinite, and mixed phosphine–phosphinite-based systems have found widespread utility as catalysts for alkane metathesis ,[48, 67, 71–74], alkyl group metathesis [62], dehydroaromatization reactions [61, 75, 76], alkane–alkene coupling reactions [77, 78], and dehydrogenation of several other substrates [64, 68, 69, 79–81].

Huang and coworkers recently reported that (^{iPr4}*PSCOP*)Ir (**30**) efficiently catalyzes the transfer dehydrogenation of COA or *n*-octane with TBE as acceptor at 200°C [64]. The transfer dehydrogenation of 3.9 M COA with equimolar TBE in the presence of 1.3 mM **30** proceeded with a rate of 2,910 TO h^{-1} [64, 68], which is twice that observed with (^{tBu4}PCP)IrH$_2$(**11-H$_2$**) (1,200 TO h^{-1}) [59] and about half that of (^{tBu4}POCOP)IrH$_2$(**21-H$_2$**) (6,900 TO h^{-1}) [59]. The (^{iPr4}PSCOP) Ir complex **30** gave almost complete consumption of TBE in about 8 h, in contrast to **21-H$_2$** which affords a maximum conversion of about 62% as the reaction levels off after about 6 h. When a lower concentration of TBE (1.3 M) was used, the rate of COA transfer dehydrogenation catalyzed by **30** showed a two-fold increase (5,600 TO h^{-1}) compared to the rate (2,910 TO h^{-1}) of the reaction with 3.9 M TBE, indicating catalyst inhibition at high concentrations of TBE.

Under the conditions used by the Huang group, (^{iPr4}PSCOP)Ir (**30**) appears to be perhaps the most efficient catalyst yet reported for *n*-octane-TBE transfer dehydrogenation, giving 1,400 TO h^{-1} (0.5 M TBE) at 200°C, as compared with (^{tBu4}PCP) IrH$_2$(**11-H$_2$**)(820 TO h^{-1}) and (^{tBu4}POCOP)IrH$_2$(**21-H$_2$**) (220 TO h^{-1}) [64, 68]. While dehydrogenation catalyzed by **21-H$_2$** gives poor selectivity for 1-octene, it is remarkable that at similar turnover numbers, the selectivity obtained with **30** was very similar (30%, ca. 115 TON) to that obtained with the bulky, highly regioselective **11-H$_2$**.

To systematically investigate steric effects on catalyst efficiency, Goldman and coworkers have replaced phosphino-*tert*-butyl groups of **11** with phosphinomethyl groups [67]. Computational studies had predicted that substitution of the first ^{t}Bu groups from the parent complex (**11**) would have a much more favorable effect in lowering the overall energy barrier in the *n*-alkane/1-alkene transfer dehydrogenation cycle than additional Me-for-^{t}Bu substitutions would. Experimental studies with (^{tBu3Me}PCP)IrH$_4$(**14-H$_4$**) and (^{tBu2Me2}PCP)IrH$_4$(**15-H$_4$**) for *n*-octane transfer dehydrogenation using TBE (0.2 and 0.4 M) or NBE (0.2, 0.4, and 1.1 M) (NBE=norbornene) revealed that **14** was indeed more active than **11** or **15** (4). As complex **15** tended to form dinuclear clusters, however, it was not clear whether the reduced activity resulted from the intrinsic properties of the monomeric catalyst or from deactivation via cluster formation. More recent studies by the Goldman group on the pincer-iridium-catalyzed *n*-pentane dehydrogenation using higher

Table 1 Transfer dehydrogenation of COA (4.6 M) with TBE (3.1 M) catalyzed by (7-6-7-^{R}PCP) Ir (0.5 mM **34**, R = ^{i}Pr; **35**, R = Ph)
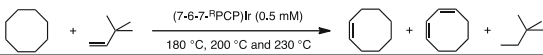
Catalyst	T (°C)	TON after 1 h		Final TON	
		Olefins	Double bonds	Olefins	Double bonds
34	180	257	259	2,328 (36 h)	2,748 (36 h)
	200	1,104	1,104	2,892 (36 h)	3,509 (36 h)
	230	3,191	3,898	3,652 (4 h)	4,550 (4 h)
35	180	698	698	2,489 (16 h)	2,765 (16 h)
	200	1,040	1,047	3,461 (36 h)	4,139 (36 h)
	230	2,827 (2 h)	3,264 (2 h)	3,955 (24 h)	4,821 (24 h)
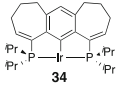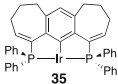
concentration of TBE (4.3 M) indicates a different trend: (^{tBu2Me2}PCP) IrH$_4$(**15-H$_4$**)> (^{tBu3Me}PCP)IrH$_4$(**14-H$_4$**)> (^{tBu4}PCP)IrH$_2$(**11-H$_2$**) [82]. At high concentrations it is likely that TBE prevents (^{tBu2Me2}PCP)IrH$_4$(**15-H$_4$**) from undergoing binuclear reactions, thus permitting high catalytic activity [82].

(4)

TON after 10 min   31   76   86   126
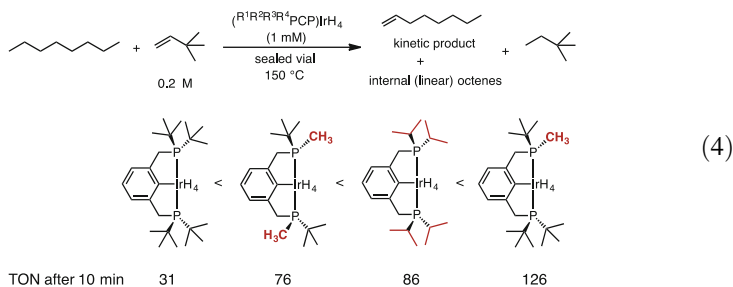
Yamamoto and coworkers have recently reported the use of 7-6-7 ring-type PCP iridium catalysts (7-6-7-^{R}PCP)Ir (**34**, R=^{i}Pr; **35**, R=Ph; Fig. 1) for alkane transfer dehydrogenation [63]. These catalysts were tested with the hope that the rigid structure would impart high thermal stability, while the flexibility of the backbone would enhance catalytic activity. With catalysts **34** and **35** (0.5 mM), the transfer dehydrogenation of COA (4.6 M) was performed with TBE (3.1 M) at various temperatures (180, 200, and 230°C; Table 1).

Comparison of the rates of dehydrogenation catalyzed by (7-6-7-^{iPr4}PCP)Ir (**34**) and (7-6-7-^{Ph4}PCP)Ir (**35**) at various temperatures indicates that **34** is more active than **35** at higher temperature whereas at lower temperatures the reverse appears to be the case. The authors rationalized this by proposing that the reaction catalyzed by the sterically more encumbered (7-6-7-^{iPr4}PCP)Ir (**34**) is entropically favored by higher temperatures. At all temperatures, the conversion obtained with (7-6-7-^{Ph4}PCP)Ir (**35**) was higher than that with **34**. Furthermore while **34** was resistant to inhibition by alkenes, but decomposed over time, **35** was claimed to be resistant to both decomposition and inhibition by alkenes. Yamamoto and coworkers have
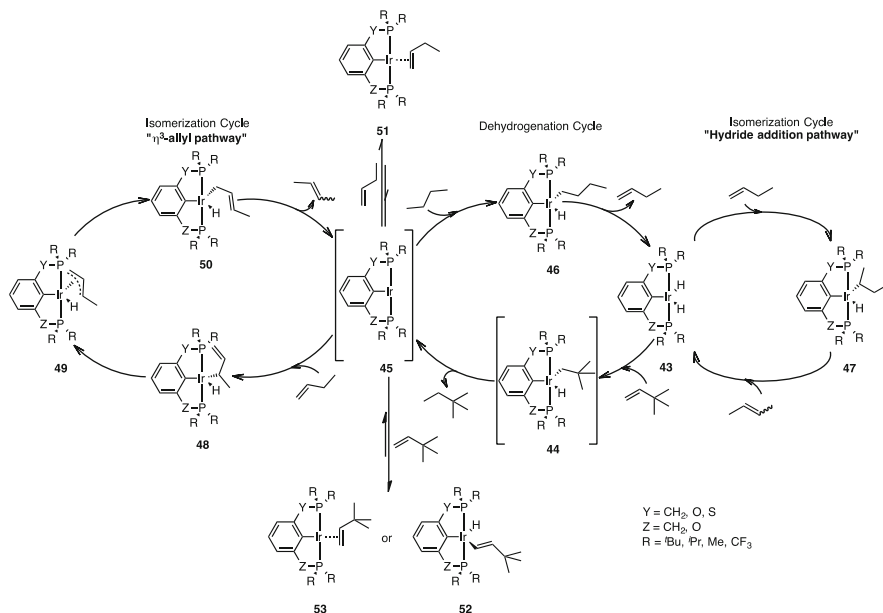
Scheme 1 Widely accepted mechanism involved in the pincer-iridium catalyzed dehydrogenation of alkane and the associated isomerization of α-olefin

also noted that **35** was more selective for primary dehydrogenation giving a higher ratio of COE:1,3-COD compared to **34**. Catalyst **34** also gave high activity for the dehydrogenation of *n*-octane (6.0 M) with NBE (1.1 M) at 150°C; **35**, however, showed poor solubility in *n*-octane and was not active for catalytic *n*-octane transfer dehydrogenation [63].

A schematic representation of our current best understanding of the catalytic cycles, illustrated for *n*-alkane/TBE transfer dehydrogenation and 1,2-α-olefin olefin isomerization by (pincer)Ir complexes, is shown in Scheme 1. While catalytic pathway is probably quite similar for the various catalysts, there are notable differences in the catalyst resting states. Hydrogenation of TBE by the dihydride complexes (**43**) results in the formation of catalytically active 14-electron three-coordinate Ir(I) species (**45**). This species undergoes C–H addition and then β-hydride elimination, in some cases to give α-olefin (as shown in Scheme 1).

The resting state of the catalyst may be the dihydride complex (**43**); this is most favorable in the case of a very crowded catalyst (e.g., (*t*Bu4PCP)Ir (**11**) and low concentrations of olefin and especially in the absence (or the presence of only very low concentrations) of strongly binding alkenes such as α-olefin. Alternatively (and probably more commonly), the resting state of the catalyst may be an Ir olefin complex. With the use of TBE, this has been found to be the Ir(III) hydrido–vinyl complex (**52**) for (*t*Bu4PCP)Ir (**11**), while for (*t*Bu4POCOP)Ir (**21**) (and probably for most pincer ligands less sterically demanding than **11**, the Ir(I) alkene complex (**53**) is more stable. In the case of *n*-alkane dehydrogenation, α-olefin product binds

more strongly than TBE (as either π-complex (**51**) or as the vinyl hydride). The differences in resting state, especially dihydride vs. olefin complex, are partly responsible for the variability of catalyst effectiveness as a function of substrate or reaction conditions. For example, considering a catalyst with a resting state of dihydride (**43**), its activity will increase with increasing concentration of acceptor or the use of a sterically less hindered acceptor such as propene; conversely, the activity of a catalyst whose resting state is olefin complex will decrease in response to the same change in conditions.

The α-olefin that is formed by the dehydrogenation of *n*-alkane catalyzed by pincer-iridium complexes such as (^{tBu4}PCP)Ir (**11**) is a kinetic product which over time undergoes an iridium-catalyzed isomerization to the thermodynamically more favored internal olefin. This isomerization can occur via either via a "hydride addition pathway" or via an "η^3-allyl pathway" (Scheme 1). Brookhart, Goldman, and coworkers have performed a computational and experimental study to elucidate the actual mechanism that is operative in this isomerization reaction catalyzed by (^{tBu4}PCP)Ir (**11**) and by (^{tBu4}POCOP)Ir (**21**) [83]. The hydride addition pathway requires the Ir–H bond of **43** to undergo 2,1-addition across the double bond of α-olefin to generate the intermediate **47** that can undergo a β-hydride elimination to give internal olefin and regenerate dihydride **43**. The "η^3-allyl pathway" was proposed to involve an initial oxidative addition of the allylic C–H bond of the α-olefin to the 14-electron 3-coordinate iridium species **45**. The resulting η^1-allyl hydride **48** then "closes" to give the η^3-allyl hydride **49** which can then "open" in the reverse sense, generating the isomeric η^1-allyl hydride **50**. The η^1-allyl hydride **50** then undergoes reductive C–H elimination to give the isomerized internal olefin and regenerate **45**. DFT calculations strongly support the involvement of the η^3-allyl pathway where the iridium has undergone a formal 1,3 shift [83].

The resting state under conditions of the olefin isomerization experiments (100 mM 1-octene, 125°C) was found to be the olefin complex **51** for both (^{tBu4}PCP)Ir (**11**) and (^{tBu4}POCOP)Ir (**21**). This of course still allows for the possibility that a small concentration of dihydride (**43**) is the species active for isomerization. To test this possibility, rates of 1-octene isomerization by (^{tBu4}PCP)Ir and (^{tBu4}POCOP)Ir were measured in both *n*-octane and *p*-xylene solutions. A steady-state concentration of dihydride, while perhaps still small, should be much greater in *n*-octane (a source of hydrogen) than in *p*-xylene. In fact, the rate of 1-octene isomerization by either **11** or **21** was identical in both solvents [83]. These studies strongly support the η^3-allyl pathway as the operative mechanism. Further support was obtained by low-temperature NMR experiments in which allene was added to (^{tBu4}POCOP)IrH$_2$ (**21–H$_2$**) resulting in the formation of (^{tBu4}POCOP)Ir(η^3-allyl)H (**54**) as well as (^{tBu4}POCOP)Ir(propenyl)H (**54′**); these both were found to convert to (^{tBu4}POCOP)Ir(η^2-propene) (**55**) (5). Chianese and coworkers have recently reported the involvement of the η^3-allyl pathway in alkene isomerization reactions catalyzed by CCC pincer-iridium complex based on **39** [84].
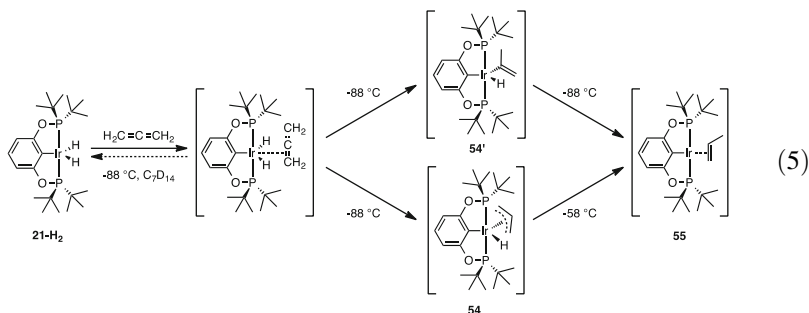
Varying the electronic component by introduction of methoxy (**16/17**), dimethylamino (**18**), and ester (**19**) functionalities to the *para*-position of the arene backbone in PCP pincer-iridium systems was found to have a modest effect on catalytic activity [54, 55, 59]. Roddick and coworkers have reported the synthesis of a series of PCP iridium complexes with bis(trifluoromethyl)phosphino groups [85–87]. The Roddick group discovered and investigated acceptorless and transfer dehydrogenation of alkanes catalyzed by (^{CF3}PCP)Ir(η^4-COD) (**56**) (COD=1,5 cyclooctadiene) [88]. The rate of COA (3.9 M)/TBE (3.9 M) transfer dehydrogenation catalyzed by **56** (1.3 mM) at 200°C was about 40 TO h^{-1}. Higher rates were found using (^{tBu4}PCP)Ir(H$_2$) (**11-H$_2$**) (1,200 TO h^{-1}) or (^{tBu4}POCOP) IrH$_2$(**21-H$_2$**) (6,900 TO h^{-1}) under identical conditions. Notably, catalyst **56** was insensitive to inhibition by product, and even in the presence of 1 M added COE, the rate of COA/TBE dehydrogenation was reduced by only 30% (24 TO h^{-1}). Operating at low TBE concentration (1.3 M), however, catalyst **56** (0.4 mM) effected transfer dehydrogenation of COA at a faster rate (155 TO h^{-1}) than with 3.9 M TBE (40 TO h^{-1}; [**56**]=1.3 mM).

In attempts by the Roddick group to determine the catalyst resting state using (^{CF3}PCP)Ir(η^4-COD) (**56**) as catalyst precursor in an equimolar mixture of COA (3.9 M) and TBE (3.9 M) at room temperature, the major species present was (^{CF3}PCP)Ir(η^4-isoprene) (**57**) [88]. The authors realized that the commercially obtained TBE (95% nominal purity) contained isoprene as the major contaminant, an important observation in view of the widespread use of TBE in transfer-dehydrogenation chemistry. The complex (^{CF3}PCP)Ir(η^4-isoprene) (**57**) was independently synthesized by the reaction of (^{CF3}PCP)Ir(H)(Cl)(η^2-C$_2$H$_4$) (**58**) with Et$_3$N at room temperature in the presence of excess isoprene (**6**).
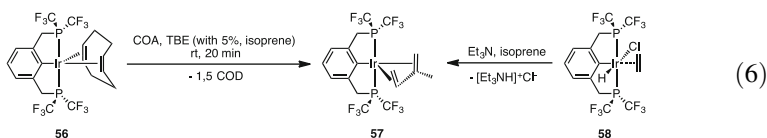
Subsequent experiments with high purity (99.6%) TBE resulted in higher rates (136 TO h^{-1}) for COA/TBE (1:1) transfer dehydrogenation catalyzed by **56** (1.3 mM). It was found that several derivatives of **20** such as (^{CF3}PCP)Ir(η^4-

isoprene) (**57**), (^{CF3}PCP)Ir(η^2-NBE) (**59**), and (NBE=norbornene) and (^{CF3}PCP)Ir (DFMP) (**60**; DFMP=MeP(C_2F_5)$_2$) catalyzed the transfer dehydrogenation of COA with TBE (1:1) at 200°C and in all cases (^{CF3}PCP)Ir(η^4-COD) (**56**) was the major resting state; the COD was presumably formed from the double dehydrogenation of COA [88].

Though (^{CF3}PCP)Ir(η^4-COD) (**56**) exhibited better conversion (660 TON after 58 h) compared with (^{tBu4}PCP)Ir(H$_2$) (**11-H$_2$**) (230 TON after 40 h) for the COA/TBE (1:1) dehydrogenation at 200°C, its catalytic activity decreased over time with decomposition and formation of free (^{CF3}PCP)H as revealed by ^{19}F NMR studies. As there was negligible change in activity in the initial presence of a large excess of COE, the authors concluded that the loss in activity of **56** was due to catalyst decomposition rather than product inhibition [88].

Quite notably, the Roddick group found that the rate of COA/TBE (1:1) transfer dehydrogenation catalyzed by **56** at 200°C and the resting state were unaffected by the presence of either N$_2$ atmosphere or excess water. This observation is in stark contrast to the behavior of (^{tBu4}PCP)Ir(H$_2$) (**11-H$_2$**) which is inhibited by N$_2$ (forming dinitrogen complexes [89, 90]) and by water (which is oxidatively added to give (^{tBu4}PCP)Ir(H)(OH) [91]). The reduced electron density on the iridium center of **56** appears to disfavor these addition reactions. For both laboratory and industrial applications, the resistance to inhibition by N$_2$ and H$_2$O makes these electron-poor catalysts quite promising candidates for further research.

Unfortunately, (^{CF3}PCP)Ir(η^4-COD) (**56**) shows relatively poor activity for the catalytic transfer dehydrogenation of linear alkanes. For example, the (^{CF3}PCP)Ir (η^4-COD)-catalyzed dehydrogenation of *n*-octane with 0.2 M TBE at 150°C gives only 81 turnovers after 48 h. Similarly the catalytic activity of **56** toward acceptorless dehydrogenation of cycloalkanes is significantly lower than that of the parent (PCP) Ir-catalyzed acceptorless dehydrogenation systems reported earlier [49, 51, 53, 54, 67]. For instance, refluxing a solution of **56** (1 mM) in cyclodecane for 24 h results in 92 TON, which is less than that obtained with (*p*-OMe-^{iPr4}PCP)IrH$_4$ (**17-H$_4$**) (2,100 TON) [54], (^{Ad4}PCP)IrH$_2$ (**13-H$_2$**) (509 TON) [53], (^{iPr4}PCP)IrH$_4$ (**12-H$_4$**) (364 TON) [53], and (^{tBu4}PCP)IrH$_2$ (**11-H$_2$**) (267 TON) [53] under similar conditions. It should be noted, however, that the specific conditions, including the apparatus design and the level of reflux activity, may significantly affect rates of acceptorless dehydrogenation; thus any comparison of activity of various catalysts for acceptorless dehydrogenation based on different reports, and especially from different laboratories, should probably be regarded as qualitative.

The pincer-iridium systems discussed thus far are all phosphine based. There are, however, reports of alkane dehydrogenation catalyzed by non-phosphine-based pincer-iridium complexes, mainly based on NCN [92, 93] and CCC [84, 94–96] pincer motifs. Goldberg and coworkers have recently reported the use of a NCN-type pincer-type complex, (^{dm}Phebox)Ir(OAc)$_2$(OH$_2$) (**36**) for the stoichiometric dehydrogenation of *n*-octane at 200°C resulting in the formation of (^{dm}Phebox)Ir(OAc)(H) (**61**) and octenes (7) [93]. This observation compares with the report by Nishiyama that **36** reacts with *n*-octane at 160°C, in the presence of an

equivalent of K_2CO_3, to give exclusive formation of (^{dm}Phebox)Ir(OAc)(n-octyl) (**62**) [97]. The Goldberg group demonstrated that the use of base stabilizes **62** by quenching the acetic acid that is released upon its formation (8); treatment of **62** with acetic acid regenerates **36** and n-octane. In the absence of a base and at high temperatures, the β-hydride elimination of 1-octene from **62** appears to drive the reaction to the formation of (^{dm}Phebox)Ir(OAc)(H) (**61**) (8); accordingly, heating an octane solution of **62** at 200°C resulted in formation of octenes and **61** [93].

$$(7)$$

$$(8)$$
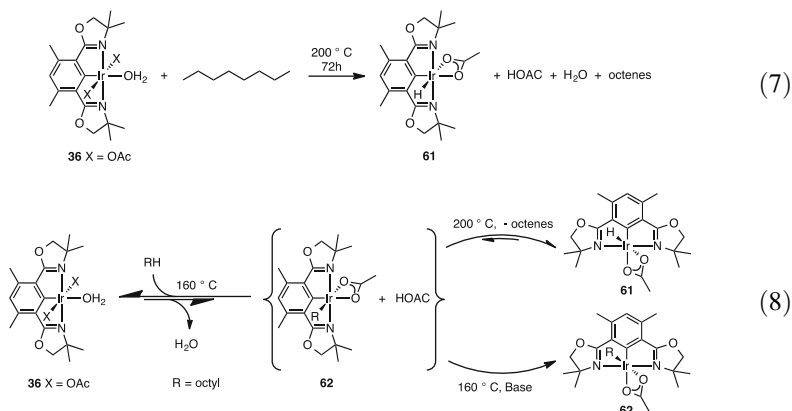
At early reaction time (3 h, ca. 30% conversion), the major octene product (66%) of the stoichiometric alkane dehydrogenation mediated by **36** was found to be 1-octene; when the reaction was complete (120 h), the product mixture comprised only internal octenes. Isomerization of 1-octene by (^{dm}Phebox)Ir(OAc)(H) (**61**) was confirmed by independent experiments [93].

Notably, the dehydrogenation reaction mediated by (^{dm}Phebox)Ir(OAc)$_2$(OH$_2$) (**36**) appears to result from C–H activation at an Ir(III) center [93, 98] in contrast with the reactions of phosphine-based pincer-iridium systems wherein an Ir (I) species is accepted to be the species that activates the C–H bond. Accordingly, in contrast to the Ir(I)-based systems, the stoichiometric alkane dehydrogenation mediated by this NCN-based Ir(III) system (**36**) is not inhibited by the presence of N$_2$, α-olefins, or water. Indeed, the Goldberg group observed that the yield of stoichiometric n-octane dehydrogenation was *increased* (by 33%) by the presence of ca. 120 equiv. water.

Goldberg and coworkers have used molecular oxygen to transform (^{dm}Phebox)Ir (OAc)(H) (**61**) quantitatively to (^{dm}Phebox)Ir(OAc)$_2$(OH$_2$) (**36**), the same species that reacts with octane to give octene and **61** [92]. This observation suggests great promise with respect to the use of oxygen to complete a catalytic cycle for alkane dehydrogenation, with a system based on Ir(III), uninhibited (or even accelerated) by water.

Chianese and coworkers have investigated the acceptorless dehydrogenation of alkanes catalyzed by CCC pincer-iridium complexes (**37–42**) [94]. Complexes **37**, **38**, and **42** were inactive for acceptorless dehydrogenation under the conditions

applied. (CCC)Ir complexes **39**, **40**, and **41**, however, generated from their hydrido-chloride precursors were found to be catalytically active. For the acceptorless dehydrogenation of cyclooctane (bp 150°C), **39**, **40**, and **41** (0.5 mM) gave TONs of 103, 84, and 35, respectively (average relative standard deviation of 29%), after 22 h. The catalytic activity of **39** was not inhibited by addition of COE (equivalent to 100 TON) indicating that the catalytic activity was not limited by product inhibition [94]. Similarly to (^{CF3}PCP)Ir(η^4-COD)(**56**) [87], the activity of **39** for acceptorless dehydrogenation was unaffected by the presence of N_2. An atmosphere of air, however, strongly decreased catalytic activity (5 TON under air vs. 100 TON under Ar and N_2), which was not restored on changing back to argon atmosphere.

Cyclodecane has a much higher boiling point than cyclooctane (201°C). Acceptorless dehydrogenation is highly endothermic and therefore might be expected to allow much greater TONs than cyclooctane. Catalyst (**39**) gave 102 TON after 22 h, no more than were obtained with COA; this would suggest that TONs are limited by catalyst decomposition, presumably more rapid at the higher reflux temperature of cyclodecane vs. COA. For comparison, the best catalytic system reported for cyclodecane dehydrogenation is based on (*p*-OMe-^{iPr4}PCP)Ir (**17**) [1 mM] [54], which gives 2,100 TOs after 24 h.

Catalyst **41**, which was less active than **39** and **40** for acceptorless dehydrogenation of cycloalkanes, showed relatively high activity for the acceptorless dehydrogenation of *n*-undecane (b.p. 196°C), giving 97 turnovers (average relative standard deviation of 9%) after 22 h; this is comparable to the most efficient catalytic systems based on PCP-type iridium catalysts. In accord with the independently established ability of CCC pincer-iridium catalysts to catalyze alkene isomerization reactions [84, 94–96], only internal undecenes were observed in the acceptorless dehydrogenation of *n*-undecane. Catalysts **39** and **40** both gave about 50 TO in the acceptorless dehydrogenation of *n*-undecane.

Several new types of pincer-iridium complexes have very recently been reported to catalyze alkane dehydrogenation (Fig. 2) [57, 69, 70]. Jensen and coworkers reported the dehydrogenation catalyst (^{tBu4}AsOCOAs)IrH$_2$ (**63**; Fig. 2) [69]. Complex **63** (1 mM) catalyzed transfer dehydrogenation of COA (3.8 M) with TBE (3.8 M) to give about 300 TON after 30 min at 200°C; this compares with 900–1,200 TON in 30 min obtained with (^{tBu4}POCOP)IrH$_2$ (**21-H$_2$**) [59, 64, 69]. The activity of **63** levels off with time giving a maximum of 930 TON after 24 h; this leveling off was attributed to both inhibition by COE product and thermal decomposition of the catalyst. Further evidence of thermal decomposition was obtained by determining the catalytic activity (after 24 h) as a function of temperature (125–200°C in increments of 15°C). The activity of **63** (1 mM) was found to steadily increase with temperature, giving 330 TON at 125°C and peaking at 175°C to give 960 TON after 24 h. Further increase in temperature gave slightly lower yields along with the observation of unidentified catalyst decomposition products.

Huang and coworkers have investigated the use of (^{R}NCOP^{tBu})Ir(H)(Cl) (**64**; 1 mM) (Fig. 2) complexes in the transfer dehydrogenation of COA and *n*-octane with 0.5 M TBE at 150°C using 2 mM NaO^{t}Bu [70]. For the COA transfer dehydrogenation, among the three derivatives of **64**, complex **64a** was by far the
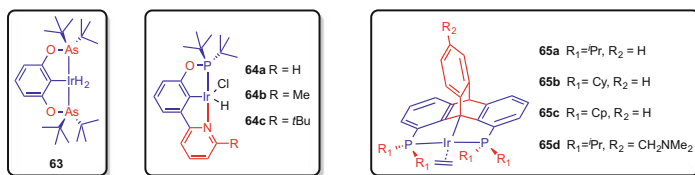
Fig. 2 Recent examples of non-PCP-type pincer-iridium catalysts for alkane dehydrogenation

most effective with initial rates of 1,010 TO h^{-1} compared to **64b** (12 TO h^{-1})and **64c** (6 TO h^{-1}). The activity of **64a** was inhibited by high TBE concentration; the initial rate of COA transfer dehydrogenation dropped from 1,010 to 425 TO h^{-1} as the TBE concentration was increased from 0.5 to 2.5 M. In the transfer dehydrogenation of COA with 0.5 M TBE catalyzed by **64a** at 150°C, about 93% of the TBE was consumed in 12 h resulting in about 470 TOs (while **64b** and **64c** gave only 6 TOs after 12 h). The authors attribute the reduced activity of **64b** and **64c** compared with **64a** to steric effects. Accordingly, complexes **64b** and **64c** exhibit better activity for the dehydrogenation of *n*-alkanes (which has a reduced steric demand) as compared with cycloalkanes. At 150°C the dehydrogenation of *n*-octane with 0.5 M TBE containing 2 mM NaO^{t}Bu (1 mM catalyst) gave initial rates of 325 TO h^{-1} with **64a**, while **64b** and **64c** gave 84 and 60 TO h^{-1}, respectively.

Brookhart and Bezier have reported the use of (^{R}triptycenePC(sp^3)P)Ir(C$_2$H$_4$) (**65**) (Fig. 2) for the transfer dehydrogenation of alkanes [57]. (PC(sp^3)P)Ir systems are of interest, partly in view of the stronger σ-donation from the bridgehead sp^3-hybridized metalated carbon, but their applicability in catalysis has been limited by the presence of α- and β-hydrogens which tend to undergo elimination [99]. Gelman [100–102] and Brookhart [57] have circumvented this problem by generating (PC(sp^3)P)Ir complexes based on triptycene. Transfer dehydrogenation of COA (3.9 M)/TBE (3.9 M) with 1.3 mM (^{iPr}triptycenePC(sp^3)P)Ir(C$_2$H$_4$) (**65a**) at 200°C gave TONs of 900 and 2,590 after 30 min and 4 h, respectively. By comparison, (^{tBu4}POCOP)IrH$_2$ (**21-H$_2$**) gave 1,400 and 1,800 TON after 30 min and 4 h. The higher TON obtained with **65a** (2,590 TO) vs. **21-H$_2$** (1,800 TOs) after 4 h is probably due to inhibition of **21** by COE. However, with both **21-H$_2$** and **65a**, the catalyst resting state is initially the TBE adduct with gradual formation of the COE complex as the reaction proceeds. But while **21** has greater binding affinity for COE vs. TBE, **65a** has similar affinity for the two olefins. Catalysts **65b** and **65c**, bearing phosphinocycloalkyl groups, gave poor results, yielding only 35 and 40 TOs, respectively, after 24 h.

Based on results by Brookhart and Goldman in which *p*-substituted ^{tBu4}PCP complexes, including (*p*-Me$_2$N-^{tBu4}PCP)Ir [55, 103] were anchored to solid supports such as γ-alumina, the Brookhart group synthesized **65d** with a dimethylamino group on the triptycene backbone. Catalysts **65a** and **65d** (1 mM) gave comparable activities (2,800 and 2,040 TON, respectively, after 20 h) for solution-phase COA (3.9 M)/TBE (3.9 M) transfer dehydrogenation at 200°C.

Attempting to anchor **65d** on basic γ-alumina and acidic γ-alumina, however, resulted in catalyst decomposition yielding only 185 and 70 TON, respectively, for the same transfer dehydrogenation (also at 200°C). Much better results, 1,250 TOs after 20 h, were obtained with **65d** anchored to neutral or low soda γ-alumina. Unfortunately such systems were not found to be recyclable. Heterogenizing **65a** (lacking a polar substituent) on either basic γ-alumina or low soda γ-alumina gave poor results (20 TON after 20 h), indicating, in accord with the studies of *p*-substituted ^{tBu4}PCP complexes, that the Ir center of the pincer complexes is deactivated by alumina in the absence of the anchoring groups.

Transfer dehydrogenation of *n*-octane at 200°C by catalyst **65a** (1 mM) using 6 M TBE as acceptor resulted in not only very high rates (40 TO min^{-1}) but also high conversions 6,000 TON after 10 h. **65a** (1 mM) is active even at 100°C for the transfer dehydrogenation of *n*-octane with 0.5 M TBE; 34 TOs were obtained after 60 min and the complete conversion of TBE to TBA was observed after 29 h (500 TO). Interestingly, in contrast with $(^{tBu4}$POCOP)Ir(η^3-allyl)H (**54**), which was generated by the reaction with allene and underwent conversion to propene complex **55** at −58°C (Eq. 5) [83], complex (**65a**) reacts with propene at room temperature to give $(^{iPr4}$triptycenePC(sp^3)P)Ir(η^3-allyl)H and $(^{iPr4}$triptycenePC (sp^3)P)Ir(η^2-C$_3$H$_6$) in a 19:1 ratio after 2 h.

3 Dehydrogenation of Alkanes by Pincer Metal Complexes Other Than Iridium

3.1 Pincer-Ruthenium Complexes in Alkane Dehydrogenation

Several PCP pincer-ruthenium complexes are known to catalyze transfer dehydrogenation of alcohols [104]. However, group 8 metal systems in general have not seen as much success in alkane dehydrogenation compared with iridium. In parallel with their study of $(^{CF3}$PCP)Ir(I) systems [85, 86, 88], Roddick and coworkers, however, found that $(^{CF3}$PCP)M complexes, where M=Ru or Os [85, 105–107], did effect catalytic alkane dehydrogenation. In contrast with catalysis by (PCP)Ir catalysts which proceeded via C–H activation by d^8 three-coordinate Ir(I) active species, Roddick proposed a d^6 four-coordinate Ru(II) hydride as the species that effected C–H addition (9).

$$(9)$$
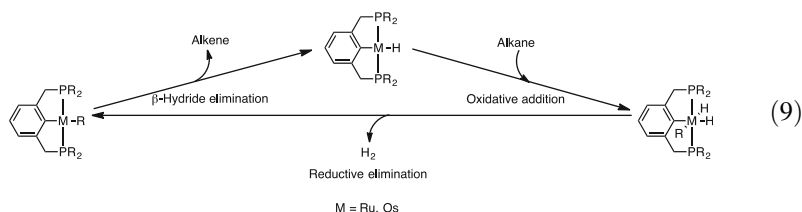
Attempts to synthesize hydride precatalyst (^{CF3}PCP)RuH(H$_2$)$_2$ (**66**) by treatment of (^{CF3}PCP)Ru(cod)H (**67**) with H$_2$ was not successful and resulted in the formation of dimeric ruthenium complex **68** (10). Complex **68** could, however, be converted back to monomeric **67** on treatment with excess COD. Thus the Roddick group used the accessible (^{CF3}PCP)Ru(cod)H **67**(12 mM) to screen for the acceptorless dehydrogenation of COA [105, 107]. This reaction resulted in only three turnovers to COE in 10 min whereupon the catalyst quantitatively decomposed to dimeric complex **68** (10). Transfer dehydrogenation of COA with equimolar amounts of TBE (3.9 M) catalyzed by (^{CF3}PCP)Ru(cod)H (**67**)(6 mM) afforded 18 TOs with complete decomposition of **67** to **68** [107]. Use of 2 equiv. of COD to prevent formation of **68** resulted in four turnovers, with **67** as the resting state of the reaction which is indicative of inhibition of catalysis by COD. When a lower catalyst loading was used (1.25 mM) to prevent dimerization of catalyst **67** to **68** in the COA/TBE transfer dehydrogenation, the reaction proceeded at initial rates of 180 TO h^{-1} and 1,000 TO h^{-1} at 150°C and 200°C, respectively. At 150°C catalytic activity leveled off after 3 h (164 TOs), while at 200°C there was no further activity after 30 min (186 TOs). Catalytic activity was found to be inhibited by COE, and catalyst **67** underwent thermal decomposition to an unidentified species. As in the case of (^{CF3}PCP)Ir(η^4-COD)(**56**), (^{CF3}PCP)Ru(cod)H (**67**) was insensitive to the presence of N$_2$ or moisture. Quite remarkably, the rate and TONs of COA/TBE transfer dehydrogenation catalyzed by **67** were identical in the presence of N$_2$, 100 equiv. of water, or even dioxygen atmosphere [107].

$$(10)$$
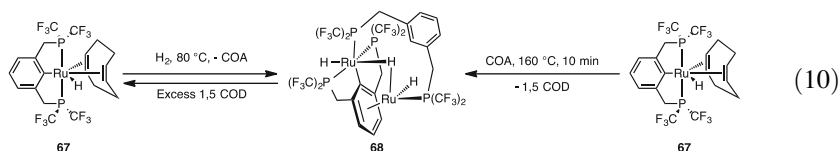
3.2 Pincer Osmium Complexes in Alkane Dehydrogenation

Following their success with pincer-ruthenium-catalyzed alkane dehydrogenation [105, 107], Roddick and coworkers investigated transfer and acceptorless dehydrogenation of alkanes catalyzed by (^{CF3}PCP)Os(COD)H (**69**) [106]. In contrast with (^{CF3}PCP)Ru(COD)H (**67**), the Os analogue shows no activity at 150°C for the transfer dehydrogenation of COA with TBE (1:1; 3.9 M). At 200°C, the initial rate of the reaction (ca. 10 min) catalyzed by **69** (1.38 mM, 1,520 TO h^{-1}) was comparable to that of (^{tBu4}PCP)IrH$_4$ (**11-H$_2$**)[59] and about 75% that of Ru complex

67 [105–107]. The osmium pincer catalyst, however, has a significantly longer lifetime than its ruthenium analogue. Thus use of **69** resulted in 610 turnovers after 8 h, whereas **67** was inactive after 20 min when a maximum of 350 TOs was obtained [106]. Control experiments to determine the stability of **69** at 200°C indicated that the decrease in activity over time resulted from catalyst decomposition to (^{CF3}PCP)Os(COD)X (**70**) where X is likely to be $CH_2CH_2{}'Bu$ [106].

As noted above, perfluoro-alkyl-substituted PCP ligands can impart remarkably decreased sensitivity toward common impurities/catalyst poisons. Thus in contrast with (^{R}PCP)Ir (R=alkyl) systems, the catalytic activity of (^{CF3}PCP)Ir toward dehydrogenation of alkanes is not altered by the presence of N_2 or water, while the (^{CF3}PCP)Ru systems is active even in the presence of O_2. Similarly, the Os analogue, (^{CF3}PCP)Os(COD)H (**69**), showed no significant change in reactivity when the transfer dehydrogenation of cyclooctane (3.9 M) with TBE (3.9 M) was performed under vacuum, under N_2, or with added water at 200°C. In the presence of O_2 (200 torr), the initial rate was unaltered, but catalytic activity decreased significantly after 1 h [106]. Analysis of the reaction mixture by ^{19}F NMR studies indicated the formation of dicarbonyl hydride cis-(^{CF3}PCP)Os(CO)$_2$H (**71**) as the major product. Control experiments point to the fact that the reaction conditions (200°C, $p_{O2} = 200$ torr) result in uncatalyzed oxidation of cyclooctane to cyclooctanone. During this process, trace acyclic hydrocarbons are also converted to aldehydes which are easily decarbonylated by **69**, resulting in catalytically inactive **71** [106].

(^{CF3}PCP)Os(COD)H (**69**) (1 mM) was found to be inactive for the acceptorless dehydrogenation of cyclooctane at 150°C. At 190°C, however, **69** (1 mM) exhibited good activity for acceptorless dehydrogenation of cyclodecane giving 125 turnovers of cyclodecenes after 1 h [106]. This activity is comparable to that of the well-studied parent PCP iridium complex (^{tBu4}PCP)IrH$_4$(**11-H$_2$**) which gives 101 turnovers after 1 h [67]. After ca. 6 h the **69**-catalyzed reaction effectively stops at 250 TOs; at 48 h the TON has increased only to 280. Determination of catalyst resting state by ^{31}P and ^{19}F NMR spectroscopy indicates that this loss of activity is due to formation of dimeric osmium species, similar to those discussed above in the case of (^{CF3}PCP)Ru(COD)H (**67**) (**10**) [105–107].

4 Applications of Alkane Dehydrogenation

4.1 Alkane Metathesis and Alkane–Alkene Coupling Reactions

The global demand for liquid fuel (diesel and jet fuel in particular) is rapidly outpacing conventional petroleum production [108–110]. The upgrading of low-molecular-weight alkanes, particularly to the desirable C_8–C_{19} range, will therefore become increasingly important, whether such light alkanes are ultimately derived

from natural gas, coal, biomass (via either reduction or gasification [111]), condensates, or (in the longer term) the reduction of CO_2 [112] using solar, wind, or nuclear energy. Fischer–Tropsch (F–T) catalysis [113–117] in particular will likely yield an increasing share of the liquid fuel supply, which in turn will lead to growing production of light alkanes as primary F–T oligomerization products and secondary products of cracking F–T wax.

4.1.1 Alkane Metathesis

Initial reports of alkane metathesis were based on heterogeneous catalysts developed by Burnett and Hughes [118] and later by the research group of Basset [119–121]. These systems gave little or no molecular weight selectivity. Goldman, Brookhart, and coworkers reported the first homogeneous alkane metathesis system, operating under mild conditions [72]. A tandem system was reported in which alkane dehydrogenation to olefin by pincer-iridium catalysts was followed by olefin metathesis by Schrock's MoF12 catalyst (72), to give olefins of higher and lower carbon numbers. These olefins in turn act as hydrogen acceptors, resulting in the "metathesized" alkane products and regenerating the pincer-Ir dehydrogenation catalyst (11).

$$(11)$$
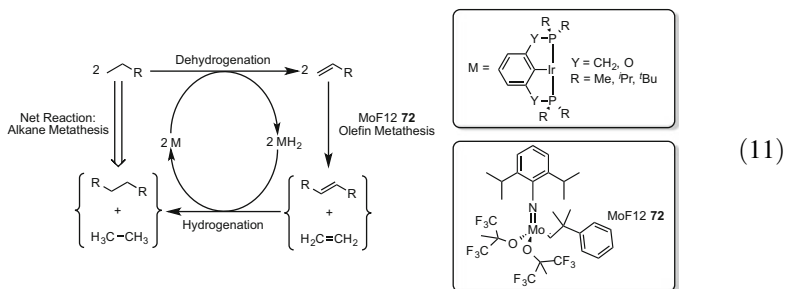
While the heterogeneous alkane metathesis systems developed by Basset, Coperet, and coworkers give mixtures of linear and branched alkanes [119–121], the pincer-Ir-based alkane metathesis systems [72] gave exclusively n-alkanes. However, in addition to C_{2n-2} n-alkane and ethane formed from C_n n-alkane (11), n-alkanes of intermediate chain length are formed, often as the major product. Among the pincer-iridium catalysts, yields for n-hexane metathesis at 125°C were as follows: (^{tBu3Me}PCP)IrH$_4$(14-H$_4$)>(^{iPr4}PCP)IrH$_4$ (12-H$_4$)> (^{tBu2Me2}PCP) IrH$_4$(15-H$_4$)>(^{tBu4}PCP)IrH$_2$(11-H$_2$) [67]. Scott and coworkers have successfully extended the application of alkane metathesis to cycloalkanes [73]. These initial reports of pincer-Ir-based alkane metathesis systems have been reviewed [46–48, 71].

Although the use of (^{tBu4}PCP)IrH$_2$(11-H$_2$) and (^{tBu4}POCOP)IrH$_2$(21-H$_2$) for alkane metathesis (with 72 as co-catalyst) gave similar rates, the corresponding resting states were found to be different: (^{tBu4}PCP)IrH$_2$ and (^{tBu4}POCOP)Ir(olefin),

respectively [74, 83]. This suggests that in the case of (^{tBu4}PCP)IrH$_2$(**11-H$_2$**), a fast dehydrogenation of alkane is paired with a rate-determining olefin hydrogenation step while, conversely, the alkane dehydrogenation segment of the cycle is rate determining in the case of alkane metathesis co-catalyzed by (^{tBu4}POCOP) IrH$_2$(**21-H$_2$**). Accordingly, Goldman and coworkers investigated the PCOP catalysts **27–29** based on the hypothesis that for such "hybrid" catalysts, the rate of each segment would be intermediate between the fast and slow steps of **11-H$_2$** and **21-H$_2$**; this would be expected to yield an overall faster rate. The increased rate of the slow (rate-determining) step is not offset by the decreased rate of the fast step [74]. These mixed phosphine–phosphinite PCOP pincer-iridium systems were indeed found to be more active than the PCP and POCOP analogues for alkane metathesis. (^{tBu4}PCOP)IrH$_4$ (**27**) gave rates about fourfold greater than bisphosphine complex (^{tBu4}PCP)IrH$_2$(**11-H$_2$**) and eightfold greater than bisphosphite complex (^{tBu4}POCOP)IrH$_2$(**21-H$_2$**). The less sterically hindered (^{tBu2}PCOP^{iPr2})IrH$_4$ (**29**) in turn gave rates another 4.4 times greater. The catalytic resting state of (^{tBu4}PCOP)Ir (**27**) was found to be a mixture of hydride and olefin species; this supports the hypothesis that motivated investigation of the PCOP complexes, suggesting comparable rates for the alkane dehydrogenation and olefin hydrogenation, segments in the overall cycle catalyzed by **27** [74].

In the metathesis of *n*-hexane, while (^{tBu4}PCP)Ir(H$_2$) (**11-H$_2$**) gave moderate selectivity toward formation of *n*-decane, very poor selectivity was obtained with (^{tBu4}POCOP)IrH$_2$(**21-H$_2$**) [67, 72, 74] or with PCOP iridium complexes **27–29** [74]. It was initially presumed that the poor selectivity afforded by **21** could be attributed to rapid olefin isomerization, specifically, more rapid than olefin metathesis catalyzed by (^{tBu4}PCP)Ir precursors under the reaction conditions. However, Goldman and Brookhart have recently shown that this difference in selectivity is due to different regioselectivities of **11** and **21** in the primary *n*-alkane dehydrogenation reaction event itself [122, 123].

While (^{tBu4}PCP)Ir (**11**) shows very high kinetic selectivity for the formation of α-olefin, (^{tBu4}POCOP)Ir (**21**) favors dehydrogenation of *n*-alkane to yield internal olefins as the primary dehydrogenation products. A combination of computational and mechanistic experimental studies indicates that the rate-determining step in the dehydrogenation sequence is different for **11** than for **21**; this accounts for the striking difference in regioselectivity by such similar species.

The rate of alkane metathesis catalyzed by various PYCYP (Y=CH$_2$, O) iridium pincer complexes in tandem with MoF12 (**72**) slowed down with time; this was found to be attributable to decomposition by MoF12 (**72**) [67, 72, 74, 124]. The use of Re$_2$O$_7$/Al$_2$O$_3$ as the olefin metathesis catalyst required higher temperatures to obtain good reaction rates; however the oxide catalyst was more stable than MoF12 (**72**), resulting in higher TONs [72]. Schrock and coworkers have screened over 40 bis(alkoxide) and mono(alkoxide)mono(pyrrolide) (MAP) complexes of Mo and W, varying the imido, alkoxide, and pyrrolide ligands [125]. In general, olefin metathesis catalysts based on tungsten were better than those based on molybdenum, and in particular, W(NAr)(CHR)(OSiPh$_3$)$_2$ (**73**) (Ar=2,6 diisopropylphenyl) was the most effective co-catalyst. Brookhart and coworkers have used pincer-

iridium complexes with polar anchoring group supported on Al_2O_3 in tandem with Re_2O_7/Al_2O_3 to obtain remarkably high TONs in alkane metathesis [103].

4.1.2 Alkane–Alkene Coupling

Bercaw and Labinger recently reported on alkane–alkene coupling as another approach toward upgrading light hydrocarbons [77, 78]. This work is based on the fact that light hydrocarbon feeds typically contain alkenes. Such a mixture could be subjected to a tandem catalytic system comprising an alkene dimerization catalyst and an alkane transfer-dehydrogenation catalyst (12). The dimerization catalyst would effect coupling of two C_n alkene fragments to give C_{2n} alkene, while the transfer-dehydrogenation catalyst could effect the dehydrogenation of C_n alkane to regenerate C_n alkene and transfer hydrogenation of C_{2n} alkene to give C_{2n} alkane. The net reaction would be the coupling of alkane with alkene to give a higher alkane without the formation of any lighter by-products [67, 72, 74, 103]. Along similar lines, in a recent patent, Goldman and coworkers report alkane coupling where alkane dehydrogenation by a pincer-iridium catalyst is accompanied by oligomerization of the resulting alkene and subsequent transfer hydrogenation of the resulting olefinic dimer or oligomer [126].

(12)
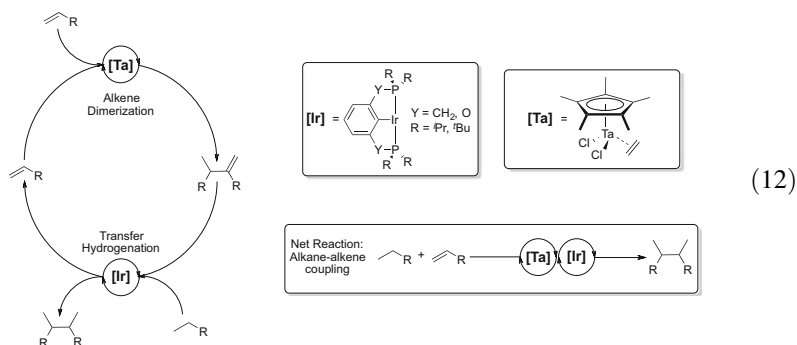
Bercaw and Labinger used $Cp*Ta(Cl)_2(C_2H_4)$ (**74**) as the alkene dimerization catalyst which was first reported by Schrock [127] and is known to be inert to internal alkenes and sterically hindered terminal alkenes. For alkane transfer hydrogenation, three catalysts, $(^{iPr4}PCP)IrH_4$(**12-H$_4$**), $(^{tBu4}PCP)IrH_4$(**11-H$_4$**), and $(^{tBu4}POCOP)Ir(C_2H_4)$(**21-C$_2$H$_4$**), were screened. Attempts to couple 1-hexene with *n*-heptane using a tandem catalytic system based on **74** and **21-C$_2$H$_4$** were not successful, though 1-hexene coupling and *n*-heptane dehydrogenation occurred in these reactions [78]. The failure to accomplish 1-hexene/*n*-heptane coupling was traced to the poor kinetic selectivity of **21-C$_2$H$_4$** [74, 83, 122, 123] which affords only internal heptenes that are inert to coupling by **74**.

$$(13)$$
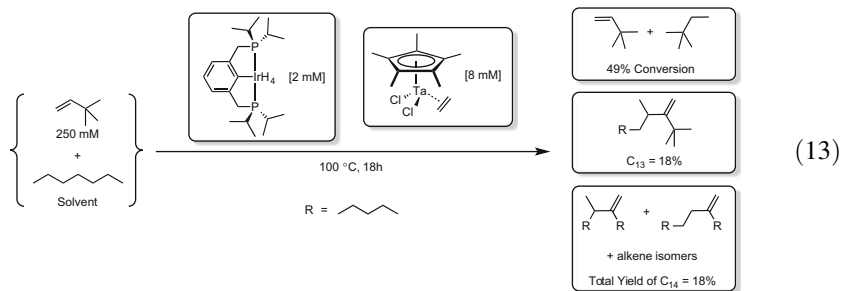
Reaction of 1-hexene with *n*-heptane at 125°C using (^{tBu4}PCP)IrH$_4$(**11-H$_4$**) (10 mM) in tandem with **74** (16 mM), resulted in C$_{13}$ (resulting from hexene/ heptene coupling) and C$_{14}$ alkenes with 35% cooperativity [78]. Bercaw and Labinger define "cooperativity" as the amount of 1-heptene generated by dehydrogenation that is incorporated into C$_{13}$ and C$_{14}$ dimers. The absence of C$_{13}$ and C$_{14}$ alkanes indicates that the catalytic cycle (12) is not completed, presumably due to the fact that the 1,1-disubstituted alkenes are poor hydrogen acceptors.

Use of (^{iPr4}PCP)IrH$_4$(**12-H$_4$**)(10 mM) improved the total turnovers compared to that obtained with (^{tBu4}PCP)IrH$_4$(**11-H$_4$**) but with identical cooperativity. However significant improvement in overall yield of alkene dimers (40%) with high cooperativity (91%) was observed when 1-hexene was slowly added via syringe pump to a refluxing *n*-heptane solution at 100°C with a lower catalyst loading ([**12-H$_4$**]=5 mM and [74]=8 mM) [78]. This tandem system was also found to accomplish catalytic dimerization of *n*-heptane with TBE (which is inert to dimerization) as acceptor (13). High yields of C$_{14}$ alkenes were also obtained using styrene as an acceptor.

4.2 Aromatics via Alkyl Group Cross Metathesis and Alkane Cyclodimerization

Growth in global demand for chemicals, including aromatics (particularly benzene, toluene, and xylenes, or "BTX"), will strongly outpace stagnant demand for gasoline. Since aromatics are obtained in large part as a by-product of gasoline refining, this creates a global shortage of these key chemical building blocks. In addition to BTX, there is also a high demand for *n*-alkyl arenes, which are precursors for surfactants with high detersive power [128]. Synthesis of *n*-alkyl arenes requires the challenging anti-Markovnikov arylation of olefins [129–131], and hence branched alkyl arenes synthesized via Friedel−Crafts alkylation currently dominate the surfactant industry. Goldman and Brookhart have reported an efficient route to *n*-alkyl arenes directly from *n*-alkane as starting materials via dehydroaromatization reaction (14) [61]. Pincer-iridium complexes were proposed to catalyze the sequential dehydrogenation of alkanes ($\geq$C$_6$) to conjugated trienes, followed by

ring closure to cyclohexadienes and then further transfer dehydrogenation to aromatics. In addition to monoalkyl benzenes, these reactions produced significant amounts of dialkyl benzenes, particularly ortho-alkyl toluenes. Obtaining better control of the product distribution remains challenging [75, 76]. Further, the requirement of 4 equiv. sacrificial olefin acceptor limits the utility of this reaction, particularly considering that the best results were obtained with TBE.

$$(14)$$
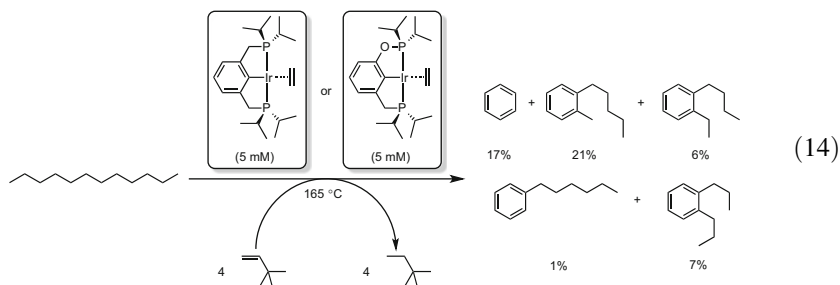
As noted above, TBE has enjoyed great popularity in the field of alkane transfer dehydrogenation since its introduction by Crabtree in 1979 [1]. However, on an industrial scale, the use of acceptors that are less expensive and easily recyclable would obviously be preferable; two obvious choices are propene and ethylene. Thus it is somewhat promising that propene gave moderately good yields as an acceptor for dehydroaromatization reaction (14), although not as good as TBE [61]. However, especially in view of the abundance of ethane resulting from the recent North American shale gas boom, the use of ethylene would generally be much more desirable [132, 133].

$$(15)$$
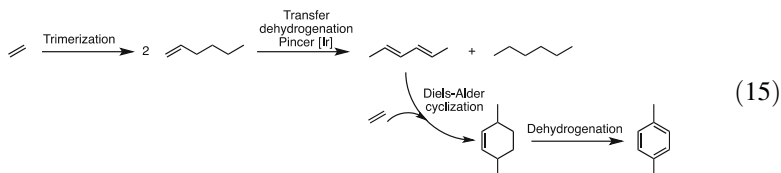
On a closely related note, Brookhart and coworkers have recently demonstrated the role of ethylene as an acceptor and as a dienophile in the syntheses of piperylene, toluene, and p-xylene [134, 135]. With the use of 1-hexene obtained (as is common) from the trimerization of ethylene, p-xylene can thus be synthesized with ethylene as the sole feedstock (15) [135]. Brookhart discovered conditions under which 1-hexene disproportionation at 180°C, using 0.04 mol% pincer-iridium dehydrogenation catalysts, is terminated at the diene stage, precluding benzene formation. In these reactions $(^{iPr4}$anthraphos$)$Ir(C_2H_4) (**31-C$_2$H$_4$**) (222 TO h^{-1}) outperformed $(^{iPr4}$PCOP$)$Ir(C_2H_4) (**28-C$_2$H$_4$**) (61 TO h^{-1}) and especially the more crowded $(^{tBu4}$POCOP$)$Ir(C_2H_4)(**21-C$_2$H$_4$**) (0.5 TO h^{-1}) and $(^{tBu4}$PCP$)$Ir(C_2H_4)(**11-C$_2$H$_4$**) (0.4 TO h^{-1}).The thermodynamically less favored 1,3-hexadiene undergoes isomerization to 2,4-hexadiene. The diene mixtures

were subsequently subjected to a Diels–Alder cyclization at 250°C with ethylene (600 psi) resulting in 96% conversion to an 8:1 mixture of 3,6-dimethylcyclohexane and 3-ethylcyclohexane. Dehydrogenation of 3,6-dimethylcyclohexane and 3-ethylcyclohexane at 400°C over Pt/Al_2O_3 gave an 8.5:1 mixture of *p*-xylene and ethylbenzene in 93% and 88% yields, respectively. Based on this multistep approach, the Brookhart group then developed a one-pot reaction. Thus heating 1-hexene at 250°C under 600 psi of ethylene for 192 h resulted in about 10% aromatic products. Piperylene and toluene have similarly been obtained via tandem transfer dehydrogenation of pentane/pentene followed by Diels–Alder cyclization with ethylene [134].

Schrock and coworkers have reported the synthesis of *n*-alkyl arenes via tandem dehydrogenation of alkyl benzenes and *n*-alkanes followed by olefins metathesis and hydrogenation of resulting alkenes (16) [62]. The net reaction, termed alkyl group cross-metathesis (AGCM), gave high yields of long-chain *n*-alkyl arenes.
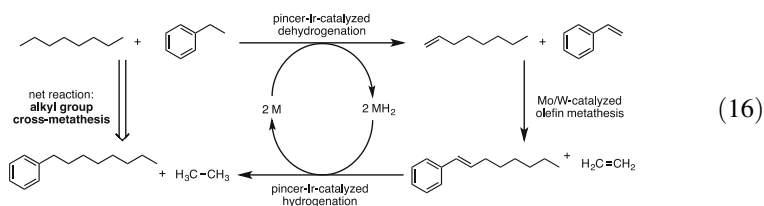
In contrast with the *n*-alkane dehydroaromatization reactions, AGCM does not require any added olefinic acceptors and also does not result in the formation of dialkyl benzenes. Excellent results were obtained for the metathesis of *n*-octane and ethyl benzene at 180°C using $W(NAr')(C_3H_6)(pyr)(OHIPT)$ (**75**)(Ar'=2,6-$Me_2C_6H_3$, OHIPT=2,6-(2,4,6-*i*-$Pr_3C_6H_2)_2C_6H_3O$) (11 mM) as the olefin metathesis catalyst and ($^{tBu4}PCP)IrH_2$ (**11-H$_2$**) (7 mM) as the dehydrogenation catalyst. This reaction not only gave the highest conversion of 1-phenyl octane (350 mM) but also resulted in the highest selectivity (17:1) for *n*-alkyl arene vs. C_{14} arising from alkane metathesis. In another route to monoalkylarenes from *n*-alkanes, Goldman and coworkers have recently patented a tandem catalytic system for alkane–arene coupling where a mixture of alkane and arene in one pot is subjected to acceptorless alkane dehydrogenation by pincer-iridium catalysts, which is followed by Friedel–Crafts coupling by zeolite-based catalysts [136].

5 Summary and Outlook

Recent years have seen great progress in increasing the applications and mechanistic understanding of alkane dehydrogenation by pincer-Ir catalysts. Highly active, regioselective, and thermally robust catalysts based on the motif of a central coordinating carbon and two P-coordinating groups (PCP-type, e.g., PCP itself, PCOP, POCOP, anthraphos, etc.) continue to be developed. Supporting such

catalysts on solids appears to be relatively straightforward and effective. Double-bond isomerization, however, continues to be a problem. Given these strengths, and this weakness, it is perhaps not surprising that very promising results continue to emerge from the development of tandem catalytic systems, in which olefin is formed and then a secondary reaction is catalyzed, e.g., olefin metathesis. Particularly attractive are those cases in which the secondary reaction is more rapid than isomerization, allowing exploitation of the exquisite regioselectivity offered by some of these dehydrogenation catalysts. Another tandem catalytic-type application of these catalysts involves multiple dehydrogenations, for example, dehydrogenation followed by a Diels–Alder reaction or dehydrogenation–cyclization–aromatization.

Recent years have also seen growth in the development of non-PCP-type iridium-based catalysts, for example, the NCN (phebox) iridium complexes, and catalysts based on metals other than iridium. Complexes of both of these categories, unlike PCP-type iridium complexes, seem to offer particular promise by showing tolerance of N_2 and more surprisingly water. Most intriguing, some of these systems including Roddick's ^{CF3}PCP-based catalysts and the (phebox)Ir complexes show promise with respect to the use of O_2; given the very favorable thermodynamics of alkane-to-dioxygen transfer dehydrogenation and C–H oxygenation reactions, this certainly presents exciting opportunities.

References

1. Crabtree RH, Mihelcic JM, Quirk JM (1979) J Am Chem Soc 101:7738–7740
2. Crabtree RH, Demou PC, Eden D, Mihelcic JM, Parnell CA, Quirk JM, Morris GE (1982) J Am Chem Soc 104:6994–7001
3. Crabtree RH, Mellea MF, Mihelcic JM, Quirk JM (1982) J Am Chem Soc 104:107–113
4. Baudry D, Ephritikhine M, Felkin H (1980) J Chem Soc Chem Commun 1243–1244
5. Baudry D, Ephritikhine M, Felkin H (1982) J Chem Soc Chem Commun 606–607
6. Baudry D, Ephritikhine M, Felkin H, Zakrzewski J (1982) J Chem Soc Chem Commun 1235–1236
7. Bergman RG (1984) Science 223:902–908
8. Janowicz AH, Bergman RG (1982) J Am Chem Soc 104:352–354
9. Janowicz AH, Bergman RG (1983) J Am Chem Soc 105:3929–3939
10. Ghosh CK, Rodgers DPS, Graham WAG (1988) J Chem Soc Chem Commun 1511–12
11. Hoyano JK, Graham WAG (1982) J Am Chem Soc 104:3723–3725
12. Rest AJ, Whitwell I, Graham WAG, Hoyano JK, McMaster AD (1984) J Chem Soc Chem Commun 624–626
13. Rest AJ, Whitwell I, Graham WAG, Hoyano JK, McMaster AD (1987) J Chem Soc Dalton Trans 1181
14. Harper TGP, Shinomoto RS, Deming MA, Flood TC (1988) J Am Chem Soc 110:7915–7916
15. Jones WD, Feher FJ (1983) Organometallics 2:562–563
16. Jones WD (2000) Science 287:1942–1943
17. Labinger JA, Bercaw JE (2002) Nature 417:507–514
18. Goldberg KI, Goldman AS (eds) (2004) Activation and functionalization of C–H bonds. In: ACS symposium series 885, Washington, DC, American Chemical Society
19. Bergman RG (2007) Nature 446:506

20. Crabtree RH (2010) Chem Rev 110:575
21. Balcells D, Clot E, Eisenstein O (2010) Chem Rev 110:749–823
22. Baudry D, Ephritikhine M, Felkin H, Holmes-Smith R (1983) J. Chem. Soc. Chem Commun 788–789
23. Goldman AS, Renkema KB, Czerw M, Krogh-Jespersen K (2004) Activation and Functionalization of C–H Bonds. ACS Symp Ser 885:198–215
24. Burk MJ, Crabtree RH, Parnell CP, Uriarte RJ (1984) Organometallics 3:816–817
25. Felkin H, Fillebeen-Khan T, Gault Y, Holmes-Smith R, Zakrzewski J (1984) Tetrahedron Lett 25:1279–1282
26. Felkin H, Fillebeen-khan T, Holmes-Smith R, Yingrui L (1985) Tetrahedron Lett 26:1999–2000
27. Afeefy, HY; Liebman, JF; Stein, SE "Neutral Thermochemical Data" in NIST Chemistry WebBook, NIST Standard Reference Database Number 69, Eds. P.J. Linstrom and W.G. Mallard, National Institute of Standards and Technology, Gaithersburg MD, 20899, http://webbook.nist.gov, (retrieved October 15, 2014)
28. Burk MJ, Crabtree RH, McGrath DV (1985) J. Chem. Soc. Chem Commun 1829–1830
29. Burk MJ, Crabtree RH (1987) J Am Chem Soc 109:8025–8032
30. Kunin AJ, Eisenberg R (1986) J Am Chem Soc 108:535–536
31. Kunin AJ, Eisenberg R (1988) Organometallics 7:2124–2129
32. Sakakura T, Sodeyama T, Tanaka M (1989) New J Chem 13:737–745
33. Sakakura T, Sodeyama T, Tokunaga Y, Tanaka M (1988) Chem Lett 17:263–264
34. Sakakura T, Tanaka M (1987) Chem Let 16:249–252
35. Sakakura T, Tanaka M (1987) J Chem Soc Chem Commun 758–759
36. Aoki T, Crabtree RH (1993) Organometallics 12:294–298
37. Fujii T, Higashino Y, Saito Y (1993) J Chem Soc Dalton Trans 517–520
38. Fujii T, Saito Y (1990) J Chem Soc Chem Commun 757–758
39. Maguire JA, Boese WT, Goldman AS (1989) J Am Chem Soc 111:7088–7093
40. Maguire JA, Goldman AS (1991) J Am Chem Soc 113:6706–6708
41. Maguire JA, Petrillo A, Goldman AS (1992) J Am Chem Soc 114:9492–9498
42. Chowdhury AD, Weding N, Julis J, Franke R, Jackstell R, Beller M (2014) Angew Chem Int Ed Engl 53:6477–6481
43. Wang K, Goldman ME, Emge TJ, Goldman AS (1996) J Organomet Chem 518:55–68
44. Gupta M, Hagen C, Flesher RJ, Kaska WC, Jensen CM (1996) Chem Commun 2083–2084
45. Gupta M, Hagen C, Kaska WC, Cramer RE, Jensen CM (1997) J Am Chem Soc 119:840–841
46. Choi J, Goldman A (2011) Top Organometal Chem 34:139–167
47. Choi J, MacArthur AHR, Brookhart M, Goldman AS (2011) Chem Rev 111:1761–1779
48. Findlater M, Choi J, Goldman AS, Brookhart M (2012) Catal Met Complexes 38:113–141
49. Xu W-W, Rosini GP, Krogh-Jespersen K, Goldman AS, Gupta M, Jensen CM, Kaska WC (1997) Chem Commun 2273–2274
50. Liu F, Pak EB, Singh B, Jensen CM, Goldman AS (1999) J Am Chem Soc 121:4086–4087
51. Liu FS, Goldman A (1999) Chem Commun 655–656
52. Haenel MW, Oevers S, Angermund K, Kaska WC, Fan H-J, Hall MB (2001) Angew Chem Int Ed Engl 40:3596–3600
53. Punji B, Emge TJ, Goldman AS (2010) Organometallics 29:2702–2709
54. Zhu K, Achord PD, Zhang X, Krogh-Jespersen K, Goldman AS (2004) J Am Chem Soc 126:13044–13053
55. Huang Z, Brookhart M, Goldman AS, Kundu S, Ray A, Scott SL, Vicente BC (2009) Adv Synth Catal 351:188–206
56. Kuklin SA, Sheloumov AM, Dolgushin FM, Ezernitskaya MG, Peregudov AS, Petrovskii PV, Koridze AA (2006) Organometallics 25:5466–5476
57. Bezier D, Brookhart M (2014) ACS Catal 4:3411–3420
58. Göttker-Schnetmann I, Brookhart M (2004) J Am Chem Soc 126:9330–9338
59. Göttker-Schnetmann I, White P, Brookhart M (2004) J Am Chem Soc 126:1804–1811

60. Göttker-Schnetmann I, White PS, Brookhart M (2004) Organometallics 23:1766–1776
61. Ahuja R, Punji B, Findlater M, Supplee C, Schinski W, Brookhart M, Goldman AS (2011) Nature Chem 3:167–171
62. Dobereiner GE, Yuan J, Schrock RR, Goldman AS, Hackenberg JD (2013) J Am Chem Soc 135:12572–12575
63. Shi Y, Suguri T, Dohi C, Yamada H, Kojima S, Yamamoto Y (2013) Chem Eur J 19:10672–10689
64. Yao W, Zhang Y, Jia X, Huang Z (2014) Angew Chem 126:1414–1418
65. Jia X, Zhang L, Qin C, Leng X, Huang Z (2014) Chem Commun 50:11056–11059
66. Morales-Morales D, Redón Ro, Yung C, Jensen CM (2004) Inorg Chim Acta 357:2953–2956
67. Kundu S, Choliy Y, Zhuo G, Ahuja R, Emge TJ, Warmuth R, Brookhart M, Krogh-Jespersen-K, Goldman AS (2009) Organometallics 28:5432–5444
68. Yao W, Zhang Y, Jia X, Huang Z (2014) Angew Chem Int Ed Engl 53:1390–1394
69. Brayton DF, Beaumont PR, Fukushima EY, Sartain HT, Morales-Morales D, Jensen CM (2014) Organometallics 33:5198–5202
70. Jia X, Zhang L, Qin C, Leng X, Huang Z (2014) Chem Commun 50:11056–11059
71. Haibach MC, Kundu S, Brookhart M, Goldman AS (2012) Acc Chem Res 45:947–958
72. Goldman AS, Roy AH, Huang Z, Ahuja R, Schinski W, Brookhart M (2006) Science 312:257–261
73. Ahuja R, Kundu S, Goldman AS, Brookhart M, Vicente BC, Scott SL (2008) Chem Commun 253-255
74. Nawara-Hultzsch AJ, Hackenberg JD, Punji B, Supplee C, Emge TJ, Bailey BC, Schrock RR, Brookhart M, Goldman AS (2013) ACS Catal 3:2505–2514
75. Goldman A, Ahuja R, Schinski W (2013) Rutgers, The State University of New Jersey, USA. US20130123552A1
76. Steffens AM, Goldman AS (2013) Abstracts of Papers, 245th ACS National Meeting & Exposition, New Orleans, LA, United States, April 7-11, 2013, INOR-1328
77. Leitch DC, Labinger JA, Bercaw JE (2014) Organometallics 33:3353–3365
78. Leitch DC, Lam YC, Labinger JA, Bercaw JE (2013) J Am Chem Soc 135:10302–10305
79. Gupta M, C. Kaska W, M. Jensen C (1997) Chem Commun 461–462
80. Jensen CM (1999) Chem. Commun 2443–2449
81. Zhang X, Fried A, Knapp S, Goldman AS (2003) Chem. Commun 2060–2061
82. Kumar A, Goldman AS (2013) Abstracts of Papers, 245th ACS National Meeting & Exposition, New Orleans, LA, United States, April 7-11, 2013, INOR-1202
83. Biswas S, Huang Z, Choliy Y, Wang DY, Brookhart M, Krogh-Jespersen K, Goldman AS (2012) J Am Chem Soc 134:13276–13295
84. Knapp SMM, Shaner SE, Kim D, Shopov DY, Tendler JA, Pudalov DM, Chianese AR (2014) Organometallics 33:473–484
85. Roddick DM (2013) Top Organomet Chem 40:49–88
86. Adams JJ, Arulsamy N, Roddick DM (2011) Organometallics 30:697–711
87. Adams JJ, Arulsamy N, Roddick DM (2011) Dalton Trans 40:10014–10019
88. Adams JJ, Arulsamy N, Roddick DM (2012) Organometallics 31:1439–1447
89. Lee DW, Kaska WC, Jensen CM (1998) Organometallics 17:1–3
90. Ghosh R, Kanzelberger M, Emge TJ, Hall GS, Goldman AS (2006) Organometallics 25:5668–5671
91. Morales-Morales D, Lee DW, Wang Z, Jensen CM (2001) Organometallics 20:1144–1147
92. Allen KE, Heinekey DM, Goldman AS, Goldberg KI (2014) Organometallics 33:1337–1340
93. Allen KE, Heinekey DM, Goldman AS, Goldberg KI (2013) Organometallics 32:1579–1582
94. Chianese AR, Drance MJ, Jensen KH, McCollom SP, Yusufova N, Shaner SE, Shopov DY, Tendler JA (2014) Organometallics 33:457–464
95. Chianese AR, Mo A, Lampland NL, Swartz RL, Bremer PT (2010) Organometallics 29:3019–3026

96. Chianese AR, Shaner SE, Tendler JA, Pudalov DM, Shopov DY, Kim D, Rogers SL, Mo A (2012) Organometallics 31:7359–7367
97. Ito J-i, Kaneda T, Nishiyama H (2012) Organometallics 31:4442-4449
98. Pahls DR, Allen KE, Wright AM, Goldberg KI, Cundari TR (2014) Abstracts of Papers, 248th ACS National Meeting & Exposition, San Francisco, CA, United States, August 10-14, 2014, INOR-804
99. Kuznetsov VF, Abdur-Rashid K, Lough AJ, Gusev DG (2006) J Am Chem Soc 128:14388–14396
100. Azerraf C, Gelman D (2009) Organometallics 28:6578–6584
101. Gelman D, Romm R (2013) Organometal Pincer Chem 40:289–317
102. Musa S, Ackermann L, Gelman D (2013) Adv Synth Catal 355:3077–3080
103. Huang Z, Rolfe E, Carson EC, Brookhart M, Goldman AS, El-Khalafy SH, MacArthur AHR (2010) Adv Synth Catal 352:125–135
104. Gagliardo M, Chase PA, Brouwer S, van Klink GPM, van Koten G (2007) Organometallics 26:2219–2227
105. Adams JJ, Gruver BC, Donohoue R, Arulsamy N, Roddick DM (2012) Dalton Trans 41:12601–12611
106. Gruver BC, Adams JJ, Arulsamy N, Roddick DM (2013) Organometallics 32:6468–6475
107. Gruver BC, Adams JJ, Warner SJ, Arulsamy N, Roddick DM (2011) Organometallics 30:5133–5140
108. Kerr RA (2011) Science 331:1510–1511
109. Murray J, King D (2012) Nature 481:433–435
110. Brandt AR, Millard-Ball A, Ganser M, Gorelick SM (2013) Environ Sci Technol 47:8031–8041
111. Huber GW, Iborra S, Corma A (2006) Chem Rev 106:4044–4098
112. Graves C, Ebbesen SD, Mogensen M, Lackner KS (2011) Renew Sustain Energy Rev 15:1–23
113. Dry ME (2002) J Chem Technol Biotechnol 77:43–50
114. Dry ME (2002) Catalysis Today 71:227–241
115. Dry ME (2004) Appl Catal A 276:1–3
116. Leckel D (2009) Energy Fuels 23:2342–2358
117. Hildebrandt D, Glasser D, Hausberger B, Patel B, Glasser BJ (2009) Science 323:1680–1681
118. Burnett RL, Hughes TR (1973) J Catal 31:55–64
119. Vidal V, Théolier A, Thivolle-Cazat J, Basset J-M (1997) Science 276:99–102
120. Coperet C, Maury O, Thivolle-Cazat J, Basset J-M (2001) Angew Chem Int Ed Engl 40:2331–2334
121. Basset JM, Copéret C, Lefort L, Maunders BM, Maury O, Le Roux E, Saggio G, Soignier S, Soulivong D, Sunley GJ, Taoufik M, Thivolle-Cazat J (2005) J Am Chem Soc 127:8604–8605
122. Biswas S, Brookhart M, Choliy Y, Goldman A, Huang Z, Krogh-Jespersen K (2010) Abstracts of Papers, 239th ACS National Meeting, San Francisco, CA, United States, March 21-25, 2010, INOR-670
123. Biswas S, Zhou T, Wang DY, Hackenberg J, Nawara-Hultzsch A, Schrock RR, Brookhart M, Krogh-Jespersen K, Goldman AS (2013) Abstracts of Papers, 245th ACS National Meeting & Exposition, New Orleans, LA, United States, April 7-11, 2013, INOR-681
124. Schrock RR (2001) Chem Rev 102:145–180
125. Bailey BC, Schrock RR, Kundu S, Goldman AS, Huang Z, Brookhart M (2008) Organometallics 28:355–360
126. Goldman AS, Stibrany RT, Schinski WL (2013) Chevron U.S.A. Inc., USA; Rutgers, The State University of New Jersey . US20130090503A1
127. McLain SJ, Wood CD, Schrock RR (1979) J Am Chem Soc 101:4558–4570
128. Yang J, Qiao W, Li Z, Cheng L (2005) Fuel 84:1607–1611

129. Bhalla G, Bischof SM, Ganesh SK, Liu XY, Jones CJ, Borzenko A, Tenn WJ III, Ess DH, Hashiguchi BG, Lokare KS, Leung CH, Oxgaard J, Goddard IIIWA, Periana RA (2011) Green Chem 13:69–81
130. Oxgaard J, Muller RP, Goddard WA, Periana RA (2003) J Am Chem Soc 126:352–363
131. Foley NA, Lee JP, Ke Z, Gunnoe TB, Cundari TR (2009) Acc Chem Res 42:585–597
132. He C, You F (2014) Ind Eng Chem Res 53:11442–11459
133. Armor JN (2013) J Energy Chem 22:21–26
134. Kundu S, Lyons TW, Brookhart M (2013) ACS Catal 3:1768–1773
135. Lyons TW, Guironnet D, Findlater M, Brookhart M (2012) J Am Chem Soc 134:15708–15711
136. Goldman AS, Dinh LV, Schinski WL (2013) Rutgers, The State University of New Jersey, USA; Chevron USA Inc. WO2013070316A1

Tethered Pincer Complexes as Recyclable Homogeneous Catalysts

Aidan R. McDonald and Harm P. Dijkstra

Abstract The utilisation of recyclable pincer complexes in applied catalysis is a vital progression in the field of homogeneous catalysis. This is routed in the high thermal and mechanical stability that most pincer complexes demonstrate. The pincer framework of a tridentate bis-chelating ligand system, with two dative appendages and a direct metal ligand σ-bond, shows higher stability than most other coordination complexes. This is essential to testing immobilisation and recycling methods for homogeneous catalysis. We review herein efforts made towards the efficient immobilisation (heterogenisation) of homogeneous pincer complexes, and their application in a variety of catalytic processes. Recycling of pincer complexes, as described herein, does not display high rates of ligand and metal leaching. The outcome of this is an array of homogeneous catalyst immobilisation techniques which can be probed using pincer complexes.

Keywords Catalysis · Catalyst recycling · Heterogenised homogeneous catalysts · Immobilised catalysts · Pincer complexes

Contents

A.R. McDonald (✉)
School of Chemistry, The University of Dublin, Trinity College, College Green, Dublin, Ireland
e-mail: aidan.mcdonald@tcd.ie

H.P. Dijkstra
Department of Organic Chemistry and Catalysis, Debye Institute for Materials Science, Utrecht University, Universiteitsweg 99, 3584 Utrecht, The Netherlands

1   Introduction

Homogeneous catalyst recycling has become an integral part of modern catalysis research. Industrial requirements of cost efficiency and low metal contamination have influenced a trend towards tethering/trapping homogeneous catalysts to maximise ease of separation from high value products [1]. Homogeneous catalysts are widely accepted to be more selective and easier to analyse and predict than heterogeneous catalysts. In homogeneous catalysis, the active site is known, and much that is occurring in catalysis is discernable and modifiable. However, the bonuses of using heterogeneous catalytic systems (e.g. ease of separation and lower costs) far outweigh the positives that lie in the use of homogeneous catalytic systems. The major impedance in using homogeneous catalytic systems lies in our inability to separate like from like.

The sustained development of catalysts for fine chemical production has led to the opinion that a method for heterogenising these homogeneous catalysts must be developed and brought to the industrial arena [2, 3]. Several methods for heterogenisation of catalysts have been explored which are mainly based on inorganic support systems [4], dendrimers [5] or functionalised organic polymers [6]. In addition significant effort has been expended to develop catalysts for biphasic reaction systems [7, 8]; however, very few industrially viable examples have come to the fore [9].

The various methods for the immobilisation of ligands on inorganic/polymeric/dendritic supports and in biphasic systems include the use of covalent/ionic bonding, applications of hydrophobic, hydrophilic and electrostatic interactions, in addition to varying the solubility properties in a liquid biphasic system [10]. The majority of these methods for immobilisation involve the functionalisation of ligands for the linking of a linker/solvator onto the support. It is observed that functionalisation/alteration of these species can modify the catalytic ability, i.e. heterogenisation of a homogeneous catalyst can affect the activity/selectivity of the catalyst. Often a decrease in activity and selectivity is observed as a result of the lower number of available catalytic sites upon immobilisation. Recovery of these various forms of immobilised catalysts is carried out by a wide range of techniques. Simple filtration is the main technique used to isolate inorganic bound catalysts and insoluble polymeric species. Considerable effort has been carried out on the development of polymeric membranes for the encapsulation and filtration of homogeneous catalysts [11]. Nanofiltration membrane [12, 13] techniques are commonly used in the case of dendritic systems.

The application of pincer complexes in this field is a vital progression in the field. This is because of the high stability that most pincer complexes demonstrate. Non-pincer coordination complexes containing mono- or bidentate phosphine and amine ligands are the most widely used ligands in homogeneous catalysis. These ligand systems often induce high reaction rates and impressive selectivity. However, recycling of these types of complexes has shown high rates of ligand and metal leaching. The pincer framework of a tridentate bis-chelating ligand system, with two dative appendages and a direct metal ligand σ-bond, shows higher thermal and mechanical stability than most other coordination complexes. This is essential to testing immobilisation and recycling methods for homogeneous catalysis.

2 Pincer Complexes Bound to Macromolecular Supports

The versatility of pincer complexes as a homogeneous catalyst has been extensively reviewed [14]. Doubtless, the main reason for the broad applicability of the pincer complex as a catalyst is its ease of ligand modification, allowing the introduction of many metal ions and the subsequent electronic and steric fine-tuning of its catalytic activity. In addition, many substituents can be introduced at the position *para* to the metal centre, opening up the opportunity to immobilise the pincer complex onto larger frameworks such as polymers, C60 and dendrimers. It was this exploratory chemistry with organometallic pincer complexes that led to a whole new research field in homogeneous catalysis: recyclable macromolecular homogeneous catalysts. Such soluble recyclable macromolecular catalysts were of special interest since they combined the advantages of heterogeneous catalysts, i.e. easy catalyst recycling and thus low costs, and homogeneous catalysts, i.e. high activity/selectivity and easy fine-tuning (for a review of catalyst recycling by nanofiltration techniques, see [12, 15] and references cited therein). In the initial work, polymers were efficiently used as soluble supports for homogeneous catalysts in order to assure easy recovery and recycling of the macromolecular catalysts from the reaction mixture [16, 17]. However, it was only when the first paper about metallodendrimers containing NCN-Ni-pincers as homogeneous catalysts was published in Nature in 1994 that this research field started to evolve and flourish [18]. In this section, we will give an overview of organometallic pincer fragments immobilised onto soluble macromolecular supports and their use in homogeneous catalysis. Moreover, the emphasis will be on the use of these multimetallic macromolecules as homogeneous catalysts in organic transformations and, if applicable, on the ability to recycle these catalysts by nano- and ultrafiltration techniques, a feature dictated by their macroscopic dimensions. Although most of this work (initially) has been conducted with pincers immobilised on soluble dendritic supports, this section will also discuss the use of polymeric supports and rigid polyaromatic supports.

2.1 Dendritic Supports

From the initial studies with polymeric supports (see Sect. 3.1), it was found that polymer-supported catalysts are rather undefined and therefore it remained difficult to accurately control the number and location of the catalytic moieties in the macromolecular material [19, 20]. To overcome that particular problem, a lot of attention was shifted to dendrimer-supported catalysts since dendrimers are well-defined tree-like polymers, and the exact catalyst loading is easy to control because dendrimers are constructed in a very controlled manner. Presently, many metallo-dendrimers are known, and their synthesis and applications have been reviewed several times [21–23].

As was mentioned earlier, the first catalytically active metallodendrimer was published in 1994 and was a collaborative project between the groups of van Koten and van Leeuwen [18]. This carbosilane dendrimer contained cyclometalated NCN-Ni(II) moieties, and it was demonstrated to be an efficient homogeneous catalyst in the atom transfer radical addition reaction (ATRA or Kharasch addition reaction) of CCl_4 with methyl methacrylate (Scheme 1). Although the rationale behind developing such macromolecular catalysts, i.e. easy and efficient catalyst recovery and recycling, was not demonstrated, this was the first example of a homogeneous catalyst immobilised on a well-defined soluble polymeric support. The synthesis of this dendrimer started from carbosilane molecules with reactive silyl-chloride functionalities on the periphery which were used to couple the diamino aryl bromide ligands. In order to prevent interaction between the different catalytic sites, a 1,4-butanediol linker was placed between the carbosilane core and the pincer moiety. In the last step, nickel(II) was incorporated into the NCN-Br ligands via oxidative addition using $Ni(PPh_3)_4$. Testing this material as a homogeneous catalyst in the Kharasch addition and comparing the results with the corresponding mono NCN-Ni-catalyst revealed that all 12 NCN-Ni sites reacted as independent catalytic sites that are well accessible for incoming substrates. The clean, regioselective 1:1 addition observed for the mononuclear catalyst was preserved. This first example immediately demonstrated the enormous advantage of using well-defined dendritic supports, i.e. the exact determination of the number of catalytically active sites makes it possible to directly compare the catalytic activity and selectivity, and thus catalyst efficiency, of the individual sites with the nonsupported monometallic analogues. This also allows screening for additional (catalytic) effects created by the macromolecular support or by the fact that many catalytic sites are gathered in a relative small volume.

Encouraged by these promising initial results, a more detailed investigation into the use of carbosilane dendrimers as supports for homogeneous catalysts was performed [24, 25]. Kleij et al. demonstrated a new procedure for the full metallation of carbosilane dendrimers bearing NCN-pincer ligands based on a poly-lithiation/transmetallation strategy using t-BuLi and $NiCl_2(PEt_3)_2$ (Scheme 2). **G0**, **G1**, **G1***, **G1*** and **G2** carbosilane dendrimers containing 4 (**G0**), 8 (**G1***), 12 (**G1** + **G1***) and 36 (**G2**) NCN-pincer groups were accessible via this route.
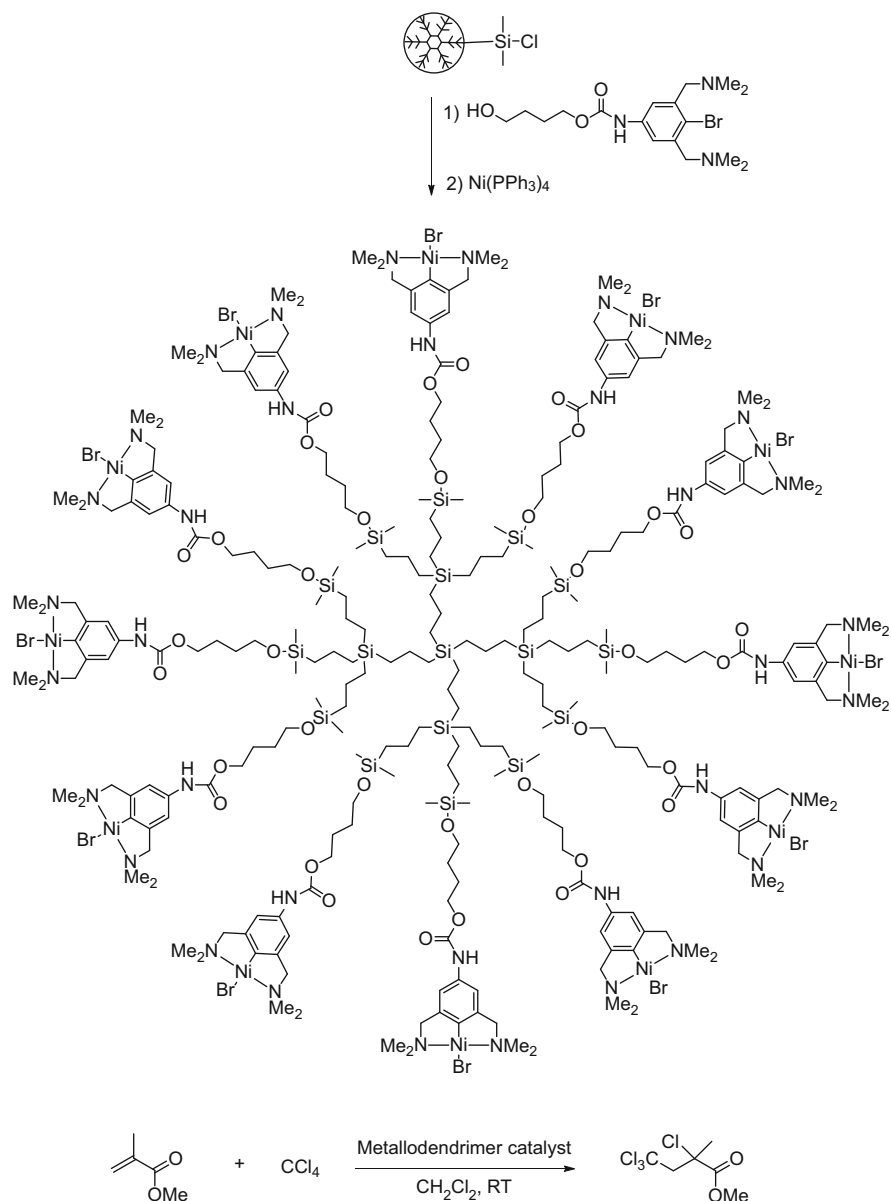
Scheme 1 First metallodendrimer catalyst and (below) Kharasch addition reaction [18]

Notably, the second-generation (**G2**) dendrimer bearing 36 NCN-Ni pincer groups was metallated up to 79% using this protocol, meaning that a polylithiated intermediate containing up to 36 aryl-lithium bonds was formed and subsequently

Synthesis strategy:
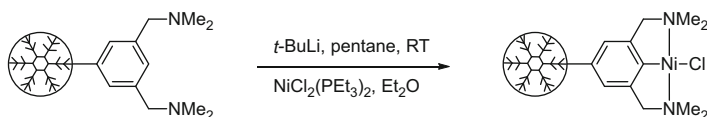
Various generation metallodendrimers:
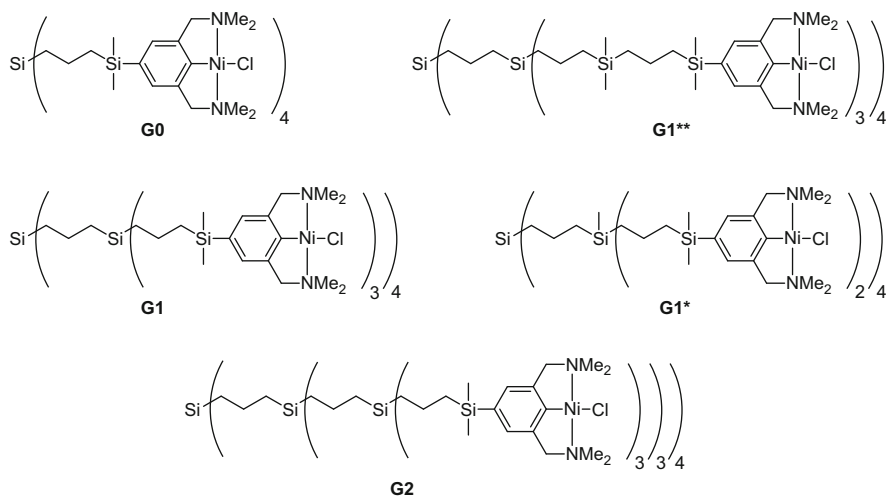
Scheme 2 Several carbosilane dendrimers functionalised with the NCN-Ni-moiety [24]

transmetallated. These homogeneous dendritic catalysts were tested in the Kharasch addition reaction of CCl_4 to methyl methacrylate (see Scheme 1).

Whereas the **G0**, **G1*** and **G1**** possessed similar activities as the mononuclear NCN-NiCl catalyst, the **G1** and **G2** dendritic catalysts showed dramatic decrease in catalytic activity. The initial reaction rate of the **G1** catalyst had dropped ca. 70% with respect to the mononuclear catalyst, while for **G2**, almost no activity was observed (<1.5% after 4 h) [24]. Closer analysis of the reaction mixtures of **G1** and **G2** revealed that in both cases, a purple precipitate had formed during catalysis that contained inactive paramagnetic Ni(III) sites. Importantly, the other two first-generation catalysts, **G1*** and **G1****, only gave formation of the inactive Ni(III) species after all methyl methacrylate was consumed. To shine more light on this matter, a more in-depth study of the origin of the purple species was conducted using a monometallic NCN-Ni complex bearing a p-trimethylsilyl substituents (as a mimic for the carbosilane dendrimer). With this mononuclear NCN-Ni(II) complex, a purple $[NiCl_2(NCN)(p\text{-}SiMe_3)]$ was obtained from reaction of $[ClNi\text{-}NCN$ $(p\text{-}SiMe_3)]$ with CCl_4, a process producing C_2Cl_6 as a coupling product just like in the case of the higher-generation dendrimers. An explanation for why this deactivation process occurs from the start of the reaction for multimetallic catalysts

Scheme 3 Schematic representation of deactivation mechanism for **G1** and **G2** [24]
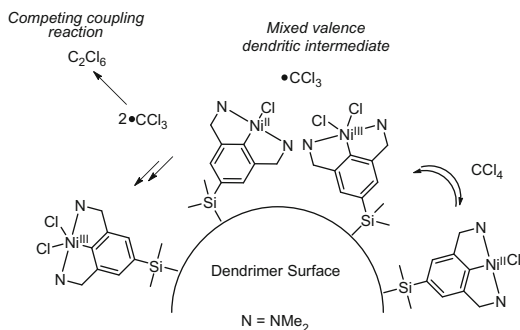
G1 and **G2** and only after the reaction for the mono-NCN-Ni catalyst was provided by modelling studies. Molecular modelling studies with **G0** and **G1** clearly revealed that in the case of **G1,** the Ni(II) sites are in much closer proximity as compared to the **G0** dendrimer. From these studies, it was concluded that the irreversible formation of the Ni(III) sites was a result of a 'proximity effect' (or dendritic effect) between the peripheral Ni(II) sites in **G1** and **G2**. This was supported by the results obtained with **G1*** and **G1****, in which the Ni(II) sites are further separated from each other as compared to **G1** and **G2**, showing no deactivation during catalysis. A deactivation mechanism was proposed (Scheme 3) in which the reduced Ni···Ni distance at the periphery favours the interaction between reactive intermediates (such as ·CCl_3-radicals) created at the dendrimer surface. This phenomenon can lead to fast coupling reactions, for example, between two ·CCl_3 radicals, that are in close proximity to each other, to form C_2Cl_6 at the dendrimer surface. This recombination process is competitive with the reaction of the radical with methyl methacrylate preventing the production of the desired product. Additionally, it also leads to a lower radical concentration thereby preventing reduction of the persistent Ni(III) radical to the catalytically active Ni(II). Thus, for dendritic catalysts in which the catalytic sites are in close proximity (**G1** and **G2**), this will ultimately lead to the complete and irreversible formation of Ni(III)-sites and thus to full deactivation of the dendritic catalyst. Although this was an undesired effect, it was the first example of the so-called dendritic effect, i.e. additional effects caused by the special design of the dendritic backbone. Secondly, this study also nicely illustrated that undesired (deactivation) effects can rather easily be resolved by careful adjustments to the dendritic architecture.

Applying **G0** and **G1** in a nanofiltration membrane reactor revealed that these dendritic catalysts were retained in 97.4 and 99.8%, respectively. This means that after exchanging one reactor volume with solvent respectively 2.6 and 0.2% had leached out of the reactor. Applying the G1 catalyst in a continuous catalytic experiment in the Kharasch, addition reaction gave very poor catalytic results, similar to the batch process. A total-turnover-number per Ni-site of only 20 was obtained (complete loss of activity within 1,000 min) even though ICP analysis of the reaction mixture after catalysis showed that only 1.4% of the G1 catalyst was washed out of the reactor per reactor volume. This number is in agreement with the
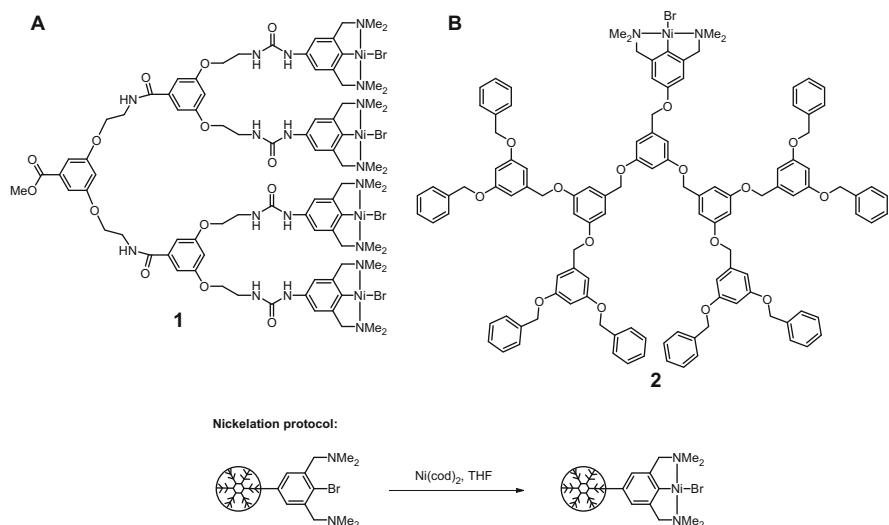
Scheme 4 Dendritic wedges containing preipheral (**A**) and core (**B**) NCN-Ni(II) catalysts [26]

99.8% retention rate found in the batch process (99.8%). Thus, since catalyst leaching cannot account for the fast loss of catalytic activity, it meant that also in the continuous process, there is a considerable amount of deactivation of the nickel (II)-catalyst. Although the catalytic results in the continuous setup were rather disappointing, this study clearly showed that dendrimers are suitable supports for homogeneous catalysts, affording well-defined macromolecular multimetallic catalysts that can easily be fine-tuned. Additionally, it revealed that it is possible to efficiently recycle specially constructed homogeneous catalyst by means of nanofiltration techniques.

The catalytically active NCN-Ni(II)-moiety has also been attached to different dendritic supports. Gossage et al. synthesised an amino acid-based dendritic support and functionalised it with pincer-Ni(II) fragments (**1**, Scheme 4a) [26]. Again the nickel(II) centre was introduced in the final step, however not in the lithiation/ transmetalation manner described earlier but rather using an oxidative addition protocol of Ni(cod)$_2$ to the aryl-bromide bond. This procedure afforded the desired nickelated dendrimer in high yields (Scheme 4). Although no recycling of the catalyst was reported, this catalytic system performed similarly to the mono-pincer analogue, again showing that lower-generation dendrimers containing a lower catalyst loading do not show the deactivation behaviour of the higher-generation NCN-Ni-carbosilane dendrimers (vide supra). Obviously, the deactivation problem can also be overcome by attaching only one catalytic pincer moiety to a dendritic wedge (**2**, Scheme 4b). It was demonstrated that by attaching a single NCN-Ni(II) fragment to three Frechet-type dendritic wedges of different generations (G1, G2 and G3-wedges, respectively), a macromolecular catalyst was obtained for the Kharasch addition reaction (see Scheme 1) that could successfully be recovered

from the reaction mixture by nanofiltration techniques [27]. By loading a vial capped with a nanofiltration membrane with the appropriate dendrimer and placing this vial in a container filled with solvent, it was shown that the catalyst functionalised with the largest dendritic wedge, i.e. G3 (**2**, Scheme 4), gave the best retention rates by the given nanofiltration. Feeding the substrates for the Kharasch addition reaction to this solution resulted in the formation of product. Although this catalytic process was considerably slower than with the non-compartmentalised catalyst, probably due to diffusion limitations of substrates into the vial containing the catalyst, this experiment showed that the homogeneous catalyst could efficiently be recovered from the reaction mixture in a nondestructive manner and reused. This experimental setup was given the name *teabag approach* since the catalyst could be removed from the reaction mixture like a teabag. Interestingly, it was suggested that this approach opens up the possibility to conduct sequential catalytic reactions without intermediate work-up since the catalyst can simply be replaced with another catalyst by replacing the *catalytic* vials. This implies very efficient use of the often expensive catalyst and also time and cost reduction due to combining several catalytic steps into a one-pot process.

A recent study performed by Klein Gebbink and co-workers focussed on the use of SCS-Pd pincer complexes tethered to both polar PAMAM-type and apolar carbosilane support materials [28]. The goal of this investigation was to understand the role the polymeric support plays in influencing the catalytic activity and selectivity. The supported complexes were applied as catalysts in cross-coupling reactions. Minor differences in reactions rates and selectivities were observed when comparing the polar and apolar support materials. Similarly, minimal marked effect of dendrimer generation was noted. Klein Gebbink suggests that this study demonstrates that while the support material can affect the catalytic activity of supported catalysts, often the intrinsic properties of a specific reaction will determine whether the support plays a role or not. Ultimately, the effect of the support material should always be considered when employing tethered catalysts in catalysis.

Another intriguing approach developed by van Koten and co-workers was to decorate dendrimers with catalytically active pincer moieties via a non-covalent attachment protocol [29–31]. Non-covalent attachment of a monometallic catalyst to a dendrimer support offers a number of advantages: (1) controlled introduction and removal of the catalytic group without having to build up the macromolecular catalyst from scratch; (2) easy replacement of one catalytic group by another (different) one, an aspect that is especially convenient in case of catalyst deactivation or sequential catalysis; and (3) reuse of the often expensive dendritic support [32–35] (for a review, see [36]). In this approach, treatment of a carbosilane core **3** containing four 3,5-bis((dimethylamino)methyl)phenyl groups with, for example, 8 equiv. of *Frechet*-type dendron **4** containing a benzyl bromide focal point resulted in the quarternisation of the amino groups, thereby affording core-shell dendrimer [**7**][Br]$_8$ with eight cationic charges in the clefts of the dendrimer (Scheme 5). Introduction of an organometallic NCN-palladium(II) pincer moiety was subsequently achieved via an ion-exchange reaction in which the halide anion in the core of the dendritic support was replaced by an NCN-palladium(II) moiety bearing a

Scheme 5 Non-covalent binding of homogeneous pincer catalysts to core-shell dendritic supports [29]

tethered sulphato anionic group (Scheme 5). Applying this methodology, several core-shell dendrimers containing different peripheral dendritic wedges and pincer-sulphato tethers were synthesised (Fig. 1). Purification was simply achieved by
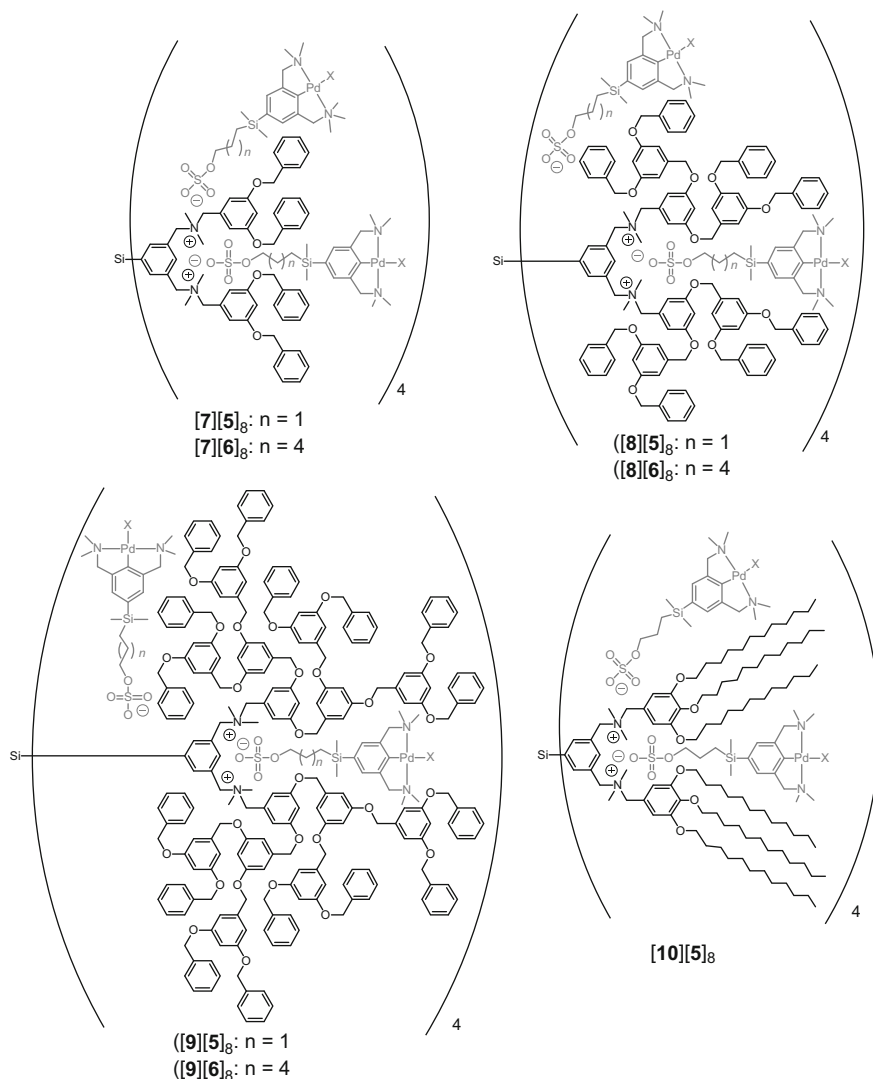
Fig. 1 Various dendritic-catalyst assemblies [29]

repeated dialysis, and these supramolecular structures were analysed by pulse gradient spin echo (PGSE) NMR spectroscopy, transition electron microscopy (TEM), mass spectrometry and elemental analysis. NMR studies clearly revealed a strong binding between the dendritic support and the sulphato-pincer complexes, providing proof for the formation of unimolecular macroscopic structures. The dimensions of these structures varied between the 2.8 and 5.0 nm as was determined by TEM, PGSE NMR spectroscopy and molecular modelling studies, while the shape of the assemblies becomes more spherical at higher generations.

Scheme 6 Catalyst activation and catalytic test reaction
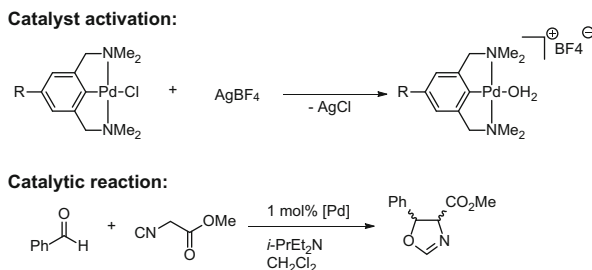
Interestingly, the sizes of the lower-generation dendritic assemblies (**7** and **8**, Fig. 1) were determined by the length of the organometallic pincer guests since the NCN-Pd(II) head group sticks out of the periphery of the dendritic support. This means that the dimensions of these structures can simply be varied by changing the length of the tether, also creating the opportunity to change the polarity around the catalytically active palladium(II) centre by exposing it to the solvent or to the interior of the dendrimer.

The resulting metallodendritic assemblies were tested as homogeneous catalysts in the aldol condensation reaction between benzaldehyde and methyl isocyano-acetate (Scheme 6), a reaction in which the pincer-palladium site acts as a Lewis acid catalyst. Since the NCN-PdCl complex is a poor Lewis acid, the catalytic species was activated prior to catalysis by chloride abstraction with AgBF$_4$ affording the stronger Lewis acidic cationic aqua complexes (X $=$ OH$_2$, Fig. 1 and Scheme 6). Applying these catalysts (1 mol% [Pd]) in the aldol condensation reaction revealed that the dendritic assemblies possessed slightly lower activity as compared to the unsupported catalysts **5** and **6**. In the case of the systems with the shorter C3 linker ([**7**][**5**], [**8**][**5**], [**9**][**5**] and [**10**][**5**], Fig. 1), conversions between the 69 and 73% were determined after 24 h, whereas the unsupported catalyst **5** reached a slightly higher conversion of 83%. The dendritic catalysts with the longer C6-linker ([**7**][**6**], [**8**][**6**] and [**9**][**6**], Fig. 1) showed similar behaviour, although the conversions were somewhat higher, approximately 83% for the dendritic assemblies versus 95% for the unsupported catalyst **6**. Although the differences are small, these results suggest that by changing the linker of the pincer-sulphato tether (**5** vs. **6**), the catalytic activity can be altered, probably a result of more efficient encapsulation of **5** by the dendritic support. Surprisingly, increasing the generation of the dendritic support (going from **7** to **10**) and thus increasing the steric bulk around the catalytically active palladium(II) centre only resulted in minute differences in catalytic activity. Assemblies [**8**][**5**] and [**9**][**5**] showed somewhat higher initial conversion rates as compared to [**7**][**5**] and **5** while dendritic catalyst [**10**][**5**] possessed the lowest initial activity after 5 h in this reaction. These results suggest that the dendritic wedges are relatively 'open' structures, meaning that substrate molecules can rather easily enter the dendritic clefts and interact with the well-exposed palladium(II) centre to form product. Thus, whereas changing the linker of the pincer-sulphato tether has a small but marked effect

(probably steric) on the catalytic activity per Pd-centre, for a given pincer-sulphato tether, the steric influence of the dendritic wedge is negligible. This observation was supported by the stereoselectivity of this catalytic reaction since the *cis/trans* ratio of the oxazoline product remained fairly constant (67–74% trans-product) using both supported and unsupported catalysts. This means that by altering the dendritic wedge, the size of the dendritic assemblies can be altered easily in order to optimise its (nano)filtration behaviour without affecting the catalytic activity of the organometallic pincer guest. Additional advantages of easy modification of the nature of the dendritic shell can be efficient adjustment of the solubility properties of the catalytic dendritic assemblies for specific media and protection of the catalytic sites against deactivation processes, a crucial aspect in continuous catalytic reaction setups as it increases the lifetime and thus the efficiency of the homogeneous catalyst.

The metallodendrimers discussed in this section have clearly illustrated that dendrimers are suitable supports for homogeneous catalysts and that the macromolecular catalysts can be easily fine-tuned to optimise their physical properties as well as their catalytic achievements. Due to the wide variety of different dendritic backbones of various chemical natures and generations and due to their easy modification procedures, dendrimers have already shown great promise as supports for homogeneous catalysts in continuous catalytic reactions in membrane reactors [33, 37–42].

2.2 Shape-Persistent (Poly)Aromatic Supports

As discussed in the previous section, the main reasons for using dendrimers as soluble supports in the field of macromolecular homogeneous catalysts and catalyst recycling are their ease of synthesis and their well-defined structures, allowing easy fine-tuning of the catalytic system and straightforward comparison with the monometallic catalytic systems. Obviously, for macromolecular catalysts to be successful in continuous catalytic reactions in membrane reactors, very efficient retention rates (>99%) of the catalysts by the nanofiltration membranes are required. For dendritic systems, it was observed that at least second-generation dendrimers with molecular weights > 2,000 Da were needed to meet this criterion. This is rather remarkable since the molecular weight cut-off masses (MWCO is defined as the molecular weight at which 90% of the solutes are retained by the membrane) of the used membranes are typically <1,000 Da, meaning that first-generation dendrimers should already be retained very efficiently by these membranes. It was postulated that this phenomenon was due to the flexible behaviour of the dendritic backbones. In earlier studies, it was already reported that dendrimers undergo shape changes in solution and that back-folding of a dendritic arm can occur, a phenomenon that becomes increasingly important when going up in generation [43, 44]. This implies that going from lower- to higher-generation dendrimers does not automatically lead to a linear increase in dendrimer size and thus retention rates by nanofiltration

11a: M = Pd, L = halide
11b: M = Pd, L = OH$_2$(BF$_4$)
For retention measurements
11c: M = Pt, L = halide

12a - c

13a - c

14a - c
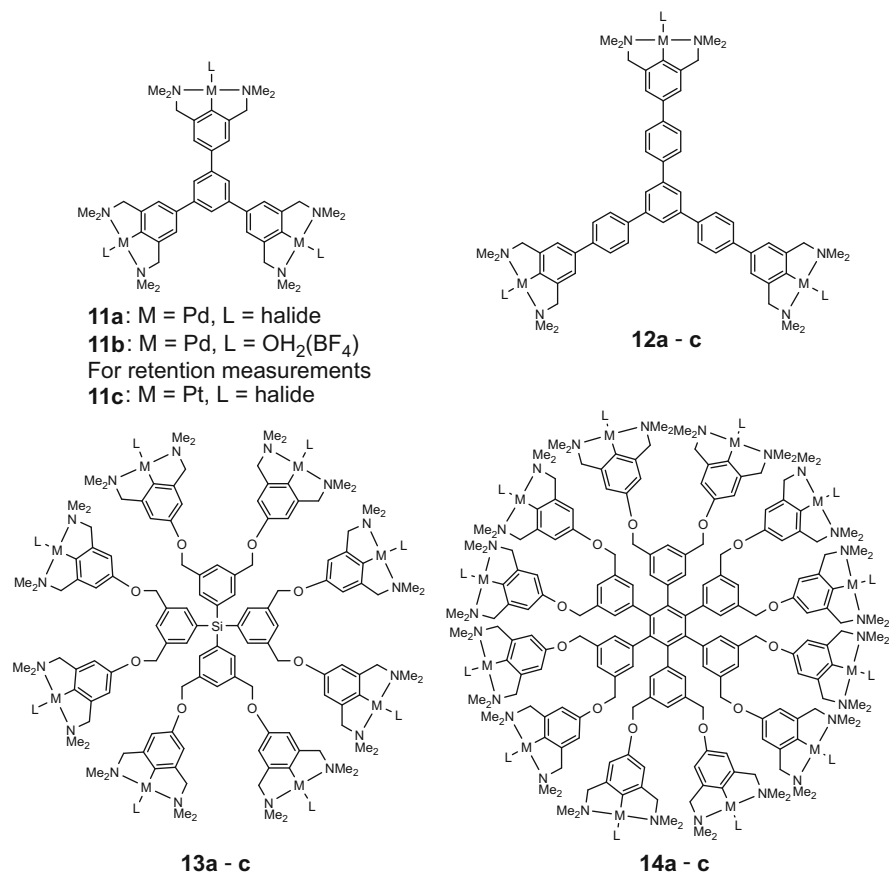
Fig. 2 Shape-persistent multimetallic pincer complexes [43]

membranes. Van Koten and co-workers decided to study this phenomenon by synthesising shape-persistent multimetallic pincer complexes and investigate the influence of rigidity and dimension of these materials on their retention behaviour. By directly comparing these results to the pincer containing dendritic systems discussed in the previous section, a good impression of the importance of shape persistence in the backbone of macromolecular catalysts could be obtained.

The shape-persistent multimetallic pincer complexes (**11–15**) used in this study are outlined in Fig. 2. Multi(NCN-MX) complexes containing palladium(II) and platinum(II) centres were prepared. The platinum complexes **11c–15c** were used to determine the retention rates of these materials by utilising the power of the NCN-PtX (X=halide) unit to absorb gaseous SO$_2$ (Scheme 7a), a process accompanied by a characteristic colour change from colourless to bright orange. This colour change allowed the use of UV–V is spectroscopy to accurately determine the concentration of the multi(NCN-Pt) complexes in the retentate and the permeate

Scheme 7 (**a**) Colour change due to SO_2 absorption by NCN-PtX; (**b**) double Michael addition reaction catalysed by NCN-Pd-catalysts
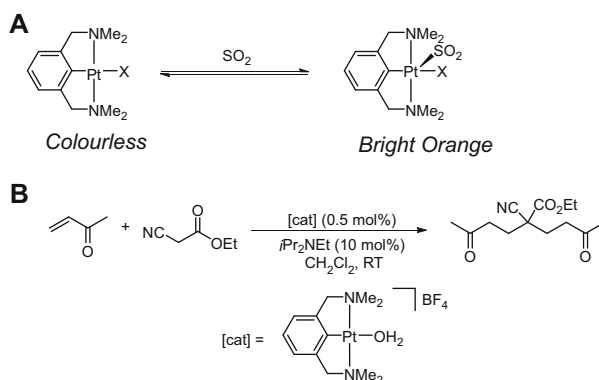
and thus the retention rates of these complexes by nanofiltration membranes. The palladium analogues on the other hand were used as homogeneous catalysts in the double Michael addition between methyl vinyl ketone and ethyl α-cyanoacetate (Scheme 7b).

Different synthesis strategies were used to prepare these shape-persistent multimetallic complexes. Trispincer complexes **11** [45] and **12** [46] were prepared via a triscondensation reaction of pincer acetophenone derivatives **16** followed by the oxidative addition of Pd(dba)$_2$ (dba = dibenzylideneacetone) or [Pt(p-tol)$_2$Et$_2$S]$_2$ [47] to the carbon-iodine bond to afford complexes **11** and **12**, respectively (Scheme 8a). For octa- and dodecapincer systems **13** and **14**, an alternative strategy to construct multimetallic materials was developed. Instead of using the 'classical' strategy, i.e. to first fully prepare the ligand system followed by multiple metallation reactions on one molecule, here the individual mono-pincer systems were first metallated prior to coupling them to the shape-persistent supports. Whereas the former (classical) route often leads to incomplete metallations, especially when an increasing number of ligand sites have to be metallated, the latter strategy assures full metallation of all ligand sites present in the final multimetallic material. Thus, octa- and dodecapincer complexes **13** and **14** were prepared via an eight- and twelvefold ether coupling of monopincer precursors **17a,b** with octa- and dodecabenzylic bromide scaffolds **18** and **19** (Scheme 8b), respectively [45]. Remarkably, full loading of the macromolecular supports was achieved, and the complexes were isolated in good yields without any observable decomposition of the organometallic pincer sites.

To obtain an impression of the dimensions of these structures molecular modelling experiments were performed. The accuracy of molecular modelling was determined by comparing the molecular modelling structure of **11a** to its X-ray crystal structure, and it was shown that the structures were in good agreement, meaning that molecular modelling gives an accurate representation of the real molecular structures of complexes **11–14** [45]. In addition, molecular modelling also revealed that changing one pincer complex for another (NCNPdX for NCNPtX) did not change the geometry and size of these complexes. This was a
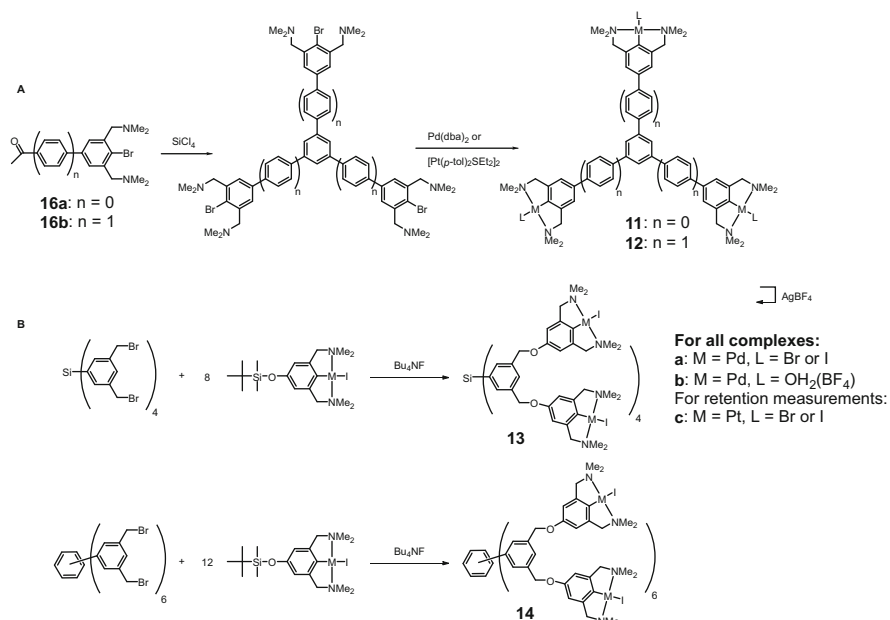
Scheme 8 Classical (**a**) and alternative approach (**b**) to synthesise shape-persistent multimetallic pincer complexes [47]

crucial aspect in this research since the NCNPt-complexes were used to determine the retention rates of these complexes by nanofiltration membranes, whereas the corresponding palladium complexes were applied as homogeneous catalysts. Thus, since the dimensions of these complexes are independent of the metal atom, the retention results obtained for the platinum complexes could be directly translated to the catalytically active Pd-analogues. It also meant that the retention results could be directly compared to those obtained with the carbosilane dendrimers bearing NCNNiCl moieties (see Sect. 2.1).

Nanofiltration studies with the pincer platinum complexes **11c–14c** using the MPF-60 nanofiltration membrane (MWCO = 400 Da) showed good retention rates with tripincer complexes **11c** ($R = 93.9\%$) and **12c** ($R = 98.7\%$) and excellent retention rates for octapincer complex **13c** ($R = 99.5\%$) and dodecapincer complex **14c** ($R = >99.9$) [45]. Remarkably, for dodecapincer complex **14c**, the concentration in the permeate was below the detection point of UV/Vis spectroscopy, meaning that the retention rate is $>99.9\%$. As a control, the mono-NCN-PtBr complex was also tested, and it was shown to have a retention rate of 82.4%, meaning that the catalyst is washed out of the reactor within 30 cycles. These results are in excellent agreement with the dimensions calculated by molecular modelling: increasing the size and three-dimensionality of these macromolecular materials going from the rather flat two-dimensional tripincer complexes **11c** (Br–Br distance = 17.5 Å, thickness ~6 Å) and **12c** (Br–Br distance = 24.6 Å,

thickness ~ 6 Å) to the more three-dimensional structure **13c** (sphere, diameter = 27.5 Å) and **14c** (flattened sphere, diameter = 32.1 Å and thickness = 24.3 Å) clearly resulted in enhanced retention rates with the largest shape-persistent multipincer complex (**14c**) showing complete retention by the nanofiltration membrane. To investigate the concept of shape persistence in the backbone of the macromolecular catalysts for attaining optimal retention rates, the calculated molecular volumes of **12c** and **14c** were related to their retention rates. Exactly the same procedure was also performed with the flexible carbosilane dendrimers G0 and G1 (Scheme 2). The calculated molecular volumes of shape-persistent complexes **12c** and **14c** were 1.2×10^3 and 4.4×10^3 Å^3, respectively, while dendrimers G0 and G1 possessed molecular volumes of 1.7×10^3 and 5.3×10^3 Å^3, respectively. Using the MPF-50 nanofiltration membranes (higher MWCO than the MPF-60 membranes, MWCO = 700 Da), retention rates of 97.6% for **12c**, 99.9% for **14c**, 97.4% for G0 and 99.8% for G1 were found. Thus, although the calculated molecular volumes of shape-persistent pincer complexes **12c** and **14c** are considerably smaller as compared to G0 and G1, respectively, they are more efficiently retained by nanofiltration membranes. It is plausible to state that this effect is due to the flexibility in the dendritic cores of G0 and G1, resulting in back-folding of the dendritic arms and thus in more dense rather than larger structures (also compared to lower-generation dendrimers). Although these differences in retention rates seem small, they can already have a significant impact when these catalysts are applied under continuously operating conditions.

As mentioned earlier, the shape-persistent multipincer systems were also tested as homogeneous catalysts in the double Michael addition reaction between methyl vinyl ketone and ethyl α-cyanoacetate (Scheme 7b) [43, 48]. In this reaction, the pincer complex acts as a Lewis acid. Since the charge neutral multi(NCN-PdX) complexes **11a–14a** are rather poor Lewis acids, also here they were first converted into the corresponding aqua complexes **11b–14b** (Scheme 8). The observed rate constants (k_{obs}) per palladium atom for catalysts **11b**, **12b** and **13b** (210–260×10^{-6} s^{-1}) were similar to the rate constant obtained for the reference monometallic NCN-Pd(OH$_2$)BF$_4$ catalyst (280×10^{-6} s^{-1}), showing that all palladium atoms efficiently act as independent catalytic sites. Remarkably, dodecapincer catalyst 14b exhibits a threefold increased activity per palladium centre ($k_{obs} = 810 \times 10^{-6}$ s^{-1}) as compared to the monometallic catalyst. Since it was ruled out that this was a consequence of the *para*-alkoxy group (*para* to the M–C bond), this activity increase must be a result of the high catalyst loading on the periphery of **14b**. It was suggested that cooperative interactions between neighbouring palladium sites during catalysis might occur. An alternative postulation was that the formation of polar micro-environments due to the highly charged periphery leading to enhanced catalytic activity.

Due to its complete retention by nanofiltration membranes and its high catalytic activity in the double Michael reaction, shape-persistent dodecapincer complex **14b** was also tested as a homogeneous catalyst in a continuous catalytic setup in a membrane reactor [49]. Two catalytic runs were performed in which the
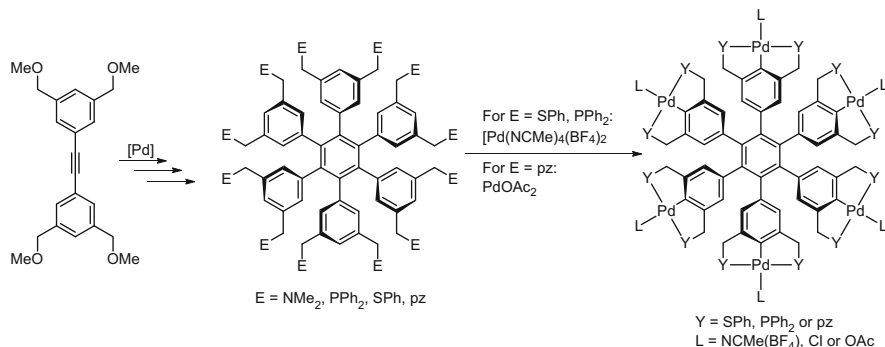
Scheme 9 Synthesis of hexa(pincer) complexes [50]

concentration of catalyst and the flow rate were varied (2.5× more catalyst and 2.5× higher flow rate in run 2 as compared to run 1). Remarkably, over the whole time range, the space-time yields in the second run were considerably higher as compared to the first run. Furthermore, in both experiments, no apparent loss of activity is observed, not even after 25 h (24 and 65 reactor volumes, respectively). Apparently, for this catalytic setup, a more efficient catalytic reaction is obtained with higher catalyst loading and flow-rates. Although no further kinetic data were obtained for this process, these results nicely illustrate that for this catalytic system, it is rather easy to obtain higher space-time yields by simply adjusting the continuous reaction conditions. The total turnover number per palladium site was increased with a factor 40 from 80 (batch process) to $>3,000$ Pd^{-1} (continuous process). This continuous catalytic system is one of the few examples in which macromolecular catalysts have been applied in a continuous catalytic setup [15]. In addition, it is rather remarkable that no loss of activity is observed not even after prolonged reaction time, a phenomenon often observed for other recyclable homogeneous catalysts. This example clearly shows the potential of soluble macromolecular complexes as recyclable homogeneous catalysts in new and more efficient catalytic processes.

Van Koten and co-workers have also reported on shape-persistent hexa(pincer) systems in which a central benzene scaffold is substituted at each position with a cyclometalated pincer moiety [43, 50]. The crucial step in the synthesis of the hexa (pincer) system was a trimerisation reaction of a symmetrically substituted acetylene under the influence of a palladium(II) catalyst to afford the hexa-pincer scaffold (Scheme 9) [51]. This route gave easy access to hexa(pincer) ligands containing pincer moieties with the NCN-, SCS- and PCP-tridentate coordination mode. Whereas the SCS- and PCP-ligands could be fully palladated using a direct electrophilic cyclopalladation procedure, a procedure earlier developed for mono-metallic systems [52, 53], the NCN-type systems appeared to be more troublesome. The NCN-system with the dimethylamino substituents could not be directly metallated using an electrophilic metallation procedure; therefore, it was attempted to use the lithiation/transmetallation procedure earlier described for the dendritic

NCN-Ni-catalysts (see 1.1.1, Scheme 2). Although complete lithiation was achieved, no fully palladated product could be obtained. It was proposed that this was caused by the poor solubility of partly metallated intermediates. To overcome this problem, the dimethylamino groups were replaced by pyrazol-1-yl moieties as it was known for the monopincer systems that the pyrazol-1-yl-based pincer systems could be directly palladated using $Pd(OAc)_2$ [54]. Applying this protocol, a fully palladated hexa(NCN-PdX) complex was obtained. Unfortunately, the solubility of this complex was too low to apply it as a homogeneous Lewis acid catalyst in the earlier mentioned double Michael addition reaction.

In order to broaden the scope of these materials, attempts were made to introduce metals other than palladium into the hexa(PCP) ligand. MonoPCP complexes containing many metal centres are known, and amongst them, the PCP-Ru complexes possess remarkably high catalytic activities in hydrogen transfer reactions. Recently, van Koten's group reported the so-called transcyclometallation (TCM) procedure as a mild and very selective method to introduce platinum(II) and ruthenium(II) centres into PCP-ligands [55, 56]. The TCM procedure involves the treatment of PCP-type ligands with cyclometalated NCN complexes resulting in a metal exchange between both pincer ligands, thus affording the metallated PCP-complex and free NCN ligand. A sixfold TCM protocol was used here to introduce selectively six platinum(II) and ruthenium(II) centres into hexa(PCP) ligand **15**. Thus, heating a mixture of hexa(PCP) ligand **15** with 6 equiv. of NCN-PtBr or NCN-Ru(PPh$_3$)Cl, afforded the corresponding hexaPCP-platinum **16** and –ruthenium complexes **17** (Scheme 10) in 70 and 79% yield, respectively [19]. No non-metallated ligand sites were observed. Interestingly, this procedure was found to be superior over the classical metallation procedures since treatment of hexa(PCP) ligand **15** with 6 equiv. PtCl$_2$(COD), for example, resulted in intractable product mixtures, probably due to nonselective metallations. Moreover, this selectivity effect was attributed to the special reaction mechanism of the TCM reaction that proceeds via a *trans*-C,Pt,C configuration, thereby preventing undesired side reactions [34–35]. Thus, the TCM procedure appeared to be ideally suited for multiple metallations within a single molecule, providing the multimetallic species in high yields.

Application of hexa(PCP-Ru(PPh$_3$)Cl) complex **17** as a homogeneous catalyst in the hydrogen transfer reaction between ketones and *i*-propanol (Scheme 11) revealed that the activity per Ru-centre in **17** was of the same order of magnitude as that of the mononuclear PCP catalyst [56]. This nicely illustrated that the all ruthenium centres act as independent catalysts, a very important feature for homogeneous catalysts containing multiple catalytic sites per molecule. Moreover, addition of another equivalent of ketone after complete conversion of the first batch revealed that the catalyst still possessed its initial catalytic activity, showing the stability of the catalyst under the applied reaction conditions. This implies that this catalyst is suitable for application under continuous reaction conditions in a membrane reactor.

The shape-persistent multi(pincer) complexes discussed in this section show great promise in the field of homogeneous catalyst recycling by means of
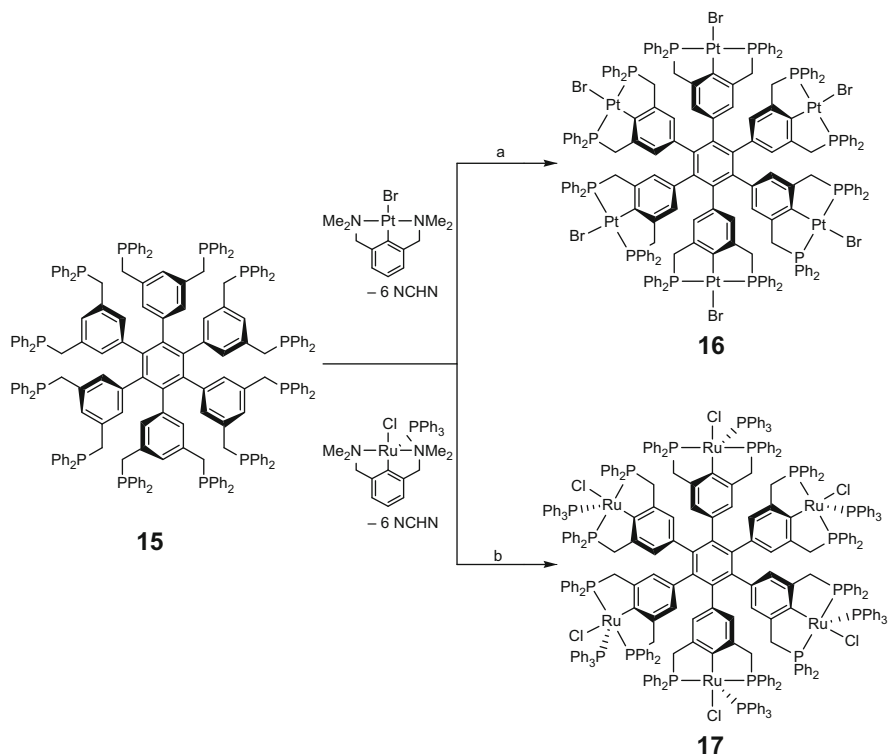
Scheme 10 Platinated and ruthenated hexa(PCP)-complexes [55]
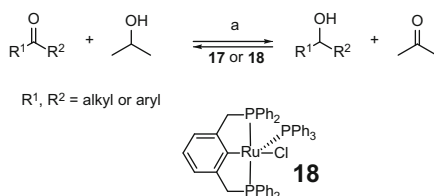
Scheme 11 PCP-ruthenium complexes as hydrogen transfer catalysts

nanofiltration techniques. Partly due to their rigidity, they are very efficiently retained by nanofiltration membranes. In addition, the metallated pincer moieties show great thermal and kinetic stability under the homogeneous catalytic conditions as was clearly illustrated by the continuous catalytic setup using dodeca (NCN) pincer catalyst **14b** and by hexa(PCP-Ru(PPh₃)Cl) catalyst **17**. For obvious reasons, this latter aspect of catalyst stability is of crucial importance in the research area of homogeneous catalyst recycling. This stability feature together with the straightforward immobilisation protocols of pincer moieties and the efficient

recycling behaviour of the macromolecular pincer catalysts explain the great success of the macromolecular pincer complexes in this research area.

3 Organic and Inorganic Polymeric Supports

The immobilisation of pincer-type complexes is not only confined to macromolecular organic supports. Silica has been widely used as a support material, while the use of clays and organic polymers has also been reported. The difference between soluble and insoluble organic supports needs to be clarified. Soluble supported catalysts are used in homogeneous reaction mixtures with the eventual goal of catalyst recycling using membrane techniques. Insoluble organic polymeric and inorganic supports have been used in biphasic catalytic solutions and can be separated from the reaction mixture by simple decantation or filtration techniques. Immobilisation of the pincer complexes should theoretically lead to easier recycling of the expensive catalyst. This is the ultimate goal when looking to immobilise homogeneous catalysts, to mimic the high recyclability and manageability of heterogeneous catalysts, while retaining the high selectivity and predictability of homogeneous catalysts. Tethering of the pincer complexes through substituents on the *para*-position of NCN-, PCP-, and SCS-Pd is the preferred mode of immobilisation.

3.1 Soluble Organic Polymeric Supports

Van Koten and Frey have collaborated to immobilise pincer complexes on hyperbranched-soluble organic supports. These compounds were easier to synthesise than their monodisperse dendrimer relatives and were thus of particular interest. Initial work focussed on hyperbranched polycarbosilane compounds which were functionalised with NCN-Pd pincer complexes [57]. Polymerisation of triallylsilane with a platinum catalyst yielded a hyperbranched allylic support (Scheme 12, polytriallylsilane, PTAS) which reacted readily with dimethylsilylchloride, in a platinum-catalysed hydrosilylation, to give a hyperbranched chlorosilane polymer. This species reacted with *para*-lithiated pincer ligand. The hyperbranched ligand and complex were purified using dialysis techniques, suggesting it was a good candidate for nanofiltration studies. Metallation followed by halide abstraction with AgBF$_4$ gave the Pd-aqua complex which was used as a catalyst in the Aldol addition of benzaldehyde and methylisocyanoacetate. The turnover frequency (TOF) of the immobilised catalysts was approximately half of the homogeneous *para*-trimethylsilyl-NCN-Pd catalyst.

Later work focussed on immobilising pincer complexes on various forms of hyperbranched polyglycerol supports (Scheme 13). Initially *para*-sulphonated NCN-Pt was immobilised in a hydrophilic polyglycerol with alkyl tails [59].

i) [(COD)PtCl₂], 40 oC; ii) HSiMe₂Cl, [(Bu₄N)₂PtCl₆], RT;
iii) LiNCN, Et₂O, -78 to RT, tBuLi, dialysis;
iv) nBuLi, [PdCl₂(SMe₂)₂], pentanes/THF;
v) AgOTf, acetone/H₂O
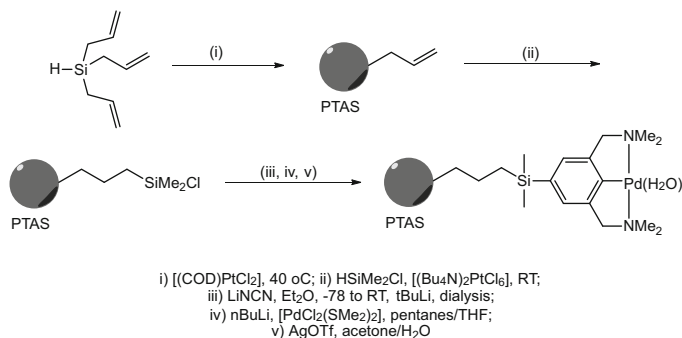
Scheme 12 Polymerisation of triallylsilane and subsequent immobilisation of NCN-Pd complex on the polysilane support [57]
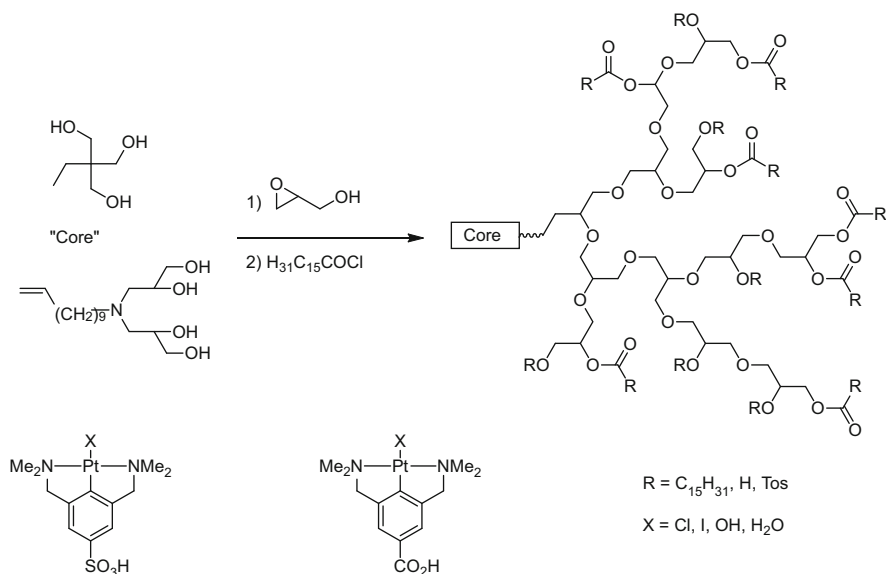
Scheme 13 *para*-Sulphonate and *para*-carboxylate pincer-platinum complexes for immobilisation in hyperbranched polyglycerolic supports [58]

The uptake of sulphonated NCN-Pt by the hyperbranched polyglycerol was monitored using UV–Vis spectroscopy. A plot of absorbance versus concentration ratio gave an inflection point, suggesting a clear effect of molecular weight on the loading capacity of the polymer. It was observed that at concentration levels above the inflection point, *increased* amounts of complex were taken into the polymer. The reason for this was suggested to be the formation of micelle-type species around a hydrophilic core (the complex or aggregate thereof). The immobilised sulphonated catalyst was tested in the double Michael addition of
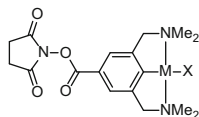
Fig. 3 Active ester-functionalised NCN-M complex [58]

ethyl cyanoacetate to methyl vinyl ketone; however, there was not a significant rate enhancement compared to the blank reaction, suggesting the aggregated/micellar species were deactivated forms of the catalyst. Subsequent work showed *para*-carboxylate-functionalised NCN-Pt complexes covalently immobilised on similar hyperbranched polyglycerol supports [60]. Activation of hyperbranched polyglycerol by tosylation was followed by reaction of the pertosylated polyglycerol with the potassium salt of *para*-carboxylato-NCN-Pt which yielded polyglycerated NCN-Pt-I. The presence of heavy Pt and I atoms meant that the compounds were visible by transmission electron microscopy (TEM). TEM showed disc-shaped structures, the size of which could be altered by varying the degree of substitution with platinum pincer moiety. Optically active hyperbranched polyglycerol was then used as a support for both *para*-sulphonated and carboxylated NCN-Pt pincer complexes [61]. As with the achiral supports, an inflection point was observed when loading the *para*-sulphonate pincer on the support. Circular dichroism (CD) experiments were carried out on both sets of immobilised catalyst. When the *para*-sulphonate complex was present, low-intensity CD bands were observed, suggesting that the complex was immobilised in the chiral support. The covalently bound chiral catalyst showed a reaction rate similar to that of the free catalyst, however, again with no enantioselection.

The van Koten group have, in a similar vein, immobilised NCN-Pt and -Pd complexes on dendrimer-functionalised polystyrene for use in the Aldol reaction [58]. Active ester chemistry was used to couple a *para*-carboxylato NCN-M complex on polyamino-functionalised polystyrene species (Fig. 3). The aldol condensation of benzaldehyde with methyl-isocyanoacetate catalysed by immobilised NCN-Pd complex showed quantitative conversion. The immobilised complex showed a substantial decrease in activity compared to its homogeneous counterpart. Upon recycling using simple filtration techniques, a decrease in activity was observed.

Immobilisation of thermally stable organometallic pincer complexes on non-ordered organic support materials has been successfully demonstrated using a number of organic support materials such as polysilanes, polyethers and polyamines. In all cases, the polymer-immobilised complexes demonstrated lower relative activity than their homogeneous analogues and in certain cases showed lower reactivity upon recycling. This lower reactivity can be assigned to mechanical decomposition of the organometallic materials, or indeed metal leaching. Most importantly, however, is that immobilisation of pincer-metal complexes on non-ordered polymeric materials is a cheap, facile method for heterogenisation of homogeneous catalysts and has been demonstrated not to affect the selectivity of the organometallic species in Lewis acid-catalysed transformations.
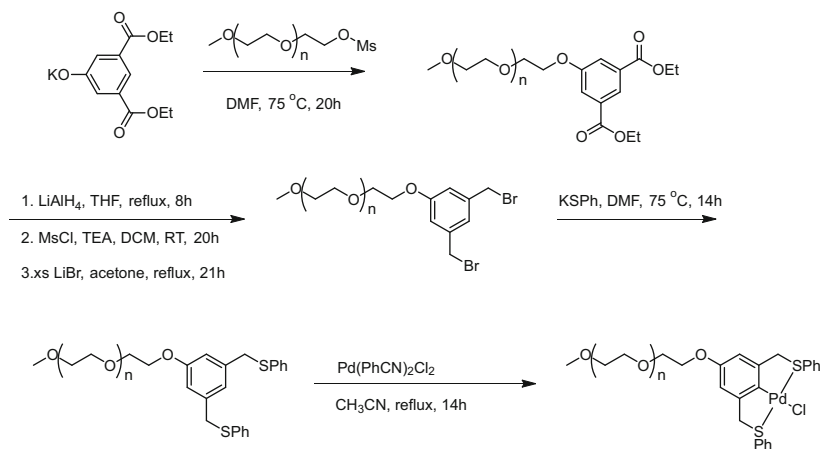
Scheme 14 Synthesis of PEG-SCS-Pd-Cl [63]

Bergbreiter and co-workers were to the fore in immobilising homogeneous catalysts on soluble organic polymeric supports [62]. Their initial work was directed towards single SCS-Pd complexes bound to linear poly(ethylene glycol) (PEG) tails with molecular weights of 5,000 [63]. Reaction of diethyl 5-hydroxy isophthalate with mesylate-terminated PEG gave the ester PEG-isophthalate (Scheme 14). Reduction of the ester to the alcohol followed by halogenation and subsequent reaction with activated thiophenol yields the PEG-SCS ligand.

The catalyst was tested in the Heck coupling reaction and was found to be an active catalyst. It was observed that the catalyst slowly decomposed, as does its homogeneous analogue, and thus was not tested in recycling experiments. A *para*-amino-functionalised SCS analogue was reacted with succinic anhydride yielding a carboxylate, which was then coupled with the PEG tail. This catalyst was also active, and did not show decomposition, and was used in recycling tests. The catalyst was recycled by adding the post-catalysis reaction mixture to diethyl ether solution, resulting in precipitation of the catalyst, which could be isolated by filtration. No loss in activity was observed upon recycling. The same group later published similar work with polyisobutylene oligomers bound to an SCS-Pd complex [64]. Later work showed multimetallic polymer-supported SCS-Pd complexes used under thermomorphic conditions [65, 66]. Poly(*N*-isopropylacrylamide) (PNIPAM) bound SCS-Pd complexes, and the previously mentioned PEG-SCS-Pd were used in a type of biphasic catalysis. At room temperature, the substrate was dissolved in heptanes and the catalysts in ethanol or dimethylacetamide. When combined at room temperature, these solutions were immiscible; however, upon heating, a homogeneous solution was obtained and catalytic conversion was observed. Re-cooling created a biphasic system again and allowed for catalyst recycling. PEG-SCS-Pd showed activity in the thermomorphic mixture and was recycled 3 times, with increasing conversion levels (run one 53%, run three >99%).

PNIPAM-bound SCS-Pd showed improved catalytic activity and also a similar pattern of increased yields upon recycling (up to 4 cycles!). This unusual increase in conversion levels was unexplained in the publications.

3.2 Pincer Complexes Immobilised on Insoluble Support Materials

Alper has been to the fore in immobilising PCP-Pd-type complexes on silica [67, 68]. Protected (as phosphine oxide) *para*-amino-functionalised PCP ligand was reacted with succinic anhydride and deprotected (Scheme 15). Carboxylic acid activation was carried out, and the resulting synthon was reacted with amino-functionalised silica, yielding the immobilised ligand. Similarly, PAMAM-functionalised silica was reacted with the activated acid yielding dendronised silica-supported ligands of various generations. Complexation was carried out using palladium bistrifluoroactate.

Catalytic intramolecular cyclocarbonylation was carried out using these catalysts. A range of allylphenols was tested. Overall selectivity was found not to be generation dependant, but CO/H_2 pressure and temperature dependant. Activity was indeed generation and tail length dependant, with the highest generation dendrimer giving the best reaction rates. The extended-tailed G1 system showed greater activity than the shorter G1 and the G0. The G0 catalyst was recycled and depending on the substrates could be reused up to 5 times. However, in most cases, recycling led to a loss in activity and/or selectivity. Interestingly, a co-ligand was always added to the reaction mixture. Diphenylphosphinobutane (DPPB) was used as the co-ligand, and without it, the reaction was very slow to non-existent. This would suggest that there was decomposition of the pincer-palladium unit and that it was not the active catalyst. This observation was backed up by the poor recyclability results, which suggest the catalyst was in the filtrate and not the filter. Other work had focussed on the G0 dendritic silica and its application in the Heck reaction. The homogeneous catalyst, used in the reaction of phenyl iodide with butyl acrylate, displayed a TOF of 1,983 h^{-1}, which was about 4 times that of the heterogenised catalyst (505 h^{-1}). Recycling tests were carried out and showed no loss in yield over 5 cycles in particular reactions. There was no mention of changes in reactions rates.

As is evident, considerable effort has been expended on immobilised pincer-palladium complexes on inorganic support materials for cross-coupling catalysis (i.e. Heck reaction). However, in almost all cases, deactivation occurs upon recycling or indeed during the initial catalytic experiments. To address this apparent catalyst decomposition, Jones and co-workers have thoroughly investigated whether or not pincer-palladium complexes are stable under cross-coupling reaction conditions, by immobilisation of several pincer-palladium complexes (Fig. 4) [69–71]. SCS- and PCP-palladium complexes were immobilised on both silica and
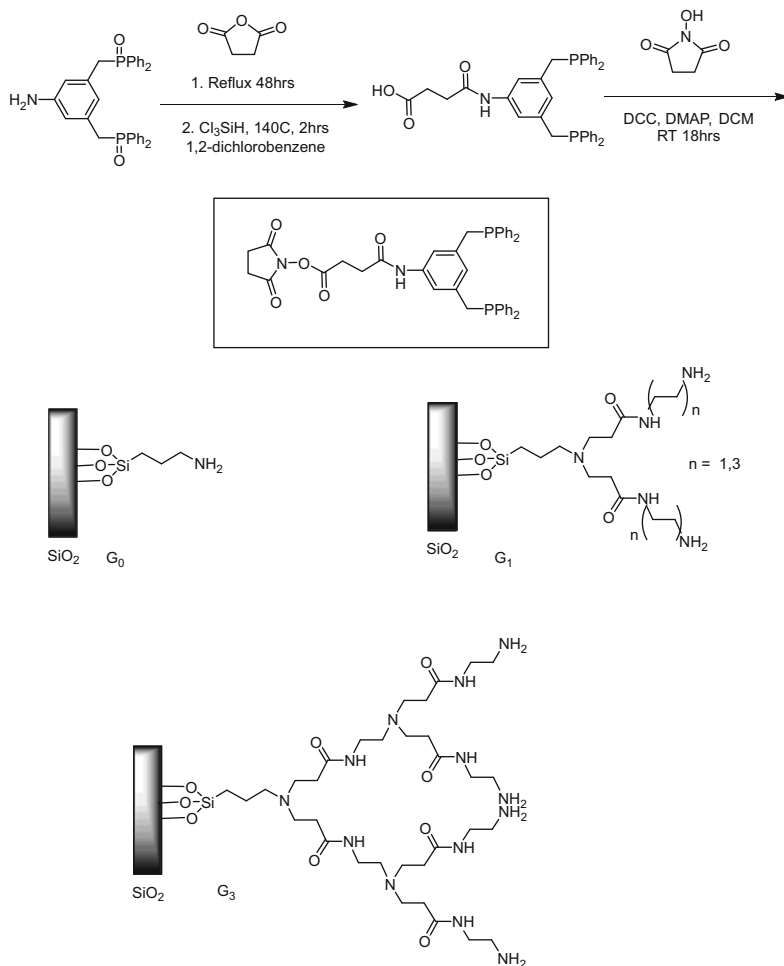
Scheme 15 Synthesis of dendritic PCP ligands on PAMAM functionalised silica support [67, 68]

organic polymeric supports using either hydroxyl or amino functionalities at the *para*-position of the pincer complex. For silica immobilisation, the *para*-hydroxy SCS- and PCP-complexes were coupled with iodopropyltrimethoxysilane, and the resulting compound could be easily grafted onto a silica support. For immobilisation of organic polymeric supports, both amino and hydroxyl functionalised pincers were reacted with activated polymer precursors or polymers themselves [72].

With all the catalysts that were used, high yields and impressive activity were observed in Heck cross-coupling reactions. Furthermore, no Pd black was observed, which is often the case when homogeneous catalysts are used under Heck conditions. The heterogenised catalysts all behaved similarly to their homogeneous counterparts. However, recycling of the catalysts (liquid biphasic separation for
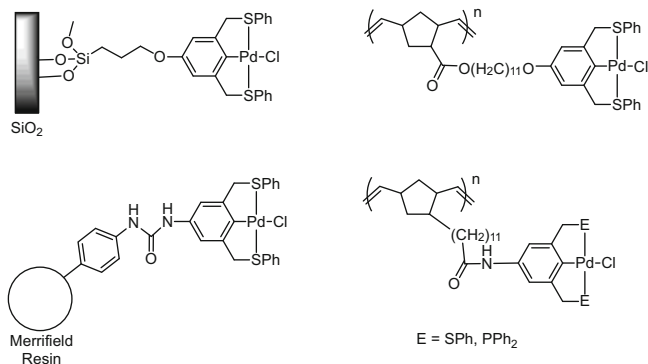
Fig. 4 Pincer-palladium complexes immobilised on silica, Merrifield resin and polynorbornene in Jones' mechanistic studies [69–71]

norbornene, frit filtration for silica/Merrifield) showed that gradual decreases in activity were occurring over successive cycles. It was also observed that approximately 20% of palladium on the support was lost per catalytic cycle. Leaching of palladium species was only occurring under catalytic conditions, and not all pincer-palladium complex was leaching palladium, as post-catalytic spectroscopy showed. When mercury(0) was added to the catalytic solution of both the multimetallic heterogeneous and multimetallic homogeneous catalysts, complete deactivation was observed. Mercury(0) forms an amalgam with palladium(0) particles and stops them from being catalytically active. When polyvinylpyridine (PVPY) was added to the multimetallic species, no activity was observed, suggesting that Heck activity comes from dissolved palladium species. Because no observation of palladium black was observed, and the filtrate of the catalysed solution was active when further substrates were added, it was presumed that soluble palladium(0) clusters were forming from the pincer-palladium(II) complexes. These soluble palladium clusters are the active catalysts in the reaction. This theory was further backed up when iodobenzene was immobilised on an inorganic support and was placed under Heck reaction conditions with silica immobilised SCS-Pd. It was observed that the supported iodobenzene reacted with butyl acrylate. This work has shown that pincer-palladium complexes are in fact pre-catalysts to soluble palladium(0) species in the Heck cross-coupling reaction and are themselves not active catalysts. This study has led others to hypothesise whether all palladium-catalysed cross-coupling reactions rely on soluble palladium(0) clusters [73].

Although tethering of organometallic pincer complexes to inorganic supports for cross-coupling reactions has shown us the pincer-organometallic is in fact a pre-catalyst, pincer complexes immobilised on inorganic support materials have been applied in an array of other transformations. Polydimethylsiloxane has been used as a support for organometallic NCN-Ni complexes [74]. Two separate synthetic routes were taken towards immobilising the catalyst: (1) carboxylate-functionalised polydimethylsiloxane was activated and reacted with 5-amino-2-
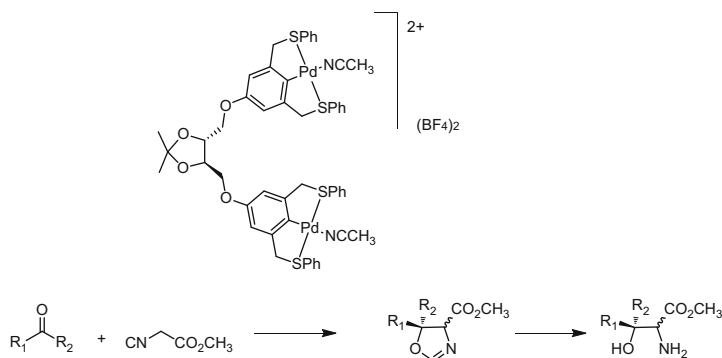
Scheme 16 Multimetallic SCS-Pd complex for asymmetric Aldol reaction [75]

bromo-1,3-bis[dimethylamino)methyl]benzene, yielding the immobilised ligand which reacted with Ni(COD)$_2$ giving the immobilised complex and (2) a commercially available organohydrosiloxane polymer was reacted with an allyl-functionalised NCN-Br ligand, yielding the immobilised ligand in a platinum catalysed hydrosilylation. IR, ^{1}H, ^{29}Si NMR and DSC were used to characterise the polymer-supported complexes. The immobilised catalysts were used in the Kharasch addition reaction of polyhalogenated compounds with alkenes. Various nickel loadings were tested, and the only system which showed equal activity with that of the free catalyst was that with the lowest density of catalytic sites on the surface (other loading levels gave diminished activity). A purple precipitate was observed from the homogeneous reaction mixtures which did not affect the catalytic results. This purple precipitate had characteristic Ni(III) properties and was suspected to be a catalyst decomposition product, vide supra.

Swager and Giménez have immobilised multimetallic SCS-Pd complexes on silica for use in asymmetric aldol addition reactions [75]. The chiral bimetallic species (Scheme 16) was synthesised to analyse the effect of a chiral pocket on the reaction of methyl-isocyanoacetate with various aldehydes. The chiral complex was synthesised using standard SCS pincer synthetic techniques, with the pincer ligands being constructed on the chiral backbone. The chiral complex did not show any increase in *cis/trans* ratio in comparison with the monometallic achiral analogue, and as with the homogeneous analogue, no enantioselectivity, thus suggesting no chiral pocket effect, or effect by neighbouring catalytic sites.

The multimetallic species was then tethered to silica via the chiral backbone of the complex (Scheme 17). Activation of silica gel by refluxing in thionyl chloride yielded a highly active silica which reacted readily with the hydrolysed ketal of the chiral complex. The complex was thus immobilised in a bidentate manner on the inorganic support. A second catalytic material, with the remaining surface silanol groups capped, was also synthesised. The principle behind immobilisation was to force the palladium centres to be in closer proximity to each other. Selectivity for *cis/trans* isomers was the same as with the unsupported catalysts. However, there
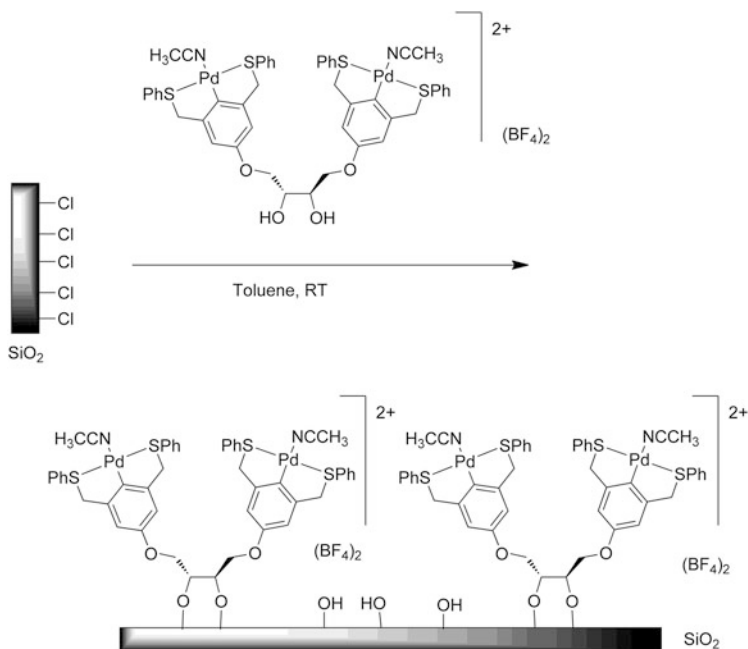
Scheme 17 Immobilised bimetallic SCS-Pd complex [76]
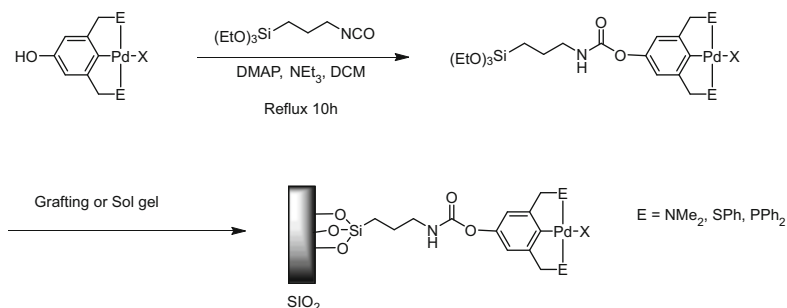
Scheme 18 Immobilised NCN-Pd pincer complex [77]

was a reproducible enantiomeric excess of 2–3%, suggesting that there was some cooperation between metallic sites which was yielding a chiral pocket.

The van Koten group has immobilised ECE-Pd-type pincers for the same reaction [76, 77]. *para*-Hydroxy-functionalised ECE-Pd pincer complexes were reacted with an activated tether (Scheme 18). The resulting complex was immobilised on silica using both grafting and sol-gel techniques. Alternatively, *silicatein protein* filaments, which had been isolated from marine demosponges, were reacted with the triethoxysilane precursor to yield an immobilised pincer complex [78]. Due to the stability of the pincer complex, it is possible to immobilise

the complex itself on the support, thus alleviating the possibility of untoward interactions between the silica and the metal centre while introducing the metal to the ligand. This is, in fact, the case with most pincer complexes immobilised on insoluble supports and is a rarity in immobilisation chemistry. Most often, the complex is constructed on the support, due to the harsh reaction conditions required to induce covalent binding of an organic moiety to an inorganic compound. However, the stability of the metal-carbon σ-bond, flanked by the dative bonds of the two arms of the pincer ligand, means that a wide range of immobilisation techniques can be availed of without developing new synthetic procedures.

The depicted complexes were converted to the aqua form of the complex and tested in the aldol reaction of benzaldehyde with methyl isocyanoacetate. Catalytic results showed the immobilised catalysts to be active as both aqua salts and as the metal halide complexes. It was also found that silver salts used to convert the metal halide to the aqua salt were active catalysts in this reaction. Recycling of the catalytic materials was carried out by centrifugation and subsequent decantation. Substantial losses in activity were observed over consecutive recycles when NCN and SCS complexes were used. The PCP complex was shown to be active over 5 recycles of the catalyst, with minimum leaching of palladium species into the reaction mixture. The decreased activity in SCS and NCN complexes was assigned to the low stability of the active catalyst. Insertion of isocyanate into the σ-aryl-palladium bond yields what was believed to be the active material [79]. It was believed that surface reconstitution led to loss of/inaccessibility to catalytic material and hence a decrease in activity.

Copper(I)-catalysed 1,3-Huisgens cycloaddition and nucleophilic reaction of an alcohol with an isocyanate have been applied to demonstrate 'click' immobilisation of pincer-palladium and platinum organometallics on silica [80]. Novel materials for this 'click' immobilisation have been developed containing both azide and isocyanate functionalities (Scheme 19). The acquired pincer-palladium-containing materials were applied in two types of C–C bond-forming reactions. In the Lewis acid-catalysed double Michael addition reaction of methyl vinyl ketone with ethyl cyanoacetate, the developed materials showed activity comparable to the
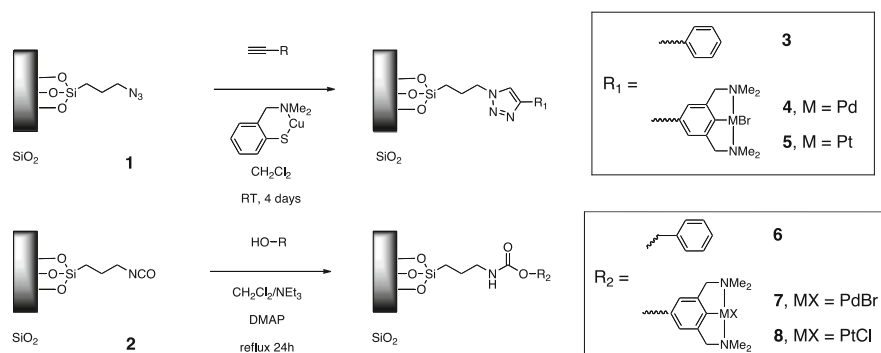
Scheme 19 'Click' immobilisation of pincer-palladium/platinum complexes on silica [80]

homogeneous catalyst. Furthermore, a model system containing only the linkers that connect the pincer organometallic to the support was found to be almost as active as the homogeneous palladium catalyst. This demonstrates the noninnocent role that the linkers can play in the 'heterogeneously' catalysed reaction. Furthermore in the successful allylic stannylation reactions, the triazole linker was again found to be noninnocent. Importantly, the synthesised materials are found to be easily recycled over numerous cycles, demonstrating the practical feasibility of the presented immobilisation technique. Catalyst stability is an important point in the developed systems. Recycling of the immobilised pincer organometallics resulted in minimal complex decompositions. The recyclability of the materials relies heavily upon the robustness and stability, both thermal and mechanical, that pincer organometallics provide.

Brookhart and Goldman have immobilised PCP-pincer iridium complexes on insoluble support materials such as Merrifield resin, silica and alumina [81, 82]. As detailed in Chap. 1 [14], Jensen, Kaska, Brookhart and Goldman have had tremendous success in applying PCP-Ir(III) complexes in the dehydrogenation of linear alkanes to yield alkenes, amongst others. Brookhart and Goldman have also had success in applying catalytic materials containing either adsorbed or tethered PCP-Ir complexes. Initial studies focussed on adsorbing Lewis-donor (alkoxide, phosphine, pyrimidine) functionalised PCP-Ir complexes on γ-Alumina (Scheme 20, top row). The polar Lewis donors were postulated to interact with the polar alumina to facilitate immobilisation. The resultant materials were robust materials that were capable of catalysing the transfer dehydrogenation between cyclooctane (COA) and *tert*-butylethylene (TBE, 2-dimethyl-1-butene) to yield cyclooctene (COE) and *tert*-butylethane (TBA, 2-dimethylbutane). Interestingly, these heterogenised catalysts demonstrated TONs considerably better than their
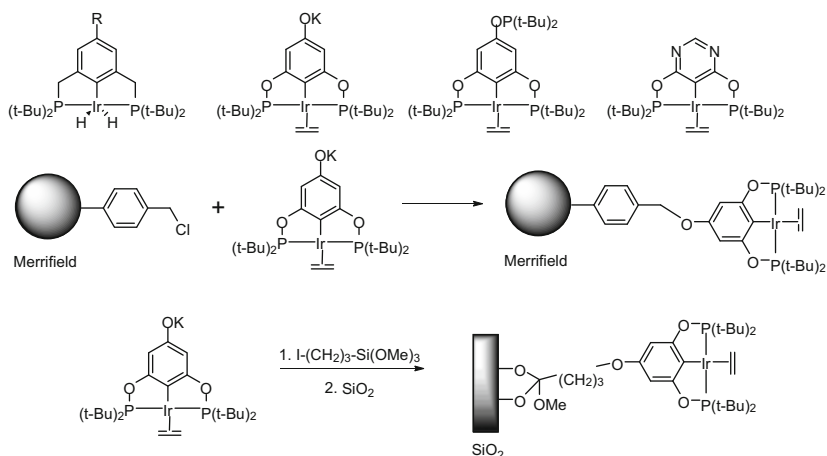
Scheme 20 Functionalised and tethered PCP-Ir complexes for heterogeneous transfer hydrogenation catalysis [81, 82]
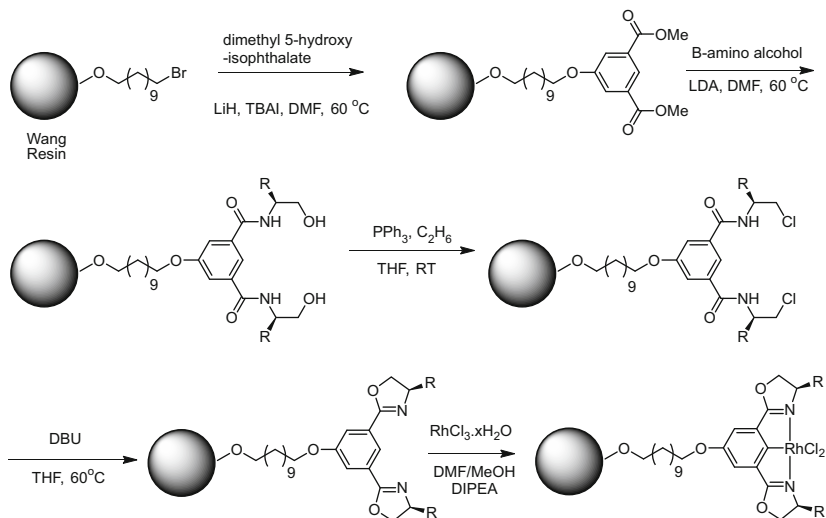
Scheme 21 Immobilised PheBox-Rh pincer complex [83]

homogeneous counterparts. The higher activity of the heterogenised catalysts was assigned to their greater stability, although insight into the reason for this stability was not provided. The adsorbed catalysts were recyclable over 8 cycles; however, considerable losses in activity (~50% decrease in TON) were observed even after the first cycle, indicating that copious leaching of the catalyst was occurring. Such leaching is to be expected when non-covalent catalyst immobilisation techniques are implemented. To overcome this problem, the authors synthesised two co-valently immobilised PCP-Ir complexes using a Merrifield resin, or silica, as the support material (Scheme 20, bottom). However, both of these materials showed diminished activity with respect to their homogeneous analogues and the adsorbed complexes.

Portnoy has constructed chiral bis-oxazoline (Box) pincer complexes on an insoluble polymeric support [83]. A brominated undecanol tether was bound to a Wang resin and was coupled with 5-hydroxyisophthalate. The immobilised isophthalate was reacted with a chiral amino alcohol. Subsequent halogenation and ring closing was performed to yield the immobilised Box ligand. Hydrated rhodium trichloride was reacted with the polymeric ligand, yielding the immobilised catalyst (Scheme 21). The catalyst was tested in the asymmetric allylation of various aldehydes. Depending on the functionalities on the Box ligand and also the substrate, *ee*'s as high as 48% were observed. Longer reaction times were necessary with the immobilised catalysts. The immobilised catalyst could be recycled with minimal losses in activity over 2–3 cycles.

4 Conclusions

The robustness that the pincer ligand framework imbues upon pincer complexes allows for thorough investigation of the potential of a tethering technique for immobilising homogeneous catalysts. Given that the pincer complex does not decay readily in multiple catalytic cycles, as demonstrated herein, the merits of any recycling technique can be adjudicated without the impediments typical of more labile coordination compounds. This ease of assessment has provided an array of tethered pincer complexes and has provided vital insights into the merits of dendritic, rigid organic, soluble polymeric and insoluble polymeric support materials. Major achievements in catalyst recycling, such as dendrimer pincer immobilisation, membrane filtration of dendritic pincer catalysts have been made. Furthermore, vital breakthroughs in the synthetic techniques required to functionalise, couple and tether coordination complexes have been demonstrated using pincer complexes. Finally, important insights into the role of colloidal metal species in cross-coupling reactions were obtained by using tethered pincer complexes in mechanistic studies. The importance of these breakthroughs cannot be understated, and they were achieved on the back of the exceptional flexibility of the pincer framework to functionalisation and, most importantly, the tremendous stability of the pincer complex.

References

1. Blaser H-U (2003) Chem Commun 293–296
2. Cole-Hamilton DJ (2003) Science 5613:1702–1706
3. Fodor K, Kolmschot SGA, Sheldon RA (1999) Enantiomer 4:497–511
4. Song CE, Lee S (2002) Chem Rev 102:3495–3524
5. Ribourbouille Y, Engel GD, Gade LH (2003) CR Chim 6:1087–1096
6. Shuttleworth SJ, Allin SM, Sharma PK (1997) Synthesis 1217–1239
7. Pozzi G, Shepperson I (2003) Coord Chem Rev 242:115–124
8. Herrmann WA, Kohlpainter CW (1993) Angew Chem Int Ed Engl 32:1524–1544
9. De Vos DE, Vankelecom IFJ, Jacobs PA (eds) (2005) Chiral catalyst immobilization and recycling. Wiley-VCH, Weinheim
10. Fan Q-H, Li Y-M, Chan ASC (2002) Chem Rev 102:3385–3466
11. Vankelecom IFJ (2002) Chem Rev 102:3779–3810
12. Dijkstra HP, van Klink GPM, van Koten G (2002) Acc Chem Res 35:798–810
13. Müller C, Nijkamp MG, Vogt D (2005) Eur J Inorg Chem 4011–4021
14. Gossage RA (2015) Pincer complexes of lithium, sodium, magnesium and copper: a discussion of solution and solid-state aggregated structure and reactivity. In: Gossage RA, van Koten G (eds) Organometallic pincer chemistry II. Topics in organometallic chemistry. Springer, Heidelberg
15. Kragl U (1996) Immobilized enzymes and membrane reactors. In: Godfrey T, West S (eds) Industrial enzymology, 2nd edn. Macmillian, Hampshire, p 275
16. Dickerson TJ, Reed NN, Janda KD (2002) Chem Rev 102:3325
17. Bergbreiter DE (2002) Chem Rev 102:3345

18. Knapen JWJ, van der Made AW, de Wilde JC, van Leeuwen PWNM, Wijkens P, Grove DM, van Koten G (1994) Nature 372:659
19. Dijkstra HP, Albrecht M, van Koten G (2002) Chem Commun 126
20. Dijkstra HP, Albrecht M, Medici S, van Klink GPM, van Koten G (2002) Adv Synth Catal 344:1135
21. Van Heerbeek R, Kamer PCJ, van Leeuwen PWNM, Reek JNH (2002) Chem Rev 102:3717
22. Kreiter R, Kleij AW, Klein Gebbink RJM, van Koten G (2001) Top Curr Chem 217:163
23. Astruc D, Chardac F (2001) Chem Rev 101:2991
24. Kleij AW, Gossage RA, Jastrzebski JTBH, Boersma J, van Koten G (2000) Angew Chem Int Ed 39:179
25. Kleij AW, Gossage RA, Klein Gebbink RJM, Reyerse EJ, Brinkmann N, Kragl U, Lutz M, Spek AL, van Koten G (2000) J Am Chem Soc 122:12112
26. Gossage RA, Jastrzebski JTBH, van Ameijde J, Mulders SJE, Brouwer AJ, Liskamp RMJ, van Koten G (1999) Tetrahedron Lett 40:1413
27. Albrecht MA, Hovestad NJ, Boersma J, van Koten G (2001) Chem Eur J 7:1289
28. Pijnenburg NJM, Lutz M, Siegler MA, Spek AL, van Koten G, Klein Gebbink RJM (2011) New J Chem 35:2356–2365
29. Kleij AW, van de Coevering R, Klein Gebbink RJM, Noordman AM, Spek AL, van Koten G (2001) Chem Eur J 7:181
30. van de Coevering R, Kuil M, Klein Gebbink RJM, van Koten G (2002) Chem Commun 1636–1637
31. van de Coevering R, Alfers AP, Meeldijk JD, Martinez-Viviente E, Pregosin PS, Klein Gebbink RJM, van Koten G (2006) J Am Chem Soc 128:12700–12713
32. Kimura M, Kato M, Muto T, Hanabusa K, Shirai H (2000) Macromolecules 33:1117
33. de Groot D, de Waal BFM, Reek JNH, Schenning APHJ, Kamer PCJ, Meijer EW, van Leeuwen PWNM (2001) J Am Chem Soc 123:8453
34. Oee M, Murata M, Takahama A, Muzugaki T, Ebitani K, Kaneda K (2003) Chem Lett 32:692
35. Oee M, Murata M, Muzugaki T, Ebitani K, Kaneda K (2003) J Am Chem Soc 125:1604
36. van de Coevering R, Klein Gebbink RJM, van Koten G (2005) Prog Polym Sci 30:474
37. de Groot D, Eggeling EB, de Wilde JC, Kooijman H, van Haaren RJ, van der Made A, Spek AL, Vogt D, Reek JNH, Kamer PCJ, van Leeuwen PWNM (1999) Chem Commun 1623
38. de Groot D, Reek JNH, Kamer PCJ, van Leeuwen PWNM (2002) Eur J Org Chem 1085
39. Hovestad NJ, Eggeling EB, Heidbüchel HJ, Jastrzebski JTBH, Kragl U, Keim W, Vogt D, van Koten G (1999) Angew Chem Int Ed 38:1655
40. Eggeling EB, Hovestad NJ, Jastrzebski JTBH, Vogt D, van Koten G (2000) J Org Chem 65:8857
41. Reetz MT, Lohmer G, Schwickardi R (1997) Angew Chem Int Ed 36:1526
42. Brinkmann N, Giebel D, Lohmer G, Reetz MT, Kragl U (1999) J Catal 183:163
43. Wooley K, Klug CA, Tasaki K, Schaefer J (1997) J Am Chem Soc 119:53
44. Chai M, Nui Y, Youngs WJ, Rinaldi PL (2001) J Am Chem Soc 123:4670
45. Dijkstra HP, Meijer MD, Patel J, Kreiter R, van Klink GPM, Lutz M, Spek AL, Canty AJ, van Koten G (2001) Organometallics 20:3159
46. Dijkstra HP, Kruithof CA, Ronde N, van de Coevering R, Ramón DJ, Vogt D, van Klink PM, van Koten G (2003) J Org Chem 68:675
47. Canty AJ, Patel J, Skelton BW, White AH (2000) J Organomet Chem 599:195
48. Dijkstra HP, Slagt MQ, McDonald A, Kruithof CA, Kreiter R, Mills AM, Lutz M, Spek AL, Klopper W, van Klink GPM, van Koten G (2003) Eur J Inorg Chem 830
49. Dijkstra HP, Ronde N, van Klink GPM, Vogt D, van Koten G (2003) Adv Synth Catal 345:364
50. Dijkstra HP, Steenwinkel P, Grove DM, Lutz M, Spek AL, van Koten G (1999) Angew Chem Int Ed 38:2186
51. Duchêne K-H, Vögtle F (1986) Synthesis 659
52. Loeb SJ, Shimizu GKH (1993) J Chem Soc Chem Commun 1396
53. Kickman JE, Loeb SJ (1994) Inorg Chem 33:4351

54. Hartshorn CM, Steel PJ (1998) Organometallics 17:3487
55. Dani P, Albrecht M, van Klink GPM, van Koten G (2000) Organometallics 19:4468
56. Albrecht M, Dani P, Lutz M, Spek AL, van Koten G (2000) J Am Chem Soc 122:11833
57. Schlenk C, Kleij AW, Frey H, van Koten G (2000) Angew Chem Int Ed 39:3445–3447
58. Suijkerbuijk BMJM, Shu L, Klein Gebbink RJM, Schlüter AD, van Koten G (2003) Organometallics 22:4175–4177
59. Slagt MQ, Stiriba S-E, Klein Gebbink RJM, Kautz H, Frey H, van Koten G (2002) Macromolecules 35:5734–5737
60. Stiriba S-E, Slagt MQ, Kautz H, Klein Gebbink RJM, Thomann R, Frey H, van Koten G (2004) Chem Eur J 10:1267–1273
61. Slagt MQ, Stiriba S-E, Kautz H, Klein Gebbink RJM, Frey H, van Koten G (2004) Organometallics 23:1525–1532
62. Bergbreiter DE (2002) Chem Rev 101:3345–3384
63. Bergbreiter DE, Osborn PL, Liu Y-S (1999) J Am Chem Soc 121:9531–9538
64. Bergbreiter DE, Li J (2004) Chem Commun 42–43
65. Bergbreiter DE, Osborn PL, Wilson A, Sink EM (2000) J Am Chem Soc 122:9058–9064
66. Bergbreiter DE, Osborn PL, Frels JD (2001) J Am Chem Soc 123:11105–11106
67. Chanthateyanonth R, Alper H (2003) J Mol Catal A Chem 201:23–31
68. Chanthateyanonth R, Alper H (2004) Adv Synth Catal 346:1375–1384
69. Yu K, Sommer W, Weck M, Jones CW (2004) J Catal 226:101–110
70. Sommer W, Yu K, Sears JS, Ji Y, Zheng X, Davis RJ, Sherrill CD, Jones CW, Weck M (2005) Organometallics 24:4351–4361
71. Yu K, Sommer W, Richardson JM, Weck M, Jones CW (2005) Adv Synth Catal 347:161–171
72. Pollino JM, Weck M (2002) Org Lett 4:753–756
73. Phan NTS, van der Sluys M, Jones CW (2006) Adv Synth Catal 348:609–679
74. Van de Kuil LA, Grove DM, Zwikker JW, Jenneskens LW, Drenth W, van Koten G (1994) Chem Mater 6:1675–1683
75. Giménez R, Swager TM (2001) J Mol Catal A Chem 166:265–273
76. Mehendale NC, Bezemer C, van Walree CA, Klein Gebbink RJM, van Koten G (2006) J Mol Catal A Chem 257:167–175
77. Mehendale NC, Sietsma JRA, de Jong KP, van Walree CA, Klein Gebbink RJM, van Koten G (2007) Ph.D. thesis, Ch 4, Utrecht University
78. O'Leary P, van Walree CA, Mehendale NC, Sumerel J, Morse DE, Kaska WC, van Koten G, Klein Gebbink RJM (2009) Dalton Trans 4289–4291
79. Mehendale NC, Klein Gebbink RJM, van Koten G (2007) Ph.D. thesis, Utrecht University
80. McDonald AR, Dijkstra HP, Suijkerbuijk BMJM, van Klink GPM, van Koten G (2009) Organometallics 28:4689–4699
81. Huang Z, Brookhart M, Goldman AS, Kundu S, Ray A, Scott SL, Vicente BC (2009) Adv Synth Catal 351:188–206
82. Huang Z, Rolfe E, Carson EC, Brookhart M, Goldman AS, El-Khalafy SH, MacArthur AH (2010) Adv Synth Catal 352:125–135
83. Weissberg A, Portnoy M (2003) Chem Commun 1538–1539

Index